Study of the Mechanical Performance of Similar and Dissimilar Titanium Alloy Joints Formed by Diffusion Bonding and Friction Stir Welding Processes

Neha Kulkarni

A dissertation
Submitted in partial fulfillment of the
requirements for the degree of

Doctor of Philosophy

University of Washington
2015

Reading Committee:
Ramulu Mamidala, Chair
Mark Tuttle
Daniel Sanders

Program Authorized to Offer Degree:
Mechanical Engineering

University of Washington

Abstract

Study of the Mechanical Performance of Similar and Dissimilar Titanium Alloy Joints Formed by Diffusion Bonding and Friction Stir Welding Processes

Neha Kulkarni

Ramulu Mamidala
Professor
Mechanical Engineering

Titanium alloys have turned strategically important in aerospace applications due to their high strength to weight ratio, corrosion resistance, and good strength sustainability at high temperatures. The joining of lightweight materials such as titanium alloys in aerospace industries offer two main benefits of near net shape manufacturing and of reduction in buy to fly ratio. Among the various joining methods, Diffusion Bonding and Friction Stir Welding (FSW) can be combined with superplastic forming, therefore, have been widely accepted technique to join titanium alloys to produce complex sheet structures with reduced weight and fabrication costs compared to mechanically fastened structures. Both the processes are mainly optimized for titanium alloy, Ti-6Al-4V, to produce defect free sheets of it. The other titanium alloys such as Ti-6242 and Ti-54MFG offer advantages of high temperature sustainability and better machinability over Ti-6Al-4V. The joining of titanium alloys with different properties can improve the utilization of titanium alloys and increase the functional properties of joints. However, a very limited research has been

conducted on joining techniques with dissimilar titanium alloys. Therefore, the current study examines the processes with dissimilar titanium alloys to broaden the application of the process with titanium alloys. The capability of diffusion bonding process for similar and dissimilar titanium alloys was studied with five titanium alloys, Ti-64SG, Ti-64FG, Ti-6242SG, Ti-54M, and Beta-21S, by maintaining two governing parameters pressure and time constant while the temperature was varied during the formation of joints. The friction stir welding of similar and dissimilar titanium joints was also studied with five titanium alloys, Ti-64SG,Ti-64FG,Ti-6242SG,Ti-6242FG, and Ti-54MFG, by varying two parameters namely, spindle speed and the feed rate, that control the quality of the process. The bond integrity of both the processes was evaluated with metallographic examination and mechanical testing. The surface and subsurface characteristics were examined to evaluate the surface characteristics and bonding strength. The mechanical strength of diffusion-bonded joints was investigated by conducting flexure testing whereas of the friction stir welded joints were examined by performing tensile tests. The probabilistic theoretical model of estimation of bonding time of dissimilar alloys was developed by computing the surface topography at the joint interface. A combined approach of numerical and experimental methodology was used to investigate the mechanical response of different titanium joints. The numerical model was developed to simulate flexural behavior of dissimilar diffusion bonded titanium joints from the material curves of its parent alloys. Similarly tensile behavior of friction stir welded similar titanium alloys for different process conditions was developed to identify the locations of maximum stress and strain in the joints. The numerical results were compared to experimentally determined behavior characteristics of the joints to gage the validity of the modeling approach. It was found that there was good agreement in the numerical and experimental results of the tensile behavior in titanium FSW joints. The diffusion bonding temperatures lower than the β transus temperature of titanium alloys were identified to obtain sound bonds in similar and dissimilar titanium alloys. The quality of bonding was improved as the bonding temperature was increased. In case of friction stir welding, the optimum values of spindle speed and feed rate for the joints formed by similar titanium alloys were 275 RPM/100 mm min-1, whereas it was 325RPM/125 mm min-1 for the joints formed by dissimilar titanium alloys.

TABLE OF CONTENTS

LIST OF FIGURES

LIST OF TABLES

ACKNOWLEDGEMENTS

I would foremost like to acknowledge the University of Washington, Department of Mechanical Engineering for giving me an opportunity to pursue a doctorate degree. I am also thankful to the department for providing me the opportunity as a Visiting Scientist to conduct research before I started my doctorate degree. My stint as a Visiting Scientist at the department greatly motivated me to pursue the doctoral degree. During my doctoral degree, I was also given the chance of being a teaching assistant for the graduate courses which has been a great learning experience. I am also thankful to department for providing the facilities to perform machining and mechanical testing for my dissertation work.

I am very grateful to my advisor, Prof. Ramulu Mamidala for his invaluable guidance throughout my research at the University of Washington. I feel fortunate to have got an opportunity to work under him. Prof. Ramulu's commitment and his willingness to provide guidance to his students anytime including the weekends has been a great source of inspiration for me. His direction has been instrumental in shaping my dissertation work. He has taught me to be goal oriented, through and comprehensive in my research. I believe that he has truly trained me to become an independent researcher.

I am thankful to Dr. Dan Sanders and the Boeing Company for supporting my research work. It has been a privilege to know and to work with Dr. Sanders whose outstanding scientific contributions have greatly motivated me. The financial support and the welds from the Boeing Company have made the project possible. Apart from supporting my research work Dr. Sanders has been a great mentor and has provided valuable advice to help my career.

I would also like to thank the members of my dissertation committee, Prof. Archis Ghate, Prof. Mark Tuttle, Prof. John Kramlich and Prof. Jiangyu Li for serving on my committee. The valuable inputs from all my committee members have contributed in improving my dissertation.

I also wish to thank my lab mates at MSTL for providing a research oriented and fun environment. Their help and valuable discussions during my research have been very useful for my work.

I am grateful to my parents for their unconditional love and warmth. They have always believed in me and have always stood by me. I am happy to have a very caring husband in Rahul. He has always been there for me and I was able to pursue doctoral degree because of his moral support. I would like to thank my parents-in-law for their backing and for their concern about my work.

I also want to thank my sisters, Pallavi and Mugdha; and brothers-in-law, Piyush and Sarang for their affection and encouragement. I also would like to thank my brother-in-law Sarang and sister-in-law Shweta for their enthusiasm and support. It has been a fun journey because of family and all my friends.

DEDICATION

I dedicate this work to my parents, husband and family.

Chapter 1. INTRODUCTION

1.1 BACKGROUND

In the aerospace industry, the buy to fly ratio is extremely important. This is both an environmental concern (energy saving) and a cost issue. The buy to fly ratio is the ratio between material procured and finished product. This ratio can be improved by using lighter materials and by minimizing material wastage. Titanium alloys are good candidates among lightweight materials. The excellent strength-to-weight ratio of titanium alloys provides a decrease of aircraft weight and therefore, a reduction in fuel consumption and emissions. The method that can be adopted to minimize the material wastage is to produce near net shape parts. In other words beginning with a shape that is closer to the final part can dramatically change the cost equations of metallics. There is big drive to get near net shape manufacturing. The other way to minimize costs is to reduce mechanical assembly by using advanced fabrication techniques such as diffusion bonding, fusion, and friction welding. In addition to reducing the material waste it also results in curtailing the nuts and bolts to join the materials.

1.2 JOINING TECHNIQUES OF TITANIUM ALLOYS

Titanium is expensive and takes long time to machine. It generally takes days to cut a blisk from solid metal. One way to overcome this is to build up near net shape by building up an engineered pre-form by depositing metal. The other method is to join simple metal shapes together to approximate final parts. In other words, the fabricated form of titanium requires joining in some form or other. Titanium joint, in order to be useful, must retain mechanical properties that meet the service requirement specification of end product.

The most common conventional joining methods used for titanium are fusion welding and friction welding [1]. Both are solid-state processes that fuse the metal without melting, thus preserving its mechanical properties. Solid state joining is a method of producing joints in which the two faying surfaces are joined at the temperature below the

melting point of the base metal without the addition of brazing or solder filler metal. These processes involve either diffusion or limited deformation with or without application of pressure to produce high quality joints between both similar and dissimilar materials. Friction stir welding is used to attach blades to disks to produce titanium compressor blisks for aeroengines, and is being applied to wing ribs and other structural components. The other important solid state welding method used in joining titanium is diffusion bonding (DB). The DB process is often described for reasons of logic in conjunction with superplastic forming. Brazing of titanium is also employed to limited degree. However the reactivity of titanium alloys poses special requirements in terms of protection of the molten pool or even solid titanium if it is exposed to atmosphere for long time. Some of the common welding techniques applied to titanium are described below.

1.2.1 *Diffusion Bonding*

Diffusion bonding is an attractive joining technique for many advanced materials, including titanium alloys, particularly when traditional fusion welding processes degrades them and when the necessity for environmental or thermal stability in thin-sheet structures impedes adhesive bonding. There is also a scope of combining diffusion bonding with superplastic forming, SPF/DB, to manufacture complex sheet structures with reduced weight and fabrication costs compared to mechanically fastened structures [1].

1.2.2 *Fusion Welding*

There are five main methods used for fusion welding titanium. These are gas tungsten arc welding (GTAW), gas metal arc welding (GMAW), plasma arc welding (PAW), electron beam welding (EAW), and laser welding (LW). Each of these methods has benefits for specific applications. Gas tungsten arc welding (GTAW) also known as tungsten inert gas welding (TIG) is the most common welding method used for titanium and its alloys [1].

1.2.3 *Friction Welding*

Friction Welding is usually practiced with alpha+beta processed or beta processed titanium alloys to obtain high integrity joints of materials. The friction welding process produces

plastic work into the weld zone and is partly responsible for the high quality bond that takes place. There are three friction welding processes that are used for titanium. These are rotational inertia welding, linear inertia welding, and friction stir welding. The rotational inertia welding is used in axisymmetric applications whereas the linear inertia welding is applied in non-axisymmetric applications. Examples of rotational inertia welding include multistage compressor rotors for large gas turbines while that of linear inertia welding includes attaching air foils to a hub for an aircraft engine rotor. The third process is the friction stir (FSW) welding. Friction Stir Welding now is a well-established solid state welding process. FSW process uses an inert, rotating mandrel or tool and a force on the tool normal to the plane of sheets (to be welded) to generate the frictional heat. During this process the two materials to be joined are tightly abutted in a line and a tool is traversed across them. The heat is generated between the joining materials and the tool. This generated frictional heat results in joining of both the surfaces. There is no melting of the materials; instead the joint is formed by plastic deformation of the pieces. This technique is capable of joining both the similar as well as the dissimilar material combinations.

Among a number of welding techniques, friction stir welding is applied extensively due to its numerous advantages over conventional welding methods. Friction stir welding offers certain advantages over fusion welding. The joining temperature of materials is lower than in fusion welding. The problems that occur in the solidification of liquid phase are not present in friction stir welding. The process does not require consumables to produce weld, there are no toxic fumes or splatter; it is a process that can be automated and thus makes it viable for industrial use.FSW is evolving as a effective joining technique that can provide localised modification and control of microstructures in the near surface layers of processed metallic components[1].

1.3 OBJECTIVES

In the aerospace industry diffusion bonding and friction stir welding have been widely adopted to produce titanium alloy structural parts. Till to date enormous research has been conducted on establishing diffusion bonding and friction stir welding with similar type of titanium alloys. Among all the titanium alloys feasible parameters have been established

for producing defect free Ti-6Al-4V structural joints. But Ti-6Al-4V can be used within limited range of temperature. The other titanium alloys such as Ti-6Al-2Sn-4Zr-2Mo has higher temperature capability. However, very limited research has been conducted on joining techniques for dissimilar titanium alloys. Therefore it is important to evaluate feasibility of joining dissimilar titanium alloys so as to increase and improve its proficiency. The joining of dissimilar metals is required in the application wherein varieties of material properties are required within the same component. The current study was conducted to gauge the performance of similar and dissimilar titanium alloys with diffusion bonding and friction stir welding process. The bond integrity was evaluated with metallographic examination and mechanical testing. The surface and subsurface characteristics were examined to evaluate the surface characteristics and bonding strength.

1.4 SUMMARY

This thesis is organized into several chapters. The current chapter is the introduction chapter. Chapter 2 reviews the literature on titanium, the joining processes evaluated in this research work which includes diffusion bonding and friction stir welding processes. Chapter 3 describes the scope, objective and methodology adopted to execute the research work. Chapter 4 provides insight to the experimental results on microstructures, mechanical behavior of joints, and on fractography. Chapter 5 highlights theoretical model developed to predict diffusion bonding time of dissimilar titanium alloys along with numerical model on diffusion bond, and mechanical behavior of joints. Chapter 6 summarizes the conclusions and identifies future scope of this study. Following summary and future scope, Bibliography and Appendixes are provided in the end. Every chapter has an introduction in the beginning with the summary at the end of the chapter.

Chapter 2. LITERATURE REVIEW

2.1 INTRODUCTION

This chapter represents the literature reviewed for the current study. The chapter is divided into three main sections. The first section reviews literature on titanium, titanium alloys, its alloying elements, and classification of tianium alloys. In the next section diffusion bonding process is presented with diffusion bonding mechanisms and the available therotical models. The last section describes friction stir welding process. The details on metallurgical aspect and the process parametes of friction stir welding process are also provided.

2.2 TITANIUM

Titanium was first introduced commercially in 1940 [2]. This is fourth abundant structural metal in the earth's crust. Three prime reasons that made Titanium important in nineties: Abundance of raw materials, location of ores, and properties of the metal. The location of ores within the borders of United States increases the importance in a metal that has high strategic value. Titanium is widely used in the aerospace industry because of its strength to weight ratio and corrosion resistance properties. Titanium and its alloys are also used in many non-aerospace applications including military, armor, medical, automotive, chemical processing, sporting goods, and power generation.

Titanium is highly reactive metal and therefore extraction of pure grade titanium is difficult. The metal reacts with oxygen and nitrogen in the air. It also reacts with other refractories in the molten state [2]. Titanium has melting point that is several hundred degrees above that of iron and over two and half times of aluminum. The density of titanium falls in the intermediate between those of aluminum and iron. The modulus of elasticity is higher than that of aluminum and slightly more than half of that of iron, and falls within the range of copper alloys.

Titanium is non-magnetic in nature. The thermal conductivity of it is low. It is $1/6^{th}$ that of iron and $1/16^{th}$ of that of aluminum. Low thermal conductivity necessitates the need of consideration in heating for fabrication at high temperatures and for welding.

Titanium is an allotropic element (exists in more than one crystallographic form) that exists in hexagonal close-packed (hcp) crystal structure (referred to as "alpha" phase) and (bcc) crystal structure (referred to as "beta" phase). Titanium exists in hcp or "alpha" phase at room temperature. This crystal structure of titanium changes from hcp or "alpha" phase to bcc or "beta" phase at 883^0C (1621^0F) [3]. The manipulation of these crystallographic variations through alloying additions, heat treatment, and thermo mechanical processing is the source for the development of a broad range of alloys and properties. The addition of alloying element divides the single temperature for equilibrium transformation into two temperatures: α transus and β transus. The 'α transus' denote the temperature above which the α phase begins to transform to β and 'β transus' is the temperature above which it is all β phase. Between these temperatures it is both α phase and β phase. The transus temperatures change with the impurity levels and the range of alloying additions. Titanium has a very high melting point 1668^0C (3035^0F). However the allotropic nature of the metal from low temperature hexagonal closed packed form to higher temperature body centered cubic form (alpha phase to beta phase) limits its application temperature. On the other hand the allotropic form offers more diverse strengthening opportunities than those of other nonferrous alloys such as aluminum or copper. This thermo-mechanical processing provides the advantage to control the microstructure and properties [3].

Commercially Pure (CP) titanium contains carbon, oxygen and nitrogen in small quantities and all three of these elements exert greater influence on properties. CP titanium is usually selected for its excellent corrosion resistance, especially in the applications requiring high ductility for fabrication but relatively low strength. The yield strength of unalloyed (commercially pure) titanium varies from 170 MPa (25 ksi) to 480 MPa (70 ksi) simply as a result of variations in the impurity and interstitial levels. The strength increases with the increasing oxygen and iron contents [3].

Titanium being a low-density element (approximately 60% of the density of steel) can be highly modified by alloying and deformation processing. Titanium and its alloys have melting points higher than those of steels [3]. Titanium is used upto temperature of about 565^0C. Beyond this point it is too high for Titanium owing to its elevated temperature properties, the concern that titanium will ignite and burn, and oxidation problems with titanium (the formation of an oxygen-stabilized alpha-case on the surface), that reduces the ductility and fatigue strength.

Titanium and its alloys have been used instead of steel and nickel alloys in the aerospace industry because titanium offers weight savings in highly loaded components that operate at low to moderately elevated temperatures. The improved elevated temperature characteristics of these alloys along with their high strength to weight ratios make them good alternative to nickel base super alloys for certain gas turbine components. Titanium alloys possess a weight reduction benefit of about 40 % over their nickel-based counterparts. Many titanium alloys have been custom-designed to have the required mechanical properties catering to their functional requirements and at the same time have adequate workability to be fabricated into mill products. Titanium and its alloys can take variety of product forms. Some specific examples of product forms with milling are ingot, billet, bar, sheet, strip, tube, and plate; non-mill products include sponge and powder; and customized product forms include forging, P/M items, and castings. Titanium can be wrought, cast, or made by P/M techniques. It can be joined by means of fusion welding, brazing, adhesives, diffusion bonding, friction welding, or fasteners. During past five decades many titanium alloys have had transient usage, however one alloy Ti-6Al-4V, mainly called, as workhorse of aerospace industry has been consistently responsible for over 50% of industry applications.

2.3 EFFECTS OF ALLOYING ELEMENTS ON TITANIUM

Titanium provides a wide range of physical and mechanical properties by adding alloying elements. Certain alloying additions, notably aluminum, tend to stabilize the alpha phase; that is, they raise the temperature at which the alloy will be transformed completely to the

beta phase. This temperature is known as the beta-transus temperature. Alloying additions such as chromium, columbium, copper, iron, manganese, molybdenum, tantalum, and vanadium stabilize the beta phase by lowering the temperature of transformation from alpha to beta. Some elements, notably tin and zirconium behave as neutral solutes in titanium and have little effect on it. Alloying elements can be classified as alpha or beta stabilizers. Alpha stabilizers, such as aluminum and oxygen, increase the temperature at which the alpha phase is stable. Beta stabilizers, such as vanadium and molybdenum, increase the stability of beta phase at lower temperatures [3]. Table 2-1 provides the list of most popular alloying elements used in titanium alloys.

Table 2-1: Titanium Alloys: Alloying Elements [4]

Alloying Element	Range (approx.),Wt. %	Effect on structure
Aluminum	2-8	α stabilizer
Chromium	2-12	β stabilizer
Copper	2-6	β stabilizer
Molybdenum	2-15	β stabilizer
Niobium	1-2	β stabilizer
Silicon	0.05 to 1	Improves creep resistance
Tin	2 to 11	α stabilizer
Vanadium	2 to 20	β stabilizer
Zirconium	2-8	β stabilizer

a. ***Aluminum***- Aluminum is an α stabilizer element that increases moduli and creep and tensile strengths while reducing alloy density. The maximum solid solution strengthening that can be obtained by aluminum is restricted because about 7% Al promotes ordering and Ti_3Al formation with associated embrittlement.
b. ***Tin***-Tin is a less strong α stabilizer and a solid solution strengthener that is often used in conjunction with aluminum to achieve higher strength without embrittlement. It is used as the main α stabilizer in IMI-679 (2Al-11Sn-5Zr-2Mo-0.1Si. This alloy is a good combination of strength and temperature capability.

c. ***Zirconium***- Zirconium is a weak β stabilizing element. It forms continuous solid solution with titanium and increases the strength at low and intermediate temperatures. However the addition of Zirconium above 5 to 6% may reduce ductility and creep strength.

d. ***Oxygen***- Oxygen content is usually kept fairly low, 0.1 to 0.15% in the titanium alloys. Although it strengthens titanium, the beneficial effect drops at temperatures above 300 ^{o}C (570 ^{o}F). Higher oxygen content also tends to lower ductility, toughness, and long-term high temperature stability.

e. ***Molybdenum***-Molybdenum is the prime β stabilizer in near α alloy as it significantly increases the heat treatment response of the alloys. It promotes high strength in quenched and aged material as well as increased hardenability. The alloys that are aimed at long-term creep strength (such as Ti-6242S) have lower molybdenum content. The addition of Molybdenum makes the alloy more difficult to weld.

f. ***Niobium***-Niobium is also a β stabilizer, is added mostly to improve surface stability (oxidation resistance) during high-temperature exposure in alloys (such as IMI-829).

g. ***Silicon*** – Silicon is an important element in high temperature titanium alloys as it increases strength at all temperatures and has a noticeable advantageous effect on creep resistance.

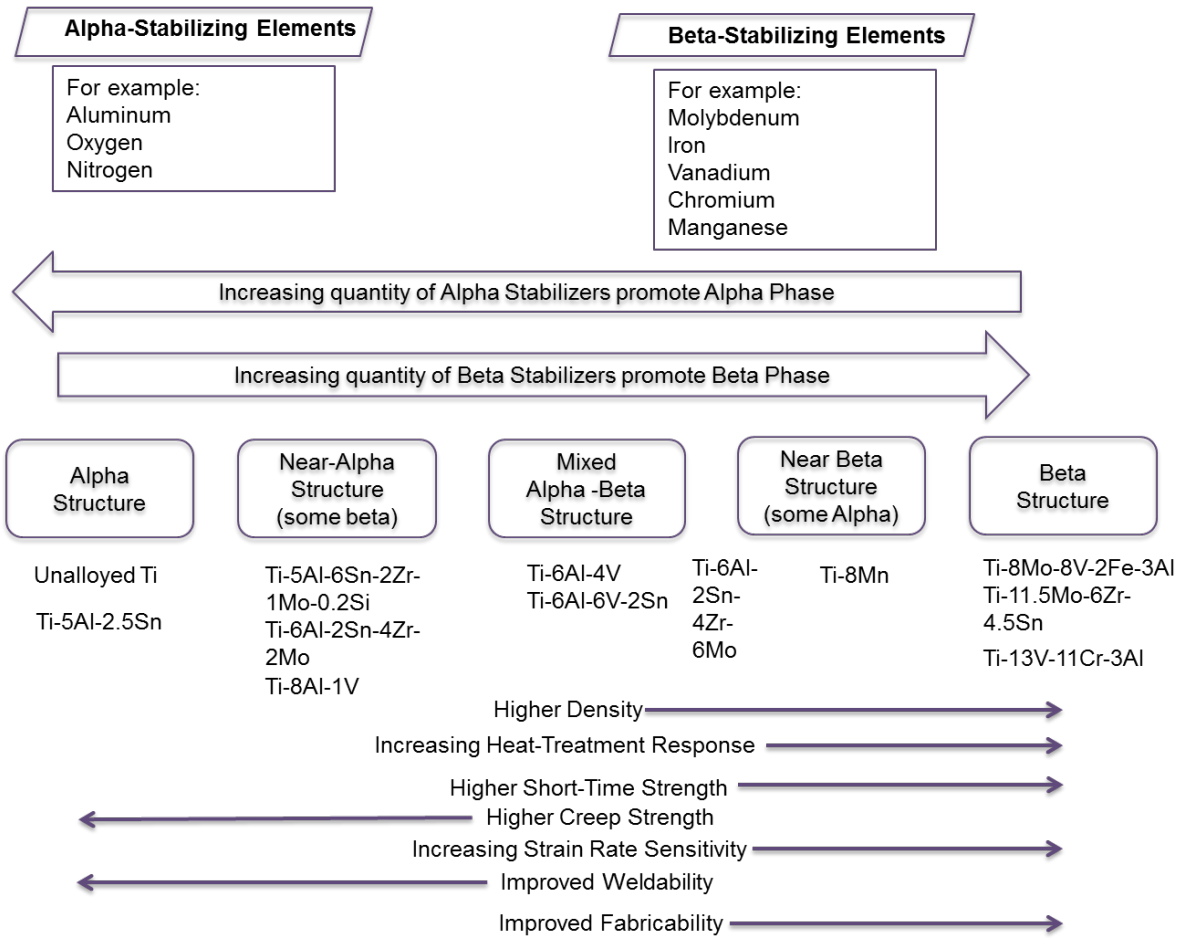

Figure 2.3-1: Effects of alloying elements on titanium alloy structure [5]

2.4 TITANIUM ALLOYS CLASSIFICATION[1]

Titanium alloys can be classified in three categories: Alpha Alloys, Alpha + Beta Alloys and Beta Alloys. This classification is based on the predominant phase or phases in their microstructure retained at room temperature favored by an alloy composition. More definite classification categorizes titanium alloys in five instead of three categories: Alpha, Near-Alpha (superalpha), Alpha+beta, Near-beta, and Beta (Figure 2.4-1).

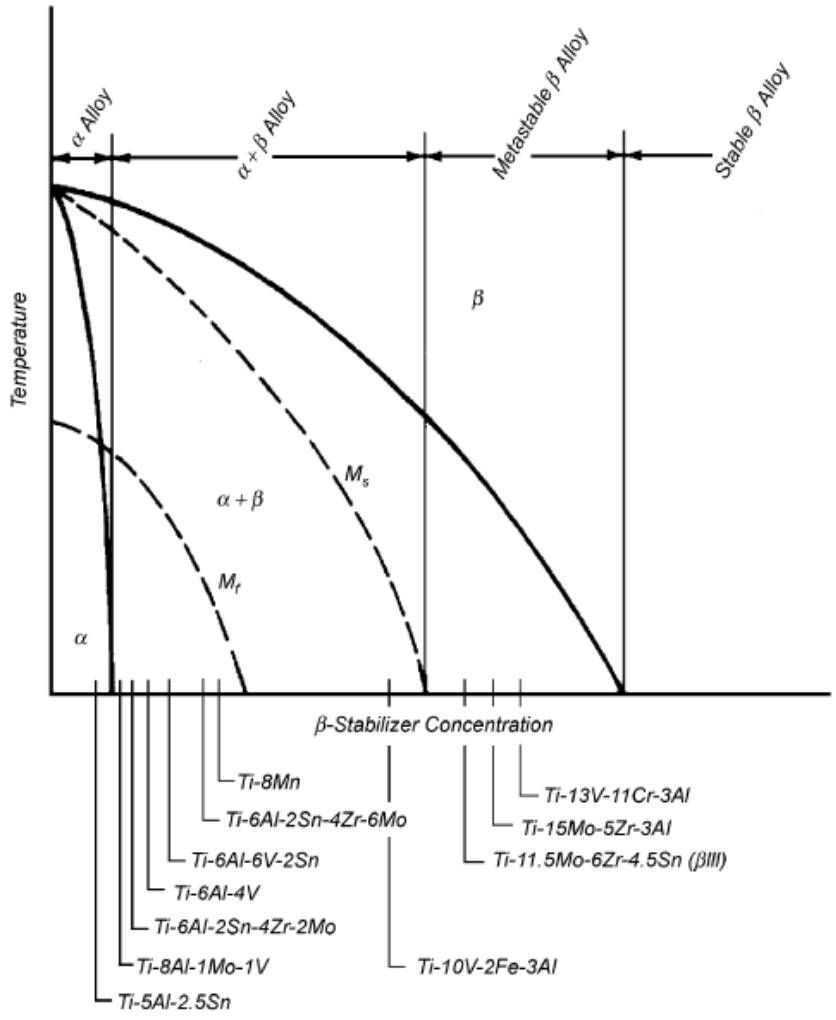

Figure 2.4-1: Pseudo binary section through a β isomorphous phase diagram [6]

Alpha titanium has hexagonal structure [hcp] that is stable up to 1625^0F. At 1625^0F, the material changes to the high temperature modification that has body-centered cubic structure [bcc] and is known as beta titanium. Alpha phase does not contain beta phase. A near-alpha (or superalpha) alloy forms a meager beta phase on heating, and therefore it looks similar to alpha phase at low temperatures. An alpha and beta alloy contains both phases. It retains beta phase and transformed beta phase. A near beta (metastable) phase retains the beta phase on initial cooling to room temperature. Beta phase has no alpha phase in it.

2.4.1 *Alpha and Near Alpha Alloys*

Alpha alloys that contain aluminum, tin, and or zirconium are selected for high temperature as well as cryogenic applications. Alpha alloys are weldable, non-heat treatable, more oxidation resistant than beta or alpha beta alloys and relatively difficult to form. These alloys contain no β stabilizers and therefore cannot be strengthened by heat treatment. These are generally annealed or recrystallized to remove residual stresses induced by cold working. Being insensitive to heat treatment they have good weld ability. They generally have poorer forge ability and narrower forging temperatures ranges than α+β or β alloys, particularly at temperatures below the β transus. Alpha rich alloys are more resistant to creep at high temperature than α+β or β alloys.

Alpha alloys that contain small proportions of β stabilizers are classified as "near- α" alloys. Although they enclose some retained β phase, these alloys consist primarily of α and behave more like conventional α alloys than α+β alloys. Near -α alloys can however, be strengthened by heat treatment or thermo mechanical processing. By heat treating these alloys above β transus temperature can improve the creep behavior of some near-α alloys.

The alpha and near alpha alloys include alloys such as Ti-3Al-2.5V (Ti-32.5), Ti-6Al-2Sn-4Zr-2Mo (Ti-6242S), Ti-5Al-2.5Sn (Ti-52.5), Ti-8Al-1Mo-1V (Ti-811). The "S" present at the end of composition denotes the addition of Silicon. Minor Si addition, in the range of 0.1 to 0.25, and higher, improves the creep resistance of high temperature alloys.

2.4.2 *Alpha Beta Alloys*

The α+β alloys contain one or more α stabilizers or α-soluble elements plus one or more β stabilizers. These alloys retain more β phase after solution treatment than the near-α alloys; the specific amount depends on the quantity of β stabilizers present and on heat treatment. The α+β alloys can be strengthened by solution treating and aging them. Solution treating is usually conducted at a temperature high in the two-phase α+β field followed by quenching in water, oil or other suitable quenchant. As an effect of quenching, the β phase present at the solution treating temperature may be retained or may be partially transformed during cooling by either martensitic transformation or nucleation and growth.

Solution treatment is followed by aging, mostly at 480 to 650^0C (900 to 1200^0F) to precipitate α and generate fine mixture of α and β in the retained or transformed β phase. Solution treating and aging can improve the strength of α+β alloys 30 to 50 %, or more, over the annealed or over-aged conditions. In α+β alloys, the hardenability increases with the increase in β stabilizers. The strength that can be obtained by heat treatment is also a function of the volume fraction of β phase present at the solution treating temperature. This category includes Ti-6Al-4V (Ti-64), Ti-6Al-6V-2Sn (Ti-662), Ti-5Al-4V-0.6Mo-0.4Fe (Ti-54M), and Ti-6Al-2Sn-4Zr-6Mo (Ti-6246).

2.4.3 *Beta Alloys*

Titanium can be made to retain the beta phase at room temperatures. Some alloying additions inhibit the alpha to beta transformations. These alloys are richer in β stabilizers and meager in α stabilizers than α+β alloys. Beta alloys are characterized by high hardenability, excellent forgeability and in sheet form can be cold formed more readily than high strength α+β or α alloys. After solution treating, β alloys are aged at temperatures of 450 to 650^0C (850 to 1200^0F) to partially transform the β phase to α. The α is present as finely dispersed particles in the retained β, resulting in the strength levels comparable to or superior to those of aged α+β alloys. Beta alloys have good ductility, and toughness, relatively low strength and good formability in the solution treated (100% retained β) conditions. Beta alloys, despite the name are actually addressed as metastable alloys because cold work at ambient temperature or heating at slightly elevated temperature can cause partial transformation into α. The major disadvantages of beta alloys in comparison with α+β alloys are high density, lower creep strength, and lower tensile ductility in the aged condition. Though tensile ductility is lower, the fracture toughness of an aged beta alloy is usually higher than that of an aged α+β alloy of comparable strength. This alloy class includes Ti-10V-2Fe-3Al (Ti-1023), Ti-15V-3Cr-3Al-3Sn (Ti-153), Ti-15Mo-3Nb-3Al (Beta-21S), and Ti-3Al-8V-6Cr-4Mo-4Zr.

2.5 SUPERPLASTIC FORMING OF TITANIUM ALLOYS

Superplastic forming and diffusion bonding are the emerging and advanced fabrication technologies. Both the processes have similar processing conditions, require an elevated temperature and benefit from fine grain size. The combined process of superplastic forming and diffusion bonding can produce parts of greater complexity than single-sheet forming alone. Therefore when applied individually or concurrently can offer significant cost and weight benefits.

Titanium has become very important material in the aerospace and other industrial applications. Titanium alloys have high yield stress and low elastic modulus that makes them difficult to handle the forming process. These properties result in formation of large elastic strains which are recovered after the load is removed during forming operation. This elastic strain is called as ‘’spring back.” The spring back mechanism makes it difficult for the titanium alloys to obtain the desired contour shapes after forming operation. Consequently, the costs that are associated with the manufacturing and the fabrication of titanium are high. The base metal titanium costs eight times as much as aluminum. Titanium exhibits superplastic behavior and the capability of diffusion bonding. Titanium alloys, especially Ti-6Al-4V poses problems in convention sheet forming, that has resulted in the commercial growth of superplastic forming. Titanium can readily absorb the thin surface oxides and dissolve minor amounts of adsorbed gases and diffuse them away from the bonding surfaces so that they will not inhibit the formation of required metallic bonding across the bond interface.

Superplastic behavior is defined with the expression that relates flow stress and strain sensitivity.

$$\sigma = \sigma_0 \left(\frac{d\varepsilon}{dt}\right)^m$$

where σ_0 represents the threshold flow stress at very low strain rate.

The material is defined as superplastic if it has a strain rate sensitivity exponent m of 0.5 or greater in the above discussed expression. As the strain rate sensitivity of the flow stress increases, the material inherits more resistant to formation of necks or other forms of

localized deformation. The flow stress and the stain rate sensitivity values are microstructure, temperature and strain rate dependent. In titanium alloys such as Ti-6Al-4V the maximum value of m is about 0.7. This typically occurs at temperature of 875^0C at strain rate of 10-4 s-1 or less [1]. The tendency of titanium to dissolve its own surface oxide when heated to >=550^0C in vacuum or high purity environment (non -oxidizing environment) makes it suitable candidate for diffusion bonding. The two titanium sheets are placed in intimate contact and modest pressure to create a high degree of contact. If this sandwich is heated to temperature (0.5Tm) or higher, the $Ti0_2$ on the surface of the sheets dissolves, leaving clean surfaces in contact. The result is that two sheets bond together by interdiffusion, resulting in bond that is indiscernible even during metallographic examination. This method of joining is called diffusion bonding (DB). This process is typically performed at temperatures in the (alpha+beta) phase field, and, hence, this process does not disturb the equiaxed microstructure of pieces being joined. Diffusion Bonding/Superplastic Forming.

The commercialization of titanium sheet components DB/SPF was developed at Rockwell Science Center in Thousand Oaks, CA, between 1971 and 1984. The diffusion bonded titanium sheets could be inflated with high pressure inert gas under SPF conditions to produce honeycomb structures that was both light weight and cost effective. Several other developments were observed in the applications o for U.S. Air Force with the refit of the F-15D aft fuselage. These monolithic structures could bear a larger engine with greater thrust resulting in improving the performance of aircraft. The other advantages offered from DB/SPF resulted in the elimination of 726 detail parts and 10,000 fasteners, increased load capabilities, 10 cubic feet of space for special requirements, and reduced weight[7].

2.6 DIFFUSION BONDING

2.6.1 *Introduction*

Diffusion bonding is a solid state welding process. In this process two clean metallic surfaces brought in contact in an inert atmosphere under a low pressure for a period of time

at elevated temperatures usually 50 to 70% of their melting point to allow some creep deformation, interface diffusion, recrystallization and grain growth to take place. Diffusion involves transfer of atoms across the boundaries due to concentration gradients. It is a clean welding process without incurring any material loss. It can be used commercially to join similar and dissimilar metals.

The International Institute of Welding (IIW) has adopted the following definition for diffusion bonding (modified definition of Kazakov):

"Diffusion bonding of materials in the solid state is a process for making a *monolithic* joint through the formation of bonds at *atomic level*, as a result of closure of the mating surfaces due to *the local plastic deformation* at elevated temperature that aids *interdiffusion* at the surface layers of the materials being joined"[8].

Technically the diffusion bonding process (DB) can be used to create joints between pieces of large section, ex: the wingbox of a large military aircraft. However in practice to create good quality bond extensive preparation of the work piece is required in terms of exacting the surface flatness and surface finish in the areas where the actual bonds occur. Moreover it is required to inspect the DB joints and this inspection is both time consuming and technically challenging.

In the early stages of DB development, the wingbox of large military aircraft was fabricated with diffusion bonding. However when this component was fatigued tested, the fatigue life was found less than the expected. The post analysis showed that several unbonded regions were present within the DB regions and these resulted in the crack initiation. The further analysis also showed that the flat surface preparation was insufficient to permit complete contact across the entire joint surface. The cost of executing adequate joint preparation is high and again this increases with the component size. Therefore the economics of this process becomes less attractive for bonding large sections and the technical risk to obtain good quality joint remains a concern. Due to above concerns, DB has never been adopted to produce large and heavy section components.

In contrast, the diffusion bonding of sheets is more productive possibility as the starting material is flat and also the inspection of these joints, if necessary, is easier to conduct. When the DB process is combined with superplastic forming enables the creation of

complex shapes with integral stiffness and becomes extremely attractive. The use of stop-off agents allows the selective bonding of regions of sheet. Moreover in sheets bonding the entire section that is formed and bonded is superplastic, and therefore the constraint of the surrounding material that prohibits complete bonding in heavy sections is not a problem. This combined processes DB and SPF have been successfully implements and are commonly referred as superplastic forming/diffusion bonding (SPF/DB). A complex honeycomb structure from a three-piece pack can be created by applying SPF/DB [1].
Unlike most welding processes, the process-time curve for diffusion bonding is almost flat in relation to job size, because the process time is independent of joint area provided adequate compressive stress is applied.

2.6.2 *Diffusion Bonding Mechanisms*

In practice, the extend of diffusion bonding and the rate at which it is obtained is governed both by material properties (such as surface, grain boundary, and volume coefficients, creep and yield strength etc.) and process parameters such as pressure, temperature, time, and surface condition. Diffusion Bonding does not occur due to one dominant mechanism but is a consequence of one or more possible mechanism that often operates in parallel. Each mechanism result in material (void) transport so that surface energy related with the interface is progressively reduces as joining proceeds. Some possible mechanisms include:

- Plastic yielding of surface asperities
- Surface source surface diffusion to void neck
- Surface source volume diffusion to void neck
- Evaporation from surface source to condensation at a neck
- Interface source grain boundary diffusion to void neck
- Interface source volume diffusion to void neck
- Power law creep mechanisms

Diffusion bonding process begins with plastic deformation in the contact region. In the bonding interface the actual area in contact is much smaller than the nominal contact area, therefore, the stresses in the bonding interface exceeds the yield strength of the material and the plastic deformation occurs. The surface and volume diffusion

particularly result in altering the shape of the void. The grain boundary and volume diffusion from the bond interface reduce the void volume.

2.6.3 *Stages in Diffusion Bonding [7]*

The stages in diffusion bonding process are shown below [Figure 2.6.1]. On the application of pressure and temperature, the initial contact takes place. The interdiffusion of atoms and the sharing of grains across the bondline will typically commence immediately upon initial contact. As the surfaces of the mating sheets are forced into closer contact, additional grains become engaged and recrystallize.

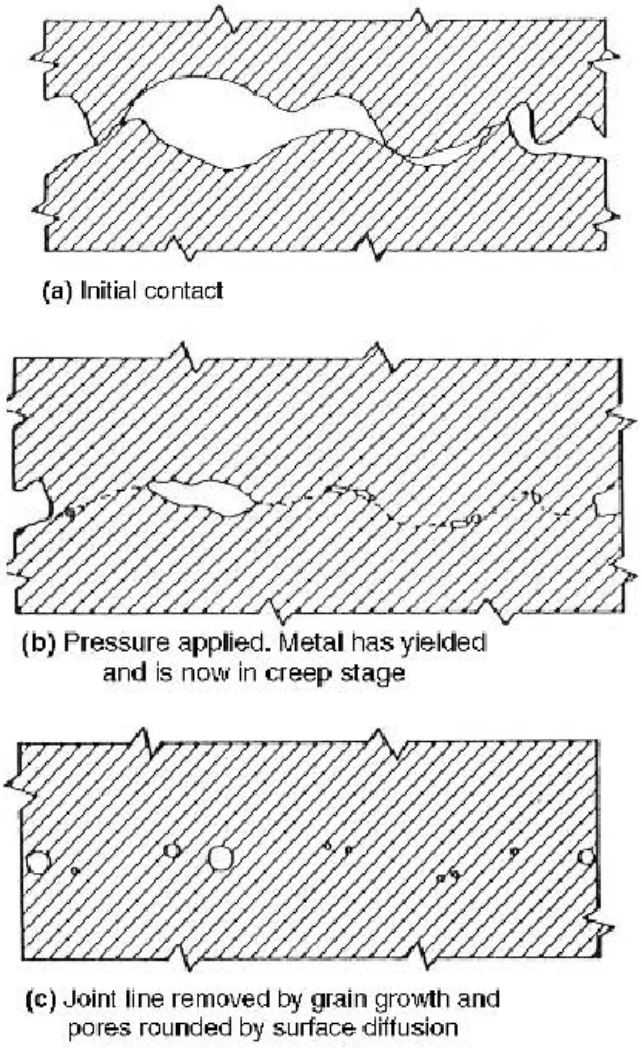

Figure 2.6-1: Stages in Diffusion Bonding [7]

The metallographic investigations of sections through the bond lines of solid state bonded samples of titanium alloy, Ti-6Al-4V with different shear strengths of the bond relative to that of the parent material are shown in Figure 2.6.2. Large, regularly spaced ellipsoid section voids were apparent on the bondlines of samples with low shear strength. The bondline was difficult to discern in the samples with high bond shear strengths. The bondline often had radii smaller than 1 μm in these samples. During bonding neither grain growth nor grain shape changes were evident, highlighting the role of superplastic over creep deformation in contributing to the solid state bonding process [10].

Figure 2.6-2: Cross-sections through bond with various parent metal shear strengths (a: 56%, b: 87%, c=95%, d>95%) [10]

A typical diffusion bonding steps occurring in the titanium alloy, Ti-6Al-4V is shown in Figure 2.6.3. As the time progresses, the diffusion bonding mechanisms operate towards the void closure and a complete closure is observed in the final stage of the bonding. However the presence of voids results in decreasing the bonding strength.

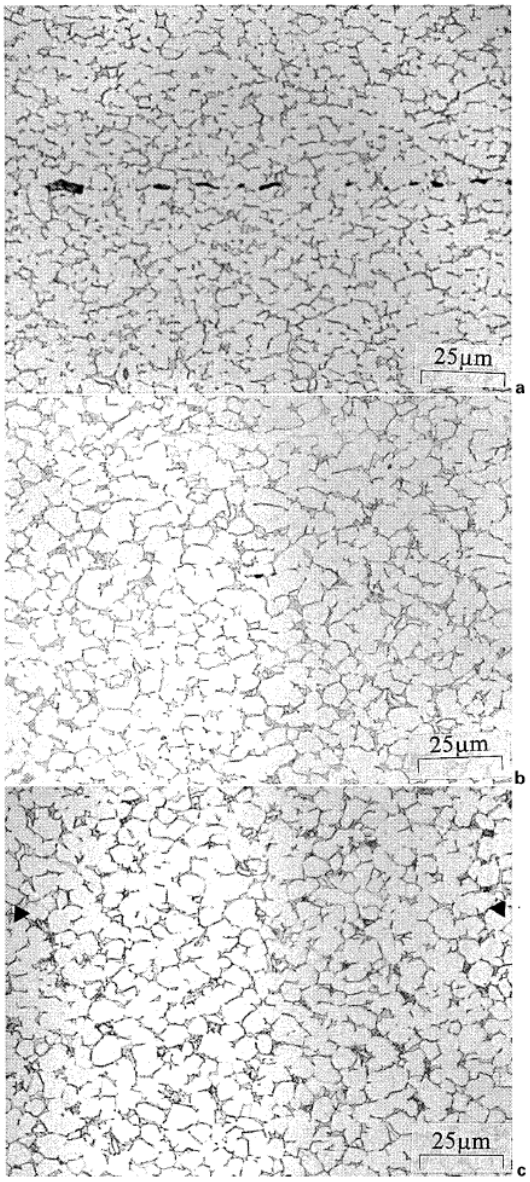

Figure 2.6-3: Optical Micrograph of bond plane region after bonding- a 10 min, b 60 min, c 90min (Ti-6Al-4V alloy, P=2.1MPa, T=920^0C, P60 finish: amplitude of 1µm and wavelength of 14.8 µm) [9]

The surface roughness profile and the kinetic conditions are required to predict the diffusion bonding process. The four main parameters that control the diffusion bonding process are pressure, temperature, time, and surface condition.

a) **Pressure**: Adequate pressure is required to establish contact on atomic scale by localized deformation of asperities on nominally flat surfaces being joined and also to permit creep mechanisms to contribute to bonding
b) **Temperature**: Thermal energy stimulates faster bonding since plastic deformation, creep, and all diffusion mechanisms are temperature dependent. Typically temperatures around 0.5 to 0.7 Tm are used, where Tm is the absolute melting temperature of lowest melting point component. Heating rates are not important.
c) **Time:** Creep and diffusion mechanisms are also strongly time dependent, and also there must be adequate time interval to allow for void closure by material transfer. As the temperature increases, the time required for bonding decreases.
d) **Surface Condition:** The height and frequency of surface asperities defining the joint will govern the extent of initial surface contact and thus influence the bonding rate. The removal of surface contaminants and oxides is necessary prior to bonding since these will either persist at joints or must be removed by solution as bonding proceeds. Therefore, it takes comparatively higher temperatures and pressures to bond aluminum-base alloys than copper-base alloys. Certain titanium alloys such as Ti-6l-4V are of particular industry interest since they can diffusion bonded and superplastically shaped in one processing operation, at temperatures above 900^0C(1650^0F), titanium can dissolve oxygen into its volume as fast as a surface scale can form. Diffusion bonded joints normally exhibit 80 to 100% of parent material strength.

2.6.4 *Diffusion Bonding Models*

The research on theoretical models of diffusion bonding was started in around mid-nineties. The early research in diffusion bonding was originated by King and Owczarski in 1967 [11]. There are basically two kinds of diffusion bonding models. One of the models is based on the pressure sintering process. The alternate model for diffusion bonding is

based on grain boundary diffusion coupled with creep. The later model gives good approximation for fine grain structures. Figure 2.6-4 summarizes model developments of diffusion bonding historically followed by details on each of these models.

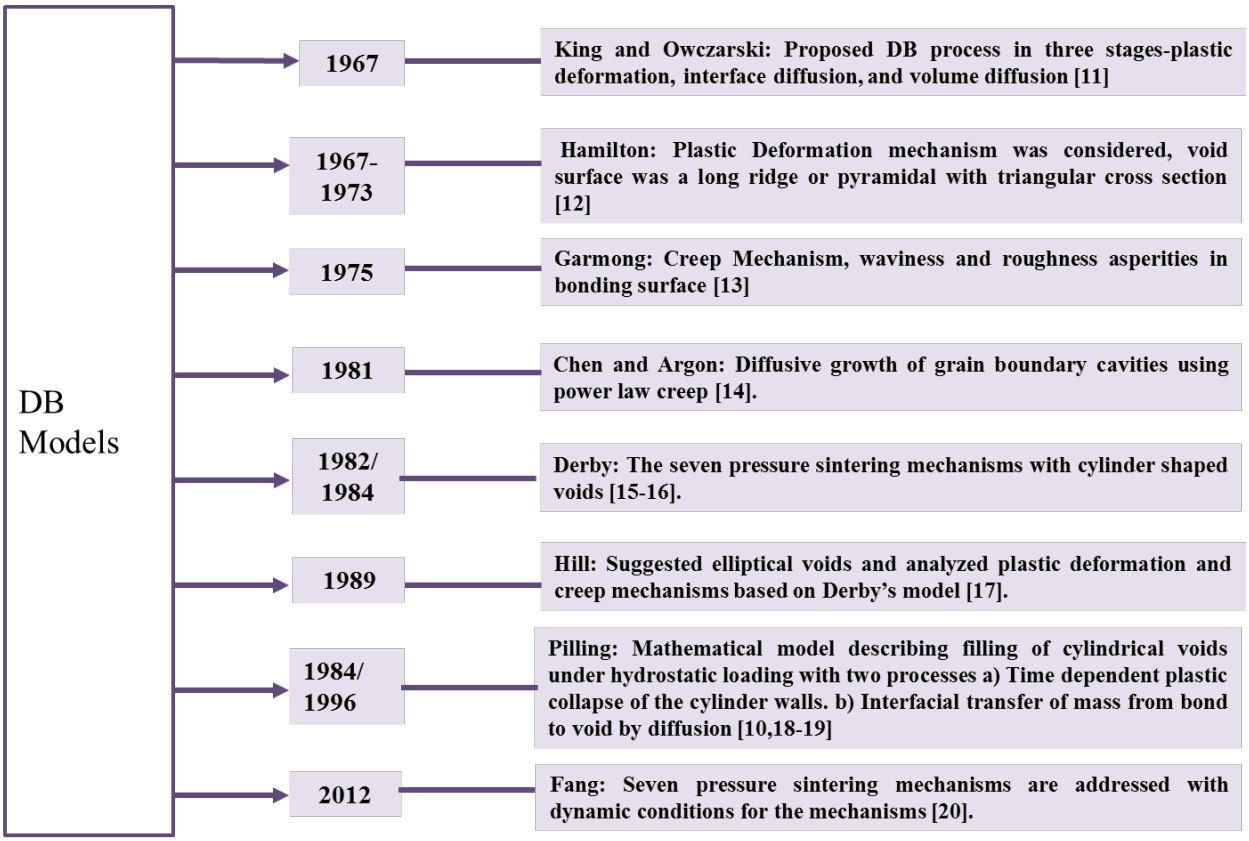

Figure 2.6-4: Historical Development of Diffusion Bonding Models

1. King and Owczarski [1967]

The early research in diffusion bonding was initiated by King and Owczarski in 1967. The diffusion bonding process was explained in three stages:

a) Stage I: Plastic deformation of asperities leads to grain boundary forming.
b) Stage II: Removal of majority voids at interface and simultaneous migration of interface away from voids
c) Stage III: Elimination of remaining voids by volume diffusion.

2. Hamilton's Model (1973)

Hamilton's model estimated diffusion bonding process with the plastic deformation mechanism [12]. The model examined the diffusion bonding in Ti-6Al-4V alloy. It was proposed that the initial requirement for diffusion bonding is the deformation of the surface structure. In the model the plastic deformation stage was characterized by representing the surface roughness as a series of long ridges (pyramidal with triangular cross section). It was shown that these ridges were in the state of plane strain. Upon the application of pressure at the elevated temperatures these ridges collapsed and eliminated the voids between them as shown in Figure 2.6-5. The bonding pressure as represented as a stress across an individual ridge. The bonding rate was predicted by correlating the bulk strain in a representative collapsing ridge to experimental creep data. A favorable agreement was found between experiment and theory.

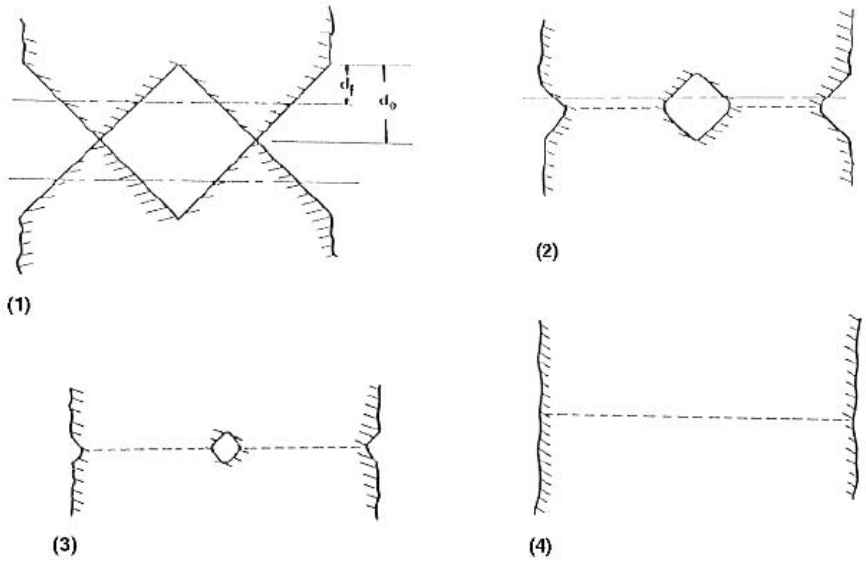

Figure 2.6-5: Steps of operation in Diffusion Bonding: (1) Initial surface contact, (2) and (3) Intermediate steps towards the closure of voids (4) Competed bonding

3. Garmong (1975)

Garmong's model improvised the geometry of voids applied in Hamilton's model of diffusion bonding [13]. In Garmong's model the waviness asperities and roughness asperities were considered in the bonding surface. The representative ridges were modeled as a series of horizontal slices. The response of each slice was summed up to the applied

stress. The model further included diffusion considerations as well. The model proposed that the disappearance of large voids caused by the waviness asperities was completed only by creep mechanism.

4. Chen and Argon (1981)

Chen and Argon developed theoretical model of diffusive growth of grain boundary cavities of both equilibrium and non- equilibrium shape in presence of power law creep [14]. The model showed that the modified rigid-grain solution that considers a creep-coupled diffusion distance can adequately prescribe the volumetric growth under creep conditions.

5. Derby and Wallach Model (1982-84)

Derby's first work on diffusion bonding started in the year 1980. Derby and Wallach gave the first comprehensive model for diffusion bonding. For the first time diffusion bonding process was considered in terms of more than one mechanism. The model postulated the mechanisms based on the pressure sintering process. Derby and Wallach proposed that some or all of the seven pressure sintering mechanisms operate in the closure of voids. The diffusion bonding model was studied mainly on the copper material. The model assumed that the void changed from triangle shape to cylinder shape in the bonding process. However the mathematical description on the process of diffusion bonding was discontinuous. Derby's first model [15] of diffusion bonding applied six bonding mechanisms:

a) Surface diffusion from surface sources to neck
b) Volume diffusion from surface sources to a neck
c) Diffusion along the bond interface from interfacial sources to a neck
d) Volume diffusion from interfacial sources to a neck
e) Power law creep deforming the ridge
f) Plastic yielding deforming the ridge

The mechanisms (a) and (b) are driven by differences in surface curvature across the surface of an interfacial void; these mechanisms rupture when a void of uniform curvature develops. The bond interface mechanisms (c) and (d) are driven by the chemical potential along the bondline; this will vary with neck curvature and applied pressure. Finally the deformation mechanisms (e) and (f) are driven primarily by the applied pressure although some surface tension effects will occur. The plastic yielding mechanism is expected to occur only in the early stages of bonding due to the large stress concentrations that are required for diffusion bonding process to take place.

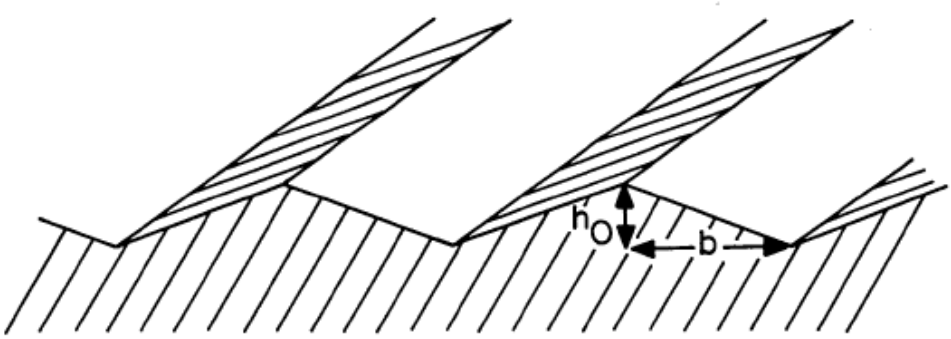

Figure 2.6-6: Derby's Model: void geometry (long triangular section ridges)

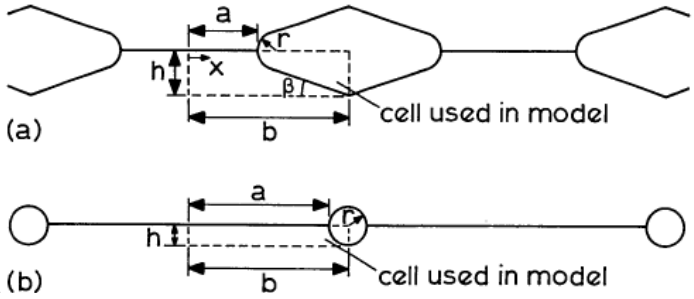

Figure 2.6-7: Derby's Model- Stage I and II (a and b): Contacting surfaces are modeled as small cells (dashed lines)

In the model the voids have a low aspect ratio and gradually shrink as bonding progresses until they reach cylindrical. In the model stage I is defined to be the time from the initial surface contact to this point, while the stage II captures the final collapse of the cylinders modeled with radial symmetry. The relationship between volume flux of mass transfer and

the corresponding rates of bond growth, void height shrinkage, and bond line neck radius growth were derived from the various geometries of the three pairs of mechanisms [15].
Derby's second model on diffusion bonding included the one mechanism that has some importance in sintering. This is bond formation by mass transfer in the vapor phase. This was excluded for diffusion bonding mechanisms, because of low vapor pressures of metals under typical bonding conditions. However this mechanism may be important when bonding non-metals, therefore, for completeness, the mechanism rate equations for such mass transfer in the vapor phase were derived [16].

6. Hills Model (1989)

Hills model on diffusion bonding suggested elliptical void shape and was based on Derby's model [17]. Likewise, the theoretical model was also studied on copper. The model assumed that when the bonding surfaces are brought together, the two sets of ridges touch tip-tip, creating between them a series of infinitely long parallel cylinders of elliptical cross section (Figure 2.6-6). The closure of a section perpendicular to the longitudinal axis is modeled and, by invoking symmetry, just one quarter of an elliptical section needs to be considered. The assumption of peak-to-peak contact will result in calculations of maximum bonding time. The parallel alignment of geometry creates condition of plane strain so allowing length of the void channels to be ignored.

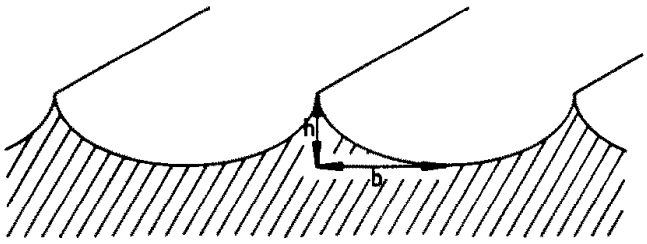

Figure 2.6-8: Hill's Model-void surface (long parallel ridges) [17]

In this model, the bonding of a single wavelength of surface roughness was assumed to occur in two stages:

a. Stage 0 (the convention used in pressure sintering): Plastic deformation is said to be instantaneous so not permitting the time dependent diffusion or creep mechanisms to

contribute bonding. Plastic deformation ends when the contact area at the interface is sufficient to support the applied load (localized stress on a ridge drops below the yield point of the material).

b. Stage I: Time dependent and one or more of the six diffusion and creep mechanisms contribute to bonding. Unlike the earlier method of Derby and Wallach, separate Stage II geometry (circular-section voids) was not required since elliptical voids can attain circular geometry naturally without a discontinuity in bonding rate. When circular geometry is reached, there is no driving force for the surface source mechanism and so contributions from these ceases. However the use of elliptical geometry allows these surface source mechanisms to reactivate naturally if aspect ratio of the voids alters from unity as a result of contributions to bonding from interface sources and creep mechanisms that operate throughout the Stage I regardless of void geometry. The routes of material transfer have been shown in Figure 2.6-9. The series of expressions for rates of each mechanism and the rates of geometric (void shape) changes for given set of process variables are derived using the manner of material distribution. The neck radius of the ellipse is derived in terms of the major and the minor semi-axes of the ellipse and its rate of change does not have to be independently. The rate of void shrinkage is expressed in terms of the rate of change of bond area and the rate of change in height.

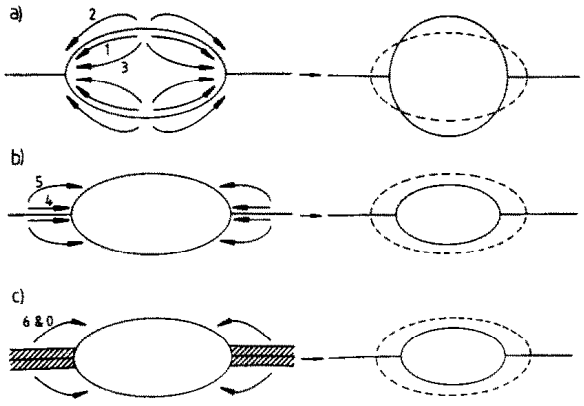

Figure 2.6-9: Hill's Model- Routes of material transfer (a) surface source mechanisms; (b) interface mechanisms; (c) bulk deformation mechanisms.

The model analyzed the creep and plastic deformation mechanisms in the diffusion bonding process. However the dynamic conditions of bonding mechanisms, such as actual action time and distance were not considered. Therefore the bonding time was overestimated.

7. Pillings Model (1984-96)

Pilling's model on diffusion bonding is based on grain boundary diffusion coupled with time based creep postulated in late nineties. The results showed that within the superplastic regime the surface roughness has more impact on diffusion bonding process than the pressure and temperature. The first model was created in 1984[9].

Pilling postulated the solid state diffusion bonding model for superplastic titanium alloy, Ti-6Al-4V. In the diffusion bonding model created in 1984, the surfaces to be bonded were assumed to have cylindrical geometry with parallel, semicircular grooves. By the use of cylindrical geometry, the effect of internal pressure was ignored as the cavities would be exposed to the atmosphere. The model had certain assumptions:

a) The two surfaces bond instantaneously on contact

b) At the bonding temperature there was a good surface diffusion to maintain the circular geometry.

In the model the bonding time was calculated by differentiating the volume of cavity with respect to time and then integrating it within limits of area fraction bonded (A_f). Figure 2.6-10 shows the shape of the void geometry.

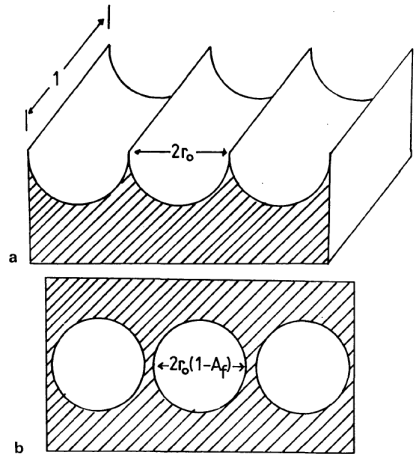

Figure 2.6-10: Pilling Model Void geometry at t = 0 [9]

Under the application of load, the points of contact between the two surfaces, that was initially negligible, deform until their area support load. The area fraction of bonded was then defined as:

$$A_f = \frac{\sigma}{\sigma_y} \tag{2.1}$$

(σ: Stress at bonding interface, σ_y: Yield Strength of Bonding material)

When the cylindrical cavity is maintained throughout the process

Volume of cavity radius

$$V = \pi r^2 . 1 \tag{2.2}$$

(Here r: instantaneous cavity radius)

$$r = r_0(1 - A_f) \tag{2.3}$$

$$\frac{dV}{dt} = -2\pi r_0^2 (1 - A_f) \frac{dA_f}{dt} \tag{2.4}$$

$$\int_0^t dt = -2\pi r_0^2 \int_{\sigma/\sigma_y}^1 \frac{1-A_f}{dV/dt} dA_f \tag{2.5}$$

(r_0: initial cavity radius)

Here dV/dt denote the rate of growth of voids. The expression was derived from Chen and Argon's [12] model of growth of voids of spherical geometry during creep. The spherical geometry was modified to the cylindrical geometry and the rate of closure of the interfacial voids.

$$\frac{dV}{dt} = \frac{16 D_B \delta \delta \Omega \sigma}{B A_f k T} \times \frac{1}{4ln\left(\frac{B+r}{r}\right) - [3-(r/r+B)^2][1-(r/r+B)^2]} \tag{2.6}$$

Here 'B' is the distance measures from the edge of the void, over which diffusive flow is the mass transfer mechanism, D_B δ: Grain boundary diffusion, Ω: Atomic volume)

The local strain rate $\dot{\varepsilon} = A_c(\sigma/G)^n$ (2.7)

$$B = \left| \frac{\pi D_B \delta \Omega |\sigma|}{A_f k T \dot{\varepsilon}} \right|^{1/3} \tag{2.8}$$

(εdot: strain rate)

Chen and Argon's theory assumed that only one grain boundary contributes towards mass transport to void cavity. However in case of superplastic materials, the grain size is strikingly less than the initial surface roughness and several grain boundaries would be

present. The contribution to mass transport from interfaces other than the bond line to overall cavity closure was introduced in the model. This was estimated by assuming material to be bonded made up multilayered sandwich where the spacing between the layers was assumed same given by the grain size d.

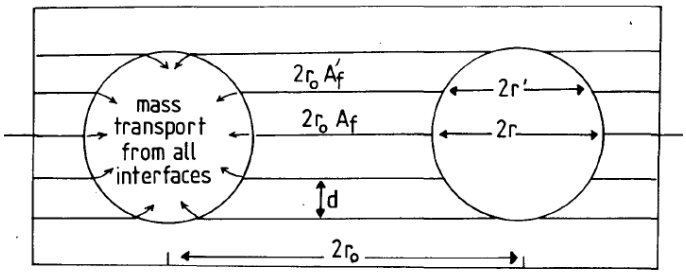

Figure 2.6-11: Pilling Model: Section through bondline showing interfaces of spacing *d* that contributes to mass transfer in bonding process [18]

The expression of rate of change of cavity volume with time was modified to include the summation of the contribution of each layer in it.

$$N_i = 2.int(r/d) + 1 \tag{2.9}$$

$$\frac{dV}{dt} = \left|\frac{dV}{dt}\right|_r + \sum_0^{(N_i-1)/2} \left|\frac{dV}{dt}\right|_r \tag{2.10}$$

Pilling further developed the diffusion bonding model to predict the time required to attain full interfacial contact during diffusion bonding under isostatic state of stress in 1988 [18]. The model proposed the rate of closure of interfacial voids using the coupled diffusion and power law creep theory based on the original work of Chen and Argon. However the law was modified to the cylindrical geometry. This work was done again the superplastic alloy Ti-6Al-4V. The model had reasonable agreement with the experimental data. The bonding mechanisms adopted in the model:

a) Plastic collapse of supporting contact areas by time dependent plasticity (power law creep/ superplastic flow)

b) Diffusion of atoms from any interface intersecting the surface of voids to that surface via both volume and interfacial paths.

c) Mass transfer from one region of void surface to another by surface diffusion or vapor phase transport.

It was concluded that the complete interfacial contact is attained primarily as a consequence of the time dependent plastic collapse of the asperities, rather than by diffusion. On application of external pressure 'P', the remote area to bond zone experiences uniform hydrostatic compression and remains undeformed. In the bond zone, the points of contact start to deform plastically. Fractional area of bond zone was defined by:

$$f_c = P/\sigma_{ys} \tag{2.11}$$

The plasticity theory was applied to calculate stress distribution in the void geometry. To calculate the stress distribution within cylinder wall, it was assumed that material first behaves elastically [19].

For radial force equilibrium

$$\frac{d\sigma_r}{dr} + \frac{\sigma_r - \sigma_\theta}{r} = 0 \tag{2.12}$$

Solving for B.C.s $\sigma_r = -P$ at $r = r_h$.

The elastic strains at a point in the cylinder wall (ε_r, ε_θ, and ε_z)

$$E\,(\epsilon_r - \alpha T) = \sigma_r - \gamma(\sigma_\theta + \sigma_z)$$
$$E\,(\epsilon_\theta - \alpha T) = \sigma_\theta - \gamma(\sigma_r + \sigma_z)$$
$$E\,(\epsilon_z - \alpha T) = \sigma_z - \gamma(\sigma_r + \sigma_\theta) \tag{2.13}$$

Plane strain case: $\epsilon_z = 0$

$$\sigma_z = \gamma(\sigma_r + \sigma_\theta) - \alpha E T$$
$$\epsilon_r = (1 + \gamma)\,\alpha T + \left(\frac{1-\gamma^2}{E}\right)\left(\sigma_r - \frac{\gamma}{1-\gamma}\,\sigma_\theta\right)$$
$$\epsilon_\theta = (1 + \gamma)\,\alpha T + \left(\frac{1-\gamma^2}{E}\right)\left(\sigma_\theta - \frac{\gamma}{1-\gamma}\,\sigma_r\right)$$
$$(\sigma_r - \sigma_\theta) = \frac{E\,(\epsilon_r - \epsilon_\theta)}{1+\gamma}$$
$$\sigma_r = \frac{E(1-\gamma)}{(1-2\gamma)(1+\gamma)}\left[\epsilon_r + \frac{\gamma}{1-\gamma}\epsilon_\theta - \alpha T\left(\frac{1+\gamma}{1-\gamma}\right)\right] \tag{2.14}$$

Substituting for $(\sigma_r - \sigma_\theta)$ and σ_r in equilibrium

$$\left(\frac{1-\gamma}{1-2\gamma}\right)\left[\frac{d\epsilon_r}{dr} + \frac{\gamma}{1-\gamma}\frac{d\epsilon_\theta}{dr} - \frac{1+\gamma}{1-\gamma}\alpha\frac{dT}{dr}\right] + \frac{\epsilon_r + \epsilon_\theta}{r} = 0$$

Noting

$$\epsilon_r = \frac{du}{dr}\ ;\ \epsilon_\theta = \frac{u}{r}$$

$$\frac{d^2u}{dr^2} + \frac{1}{r}\frac{du}{dr} - \frac{u}{r} = \frac{1+\gamma}{1-\gamma}\alpha\frac{dT}{dr}$$

$$\frac{d}{dr}\left[\frac{1}{r}\frac{d(ru)}{dr}\right] = \frac{1+\gamma}{1-\gamma}\alpha\frac{dT}{dr}$$

$$\frac{1}{r}\frac{d(ru)}{dr} = \frac{u}{r} + \frac{du}{dr} = \frac{1+\gamma}{1-\gamma}\alpha T + c_1$$

$$ru = \frac{1+\gamma}{1-\gamma}\alpha\int Tr\ dr + \int c_1 r\ dr$$

$$u = \frac{\alpha}{r}\left(\frac{1+\gamma}{1-\gamma}\right)\int_a^r Tr\ dr + \frac{c_1 r}{2} + \frac{c_2}{r}$$

$$\epsilon_\theta + \epsilon_r = \frac{1+\gamma}{1-\gamma}\alpha T + c1$$

Substituting

$$\sigma_r = \frac{E}{1+\gamma}\left[\frac{c_1}{2(1-2\gamma)} - \frac{c_2}{r^2}\right] - \frac{\alpha E}{(1-\gamma)r^2}\int_a^r Tr\ dr$$

$$\sigma_r - \sigma_\theta = \frac{E\alpha T}{1-\gamma} - \frac{2\alpha E}{r^2(1-\gamma^2)}\int_a^r Tr\ dr - \frac{2c_2 E}{r^2(1+\gamma)}$$

$$\sigma_\theta = \frac{E}{1+\gamma}\left[\frac{c_1}{2(1-2\gamma)} + \frac{c_2}{r^2}\right] - \frac{\alpha ET}{(1-\gamma)} + \frac{\alpha E}{r^2(1-\gamma)}\int_a^r Tr\ dr$$

$$\sigma_z = \frac{rEc_1}{(1+\gamma)(1-2\gamma)} - \frac{\alpha ET}{(1-\gamma)}$$

$\sigma_r = P_i$ at $r = r_h$; $\sigma_r = P_i$ at $r = r_o$

$$c_1 = \frac{2(1+\gamma)(1-2\gamma)}{E({r_o}^2 - {r_h}^2)}(P_i r_h^2 - P r_o^2)$$

$$c_2 = \frac{(1+\gamma)(P_i - P)(r_h^2 r_o^2)}{E(r_o^2 - r_h^2)}$$

The material does not behave elastically but rater in time dependent plastic manner. The radial and circumferential stresses vary with radial displacement, and superplastic flow would normally tend to even out any stress gradients, which develop in the walls of the cylinder. The average radial stress:

$$\sigma_r = \frac{r_h^2 r_o^2 (P - P_i)}{(r_o^2 - r_h^2)}\frac{1}{r^2} + P_i\frac{r_h^2 - r_o^2}{r_o^2 - r_h^2} \qquad (2.15)$$

The average circumferential stress:

$$\sigma_\theta = \frac{-r_h^2 r_o^2 (P - P_i)}{(r_o^2 - r_h^2)}\frac{1}{r^2} + P_i\frac{r_h^2 - r_o^2}{r_o^2 - r_h^2} \qquad (2.16)$$

The axial stress was calculated by assuming that external pressure acts through rigid plates covering the top and bottom surfaces of the cylinder.

$$\sigma_z = \frac{-P_i r_o^2}{(r_o^2 - r_h^2)} \tag{2.17}$$

The material doesn't behave elastically but rather in the time dependent plastic manner. Therefore average radial stress would be given by the following equation. The fractional area 'f_h' for non-bonded surface could be defined by $\frac{r_h^2}{r_o^2}$. The dividing the equation of radial stress byr_o^2, and substituting surface tension $\frac{-2\Gamma}{r_h}$ for P_i provides refined radial stress equation (2.19). Similarly average circumferential stress would be given by equation 2.20. The effective stress is then defined in equation 2.21. $f_h = 0$ when the bonding is completed. (Stress State → Isostatic compression → $\sigma_r = \sigma_\theta = \sigma_z = -P$, Surface Tension = 0 when $f_h = 0$). The effective plastic strain rate was related to effective stress through creep equation defined in equation 2.22. The individual components of strain rate using Levy-Mises associated flow rate are given in equation 2.23.

$$\overline{\sigma_r} = \frac{\int_{r_h}^{r_o} \sigma_r dr}{\int_{r_h}^{r_o} dr} = \frac{P(r_h r_o - r_o^2) + P_i(r_h^2 - r_h r_o)}{r_o^2 - r_h^2} \tag{2.18}$$

$$\overline{\sigma_r} = \frac{\left(P - {}^{-2\Gamma}/_{r_o}\right) + \left(f_h^{1/2} - 1\right)}{1 - f_h} \tag{2.19}$$

$$\overline{\sigma_\theta} = \frac{\left(-P - {}^{-2\Gamma}/_{r_o}\right) + \left(f_h^{1/2} + 1\right)}{1 - f_h} \tag{2.20}$$

$$\sigma = \left\{\tfrac{1}{2}((\sigma_r - \sigma_\theta)^2 + (\sigma_\theta - \sigma_z)^2 + (\sigma_z - \sigma_r)^2)\right\}^{1/2} \tag{2.21}$$

$$\dot{\varepsilon} = \frac{A_{sp} exp^{(-Q_{sp}/RT)}\, \sigma^{nsp}}{T} + \frac{A_{pl} exp^{\left(-Q_{pl}/RT\right)}\, \sigma^{npl}}{T} \tag{2.22}$$

$$\frac{\dot{\varepsilon_z}}{\sigma_z - \frac{1}{2}(\sigma_\theta + \sigma_r)} = \frac{\dot{\varepsilon_r}}{\sigma_r - \frac{1}{2}(\sigma_\theta + \sigma_z)} = \frac{\dot{\varepsilon_\theta}}{\sigma_\theta - \frac{1}{2}(\sigma_r + \sigma_z)} = \frac{\dot{\varepsilon}}{\sigma} \tag{2.23}$$

(Here$A_{sp}, n_{sp}, \sigma^{nsp}$: Rate constants, Stress dependencies, and Temperature dependencies of strain rate for superplastic process. $A_{pl}, n_{pl}, \sigma^{pl}$: Rate constants, Stress dependencies, and Temperature dependencies of strain rate for creep flow).

Axial collapse results in an increase in both the inner and outer radii of cylinder by amount δr_h and δr_o as height of cylinder decreases by δh. Volume of Material removed from outer reaches of cylinder walls would be:

$$\delta V = \pi\{(r_o + \delta r_o)^2 - r_o^2\}(h - \delta h) \quad (2.24)$$

= Volume of material added to bore

$$= \pi\{(r_h + \delta r_h)^2 - r_i^2\}(h - \delta h)$$

Eliminating 2nd order term; dividing by r_o^2

However $\frac{\delta r_o}{r_o} = \frac{\delta r_h}{r_h} = \varepsilon_r$, Recalling $f_h = \frac{r_h^2}{r_o^2}$; Defining $\delta f_h = \frac{r_i^2}{r_o^2} - \frac{r_h^2}{r_o^2}$

Combining above three equations; dividing by δt

$$\frac{r_i^2}{r_o^2} - \frac{r_h^2}{r_o^2} = \frac{2\delta r_o}{r_o} + \frac{\delta r_h}{r_h}\frac{r_h^2}{r_o^2}$$

$$\delta f_h = 2\varepsilon_r + 2\varepsilon_r f_h$$

$$\frac{\delta f_h}{\delta t} = -\frac{2\varepsilon_r}{\delta t} + \frac{2\varepsilon_r f_h}{\delta t}$$

$$\left.\frac{df_h}{dt}\right|_{pl} = -2\dot{\varepsilon_r}\,(1 - f_h) \quad (2.25)$$

δV = Volume of material removed from each interface, therefore change in height of cylinder δh per interface

$$\delta h = \frac{\delta V}{\pi(r_o^2 - r_h^2)}$$

Internal radius decreases from r_h to r_i

$$\delta V = \pi(r_h^2 - r_i^2)(h - \delta h)$$

Expanding and ignoring 2nd order terms

$$\delta V = -\pi r_o^2 h \delta f_h$$

Dividing by δt

$$\frac{df_h}{dt} = \frac{-1}{\pi r_o^2 h}\frac{dV}{dt} \quad (2.26)$$

The 'r_o' was defined by surface roughness, while 'h' vary throughout the process. From the previous model, the contribution of more than one grain boundary layers was considered in the calculation. The number of interfaces N_i intersecting the surface of void will be determined by ratio of grain size to void size. If all grain boundaries are assumed to lie parallel to bonding interface at spacing equal to grain size 'd'. The 'h', instantaneous height of cylindrical bore will vary throughout the process. To simplify the analysis it was assumed that instantaneous height decreases at the same rate as f_h (fractional area of non-

bonded interface) provided by equation 2.27. Total rate of change in fractional area of interfacial voids with time as a result of diffusion from grain boundaries and from bond interface intersecting the surface of void are provided in equations 2.28 and 2.29 respectively. Time required was estimated by integrating $\frac{\mathrm{df_h}}{\mathrm{dt}}$ in limits $\left(1-\mathrm{P}/\sigma_{\mathrm{ys}}\right)$ at start of bonding to zero (bonding complete).

$$N_i = int\ (1 + h/d) \tag{2.27}$$

$$= int\ (1 + h_o f_h/d)$$

$$\left.\frac{df_h}{dt}\right|_d = N_i \left(\frac{1}{\pi r_o^2 h_o f_h}\frac{dV}{dt}\right) \tag{2.28}$$

$$\frac{dV}{dt} = \frac{2\pi D g b \delta \Omega \delta \sigma_z}{KT}\frac{1-f_h}{\ln(1/f_h)-(1-f_h)/2} \tag{2.29}$$

(Here $D_{gb}\delta$: Grain Boundary diffusion, K: Boltzmann constant),

The diffusive mass transfer collapse in the previous model was modified in Pilling's results on diffusion bonding in super alpha-2 materials [20]. The cylindrical voids were filled by two processes; the time dependent plastic collapse of cylindrical walls and the interfacial transfer of mass from bond to void by diffusion. The rate of void removal by diffusional mass transfer from bond interface to void surface was determined by solving Fick's law, using stress dependent chemical potential present between the bonded interface and the void surface. Time dependent plastic collapse of cylindrical walls for area fraction of voids, 'f' was given by equation and the rate of reduction of void height was established in equations 2.30 and 2.31 respectively. The diffusive mass transfer through volume and grain boundary diffusion is provided by equations 2.32 and 2.33 respectively. The rate of reduction of void area due to each mechanism was added to give the overall rate of bonding. The bonding time can be determined by integrating the rate equations over shorter of $f = f_o \to 0, h = h_o \to 0$.

$$\left.\frac{df}{dt}\right|_{pl} = -2\dot{\varepsilon_r}\ (1-f) \tag{2.30}$$

$$\frac{dh}{dt} = \dot{\varepsilon_z}\ h \tag{2.31}$$

$$\left[\frac{df}{dt}\right]_{vol} = -\frac{4\Omega D_v}{kT}\left[\frac{f}{ln\left(\frac{1}{f}\right)-\frac{1-f}{2}}\right]\frac{1}{r_o^2}p \tag{2.32}$$

$$\left[\frac{df}{dt}\right]_{gb} = -\frac{2\Omega D_{gb}\delta}{kT}\left[\frac{1}{ln\left(\frac{1}{f}\right)-\frac{1-f}{2}}\right]\frac{1}{r_o^2}p\left(\frac{1+\frac{h}{d}}{h}\right) \quad (2.33)$$

(D_v: Volume Diffusion)

8. Li's Model (2005)

Li's model is based on Pilling's work of predicting diffusion bonding time. In this model stochastic characteristics of surface finish are taken into consideration. The probabilistic feature of the surfaces to be bonded is considered. A probabilistic model is developed by assuming void radius and height as random variables. Monte Carlo simulation technique in conjunction with numerical integration is used to calculate the bonding time and its probabilistic distribution for the diffusion bonding of Ti–6Al–4V alloy. The probabilistic model was constructed in the following steps:

(i) Identification and characterization of variables.

Inorder to determine deterministic variables and random variables, the variables were separated into two categories: external variables and internal variables. External variables included parameters, which described the environmental conditions, such as pressure and temperature; internal variables included material properties and its geometric characters like surface roughness in diffusion bonding.

(ii) Determination of the probability density function (PDF) and cumulative distribution function (CDF) for random variables based on existing experimental data and experience.

(iii) Combination of the deterministic model with CDF of random variables to construct a probabilistic model.

From the SEM observation of a diffusion-bonding surface joint used in the study whose strength is about 40% of that of parent material, the surface was represented of a semicircular. Pilling's model was utilized to calculate diffusion bonding time for the probabilistic feature of joining surfaces. In this model, it is assumed the interface was as defined in Pilling's previous model (Figure 2.6-8). Equation 2.1 ($A_{f0} = \frac{\sigma}{\sigma_y}$), defined the area of fraction 'A_{f0}' at the initial contact (t = 0), where σ and σ_y are the applied stress and yield stress corresponding to the bond temperature respectively. The bonded fraction can

be defined by equation 2.34 (where r_0 is the initial void radius and 'r' is the instantaneous void radius and 'f' is set as$f = (r/r_0)^2$). When the bonding is complete, A_f =1.

$$A_f = \frac{r_0 - r}{r_0} \tag{2.34}$$

The void closure is attributed to four of the diffusion bonding mechanisms that include plastic deformation, power law creep, grain boundary diffusion and volume diffusion. The equations from the chapter 2, 2.32, 2.32 and 2.33 describe the power law creep, grain boundary diffusion and volume diffusion respectively. The rate of change in area of fraction 'f' due to plastic deformation is defined in equation 2.35. This equation is obtained through substitutions in the pilling's equation of rate of change of fractional area due to plastic deformation. The rate of change of fractional area due to above three mechanisms is summarized in Equation 2.36. The total bonding time is obtained by integrating the rate equation given by equation 2.37.

$$\dot{\varepsilon} = \frac{A_{sp} exp^{(-Q_{sp}/RT)}\, \sigma^{nsp}}{T} + \frac{A_{pl} exp^{(-Q_{pl}/RT)}\, \sigma^{npl}}{T} \tag{2.22}$$

$$\left[\frac{df}{dt}\right]_{plasticity} = \frac{\dot{\varepsilon}}{\sigma_e}\left(3p\sqrt{f} - \frac{2\gamma\sqrt{f}}{r_0} + \frac{6\gamma}{r_0}\right) \tag{2.35}$$

$$\left[\frac{df}{dt}\right]_{vol} + \left[\frac{df}{dt}\right]_{gb} + \left[\frac{df}{dt}\right]_{plasticity} =$$

$$-\frac{4\Omega D_v}{kT}\left[\frac{f}{ln\left(\frac{1}{f}\right) - \frac{1-f}{2}}\right]\frac{1}{r_o^2}p - \frac{2\Omega D_{gb}\delta}{kT}\left[\frac{1}{ln\left(\frac{1}{f}\right) - \frac{1-f}{2}}\right]\frac{1}{r_o^2}p\left(\frac{1+\frac{h}{d}}{h}\right) + \frac{\dot{\varepsilon}}{\sigma_e}\left(3p\sqrt{f} - \frac{2\gamma\sqrt{f}}{r_0} + \frac{6\gamma}{r_0}\right)$$

(2.36)

$$t = \int_{f_0}^{f} \frac{-\sigma_e/\dot{\varepsilon}}{\left(3p\sqrt{f} - \frac{2\gamma\sqrt{f}}{r_0} + \frac{6\gamma}{r_0}\right) + \frac{4\Omega D_v}{kT}\left[\frac{f}{\ln\left(\frac{1}{f}\right) - \frac{1-f}{2}}\right]\frac{1}{r_o^2}p + \frac{2\Omega D_{gb}\delta}{kT}\left[\frac{1}{\ln\left(\frac{1}{f}\right) - \frac{1-f}{2}}\right]\frac{1}{r_o^2}p\left(\frac{1+\frac{h}{d}}{h}\right)} df \tag{2.37}$$

Where $A_{sp}, n_{sp}, \sigma^{nsp}$ are rate constants, stress dependencies, and temperature dependencies of strain rate for superplastic process; $A_{pl}, n_{pl}, \sigma^{pl}$ are rate constants, stress dependencies, and temperature dependencies of strain rate for creep flow; Ω is atomic

volume; D_{gb} and D_v and grain boundary and volume diffusivities; δ, d and h are the grain boundary width, grain size and void height respectively.

9. Fangs Model (2012)

Fang's model is based on Derby's work on diffusion bonding [21]. The model proposes the dynamic conditions for diffusion bonding mechanisms, plastic deformation, surface source mechanism, interface source mechanism and creep mechanism based on these mechanisms. The model for void closure in the diffusion bonding is derived based on these dynamic conditions. The model adopts six bonding mechanisms, in which two are surface source mechanism and two are the interface source mechanisms. The six bonding mechanisms are as follows:

1. Initial plastic deformation
2. Surface diffusion from surface sources to void neck
3. Volume diffusion from surface sources to void neck
4. Grain boundary diffusion from interface sources to void neck
5. Volume diffusion from interface sources to void neck
6. Power law creep

The mechanisms (2) and (3) refer to the surface source mechanisms, and mechanisms (4) and (5) refer to the interface source mechanisms.

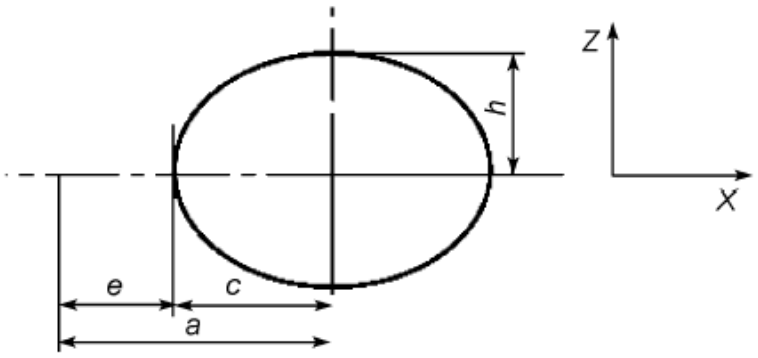

Figure 2.6-12: Fang's Model: Geometry of Void (e: half bonding length in the bonding interface (μm), a: half of the distance from the centers of two adjacent voids (μm), h: half of void height (μm), c: half of void width(μm) [21]

1. Initial Plastic Deformation

As the actual area in the bonding interface is much smaller than the nominal contact area the stresses in the bonding interface exceeds the yield strength of the material and the plastic deformation occurs. This is the dynamic condition of initial plastic deformation proposed in the model. The plastic deformation occurs when the stress in the bonding interface (σ') is greater than the yield strength of the material (σ_y) and when this stress in the bonding interface is smaller than the yield strength of the material the plastic deformation mechanism stops.

The mathematical model calculates the bonding length and the bonding height after the plastic deformation from the stress equation based on the slip line theory. The stress in the bonding interface is given by equation 2.38. Then applying slip-line theory and integrating equation 2.39 is obtained.

$$\sigma' = \frac{pa-\gamma}{e} \tag{2.38}$$

Slip line theory

$$\sigma(x) = 2K\left[1 + ln\left(1 + \frac{x}{r_A}\right)\right]$$

K: Material shear yield strength $= \frac{\sigma_y}{\sqrt{3}}$

r_A: radius of curvature of void neck

$$\bar{\sigma} = \int_0^a \frac{\sigma(x)}{e}\,dx$$

$$\bar{\sigma} = 2K\left(1 + \frac{r_A}{e}\right) ln\left(1 + \frac{e}{r_A}\right) \tag{2.39}$$

The bonding length after initial plastic deformation (e_y) was calculated by substituting the equation (2) in equation (1) and then solving for the bonding length. The constancy of volume in the initial plastic deformations of material in the bonding interface was applied to calculate the void height (hy) after initial plastic deformation. Using the iteration method the equations (3) and (4) can to solved to find out the void height and the bonding length in the bonding interface when this mechanism stops. Bonding length at yield (e_y) and height (h_y) are given by equations 2.40 and 2.41 respectively.

$$e_y = \frac{pa-\gamma}{2K\left[1+\frac{h_y^2}{\varepsilon_{y(a-e_y)}}\right]ln\left[1+\frac{e_y(a-e_y)}{h_y^2}\right]} \quad (2.40)$$

$$h_y = h' \frac{a-\frac{\pi}{4}c'}{a-\frac{\pi}{4}(a-e_y)} \quad (2.41)$$

The results of void height and bonding length obtained from the initial plastic deformation mechanism are served as the initial conditions of other mechanisms.

2. Surface Source Mechanism

The driving force for surface source mechanism was given as the difference in the void curvature. The surface mechanism continues till there is difference of void curvature and then stops when the curvature is same, i.e., the void shape is circular. The distance limit of this rounding effect was taken from Mullin's equation (eq. 2.42) to calculate the spread length ds of surface diffusion in definite time.

$$d_s = 0.46\left(\frac{D_s\delta_s\gamma\Omega t}{KT}\right)^{1/4} \quad (2.42)$$

D_s: Surface diffusion coefficient (m^2/s); Ω: Atomic Volume (m^3), K: Boltzmann constant (1.38E-223 J/K); T: Absolute Bonding temperature (K), T: Diffusion time (s); δ_s: Thickness of surface diffusion layer (m)

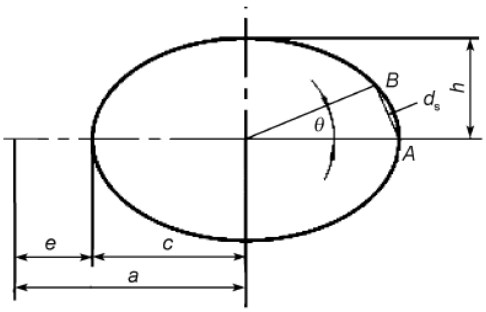

Figure 2.6-13: Mass Transfer along interface [21]

$$r_B = \left(\frac{c^2\sin^2\theta+h^2\cos^2\theta}{ch}\right)^{3/2} \quad (2.43)$$

Condition: $r_A \neq r_B$ surface source mechanism acts.

$r_A = r_B$ surface source mechanism stops.

Gibbs Thompson Relationship

$\dot{V} = \frac{2AD\Omega}{rKT}\frac{\gamma}{r}$

A: cross sectional area of diffusion flow (μm^2)

D: Diffusion coefficient (m^2/s)

When $r_A = r_B$ surface source mechanism stops, then rate of matter transfer will be zero. Hence correction factor must be included in the above equation. $\dot{V}_1$: rate of mass transfer by surface diffusion from surface sources to void neck as defined by equation 2.45 and $\dot{V}_2$: rate of mass transfer by volume diffusion from surface sources to void neck as defined by equation 2.46.

$$\dot{V} = \frac{2AD\Omega}{r_A KT}\left(\frac{1}{r_A} - \frac{1}{r_B}\right) \quad (2.44)$$

$$\dot{V}_1 = \frac{2\Omega D_s \delta_s \gamma}{r_A KT}\left(\frac{1}{r_A} - \frac{1}{r_B}\right) \quad (2.45)$$

$$\dot{V}_2 = \frac{2\Omega D_v \gamma}{KT}\left(\frac{1}{r_A} - \frac{1}{r_B}\right) \quad (2.46)$$

D_v: Volume diffusion coefficient (m^2/s)

The surface source mechanism changes the void shape, but not its volume.

Assuming height,'h', increases, and therefore the radius,'c', decreases.

$Volume: \frac{\pi}{4}h(c+\delta c) = \frac{\pi}{4}c(h+\delta h)$

$c\delta h = h\delta c$

Volume of matter transferred by surface source mechanism

$\delta V = \frac{1}{2}\left[\frac{\pi}{4}(h+\delta h)(c+\delta c) - \frac{\pi}{4}hc\right]$

Ignoring higher order terms, change rate $\dot{h_{12}}$ of void height by two mechanisms:

$$\dot{h_{12}} = \frac{4\dot{V}_{12}}{\pi c} \quad (2.47)$$

Due to constant void volume, change rate of bonding length in bonding interface:

$$\dot{e}_{12} = \frac{\dot{h}_{12} c}{h} \quad (2.48)$$

3. Interface Source Mechanism

In the model the stress distribution along the bonding interface is divided into two regions, region I is adjacent to the void geometry whereas the region II is away from the void

geometry. The stress in the region I gradually decrease whereas the stress in region II remains constant. As the stress gradient is the driving force for the interface source mechanism, the grain boundary diffusion takes place in region I while the creep occurs in region II.

The mathematical model is based on Chen [14] growth model of void in grain boundary by combining the effect of grain boundary diffusion and creep. The characteristic length for effective grain boundary diffusion introduced in this model indicated that grain boundary mechanism is more effective than that of creep. It was also suggested that the distance of grain boundary diffusion is shorten by matrix creep and the atoms flow is dominated by the grain boundary diffusion. The expression of characteristic length d_b was given by:

$$d_B = \left[\frac{D_B \delta_B \Omega p}{A_c K T (p/G)}\right]^{1/3} \tag{2.49}$$

Ac: Creep coefficient; G: Shear Modulus

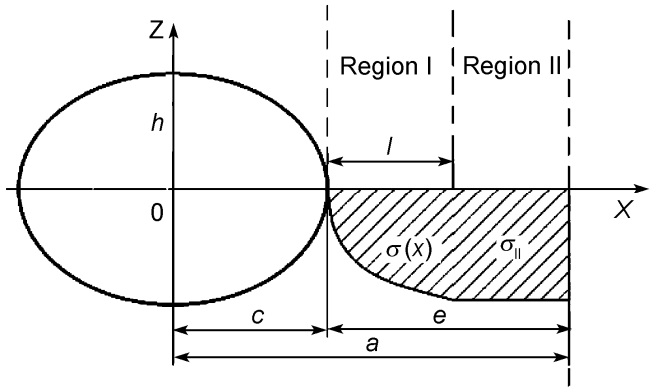

Figure 2.6-14: Stress distribution along bonding interface [21]

Dynamic Condition:

When dB > e, l = e, and dB < e, l = dB, if dB = e (Region II doesn't exist)

The rate of mass transfer by interface sources was derived using sintering theory proposed by Johnson [22]. The atom flux and chemical potential gradient of atoms relationship were used to derive the stress gradient along the bonding interface by the interface source mechanism.

$$\sigma_I = \frac{2alp+\left[3(1-2c)(e-l)\left[\frac{1}{l}+\frac{1}{r_A}\right]-\frac{2l(e-l)}{r_A}\right]\gamma}{2l^2+3(l-2c)(e-l)} \quad (2.50)$$

The mass transfer by grain boundary diffusion from interface source to void neck ($\dot{V}_3$)and by volume diffusion ($\dot{V}_4$) is given by equations 2.51 and 2.52 respectively:

$$\dot{V}_3 = \frac{3D_B\delta_B\Omega}{2KTl}\left(\sigma_I - \frac{\gamma}{l} - \frac{\gamma}{r_A}\right) \quad (2.51)$$

$$\dot{V}_4 = \frac{3D_v\Omega r_A}{KTl}\left(\sigma_I - \frac{\gamma}{l} - \frac{\gamma}{r_A}\right) \quad (2.52)$$

Assumption: Material volume remains constant, but both shape and volume alter in interface source mechanism (volume transfer: $\delta V = e\delta h$). Then the bonding height and the bonding length are defined by equations 2.53 and 2.54 respectively.

Bonding height**:** $\dot{h}_{34} = \frac{\dot{V}_{34}}{e}$ (2.53)

Bonding length*:* $\dot{e}_{34} = \frac{\dot{h}_{34}}{h}\left[a\left(\frac{4}{\pi}-1\right)+e\right]$ (2.54)

When the stress gradient in region I tends to zero, interface source stops.

4. Power Law Creep

In the diffusion bonding the micro creep is also said to impact the void closure. The stress and strain rate near the bonding interface alters with the change of void size. The power law creep condition was derived in the interface source mechanism. The dynamic condition for creep is given by:

$d_B < e$

The mathematical model was postulated by dividing the material near the bonding interface into N slices, where N can be any integer (1,2.3, …,N)

Therefore, Thickness per layer = h/N

Stress σi acting on ith slice

$$\sigma_i = \left(\frac{a}{x_1}\right)p \quad (2.55)$$

$$x_1 = a - c\sqrt{1-\frac{x_i^2}{h^2}}$$

Thus, the strain rate $\dot{\varepsilon}_i$ of the ith slice :

$$\dot{\varepsilon}_i\left(i^{th}slice\right) = SA\left|\frac{\sigma_i}{G}\right|^n \quad (2.56)$$

(S: Sign function +ve : tensile stress, -ve: compressive stress, 'n' exponent of creep)
Definition of strain and strain rate:

$$\frac{dh_i}{h_i} = \frac{dh_i}{h/N} = d\varepsilon_i = \dot{\varepsilon}_i dt = SA\left|\frac{\sigma_i}{G}\right|^n$$

By definition of limiting and integral

$$\frac{dh}{dt} = \delta A_c \left|\frac{P}{G}\right|^n \int_0^h \left(\frac{a}{x_i}\right)^n dx$$

Change rate of void height by creep

$$\dot{h}_5 = SA_c \left|\frac{P}{G}\right|^n \int_0^h \left(\frac{a}{a - c\sqrt{1-\frac{z^2}{h^2}}}\right)^n dz \tag{2.57}$$

The expression of change in bonding length in the power law creep was same as that in the interface source mechanism:

$$\dot{e}_5 = \frac{-\dot{h}_5}{h}\left[a\left(\frac{4}{\pi} - 1\right) + e\right] \tag{2.58}$$

5. Calculation of Fang's Model

In the Fang's model, the bonding parameters, the void height and the bonding length are the function of both the material properties and the process parameters. For a given metal, according to the initial void's surface height h' and the width c', the void height h_{yield} and e_{yield} after initial plastic deformation at certain bonding pressure, temperature and time were obtained by iteration method. These values were used as the initial conditions for the remaining bonding mechanisms. Then, these bonding mechanisms were solved independently using the above initial conditions and the stated dynamic conditions. By solving these mechanisms the void height and bonding length were obtained for each of them. In the end, the void height and bonding length in the bonding interface by all the mechanisms were summed up to find the total void height 'h' and bonding length 'e' in the bonding interface at certain bonding time. The bonding area fraction (A_f) was defined in terms of bonding length to describe extend of bonding achieved in the bonding interface.

Void height

$$h = \sum_{i=0}^{5} h_i \tag{2.59}$$

Bonding Length

$$e = \sum_{i=0}^{5} e_i \tag{2.60}$$

i = 0: Initial plastic deformation

1: Surface diffusion

2: Volume diffusion (Surface)

3: Grain boundary diffusion

4: Volume diffusion (Interface)

5: Power law creep

Bonding area fraction

Bonding area fraction A_{fi} in the bonding interface by the i^{th} mechanism

$$A_{fi} = \frac{e_i}{a} \tag{2.61}$$

The summation of the bonding area fraction by all mechanisms gave the total bonding fraction as defined by equation 2.62.

Σ Bonding area fraction

$$A_f = \sum_{i=0}^{5} A_{fi} \tag{2.62}$$

2.6.5 *Diffusion Bonding of Titanium Alloys*

There are several conditions that must be fulfilled for successful DB without disbanding, bondline porosity, or other defects [7]. It is generally accepted that DB of titanium occurs between 900 and 950^0C with the actual extreme upper limit being the β transus temperature for Ti-6Al-4V (990^0C). Clean surface must be used to avoid contamination of titanium surface and bondline. All surface oxides, oils, dirt, dust, hair, particles, and other debris must be completely removed. An inert atmosphere is required around the surfaces of parts being bonded to prevent the formation of high-temperature oxides (α case), which would inhibit or completely prevent bonding. A vacuum of 10^{-4} to 10^{-6} is desired to completely eliminate air between the two mating surfaces. Titanium forms a very tough oxide that can prevent diffusion; however it takes 30 days for this layer to form under standard atmospheric conditions. A flash pickle using nitric-hydrofluoric acid is required at least a month prior to bonding of the sheets to ensure that a thick oxide layer is not present. The superplastic flow stress of titanium plays an important role in deformation of the sheet and influences the bonding time. The pressure or force is required to establish initial contact between the sheets and later to deform/flatten the high points to make contact over

interfacial planes. Superplastic deformation with gas pressure is preferred method because it speeds up the process over other methods such as squeezing two sheets between hot tooling plates. A bonding pressure of 2 to 8 MPa is generally accepted range for DB using modern hot presses and heated pressure chambers. It is required to provide sufficient time so that the micro porosity between the sheets will disperse and for the trapped inert gas and oxides to diffuse into grain boundaries of the titanium matrix. Grain boundary migration is a necessary element of diffusion, and this requires soaking time at DB temperature to ensure that homogenous grain structure is obtained across the bond line. The grain size before heating affects bonding. Smaller grains diffuse faster than larger gains. As the time goes by, grain growth occurs due to effect of temperature, and excessive grain growth can result in lack of diffusion. Contaminant metals or oxides attached to titanium alloy sheet or on the surface of the sheets must be absorbed into the grain boundaries during bonding. Likewise, any trapped argon (or other inert gas) must diffuse into grain boundaries surrounding the bondline or there will be microscopic pores left at the bondline. Pores that reach a percentage surface area greater than 3%, or a size larger than 0.250mm, are generally unacceptable, though these factors can be relaxed for design of noncritical structures. An extensive experimental work on diffusion bonding has been conducted with Ti-6Al-4V alloy [9-18, 20-21]. Pilling's model works reasonably good to predict bonding time of Ti-6Al-4V. For diffusion bonding process within the superplastic regime, it was shown that temperature and pressure have little effects on the kinetics of bonding. However the variations in surface roughness have a significant effect on bonding time. The time required to attain full interfacial contact over the entire bonding surface appeared to depend on the dimensions of both the short wavelength roughness and the long-range waviness of the surfaces to be joined [23].

2.6.6 *Effect of Process Parameters on DB of Ti-6Al-4V*

The important diffusion bonding process parameters that influence the process are the bonding temperature, pressure, grain size and surface profile of the mating surfaces. The effect of these process parameters on titanium alloy, Ti-6Al-4V are discussed below.

1. **Temperature:** The bonding time reduces with the increasing temperature. Orhan [24] studied the temperature-bonding time relationship of Ti-6Al-4V (Figure 2.6-14). In the study, the proximity was found in total bonding times between 990 and 970^0C from the difference in diffusion coefficients of the different microstructures. It was attributed to the bigger amount of phase with a lower surface and grain boundary diffusion coefficients in 990^0C that results in the deceleration of diffusion at this temperature thus decreasing contribution of grain boundary in void closure. The temperature effect is also observed on the diffusion bonding mechanisms. As seen in Figure 2.6-15, At higher diffusion bonding pressures (10MPa), the increase in temperature results in increase in bonding area fractions by both the surface source and creep mechanisms, however the bonding area fraction by interface mechanism decrease. The interface source mechanism play key role in diffusion bonding at low diffusion bonding temperatures, whereas the creep mechanism plays main role at higher diffusion bonding temperatures. The spread length of surface diffusion increases with the increase in diffusion bonding temperature, therefore the bonding area fraction by surface source mechanism increases. At higher temperatures, the amount of atoms depositing to the void neck increases, the stress gradient and the characteristic length for effective grain boundary diffusion in the region adjacent to the void decreases. This also causes the stress gradient in the region away from the void to increase and creep to occur. Therefore the interface mechanism weakens and the creep mechanism enhances [21].

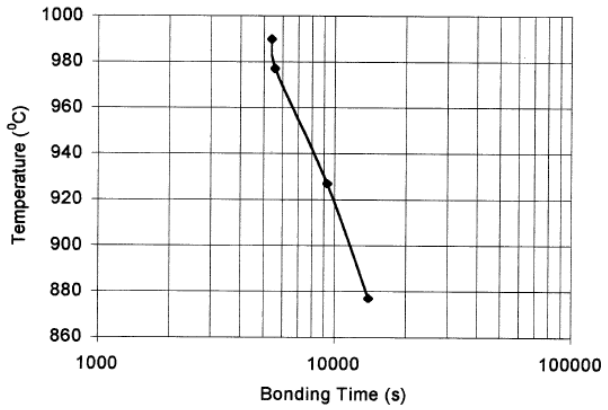

Figure 2.6-15: The dependence of bonding time on temperature [24]

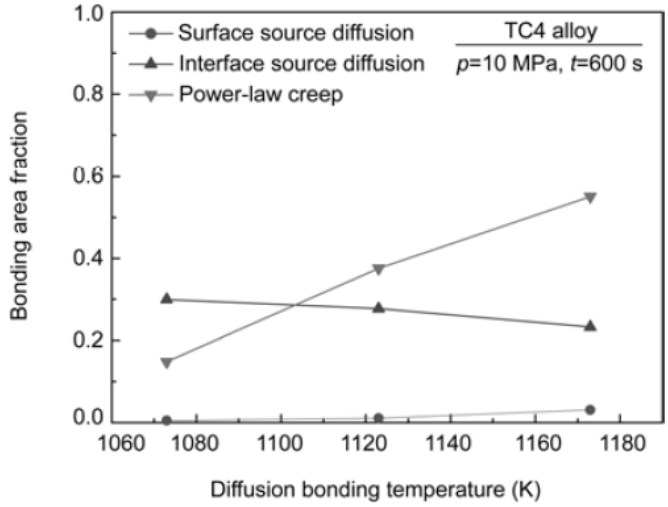

Figure 2.6-16: Bonding Temperature effect on DB Mechanisms [21]

2. **Pressure:** The increase in pressure decreases the bonding time (Figure 2.6-16). As compared to other models, the result of initial stages of bonding is different for low values of pressure. The bonded area is very small part of the total area. This was credited partly due to the difference between the radius of neck and ridge that causes a decrease in mass transfer as a result of the distribution of mass to the all free surface of void by surface diffusion. The deviation's in the curve (shown by a) show the decrease in the effect of grain boundary diffusion. The other reason was of the decreased in the number of grain boundaries intersecting the free surface of void as a result of the decrease in the length of the surface of void by mass transfer. The deviation reduces depending on pressure which is one of the major factors accelerating diffusional creep and grain boundary diffusion. As the pressure increases the deviation decreases, infers that diffusional creep becomes more effective than grain boundary diffusion at higher pressures.

   The bonding pressure effect on diffusion bonding in TC4 alloy is illustrated in Figure 2.6-17. The increase in bonding pressure enhances the surface source mechanism, and the interface source mechanism initially enhances and then weakens. The bonding area fraction by creep mechanism enhances continuously with the

increase in pressure. The interface source mechanism is dominant at low bonding pressures, while the creep is dominant at high bonding pressures.

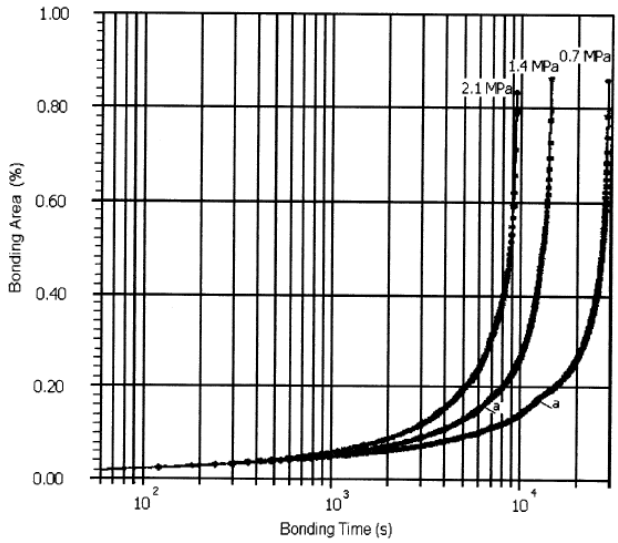

Figure 2.6-17: Effect of bonding pressure on DB (temperature 927^0C, grain size 5 μm, surface roughness height 30μm, wavelength 60μm) [24]

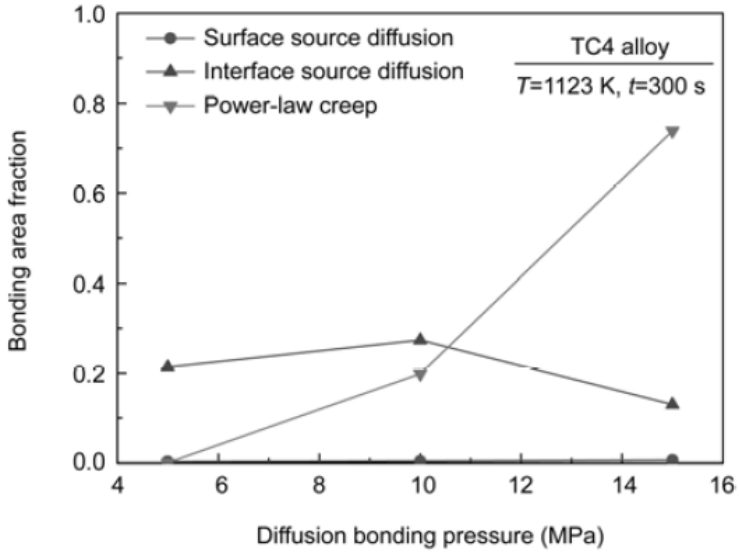

Figure 2.6-18: Bonding Pressure effect on DB Mechanisms [21]

3. **Grain Size:** Figure 2.6-18 shows the effect of grain size on bonding time. All the diffusion bonding models have shown that the diffusion bonding time reduces with the

smaller grain sizes. The smaller grain size results in lesser diffusion paths, and less mass transfer.

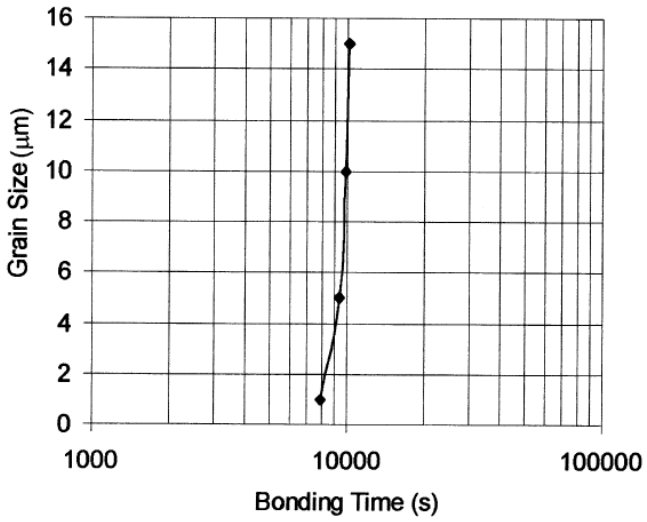

Figure 2.6-19**:** Grain size influence on bonding time [24]

4. **Surface Profile:** At low pressures the predicted bonding time is very sensitive to the value of Ra (surface roughness amplitude), whereas as high pressures is scale dependent (Figure 2.16-19) [23]. Figure 2.6.18 shows the influence of void radius or surface roughness of the bonded area on the bonding time. It can be seen that the bonding time can be greatly reduced by decreasing the void radius or in other words by improving the surface finish quality. The presence of large asperities on bonding area inhibits extensive plastic deformation of surface asperities due to poor contact. This result in reduction of the total area, consequently the bonding time will increase [25].

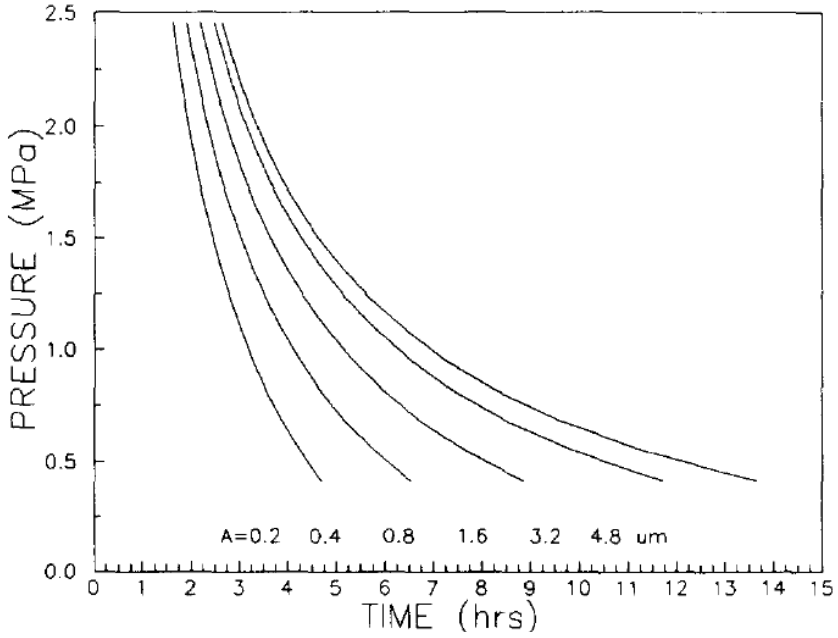

Figure 2.6-20: Predicted Bonding time variation with pressure for increasing surface roughness, A (T=1160K) [23]

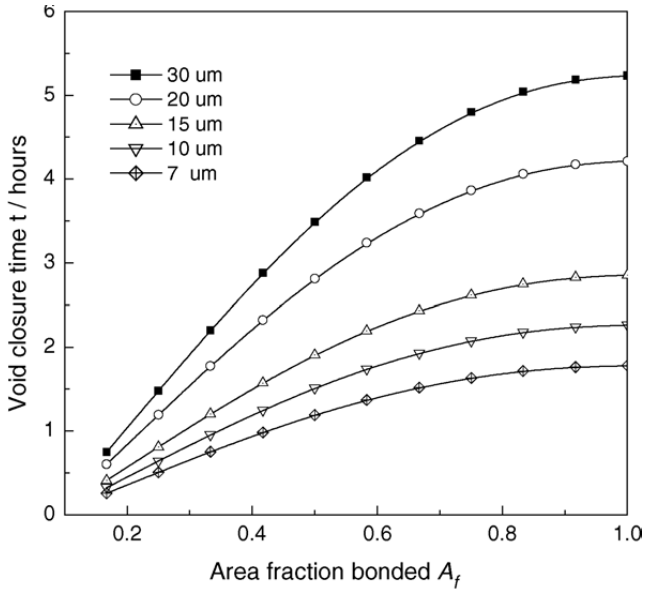

Figure 2.6-21: Effect of void radius on DB Time (P=2MPa, T=1200K) [25]

2.6.7 *Diffusion Bonding of Titanium with Dissimilar Metals*

The commercial requirements for higher performance, higher productivity and low cost in joining operations are becoming more demanding [26]. Diffusion bonding has been widely applied to join steels, aluminum alloys and titanium alloys. Maehara [27] showed that good bonds can be obtained in α-γ stainless under conditions of hot isostatic compression although bonding pressures (about 20 MPa) were appreciably higher than those associated with the diffusion bonding of titanium and aluminum sheets. Ridely et al. [28] conducted diffusion bonding in microduplex stainless steel materials in the temperature and pressure range where it exhibits superplasticity.

Interlayers are often used to diffusion bond dissimilar metals. For example, silver foil is used to bond steel to titanium and nickel foil is often used in bonding high carbon steel to itself and other materials. Basically the interlayers that can melt are adopted, thereby increasing diffusion rates, helping to fill joint gap and disrupt surface films; this is characteristic feature of diffusion-soldering and diffusion-brazing process.

Titanium alloy and stainless steel form inevitable hard and brittle Ti-Fe intermetallic compounds by diffusion bonding. Shuying Liu [29] showed that by introducing copper interlayer between titanium alloy Ti-6Al-4V and stainless steel, the diffusing of Fe and alloying elements from stainless steel to titanium matrix can be prevented, but, it failed to inhibit Ti element diffusing to the stainless steel.

Titanium and aluminum are widely used materials. Moreover, in some locations the performance requirements for Ti and Al components are special. Therefore welding of Ti and Al to form compound structure is necessary, and can result in weight and cost savings. The Ti/Al compound structure is used in the wings of airplanes, in which titanium alloy crust and aluminum alloy honey-comb are welded together. It is hard to weld Ti and Al using traditional fusion welding as the performances of Ti and Al have great differences in crystal microstructure, melting point, heat conductivity, coefficient of linear expansion, etc. The melting point of titanium and aluminum is very much different; aluminum is severely lost at the temperature below the melting point of Ti. In addition to that, the solubility of Ti or Al at room temperature is slight. The laminated intermetallics such as

Ti_3Al, TiAl, $TiAL_3$, etc. are easily formed at contacting surface between Ti and Al. Thus makes it hard to weld Ti/Al compound structure by fusion welding. Jiangwei et al. [30] joined Ti/Al dissimilar metals successfully by means of vacuum diffusion bonding after aluminizing on the surface of Ti sheet. Though intermetallics Ti/Al and Ti_3Al were formed in the transition zone on Ti substrate and aluminized coating. However the formation of intermetallics in the interface zone of Ti/Al has a delay time, and controlling the technology of diffusion bonding may reduce the formation of intermetallics.

2.6.8 *Diffusion Bonding of Dissimilar Titanium Alloys [31-33]*

Some effort has been made to assess the potential of dissimilar titanium alloys. Diffusion bonding between Ti-6Al-4V and several other titanium alloys, including Ti-6Al-2Sn-4Zr-2Mo, Ti-5.8Al-4Sn-3.5Zr-0.7Nb-0.5Mo-0.35Si (Titanium IMI834), Super Alpa-2, and Ti-4Al-4Mo-2Sn (Ti-550) has been investigated to find to produce sound bonds between the different titanium alloys. The fatigue assessment on Ti-6Al-4V/ Ti-550 showed that the control parameters adopted for Ti-6Al-4V have proved successful (i.e. temperature, time, and pressure). The metallographic inspections did not identify evidence of bond defects or abnormal grain structures. The bond width of the order 4μm was achieved. The tensile test showed that no failures were induced from the bond line but rather was controlled by the bulk response of the relatively weaker Ti-6Al-4V parent material. These hybrid specimens demonstrated a comparable fatigue response to conventional Ti-6Al-4V plate material [29].

In the past, investigations on superplastic deformation characteristics of Ti-6Al-4V with Ti-6Al-2Sn-4Zr-2Mo showed that large superplastic strains were exhibited by these alloys when they were deformed under optimum conditions of temperature and strain rate. The optimum deformation temperature for Ti-6Al-4V was found approximately 60^0C lower than for Ti-6Al-2Sn-4Zr-2Mo. The highest elongations where reached when each alloy contained approximately 40% by volume of β phase. It was observed that for each temperature and strain rate the flow stress of Ti-6Al-2Sn-4Zr-2Mo was higher than that of Ti-6Al-4V. This was attributed to the lower proportion of β phase in Ti-6Al-2Sn-4Zr-2Mo and to slow diffusivity of molybdenum atoms in the alloy. The high superplastic strains

observed for Ti-6Al-2Sn-4Zr-2Mo sheet showed that it was a suitable material for superplastic forming into components which required an improved creep resistance an improved creep resistance over that given by Ti-6Al-4V.

The other study on diffusion bonding of Ti-6Al-4V with other titanium alloys showed that Ti-6Al-4V, which had the lower optimum temperature for superplastic flow, played a major role in the diffusion bonding process. For instance it was found that the bond area fraction for Ti-6Al-4V/ Titanium IMI834 at a given temperature is very close to that for Ti-6Al-4V/Ti-6Al-4V, but far away from that for Titanium IMI834/ Titanium IMI834. For temperatures from 910 to 940^0C, Ti-6Al-4V contains 40-60% β phase while Titanium IMI834 contains only 20-30% β phase. Subsequently, the flow stress for Titanium IMI834 is much higher than that for Ti-6Al-4V. Therefore, the removal of interfacial voids will be mainly accomplished by the superplastic flow (on a microscopic scale) of Ti-6Al-4V, when bonding mechanism is dominated by plastic flow. Sound bonds were achieved between the titanium alloys, Ti-6Al-4V and Super Alpha-2. The diffusion zone was devoid of equiaxed alpha grains, revealing only fine alpha platelets less than one micron wide. For the given surface finish P1200 (h=0.2 and R=5μm), a narrow diffusion affected zone of about 20μm wide, appeared to be located mainly in the Ti-6Al-4V side of the bond.

2.7 FRICTION STIR WELDING PROCESS

2.7.1 *Introduction*

Friction Stir Welding is a relatively new solid-state joining technique invented at the Welding Institute (TWI) (Cambridge United Kingdom) in 1991[34]. Friction Stir Welding (FSW) is a well-established solid state welding process. The material could be bonded before reaching the fusion heat. This is a ‘green’ joining technique due to its energy efficiency, environment friendliness, and versatility. FSW method has generated tremendous interest from the technical and industrial community because it provides a means to join materials together without melting of the metal and causes very little thermal

distortion because far less heat is generated and the cost is low. FSW also generates no fumes or splatter, creates far less distortion, is more energy efficient, and FSW tool is non-consumable. Furthermore, FSW can be used on very thin sheets of material where making a fusion weld would be extremely hard or even impossible.

FSW has been successfully implemented in avionics, automotive and ship-building industries. It has become a viable and important manufacturing alternative or fabrication component, especially in aerospace applications. Since its inception in 1991, FSW began as a joining alternative involving aluminum alloys; it has now progressed to higher temperature systems including stainless steel, titanium, and titanium alloys [36-37]. However in case of high temperature alloys such as steel, nickel, and titanium, it is difficult to obtain FSW joints with the conventional welding tools that are made of tool steel as it leads to tool's erosion. By using commercial pure tungsten and tungsten alloys rod as welding tool, FSW was successfully applied to Ti-alloys such as Ti-6Al-4V and β Ti-alloy [38]. Since FSW process retains the relatively fine grained microstructure of the parent material, it lends itself to the superplastic forming (SPF) process. Superplastic forming requires a fine-grained microstructure to enable the deformation mechanism of grain boundary sliding. The resulting weld is far stronger and more reliable than traditional welds.

During FSW process two sheets or plates are tightly abutted in a line and a tool is traversed across them. The heat is generated between the joining materials and the tool. This generated frictional heat results in joining of both the surfaces. There is no melting of the materials; instead the joint is formed by plastic deformation of the pieces. Figure 2.7.1 shows the schematic of friction stir welding process. This technique is capable of joining both similar as well as the dissimilar material combinations that are difficult or that cannot be welded using conventional welding methods. By using friction stir welding it is possible to produce strong and high quality welding. Friction stir welding (FSW) produces a microstructure similar to that of the wrought material as opposed to the large, coarse grained, cast type microstructures formed in fusion welds. The steps in friction stir welding process are as follows:

1) The pin and shoulder of the rotating weld tool are plunged into the metal.

2) The metal is first heated by the frictional interaction of the tool with metal as it comes into contact with the head of the pin, then sides of the pin.
3) As a result, the shoulder becomes engaged.
4) Heat is maintained through friction during the steady state weld, whereby the pin tool is advanced forward to create butt weld between two sheets of metal.
5) As the tool advances, the shoulder of the pin exerts a downward forging force on the plasticized metal and since it also rotated, the softened material is being extruded around the pin from the front to the back of the weld nugget.
6) Each revolution is basically one extrusion/forging event and a solitary semi-circular pin tool feed mark is left behind on the top surface.
7) After one rotation occurs, most of the previous rotation is re-imprinted and covered up by the mechanical action of the next pin tool rotation, such that the length of the weld appears to a long series of individual semi-circular coined outlines that cover each other, with a prominent protruding burr left behind on the top surface for each rotation.

Friction Stir Welding encompasses complex material movement and plastic deformation. In friction stir welding process, forge loads are recorded in the z- direction. These loads are not the input parameter for the process, because generally position control is used. These are a resultant of the other parameters. However, loads are used to compensate for the deflection in the equipment and maintain the desired plunge depth. The stirring pins are subjected to high temperatures and stresses, making their design and material choice a critical element of the process.

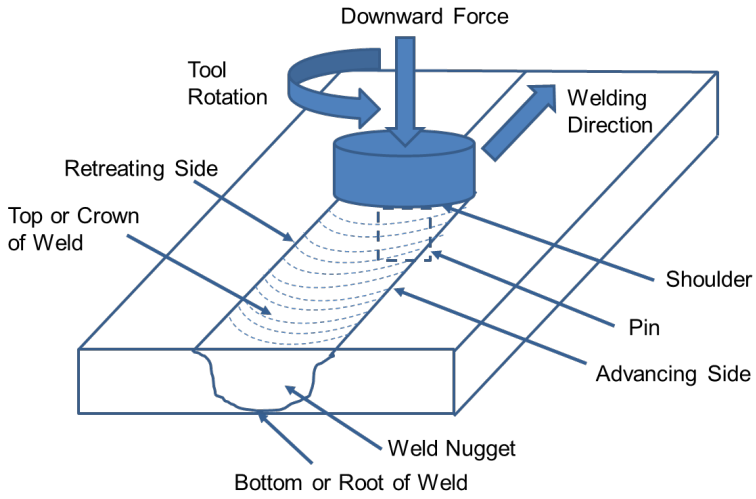

Figure 2.7-1: Friction Stir Welding Process [35]

During friction welding, the tool geometry, welding parameters, and joint design exert significant influence on temperature distribution and the material flow pattern, thereby influencing the micro structural evolution of material. In FSW, the semi-circular shaped pin tool feed marks that are left behind varied in depth and shape proves detrimental not only in fatigue performance but also in further processing such as superplastic forming. In this section, friction stir welding metallurgy, and a few major factors affecting FSW/FSP process, such as welding parameters, and tool geometry are addressed.

Numerical simulation of the FSW process is a complex problem which involves physical couplings between mechanics and heat transfer, very large deformations and strain rates in the stirring zone around the pin. However the simulation of FSW processes enables estimation of different process parameters such as tool geometry and speeds etc. Significant progress has been made in the fundamental understanding of both the FSW process and the properties of the resulting welded joints. Still accurate and reliable numerical analysis of the FSW is a very challenging task as the behavior of the FSW joints is influenced by many factors in combination [39].

2.7.2 *Friction Stir Welding Metallurgy*

Friction Stir Welding is asymmetric in nature and results in highly characteristic microstructure. The advancing side of the weld is where the rotation and translation of the tool are in same direction, whereas the retreating side of the weld is where the rotation of tool opposes the translation direction. Figure 2.7.2 shows a cross section of an aluminum weld showing the difference in the advancing and the retreating side.

The weld nugget, or stir zone is where the intense heat and plastic deformation from the tool pin generates a fine grained recrystallized microstructure. The interface between nugget and parent material is gradual on the retreating side but sharp on the advancing side [35]. The area adjacent to weld nugget is called the thermo-mechanical affected zone (TMAZ). This zone experiences both temperature and deformation during FSW, however in the TMAZ, there is no recrystallization. Beyond TMAZ, there is heat affected zone (HAZ). The HAZ undergoes a thermal cycles but is not prone to any plastic deformation.

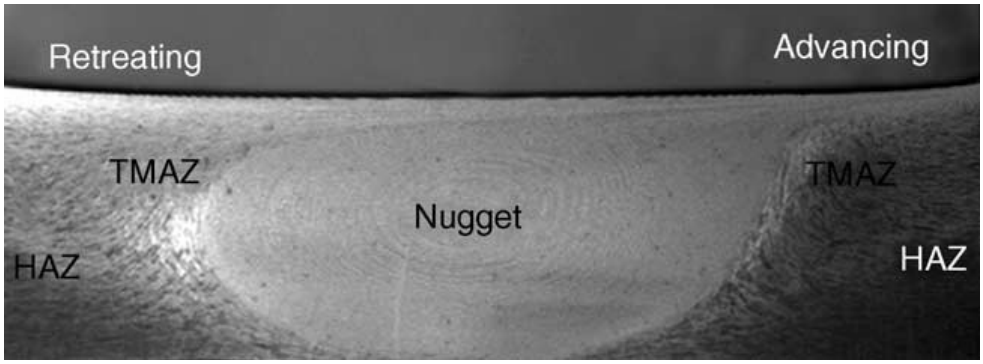

Figure 2.7-2: A typical macrograph showing various microstructural zones in FSP 7075Al-T651 [34]

The dynamic recrystallization during FSW/FSP results in generation of fine and equiaxed grains in the nugget zone [35]. Measured grain sizes differ from 1 to 20 microns. Figure 2.7.3 shows typical grain size distribution in various locations in an aluminum friction weld. The various locations include the center of the weld, the mid thickness on the advancing and retreating sides of the nugget, and on the weld centerline near the top and

bottom of the weld. It can be observed that the grain size is fine and equiaxed in weld nugget zone, but also varies in size. The variation in size from top to bottom is supposed to be related with the thermal gradient through the thickness of the joint. The top of the weld is exposed to the temperatures developed by the shoulder of the tool and therefore results in larger grains near the top of the weld. The bottom of the weld is in contact with a backing fixture that will conduct heat out of the weld zone and thus results in smaller grains in the bottom. The grain size variation is also observed from the advancing to retreating side of the nugget. This is mostly associated with thermo-mechanical gradients due to the asymmetrical nature of the process.

In addition to grain size variations within any particular weld, it can also be noted that the grain size is dependent, and can be controlled with the welding parameters. The weld nugget grain size can be decreased by reducing the tool rate and / or increasing the tool feed rate, or decreasing the ratio of the tool rotation to transverse speed [35]. The lower rotation with higher transverse rates has finer microstructures than higher rotation with slower transverse rate weld. This is due to the lower processing temperatures produced by the lower rotation rates and decreased time at temperature for increased transverse rate. On the contrary, the higher temperatures produced by the increased rotation rates and the increased time at temperature from the lower transverse rates permit for more grain growth upon recrystallization after being stirred.

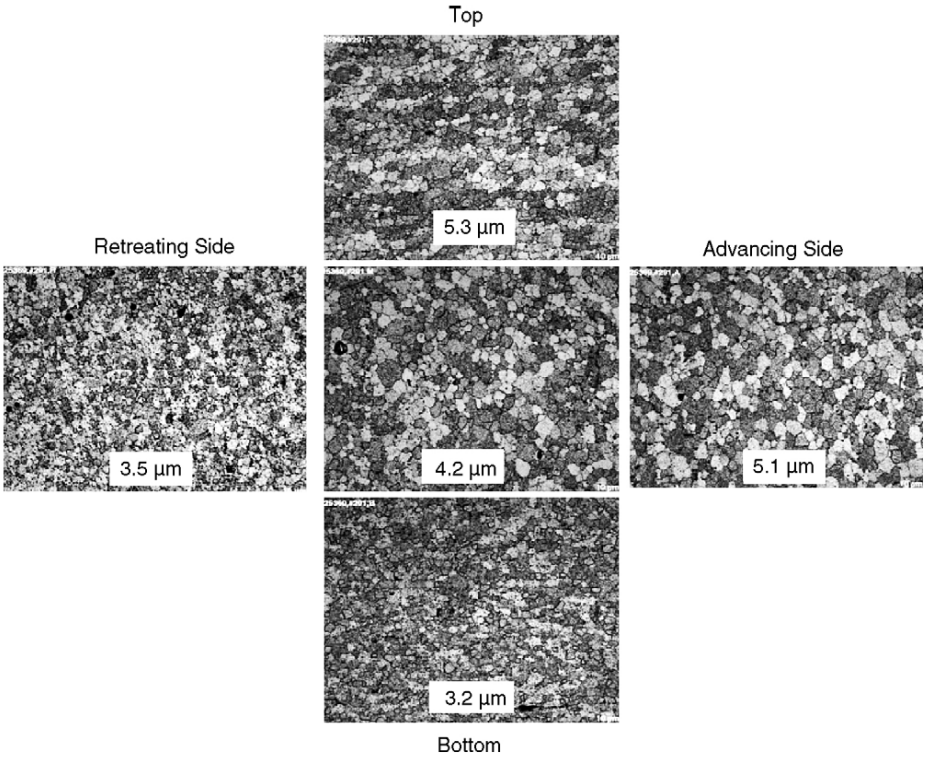

Figure 2.7-3: Grain size distributions in various locations of Al-7075 weld nugget [35]

2.7.3 *Process Parameters in Friction Stir Welding*

2.7.3.1 Tool geometry[40]

The rotating tool of friction stir welding consists of a shoulder and or probe. The friction stir welding tools are mainly classified into three types that include fixed, adjustable and self-reacting, as shown in Figure 2.7-4. The fixed probe tool consists of a single piece comprising both the shoulder and probe. This type of tool can only weld a work piece with a constant thickness due to fixed probe length. In case the probes wears or breaks, the whole tool needs to be replaced. The adjustable tool consists of two independent parts, separate shoulder and probe, to allow adjustment of probe length during FSW. In this design, the probe and shoulder can be manufactured of different materials and the probe can be easily replaced when worn or damaged. In addition to that, the adjustable probe length allows controlling welding variables and can accommodate multiple thickness work

pieces. Both the fixed and the adjustable tools often require a backing anvil. The fixed and adjustable tools can be tilted longitudinally and laterally. The third type of tool is self-reacting or bobbin type tool that is made up of three pieces: top shoulder, probe and bottom shoulder. This tool allows multiple gauge thickness joints due to adjustable probe length between the top and bottom shoulders. The bobbin type of tool can only work perpendicularly to the work piece surface and doesn't need a backing anvil.

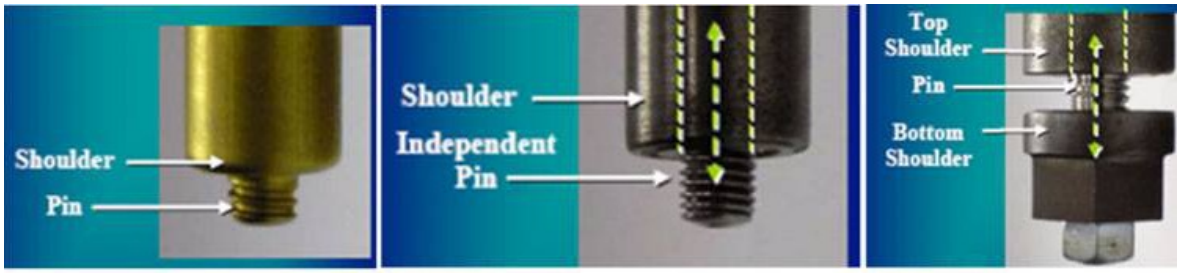

Figure 2.7-4: Tools in Friction Stir Welding [40]

The tool shoulder is responsible for applying downward pressure to the workpiece surface. It constrains the plasticized material around the probe, generates heat through the friction and causes plastic deformation in a relatively thin layer under the bottom surface of the shoulder. The rotating probe mainly drags along, plasticizes, and mixes the adjacent material in the stir zone, and thus creating a joint without fusion. Figure 2.7-5 illustrates typical tool shoulder outer surfaces, the bottom end surfaces and the end surfaces. The shape of the shoulder outer surface has an insignificant effect on the welding quality as the shoulder plunge depth is typically small (1 to 5% of gauge thickness). As shown in Figure, typically three types of shoulder end surfaces are used: flat, concave and convex. Among these, the simplest design is of the flat shoulder end surface. However the main disadvantage of this design is that the end surface is not effective for trapping the flowing metal material under the bottom shoulder, promoting excessive material flash. To overcome this, a concave shoulder end surface was designed and has become popular for restricting material extrusion from the sides of shoulder. The convex shoulders provides benefit of attaining contact with the workpiece at any location along the convex end surface, and thereby, accommodate differences in flatness or thickness between the two adjoining workpieces, the inability of the smooth end surface to prevent material

displacement away from probe causes weld integrity issues. The shoulder end surfaces can also contain some features to increase material friction, shear and deformation for increased workpiece mixing and higher weld quality. The typical shoulder end styles include flat (smooth or featureless), scrolls, ridges, knurling, grooves and concentric circles as shown in Fig. 2.7-5.

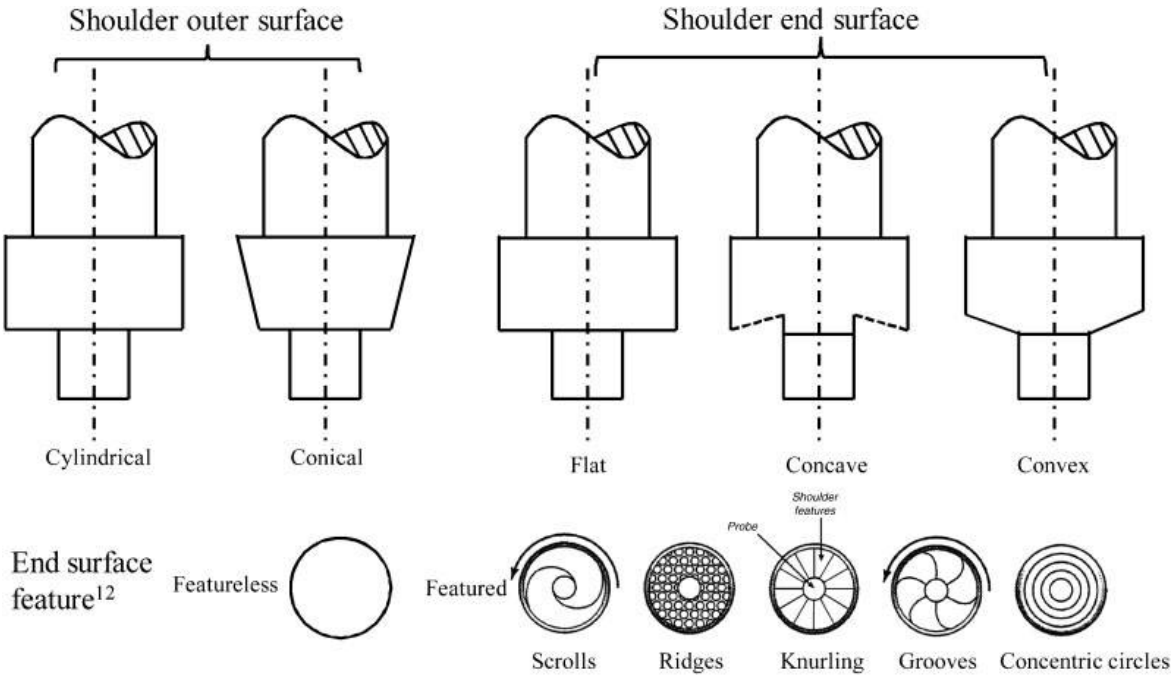

Figure 2.7-5: Tool shoulder shapes and features [40]

The friction stirring probe can produce deformational and frictional heating. Ideally, it is designed to disrupt the contacting surfaces of the workpiece, shear the material in front of the tool and move the material behind the tool. The depth of deformation and tool travel speed are mainly governed by the probe. Figure 2.7-6 illustrates the probe shapes and their main features. The end shape of the probe is either flat or domed. The flat bottom probe is easy to manufacture, therefore is the most commonly used form. However the flat probe produces the high forge force during plunging. On the other hand, a round or domed end shape can reduce the forge force and tool wear upon plunging, thereby increasing tool life by eliminating local stress concentration and improving the quality of the weld root directly at the bottom of the probe. As the dome radius decreases, the weld

quality was often comprised, while these advantages are maximized when the dome radius is 75% of the probe diameter.

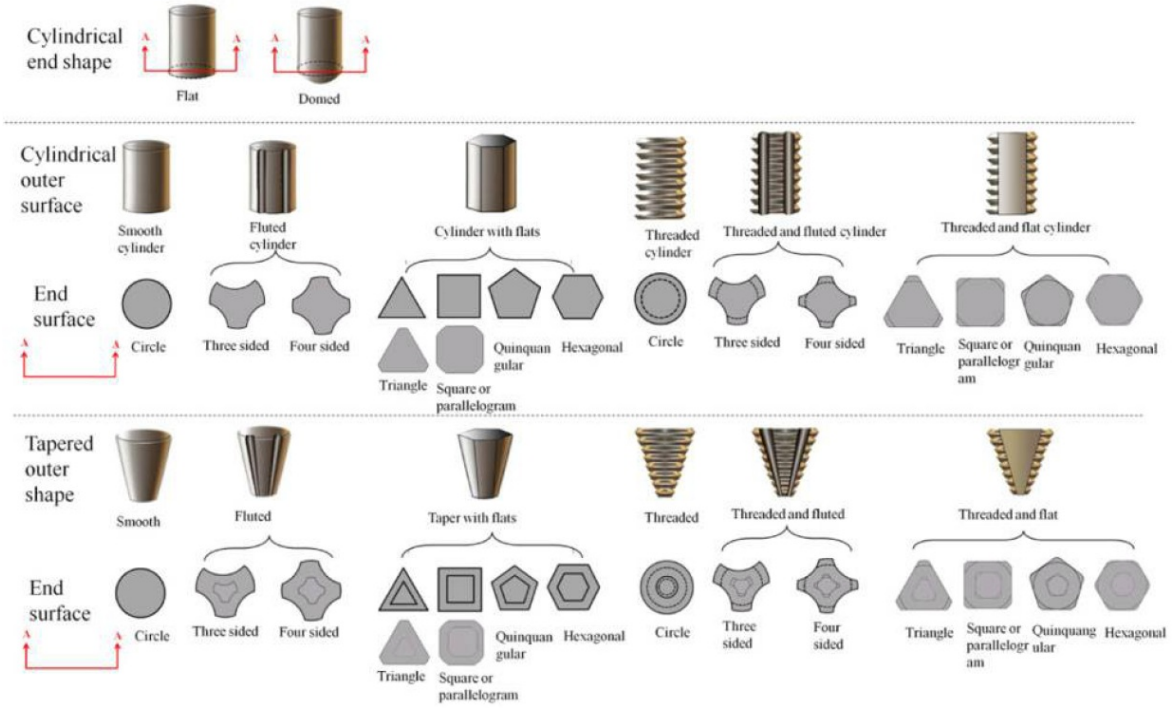

Figure 2.7-6: Tool Probes in Friction Stir Welding [40]

Tool material characteristics are important in FSW. The tool material is selected depending on the workpieces to be joined and the desired tool life as well as the user's own experiences and preferences. The candidates for tool material should have good mechanical and thermal properties. The essential mechanical tool properties are higher compressive yield strength at elevated temperature than the expected forge forces onto the tool, good strength, dimensional stability, creep resistance, good fracture toughness to resist the damage during plunging and dwelling. The important thermal properties are good thermal fatigue strength to resist repeated heating and cooling cycles, and low coefficient of thermal expansion between the probe and the shoulder materials to reduce the thermal stresses (e.g. the use of a thermal barrier coating for polycrystalline cubic boron nitride (PCBN) tools to prevent heat from moving into the tungsten carbide shank). The other tool properties that should be advantages would be no harmful reaction with the workpiece material, good machinability to ease manufacture of complex features on the shoulder and

probe and low or affordable cost. The different tool materials used for FSW include Tool steel, Ni and Co based superalloys, Refractory metals, Carbides and metal matrix composites (MMCs) and PCBN. Among different tool materials, Tool steel is the most widely used tool material for aluminum alloys. Within the tool steels, AISI H13, chromium–molybdenum hot worked air hardening steel, has been the most commonly used. Nickel and cobalt based superalloys, which were initially designed for aircraft engine components offer high strength, ductility, good creep and corrosion resistance as tool materials. Nickel based alloys are widely used for friction stir welding Titanium alloys.

2.7.3.2 Welding Parameters

The strength of friction stir welding depends on the primary process parameters that include spindle speed, feed rate and depth of penetration. The other variables that control the process include tooling design, material, thermal management, plunge depth, etc. Feed rate is the velocity at which the tool is advanced against the work piece. Feed rate is typically expressed in units of distance per revolution (generally inches per revolution (ipr) or millimeters per revolution). The spindle speed is the rotational frequency of the spindle of the machine, measured in revolutions per minute (RPM). The rotation of tool results in stirring and mixing of material around the rotating pin and the translation of tool moves the stirred material from the front to the back of the pin and completes welding process. The material to be cut determines the preferred speed. More spindle speed will affect tool and cause premature tool wear, breakages, and tool chatter, all of which can lead to potentially dangerous conditions. Using the correct spindle speed for the material and tools will significantly affect tool life and the quality of the surface finish. The spindle speeds may be calculated for all machining operations once the welding speed is known. The best speed depends on the welding requirements of weldment quality and weld strength required. Higher quality of weld and strength can be acquired at high speed operations. The other parameter is size of weld. Typically large welds require low speed operation. It also depends on material to be welded and the thickness of the work piece to be welded. Harder the material higher is the speed operation required. In FSW higher spindle speeds overheat and over soften the weld material resulting in unconsolidated joint formation. On the contrary slow spindle speeds with high travel rate will not produce sufficient heat to

promote material flow during the process resulting in extremely high loads, shoulder disengagement and tool wear. Even the low spindle speeds with slow travel rate result in lack of penetration and to produce sufficient material flow can result in tool wear [41]. In addition to spindle speed and feed rate, a suitable tilt of the spindle towards trailing direction is an important parameter that ensures that the shoulder of the tool holds the stirred material by threaded pin and move material efficiently from the front to the back of the pin. Further, the insertion depth of pin into the work pieces (also called target depth) is important for producing sound welds with smooth tool shoulders. The insertion depth of pin is associated with the pin height. When the insertion depth is too shallow, the shoulder of tool does not contact the original work piece surface. Thus, rotating shoulder cannot move the stirred material efficiently from the front to the back of the pin, resulting in generation of welds with inner channel or surface groove. When the insertion depth is too deep, the shoulder of tool plunges into the work piece creating excessive flash.

Weldability is defined by the capability of the alloy to produce a weld that is free of defects and discontinuities. However, the micro-macro irregularities that are typically formed in a friction stir welding nugget, due to solid state deformation process, has a deleterious effect on the surface and subsurface. Defects that may be faced when welding titanium alloys are solidification segregation (macro segregation and micro segregation, solidification cracking, contamination cracking, hydrogen embrittlement, subsolidus (ductility cracking) and porosity. The hardness and microstructure properties of friction stir welded joints were found to be dependent on weld thickness, which suggests significantly different thermo mechanical conditions. Typically, thicker welds produce larger grains and lower hardness. This has been attributed to higher processing temperatures and longer exposure times to the elevated temperatures, permitting grain growth after mixing of the material.

2.7.4 *Friction Stir Welding of Ti-6Al-4V*

Friction stir welding of titanium has been reported by many researchers. Lienert [42] provided excellent review on FSW titanium that included tool materials, tool designs,

welding parameters, microhardness, microstructures, and mechanical properties for commercial pure titanium (CP Ti). Much research has been focused on the workhorse of aerospace industry Ti-6Al-4V. Reynolds et al. [43] reported shear textures in FSW welds of Timetal 21S β -titanium alloy. Zhang et al. [44] conducted FSW of Ti-6Al-4V 3 mm plates under different rotational speeds of 400 and 500 rpm and stated microstructural characteristics produced in stir zone (fine lamellar α+β) and heat affected zone (bimodal microstructure). Liu et al. [45] performed FSW at constant rotation speed of 400 rpm with welding speeds ranging from 25 to 100 mm/min. The study reported bimodal microstructure in stir zone, the size of primary α increased with the welding speed, and microstructure of the heat zone matched with the base metal.

Friction Stir Welding has proved to be a successful solid-state joining technique that can be used to fabricate near net titanium structures at a reduced cost compared to traditional manufacturing processes. FSW can be combined with superplastic forming to produce near-net shape manufacturing of large titanium parts [46-47]. Superplastic forming of titanium alloy Ti-6Al-4V has found widespread applications for the manufacture of many commercial jet aircraft fuselage parts, wing, empennage and jet engines components. The SPF process has found to be specifically effective when applied to areas of the aircraft where large structural loads and exposure to high temperature combine together to result in complex engineering stress problems. One limitation to the SPF opportunity has been the size of available raw sheet material, which has generally been 1.2 meters to 3.7 meters. In order to overcome the size limitation, it was important to develop a suitable joining process for titanium alloys that is compatible with the subsequent operation of superplastic forming.

Ramulu et.al [46] studied the performance of friction stir welded (FSW) and friction stir welded-superplastically formed Ti–6Al–4V alloy sheets by evaluating tensile properties of friction stir welded and superplastically formed friction stir welded Ti–6Al–4V of both standard grain and fine grained titanium. The fine and standard grain alloys were tested in the as welded, stress relieved (SR) and superplastically formed (SPF) conditions. The study showed that friction stir welds in Ti–6Al–4V alloy can possess yield and ultimate tensile strengths that are superior to the parent material properties. However,

elongation to failure in the welded samples was reduced. The increased strengths were associated to grain refinement in the weld nugget while the decreased elongations were related with root defects leading to pre-mature failure in addition to the refined grain structure. Welds in fine grain material and stress relived welds produced improved strengths and elongations. It was observed that superplastic forming had an adverse effect on the mechanical properties of the joints, but the strength properties were still comparable to as received parent material.

Sanders et.al [48] optimized the friction stir welding process (FSW) for superplastic forming and surface to improve surface texture for titanium aerospace structures by applying FSW to 3 mm-thick Ti-6Al-4V plates under different rotational speeds. Defect-free welds were successfully produced at rotational speeds of 400 and 500 rpm. In the optimization process, a number of experiments were conducted to determine the effects of changes of FSW process parameters on the surface roughness of fine grain 2mm thick titanium alloy. The process was optimized to find the spindle speed and feed rate to produce a uniform deformation in both weld and parent metal when the joint was superplastically formed. A typical surface profile of FSW surface welded at spindle speed of 600 RPM and feed rate of 1.7 mm/s is shown in Figure 2.7-7. The titanium FSW has crack like features that extend inwards from the backside of the individual feed mark protrusions. The surface roughness data showed that the FSW process variables influence the surface topography and roughness of the FSW weld in both profile shape and computed average statistical parameters.

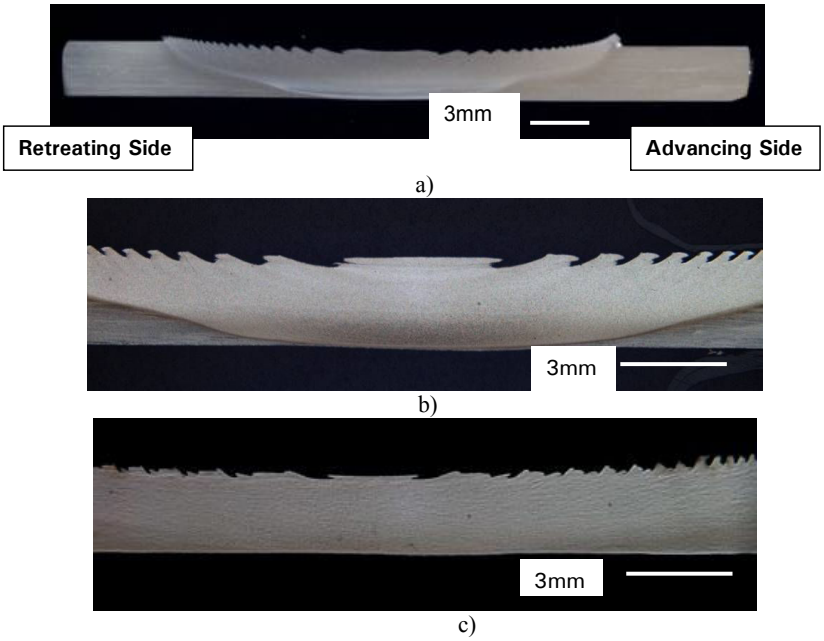

Figure 2.7-7:Macrograph showing width of three different FSW titanium butt weld nuggets and the surface texture (600 RPM and 1.7 mm/s feed rate) [48]

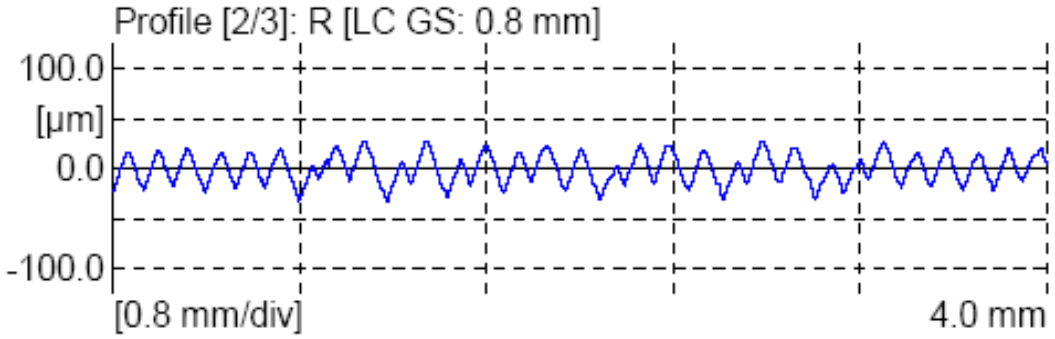

Figure 2.7-8: Surface Profile of FSW surface on advancing side of the weld bead [48]

The surface roughness study [Figure 2.7-8] showed that the center of FSW has a significantly higher (near 50% greater) Ra than the sides of the weld nugget. The comparison of the Maximum Height of the Profile (Rt) and Average Maximum Height of the profile (Rz) to either the advancing side or the retreating side of the weld surface indicated that the center surface of the FSW appears to have more severe roughness. Since the height of the tool marks is very small, the range of 25 to 48 µm, it was very likely that the contribution of the depth of the roughness profile would be another key factor for the loss of fatigue strength in addition to the effects of extremely small notch located at the

bottom of the tool marks valleys. Since the Rt and Rz values were measured very close together in almost all cases, it was concluded that the peak height of the individual pin tool feed marks repeated very closely and that there is small variation in the actual height of the tooling marks. The superplastic characteristics were studied to determine whether it would be suitable for fabricating complex shapes of deeply formed parts. The superplastic properties were measured using a forming temperature of 774^0 C and a constant strain rate of 2.7 X 10^{-4} s^{-1} by pulling to a total superplastic strain level between 70 and 100%. The typical process parameters were obtained for achieving titanium FSW with an equivalent strain between the parent and FSW weld zone to have an RPM range of 150 to 400, feed rate of 0.83 to 5.00 mm/s, and forge loads of approximately 25 to 65 kN. The study on fine grain Ti-6A-4V (grain size 0.8 to 2μm) showed that the pin tool marks on the top surface of the weld could be detrimental to both the superplastic forming (SPF) characteristics and the fatigue performance of the welds. In the study test pieces made of 2.5 and 3.0 mm thick Ti-6Al-4V fine grain sheet metal were FSW butt joined together to build 20 test panels that were 20 mm wide by 60 mm long (FSW parameters: 300 RPM, 1.27 mm/s feed rate, a 3^0 tilt of the spindle away from the direction of travel and forge load in z-direction of 31 to 40 KN). The fatigue test samples were cut from FSW panel with transverse FSW welds. The performance of transverse FSW coupons improved when the stirring pin tool marks were removed from the surface by machining and also had low plasticity burnishing (LPB) performed to induce fatigue-resistant compressive stresses. In this case, the fatigue results showed 91% of the observed parent metal's endurance limit. On the FSW coupons that simply had the stirring pin marks removed by machining performed nearly as good as the parts with the LPB, with an observed endurance limit of 81% of the parent metal strength. This was remarkable compared to the other titanium welding processes that have much larger drop in fatigue performance.

Edward's [49] study on identification of process parameters for Ti-6Al-4V revealed the FSW process window. Typical macrographs and micrographs from the study are shown in Figure 2.7-9. This process window was identified for a certain range of tool design and thickness (Figure 2.7-10). In general, formation of void type defects was noticed for high spindle speeds and low feed rate. At low feed rate and high spindle speed, the heat

generated by the tool during the process is insufficient to produce a joint. However a correct combination of spindle speed, feed rate, and tool design is needed to produce a defect free joint in virtually any thickness of Ti-6Al-4V. The process window identified for the thicknesses shown in Figure 2.7-10 is dependent on the tooling material, thermal management, tool designs, weld machine, fixturing equipment, etc. The experiments used tungsten based backing anvil for all trails. It was found that achieving full penetration welds with this anvil material was difficult. This was related to the high thermal conductivity of tungsten, which rapidly extracts heat, keeps the root of the joint cold, prevents material flow, and limits penetration. By using other lower conductivity materials, such as ceramics and steels, more heat is retained in the root of the weld, highly enhancing penetration and widening the process window. However there are some limitations of using alternate materials, such as alloying between the hot titanium and steel, or cracking of ceramics. This was prevented with tungsten-based anvils because they do not react with titanium at elevated temperatures. These relationships should be addressed when selecting the tooling materials and subsequent process parameters. The microstructure of welds varies with joint thickness.

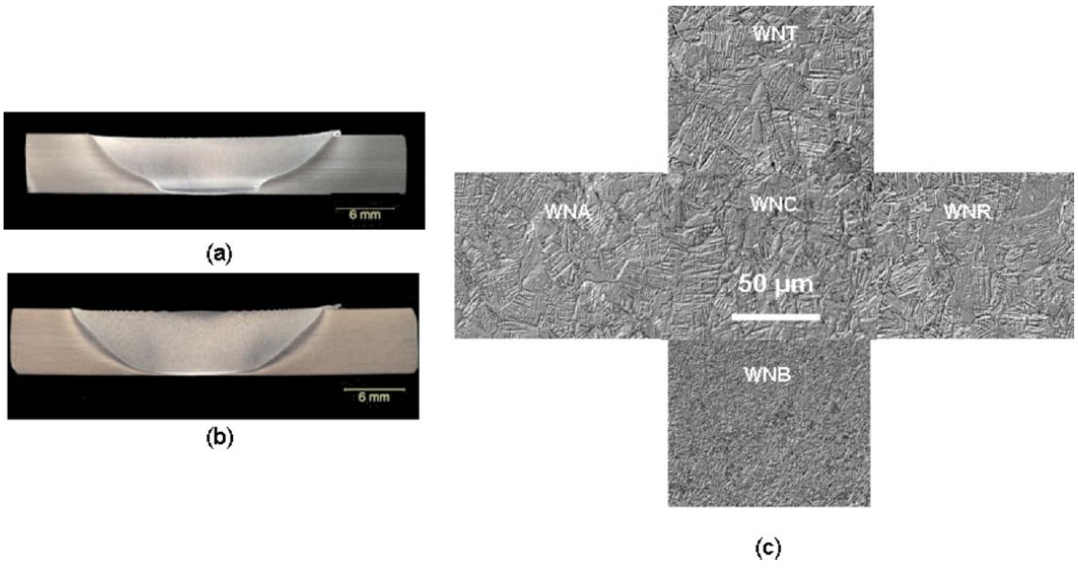

Figure 2.7-9: Typical Macrographs of 6mm Ti-6Al-4V FSW's (a) 280 rpm at 45 mm/min and (b) 280 rpm at 100 mm/min (c) micrographs from 280 rpm at 100 mm/min weld [49]

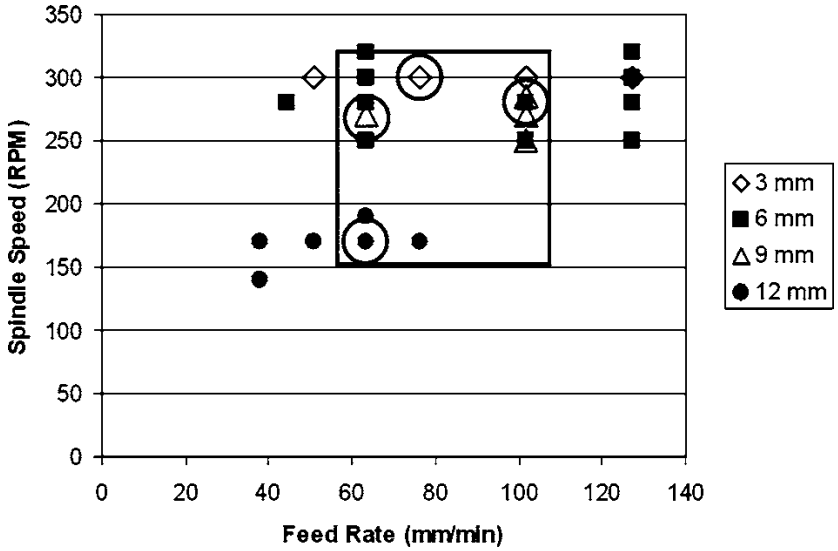

Figure 2.7-10: Schematic for Ti FSW Process Window [49]

It was observed that the grain size increases with weld thickness (Figure 2.7-11). The increase in weld thickness increases the heat input and therefore slows down the cool down of the weld nugget after stirring. Slower feed rates increase the exposure time of the weld to the process temperatures and allow for grain growth. A grain size gradient also exists through the thickness of the welds. The grains at the top of the weld are considered larger than those in the bottom due to the tapered tool geometry and the low thermal conductivity of the workpiece. The heat input is lower in the weld region, as the pin tapers down. The root is also exposed to less of heat generated by the shoulder of the tool due to low thermal conductivity of titanium. The grain size gradient is more dominant in thicker welds than thinner section as the pin length to shoulder diameter ratio is smaller, and the thermal gradient thru the thickness of the joint is smaller than the thicker welds. No significant grain size gradient occurred across the width of the welds, from the advancing to the retreating side. Therefore a fairly uniform temperature gradient exists across the face of the welds. For thin welds less than 3 mm subtransus process was noticed since primary alpha and only a small amount of transformed beta were observed in the weld nugget microstructure. For thicker welds, the microstructure revealed coarser acicular alpha grains, implying supertransus process temperatures. The high cycle fatigue performance of titanium friction stir welds was comparable to the parent material properties. Tensile

properties of titanium FSWs produced higher ultimate and yield strengths compared with the parent material, but elongations were reduced.

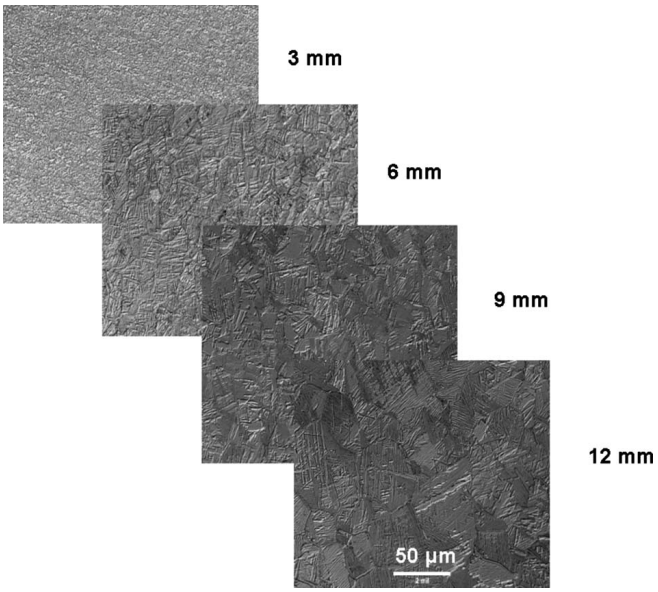

Figure 2.7-11: Weld Nugget grain size vs thickness comparison [50]

Edward's exhibited the effect of heat treatment on friction stir welded Ti-6AL-4V joints [50]. The study was conducted on 6 mm thickness Ti-6Al-4V butt welds were subjected to heat treatments ranging from 700 to 900^0C (spindle speed: 250 RPM and feed rate: 100 mm/min). The heat treatment was performed for 30 minutes in a vacuum and then furnace cooled. The study showed that increased heat treatment in Ti-6Al-4V friction stir welds lead to lower hardness and tensile strengths, higher elongation to failure and improved high cycle fatigue performance. Edwards's another study on the processing conditions of friction stir welding on Ti-6Al-4V determined the peak temperatures during the process [51]. This study was conducted as a function of the processing conditions such as tool rotation speed and feed rate. The study revealed that the spindle speed has dominant effect on peak temperatures while feed rate controls exposure time. The macrostructural evaluation show that for the considered range of spindle speed and feed rate (Figure 2.7-12), all welds appeared to be free of major defects, but the low travel speed (50 mm min-1) and low spindle speed (200 rev min-1) welds have visual indicators of unusual flow

patterns near the root of the weld and that could be a sign of void type defect beginning at the form. Higher spindle speeds and lower federate result in increasing the grain size due to increased temperatures and longer exposure time [52].

Edward's study of effect of process conditions on superplastic forming behavior in Ti-6Al-4V welds showed that balance between the rotation speed and feed rate of the tool can be used to produce a quality joint. The effect of speed and feed rate on macro and micrograph of weld region is shown in Figure 2.7-12 [52]. The peak temperature of the weld is mainly influenced by the spindle speed, while travel speed of the tool dictates the time the work piece material is subjected to the peak temperatures caused by tool rotation. The high spindle speeds at low feed rates (such as 750 rev min^{-1} at 50 mm min^{-1}) heat in the material excessively causing near melting temperatures and a low flow stresses of the work piece. On the contrary, 150 rev min^{-1} at 150 mm min^{-1} low spindle speeds and high travel speeds, do not produce enough heat to promote material flow and therefore cannot produce weld (Figure 2.7-13 and 14) [52].

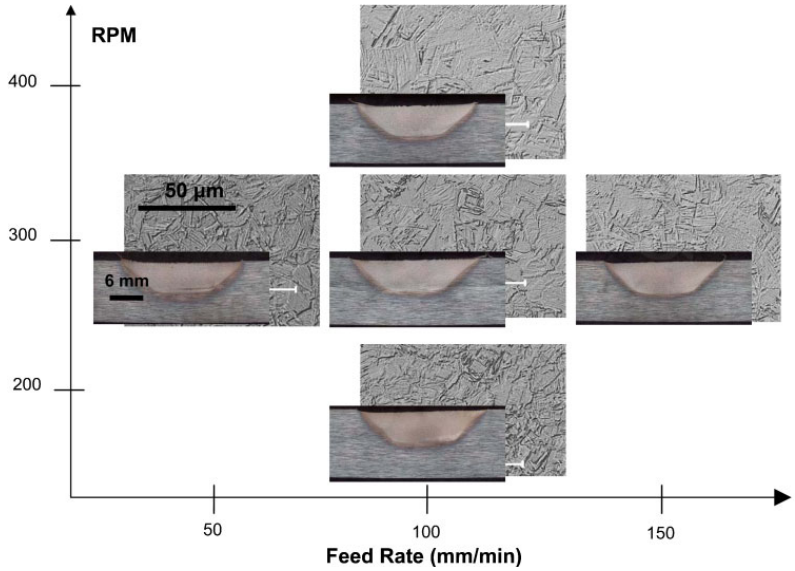

Figure 2.7-12: Macro and micrographs of welds as a function of spindle speed and feed rate [52]

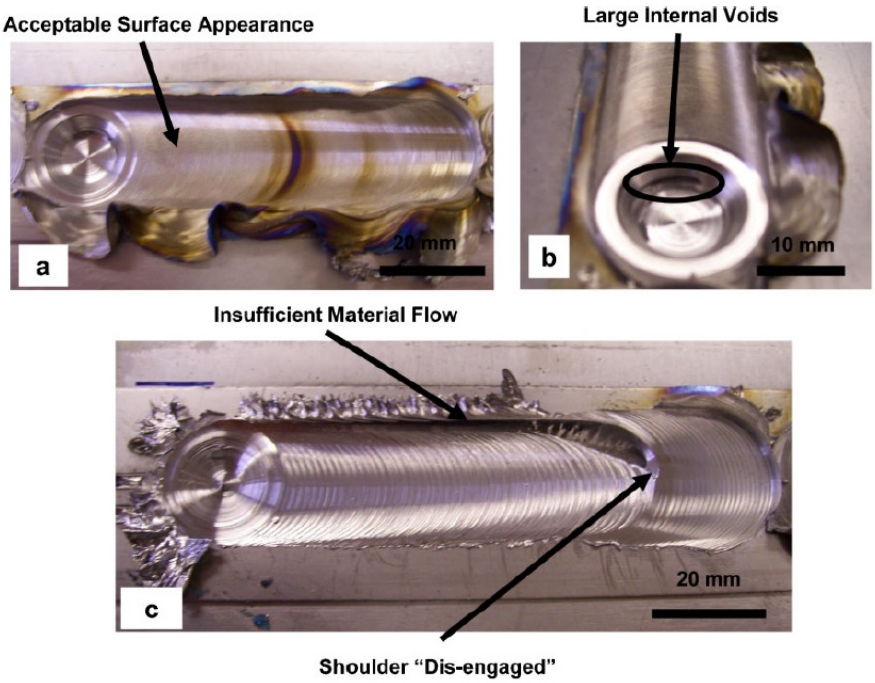

a weld surface made at 750 rev min^{-1} at 50 mm min^{-1}; *b* tool extraction point of same weld showing the massive void present; *c* weld surface made at 150 rev min^{-1} at 150 mm min^{-1}
Examples of welds made under unacceptable process conditions

Figure 2.7-13:a Weld Surface made at 750 rev min^{-1} at 50 mmmin^{-1}; b tool extraction point of same weld showing massive void present; c weld surface made at 150 rev min^{-1} at 150 mm min^{-1} [52]

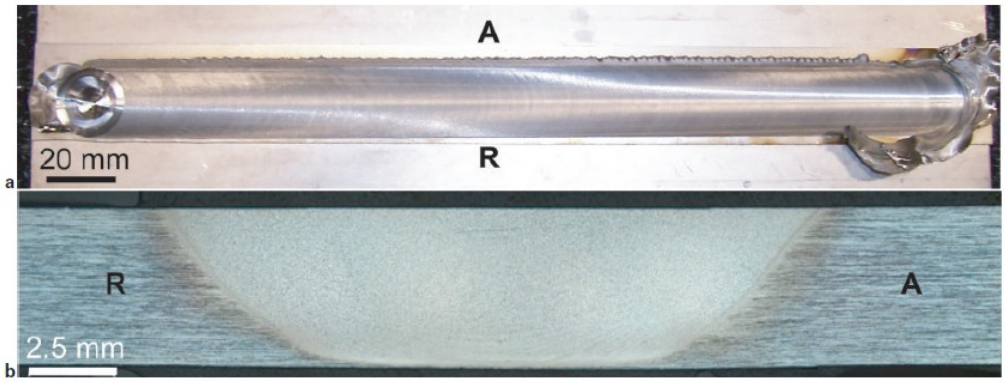

a surface photograph; *b* cross-section macrograph
4 Weld produced under optimal welding conditions: 300 rev min^{-1} at 100 mm min^{-1}

Figure 2.7-14:Cross-sections of non-optimal condition welds (a 150 rev min^{-1} at 50 mm/min, b 750 rev min-^{1} at 200 mm/min) [52]

The mechanical properties of friction stir welded Ti-64 joints have been studied by several authors [53-55]. Table 2-2 displays the tensile properties for Ti-64 weldments for number of process conditions and joint thickness.

Table 2-2 Mechanical Properties of FSW Ti-64SG [53-55]

Year	Author	Process Conditions		Joint Thickness	Mechanical Properties	
		Travel Rate	Rotational Speed		Transverse Tensile	Stir Zone Tensile
2008	Zhang [51]	1mm/s - Constant with plunge depth 2 mm	300 RPM	3 mm	TS :925 MPa, YS: 825 MPa, %E:10	TS :1050 MPa, YS: 950 MPa, %E:33
			600 RPM		TS :900 MPa, YS: 800 MPa, %E:7	TS :1040 MPa, YS: 920 MPa, %E:28
2010	Liu [52]	Base Material		2 mm	TS: 1030 MPa, %E: 14.2	
		25 mm/min	400 RPM		TS:930MPa, %E: 5.8	
		50 mm/min			TS:950MPa, %E: 6	
		100 mm/min			TS:980MPa, %E: 7	
2010	Liu Hui-jee [53]	50 mm/min, 2.5 degree tilt with pin tool	400 RPM		TS: 953 MPa	

2.7.5 *Friction Stir Welding of Dissimilar Metals*

Friction Stir Welding was started as a joining alternative for aluminum alloys. However it has now advanced to higher temperature systems including stainless steels, titanium and titanium alloys. FSW has been demonstrated to be extensively effective for joining dissimilar alloys and metals those were not possible to weld by conventional, fusion welding. It has been successfully applied in joining aluminum metal matrix composites such as Al-6061 with 20% Al_2O_3 and aluminum alloy containing 20% SiC, and aluminum alloys welded to magnesium alloys. Murr's [37] review on FSW research on dissimilar metal and alloy systems provides testament to the diversity of applications, particularly

commercial for FSW. The FSW of dissimilar, lightweight alloys such as Al-alloys to Mg-alloys is promising for a host of aerospace and automotive applications.

Murr [37] has conducted comparative study on FSW of dissimilar aluminum alloys Al-2024/Al-1100, Al-2024/Al-6061, and Al-2024/Al-2195 alloy systems. The difference between FSW of Al-2195 and Al-2024 and dissimilar Al-2024/Al-2195 showed a general trend toward Al2195 within the weld zone while the edges of HAZ for the retreating Al-2024 side and the advancing Al-2195 reflect the features of FSW for each of these component workpieces. A very similar intercalation structure for the Al-2195 and the dissimilar Al-2024/Al-2195 system as illustrated in Figure 2.7.15 .The study showed that the principal difference in the FSW of the same system of metals and alloys versus dissimilar system of FSW alloys is the variation in asymmetry or the degree of symmetry with the reference to the weld centerline at zero of the residual hardness. This difference was observed irrespective of the rotation direction (cw or ccw) or the advancing side of the tool. The material flow in dissimilar material flow systems is complex and intercalated and that causes fluctuation in micro indentation hardness profiles, especially in the weld zone. This fluctuation is often in the region at the edges of the weld zone, depending on the advancing versus retreating side materials.

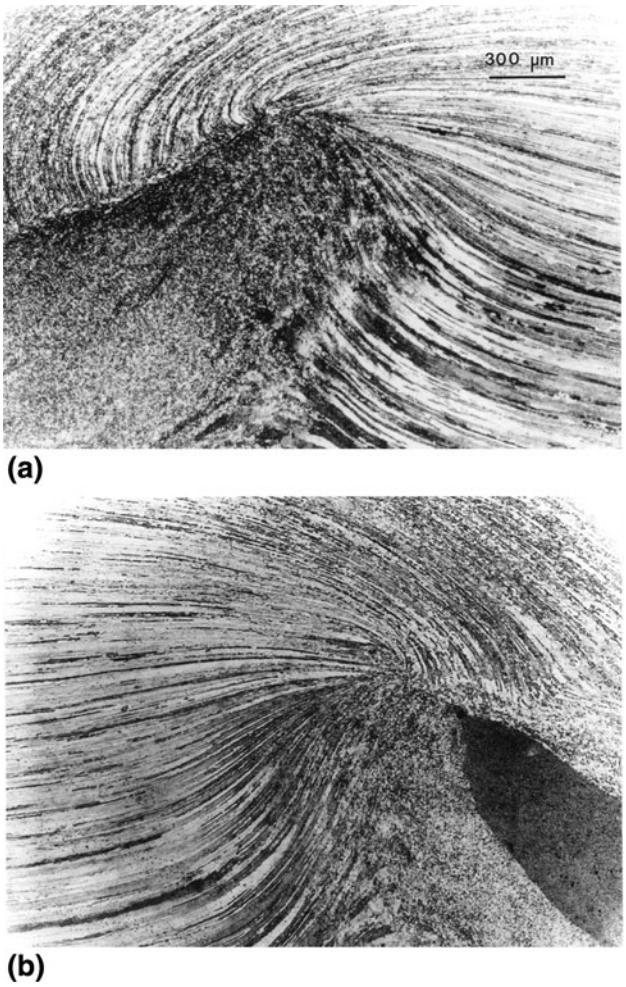

Figure 2.7-15: Weld zone intercalation structure for the Al-2195 (a) and dissimilar Al-2024/Al-2195 (b) [37]

Alvarez [56] studied the material flow and mixing patterns during dissimilar friction stir welding of Al-7075-T6 and Al-2024-T3. The impact of welding parameters, rotational speed on material mixing of these aluminum alloys was performed through 'stop action' technique. It was observed that mixing greatly depends on the heat input. By keeping the other welding variables constant, the rotational speed was varied in the range from 400 to 2000-revolution min^{-1}. Figure 2.7.16 shows cross section of welds performed at different rotational speeds. At the lowest rotational speed, a clear boundary between two alloys is distinguished. As compared to the rest of welding conditions, the sample showed larger thermomechanical affected zone (TMAZ), especially below the shoulder, and a characteristic basin shape (Figure (a)). This suggests that the volume of material that has

been plastically deformed due to the interaction with the tool is greater at this welding condition, though a distinguishable weld nugget has not developed inside the TMAZ. A well-developed stir zone was seen at the fastest rotational speed of 2000 rev min^{-1} (Figure 2.7.16 (c, d, e)). This stir zone was located mainly in the bottom half and was composed by intercalated bands of Al-7075 and Al-2024, which adopt an elliptical shape. Above the weld nugget, nearby the tool shoulder, dissimilar materials were not mixed at all. In the intermediate mixing state of 1000 rev min^{-1}, although there are no intense onion ring features, some evidence of intermixing and banding is observed at the bottom of SZ. In the weld nugget of this intermediate mixing stage, a thin layer of Al-7075 (tongue-shaped) has been pushed toward the retreating side (Figure 2.7.16 (b)). At the same time there has been bulk transference of Al-2024 material from the RS to the AS at the sheet top and bottom.

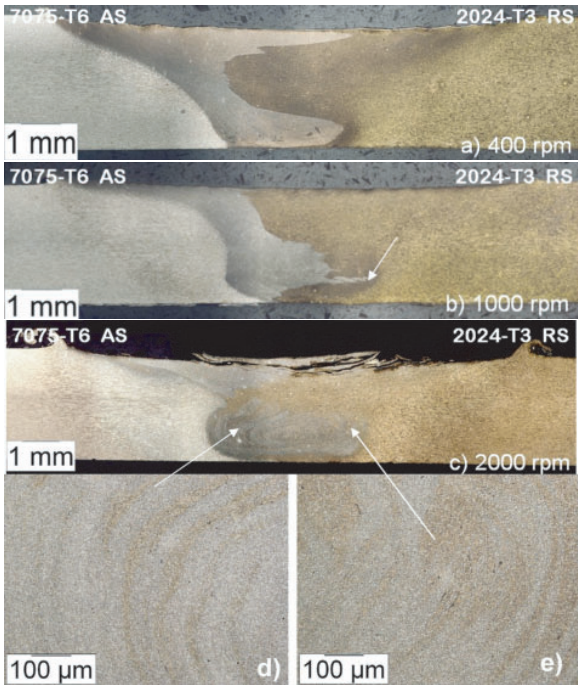

Figure 2.7-16: Cross sections of Al-7075/ Al-2024 at feed rate (400, 1000, and 2000 rev min^{-1} and enlargements of banded mixing patterns obtained at 2000 rev min^{-1} in advancing side and retreating side) [56]

Esmaeili et al. [57] studied the dissimilar friction stir welding of aluminum to brass by investigating the weld defects through radiography. The primary detected defect was

coarse and continuous distribution of fragments of brass in aluminum matrix called fragment defects. These defects are accompanied by tunneling and void defects in vicinity of fragments. The formation of fragments was attributed to the utilized rotational speed in joining of aluminum to brass that was found not enough to plasticize the brass as well as aluminum. The required rotational speed for joining the similar plates of brass (>1000 rev min^{-1}) is significantly higher than what is needed for welding the brass plate to aluminum (450 $revmin^{-1}$). Such a lack of plasticization results in the formation of coarse brass particles. These coarse fragments can be removed by using a proper offset value to crumble the coarse particles of brass. The crumbling phenomenon generates a metal matrix composite through the nugget zone where fine brass particles act as a reinforcing component in aluminum matrix, and subsequently detrimental effect of fragment defects disappears.

Masayuki [58] studied friction Stir Welding of Titanium and Titanium alloy Ti-6Al-4V with aluminum alloys Al-7075 and Al-2024. The macrostructure of the cross section of joints (Figure 2.7.17) show the weld between the two dissimilar alloys. The cross sectional microstructure mixed region (Figure 2.7.18) of Al alloy and pure Ti joints showed black regions at the joint interface. These regions contained a mixture of pure Ti and Al alloy. The mixed regions did not cover all the joint interfaces and were observed partly at the interface and many of them were observed at the upper half of the plate and at the interface. The width of the plastically deformed region near the interface of pure Ti increased with a decrease in the travel speed.

Figure 2.7.19 shows cross sectional microstructures of the joint interface of Ti-6l-4V/ Al alloys joints. In these joints, the plastically deformed region of Ti-6Al-4V near the interface was narrower than that in the Ti/Al alloys joints. The width of the region less than 200 μm at a travel speed of 100 mm/min, also no refined grains by dynamic recrystallization were observed. The weldability of the Ti and Al-2024 alloy was better than of the Ti and Al-2024, the tensile strengths of the Ti/Al-2024 joints were higher than the other joints of the study. The travel speed in FSW was seed to affect the tensile strength of the joint. The increase in travel speed tends to increase the tensile strength of the Ti and Al alloy joints. The tensile strength of Ti-6Al-4V and Al joint is lower than the Ti and Al

alloy joint. The hardness of the base materials affects the weldability of Ti alloy and Al alloy joined by FSW.

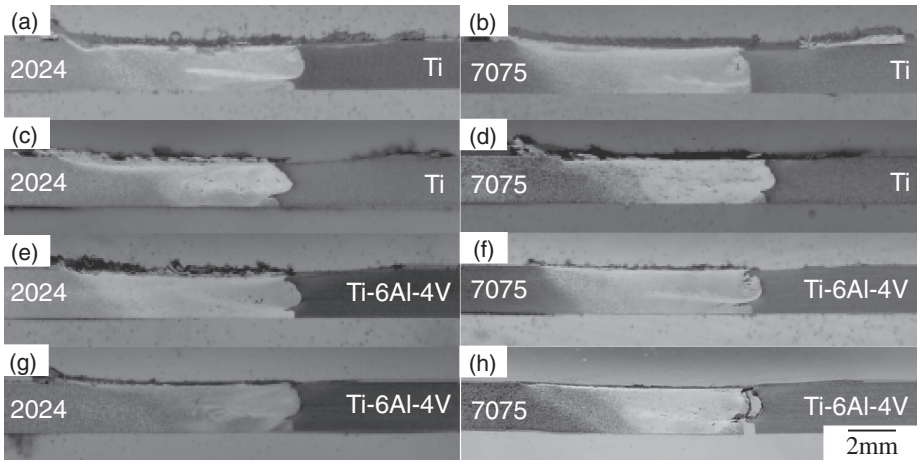

Figure 2.7-17:Macrostructure of joints at different speeds of Ti/ Al alloys a) Ti/Al-2024 (100 mm/min), b) Ti/Al-7075 (100 min/min), c)Ti/Al-2024 (300 mm/min), d) Ti/ Al-7075 (300 mm/min), e) Ti-6Al-4V/Al-2024 (100 mm/min), f) Ti-6Al-4V/Al-7075 (100 mm/min), g) Ti-6Al-4V/Al-2024 (300 mm/min), and h) Ti-6Al-4V/Al-7075 (300 mm/min) [58]

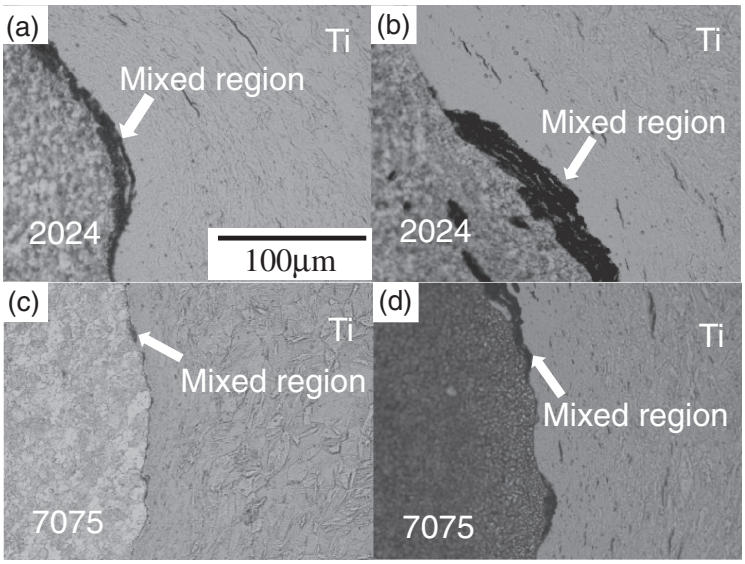

Figure 2.7-18:Cross-section microstructures of the joint interface at different travel speeds of Ti/Al-2024 a) Ti/Al-2024 (100 mm/min), b) Ti/Al-7075 (100min/min), c) Ti/Al-2024 (300 mm/min), d) Ti/ Al-7075 (300 mm/min) [58]

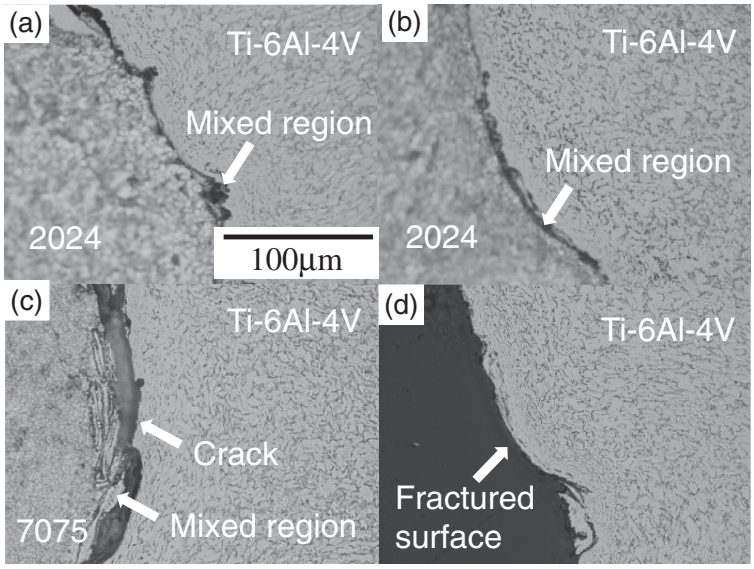

Figure 2.7-19:Cross section microstructures of the joint interface at different travel speeds of Ti-6Al-4V/Al-2024 a) Ti-6Al-4V/Al-2024 (100 mm/min), b) Ti-6Al-4V/Al-7075 (100mm/min), c) Ti-6Al-4V/Al-2024 (300mm/min), and d) Ti-6Al-4V/Al-7075 (300mm/min) [58]

2.8 SUMMARY

To improve buy to fly ratio and to obtain near net shapes of titanium parts, it is vital to join titanium alloys. The established processes of diffusion bonding and friction stir welding have shown good promise in achieving good quality titanium joints. Diffusion bonding combined with superplastic forming is a well-established process for manufacture of components largely from Ti-6Al-4V sheet material. However relatively low temperature of Ti-6Al-4V sheets limits its range of applications. The increase in demand for advanced lightweight materials with elevated temperature properties superior to that of conventional titanium alloys such as Ti-6Al-4V has stimulated the development of more advanced alloys that can work at high temperatures. However there is interest in the ability of the titanium alloys to form sound diffusion bond with Ti-6Al-4V and other titanium alloys to produce structures with superior properties for elevated temperature applications. Previous work on titanium alloys has shown that optimum superplastic behavior is usually obtained at temperatures near to those at which materials contain 40-50% by volume of β phase.

Sounds bonds could be obtained at temperatures between those considered optimum for superplastic flow for the dissimilar alloys.

A considerable research has been conducted on application of friction stir welding with titanium. Till date limited research has been conducted on diffusion bonding and friction stir welding of a titanium alloy with the other titanium alloys. The past studies on dissimilar titanium joining with diffusion bonding have showed positive results. However diffusion bonding of very few combinations of titanium alloys has been investigated. Therefore, the main purpose of the current study was to examine the joining one titanium alloy with the other titanium alloys through both these processes.

Chapter 3. RESEARCH METHODOLOGY

3.1 INTRODUCTION

This section presents the proposed research and methodology adopted for studying the joining of dissimilar titanium alloys. In the first segment, the objectives of the research are defined and the research goals are established. In the later segment, the experimental procedure to analyze both joining processes, diffusion bonding and friction stir welding respectively are discussed. The details on the sample preparation, the bond quality assessment methods to evaluate the joining of titanium alloys to establish the surface and mechanical properties are discussed.

3.2 OBJECTIVES OF RESEARCH

The use of titanium alloys has increased over the years in the aerospace industry. Ti-6Al-4V is known as the workhorse of aerospace industry. Other titanium alloys like Ti-15Mo-3Nb-3Al, and Ti-54M has also found place in the aerospace applications. The particular properties of titanium alloys decide their applications, while some of their properties limit their use. The joining of titanium alloys with other materials is increasingly demanded from the industry as it can effectively reduce material costs and improve the design. Successful results have been found on joining titanium with nickel-based alloys, aluminum alloys, and steel among the others. Therefore if the titanium alloys with different properties are joined, it can improve the utilization of titanium alloys and improve the functional properties of titanium.

Titanium and its alloys are good materials for diffusion bonding since their surface oxide films are readily dissolved at the temperatures encountered in the process. As stated earlier, there is also a scope of combining diffusion bonding with superplastic forming, SPF/DB, in joining titanium alloys to reduce weight and fabrication costs compared to mechanically fastened structures. Developments in FSW of dissimilar titanium alloys enable monolithic structures of heterogeneous materials that can utilize the varied properties of titanium alloys to enable high performance designs that remain cost effective.

Therefore, the main objective of this study was to understand the feasibility of joining dissimilar titanium alloys using diffusion bonding and friction stir welding processes.

a) The microstructural evolution during DB and FSW remains a critical consideration in determining which processing routes (eg, heat treatment, superplastic forming) are viable for subsequent component fabrication.
b) Experimental characterization of mechanical properties of the titanium joint alloys.
c) The modeling of dissimilar joining of titanium alloys has not been studied. An attempt will therefore be made to theoretically model the diffusion bonding of dissimilar materials to optimize the diffusion bonding process
d) A numerical model will also be developed of diffusion bonding process and numerical experiments will be conducted to simulate the process with varying parameters.

3.3 RESEARCH GOALS

The section provides the methodology and the tasks to achieve the stated objective. The samples of both the similar and dissimilar titanium alloys were prepared for studying diffusion bonding and friction stir welding processes. The joining methods were examined as a function of the influencing parameter of the process. The other process parameters were selected from the previous investigations conducted to obtain good quality joints. In order to study the capability of diffusion bonding process for dissimilar titanium alloys, two governing parameters pressure and time were held constant while the temperature was varied for making the samples. The viability of friction stir welding process was studied by varying the two parameters that control the quality of the process, mainly the velocity and the feed rate. The specific goals of research study were divided in following tasks:

1. Diffusion Bonding Evaluation

The quality of diffusion-bonded joints was examined by assessing the mechanical behavior of the joints.

a) Mechanical Behavior: The mechanical testing was conducted to evaluate the quality and sustainability of dissimilar titanium joints. The mechanical behavior of diffusion bonded titanium joints was established through hardness and flexure testing
b) Microstructural Characterization: The microstructural study was made to examine the quality of diffusion bonding at the interface. The bonding interface was observed to find the presence of voids and the thickness of bondline.
c) Hardness Distribution: The hardness of the joint can provide insight into the expected performance of the joint.
d) Surface Measurements: The surface quality of the diffusion-bonded joints was also assessed by surface profile measurements.

2. *Friction Stir Welding Evaluation*

a) Mechanical Properties: The mechanical testing was conducted to evaluate the quality and sustainability of dissimilar titanium joints. The mechanical behavior of friction stir welded titanium joints was established through tensile testing.
b) Microstructural Characterization: The microstructure study will be conducted to provide the qualitative aspect of the process in terms of the material flow and mixing characteristics in the different zones of friction stir welding process.
c) Surface Measurements: The surface quality of the friction stir welded joints was also assessed by surface profile measurements. The surface profile measurements were made to study the influence of process parameters on the surface roughness of the welded joints.
d) Hardness Distribution: The hardness of the joint can provide insight into the expected performance of the joint through friction stir welding.

3. *Theoretical Modeling*

The diffusion bonding process is not very simple to model because of the complexity of the mechanisms that occur individually or in synchronization towards the closure of voids. Furthermore in case of dissimilar materials the complexity aggravates, the void

geometry becomes more complex due to variance in the surface profile and grain sizes, the difference in the superplastic properties of the joining materials. The first step should be to verify established theoretical models for similar titanium alloys. Then to develop the model for dissimilar materials; it is essential to make modification in the void geometry, superplastic properties, the interface, grain boundary, and creep mechanisms of the joining materials.

4. *Numerical Modeling*

The modeling of diffusion bonding mechanism for similar materials will be developed. Next step would be to apply the model to dissimilar materials. The numerical model can be used as an optimization tool to develop the diffusion bonding process for similar as well as dissimilar materials. Additionally the numerical modeling of mechanical testing of diffusion bonding and friction stir welding will also be developed. The numerical results can provide the insight to the stress strain distribution at the critical locations and failure location for the joints.

3.4 TITANIUM ALLOYS: PROPERTIES AND APPLICATIONS[59]

This section highlights the titanium alloys adopted in the study along with their properties and applications. Six titanium alloys were included in this study. They were Ti-15Mo-3Nb-3Al (β-21S), Ti-5Al-4V-0.6Mo-0.4Fe (Ti -54M), Ti-6Al-4V (Ti-64), Ti-6Al-4V fine grained (Ti-64 FG), Ti-6Al-2Sn-4Zr-2Mo (Ti-6242), Ti-6Al-2Sn-4Zr-2Mo fine grained (Ti-6242 FG). From the six alloys, two alloys belong to the near alpha type of titanium alloys, (Ti-6242, Ti-6242FG); the other three are alpha-beta titanium alloys (Ti-64, Ti-64FG, and Ti-54M); and the last one is a beta titanium alloy (β-21S). The alpha stabilizer, aluminum, is present in all of the alloys. Ti-6Al-4V and Ti-6Al-2Sn-2Zr-2Mo have equal proportion of aluminum; while it is 5 % in Ti-5Al-4V-0.6Mo-0.4Fe and 3 % in Ti-15Mo-3Nb-3Al. β21S has two beta stabilizer, molybdenum (15%) and niobium (3%). In Ti-6Al-4V, beta proportion is compensated by 4% vanadium. Ti-6Al-2Sn-4Zr-2Mo replaces 4V of

Ti-6Al-4V with 2Mo, a strong beta stabilizer than former, and inserts neutral elements with this regard, tin and zirconium, for beta stability. Ti-5Al-4V-0.6Mo-0.4Fe has two beta stabilizers, 4% vanadium and 0.6 % molybdenum.

3.4.1 *Ti-15Mo-3Nb-3Al (β-21S or Beta-21S)*

Ti-15Mo-3Nb-3Al is a metastable β alloy that provides the high strength and good cold formability of a metastable β alloy, but has been specifically developed for improved oxidation resistance, elevated temperature strength, creep resistance, and theramol stability. The main product form of β-21S is strip and is also well suited for metal matrix composites as it can be rolled to foils economically and is compatible with most fibers.
The composition is Beta-21S, with molybdenum and niobium working synergistically to raise corrosion resistance to very high levels. This alloy can be made into the thickness of the foil 0.064mm. Metastable beta alloys usually fall to the left of (lower creep resistance) of Ti-64 band, however Beta-21S is to the right of Ti-64 curve, indicating an approximately 30^0C (50^0F) advantage in creep over Ti-64. Ti-6242 is however more creep resistant than Beta-21S. It provides good oxidation resistance as compared to other beta alloys and commercial titanium. It is very resistant to corrosion and hydrogen adsorption in hot reducing acids. This corrosion resistance behavior has led to testing of this alloy in commercial aircraft hydraulic fluid. Prior to the development β-21S, the use of titanium and its alloys was restricted for certain warm (205 to 370^0C or 400 to 700^0F) engine components on commercial aircraft due to the risk of catastrophic failure of titanium components due to corrosion and hydrogen embrittlement caused by contact with hydraulic acid. Beta-21S can take product forms such as cut sheet, strip, plate, bar, billet, and bloom. It is typically beta-solution treated to precipitate alpha and thereby results into strengthening on aging. It also offers one of the lowest hydrogen uptake efficiency levels of any titanium alloy.

Beta-21S is very favorable for applications above 290^0C (550^0F), with thermal stability up to 625^0C (116^0F) and creep resistance comparable to Ti-64.The combination of high strength and high corrosion resistance make it an ideal candidate for orthopedic implants, deep sour oil wells, and geothermal brine wells. Beta-21S has fairly good high

temperature properties. The creep properties of Beta-21S are superior to that of Ti-64. Beta-21S is used by Boeing and P&W for temperatures upto 650^0C. The other real advantage of this is its resistance to hot hydraulic fluid, which is one of the very few corrosive media for titanium in the aerospace environment. TIMET Beta-21S has provided significant weight savings in the 777 nacelles. TIMET Beta-21S is used on the aircraft cover and plug and nozzle for all three 777 engines, the P&W 4084, GE-90, and the Trent 800 [4, 24]. Beta-21S can withstand temperature as high as 800^0C (1500^0F) when combined with SC (silicon carbide).

3.4.2 *Ti-5Al-4V-0.6Mo-0.4Fe (Ti-54M)*

Ti-54M is an alpha- beta titanium alloy. It was developed to improve upon the overall production costs of Ti-64 while providing similar properties. TIMET has produced significant quantities of Ti-54M via electron-beam-single-melting (EBSM). As compared to Ti-64, Ti-54M contains lower Al content which improves forgeability and machinability, whereas slight addition of Mo and Fe promote alpha grain refinement and diffusion acceleration respectively. It reduces the β-transus temperature of Ti-54M resulting in low flow stresses at elevated temperatures and reduction in the working temperature necessary in (α+β) thermomechanical zone. Therefore, Ti-54M shows superior superplastic forming characteristics as compared to Ti-64. Though Ti-54M and Ti-64 have similar mechanical properties; however the former has improved machinability of 10-15% [60].

3.4.3 *Ti-6Al-4VStandard Grain (Ti-64SG)*

Ti-64SG is the most popular α+β titanium alloy. The grain size of the standard Ti-64 is about 8 μm. Ti-64 is unique in the sense it combines desired mechanical properties with inherent workability. This alloy has good corrosion resistance properties, good fatigue and fracture properties and is used at a minimum tensile strength of 896MPa. The fatigue and fracture properties can be optimized through heat treatment. Ti-64 is commonly used in the mill-annealed form and can take various forms that include forgings, bar, sheet, plate, castings, extrusions, tubing and fasteners.

Ti-64 may have different fractions of alpha and beta phases, depending on heat treatment and interstitial (primarily oxygen) content. In addition, Ti-64 can acquire huge variations of microstructures with different geometrical arrangements of the alpha and beta phases, depending on particular thermomechanical treatment. These different alpha morphologies and microstructures can be classified into three different categories: lamellar, equiaxed, or a mixture of both (bimodal). The lamellar is a fairly coarse structure and is often referred to as plate-like alpha. It is resulted from slow cooling into the two phase region from above β transus which leads to nucleation and growth of the alpha-phase in plate form starting from beta boundaries. On the other hand air cooling results in a fine needle-like alpha phase referred to as acicular alpha. Some intermediate cooling rates develop Widmanstätten structures. Fine lamellar structure can be developed by water quenching from the β phase field followed by annealing in the (α+β)-phase region. The equiaxed microstructure are obtained by extensive (> 75% reduction) mechanical working the material in the (α+β)-phase field, where the breakup of lamellar alpha into equiaxed alpha depends on the deformation procedure. The bimodal type microstructures consist of isolated primary α-grains in a transformed beta matrix. These microstructures are best obtained by a 1 h anneal at 995^0C (1750^0F) followed by water quenching (or more commonly an air cool) and aging at 600^0C (1100^0F).

Ti-64 is highly resistant to natural environment and to many aqueous chemicals up to at least their boiling temperatures. It is resistant to general corrosion by sea water and brine, oxidizing acids, aqueous chloride solutions, wet chlorine gas and sodium hypochlorite at typical product-operating temperatures. Additionally it is generally immune to galvanic corrosion in contact with other structural materials and is compatible with nickel alloys and stainless steels. However, it is vulnerable to reducing acids such as hydrofluoric, hydrochloric, sulfuric, oxalic, formic, and phosphoric acids; and can promote galvanic attack when in contact with less noble metals such as aluminum, carbon steel, and magnesium alloys. The thermal conductivity of Ti-64 is less than that of titanium, while its thermal expansion and specific heat are close to titanium. The liquidus temperature of Ti-64 is below the melting point (1688^0C, or 3070^0F). This has prime application in aerospace

due to its excellent benefit of corrosion resistance with the advantage of less weight. Due to its numerous benefits, Ti-64 has become a standard alloy against which other alloys must be compared when choosing titanium alloy for a specific application. The classic example of the use of this alloy is in Boeing 757 landing gear and the windshield frames. The windshield frames on 767 and 777 are machined from the Ti-64 forgings. The other typical uses include pressure vessels, aircraft turbine and compressor blades and disks, surgical implants, etc. [61].

3.4.4 *Ti-6Al-4V Fine Grain (Ti-64 FG)*

Ti-6Al-4V FG is the fine grain version of Ti-6Al-4V alloy. Verknaya Salda Metallurgical Production Association in Russia developed this fine grain form of Ti-6Al-4V alloy, of the grain size of about 1μm. The fine grain version of Ti-6Al-4V offers some advantages over the regular grain of Ti-6Al-4V. The superplastic forming can be performed at lower temperatures of around 775^0C as compared to typical temperatures of 900^0C to 920^0C used with the standard grain size. This high temperature causes degradation of press platens and wear and oxidation of tooling materials [63]. The grain size influences the oxygen diffusion in superplastic forming. As the grain size decreases, the rate of oxygen diffusion increases [63]. The fine grains require much lower flow stress to accomplish superplastic process as compared to the conventional Ti-64 alloy. Ti-6Al-4VFG can diffusion bond to itself and as well as to other standard size titanium alloys. Because of the above advantages, this alloy is used in the production of SPF and SPF/DB aerospace components.

3.4.5 *Ti-6Al-2Sn-4Zr-2Mo (Ti-6242)*

Ti-6Al-2Sn-4Zr-2Mo-0.08Si (Ti-6242S or Ti-6242Si) is a near-alpha titanium alloy developed in the late 1960's as an elevated temperature alloys. This alloy has excellent combination of creep strength, tensile strength, toughness, and high temperature stability for long term applications at temperatures upto 425^0C (800^0F). It is a most creep resistant alloy that shows creep resistance upto 565^0C (1050^0F). It has been reported that 1000 hours exposure upto 540^0C (1000^0F) without load has no detrimental effect on subsequent room temperature tensile properties of duplex annealed sheet. On the contrary, 1000-hour

exposure with load produces a serious loss of ductility at 480^0C (137 MPa) for duplex annealed sheet. Souni [64] investigated the creep behavior of a high temperature near alpha alloy Ti-6242 Si in the stress range from 160 to 350 MPa and a temperature range from 500 to 600°C, using constant stress tensile creep experiments. The emphasis of his work was on primary and anelastic creep behavior and their dependencies on stress, strain and processes microstructures. It was shown that both primary and anelastic creep strongly depend on creep strain and applied stress.

The chemical composition of Ti-6242 consist of 6% aluminum addition, a potent alpha-phase stabilizer, while the 2% molybdenum addition represents only a moderate quantity of potent beta-phase stabilizer. The addition of other elements tin and zirconium that are neutral with respect to the phase provide solid solution strengthening to the alloy. The net effect of this combination of elements makes it a weak beta stabilized; therefore the alloy is properly described as a near-alpha, alpha-beta alloy. The original composition of this alloy doesn't contain silicon, but RMI introduced nominal 0.08% silicon content that allowed the alloy to meet the creep requirements for its intended jet engines applications.

Ti-6242S is sometimes described as near-alpha or super-alpha alloy, but in its normal heat treated condition this alloy has a structure better described as alpha-beta. It requires proper heat treatment to develop good creep resistance, while limited hardening of Ti-6242S can be obtained by solution treating and aging. The available mill forms of Ti-6242S include billet, bar, plate, sheet, strip, and extrusions. Some forging operations can be carried out at room temperature, and warm forging (425 to 705^0C or 800 to 1300^0F) can be employed when necessary. The alloy has fair weld ability; however the molten weld metal and adjacent heated zones must be shielded from active gases (nitrogen, oxygen, and hydrogen).

The ultimate tensile strength is about 930 MPa and had density 4.54 g/cm^3 (0.164 lb /in^3). Ti-6242S is primarily used in the gas turbine industry for rotating components such as blades, discs and rotors upto about 540^0C, and also in sheet-metal form for engine afterburner structures and for various 'hot' airframe skin applications, where high strength and toughness, excellent creep resistance, and stress stability at temperatures up to 565C

(1005^0F) are required. Ti-6242 is used in the application that requires higher temperature, not supported by Ti-64. The alloy is used in the high-pressure compressor at temperatures too high for Ti-64 (above about 315^0C) for structural applications.

3.4.6 *Titanium Alloys Mechanical Properties*

The composition, β transus and useful temperature and mechanical properties of different titanium alloys are discussed in this section in Table 3-1, 3-2, and 3-3 respectively.

Table 3-1: Composition of Parent Titanium Alloys [59]

No.	Alloy Name	Alloy Type	Alloy Composition (%)									
			Al	Fe	Mo	Nb	O	Sn	Si	Ti	V	Zr
1	Beta-21S	β	3		15	2.7			0.2			
2	Ti-54MFG	α +β	5	0.4	0.6					90	4	
3	Ti-6Al-4VSG and FG	α +β	6	0.25 (Max)			0.2 (Max)			90	4	
5	Ti-6242SG and FG	Near α	6		2			2				4

Table 3-2: β Transus and Useful Temperature of Parent Titanium Alloys [59]

Alloy	Alloy type	Year of introduction	Useful Maximum temperature		βTransus temperature	
			^{o}C	^{o}F	^{o}C	^{o}F
Beta-21S	β	1988	590	1100	793 to 810	1460 to 1490
Ti-64SG	α +β	1954	300	580	995	1825
Ti-6242	Near α	1967	450	840		
Ti-6242S	Near α	1974	520	970	995±15	1825±25

Table 3-3: Mechanical Properties of Parent Titanium Alloys [65]

Base Alloy	Melting Point (°C)	Vickers Hardness	Ultimate Strength (MPa)	Yield Strength 0.2 % (MPa)	Elongation (%)	Elastic Modulus (GPa)	Poisson's Ratio
Beta-21S			915	880	15	83	
Ti-54M			972	889	16.5		
Ti-64SG	1660	349	950	880	14	113.8	0.342
Ti-6242	T8	333	1010	990	3	120	0.32

3.5 DIFFUSION BONDING OF SIMILAR AND DISSIMILAR TITANIUM ALLOYS

3.5.1 *Specimen Preparation*

The diffusion bonded titanium alloy joints were formed in the Boeing facility. The samples comprised the combinations of similar and dissimilar titanium alloys. The diffusion bonded samples were prepared with pair of 75 x 75 mm squares sheets as shown in Figure 3.4-1. These sheets were first deburred and then cleaned using nitric hydrofluoric pickle acid bath to remove contaminants and oxides. The pairs were then mated together and edges were TIG welded to make seal. Before the welding, gas tube was inserted to create vacuum (1EE-01Pa). The vacuum established tube was sealed, to avoid formation of alpha case that causes dis-bonding. The pressure of 1-5 MPa was held constant throughout the process. The bonding time selected was 1-5 hours for all the samples. The temperature (between 0.4 to 0.7 melting point temperature (Tm) of the bonding material) was varied while joining the similar and dissimilar titanium alloys. The experimental procedure adopted to evaluate diffusion bonded specimens is described in Figure 3-4.2.

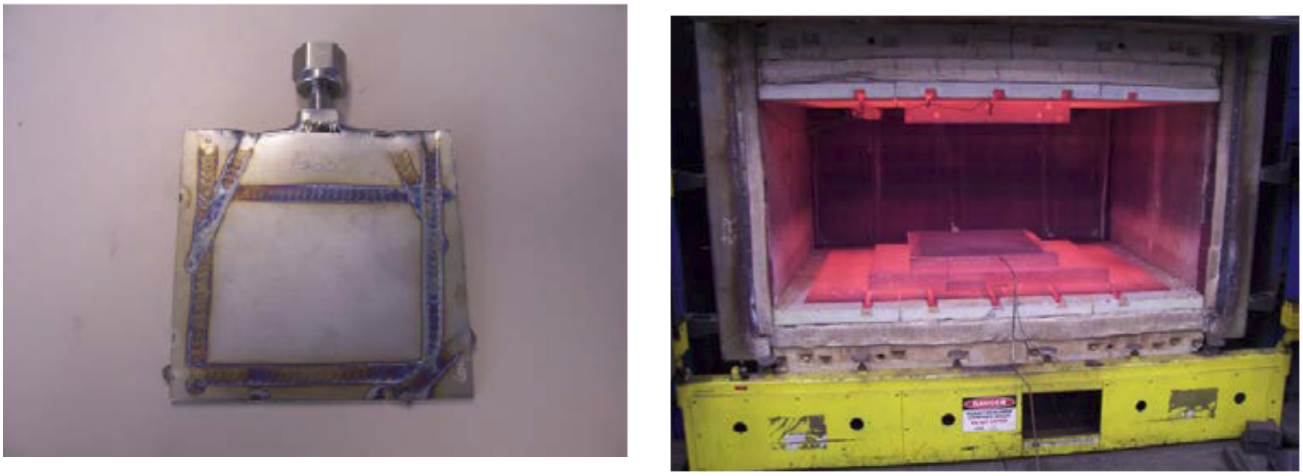

Figure 3.5-1: Diffusion Bonding: Sample Preparation (Left: Representative diffusion pack configuration, after evacuation and close out, Right: Completed diffusion pack, in press)

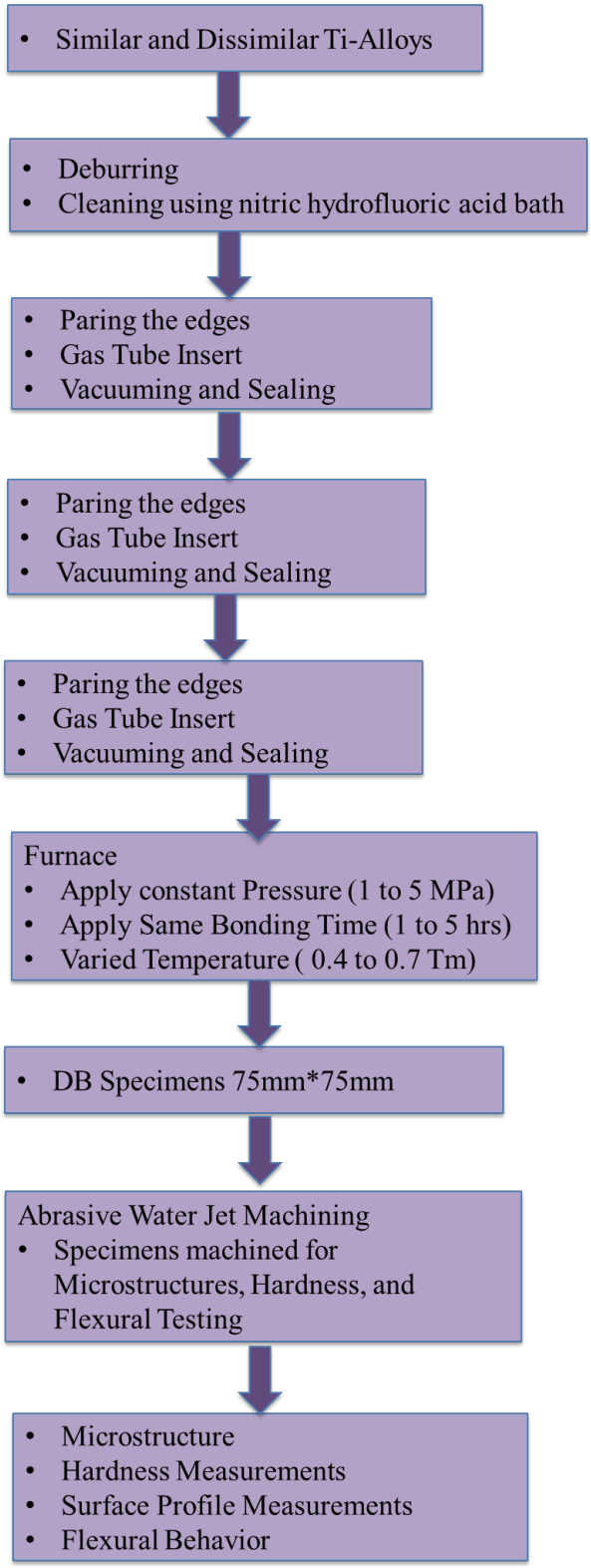

Figure 3.5-2: Diffusion Bonding Joining Evaluation

3.5.2 *Specimen List*

Six parent alloys were selected for analyzing the diffusion bonding process of dissimilar titanium alloys. The samples for each alloy combinations were prepared in a temperature range of 0.4 to 0.7 Tm of the bonding titanium alloys. The temperature values T1 to T8 are in the increasing order in the range of 0.4 to 0.7 Tm of Ti-64 alloy. The range of temperatures was between 730^0C to 950^0C. The actual values of temperature are protected due to proprietary nature of the work. Diffusion bonding specimens were prepared at the Boeing facility and were received in three batches. In the third batch, the specimens were not diffusion bonded and separated during the machining operation. Therefore, quality of diffusion bonding was evaluated for two batches. In the first and the second batches, the parent alloys were Ti-15Mo-3Nb-3Al (Beta-21S), Ti-54M, Ti-6Al-4VSG, Ti-6Al-4VFG, and Ti-6242. In total 81 combinations of diffusion bonded titanium alloys were made from these five parent alloys that included both the similar and dissimilar combinations of alloys as shown in Table 3-4. The diffusion bonded samples included five types of similar and ten types of dissimilar titanium alloys.

Table 3-4: List of Diffusion Bonded Specimens

Batch 1	Temperatures							
Celsius	T1	T2	T3	T4	T5	T6	T7	T8
	β-21S/ β21S	β-21S/ β-21S			β-21S/ β-21S	β-21S/ β-21S	β-21S/ β-21S	β-21S/ β-21S
				β21S/ Ti-64	β-21S/ Ti-64	β-21S/ Ti-64	β-21S/ Ti-64	β-21S/ Ti-64
			β-21S/ Ti-64FG	β-21S/ Ti-64FG	β-21S/ Ti-64FG			
					β-21S/ Ti-6242	β-21S/ Ti-6242	β-21S/ Ti-6242	β-21S/ Ti-6242
				Ti-64/ Ti-64	Ti-64/ Ti-64	Ti-64/ Ti-64	Ti-64/ Ti-64	Ti-64/ Ti-64
				Ti-6242/ Ti-64	Ti-6242/ Ti-64		Ti-6242/ Ti-64	Ti-6242/ Ti-6242
					Ti-6242/ Ti-6242	Ti-6242/ Ti-6242	Ti-6242/ Ti-6242	Ti-6242/ Ti-6242

Batch 2	Temperatures						
Celsius	T1	T2	T3	T4	T5	T6	T7
	Ti-54M/ Ti-54M	Ti-54M/ Ti-54M	Ti-54M/ Ti-54M	Ti-54M/ Ti-54M	Ti-54M/ Ti-54M		
	Ti-54M/ Ti-6242	Ti-54M/ Ti-6242	Ti-54M/ Ti-6242	Ti-54M/ Ti-6242	Ti-54M/ Ti-6242	Ti-54M/ Ti-6242	Ti-54M/ Ti-6242
	Ti-54M/ β-21S	Ti-54M/ β-21S	Ti-54M/ β-21S	Ti-54M/ β-21S	Ti-54M/ β-21S	Ti-54M/ β-21S	Ti-54M/ β-21S
	Ti-54M/ Ti-64	Ti-54M/ Ti-64	Ti-54M/ Ti-64	Ti-54M/ Ti-64	Ti-54M/ Ti-64	Ti-54M/ Ti-64	Ti-54M/ Ti-64
	Ti-64FG/ Ti-64FG	Ti-64FG/ Ti-64FG	Ti-64FG/ Ti-64FG	Ti-64FG/ Ti-64FG			
	Ti-64FG/ Ti-6242	Ti-64FG/ Ti-6242	Ti-64FG/ Ti-6242	Ti-64FG/ Ti-6242	Ti-64FG/ Ti-6242		
	Ti-64FG/ Ti-β-21S	Ti-64FG/ β-21S	Ti-64FG/ β-21S	Ti-64FG/ β-21S	Ti-64FG/ β-21S		
	Ti-64FG/ Ti-64	Ti-64FG/ Ti-64	Ti-64FG/ Ti-64	Ti-64FG/ Ti-64	Ti-64FG/ Ti-64		
	Ti-64FG/ Ti-54M	Ti-64FG/ Ti-54M	Ti-64FG/ Ti-54M	Ti-64FG/ Ti-54M	Ti-64FG/ Ti-54M		

Batch3	Temperatures					
Celsius	T1	T2	T3	T4	T5	T6
	β-21S/ Ti-6242FG	β-21S/ Ti-6242FG	β-21 / Ti-6242FG	β-21S/ Ti-6242FG	β-21S/ Ti-6242FG	β-21S/ Ti-6242FG
	Ti-54M/ Ti-6242FG	Ti-54M/ Ti-6242FG	Ti-54M/ Ti-6242FG	Ti-54M/ Ti-6242FG	Ti-54M/ Ti-6242FG	
	Ti-64/ Ti-6242FG	Ti-64/ Ti-6242FG	Ti-64/ Ti-6242FG	Ti-64/ Ti-6242FG	Ti-64/ Ti-6242FG	Ti-64/ Ti-6242FG
	Ti-64FG/ Ti-6242FG	Ti-64FG/ Ti-6242FG	Ti-64FG/ Ti-6242FG	Ti-64FG/ Ti-6242FG		
	Ti-6242/ Ti-6242FG	Ti-6242/ Ti-6242FG	Ti-6242/ Ti-6242FG	Ti-6242/ Ti-6242FG	Ti-6242/ Ti-6242FG	Ti-6242/ Ti-6242FG
		Ti-6242FG/ Ti-6242FG	Ti-6242FG/ Ti-6242FG	Ti-6242FG/ Ti-6242FG	Ti-6242FG/ Ti-6242FG	Ti-6242FG/ Ti-6242FG

3.5.2.1 Specimens List with Titanium Alloys Classification

3.5.2.1.1 Similar Titanium Alloys

In similar titanium alloys, diffusion bonded joints were obtained from three types of titanium alloys that included: Near-α to Near-α, α + β to α + β and β to β titanium diffusion joints. Table 3-5 shows the list of five similar types of diffusion bonded titanium alloys with the alloy classification.

Table 3-5: Similar DB Titanium Joints with Alloy classification

Type of Ti-Alloy	Type of Ti-Alloy	Ti-Alloy/Ti-Alloy	Diffusion Temperatures (Celsius)							
			T1	T2	T3	T4	T5	T6	T7	T8
Near-α	Near-α	Ti-6242/Ti-6242					✓	✓	✓	✓
α + β	α + β	Ti-54M/Ti-54M	✓	✓	✓	✓	✓			
		Ti-64SG/Ti-64SG				✓	✓	✓	✓	
		Ti-64FG/Ti-64FG	✓	✓	✓	✓				
β	β	β-21S/ β-21S	✓	✓			✓	✓	✓	✓

3.5.2.1.2 Dissimilar Titanium Alloys

In dissimilar titanium alloys, four combinations were made from three types of titanium alloys that included: Near-α to α + β, Near-α to β, α + β to α + β, and α + β to β dissimilar titanium alloys. In case of Ti-64FG/ β-21S (α + β to β ti- alloy) two specimens were present at temperatures T3^{0}C, T4^{0}C, T5^{0}C. Table 3-6 lists the dissimilar diffusion bonded titanium joints with alloy classification obtained at different temperatures.

Table 3-6: Dissimilar DB Titanium Joints with Alloy classification

Type of Ti-Alloy	Type of Ti-Alloy	Ti-Alloy/Ti-Alloy	Diffusion Temperatures (Celsius)							
			T1	T2	T3	T4	T5	T6	T7	T8
Near-α	α + β	Ti-6242/Ti-54M	✓	✓	✓	✓	✓	✓	✓	
		Ti-6242/ Ti-64SG				✓	✓		✓	✓
		Ti-6242/ Ti-64FG	✓	✓	✓	✓	✓			
Near-α	β	Ti-6242/ β-21S					✓	✓	✓	✓
α + β	α + β	Ti-54M /Ti-64SG	✓	✓	✓	✓	✓	✓	✓	✓
		Ti-54M/ Ti-64FG	✓	✓	✓	✓	✓			
		Ti-64SG /Ti-64FG	✓	✓	✓	✓	✓			
α + β	β	Ti-54M/ β-21S	✓	✓	✓	✓	✓	✓	✓	
		Ti-64SG/ β-21S				✓	✓	✓	✓	✓
		Ti-64FG/ β-21S	✓	✓	✓✓	✓✓	✓✓			

3.5.3 *Diffusion Bonding Experimental Work*

The surface quality of diffusion bonded titanium joints was evaluated through hardness measurements, and surface roughness measurements. The mechanical quality of joints was established by flexure testing. The specimens of hardness test and three-point bend test were cut using Abrasive Water Jet machine. The specimen mounts were prepared for performing hardness testing. The microstructures were obtained while performing the hardness testing. Out of the three batches, the two batches were evaluated with hardness testing, surface profile measurements, and flexure testing as shown in Table 3-7.

Table 3-7: Diffusion Bonded Specimens Experimental Work

Batch	**Hardness Testing**	**Flexure Testing**	**Surface Profile**
1	✓	✓	✓
2	✓	✓	✓
3	×	×	×

3.5.3.1 Hardness Testing

The hardness measurements on diffusion bonded alloys were performed using Vickers Hardness test on *LECO AMH 43 Micro hardness Testing* System. All microhardness indents used Vickers indenters with a 500 gram load and a dwell time of 13 seconds. The hardness was measured across the diffusion-bonded samples at eleven locations. The first five measurements were made on the upper alloy; the sixth one was made on and near the bondline and the remaining five measurements were made on the lower alloy as shown in Figure 3.4-3. This arrangement helped in capturing the hardness variation present across alloy. The hardness results are plotted from the bond line as a function of temperature. In addition to this, the bondline hardness was plotted to understand the effect of temperature change on the bonding process.

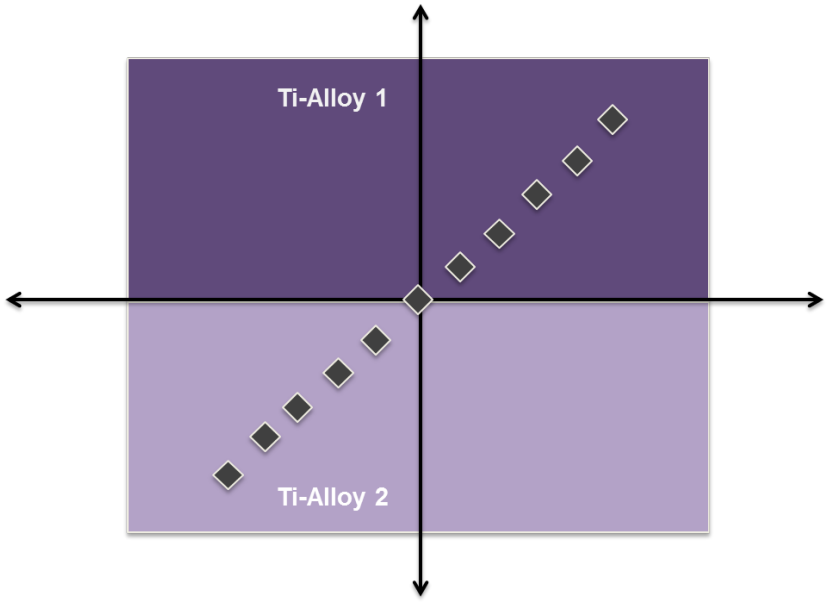

Figure 3.5-3: Layout of Hardness Measurement Positions

3.5.3.2 Surface Profile Measurements

The surface profile measurements were performed on Mahr Surface (Profilometer) Analysis System. All the measurements were obtained with a diamond stylus probe of radii 2.54 µm. Surface roughness parameters were evaluated based on a cut off length of 0.8 mm. The measurement length of the surface profile was approximately 3 to 3.5 mm. The width of the specimens allowed the measurement in the longitudinal direction only. The surface profile parameters were measured at three locations: the upper alloy, approximately on or near the bondline, and the lower alloy.

3.5.3.3 Flexural Test

The mechanical behavior of the parent titanium alloys and diffusion bonded titanium alloys was analyzed using flexural testing. The three point bend test was performed on *Instron* machine to gauge the mechanical strength of diffusion bonded specimens. Figure 3.4-4 illustrates the set up used to perform three point bend test of diffusion bonded joints. The specimen dimensions are provided in Table 3-8. Flexural properties such as modulus of elasticity, and ultimate stress were compared with the parent alloys.

Table 3-8 Specimen Dimensions in Three Point Bend Test

Batch	Support Span (mm)	Width (mm)	Thickness (mm)
1	50	8.619±2.441	1.87±0.228
2	50	13.134±0.221	3.964±1.122

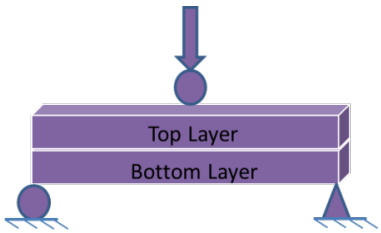

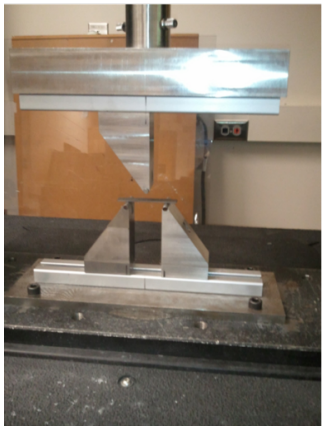

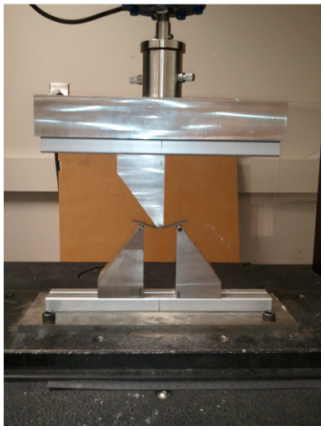

Fractured Thickness **Fractured Surface**

Figure 3.5-4**:** Diffusion Bonding: Flexure Test Set Up (Ti-54M/ Ti-54M Results)

3.6 FRICTION STIR WELDING OF DISSIMILAR TITANIUM ALLOYS

3.6.1 *Sample Preparation*

The friction stir welded similar and dissimilar titanium alloy samples were prepared in the Boeing facility. The viability of friction stir welding process was studied by varying the two parameters that control the quality of the process, mainly the spindle speed and the feed rate. The optimum conditions are necessary in order to produce good quality welded joints. Edward's [49] identified process parameters for Ti-6Al-4V and revealed titanium FSW process window for a certain range of tool design and thickness as shown in Figure 3.5-9.

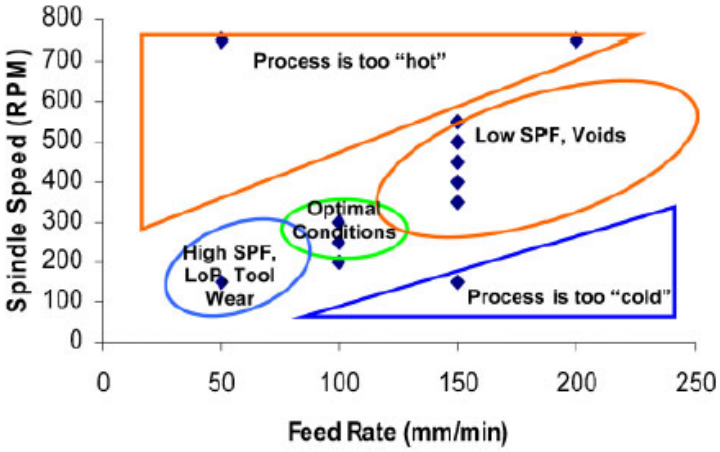

9 Schematic of FSW process window for SPF

Figure 3.6-9: Schematic of FSW Process window for SPF [49]

The conditions found in Edward's study of friction stir welding of Ti-6Al-4V were used to produce the friction stir welded joints of Ti-6Al-4V and other titanium alloys [49]. The spindle speed was changed from 225 RPM to 325 RPM. The travel rate was varied from 100 mm/min to 150 mm/min. Five combinations were made from the spindle speed and travel rate. The spindle speed was kept constant at 275 RPM and the travel rate was changed from 100 to 125, to 150 mm/min. For the travel rate of 125 mm/min three spindle speeds were present 225 RPM, 275 RPM and 325 RPM.

3.6.2 *Specimen List*

Three types titanium alloys were employed in the study that involved two ‘α+β’ types and one ‘Near-α’ type of titanium alloy. The ‘α+β’ type of alloys included Ti-5Al-4V-0.6Mo-0.4Fe Fine Grain (Ti-54MFG), and Ti-6Al-4V Standard Grain and Fine Grain (Ti-64SG, Ti-64FG) whereas the ‘Near-α’ type included Ti-6Al-2Sn-4Zr-2Mo. Standard Grain and Fine Grain (Ti-6242SG, Ti-6242FG). The alpha stabilizer, aluminum, is present in all the alloys. Ti-6Al-4V and Ti-6Al-2Sn-4Zr-2Mo have equal proportion of aluminum, while it is 5 % in Ti-5Al-4V-0.6Mo-0.4Fe. In Ti-6Al-4V, beta proportion is compensated by 4% vanadium. Ti-6Al-2Sn-4Zr-2Mo replaces 4V of Ti-6Al-4V with 2Mo, a strong beta stabilizer than former, and inserts neutral elements with this regard, tin and zirconium, for beta stability. Ti-5Al-4V-0.6Mo-0.4Fe has two beta stabilizers, 4% vanadium and 0.6 % molybdenum.

The above five titanium alloys were friction stir welded with each other to form five similar types and seven dissimilar types of combinations. Figure 3.5.1 represents the typical titanium alloy welded plate obtained through friction stir welding joints. The list of friction stir welded specimens is provided in Table 3-9. The thickness of the welded specimens was around 4.6 mm.

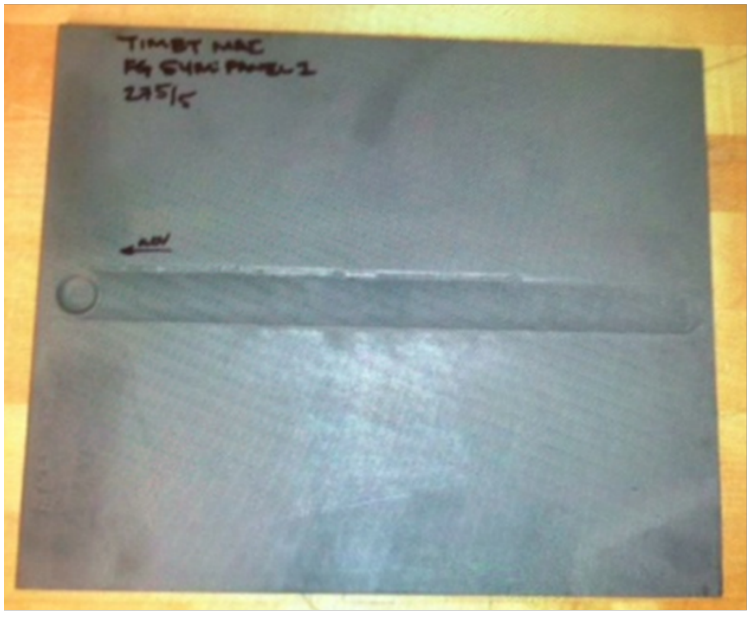

Figure 3.6-1: Typical Friction Stir Welded plate

Table 3-9**:** Friction Stir Welded Samples

S. No.	Titanium Alloy	Speed (rpm)/Feed Rate (mm/min)				
		Panel 1	*Panel 2*	*Panel 3*	*Panel 4*	*Panel 5*
1	Ti-54MFG/Ti-54MFG	275/125	275/150	325/125	275/100	225/125
2	Ti-64SG/ Ti-64SG	275/125	275/150	325/125	275/100	225/125
3	Ti-64FG/ Ti-64FG	275/125	275/150	325/125	275/100	225/125
4	Ti-6242SG/Ti-6242SG	275/125	275/150	325/125	275/100	225/125
5	Ti-6242FG/Ti-6242FG	275/125	275/150	325/125	275/100	225/125
6	Ti-54MFG/Ti-64SG	275/125	275/150	325/125	275/100	225/125
7	Ti-54MFG/Ti-6242SG	275/125	275/150	325/125	275/100	225/125
8	Ti-54MFG/ Ti-64FG	275/125	275/150	325/125	275/100	225/125
9	Ti-54MFG/Ti-6242FG	275/150	325/125	275/100	225/125	
10	Ti-64SG/Ti-6242SG	275/125	275/150	325/125	275/100	22512/5
11	Ti-64SG/Ti-6242FG	275/150	325/125	275/100	225/125	
12	Ti-64FG/Ti-6242FG	275/150	325/125	275/100	225/125	

3.6.2.1 Similar Titanium Alloys

Two types of titanium alloys: Near-α to Near-α (Ti-6242SG, Ti-6242FG) and α + β to α + β (Ti-54MFG, Ti-64SG, and Ti-64FG) were friction stir welded at different feed rate and travel speed to obtain five types of similar friction stir welded titanium joints as shown in Table 3-10.

Table 3-10 Similar FSW Titanium Joints with Alloy classification

Type of Ti-Alloy	Type of Ti-Alloy	Ti-Alloy/Ti-Alloy	Speed (rpm)/Feed Rate (mm/min)				
			275/125	275/150	325/125	275/100	225/125
Near-α	Near-α	Ti-6242SG/Ti-6242SG	✓	✓	✓	✓	✓
		Ti-6242FG/Ti-6242FG	✓	✓	✓	✓	✓
α + β	α + β	Ti-64SG/Ti-64SG	✓	✓	✓	✓	✓
		Ti-64FG/Ti-64FG	✓	✓	✓	✓	✓
		Ti-54MFG/Ti-54MFG	✓	✓	✓	✓	✓

3.6.2.2 Dissimilar Titanium Alloys

Seven combinations of dissimilar titanium joints were obtained by welding five Near-α to α + β titanium alloys and two α + β to α + β titanium alloys as shown in Table 3-11.

Table 3-11 Dissimilar FSW Titanium Joints with Alloy classification

Type of Ti-Alloy	Type of Ti-Alloy	Ti-Alloy/Ti-Alloy	Speed (rpm)/Feed Rate (mm/min)				
			275/125	275/150	325/125	275/100	225/125
Near-α	α + β	Ti-6242SG/ Ti-54MFG	✓	✓	✓	✓	✓
		Ti-6242SG/ Ti-64SG	✓	✓	✓	✓	✓
		Ti-6242FG/ Ti-64SG	✓	✓	✓	✓	
		Ti-6242FG/ Ti-64FG	✓	✓	✓	✓	
		Ti-6242FG/ Ti-54MFG	✓	✓	✓	✓	
α + β	α + β	Ti-54MFG/Ti-64SG	✓	✓	✓	✓	✓
		Ti-54MFG/Ti-64FG	✓	✓	✓	✓	✓

3.6.3 *Friction Stir Welding Experimental Work*

3.6.3.1 Tensile Test

Tensile tests were conducted at room temperature to determine the global stress strain behavior of welded joints. The tensile specimens were cut from welded plates using Abrasive Water Jet Machining. All the samples were cut transverse to the weld so that the weld was in the center of the tensile specimens gage length. Four tensile coupons were obtained per plate (Figure 3.5.2 (a)). The dimension of the tensile test specimen per ASTM E-8 is shown in Figure 3.5.2 (b). Two tensile coupons from the four samples obtained from the plate of friction stir welded titanium alloys were tested on a 250 kN capacity 5585 Instron Load Frame. The tensile tests were conducted under displacement control at a constant cross head extension speed of 1.27 mm/min. Every sample was tested to failure. A load cell built into the load frame monitored the load data. The axial strain data was examined by a video extensometer. The gage length of 50 mm was monitored to collect the axial strain data. Through a data acquisition system, plots of engineering stress vs. engineering strain are produced in addition to calculating Elastic modulus; yield strength at

0.2% strain, tensile strength, and elongation. Figure 3.5.3 shows the experimental set up used during tensile testing. There was not much scatter present in the stress-strain data of two samples of each specimen; therefore the testing was limited to two tensile coupons.

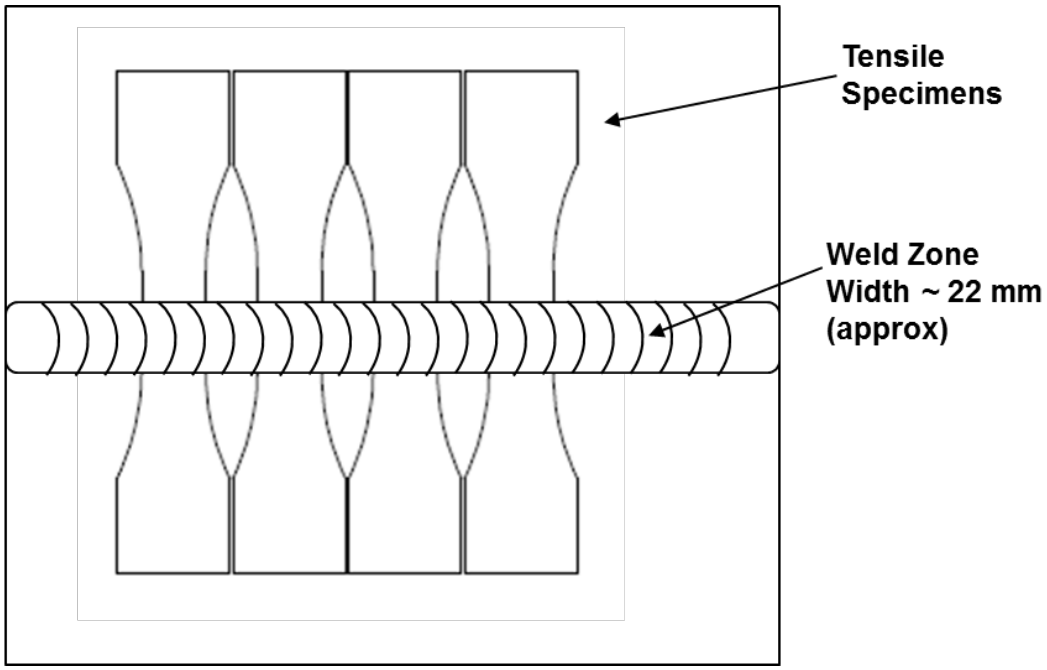

(a)

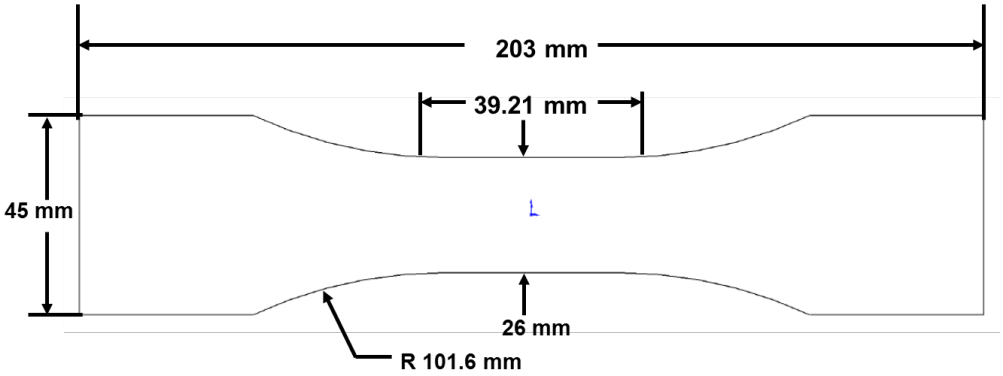

(b)

Figure 3.6-2: (a) Layout of machining tensile coupons (b) Tensile Specimen Dimensions

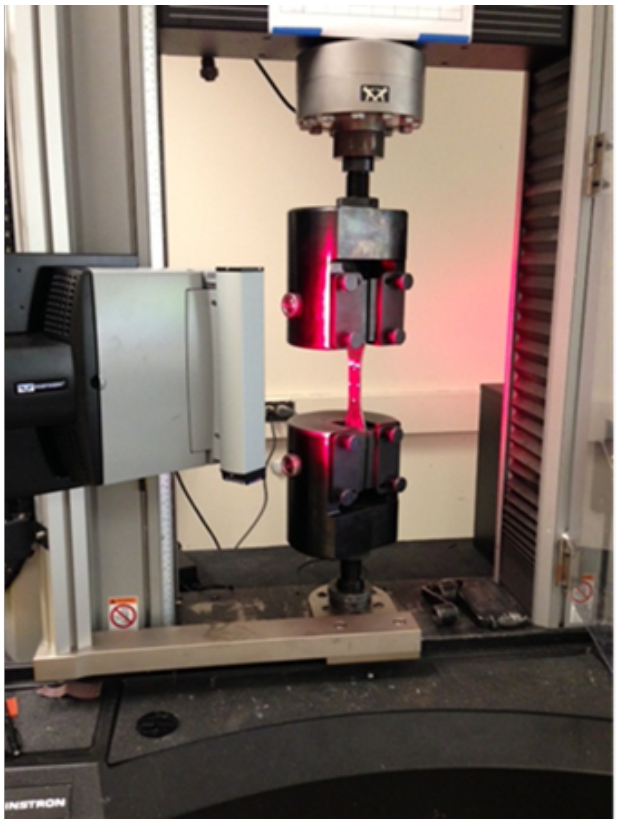

Figure 3.6-3: Tensile Test Experimental Set up

Table 3-12: Tensile Test Specimen Dimensions

Thickness	4.5 ± 0.6mm
Width	25.48 ± 0.8mm
Gauge Length	50 mm
Strain Rate	1.27mm/min

3.6.3.2 Surface Profile measurements

The surface profile measurements were performed on *Mahr Surface Profilometer Analysis* System. All the measurements were obtained with a diamond stylus probe of radii 2.54µm. Surface roughness parameters were evaluated based on a cut off length of 0.8mm. The measurement length of the surface profile was approximately 3 to 3.5mm. Six measurements were obtained for each of the alloy. Three measurements were made along

the transverse direction of the welded plate and the other three were made in the longitudinal direction. Figure 3.5-4 below represents the direction on the welded plate. The three measurements in both the cases included one in the welded region and the other two on the either side of the welded region (the two alloys).

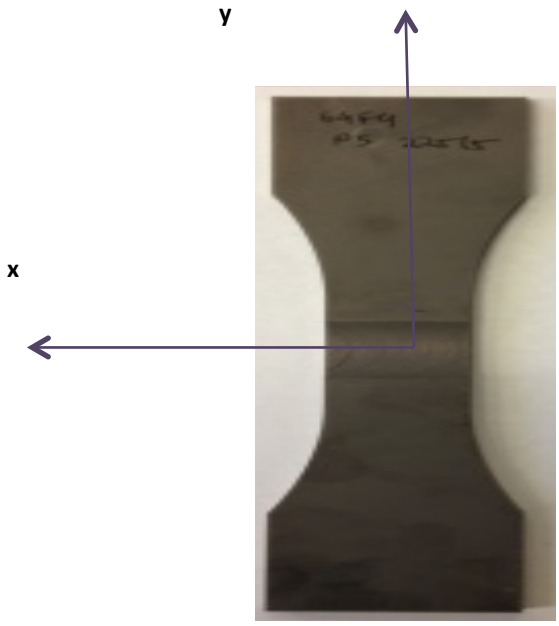

Figure 3.6-4: Friction Stir Welding: Profile Measurement Direction- x: Transverse and y: Longitudinal

Chapter 4. EXPERIMENTAL RESULTS

4.1 INTRODUCTION

The chapter four presents the results of titanium joints obtained from diffusion bonding and friction stir welding processes. At the beginning of the chapter the results of diffusion bonded joints are discussed followed by the friction stir welding results. The section 4.2 highlights the experimental results of quality assessment of diffusion bonded similar and as well as dissimilar titanium joints. The results of the microstructures, hardness testing, surface roughness, and flexure testing are discussed in the section 4.2. The succeeding sections discuss the results on friction stir welded titanium joints. Section 4.3 highlights the experimental work on strength valuation of similar and dissimilar welded titanium joints.

4.2 DIFFUSION BONDING OF SIMILIAR AND DISSIMILAR TTIANIUM JOINTS QUALITY ANALYSIS

4.2.1 *Microstructures*

The microstructures of diffusion bonded titanium alloys are shown below. Figure 4.2-1 shows the microstructures of some of the diffusion bonded titanium alloys. It was observed that good quality of diffusion bonding was achieved in the temperature range of $T5^0C$ to $T8^0C$. In Ti-64SG/Ti-64SG a good quality of bonding was obtained at all temperatures. There was a visible mismatch between microstructures across the bond line at lower temperatures. This mismatch decreased with the increase in temperature and fully homogenized microstructure was obtained at $T8^0C$. In Ti-64FG/Ti-64FG the bonding quality obtained at interface was not good for the experimental conditions. The bond line was visibly thick at the interface. Among all the temperatures, thinner bond line was obtained at $T4^0C$. In Ti-54M/Ti-54M good parent-parent joining could not be obtained in Ti-54M/Ti-54M within the temperature range $T1^0C$ to $T8^0C$. The bond line was visible for most of the temperatures. In the temperature range, comparatively good quality joints were obtained at $T5^0C$ and $T1^0C$. In the middle range of temperature, a visibly thick bond line

was observed. However, the thickness of bond line at the interface in the middle range of temperature decreased, as the temperature was increased. Table 4-1 shows the quality of similar and dissimilar titanium joints obtained through diffusion bonding.

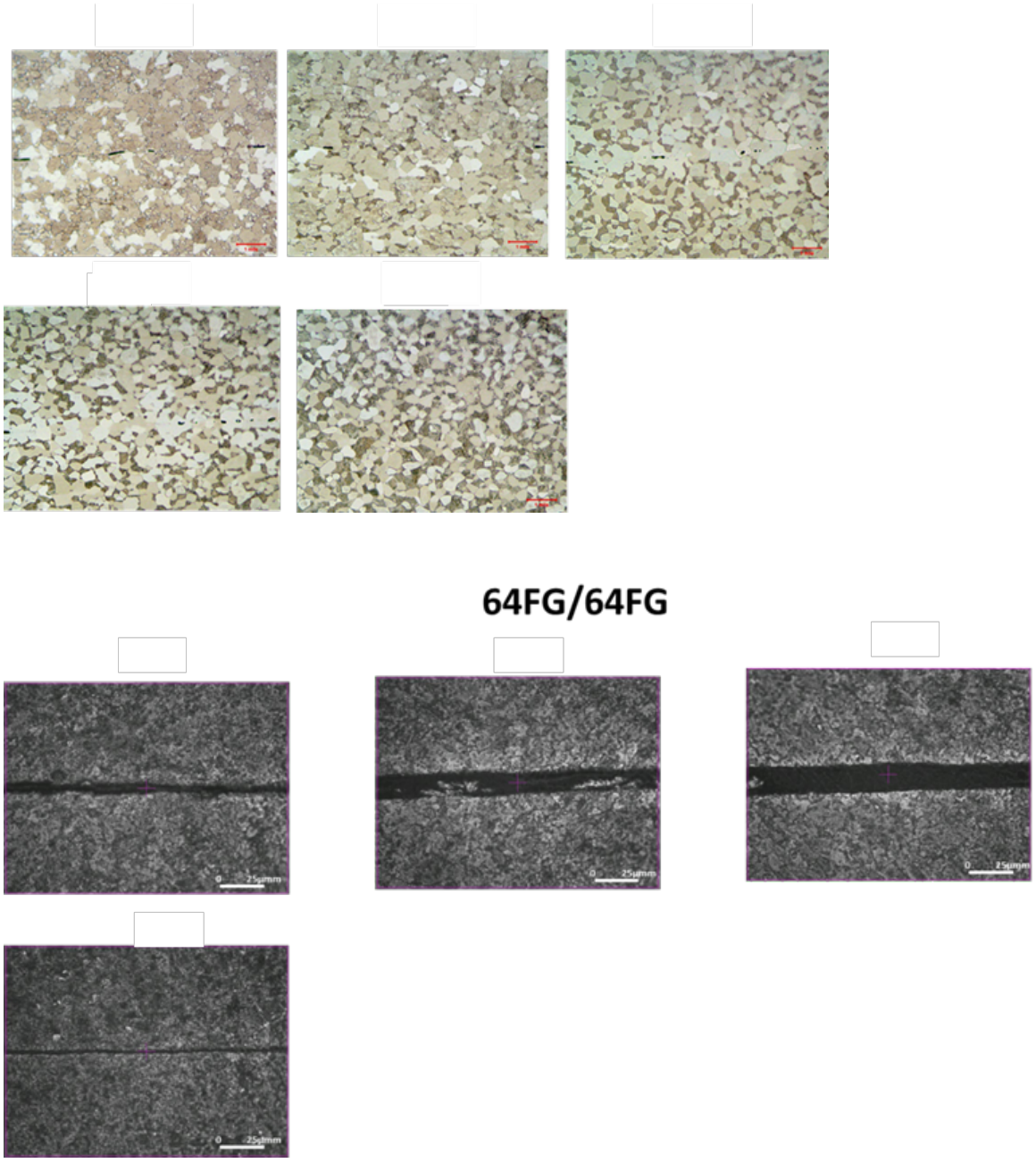

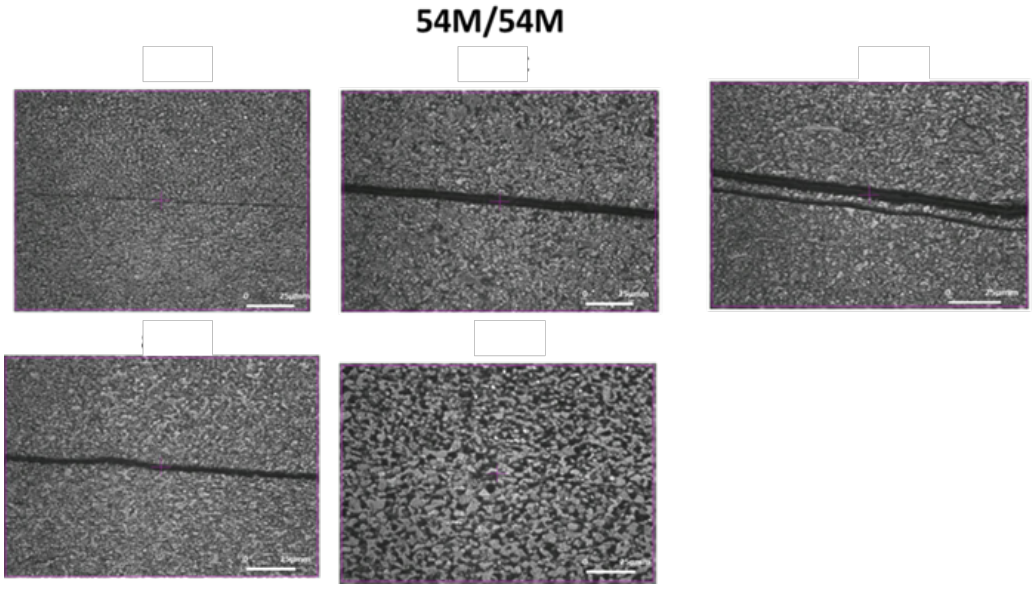

Figure 4.2-1: Microstructure of diffusion bonded Ti-64SG/Ti-64SG, Ti-64FG/Ti-64FG, and Ti-54M/Ti-54M in the increasing order of temperature

Table 4-1: Diffusion Bonding Quality for Ti -Alloys (Red: Not good bonding quality, Yellow: Moderate Quality)

Ti Alloy	Temperature (Celsius)							
	T1	**T2**	**T3**	**T4**	**T5**	**T6**	**T7**	**T8**
64/64				64/64	64/64	64/64	64/64	64/64
6242/ 6242					6242/ 6242	6242/ 6242	6242/ 6242	6242/ 6242
21S/ 21S	21S/ 21S	21S/ 21S			21S/ 21S	21S/ 21S	21S/ 21S	21S/ 21S
54M/ 54M	54M/ 54M	54M/ 54M	54M/ 54M	54M/ 54M	54M/ 54M			
64FG/ 64FG	64FG/64 FG	64FG/6 4FG	64FG/6 4FG	64FG/6 4FG	64FG/64 FG			
64/ 6242				64/ 6242	64/ 6242	64/ 6242	64/ 6242	64/ 6242
64/21S				64/21S	64/21S	64/21S	64/21S	64/21S
64/ 54M	64/ 54M	64/ 54M	64/ 54M	64/ 54M	64/ 54M	64/ 54M	64/ 54M	
6242/ 54M	6242/ 54M	6242/ 54M	6242/ 54M	6242/ 54M	6242/ 54M	6242/ 54M	6242/ 54M	
64/ 64FG	64/ 64FG	64/ 64FG	64/ 64FG	64/ 64FG	64/ 64FG			
64FG/ 54M	64FG/ 54M	64FG/ 54M	64FG/ 54M	64FG/ 54M	64FG/ 54M			
6242/ 21S					6242/ 21S	6242/ 21S	6242/ 21S	6242/ 21S
6242/ 64FG	6242/ 64FG	6242/ 64FG	6242/ 64FG	6242/ 64FG	6242/ 64FG			
21S / 54M	21S / 54M	21S /54M	21S / 54M	21S / 54M	21S /54M	21S / 54M	21S /54M	
21S / 64FG	21S / 64FG	21S/ 64FG	21S / 64FG	21S /64FG	21S / 64FG			

Good/ Total	**2/10**	**2/10**	**1/9**	**7/11**	**10/15**	**9/9**	**7/9**	**4/6**

4.2.2 *Hardness Results*

This section shows the hardness results of diffusion bonded Ti-alloys. The hardness measurements made at eleven locations (the first five in one of the Ti-alloy, sixth at the bondline and the remaining five in the other alloy) in the diffusion bonded Ti-alloys are plotted as a function of temperature. Figure 4.2-2 and 4.2-3 show the cases of parent and bondline hardness measurements for good and not so good quality bonded joints. In addition to this, the hardness at the bondline interface of each diffusion bonded Ti-alloy is plotted with respect to the temperature. More specifically the hardness near the bonded region and in the parent regions was studied to understand the hardness distribution in the similar and the dismiliar titanium alloys. The hardness results are divided into two sections, similar titanium alloys and into dissimilar titanium alloys. In the Figures of hardness distribution of dissimilar titanium joints, the hardness distribution of the dissimilar joint is as per the title of joint in the diagram. (For eg: In case of dissimilar joint Ti-6242/Ti-54M- the title of hardness distribution is 6242/54M, then the left hand side '6242' denotes the hardness distribution of Ti-6242 region, while the right hand side denotes that of Ti-54M region). For all the diffusion bonded Ti-joints, the bondline hardness was compared with the most popular and widely used alloys, Ti-64 and Ti-6242 (Table 4.2). The cases of good quality diffusion bonded joints were adopted to understand the effect of temperature on the hardness results.

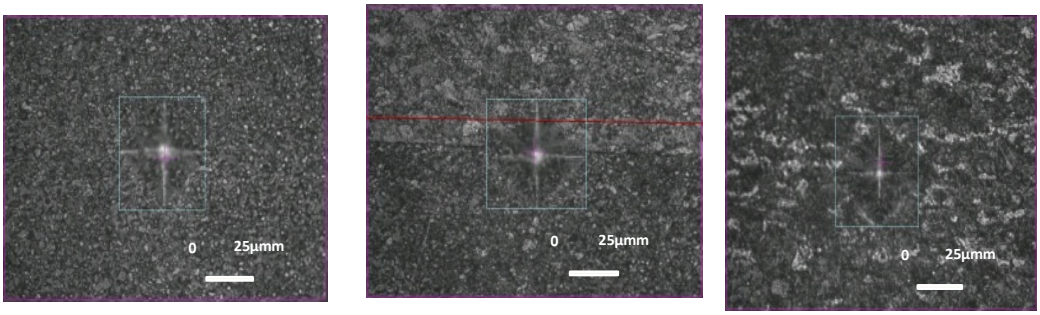

Figure 4.2-2: Hardness indent measurements with good quality bond interface: Ti-64SG/ Ti-54M (T=T4^{0}C, Ti-54M on left, Ti-64SG on right)

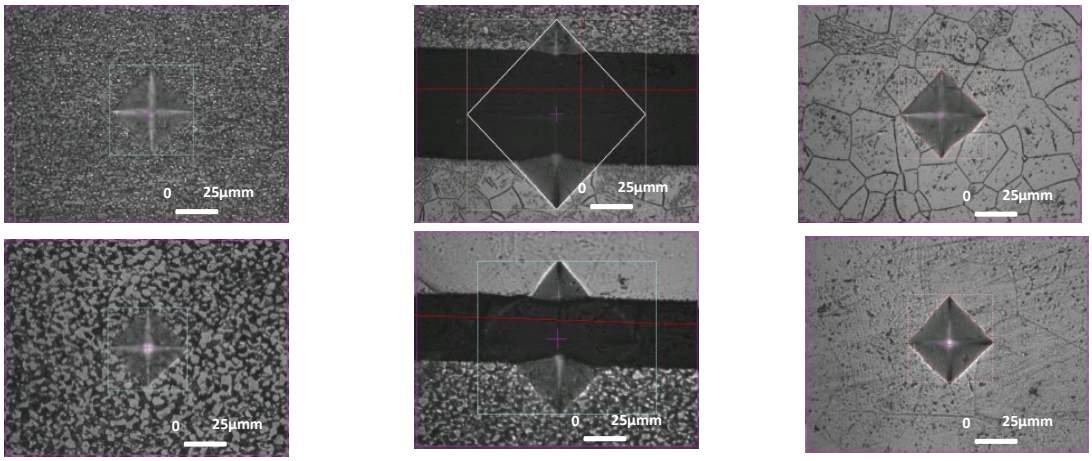

Figure 4.2-3: Hardness indent measurements when thick bondline is present: β-21S / Ti-54M (T=T2^{0}C and T4^{0}C, Ti-54M on left; Beta 21S on right)

4.2.2.1 Hardness Results – DB Similar Titanium Alloys

4.2.2.1.1 Near-α to Near-α Similar Ti-Alloys

In near-α to near-α similar diffusion bonded titanium alloy, Ti-6242/ Ti-6242, the bondline hardness increased with the increase in temperature. There was no much significant change in the hardness between the parent and the bonded region at higher temperatures.

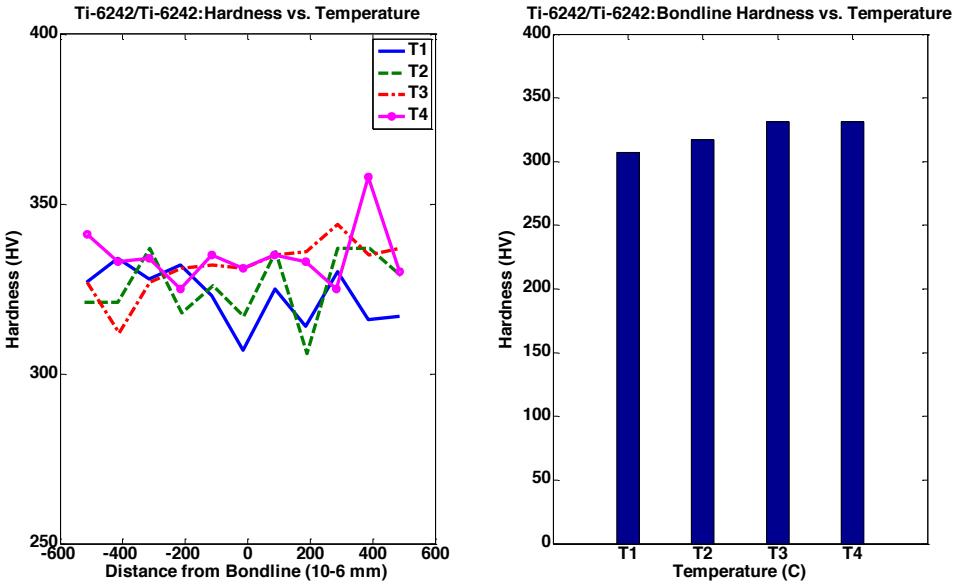

Figure 4.2-4: Hardness Distribution and Bondline Hardness of DB Similar Near-α Ti-Alloys (Ti-6242/Ti-6242) with respect to temperature

4.2.2.1.2 α + β to α + β Similar Ti-Alloys

In the α + β to α + β diffusion bonded titanium alloys, Ti-54M/Ti-54M and Ti-64FG/Ti-64FG, hardness decreased at the bondline with respect to parent region, while in Ti-64SG/Ti-64SG the bondline hardness increased with respect to parent region. In Ti-54M/ Ti-54M the hardness across the bonded region mostly increased with the temperature.

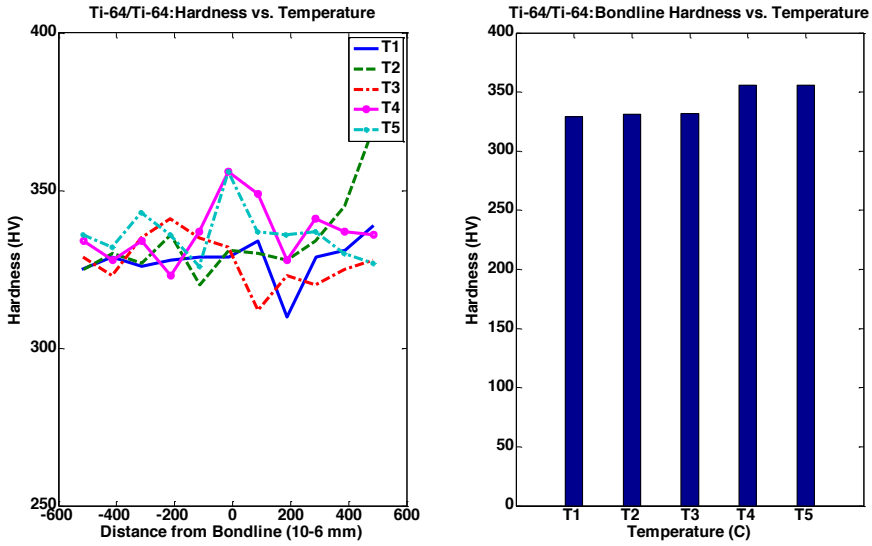

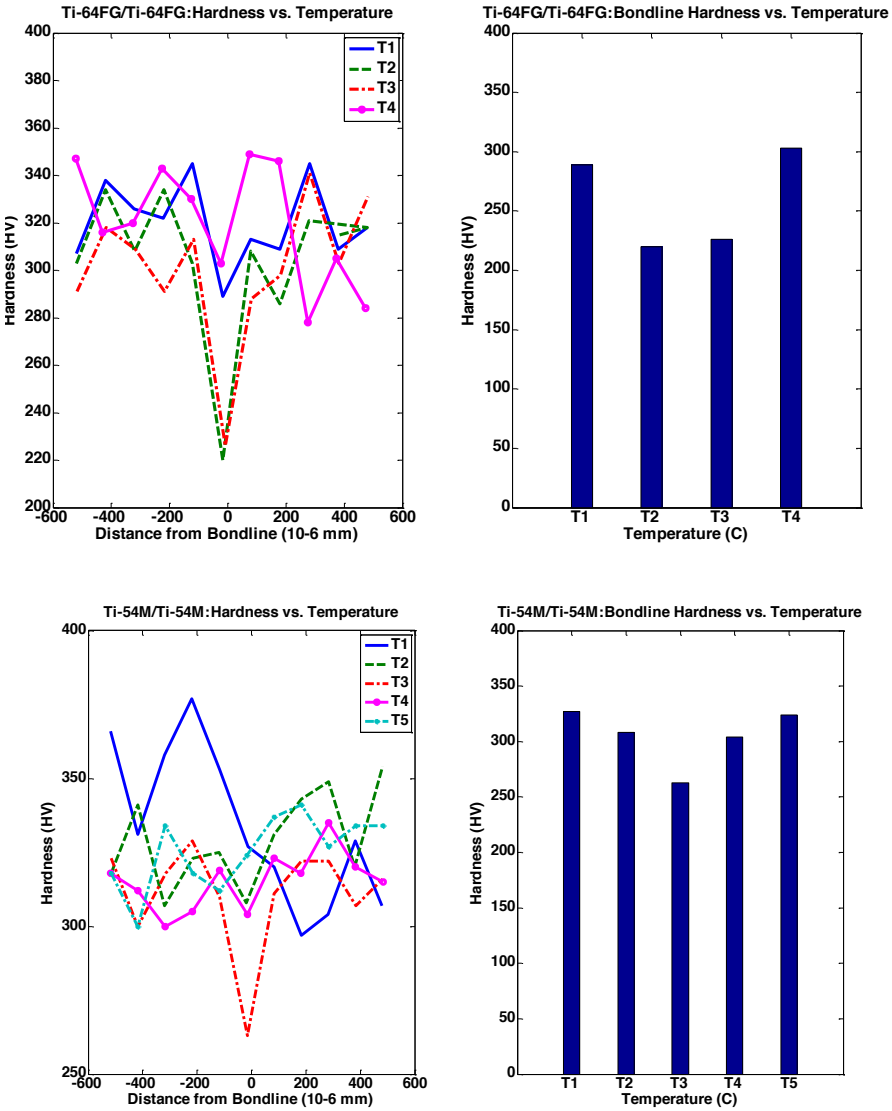

Figure 4.2-5: Hardness Distribution and Bondline Hardness of DB Similar α + β Ti-Alloys (Ti-64SG/Ti-64SG, Ti-64FG/Ti-64FG and Ti-54M/Ti-54M) with respect to temperature

4.2.2.1.3 β to β Similar Ti-Alloys

In β-21S/ β-21S diffusion bonded titanium alloys the hardness distribution was found mostly unaffected by temperature. There was no much change in the hardness across the bond and the parent material region.

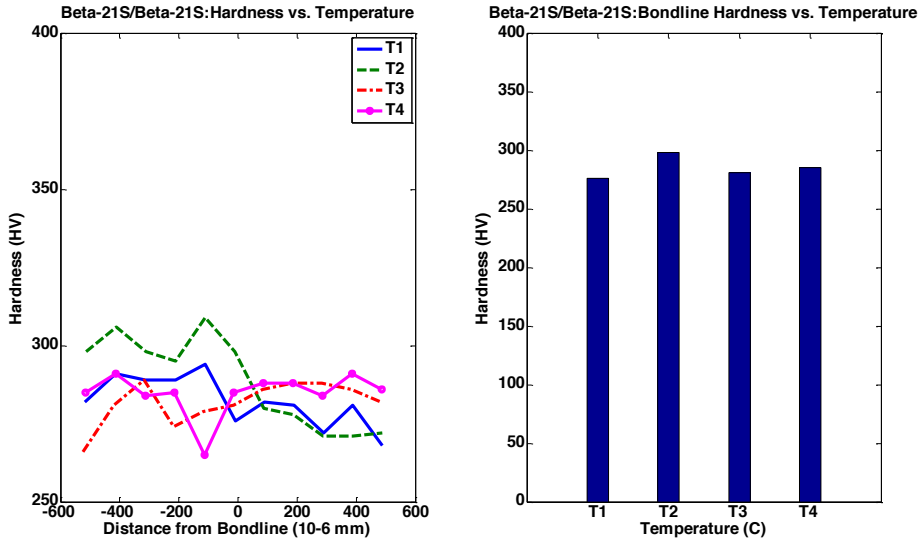

Figure 4.2-6: Hardness distribution and Bondline Hardness of DB Similar β Ti-Alloys (β-21S/ β-21S) with respect to temperature

4.2.2.2 Hardness Results – DB Dissimilar Titanium Alloys

4.2.2.2.1 Near α to α + β Dissimilar Titanium Alloys

In α to α + β dissimilar titanium alloy, Ti-6242/Ti-54M, the hardness in Ti-6242 region was higher than the hardness observed in Ti-54M region. The bondline hardness was close to the hardness observed in Ti-6242 region. The bondline hardness mostly increased with the increase in the diffusion bonding temperature. In Ti-6242/Ti-64 the bondline hardness increased with the increase in the diffusion bonding temperature. The hardness in the Ti-64 region was higher than the hardness in the Ti-6242 region. The bondline hardness was observed close to the hardness observed in the Ti-6242 region. In Ti-6242/Ti-64FG the hardness in Ti-64FG region is slightly higher than the hardness observed in the Ti-6242 region. At $T4^0C$, there is not much change in the hardness distribution across both the parent alloys including the bondline hardness.

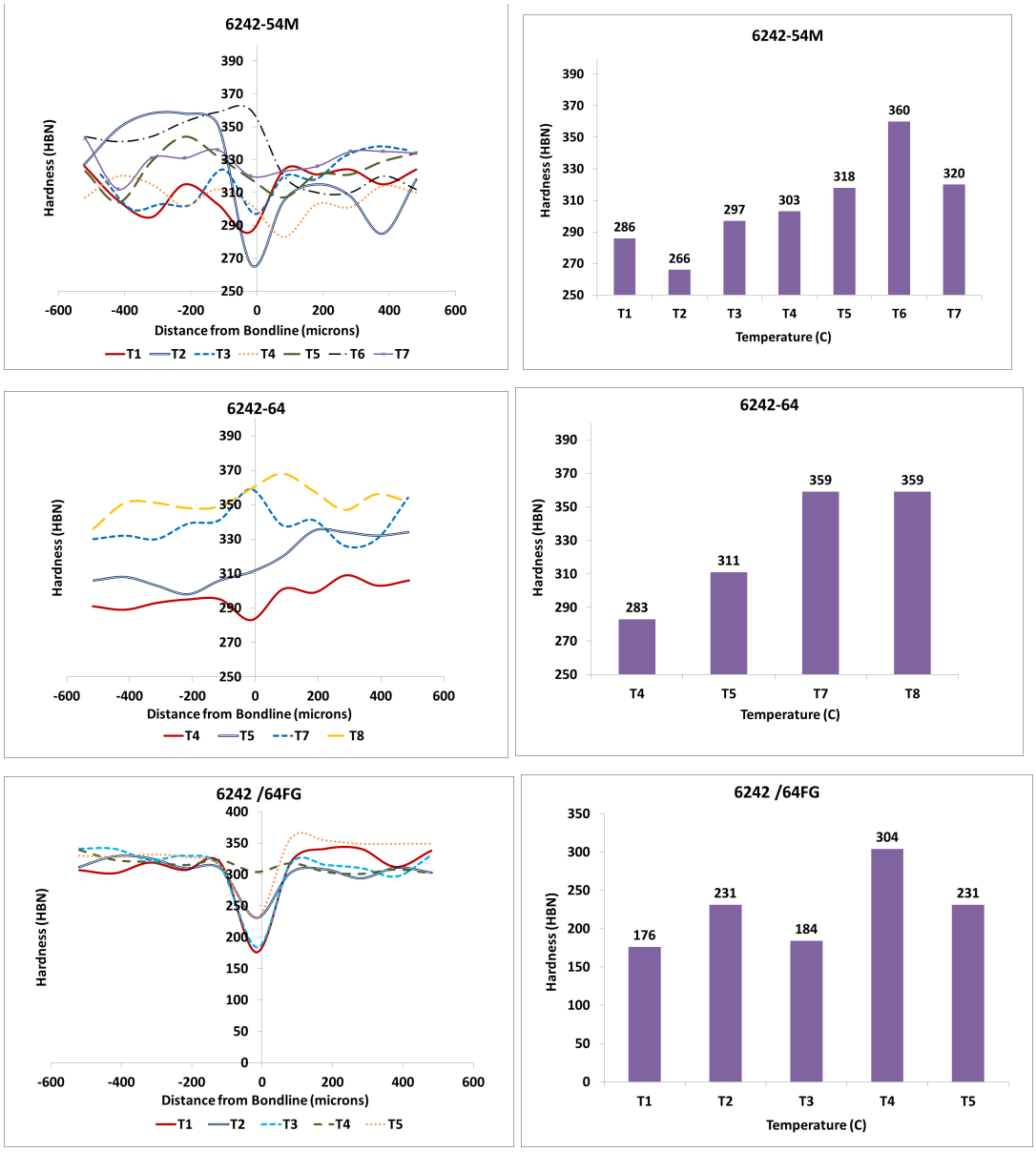

Figure 4.2-7: Hardness Distribution and Bondline Hardness of Near α to α + β DB Dissimilar Ti- Alloys (Ti-6242/ Ti-54M and Ti-6242/Ti-64SG, and Ti-6242SG/Ti-64FG) with respect to temperature

4.2.2.2.2 Near-α to β Dissimilar Titanium Alloys

In Ti-6242/ β-21S the bondline hardness increased with the increase in the temperature. In most of the cases the hardness in the β-21S region was higher than the hardness in the Ti-6242 region. The bondline hardness was close to the hardness in the β-21S region.

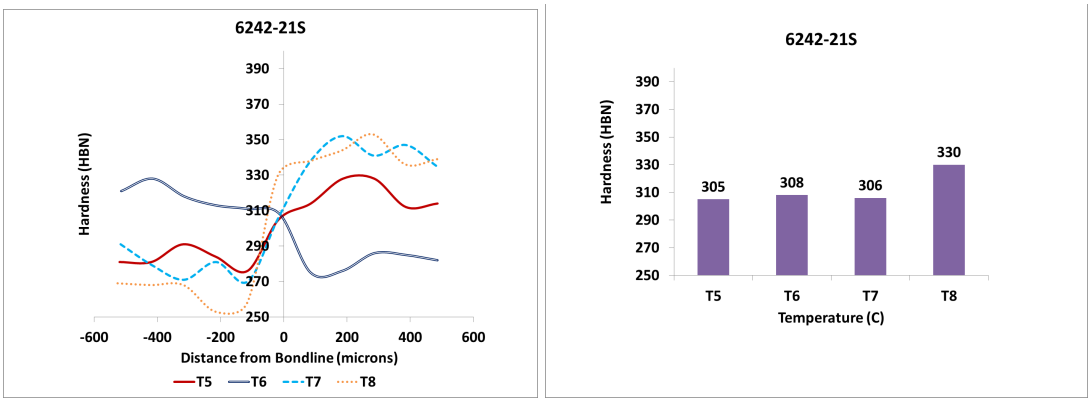

Figure 4.2-8: Hardness Distribution and Bondline Hardness of Near α to β Dissimilar DB Ti-Alloys (Ti-6242/β-21S) with respect to temperature

4.2.2.2.3 α + β to α + β Dissimilar Titanium Alloys

In Ti-64SG/Ti-54M the hardness in the Ti-54M region was higher than the hardness in the Ti-64SG region. The bondline hardness was closer to the hardness in the Ti-64SG region. Though the bondline hardness did not affect much with respect to the temperature, the highest bondline hardness was observed at T7^{0}C. In Ti-64FG/Ti-54M the hardness in the parent region Ti-54M was slightly higher than the hardness in the parent regionTi-64FG. The bondline hardness was lower than the hardness in both of the parent region, Ti-54M and Ti-64FG. The increase in temperature resulted in increase in the hardness at the bonded interface. In Ti-64SG/Ti-64FG most of the cases the hardness in the Ti-64 region was higher than the hardness in the Ti-64FG region. At T5^{0}C, the hardness in the Ti-64FG region is higher than the hardness in the Ti-64 region. The bondline hardness was close to the parent alloy of higher hardness value. There was slight increase in the bondline hardness with the increase in the diffusion bonding temperature.

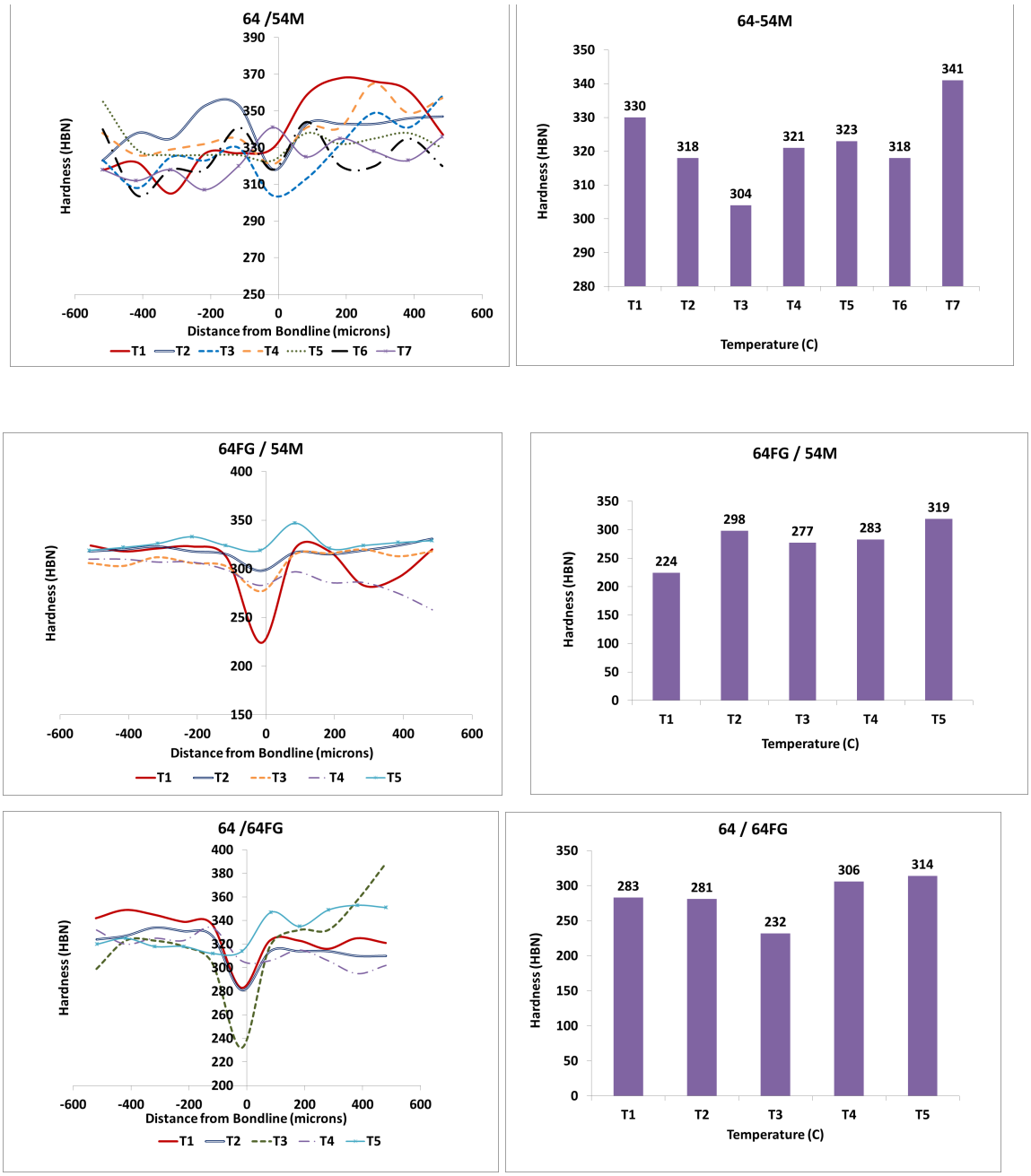

Figure 4.2-9: Hardness Distribution and Bondline Hardness of α + β to α + β DB Dissimilar Ti-Alloys (Ti-64SG/ Ti-54M, Ti-64FG/Ti-54M, and Ti-64/Ti-64FG) with respect to temperature

4.2.2.2.4 α + β to β Dissimilar Titanium Alloys

In α + β to β dissimilar titanium alloy, β-21S /Ti-54M, the hardness in β-21S region was higher than the hardness in the Ti-54M region. The bondline hardness value was close to

the parent alloy β-21S. There was not much effect of temperature on the hardness distribution across the bonded region. In β-21S /Ti-64 most of the cases, the hardness in the Ti-64 region was higher than the hardness in β-21S region. The hardness across the bonded region in the dissimilar Ti- alloy, β-21S-Ti-64, was closer to the Ti-64 region. There was slight increase in the bondline hardness with the increase in the diffusion bonding temperature. In β-21S /Ti-64FG - Batch 1 the hardness in the β-21S region was higher than the hardness in the Ti-64FG region. The hardness values across the bonded region increased with the increase in temperature.

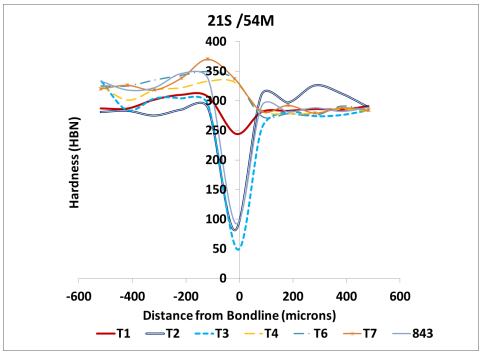

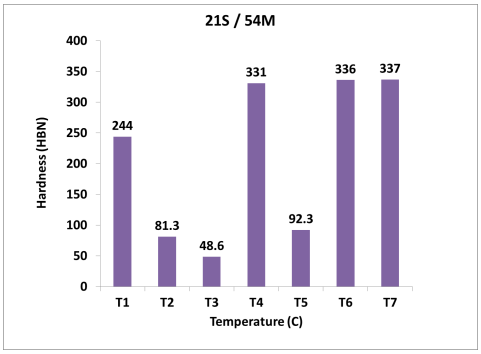

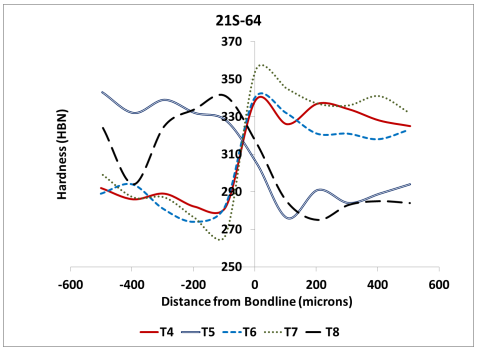

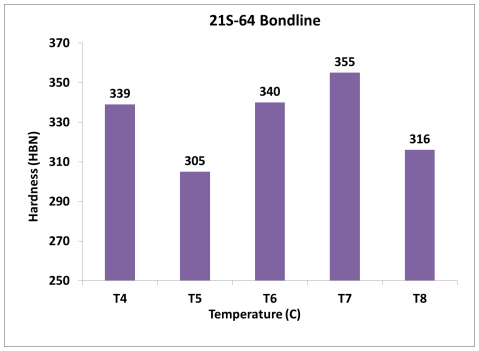

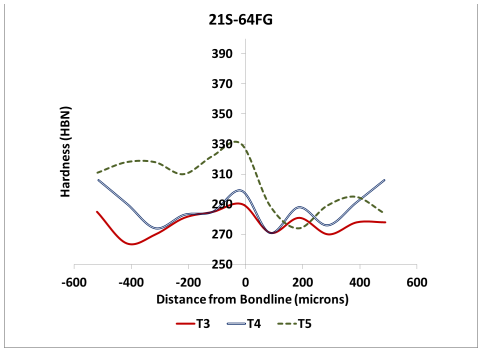

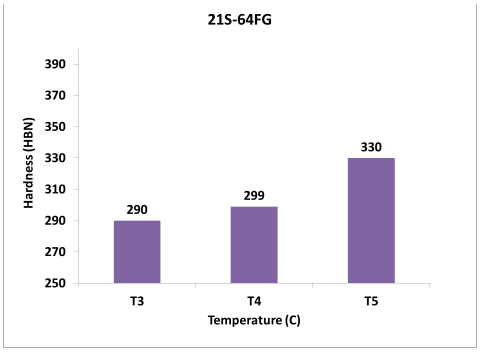

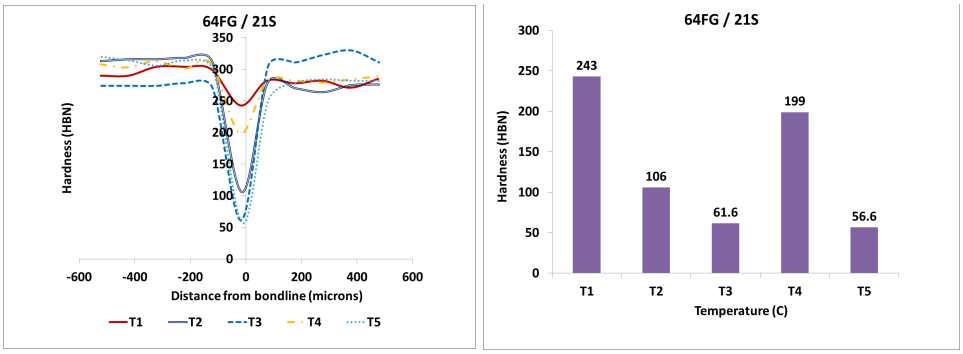

Figure 4.2-10: Hardness Distribution and Bondline Hardness of DB α + β to β Dissimilar Ti-Alloys (β-21S/Ti-54M, β-21S /Ti-64SG, and β-21S /Ti-64FG Batch 1 and 2) with respect to temperature

4.2.2.3 Comparison of Bondline Hardness of Diffusion bonded Ti-Alloy joints with Ti-64 and Ti-6242 Hardness

The bondline hardness of diffusion bonded Ti- Alloy joints was compared with the Vickers hardness of Ti-64 (~349 HBN) and Ti-6242(~333HBN) respectively. The increase and the decrease in the hardness with respect to these two parent alloys are shown in the Table 4.2-2. The diffusion bonded joints of Ti-64SG /Ti-64SG showed increase in the hardness of the joint with respect to the parent alloy hardness. The dissimilar combination of Ti-64SG/ Ti-6242SG also showed the similar observation. The bondline hardness as close to 80 % of Ti-64 was achieved with the diffusion bonding process.

Table 4-2: Comparison of Bondline Hardness of Diffusion bonded Ti-Alloy joints with Ti-64 and Ti-6242 Hardness

Ti Alloy	**Temperature (Celsius)**							
	T1	**T2**	**T3**	**T4**	**T5**	**T6**	**T7**	**T8**
β-21S/β-21S					281	285	286	282
wrto Ti-64					**-19.5**	**-18.3**	**-18.1**	**-19.2**
Ti-54M/Ti-54M	327	308	263	304	324			
wrto Ti-64	-6.3				**-7.2**			
Ti-64/Ti-64				329	331	332	356	356
wrto Ti-64				**-5.7**	**-5.2**	**-4.9**	**2.0**	**2.0**
Ti-64FG/Ti64FG	289	220	226	303				

wrto Ti-64				**-13.2**				
Ti-6242/Ti-6242					307	317	331	331
wrto Ti-64					**-12.0**	**-9.2**	**-5.2**	**-5.2**
wrto Ti-6242					**-7.8**	**-4.8**	**-0.6**	**-0.6**
β-21S / Ti-54M	244	81.3	48.6	331	92.3	336	337	
wrto Ti-64				**-5.2**		**-3.7**		
Ti-64/ β-21S				339	305	340	355	316
wrto Ti-64				**-2.9**	**-12.6**	**-2.6**	**1.7**	
β-21S /Ti-64FG (B1)			290	299	330			
wrto Ti-64			**-16.9**	**-14.3**	**-5.4**			
β-21S /Ti-64FG (B2)	243	106	61.6	199	56.6			
wrto Ti-64	**-30.4**							
Ti-6242/ β-21S					305	308	306	330
wrto Ti-64					**-12.6**	**-11.7**	**-12.3**	
wrto Ti-6242					**-8.4**	**-7.5**	**-8.1**	
Ti-64/Ti-54M	330	318	304	321	323	318	341	
wrto Ti-64	**-5.4**	**-8.9**	**-12.9**	**-8.0**	**-7.4**	**-8.9**		
Ti-64FG/Ti-54M	224	298	277	283	319			
wrto Ti-64		**-14.6**			**-8.6**			
Ti-54M/Ti-6242	286	266	297	303	318	360	320	
wrto Ti-64	**-18.1**			**-13.2**	**-8.9**	**3.2**	**-8.3**	
wrto Ti-6242	**-14.1**			**-9.0**	**-4.5**	**8.1**	**-3.9**	
Ti-64/Ti-64FG	283	281	232	306	314			
wrto Ti-64				**-12.3**	**-10.0**			
Ti-64/Ti-6242				283	311		359	359
wrto Ti-64				**-18.9**	**-10.9**		**2.9**	**2.9**
wrto Ti-6242				**-15.0**	**-6.6**		**7.8**	**7.8**
Ti-6242/Ti-64FG	176	231	184	304	231			
wrto Ti-64				**-12.9**				
wrto Ti-6242				**-8.7**				

4.2.2.4 Effect of Temperature on Hardness in DB Similar and Dissimilar Ti-Joints

The hardness of good quality joints obtained with diffusion bonding process was plotted with respect to temperature in Figure 4.2-11. It includes both the similar and dissimilar titanium joints at different temperatures. It can be seen that the hardness varies linearly with respect to temperature. In most of the cases, increase in hardness is observed with the

increase in temperature. Table 4-3 defines the linear equation of hardness as a function of temperature with their corresponding regression values.

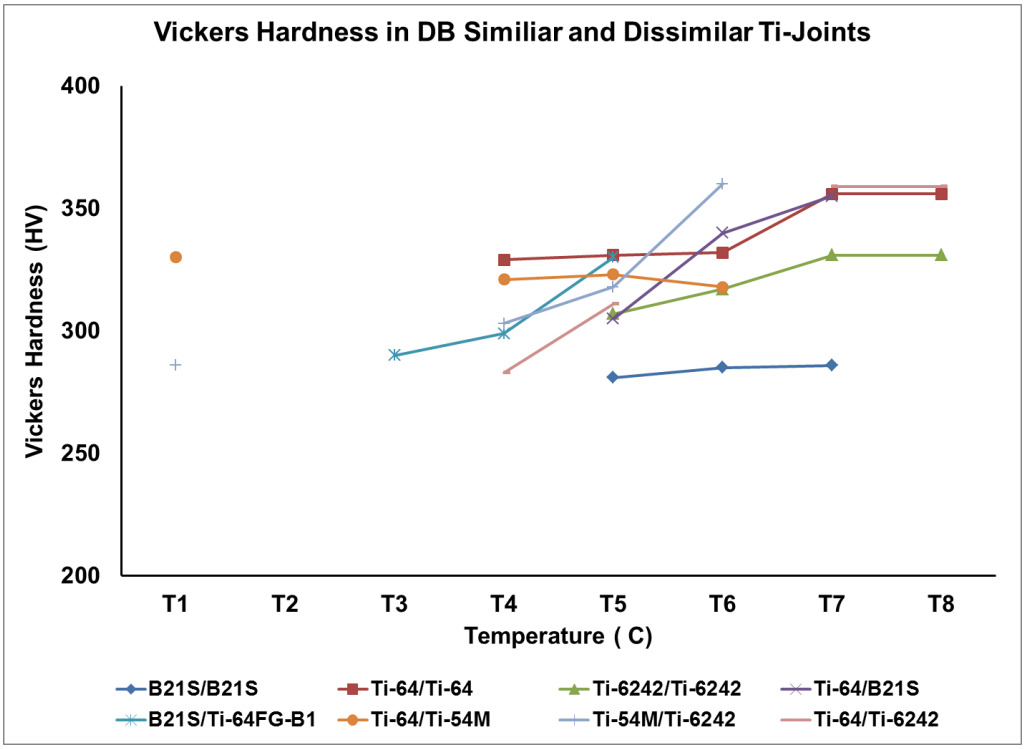

Figure 4.2-11: Effect of Temperature on Hardness in DB Similar and Dissimilar Ti-Joints

Table 4-3: of Hardness in Similar and Dissimilar DB Ti-Joints as function of temperature

Ti-Alloy	Linear Equation	Regression Value
B21S/B21S	y = 0.0893x + 206.23	R^2 = 0.8929
Ti-64/Ti-64	y = 0.2847x + 92.791	R^2 = 0.8084
Ti-6242/Ti-6242	y = 0.3071x + 49.679	R^2 = 0.8998
Ti-64/B21S	y = 0.8929x - 370.24	R^2 = 0.9494
B21S/Ti-64FG-B1	y = 0.7143x - 236.52	R^2 = 0.9084
Ti-64/Ti-54M	y = -0.0798x + 388.11	R^2 = 0.8834
Ti-54M/Ti-6242	y = 0.4622x - 60.142	R^2 = 0.7678
Ti-64/Ti-6242	y = 0.7187x - 298.21	R^2 = 0.9425

4.2.3 *Surface Roughness Results*

The surface roughness measurements were performed on the diffusion bonded titanium alloys near the bondline and in the parent alloy region. Surface roughness was assessed by examination of the effectiveness of average surface parameter Ra, arithmetic average roughness, Rz, ten point height; average distance between the five peaks and five deepest valleys and RSm, Mean value of the profile element width within a sampling length. The arithmetic average of the absolute values 'Ra' provided good measure of the microscopic peaks and valleys of the surface [66]. Table 4.4 displays the surface roughness of parent alloys measured in the longitudinal and the transverse direction. Figure 4.2-12 shows the surface roughness profile of Ti-64SG in the transverse and the longitudinal direction. In the following section the surface roughness parameter, 'Ra', as a function of temperature is plotted for the diffusion bonded titanium alloys. In these figures, 'BD' denotes the surface roughness value obtained at the bondline interface for the diffusion bonded titanium alloys.

Table 4-4**:** Surface Roughness measurements of Parent Alloys

	Ra (µm)		**Rz (µm)**		**RSm (µm)**	
Ti- Alloy	Longitudinal	Transverse	Longitudinal	Transverse	Longitudinal	Transverse
Ti-64	1.28	1.42	8.92	10.13	26.48	35.61
Ti-64 FG	1.16	1.30	6.12	8.99	20.06	30.11
Ti-6242	0.83	0.81	5.38	5.74	21.64	24.00
Ti-6242 FG	0.99	0.65	7.07	3.91	34.91	17.78
Ti-54M	1.74	1.88	10.89	13.87	27.17	44.82

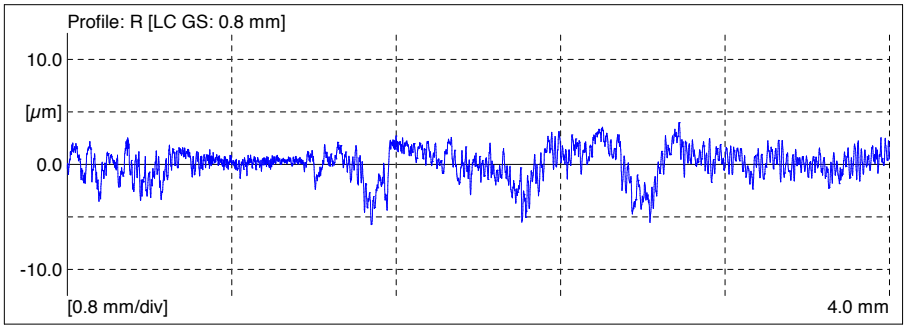

Transverse Direction

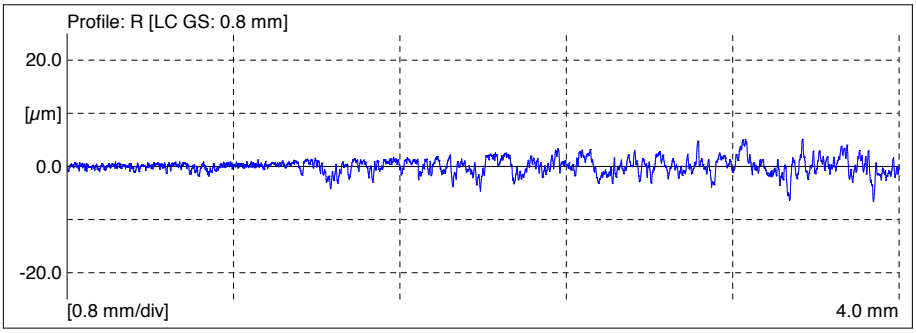

Longitudinal Direction

Figure 4.2-12**:** Surface Profile of Ti-64SG in Transverse and Longitudinal direction

4.2.3.1 Surface Roughness Results– DB Similar Titanium Alloys

4.2.3.1.1 Near-α to Near-α Similar Ti-Alloys

In Ti-6242/ Ti-6242 the surface roughness value of 'Ra' did not change across the bondline and in both of the parent regions with respect to the temperature except at T7^{0}C. The good quality diffusion bonding of Ti-6242/Ti-6242 was evident in the surface roughness results (Figure 4.2-13).

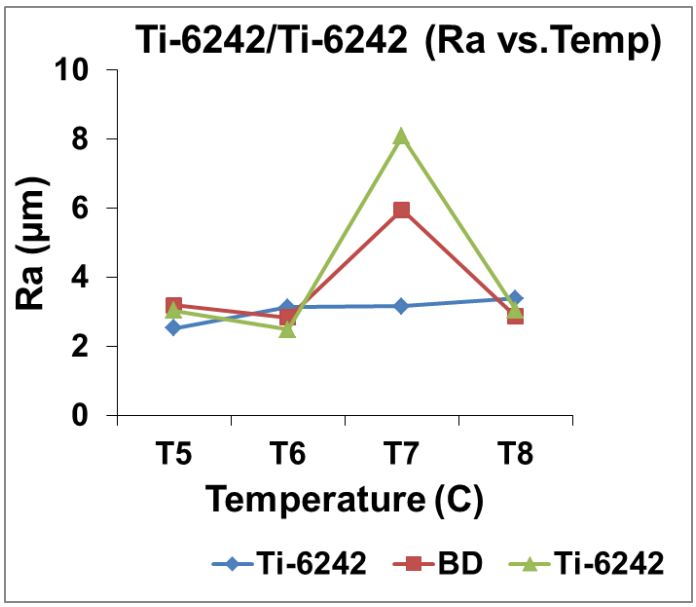

Figure 4.2-13: 'Ra' as function of temperature in DB Similar Near-α Ti-Alloys (Ti-6242/Ti-6242)

4.2.3.1.2 α + β to α + β Similar Ti-Alloys

In Ti-64SG/Ti-64SG the surface roughness value of 'Ra' did not change across the bondline with respect to the temperature except at T4^{0}C. The 'Ra' values in the parent region were also unaffected as a function of temperature. The good quality diffusion bonding of Ti-64/Ti-64 was evident in the surface roughness results. In Ti-64FG/ Ti-64 FG the surface roughness value of 'Ra' in the bondline interface decreased with the increase in temperature. The 'Ra values varied in the parent region as a function of temperature, comparatively higher values were obtained in one of the parent region than the other parent region from temperature T1^{0}C to T5^{0}C.

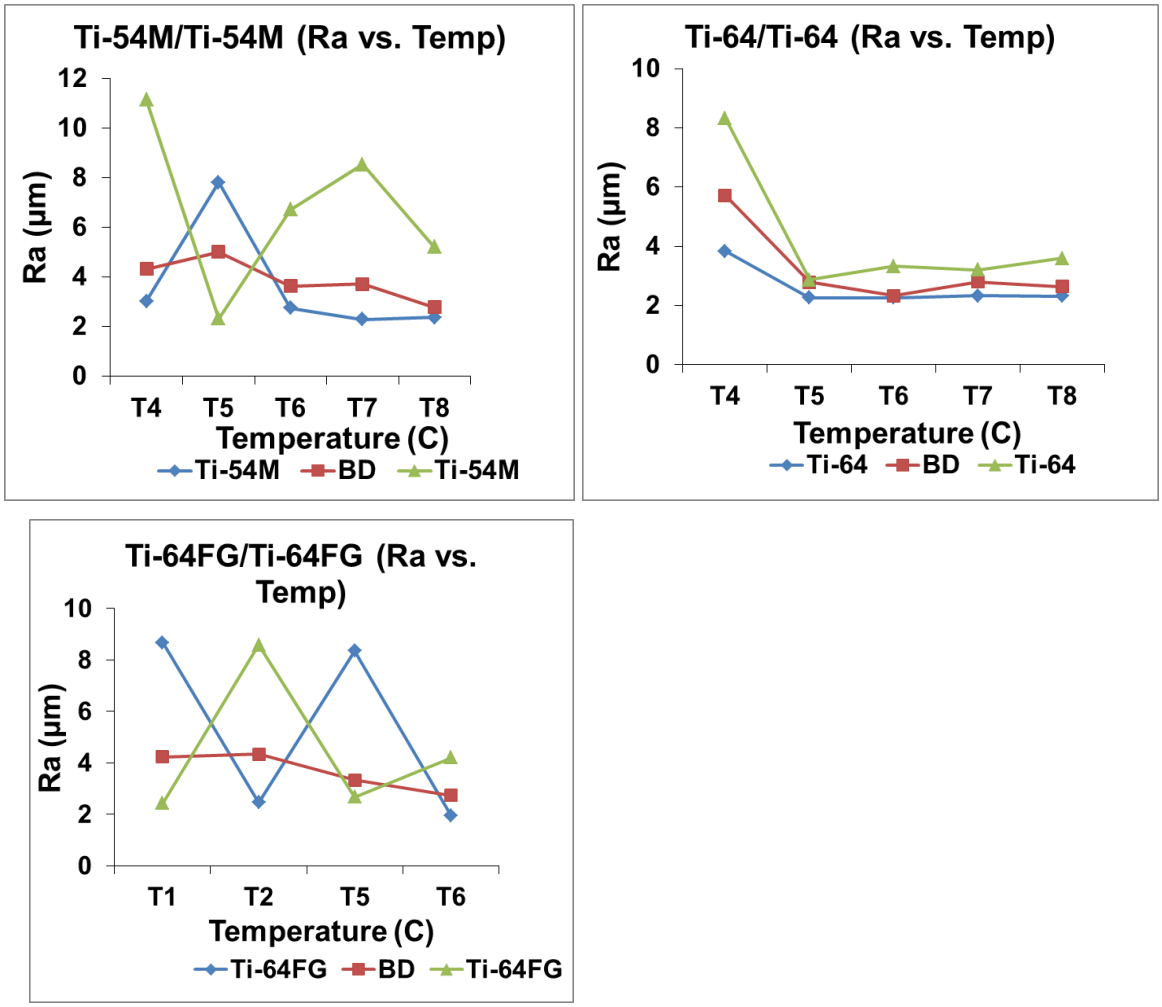

Figure 4.2-14: 'Ra' as function of temperature in DB Similar α+ β Ti-Alloys (Ti-54M/Ti-54M, Ti-64/Ti-64, Ti-64FG/Ti-64FG)

4.2.3.1.3 β to β Similar Ti-Alloys

In β-21S/ β-21S the surface roughness value of 'Ra' did not change across the bondline with respect to the temperature except at T8^{0}C. The 'Ra' values in the parent region were also unaffected as a function of temperature.

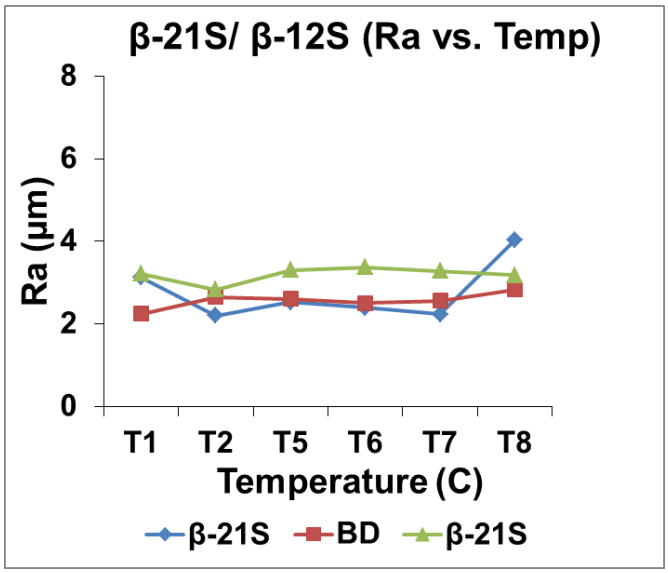

Figure 4.2-15: 'Ra' as function of temperature in DB Similar β Ti-Alloys (β-21S/ β-21S)

4.2.3.2 Surface Roughness Results– DB Similar Titanium Alloys

4.2.3.2.1 Near-α to α+ β Dissimilar Ti-Alloys

In Ti-6242/Ti-54M the surface roughness value of 'Ra' in Ti-6242 was higher than in the Ti-54M region. In most of the cases, the bondline 'Ra' values were found close to the values in the Ti-54M region. The bondline 'Ra' values did not change much with respect to the temperature. In Ti-6242/Ti-64 the surface roughness value of 'Ra' in Ti-6242 was higher than in the Ti-64 region. In most of the cases, the bondline 'Ra' values were found close to the values in the Ti-64 region. The bondline 'Ra' values did not change much with respect to the temperature. In Ti-6242/Ti-64FG the bondline 'Ra' values did not change much with respect to the temperature. In most of the cases, the bondline 'Ra' values were found close to the values in the Ti-64FG region.

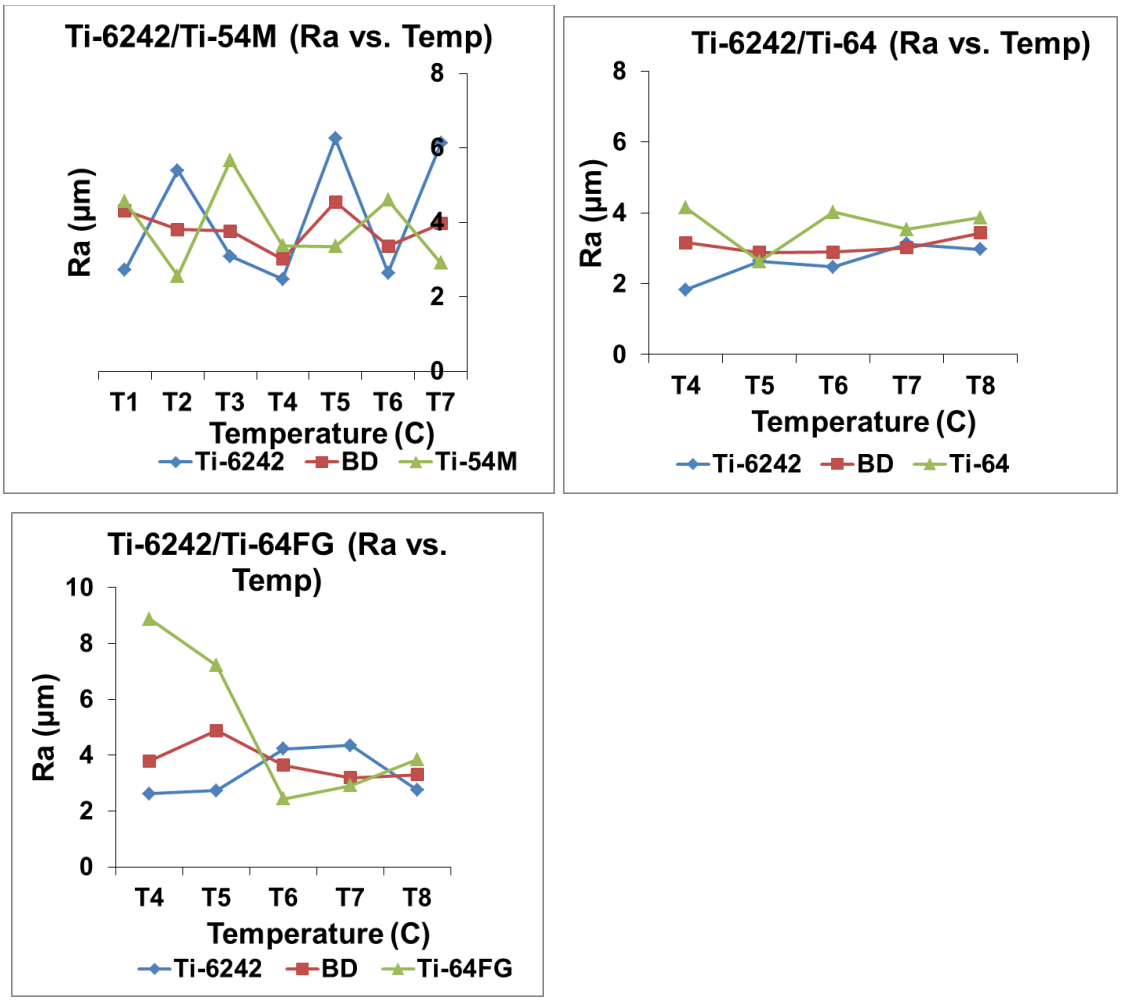

Figure 4.2-16: 'Ra' as function of temperature in DB Dissimilar Near-α to α+ β Ti-Alloys (Ti-6242/Ti-54M, Ti-6242/Ti-64SG, Ti-6242/Ti-64FG)

4.2.3.2.2 Near-α to β Dissimilar Ti-Alloys

In Ti-6242/ β-21S the surface roughness value of 'Ra' did not change across the bondline and in both of the parent regions, β-21S and Ti-6242, with respect to the temperature except at $T7^0C$. The good quality diffusion bonding of β-21S/Ti-64 at the temperatures T4and $T6^0C$ was evident in the surface roughness results. The surface roughness value 'Ra' at the bondline was observed close to the values of β-21S region.

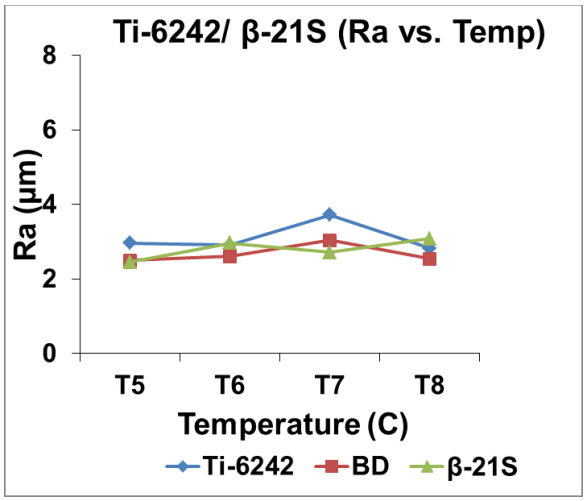

Figure 4.2-17: 'Ra' as function of temperature in DB Dissimilar Near-α to β Ti-Alloys (Ti-6242/ β-21S)

4.2.3.2.3 α+ β to α+ β Dissimilar Ti-Alloys

In Ti-64/Ti-54M the surface roughness value of 'Ra' in in Ti-64 was higher than in Ti-54M at lower temperatures, whereas in the higher temperature range, the 'Ra' values in Ti-54M region was higher than in the Ti-64 region. The bondline 'Ra' values did not change much with the increase in temperature.InTi-64FG/Ti-54M the surface roughness value of 'Ra' in Ti-54M was higher than in the Ti-64FG region. The bondline 'Ra' values were found close to the values in the Ti-64FG region did not change much with respect to the temperature. In Ti-64/Ti-64FG the surface roughness value of 'Ra' in Ti-64FG was higher than in the Ti-64 region from temperature T1^{0}C to T3^{0}C. The bondline 'Ra' values did not change much with respect to the temperature

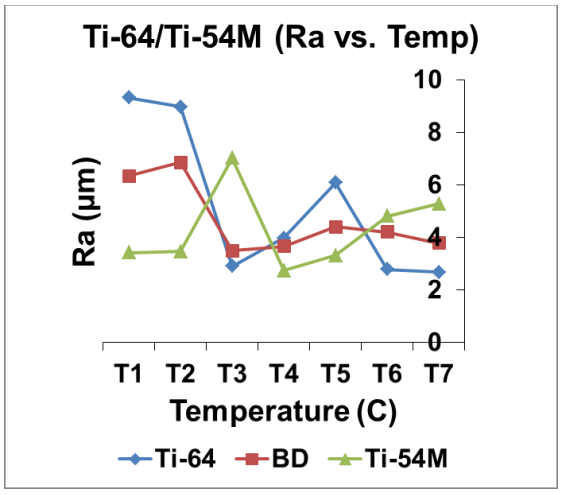

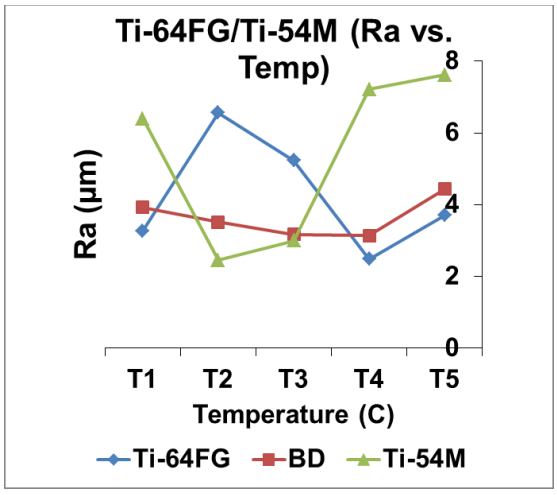

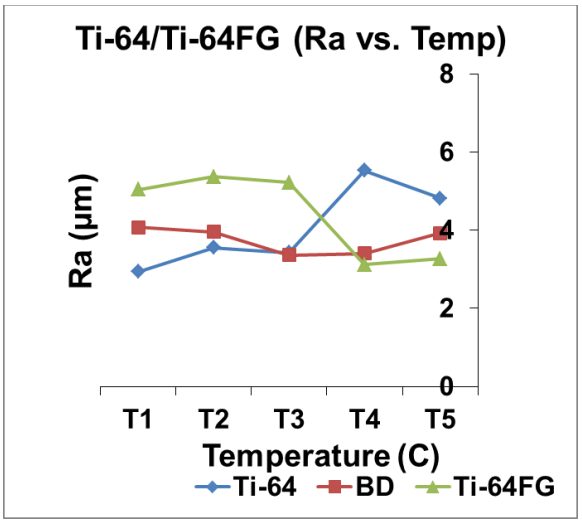

Figure 4.2-18: 'Ra' as function of temperature in DB Dissimilar α+ β to α+ β Ti-Alloys (Ti-64SG/Ti-54M, Ti-64FG/Ti-54M, Ti-64SG/Ti-64FG)

4.2.3.2.4 α + β to β Dissimilar Titanium Alloys

In β-21S /Ti-54M the surface roughness value of 'Ra' in Ti-54M was higher than β-21S region. At the temperatures T4 and T6^{0}C, where good quality diffusion bond was obtained, similar values of 'Ra' were obtained across the bondline. In β-21S /Ti-64 the surface roughness value of 'Ra' did not change across the bondline and in both of the parent regions, β-21S and Ti-64, with respect to the temperature except at T7^{0}C. A good quality diffusion bonding of β-21S/Ti-64 at the temperatures T4, T5, and T6^{0}C was evident in the surface roughness results. In β-21S /Ti-64FG-Batch1, the surface roughness value of 'Ra' in Ti-64FG region was found higher than in β-21S region. However in the Batch 2, the 'Ra' value in in β-21S region was higher than in Ti-64FG region. In the Batch1, the bondline 'Ra' values did not change with respect to temperature, whereas in the Batch2, decreased with the increase in temperature except at T7^{0}C.

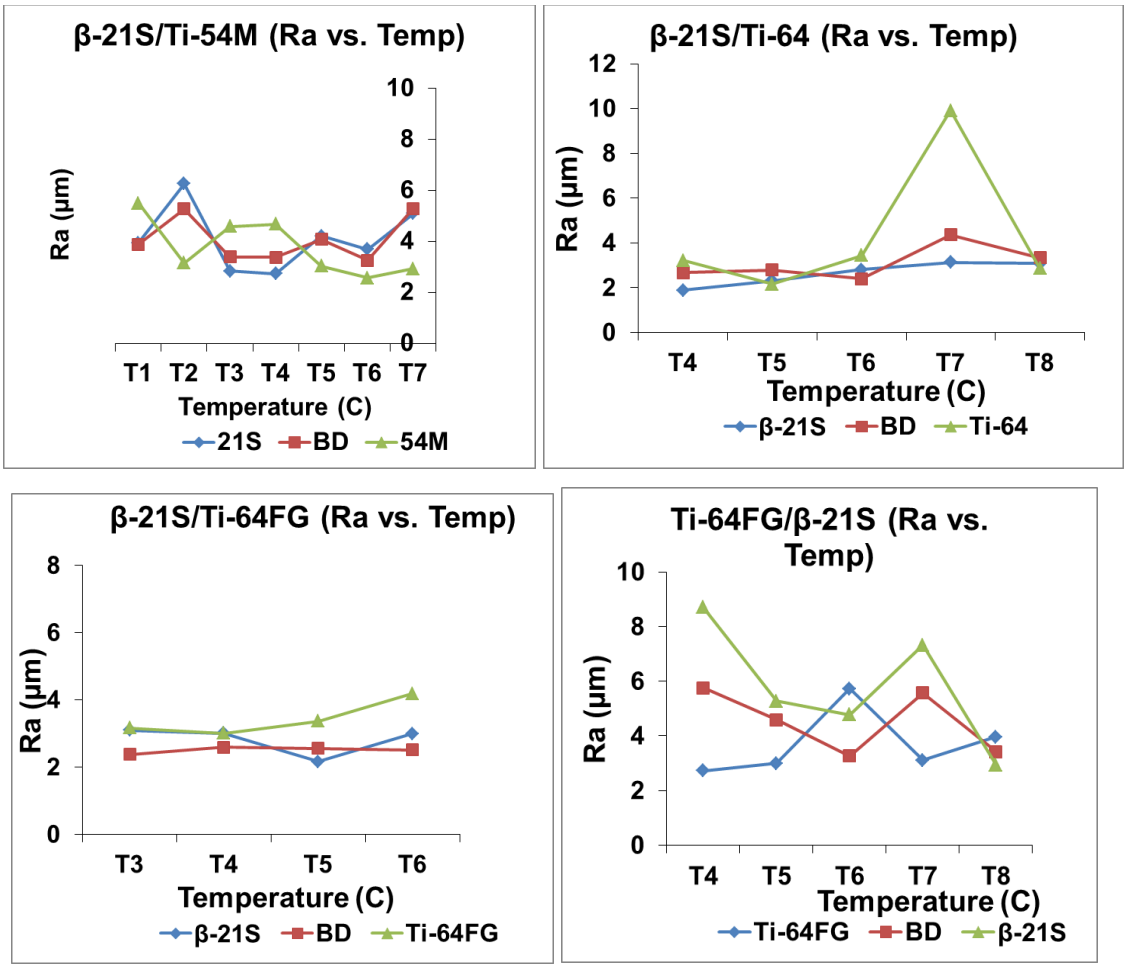

Figure 4.2-19: 'Ra' as function of temperature in DB Dissimilar α+ β to β Ti-Alloys (β-21S/Ti-54M, β-21S /Ti-64SG, and β-21S /Ti-64FG Batch 1 and 2)

4.2.3.3 Effect of Temperature on Surface Roughness in DB Similar and Dissimilar Ti-Joints

The effect of temperature on surface roughness 'Ra' measured along the bonding interface for the diffusion bonded dissimilar titanium alloys are shown in Figure 4.2-20. The cases of good quality bond cases were only considered here. It was observed that in almost all cases, except Ti-64/ Ti-54M, the surface roughness values remained unaffected at the bonding interface with the change of temperature. The change in temperature did not impact the average roughness of the bonded surface.

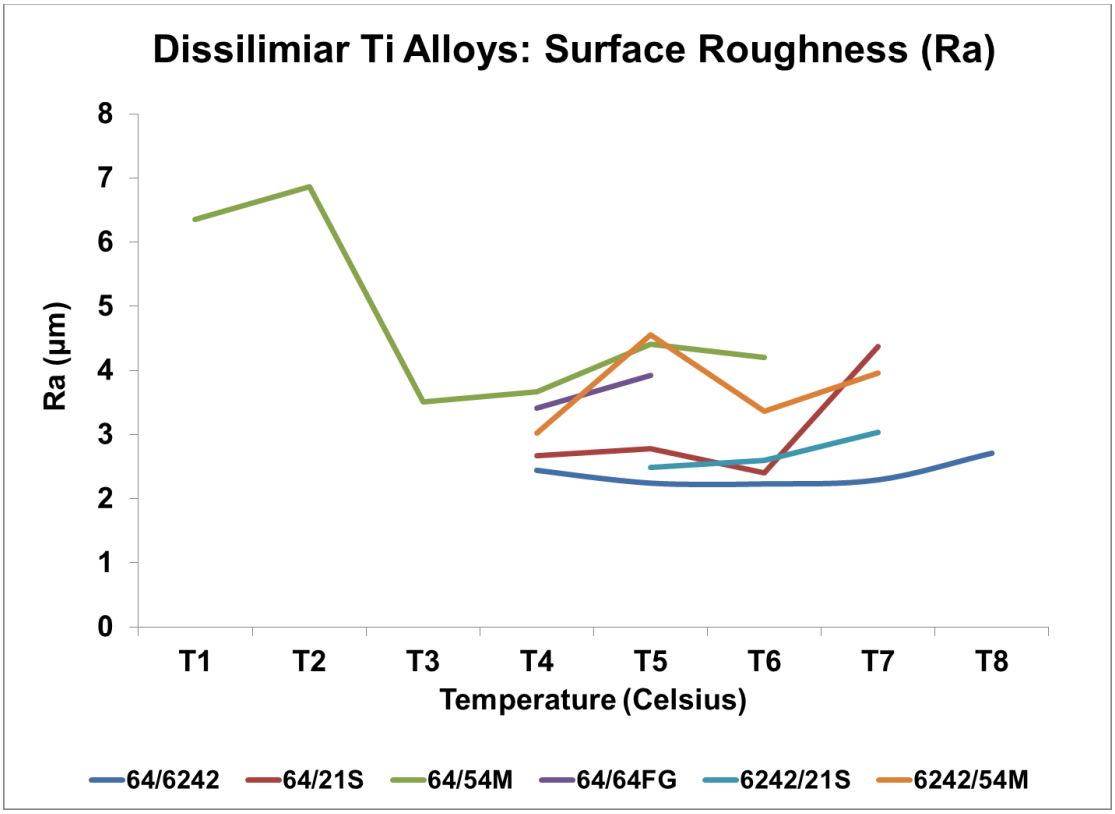

Figure 4.2-20: Diffusion Bonded Dissimilar Ti-Alloys: Surface Roughness – function of Temperature

4.2.4 *Flexural Test Results*

The current section discusses the flexural test results of parent alloys, diffusion bonded similar and dissimilar titanium joint. As the displacement of machine was measured during flexural testing, therefore the stress curves are plotted with respect to displacement instead of the strain. The ultimate stress and the modulus of elasticity results were compared with the results diffusion bonded parent alloys. The joint efficiency was calculated from the ultimate stresses.

4.2.4.1 Parent Alloys

The parent alloys, Ti-64, Ti-64FG, Ti-54M, Ti-6242SG, and Ti-6242FG stress strain properties were obtained through the flexural testing. Table 4-5 represents the flexural properties of the parent alloys obtained in the three point bend test, whereas Figure 4.2-21

shows the load displacement curve and stress extension curve for parent alloys Ti-6242FG showed highest flexural strength while Ti-54MFG produced highest elongation. Ti-64SG and Ti-64FG showed similar strength properties while the ductility was higher in Ti-64SG than in Ti-64FG.

Table 4-5: Flexural properties of the parent Ti-Alloys

Parent Alloy	Elastic Modulus (MPa)	Max Flexure Load (N)	Flexure Stress at Max Load (MPa)	0.02% Yield Stress (MPa)	% Elongation
Ti-64SG	80977	14542	2144	1600	12.89
Ti-64FG	81819	14343	2175	1600	8.00
Ti-54MFG	78970	14611	2163	1570	14.49
Ti-6242SG	76098	13334	1937	1550	11.09
Ti-6242FG	73866	14461	2083	1560	8.92

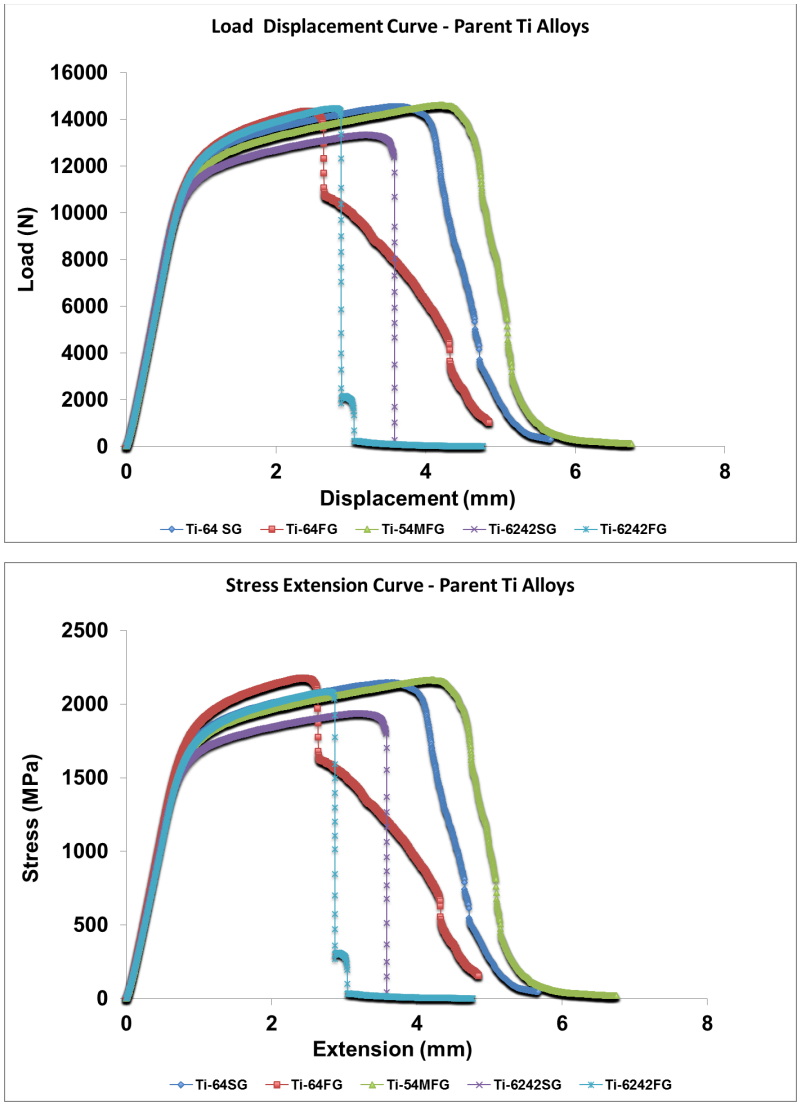

Figure 4.2-21: Load displacement and stress displacement curves of parent Ti- Alloys

4.2.4.2 Flexural Results – DB Similar Titanium Alloys

The load displacement and stress extension of diffusion bonded similar titanium joints obtained through the flexure tests at different diffusion temperatures are shown in following section. The results of different types of titanium alloys, near-α, α + β, and β alloys are plotted with respect to temperature. Table 4-6, 4-7, and 4-8 present the flexural properties elastic modulus, ultimate stress, and yield stress respectively for the diffusion bonded similar titanium joints.

Table 4-6: Elastic Modulus Results of Diffusion bonded Similar Ti-Alloys

Ti-Joints	Temperatures (C)							
	T1	T2	T3	T4	T5	T6	T7	T8
	E (MPa)	E (MPa)	E (MPa)	E (MPa)	E (MPa)	E (MPa)	E (MPa)	E (MPa)
β21S/β21S	24386	43929			43897	40445	32640	33618
Ti-54M/Ti-54M	95902	46720	44780	45513	92374			
Ti-64/Ti-64				63168	58956	61564	62589	62334
Ti64FG/Ti64FG	45867	31604	49710	45985				
Ti-6242/Ti-6242					66179	56999	51484	54926

Table 4-7: 0.2 % Yield Stress Results of Diffusion bonded Similar Ti-Alloys

Ti-Joints	Temperatures (C)							
	T1	T2	T3	T4	T5	T6	T7	T8
	0.2% YS (MPa)	0.2% YS (MPa)	0.2% YS (MPa)	0.2% YS (MPa)	0.2% YS (MPa)	0.2% YS (MPa)	0.2% YS (MPa)	0.2% YS (MPa)
β21S/β21S					400	390	225	310
Ti-54M /Ti-54M	1480	1000	1000	1000	1100			
Ti-64/Ti-64				700	700	610	640	710
Ti-64FG/Ti-64FG	1050	700	1075	1000				
Ti-6242/Ti-6242					840	800	790	800

Table 4-8: Ultimate Stress Results of Diffusion Similar bonded Ti-Alloys

Ti-Joints	Temperatures (C)							
	T1	T2	T3	T4	T5	T6	T7	T8
	US (MPa)	US (MPa)	US (MPa)	US (MPa)	US (MPa)	US (MPa)	US (MPa)	US (MPa)
β21S/β21S					426	403	239	324
Ti-54M /Ti-54M	1563	1508	1492	1547	1660			
Ti-64/Ti-64				723	754	625	651	750
Ti-64FG/Ti64FG	1649	1083	1710	1558				
Ti-6242/Ti6242					936	854	854	929

4.2.4.2.1 Near-α to Near-α Similar Ti-Alloys

Figure 4.2-22 shows the effect of temperature on the flexural test results in case of near α to near-α diffusion bonded similar titanium joints, Ti-6242SG/Ti-6242SG. The elastic modulus did not change much with respect to diffusion bonding temperature. The change in flexural strength of joints was in the range of 40MPa with respect to temperature. Higher ductility was observed with the T6 and T7^{0}C.

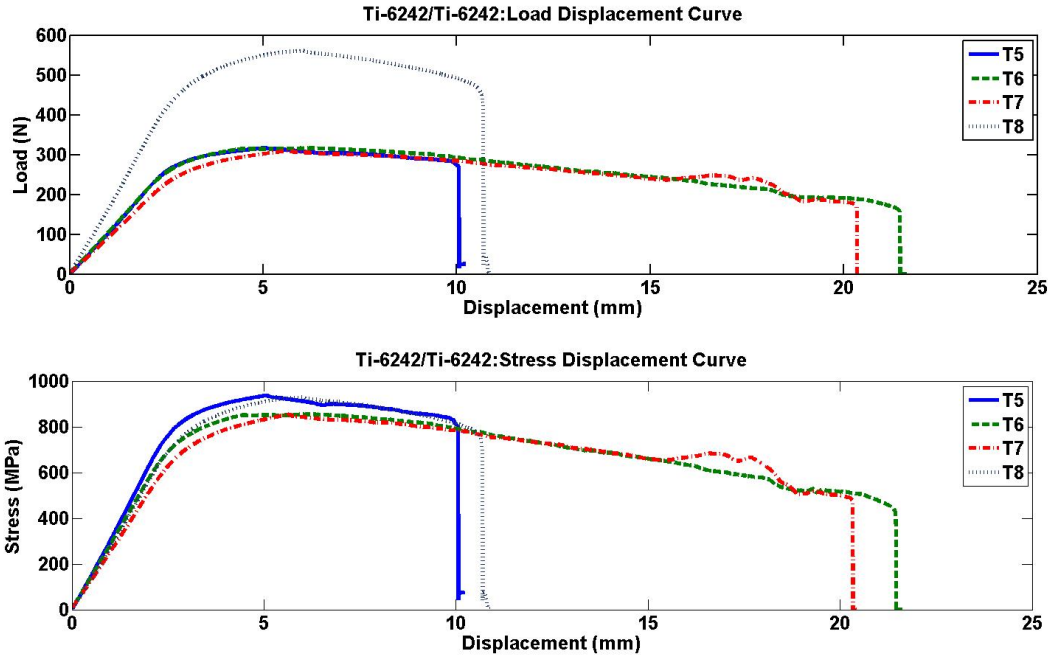

Figure 4.2-22: Load Displacement and Stress Extension Curve in DB Similar Near-α Ti-Alloys (Ti-6242/Ti-6242)

4.2.4.2.2 α + β to α + β Similar Ti-Alloys

The flexural test results of diffusion bonded similar α+ β Ti-Alloys-Ti-54M/Ti-54M, Ti-64/Ti-64, and Ti-64FG/Ti-64FG at different diffusion bonding temperatures are shown in Figure 4.2-23. The similar α+ β titanium alloys, Ti-54M/Ti-54M and Ti-64FG/Ti-64FG, did not show good bond quality as compared to the quality of bond obtained from Ti-64SG/Ti-64SG. However the flexural strength results were contrary to the microstructural observation. Even though the bonded alloys with the presence of defects at the bondline showed reasonable joint strength during flexural testing but they might

not have good fatigue life. This can be attributed to the fact that the defects would produce crack propagation and reduce fatigue life. Hence the cases where the microstructure showed good defect free bond should be considered the successful cases of diffusion bonding. In case of Ti-64SG/Ti64SG the lower side and higher side (T4 and $T8^0C$) temperatures showed good flexural strength. However the ductility was higher in the mid bonding temperatures.

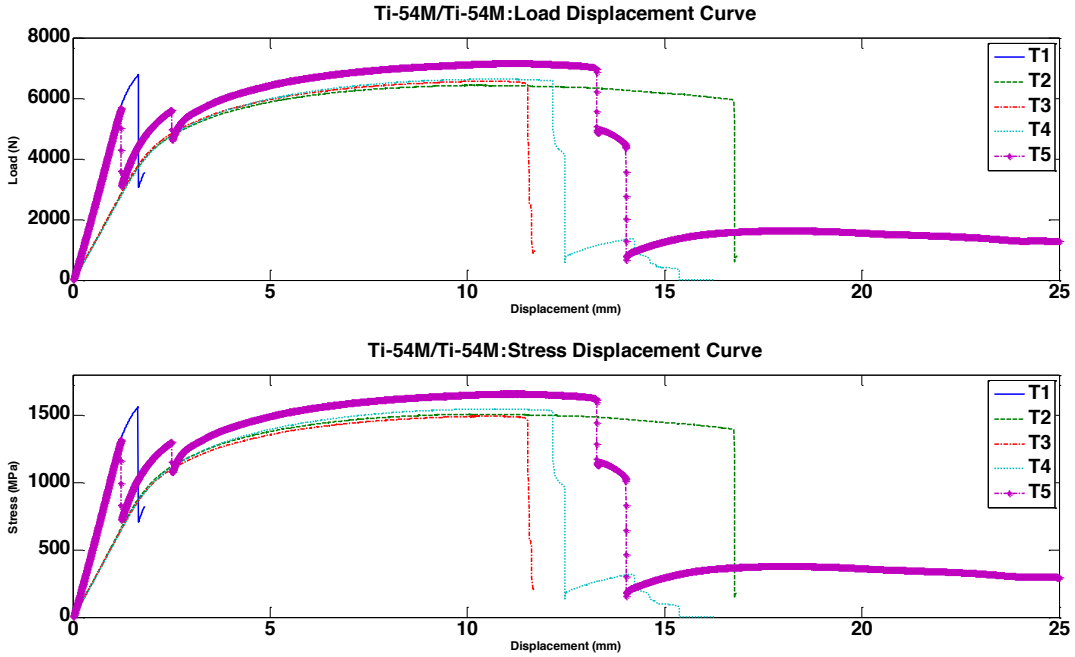

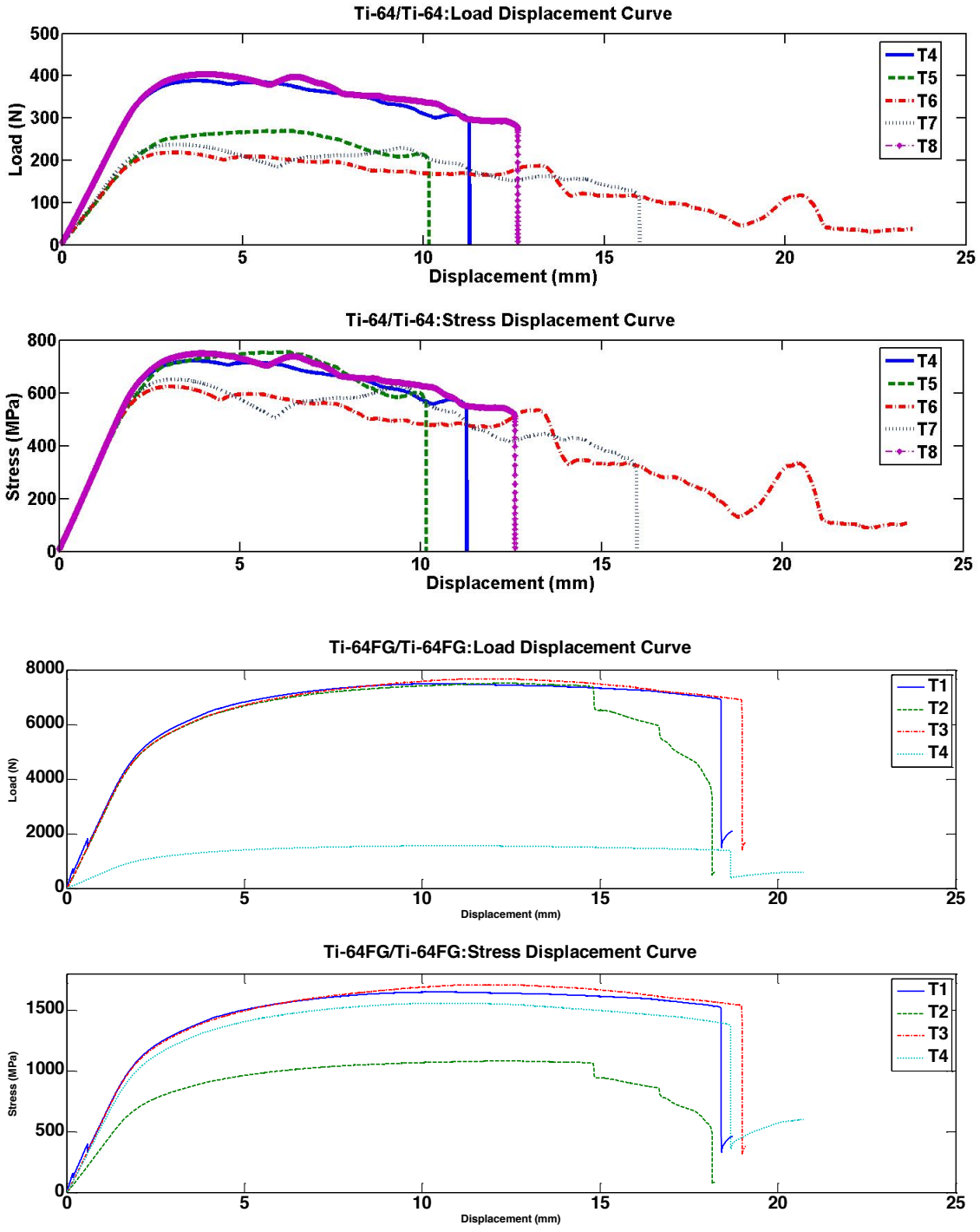

Figure 4.2-23: Load Displacement and Stress Extension Curve in DB Similar α+ β Ti-Alloys (Ti-54M/Ti-54M, Ti-64/Ti-64, Ti-64FG/Ti-64FG)

4.2.4.2.3 β to β Similar Ti-Alloys

Figure 4.2-24 shows the results of flexural strength of β to β Similar Ti-Alloy, β-21S/ β-21S at different diffusion bonding temperatures. In case of β-21S/ β-21S, except T1^{0}C, other bonding temperatures yielded good bonding results. In terms of flexural strength and elastic modulus, T2^{0}C showed higher values than at other temperatures. The ductility of the bonded joints did not change much with respect to the bonding temperatures.

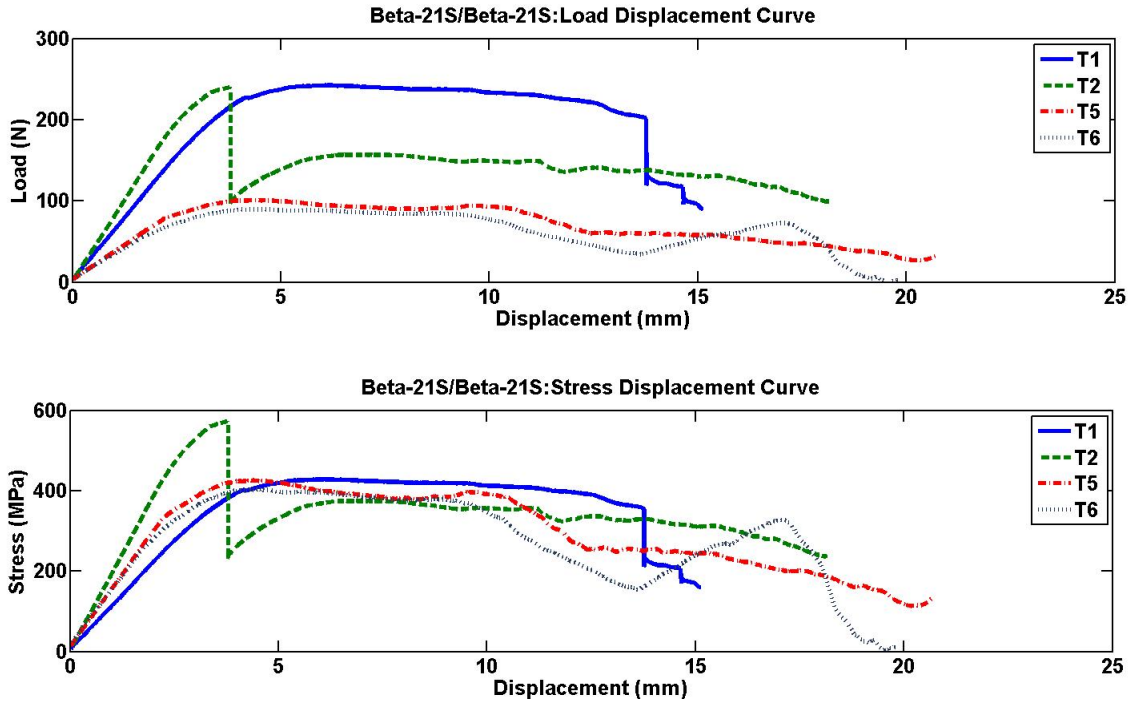

Figure 4.2-24: Load Displacement and Stress Extension Curve in DB Similar β Ti-Alloys (β-21S/ β-21S)

4.2.4.3 Flexural Results– DB Dissimilar Titanium Alloys

The load displacement and stress extension of diffusion bonded dissimilar titanium joints obtained through the flexure tests at different diffusion temperatures are shown in following section. The results of different types of dissimilar titanium joints, near-α to α+ β, near-α to β, and α+ β to α+ β, are plotted with respect to temperature. Table 4-9, 4-10, and 4-11 present the flexural properties elastic modulus, ultimate stress, and yield stress respectively for the diffusion bonded dissimilar titanium joints.

Table 4-9: Elastic Modulus Results of Diffusion bonded Diffusion Bonded Ti-Alloys

Ti-Joints	Temperatures (C)							
	T1	T2	T3	T4	T5	T6	T7	T8
	E (MPa)	E (MPa)	E (MPa)	E (MPa)	E (MPa)	E (MPa)	E (MPa)	E (MPa)
β21S/ Ti54M	65184	53286	53740	90887	60400	88866	89029	
β21S/Ti-64				52171	52362	53087	81661	50250
β21S/ Ti-64FG			56627	53561	52242	50814		
β21S/ Ti-64FG	95663	53238	53946	61769	50038			
β21S/Ti-6242					43002	46442	41253	42900
Ti-54M/ Ti-64	97770	99061	100385	96944	102553	105004	101840	
Ti-54M/Ti-64FG	48170	86905	45926	48213	90740			
Ti-54M/Ti-6242	103450	63115	58473	101105	103101	102117	108522	
Ti-64/ Ti-64FG	106330	61680	63295	102664	102928			
Ti-64/Ti-6242				49366	54188	53030	53173	51904
Ti-64FG/Ti-6242	63605	62014	63034	99405	64110			

Table 4-10: 0.2 % Yield Stress Results of Diffusion bonded Dissimilar Ti-Alloys

Ti-Joints	Temperatures (C)							
	T1	T2	T3	T4	T5	T6	T7	T8
	0.2% YS (MPa)	0.2% YS (MPa)	0.2% YS (MPa)	0.2% YS (MPa)	0.2% YS (MPa)	0.2% YS (MPa)	0.2% YS (MPa)	0.2% YS (MPa)
β21S/ Ti54M	875	975	925	1400	1025	1450	1400	
β21S/Ti-64				600	645	625	950	510
β21S/Ti-64FG			450	600	700	580		
β21S/Ti-64FG	1050	700	1075	1000	750			
β21S/Ti-6242					580	600	480	480
Ti-54M/Ti-64	1100	1025	1450	1450	1550	1600	1500	
Ti54M/Ti64FG	1050	1040	1010	1000	1460			
Ti-54M/Ti6242	1500	1150	1075	1475	1500	1575	1575	
Ti-64/Ti64FG	750	1100	1100	1450	1500			
Ti-64/Ti-6242				700	720	760	760	780
Ti-64FG/Ti6242	1050	1100	1125	1125	1100			

Table 4-11: Ultimate Stress Results of Diffusion bonded Dissimilar Ti-Alloys

Ti-Joints	Temperatures (C)							
	T1	T2	T3	T4	T5	T6	T7	T8
	US (MPa)	US (MPa)	US (MPa)	US (MPa)	US (MPa)	US (MPa)	US (MPa)	US (MPa)
β21S/ Ti54M	1175	1368	1028	1666	1556	1704	1693	
β21S/Ti-64				626	705	685	1059	527
β21S/Ti-64FG			494	637	721	592		
β21S/Ti-64FG	1752	1567	1165	1416	1133			
β21S/Ti-6242					613	636	518	523
Ti-54M/ Ti-64	1725	1692	1703	1786	1828	1960	1882	
Ti-54M/Ti-64FG	1590	1545	1584	1577	1794			
Ti-54M/Ti-6242	1722	1744	1302	1523	1740	1948	2008	
Ti-64/Ti-64FG	1512	1474	1471	1892	1848			
Ti-64/Ti-6242				751	814	832	870	984
Ti-64FG/Ti-6242	1483	1513	1469	1807	1356			

4.2.4.3.1 Near-α to α+ β Dissimilar Ti-Alloys

The flexural results of load displacement and stress extension of near- α to α+ β titanium joints are shown in Figure 4.2-25 at different diffusion bonding temperatures. It included the cases of Ti-6242/Ti-54M, Ti-6242/Ti-64SG, Ti-6242/Ti-64FG. The dissimilar joint Ti-6242SG/Ti-64SG yielded good quality bonding at all the bonding temperatures, whereas with fine grain of Ti-64, i.e. in Ti-6242SG/Ti-64FG only the temperature $T4^0C$ produced good quality results. Even Ti-6242SG/Ti-54M produced good diffusion bond between them at all temperatures except $T7^0C$ where moderate quality of bond was obtained through diffusion bonding process. In case of Ti-6242SG/Ti-64SG, the elastic modulus did not change much with respect to bonding temperature, while the flexural strength of joint was greater at higher temperature $T8^0C$, and the ductility was higher at lower temperature than $T8^0C$. The stress displacement curve of Ti-6242SG/Ti-64FG showed that higher elastic modulus, flexural strength, and ductility were found at $T4^0C$ which was in agreement with its microstructure bonding quality results. In case of Ti-

6242SG/Ti-54M, bonding temperature T6^{0}C yielded higher joint strength. The stiffness in this case was lower at temperatures T2 and T3^{0}C whereas at other temperatures it was higher as well as consistent than at these temperatures. In these different types of near- α to α+ β dissimilar titanium joints, Ti-6242/Ti-54M yield higher joint strength than the other dissimilar titanium joints present in these combination of joints.

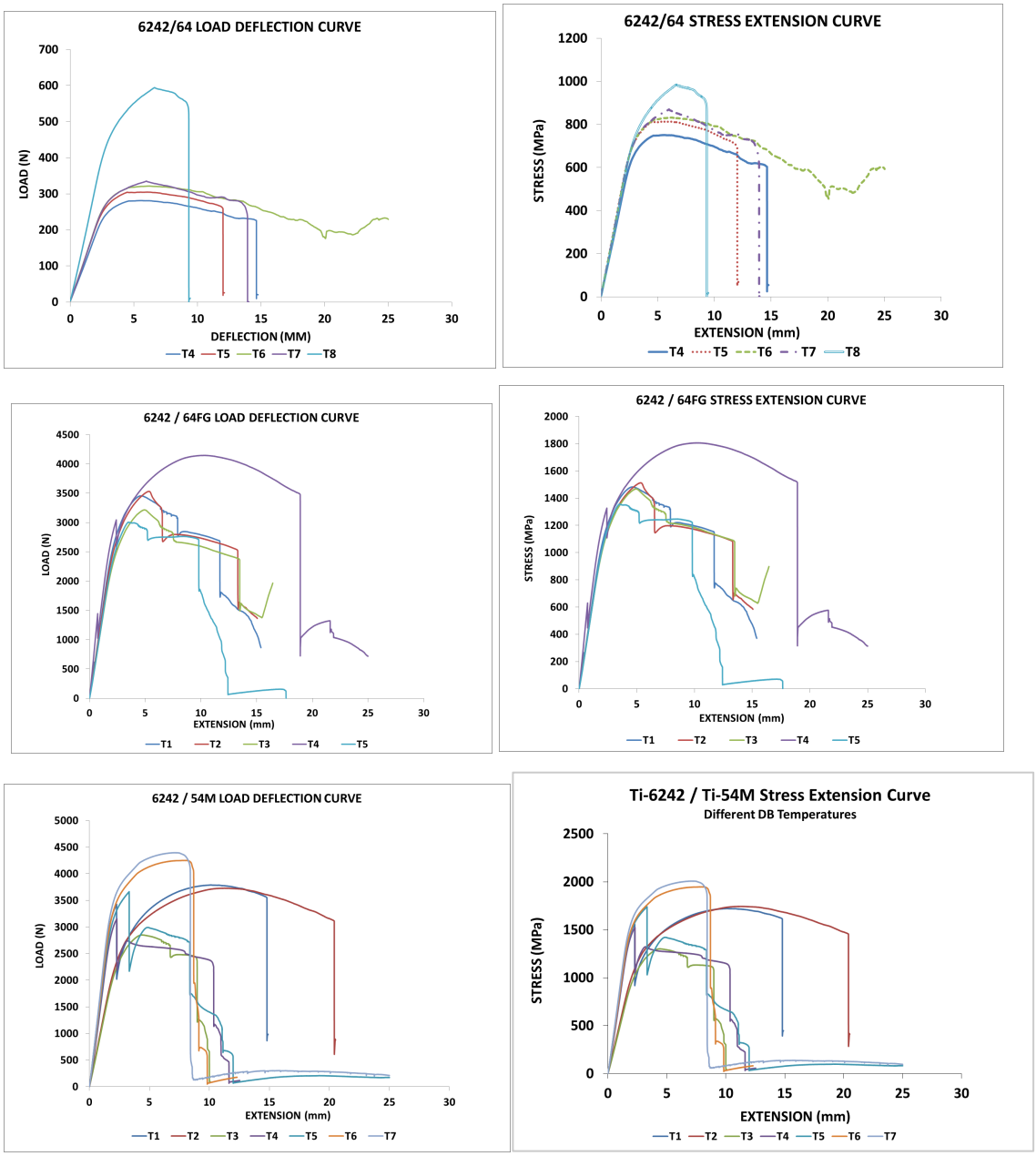

Figure 4.2-25: Load Displacement and Stress Extension Curve in DB Dissimilar Near-α to α+ β Ti-Alloys (Ti-6242/Ti-54M, Ti-6242/Ti-64SG, Ti-6242/Ti-64FG)

4.2.4.3.2 Near-α to β Dissimilar Ti-Alloys

Another type of diffusion bonded dissimilar titanium joint present was Near-α to β which included Ti-6242SG/Beta 21S joint. The flexural results of this joint are shown in Figure 4.2-26 at different bonding temperatures. Here, good quality bonds were obtained at all temperatures except at T8^{0}C where the higher bonding temperature showed defects affecting the quality of joint while the flexural strength was highest at T6^{0}C among different bonding temperatures.

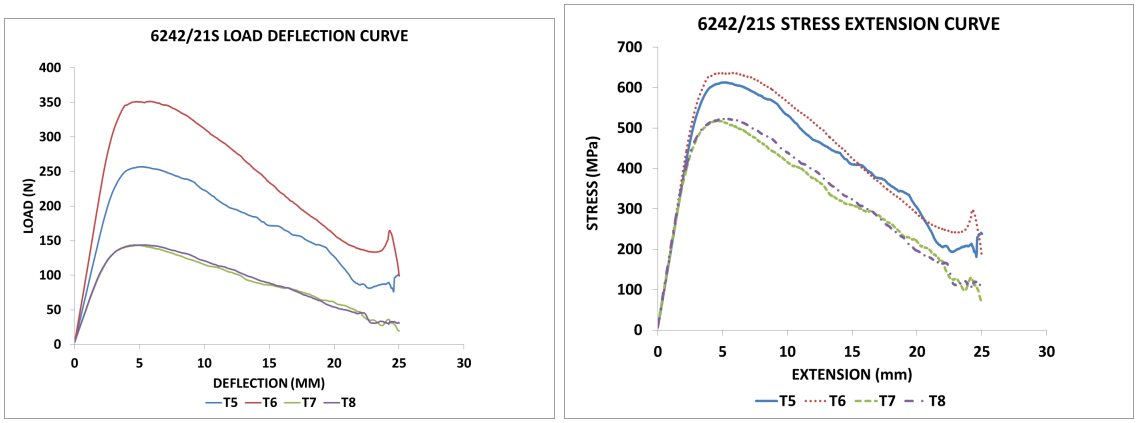

Figure 4.2-26: Load Displacement and Stress Extension Curve in DB Dissimilar Near-α to β Ti-Alloys (Ti-6242/ β-21S)

4.2.4.3.3 α+ β to α+ β Dissimilar Ti-Alloys

The flexural results of α+ β to α+ β dissimilar titanium joints are displayed in Figure 4.2-27 at different bonding temperatures. It included the combinations of Ti-64SG/Ti-54M, Ti-64FG/Ti-54M, and Ti-64SG/Ti-64FG. The bonding quality was good for Ti-64SG/Ti-54M at all bonding temperatures except at T7^{0}C where moderate quality of joint was achieved though diffusion bonding. Ti-64FG/Ti-54M did not produce good quality bond at lower temperatures, while at higher temperatures moderate quality bond was obtained as a result of diffusion bonding process. In case of Ti-64SG/Ti-64FG better quality of bond could be achieved at T4 and T5^{0}C than other bonding temperatures. The flexural properties of Ti-64/Ti-54M joint showed that elastic modulus did not change much with respect to bonding temperatures while higher strength and ductility was obtained at T6^{0}C and T1^{0}C respectively. The stress displacement curve of Ti-64FG/Ti-54M showed lot of noise which

could be the result of opening of voids present across the bondline of the joint as the microstructures of Ti-64FG/Ti-54M had also shown that good quality of bond was not obtained between them. In this case higher strength was attained at $T5^0C$ which in agreement with its microstructure where it showed moderate quality. In Ti-64SG/Ti-64FG higher flexural strength was obtained at T4 to $T5^0C$ again in agreement with its microstructure results. Therefore the combination of Ti-64SG/T-54M produced good quality bond among the α+ β to α+ β dissimilar titanium joints.

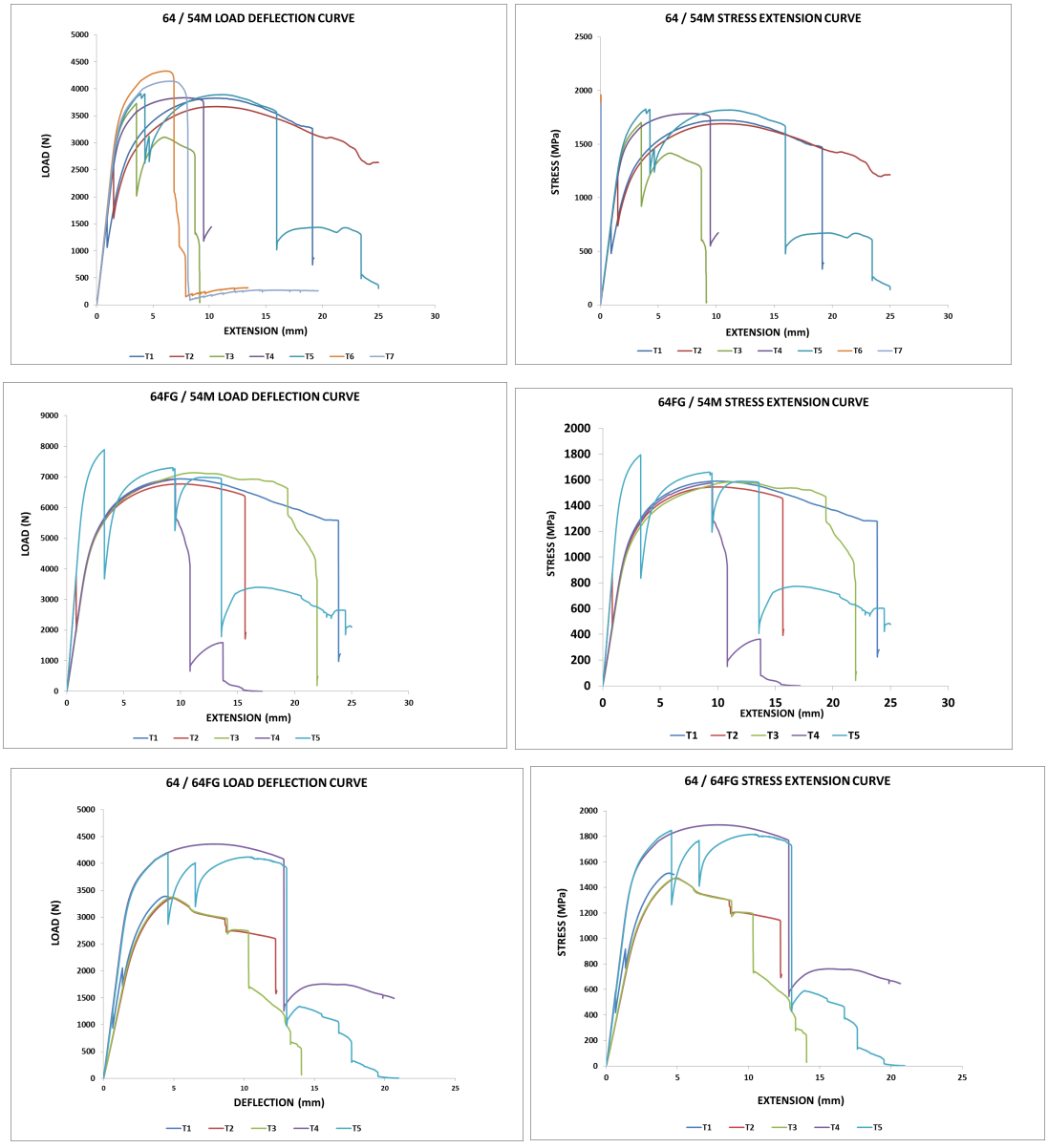

Figure 4.2-27: Load Displacement and Stress Extension Curve in DB Dissimilar α+ β to α+ β Ti-Alloys (Ti-64SG/Ti-54M, Ti-64FG/Ti-54M, Ti-64SG/Ti-64FG)

4.2.4.3.4 α + β to β Dissimilar Titanium Alloys

The flexural curves of load displacement and stress displacement of α + β to β dissimilar titanium joints are shown in Figure 4.2-28 at different diffusion bonding temperatures. This includes the alloy combinations of α + β type of titanium alloys Ti-54M, Ti-64SG, and Ti-64FG with β type of alloy Beta-21S. In case of Ti-54M/Beta 21S, bonding temperatures T4 and T6^{0}C yielded good quality joints while T7^{0}C produced moderate quality of joint. In this case, the elastic modulus and flexural strength was higher at T4, T6 and T7^{0}C while the ductility was higher at T7^{0}C only. In Ti-64SG/Beta 21S, good quality of joints was obtained at most of the bonding temperatures except at T8^{0}C where moderate quality was obtained with diffusion bonding. For dissimilar joint of Ti-64SG/Beta 21S, T7^{0}C produced higher flexural properties than other temperatures. Interestingly, the temperatures other than T7^{0}C also showed similar flexural properties. The alloy combination of Ti-64FG/Beta-21S did not produce good quality joints except at T1^{0}C where moderate quality of joint was obtained with diffusion bonding. The stress displacement curves also showed comparatively higher flexural properties for this temperature.

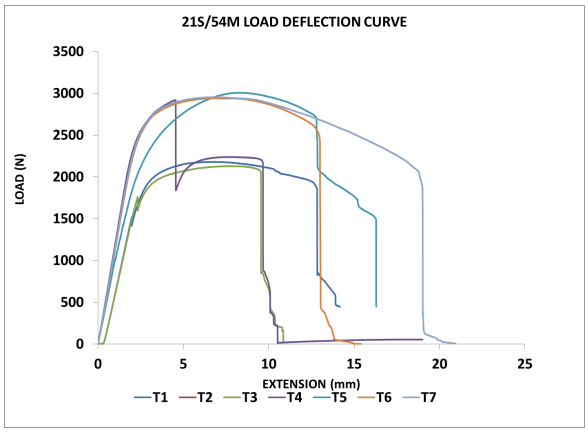

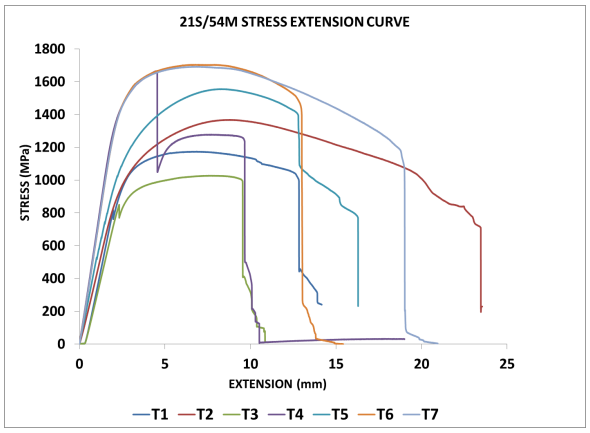

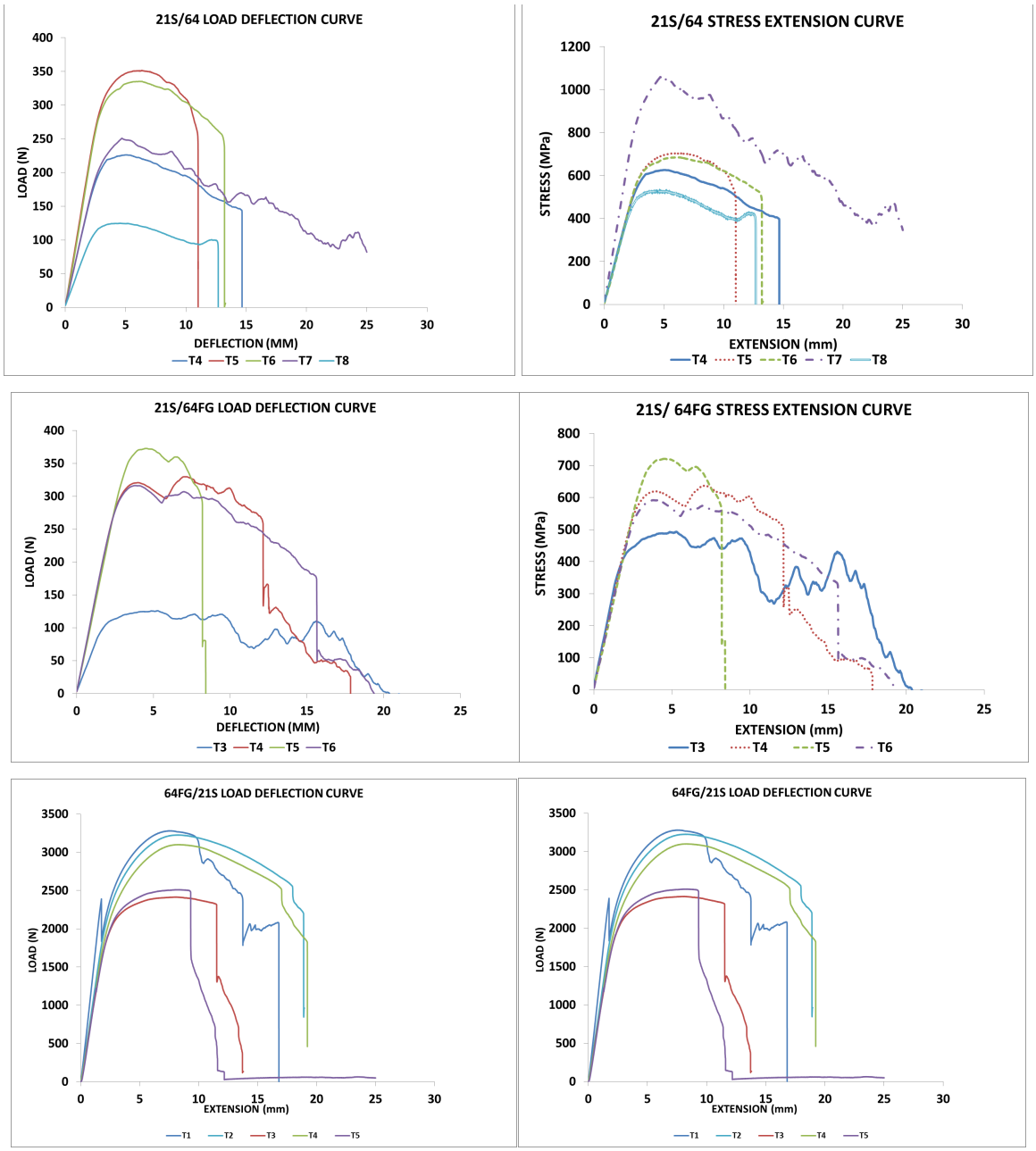

Figure 4.2-28: Load Displacement and Stress Extension Curve in in DB Dissimilar α+ β to β Ti-Alloys (β-21S/Ti-54M, β-21S /Ti-64SG, and β-21S /Ti-64FG Batch 1 and 2)

4.2.4.4 Comparison of Elastic Modulus results of diffusion bonded Ti-Alloys

The flexural property results of elastic modulus of different dissimilar titanium joints were compared with different types of similar titanium joints. Figure 4.2.29 to Figure 4.2.31

show the elastic modulus of near-α type Ti-6242; α + β types Ti-54M, Ti-64, Ti-64FG; and β- type β21S with other dissimilar titanium alloys.

4.2.4.4.1 Near-α to other dissimilar Ti-Alloys

The parent alloy Ti-6242/Ti-6242 elastic modulus remained unaffected with the increase in the temperature. The diffusion bonding with β21S and Ti-64SG yielded lower elastic modulus than Ti-6242/Ti-6242 elastic modulus.

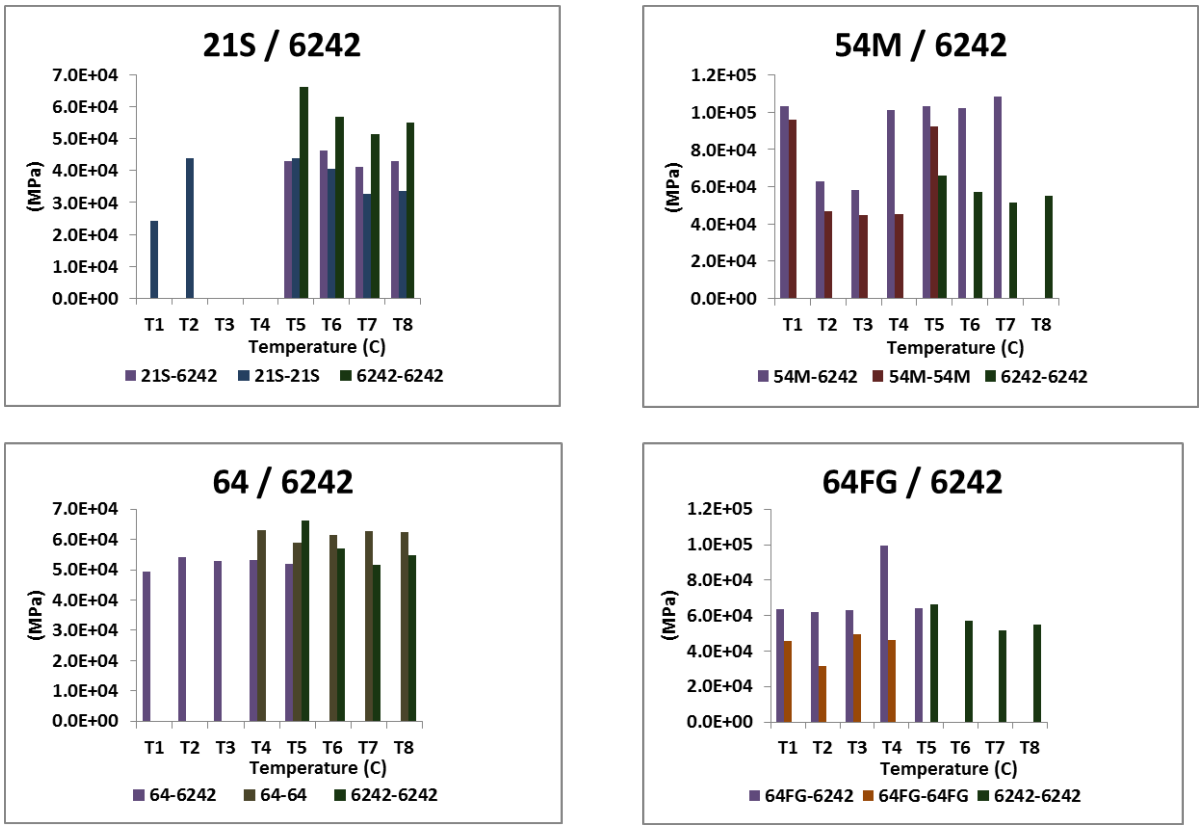

Figure 4.2-29: Elastic Modulus in DB Near-α Ti-Alloys (Ti-6242 Ti-6242) with other Dissimilar Ti- Alloys

4.2.4.4.2 α + β to other dissimilar Ti-Alloys

The parent alloy Ti-54M/Ti-54M elastic modulus varied with the increase in the temperature. The elastic modulus was same for the lower and the higher temperature. The microstructure showed that the Ti-54M/Ti-54M bonded well at the lower and the higher temperature whereas they did not bond well for the remaining temperature range. The diffusion bonding of Ti-54M with the dissimilar alloys, Ti-64SG and Ti-6242 improved the

elastic modulus than from bonding with itself. The parent alloy Ti-64SG/ Ti-64SG elastic modulus remained unaffected with the increase in the temperature. The microstructure showed that the bonding improved with the higher temperature and became fully bonded at T8^{0}C. The diffusion bonding with the dissimilar alloys, Ti-54M, and Ti-64FG improved the elastic modulus of Ti-64SG alloy than bonding with itself. The parent alloy Ti-64FG/Ti-64FG elastic modulus varied with the increase in the temperature. The microstructure showed that the poor bonding quality for the entire temperature range. The diffusion bonding with the dissimilar alloys, β21S, Ti-64SG, and Ti-6242 improved the elastic modulus of Ti-64FG.

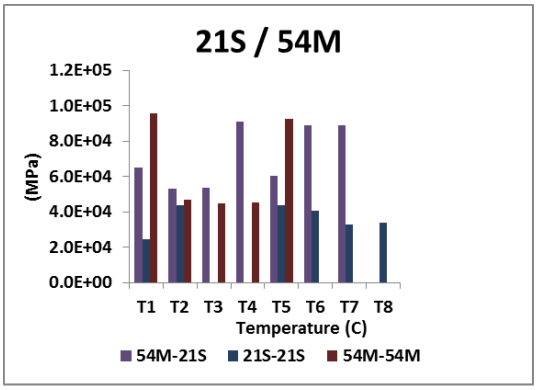

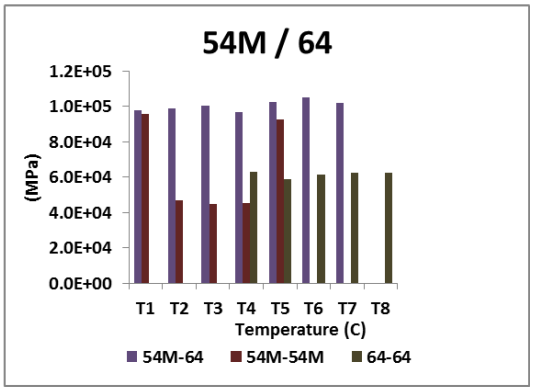

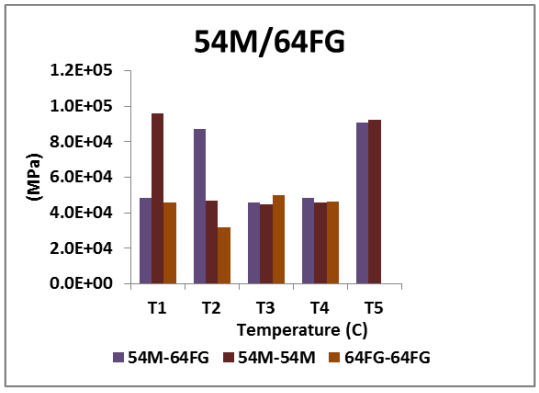

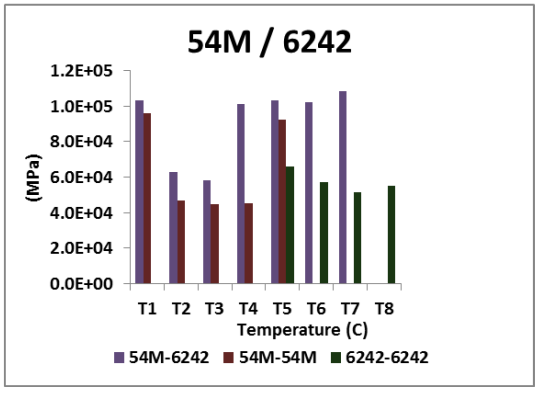

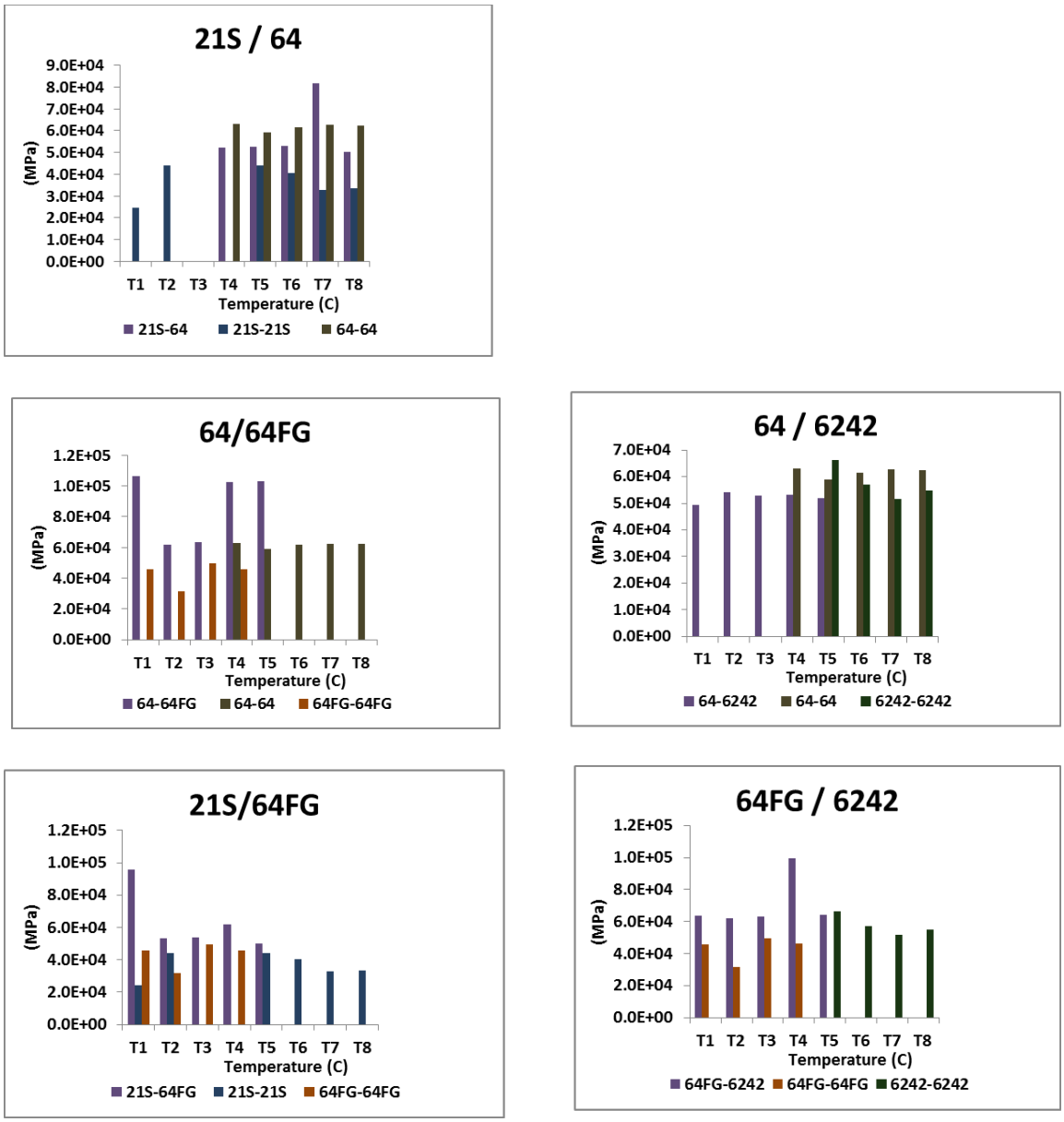

Figure 4.2-30: Elastic Modulus in DB Similar α + β Ti-Alloys (Ti-54M/Ti-54M, Ti-64/Ti-64, Ti-64FG/Ti-64FG) with other Dissimilar Alloys

4.2.4.4.3 β to other dissimilar Ti-Alloys

The parent alloy β-21S/β-21S elastic modulus increased initially with the temperature, however then remains unaffected with the change in temperature. β-21S alloy has elastic modulus of 105 GPa. The diffusion bonded β-21S alloys have values lower modulus values than the beta β-21S alloy. This can be attributed to the inadequate bonding quality present at the bonding interface. The diffusion bonding occurs at higher temperature therefore

some decrease in the elastic modulus is expected. The diffusion bonding with other dissimilar alloys, Ti-54M, Ti-64SG, Ti-64FG, and Ti-6242 improved the elastic modulus of β-21S alloy than with the diffusion bonded β-21S alloy. The increase in temperature did not affect the elastic modulus of β-21S /Ti-6242 alloy.

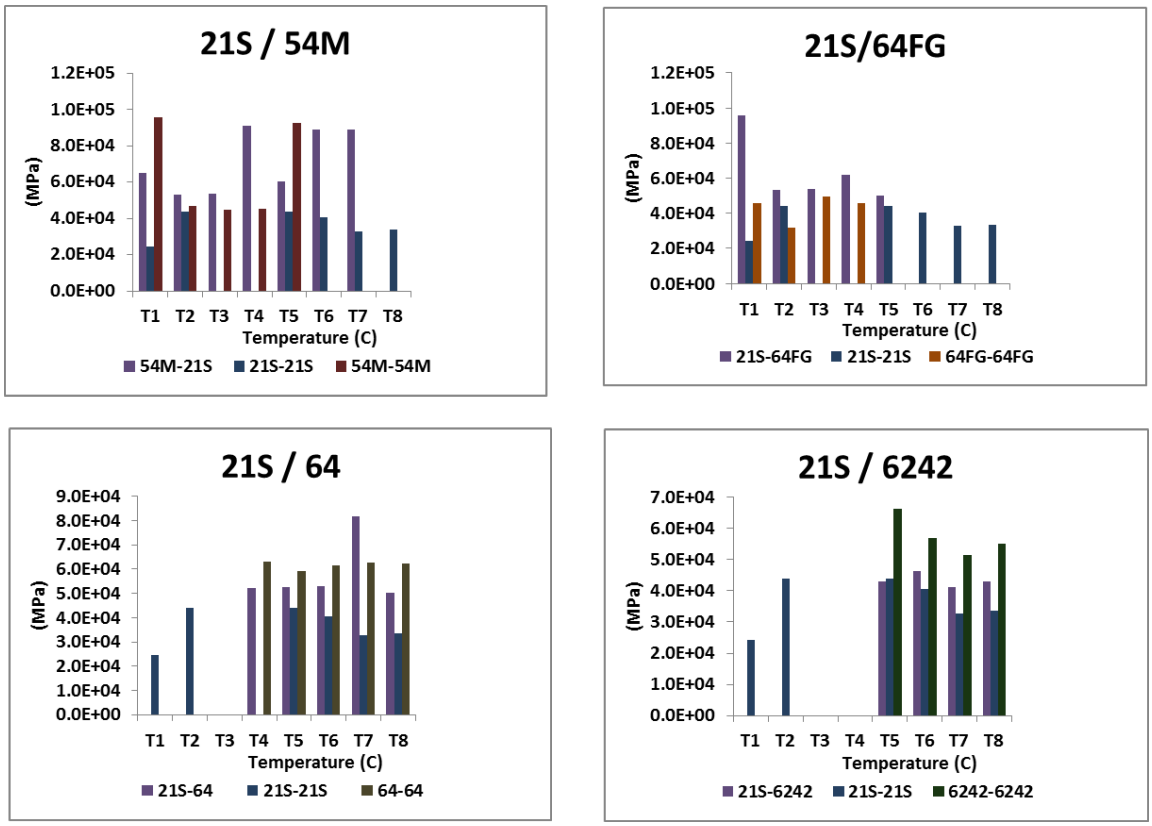

Figure 4.2-31: Elastic Modulus in DB Similar β Ti-Alloys (β-21S/ β-21S) with other dissimilar Ti- Alloys

4.2.4.5 DB Joint Efficiency Results

The ultimate stresses results of dissimilar titanium alloys were compared with their respective parent-parent alloys and joint efficiency was evaluated with respect to the parent diffusion bonded alloys. The positive and the higher values of efficiency denote that the diffusion bonding of the titanium alloys with the dissimilar alloys helped in improving the diffusion joining process and the bonding strength of the alloys. The negative values show the retarding of the bonding strength.

4.2.4.5.1 Near-α to other dissimilar Ti-Alloys

Ti-6242 showed negative bonding efficiency with Beta-21S and Ti-64SG as the bonding temperature was increased, whereas with Ti-54M the efficiency improved with temperature.

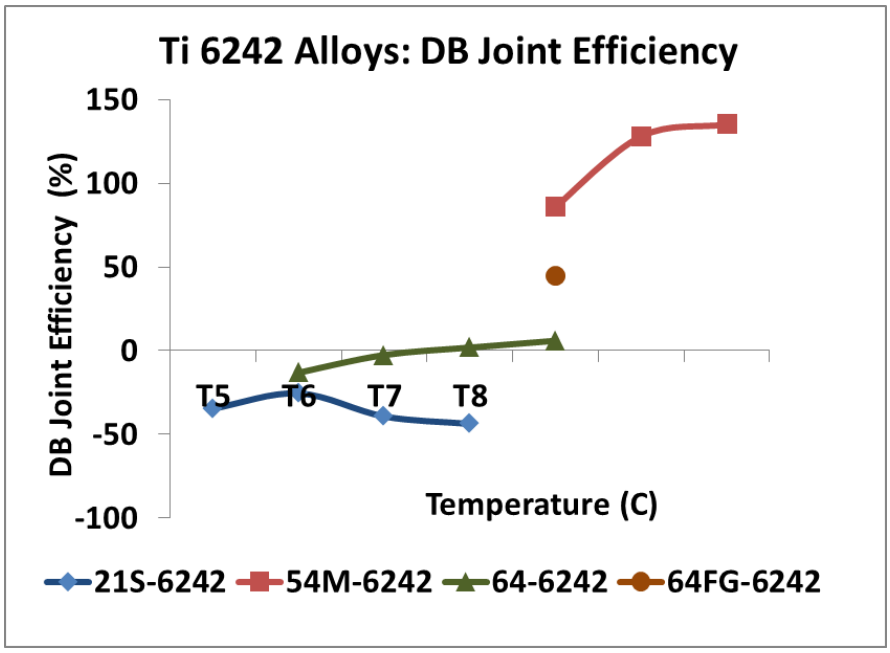

Figure 4.2-32: DB Joint Efficiency in DB Near-α Ti-Alloys with other dissimilar Ti-Alloys (Ti-6242/Ti-6242)

4.2.4.5.2 α + β to other dissimilar Ti-Alloys

The bonding efficiency of Ti-54M with other titanium alloys was in the range -30% to 20 %. The bonding efficiency of Ti-54M with Ti-64SG remained unaffected with the temperature. Some slight variation in the efficiency was observed for Ti-54M with Ti-64FG. The efficiency of Ti-54M with β21S was negative as expected. The highest efficiency (16%) could be achieved with Ti-6242 alloy at T2^{0}C. In Ti-64SG**,** the flexure test results had produced lower ultimate stresses. Hence, Ti-64SG showed higher bonding efficiency with other titanium alloys except the β21S alloy. Ti-64FG showed similar trends of the bonding efficiency with all other titanium alloys. The efficiency initially increased and then decreased followed by rise with the temperature.

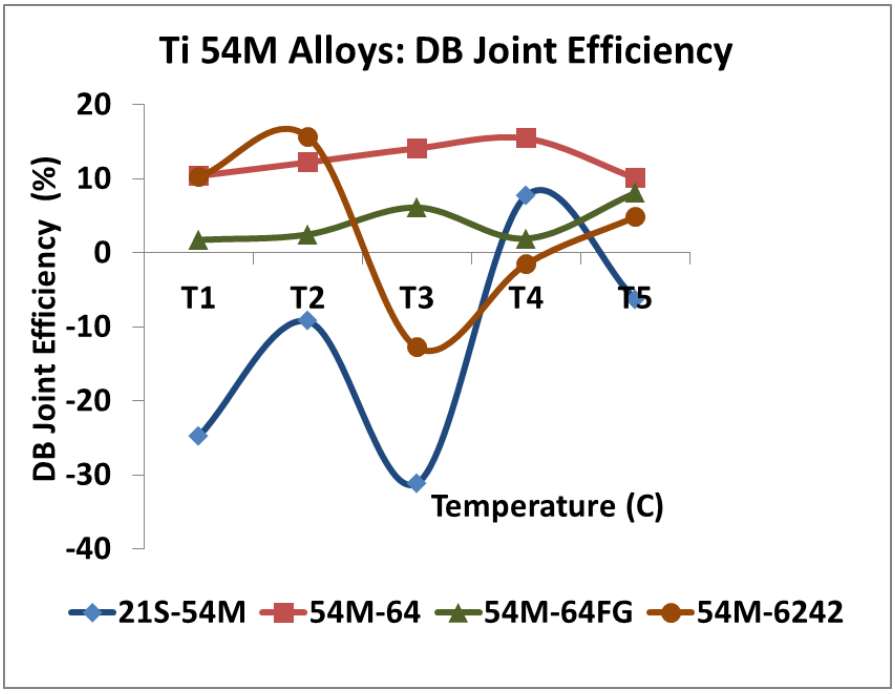
Ti 54M Alloys: DB Joint Efficiency
DB Joint Efficiency (%)
20
10
0
-10
-20
-30
-40
T1
T2
T3
T4
T5
Temperature (C)
21S-54M
54M-64
54M-64FG
54M-6242

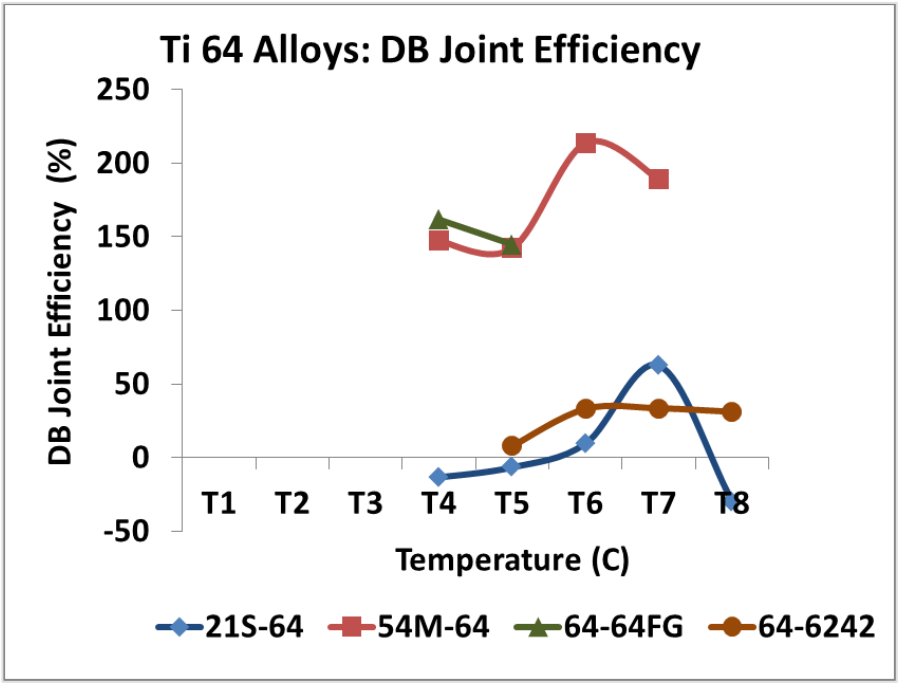
Ti 64 Alloys: DB Joint Efficiency
DB Joint Efficiency (%)
250
200
150
100
50
0
-50
T1
T2
T3
T4
T5
T6
T7
T8
Temperature (C)
21S-64
54M-64
64-64FG
64-6242

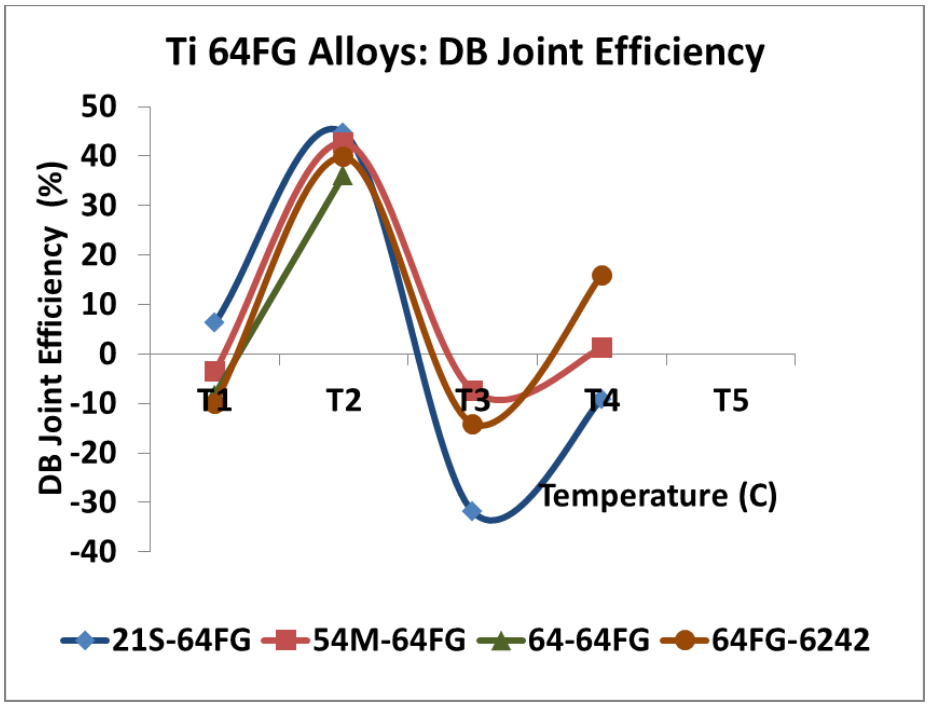

Figure 4.2-33: DB Joint Efficiency in DB Similar α + β Ti-Alloys Alloys with other Dissimilar Ti-Alloys (Ti-54M/Ti-54M, Ti-64/Ti-64, Ti-64FG/Ti-64FG)

4.2.4.5.3 β to other dissimilar Ti-Alloys

The diffusion bonded β21S/ β21S showed lower values of ultimate stress. The microstructure captured the poor bonding quality at the interface of the joints. This was evident in their flexure test results. Therefore β21S alloy provided very high bonding efficiency with all other titanium alloys.

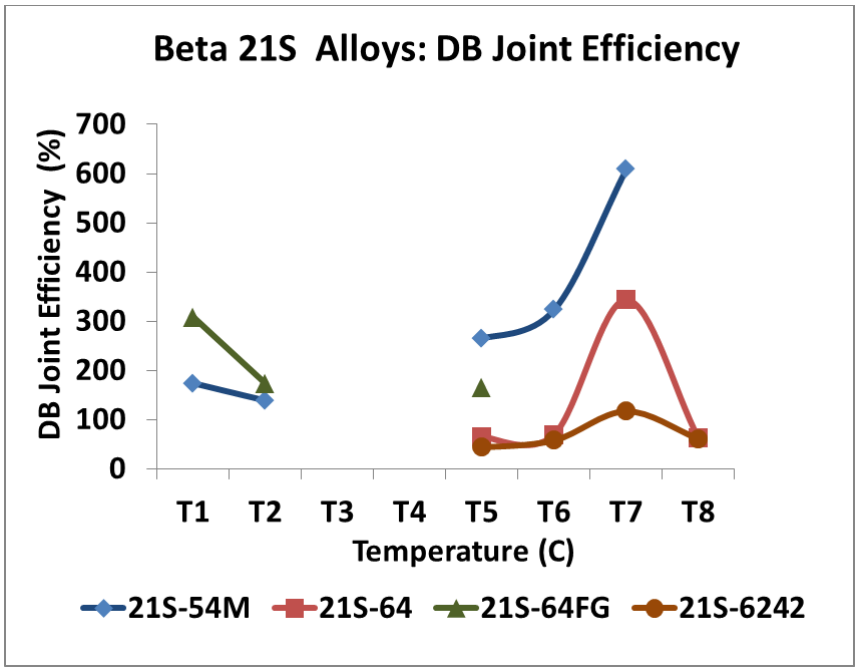

Figure 4.2-34: DB Joint Efficiency in DB Similar β Ti-Alloys with other Dissimilar Ti-Alloys (β-21S/ β-21S)

4.2.5 *Flexural Fractured Specimens*

The current section discusses results on fracture of similar and dissimilar diffusion bonded titanium joints. The diffusion bonded samples were subjected to flexural tests until failure to study the mechanical behavior of diffusion joints. In case of similar joints, the thickness was same whereas in dissimilar joints, both the cases of same thickness and different thickness of the joining materials were present. The effect of different thickness at the joint was observed on the fracture of the joints. In the later section metallographic examination of sections through the bond lines is discussed for diffusion bonded Ti-64/Ti-64, Ti-6242/Ti-6242, and Ti-64/Ti-6242 alloys.

4.2.5.1 Fracture Results – DB Similar Titanium Joints

The current section discusses fracture results of similar type of diffusion bonded titanium joints. Figures 4.2-35 to 4.2-37 displays the fractured specimens of different types of titanium joints, near-α to near-α, α + β to α + β, β to β titanium joints at different bonding temperatures. In Figures, the fractured specimens are showcased from lower temperature to

higher temperature from up to the down. Table 4-12 presents the details of the fracture observed after the three point bend test of these similar type of diffusion bonded titanium joints.

4.2.5.1.1 Near-α to Near-α Similar Ti-Alloys

In case of near-α to near-α similar type of diffusion bonded joint, Ti-6242SG/Ti-6242SG, the thickness of the joint was same. The microstructures of these joints showed good quality of bond at higher bonding temperatures T7 and T8^{0}C. The good quality of joints was evident in the fractured samples as there was no bondline separation even after the flexural testing at all diffusion bonding temperatures.

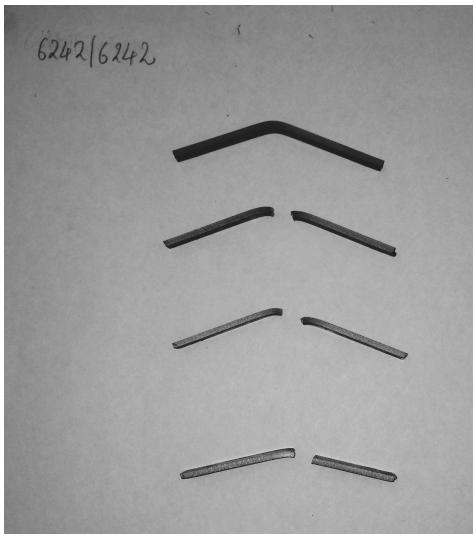

Figure 4.2-35: Fractured Specimens from lower to higher temperatures in DB Similar Near-α Ti-Alloys (Ti-6242/Ti-6242)

4.2.5.1.2 α + β to α + β Similar Ti-Alloys

The fracture results of α + β to α + β similar titanium joints, Ti-54M/Ti-54M, Ti-64/Ti-64, Ti-64FG/Ti-64FG, showed no bondline separation in case of Ti-64SG/Ti-64SG. However post flexural testing there was bondline separation in case of Ti-54M/Ti-54M and Ti-64FG/Ti-64FG fractured joints. Ti-64SG/Ti-64SG joints fractured completely except at T6^{0}C while Ti-54M/Ti-54M did not fracture completely except at T4^{0}C where it fractured completely.

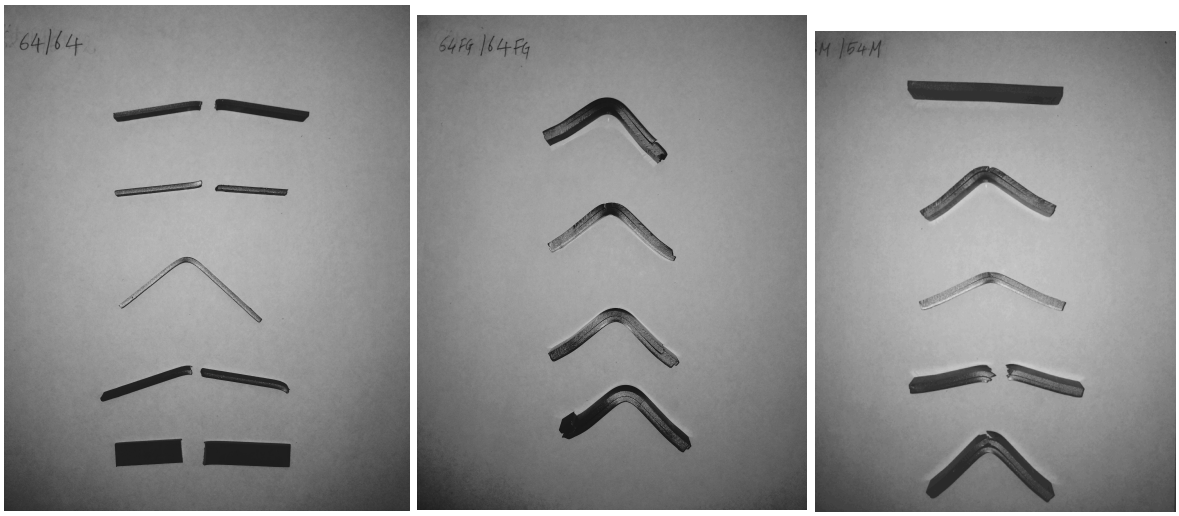

Figure 4.2-36: Fractured Specimens from lower to higher temperatures in DB Similar α + β Ti-Alloys (Ti-54M/Ti-54M, Ti-64/Ti-64, Ti-64FG/Ti-64FG)

4.2.5.1.3 β to β Similar Ti-Alloys

β to β diffusion bonded flexural tested joints did not fracture completely. In these joints, delamination was observed at lower bonding temperatures.

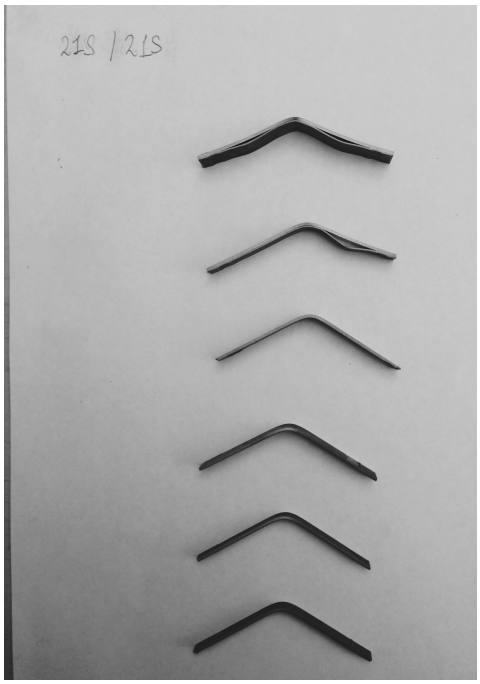

Figure 4.2-37: Fractured Specimens from lower to higher temperatures in DB Similar β Ti-Alloys (β-21S/ β-21S)

Table 4-12: Flexure Test Fracture Results of Similar Titanium Joints - EQ: Equal Thickness BS: Bondline Separation, N BS : No Bondline Separation, CF: Complete Fracture, N CF: Did not Fracture completely

Alloy Name	Temp (C)	Bondline	Fracture	Thickness/Top Alloy	Bend Test Observation
β-21S/ β-21S	T5	N BS	N CF	EQ	
	T6	N BS	N CF	EQ	
	T7	N BS	N CF	EQ	
	T8	N BS	N CF	EQ	
Ti54M/ Ti-54M	T1			EQ	
	T2	BS	N CF	EQ	Lower sheet fractured
	T3	BS	N CF	EQ	Lower sheet fractured
	T4	BS	CF	EQ	
	T5	BS	N CF	EQ	Lower sheet fractured
Ti-64/ Ti-64	T4	N BS	CF	EQ	
	T5	N BS	CF	EQ	
	T6	N BS	N CF	EQ	
	T7	N BS	CF	EQ	
	T8	N BS	CF	EQ	
Ti-64FG/ Ti-64FG	T1	BS	N CF	EQ	
	T2	BS	N CF	EQ	
	T3	BS	N CF	EQ	
	T4	BS	CF	EQ	Separation of dissimilar Ti sheets near the weld
Ti-6242/ Ti-6242	T5	BS	N CF	EQ	
	T6	N BS	CF	EQ	
	T7	N BS	CF	EQ	
	T8	N BS	CF	EQ	

4.2.5.2 Fracture Results – DB Dissimilar Titanium Joints

The next section discusses fracture results of dissimilar type of diffusion bonded titanium joints. Figures 4.2-38 to 4.2-41 displays the fractured specimens of different types of dissimilar titanium joints, near-α to α + β, near-α to β, α + β to α + β, α + β to β joints, at different bonding temperatures. In Figures, the fractured specimens are showcased from lower temperature to higher temperature from up to the down. Table 4.13 presents the details of the fracture observed after the three point bend test of diffusion bonded dissimilar titanium joints.

4.2.5.2.1 Near-α to α+ β Dissimilar Ti-Alloys

In near-α to α+ β dissimilar titanium joints, the sheet thickness was same in Ti6242/Ti-64SG whereas it was unequal in Ti-6242/Ti54M and Ti-64FG with Ti-6242 thinner than the other alloy in both the cases. In Ti6242/Ti-64SG the bonded joints did not fracture completely at lower temperatures whereas it fractured completely at higher temperatures. This is in agreement with the flexural curves where higher ductility was observed at lower temperatures. In other dissimilar joints, effect of thickness was evident on the fracture. In Ti-6242/Ti-64FG, when thinner sheet was present on the top during flexural testing, delamination was observed near the interface of the joint. In the same dissimilar joint when thinner sheet was present on the bottom, instead of delamination fracture was seen near the interface of lower thinner sheet. At $T8^0C$, separation of joints was observed at the welded region. Similarly in case of Ti-6242/Ti-54M when thinner sheet of Ti-6242 was present on the top same delamination phenomena at the lower bonding temperatures and when thinner sheet was on the bottom during the test, complete fracture of thinner sheet near the interface was repeated in the fractured joints.

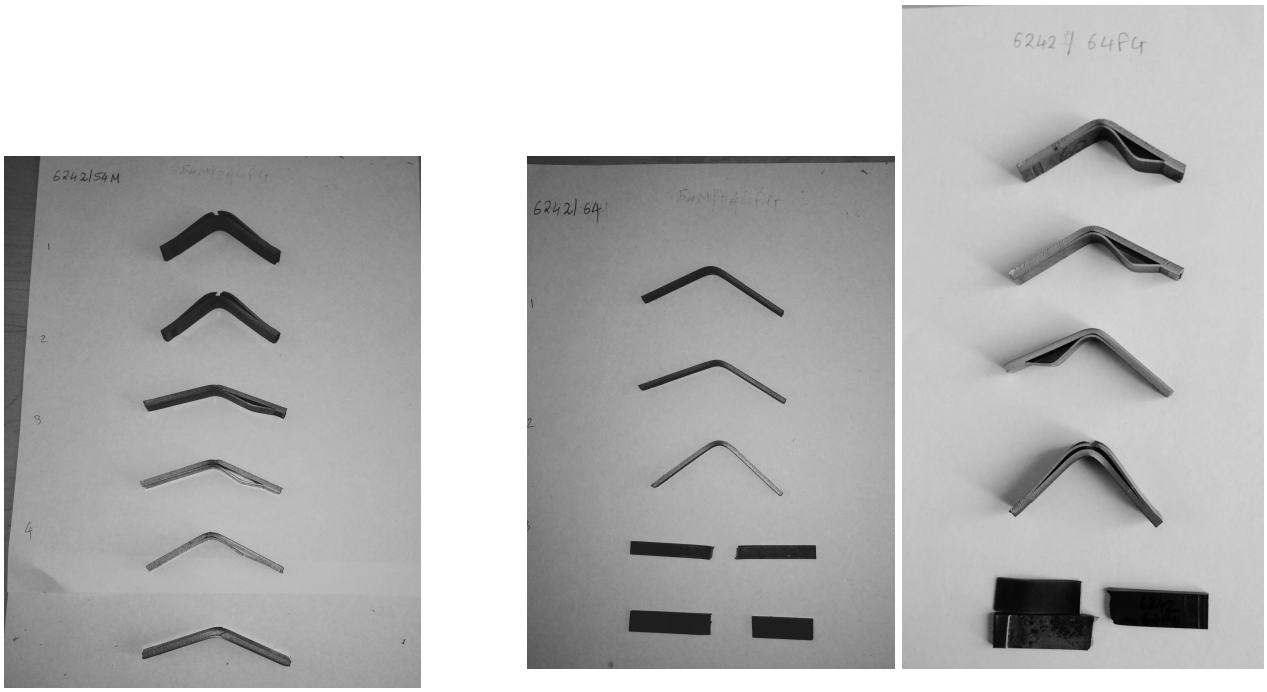

Figure 4.2-38: Fractured Specimens from lower to higher temperatures in DB Dissimilar Near-α to α+ β Ti-Alloys (Ti-6242/Ti-54M, Ti-6242/Ti-64SG, Ti-6242/Ti-64FG)

4.2.5.2.2 Near-α to β Dissimilar Ti-Alloys

In fracture of near-α to β dissimilar titanium joint, Ti-6242/Beta-21S, even after the flexural testing the bondline did not separate and also did not fracture completely .Thus shows good strength in the joints obtained from diffusion bonding.

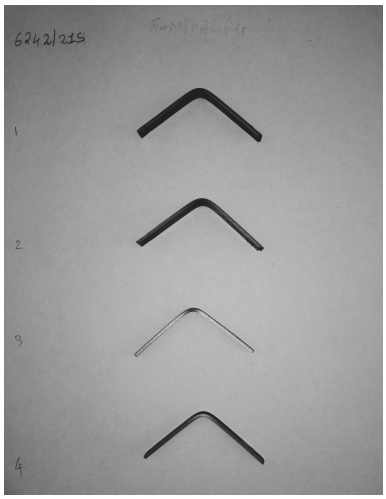

Figure 4.2-39: Fractured Specimens from lower to higher temperatures in DB Dissimilar Near-α to β Ti-Alloys (Ti-6242/ β-21S)

4.2.5.2.3 α+ β to α+ β Dissimilar Ti-Alloys

In dissimilar α+ β to α+ β titanium joints showed common occurrence of bondline separation after flexural testing. In the dissimilar joints Ti-64SG/Ti-54M and Ti-64FG/Ti-54M wherein unequal joint thickness was present, with thinner sheet present on the top it resulted in delamination of thinner sheet at lower bonding temperatures, whereas when thinner sheet was present at the bottom, the fracture was seen from the bottom till the interface of the joint. However when thinner sheet was present on the top at higher, temperatures, it resulted in fracture of lower thicker sheet. In case of equal thickness diffusion sheets, Ti-64FG/Ti-54M the diffusion bonded joints did not fractured completely except at T4^{0}C which showed complete fracture after the flexural test.

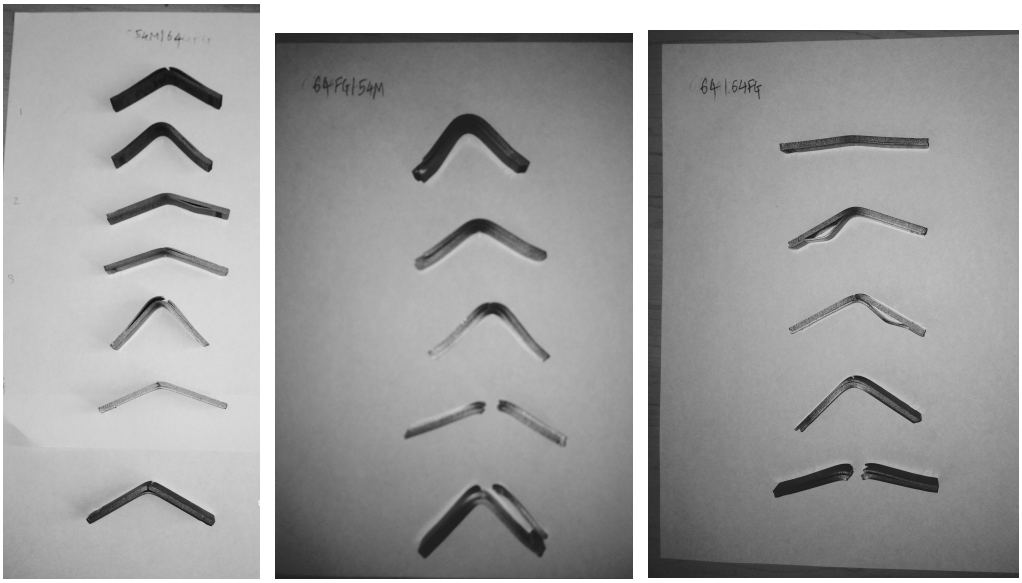

Figure 4.2-40: Fractured Specimens from lower to higher temperatures in DB Dissimilar + β to α+ β Ti-Alloys (Ti-64SG/Ti-54M, Ti-64FG/Ti-54M, Ti-64SG/Ti-64FG)

4.2.5.2.4 α + β to β Dissimilar Titanium Alloys

In α + β to β dissimilar titanium joints, Beta-21S /Ti-54M the fractured specimens showed bondline separation without complete fracture at most of the bonding temperatures except at T6^{0}C where complete fracture was observed without bondline separation. In case of Ti-64SG/Beta 21S, the fractured joints did not show separation at higher temperatures. Additionally the joints did not show complete fracture till T6^{0}C, while it completely fractured at T7^{0}C after being subjected to flexural test. In case of Ti-64FG/Beta-21S

similar phenomenon of effect of thickness of sheets on fracture was as observed in the previous cases of delamination of upper thinner sheet and fracture of thinner bottom sheet.

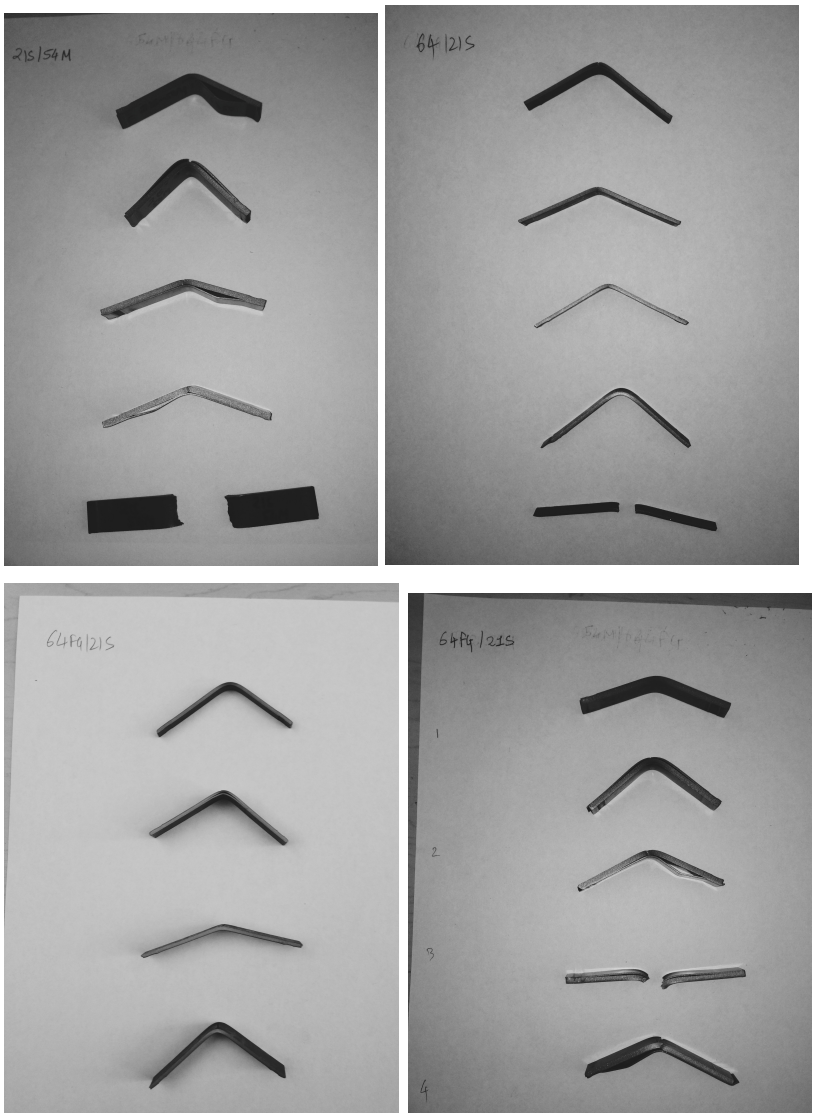

Figure 4.2-41: Fractured Specimens from lower to higher temperatures in DB Dissimilar α+ β to β Ti-Alloys (β-21S/Ti-54M, β-21S /Ti-64SG, and β-21S /Ti-64FG Batch 1 and 2)

Table 4-4-13: Flexure Test Fracture Results of Dissimilar Titanium Joints - EQ: Equal Thickness BS: Bondline Separation, N BS : No Bondline Separation, CF: Complete Fracture, N CF: Did not Fracture completely

Alloy Name	Temp (C)	Bondline	Fracture	Thickness/Top Alloy	Bend Test Observation
β-21S/ Ti-64	T4	BS	N CF		
	T5	N BS	N CF		
	T6	N BS	N CF		
	T7	N BS	CF		
β-21S/ Ti-64FG	T3	N BS	N CF		
	T4	BS	N CF		
	T5	N BS	N CF		
	T6	N BS	N CF		
β-21S / Ti- 64FG	T1	BS	N CF	Ti-64FG	
	T2	BS	N CF	Ti-64FG	Thinner lower sheet fractured
	T3	BS	N CF	β-21S	Delamination of thinner top portion
	T4	BS	CF	Ti-64FG	
	T5	BS	N CF	β-21S	Delamination of thinner top portion, bottom thick sheet fractured
β-21S/ Ti-6242	T5	N BS	N CF		
	T6	N BS	N CF		
	T7	N BS	N CF		
	T8	N BS	N CF		
Ti-64/ Ti-6242	T4	BS	N CF		
	T5	BS	N CF		
	T6	N BS	N CF		
	T7	N BS	CF		
	T8	N BS	CF		
Ti-54M/ Ti-6242	T1	BS	N CF	Ti-54M	Thinner lower sheet fractured
	T2	BS	N CF	Ti-54M	Thinner lower sheet

					fractured
	T3	BS	N CF	Ti-6242	Delamination of thinner top portion
	T4	BS	N CF	Ti-6242	Delamination of thinner top portion
	T5	BS	N CF	Ti-6242	Delamination of thinner top portion
	T6	BS	N CF	Ti-6242	Thicker lower sheet fractured
	T7	BS	N CF	Ti-6242	Thicker lower sheet fractured
β-21S / Ti-54M	T1	BS	N CF	β-21S	
	T2	BS	N CF	Ti-54M	
	T3	BS	N CF	β-21S	
	T4	BS	N CF	β-21S	
	T5	BS	N CF	Ti-54M	
	T6	N BS	CF	Ti-54M	
	T7	BS	N CF		
Ti-54M/ Ti-64	T1	BS	N CF	Ti-54M	Thinner lower sheet fractured
	T2	BS	N CF	Ti-54M	
	T3	BS	N CF	Ti-64	Delamination of thinner top portion
	T4	BS	N CF	Ti-54M	Thinner lower sheet fractured
	T5	BS	N CF	Ti-54M	Thinner lower sheet fractured
	T6	BS	N CF	Ti-64	Thicker lower sheet fractured
	T7	BS	N CF	Ti-64	Thicker lower sheet fractured
Ti6242/ Ti-64FG	T1	BS	N CF	Ti-6242	Delamination of thinner top portion
	T2	BS	N CF	Ti-6242	Delamination of thinner top portion
	T3	BS	N CF	Ti-6242	Delamination of thinner top portion
	T4	BS	N CF	Ti-64FG	Thinner lower sheet fractured

	T5	BS	CF		Separation of dissimilar Ti sheets near the weld
Ti-64/ Ti-64FG	T1	BS	N CF	Ti-64	
	T2	BS	N CF	Ti-64	Delamination of thinner top portion
	T3	BS	N CF	Ti-64	Delamination of thinner top portion
	T4	BS	N CF	Ti-64FG	Thinner lower sheet fractured
	T5	BS	CF	Ti-64FG	Thinner lower sheet fractured
Ti-64FG/ Ti-54M	T1	BS	N CF	EQ	
	T2	BS	N CF	EQ	
	T3	BS	N CF	EQ	
	T4	BS	CF	EQ	
	T5	BS	CF	EQ	Separation of dissimilar Ti sheets near the weld

4.2.5.3 Fractured Specimens Metallographic Examination

Metallographic examination was conducted of sections through the bond lines of solid-state bonded samples after flexure testing. Figure 4.2-42 and Figure 4.2-43 show metallographic images of Ti-64SG/ Ti-64SG at T5 and T8^{0}C. The bond line is evident at T5^{0}C. The failure did not occur near the bond line. In case of Ti-64SG / Ti-64SG, Ti-6242/Ti-6242(Figure 4.2-44) and Ti-64SG /Ti-6242 (Figure 4.2-45) at T8^{0}C, the bond line remained unaffected after performing flexure testing. Therefore demonstrates that a good quality joining strength was achieved through diffusion bonding. The fractured surfaces appear rough and irregular. The surface consists of many micro voids and dimples, therefore demonstrates the case of ductile failure.

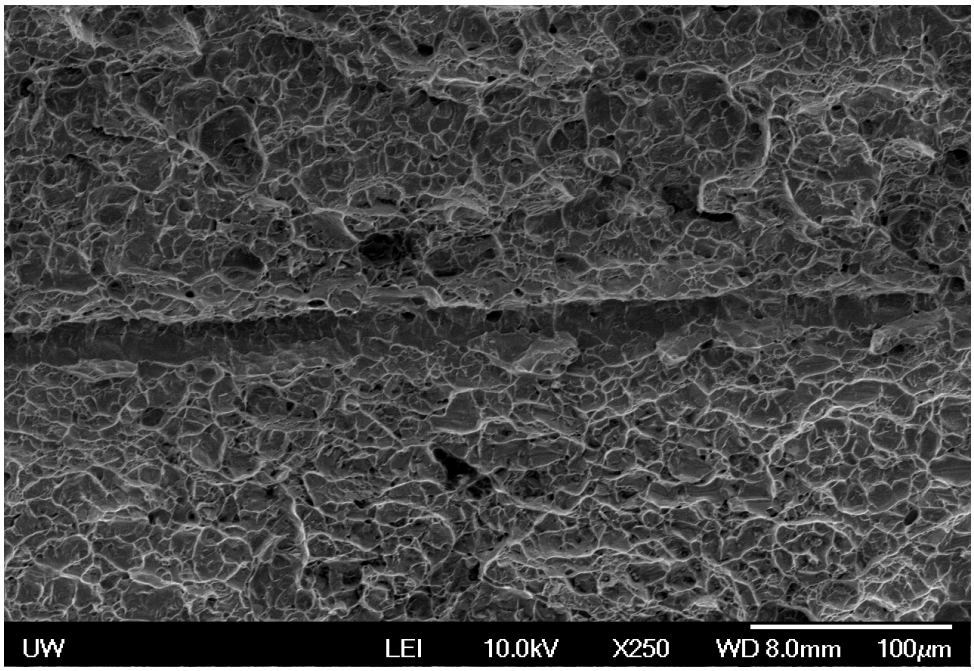

Figure 4.2-42: Microstructure of Fractured surface along bonding interface: Ti-64SG / Ti-64SG, T5^{0}C

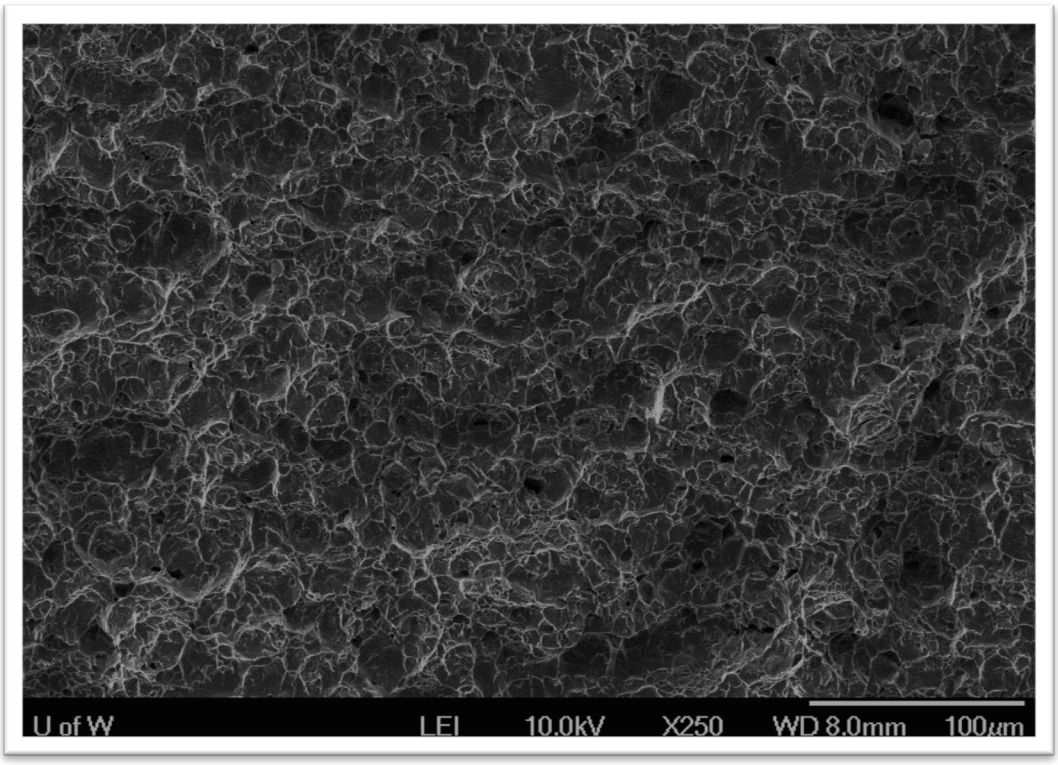

Figure 4.2-43: Microstructure of Fractured surface along bonding interface: Ti-64SG / Ti-64SG, T8^{0}C

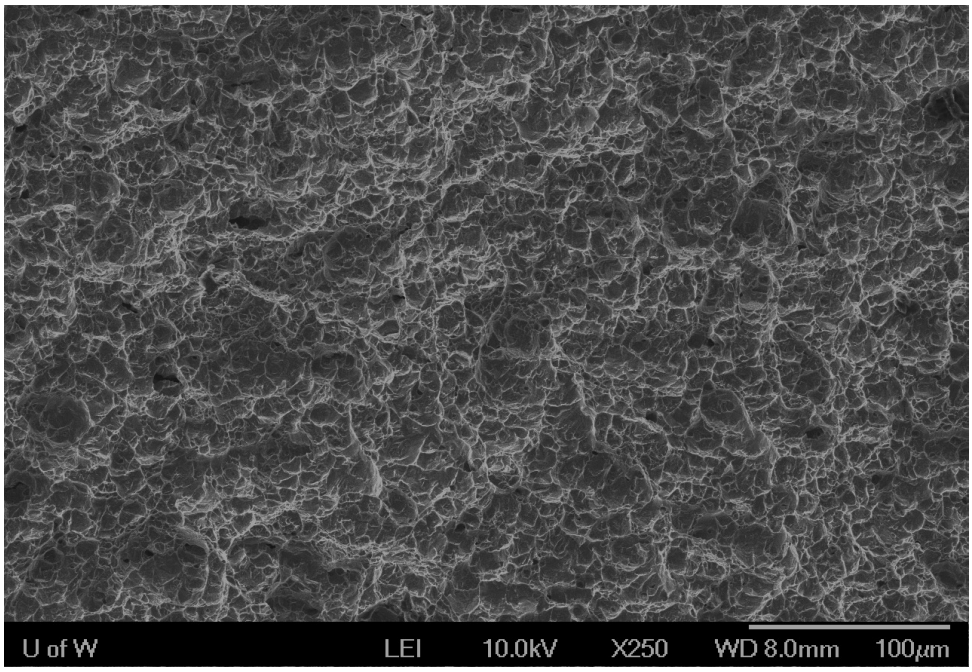

Figure 4.2-44: Microstructure of Fractured surface along bonding interface: Ti-6242/Ti-6242, T8^{0}C

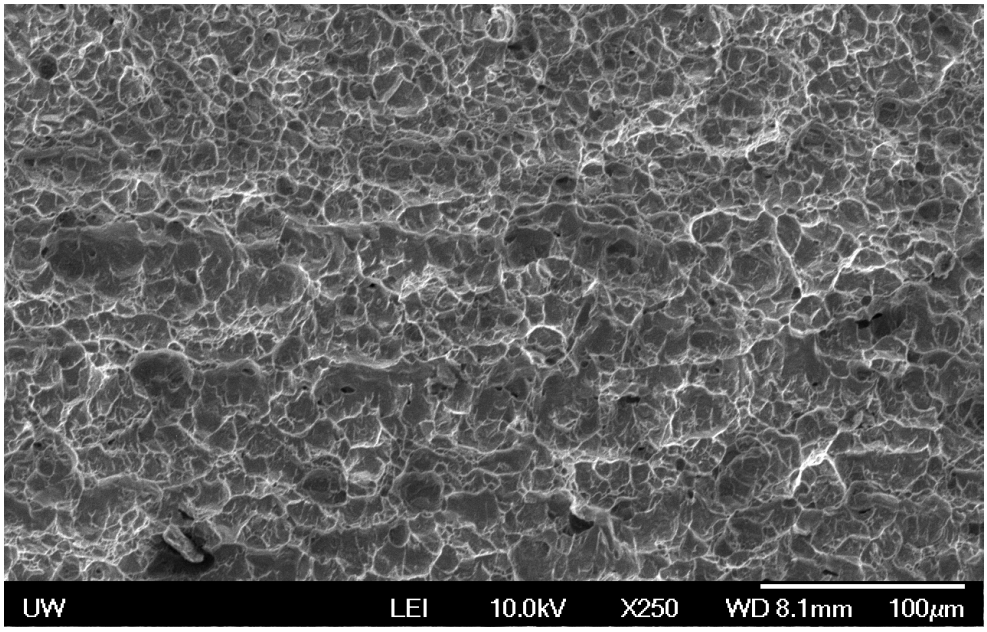

Figure 4.2-45: Microstructure of Fractured surface along bonding interface: Ti-64SG /Ti-6242, T8^{0}C

4.3 FRICTION STIR WELDING OF SIMILAR AND DISSIMILAR TTIANIUM JOINTS QUALITY ANALYSIS

4.3.1 *Macrostructure*

Optical macrographs from typical FSW butt joint transverse sections of titanium alloy Ti-6242SG/Ti-6242SG oriented to show the top surface and thickness cut of the titanium stir weld coupons as shown in Figure 4.3-1. The top surface is saw-toothed in appearance. The sharpness of the spikes was observed more for higher spindle speeds. Large sized burrs occur on the advancing side. Both the surface texture and the burr geometry vary across the weld nugget.

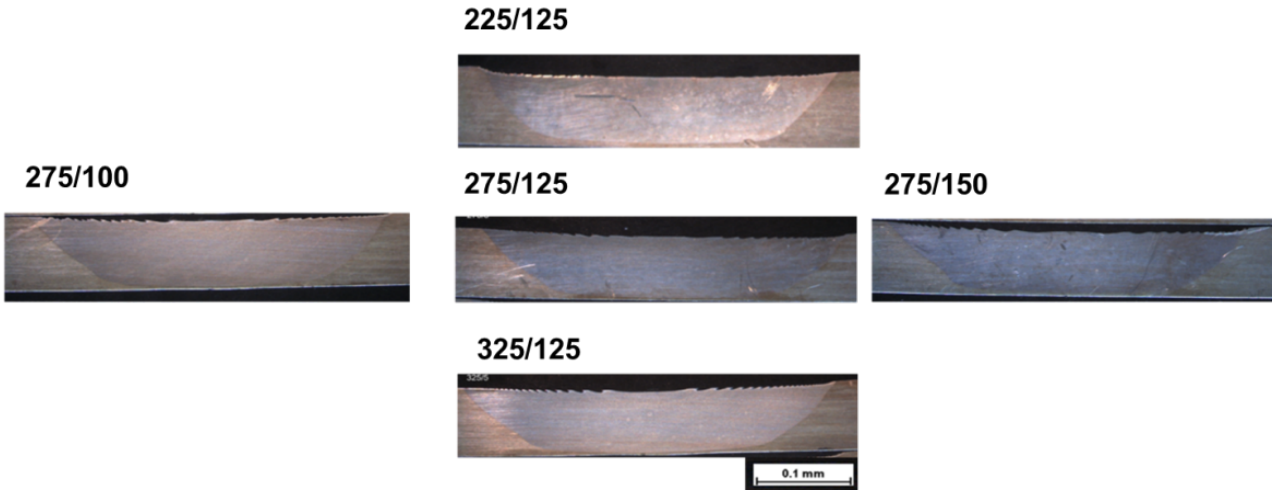

Figure 4.3-1: Macrographs of butt joined Ti-6242SG/Ti-6242SG at different Spindle Speeds (RPM)/ Feed Rate (mm/min)

Figure 4.3-2 shows typical macrograph of friction stir welded joint between Ti-6242SG and Ti-64SG. During the welding process, the material moves from retreating side to advancing side in the welded zone. The change in feed rate and rotation speed shows different mixing patterns in the welded zone of dissimilar alloys. Note that these experimental conditions produced defect free butt joints with dissimilar titanium alloys. In Ti-6242SG/Ti-64SG, the material flows from Ti-64SG (retreating side) to Ti-6242SG (advancing side). In case of constant spindle speed at 275RPM, the increase in feed rate

from 125 mm min-1 to 150 mm min-1 moved less amount of material from Ti-64SG towards Ti-6242SG side. For constant feed rate at 125 mm min-1, higher amount of material passed from the retreating side at 275 RPM than at 325 RPM. Table 4.14 provides the details of materials assignment in advancing and retreating side while producing dissimilar titanium joints through friction stir welding. Ti-54MFG was held at retreating side while making dissimilar joints. In case of dissimilar joints with fine grain and standard grain titanium, the fine grain alloy was placed at advancing side. In the combination of same grain type, standard grain to standard grain and fine grain to fine grain (Ti-64SG/Ti-6242SG and Ti-64FG/Ti-6242FG), Ti-6242 was placed in the advancing side.

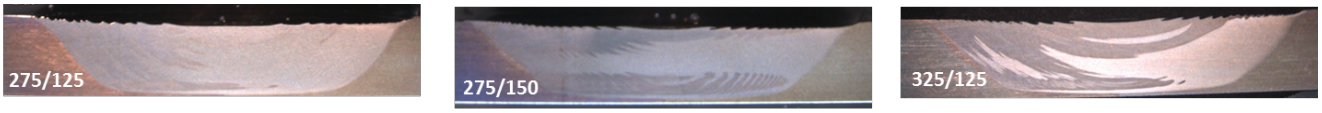

Figure 4.3-2: Macrograph of FSW Ti-62424SG/Ti-64SG at different rotation speed and feed rates (RPM/mm min-1)

Table 4-14: Material Assignment in Advancing and Retreating side in Dissimilar Friction Stir Welded Titanium Alloys

Dissimilar FSW Ti-Joints	Advancing	Retreating
Ti-54MFG/Ti-64SG	Ti-64SG	Ti-54MFG
Ti-54MFG/Ti-6242SG	Ti-6242SG	Ti-54MFG
Ti-54MFG/ Ti-64FG	Ti-64FG	Ti-54MFG
Ti-54MFG/Ti-6242FG	Ti-6242FG	Ti-54MFG
Ti-64SG/Ti-6242SG	Ti-6242SG	Ti-64SG
Ti-64SG/Ti-6242FG	Ti-6242FG	Ti-64SG
Ti-64FG/Ti-6242FG	Ti-6242FG	Ti-64FG

4.3.2 *Mechanical Behavior of Welded Joints*

The stress strain data of the tensile test was plotted to study the mechanical properties of the friction stir welding process. The stress strain curves were plotted for all the specimens. The important mechanical properties such as the Modulus of Elasticity, Yield Stress, Ultimate Stress, and Elongation were established from the plots. Table 4.15-18 refers mechanical properties of similar and dissimilar friction stir welded titanium joints. In order

to understand the influence of tooling conditions on the process, the results were analyzed as a function of feed rate and the speed.

Table 4-15: Elastic Modulus (GPa) of Friction Stir Welded Similar and Dissimilar Joints

FSW Ti-Alloy Joints	Speed (RPM)/Feed Rate (mm/min)				
	225/ 125	275/100	275/125	275/150	325/ 125
Ti-54MFG/Ti-54MFG	90540	90770	96401	91720	92780
Ti-64SG/ Ti-64SG	104194	96908	104375	94628	101865
Ti-6242SG/Ti-6242SG	129449	123190	129539	136317	99117
Ti-64FG/ Ti-64FG	100124	82789	79653	85667	87605
Ti-6242FG/Ti-6242FG	132721	130823	118696	114634	97630
Ti-54MFG/Ti-64SG	93103	96448	95109	101511	87679
Ti-54MFG/Ti-6242SG	158624	120465	120530	144185	102818
Ti-54MFG/Ti-64FG	76222	100858	93342	93643	77738
Ti-54MFG/Ti-6242FG	156259	119913		116497	117365
Ti-64SG/ Ti-6242SG	131140	140350	106087	125140	132654
Ti-64SG/Ti-6242FG	134957	147766		125887	126027
Ti-64FG/ Ti-6242FG	176334	141140		157275	126756

Table 4-16: 0.2% Yield Strength (MPa) of Friction Stir Welded Similar and Dissimilar Joints

FSW Ti-Alloy Joints	Speed (RPM)/Feed Rate (mm/min)				
	225/ 125	275/100	275/125	275/150	325/ 125
Ti-54MFG/Ti-54MFG	697	755	739	677	728
Ti-64SG/ Ti-64SG	679	713	690	688	697
Ti-6242SG/Ti-6242SG	726	795	769	717	760
Ti-64FG/ Ti-64FG	618		693	690	715
Ti-6242FG/Ti-6242FG	768	803	808	T5	851
Ti-54MFG/Ti-64SG	669	706	684	611	714
Ti-54MFG/Ti-6242SG	867	824	878	723	897
Ti-54MFG/Ti-64FG	630	685	689	690	
Ti-54MFG/Ti-6242FG	355	848		856	840
Ti-64SG/ Ti-6242SG	784	839	768	802	829
Ti-64SG/Ti-6242FG	896	873		897	721
Ti-64FG/ Ti-6242FG	665	713		695	723

Table 4-17: Ultimate Strength (MPa) of Friction Stir Welded Similar and Dissimilar Joints

FSW Ti-Alloy Joints	Speed (RPM)/Feed Rate (mm/min)				
	225/ 125	275/100	275/125	275/150	325/ 125
Ti-54MFG/Ti-54MFG	903	949	919	895	915
Ti-64SG/ Ti-64SG	884	907	880	913	898
Ti-6242SG/Ti-6242SG	945	950	941	929	960
Ti-64FG/ Ti-64FG	848	880	877	864	886
Ti-6242FG/Ti-6242FG	955	867	937	984	899
Ti-54MFG/Ti-64SG	891	917	896	853	924
Ti-54MFG/Ti-6242SG	956	993	995	842	1006
Ti-54MFG/Ti-64FG	869	876	867	881	930
Ti-54MFG/Ti-6242FG	508	961		976	994
Ti-64SG/ Ti-6242SG	892	958	916	872	981
Ti-64SG/Ti-6242FG	896	1000		990	960
Ti-64FG/ Ti-6242FG	761	910		886	955

Table 4-18: Ductility (%Elongation) of Friction Stir Welded Similar and Dissimilar Joints

FSW Ti-Alloy Joints	Speed (RPM)/Feed Rate (mm/min)				
	225/ 125	275/100	275/125	275/150	325/ 125
Ti-54MFG/Ti-54MFG	7	6	6	8	8
Ti-64SG/ Ti-64SG	5	8	7	7	7
Ti-6242SG/Ti-6242SG	2	4	3	2	5
Ti-64FG/ Ti-64FG	4	10	9	9	9
Ti-6242FG/Ti-6242FG	1	2	2	1	3
Ti-54MFG/Ti-64SG	6	7	7	5	8
Ti-54MFG/Ti-6242SG	1	4	4	3	6
Ti-54MFG/ Ti-64FG	8	5	7	8	11
Ti-54MFG/Ti-6242FG	0	2		2	3
Ti-64SG/ Ti-6242SG	1	2	14	1	3
Ti-64SG/ Ti-6242FG	1	2		2	2
Ti-64FG/ Ti-6242FG	1	2		2	2

4.3.2.1 Friction Stir Welded Similar Ti-Alloys

The standard Ti-6Al-4V sheet has elastic modulus of 113.8 GPa, yield strength of 1103 MPa, ultimate strength of 1172 MPa and elongation at failure of about 10 %. Figure 4.3-3 show the stress strain behavior of the different titanium alloys. The stress strain behavior obtained from the two samples of each specimen was similar; therefore, one of the results from the two of them was plotted. The other mechanical properties varied with the change in feed rate and spindle speed. The stress strain trends were similar in titanium alloys, Ti-54MFG/Ti-54MFG, Ti-64SG/Ti-64SG, and Ti-64FG/Ti-64FG. The ductility values were comparatively higher in these alloys than the other titanium alloys Ti-6242SG/Ti-6242SG and Ti-6242FG/Ti-6242FG. Ti-6242FG/Ti-6242FG showed very low ductility. The average mechanical properties were close to the standard properties of Ti-6Al-4V. The joint strength of 70% was obtained through the friction stir welding of titanium alloys. Ti-6242SG/Ti-6242SG showed highest elastic modulus whereas Ti-64FG/Ti-64FG displayed low elastic modulus for the combination of feed rate and spindle speed used in the study. The mechanical properties of the welded titanium alloys were affected by the feed rate and the spindle speed. Ti-6242SG/Ti-6242SG showed highest average ultimate tensile strength amongst all the titanium alloys. The average yield strength was higher in case of Ti-6242FG/Ti-6242FG, whereas Ti-64FG/Ti-64FG achieved the maximum elongation in all the titanium alloys.

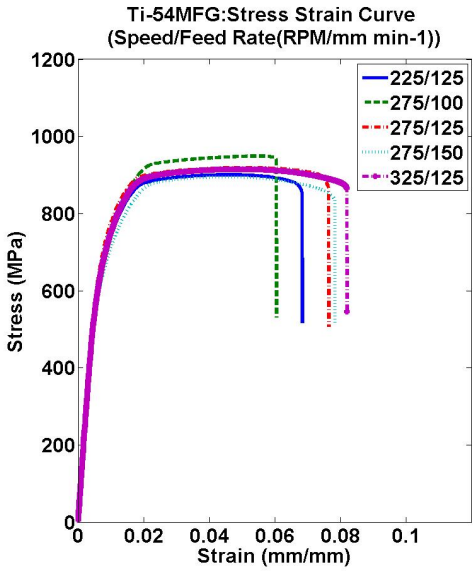

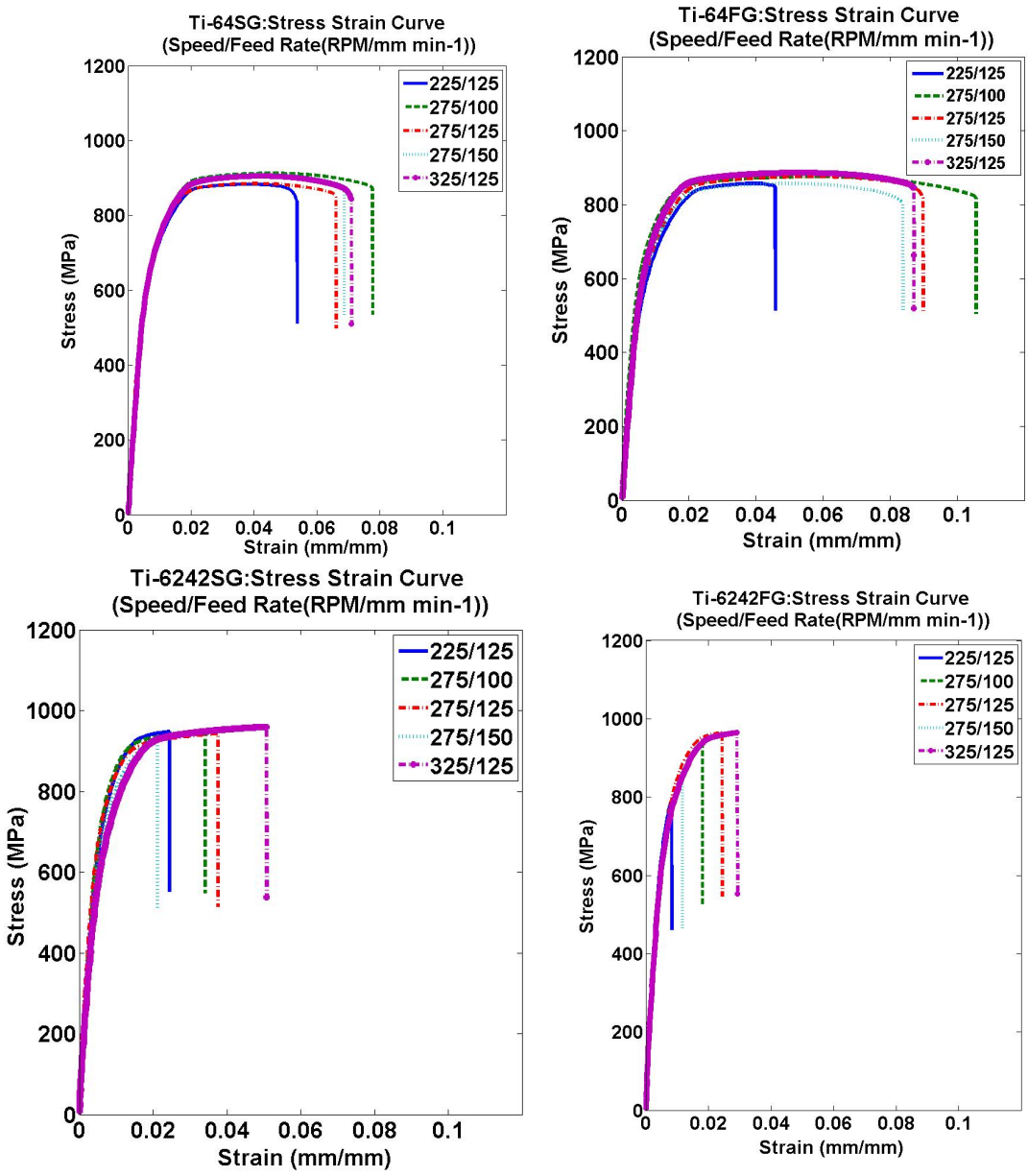

Figure 4.3-3: FSW Stress Strain Curve Ti-54MFG, Ti-64SG, Ti-64FG, Ti-6242SG, and Ti-6242FG

4.3.2.1.1 Influence of Spindle Speed

The impact of spindle speed from 225 RPM to 325RPM was studied on the mechanical properties of the joints by keeping the feed rate constant at 125 mm/min. The elastic modulus did not affect with the change in spindle speed for friction stir welded titanium alloys. Figure 4.3-4 shows the effect of speed on mechanical properties of the different

titanium joints. The increase in speed from 225 RPM to 275 RPM increased the yield strength in the titanium alloys. The further increase in speed to 325 RPM increased the yield strength in Ti-64SG/Ti-64SG and Ti-64FG/Ti-64FG but slightly decreased the yield strength in Ti-54MFG/Ti-54MFG, Ti-6242SG/Ti-6242SG, and Ti-6242FG/Ti-6242FG. There was influence of speed on yield strength and ultimate strength in Ti-64FG/Ti-64FG and Ti-6242FG/Ti-6242FG.There was 15 % increase in yield strength observed for Ti-64FG/Ti-64FG. The ultimate strength increased with the spindle speed in case of Ti-64FG/Ti-64FG by 5%, while it decreased with the increase in speed for Ti-6242FG/Ti-6242FG. In the rest of titanium alloys, the ultimate strength did not vary significantly with the change in spindle speed. The elongation increased with the increase in the spindle speed for all friction stir welded titanium alloys.

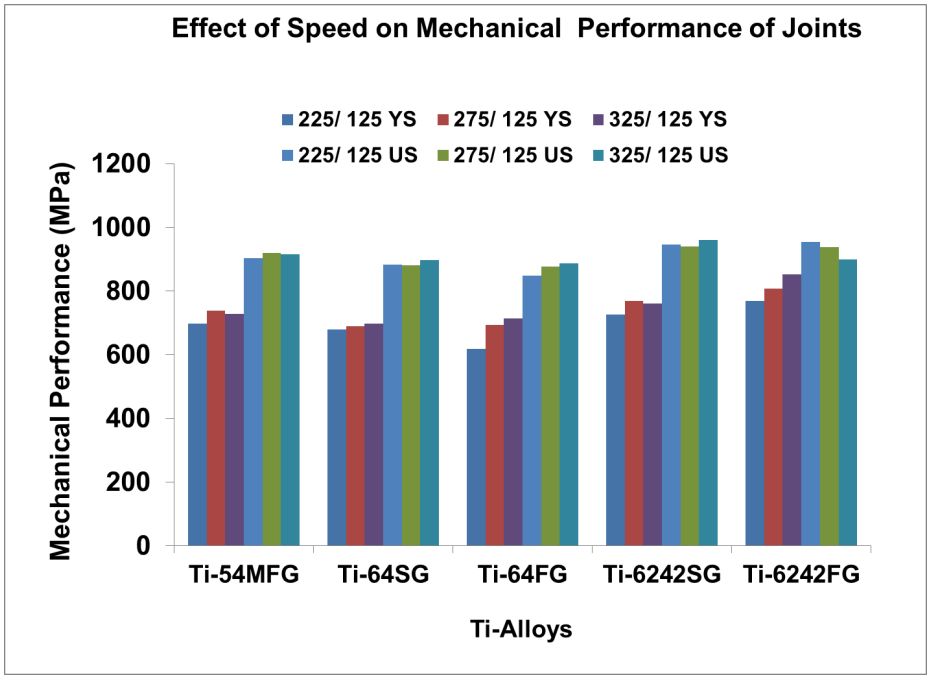

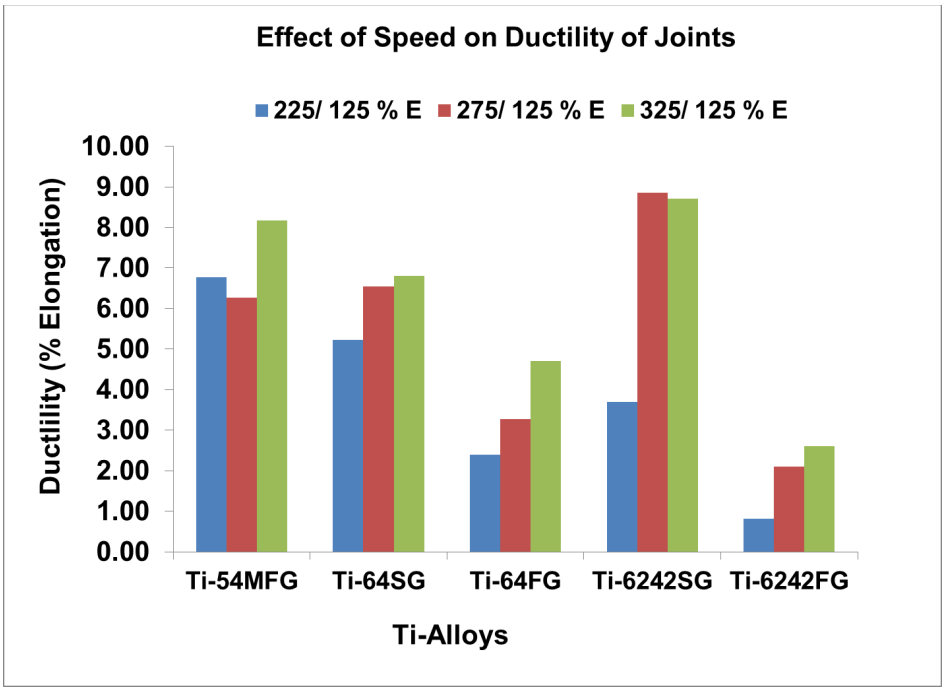

Figure 4.3-4: Effect of Tool Speed on Mechanical Properties and Ductility of FSW Ti-Joints

4.3.2.1.2 Influence of Feed Rate

The effect of feed rate from 100 mm/min to 150 mm/min was studied on the mechanical properties of the friction stir welded titanium alloys by maintaining the spindle speed at 275 RPM (Figure 4.3-5). The elastic moduli of the friction stir welded titanium alloys did not change significantly with the feed rate. The impact of feed rate on other mechanical properties of titanium joints is shown in Figure 4.4-5.The yield strength measured at 0.2% strain and the ultimate tensile strength decreased with the increase in feed rate for all the welded titanium alloys except the ultimate strength of Ti-64SG/Ti-64SG and Ti-6242FG/Ti-642FG. The ultimate tensile strength increased by 4 % in Ti-64SG/Ti-64SG when the feed rate was changed from 125 mm/min to 150 mm/min and by 5 % in Ti-6242FG/Ti-642FG when the feed rate was changed from 100 mm/min to 125 mm/min at the constant spindle speed of 275 RPM. The increase in feed rate increased the elongation in Ti-54MFG/Ti-54MFG, while it decreased in Ti-64FG/Ti-64FG and Ti-6242SG/Ti-6242SG. In rest of titanium alloys, the elongation varied with the change in the feed rate.

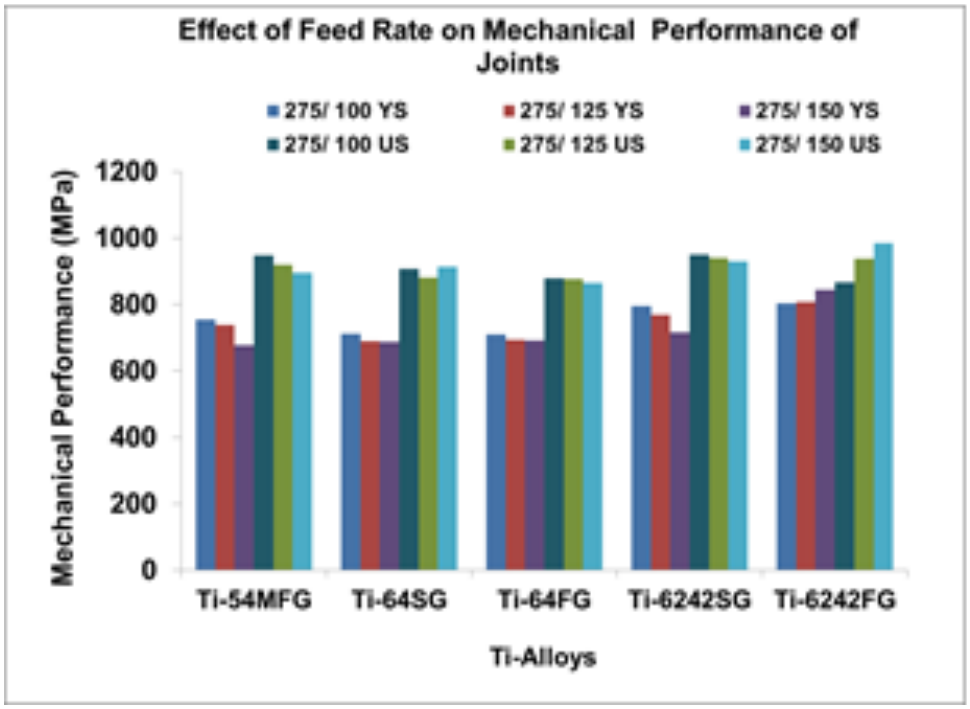

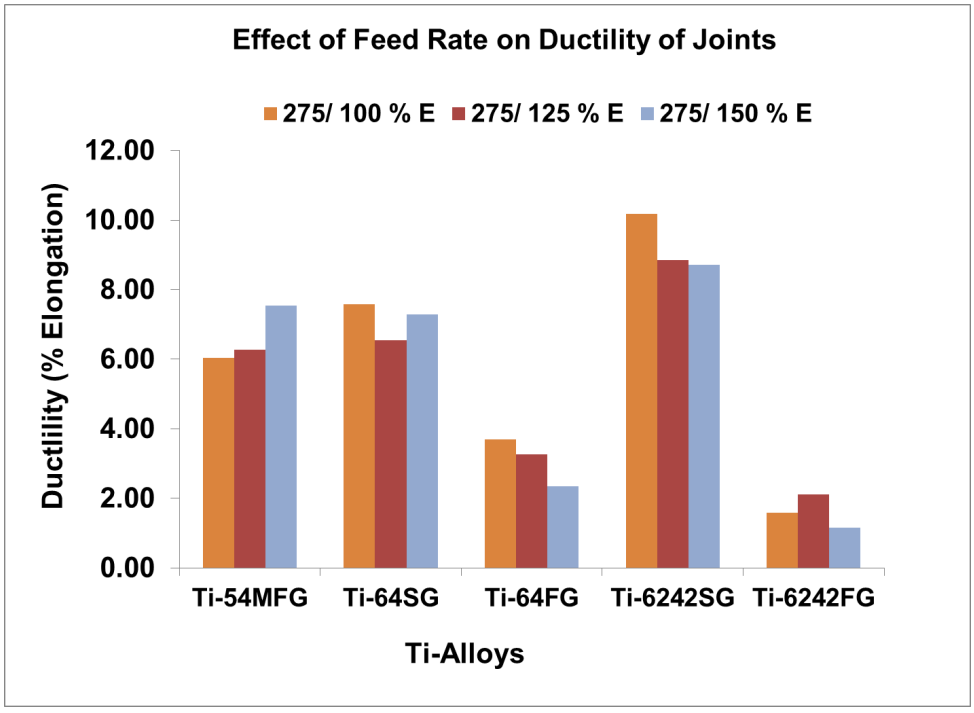

Figure 4.3-5: Effect of Feed Rate on Mechanical Properties and Ductility of FSW Ti-Joints

4.3.2.2 Friction Stir Welded Dissimilar Ti-Alloys

The mechanical behavior was assessed from the stress strain curve in the friction stir welded dissimilar titanium alloys. The results in this subsection are divided into two parts according to the grain size. The two parts of this subsection include results on joints made with standard grain titanium alloy and Ti-54MFG and the joints made with fine grain titanium alloy and Ti-54MFG.

4.3.2.2.1 Joints with Ti-54MFG and Standard Grain Titanium Alloys

The stress strain for dissimilar titanium alloys Ti-64SG/ Ti-54MFG, Ti-6242SG/ Ti-54MFG, and Ti-6242SG/Ti-64SG at different rotation speeds and feed rates are shown in Figure 4.3-6. The joint strength of dissimilar friction stir weldment was at most 90% and above of the parent alloys. The stress strain curve shows that the elastic modulus did not affect with the change in process parameters. The average elastic modulus for dissimilar alloys Ti-64SG/ Ti-54MFG, Ti-6242SG/ Ti-54MFG, and Ti-6242SG/Ti-64SG was 94.8 GPa, 129.4 GPa, and 127.1 GPa respectively. Ti-6242SG/Ti-54MFG showed highest elastic modulus of 158.6 GPa at 225RPM/125 mm min-1. The impact of feed rate and rotation speed was evident on ultimate strength and ductility than the yield strength. In case of dissimilar alloys with Ti-54MFG, the mechanical properties were higher with Ti-6242SG than with Ti-64SG. Both the ultimate strength and yield strength were higher in friction stir welded Ti-6242SG/Ti-54MFG alloy. In terms of ductility, highest value was reached in Ti-6242SG/Ti64SG at 275RPM/125 mm min-1. In the rest of the cases, the elongation was less than 10%.

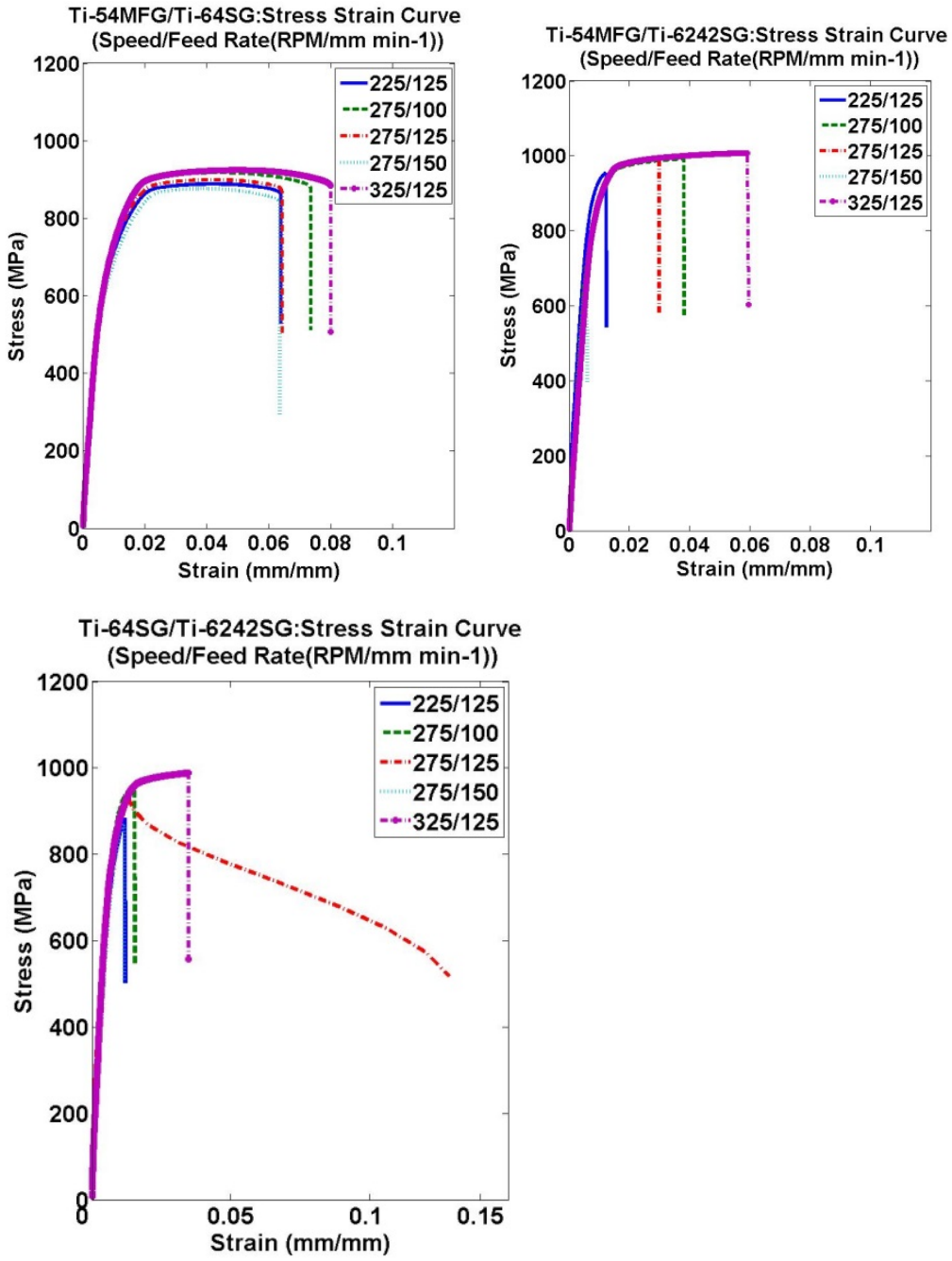

Figure 4.3-6: Stress Strain in Dissimilar Titanium Alloys with Standard Grain- Ti-54MFG/Ti-64SG, Ti-54MFG/Ti-64SG, Ti-54MFG/Ti-6242SG, and Ti-64SG/Ti-6242SG

a. *Influence of Feed Rate*

The influence of feed rate on the strength of the joint was examined by changing the feed rate from 100 mm min-1 to 150 mm min-1 maintaining the rotation speed constant

at 275RPM as shown in Figure 4.3-7. The increase in feed rate caused the increase in modulus of elasticity in the alloys joined with Ti-54MFG, while decreased in Ti-6242SG/Ti-64SG. The other mechanical properties, the yield strength measured at 0.02%, the ultimate strength, and the elongation lowered with increase in the feed rate in Ti-64SG/Ti-54MFG. In case of Ti-6242SG/Ti-54MFG, the yield strength increased followed by a decrease; while the ultimate strength slightly increased with the first step of increase in the speed, followed by a decrease from the feed rate of 125 mm min-1 to 150mm min-1. The ductility of Ti-6242SG/Ti-54MFG decreased with the increase in feed rate. The highest value of ductility was reached at the feed rate of 125 mm min-1 in Ti-6242SG/Ti-64SG welded joint. The decrease in strength as a result of increase in feed rate was less than 14% and 16% for yield strength and ultimate strength respectively. Therefore, the effect of rotation speed was more evident than the feed rate on the friction stir welded dissimilar titanium alloys. However the strength was a good as 90% with respect to original strength of the parent alloys. During the friction stir welding, when the rotation speed was held constant, the feed rate of 125 mm min-1 recorded the maximum strength for the joint. In terms of dissimilar joined alloys, Ti-6242SG/Ti-54MFG showed higher strength properties than the other titanium joined alloys.

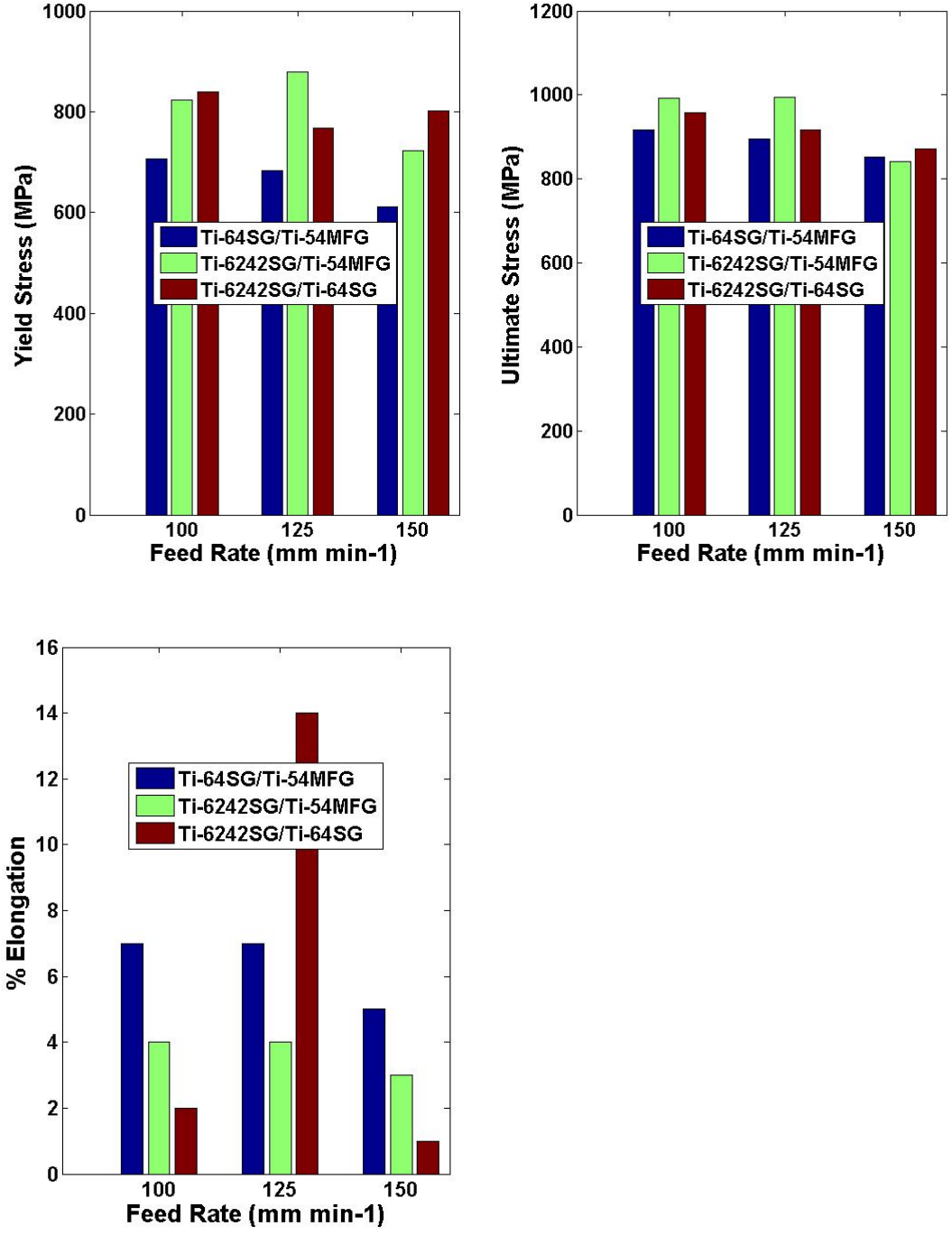

Figure 4.3-7: Effect of Feed Rate on mechanical strength and ductility of joints in dissimilar joined Ti-Alloys with Standard Grain (Ti-54MFG/Ti-64SG, Ti-54MFG/Ti-64SG, Ti-54MFG/Ti-6242SG, and Ti-64SG/Ti-6242SG)

b. *Influence of Spindle Speed*

The effect of rotation speed on the mechanical behavior of friction stir welded joints was observed by increasing the rotation speed from 225RPM to 325RPM keeping the feed rate constant at 125 mm min-1 as shown in Figure 4.3-8. The increase in rotation speed resulted in increase in yield strength; ultimate strength and the elongation in dissimilar alloy Ti-64SG/Ti-54MFG and Ti-6242SG/Ti54MFG. In Ti-6242SG/Ti64SG, the increase in rotation speed from 225RPM to 275RPM decreased the yield strength, followed by the increase from 275RPM to 325RPM. However the ultimate strength in this case increased with the increase in rotation speed. The ductility in case of Ti-6242SG/Ti-64SG increased with the rotation speed 225RPM to 275RPM where it recorded 14%. In the process when the feed rate was constant, maximum properties in terms of strength were observed at the rotation speed 325RPM for all three of the welded alloys, while the maximum ductility was reached with rotation speed 275RPM. Ti-6242SG/Ti-54MFG alloy showed higher strength than the other dissimilar welded titanium alloys. The rise of maximum 7% in yield strength and of 10 % in ultimate strength was observed in the dissimilar alloys as an effect of increase in rotation speed.

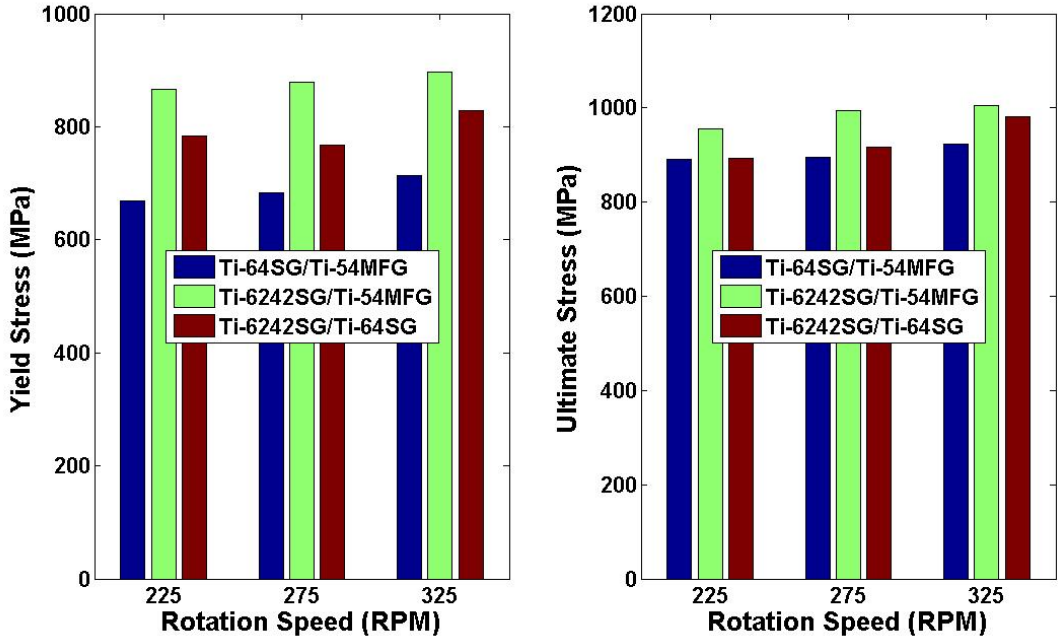

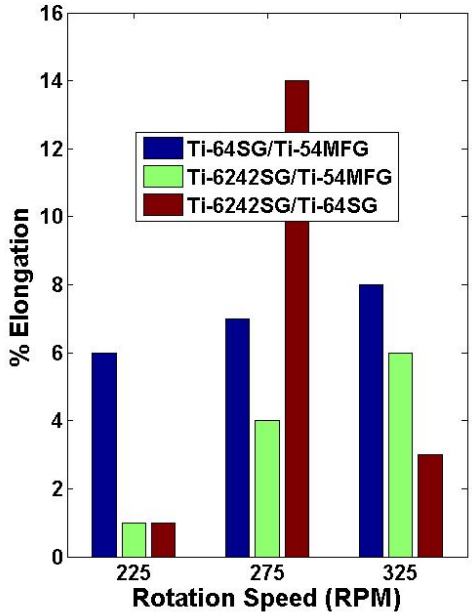

Figure 4.3-8: Effect of Spindle Speed on mechanical strength and ductility of joints in dissimilar joined Ti-Alloys with Standard Grain (Ti-54MFG/Ti-64SG, Ti-54MFG/Ti-64SG, Ti-54MFG/Ti-6242SG, and Ti-64SG/Ti-6242SG)

4.3.2.2.2 Joints with Ti-54MFG and Fine Grain Titanium Alloys

The stress strain for dissimilar titanium alloys Ti-54MFG/Ti-64FG, Ti-54MFG/Ti-6242FG, Ti-64SG/Ti-6242FG, and Ti-64FG/Ti-6242FG at different rotation speeds and feed rates are shown in Figure 4.3-9. The elastic modulus did not affect much with the change in process parameters. The average elastic modulus for dissimilar alloys with fine grain Ti-54MFG/Ti-64FG, Ti-54MFG/Ti-6242FG, Ti-64SG/Ti-6242FG, and Ti-64FG/Ti-6242FG was 88.36 GPa, 127.5 GPa, 133.66 GPa, and 150.38 respectively. Ti-64FG/Ti-6242FG showed highest elastic modulus of 176.33 GPa at 225RPM/125 mm min-1. The impact of feed rate and rotation speed was evident on ultimate strength and ductility than the yield strength. The stress strain curve showed that Ti-54MFG/Ti-64FG yielded higher ductility than other combination of dissimilar titanium joints with fine grain. In terms of ductility, highest value was reached in Ti-54MFG/Ti-64FG at 325RPM/125 mm min-1. In the rest of the cases, the elongation was less than 5%.

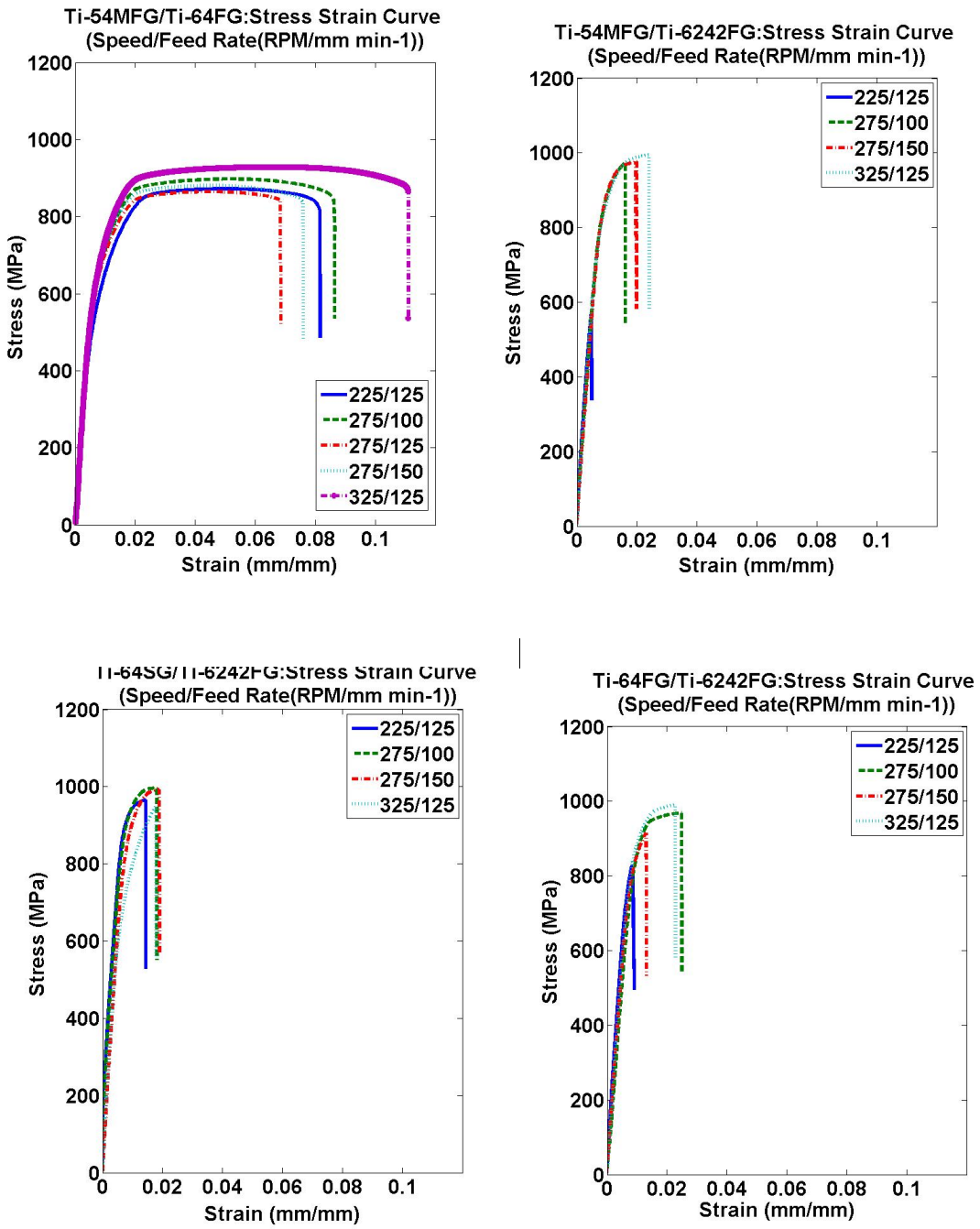

Figure 4.3-9: Stress Strain in Dissimilar Titanium Alloys with Fine Grain (Ti-54MFG/Ti-64FG, Ti-54MFG/Ti-6242FG, Ti-64SG/Ti-6242FG, and Ti-64FG/Ti-6242FG)

a. *Influence of Feed Rate*

The influence of feed rate on the strength of the joint was examined by changing the feed rate from 100 mm min-1 to 150 mm min-1 maintaining the rotation speed constant at

275RPM as shown in Figure 4.3-10. The yield strength measured at 0.02 strain increased with the feed rate for Ti-54MFG/Ti-64FG, Ti-54MFG/Ti-6242FG, and Ti-64FG/Ti-6242FG except for Ti-64SG/Ti-6242FG. The ultimate stress and elongation increased with the increase in feed rate for dissimilar friction stir welded titanium fine grain joints. The feed rate 150mm min-1 yield higher results in the fine grain dissimilar joints.

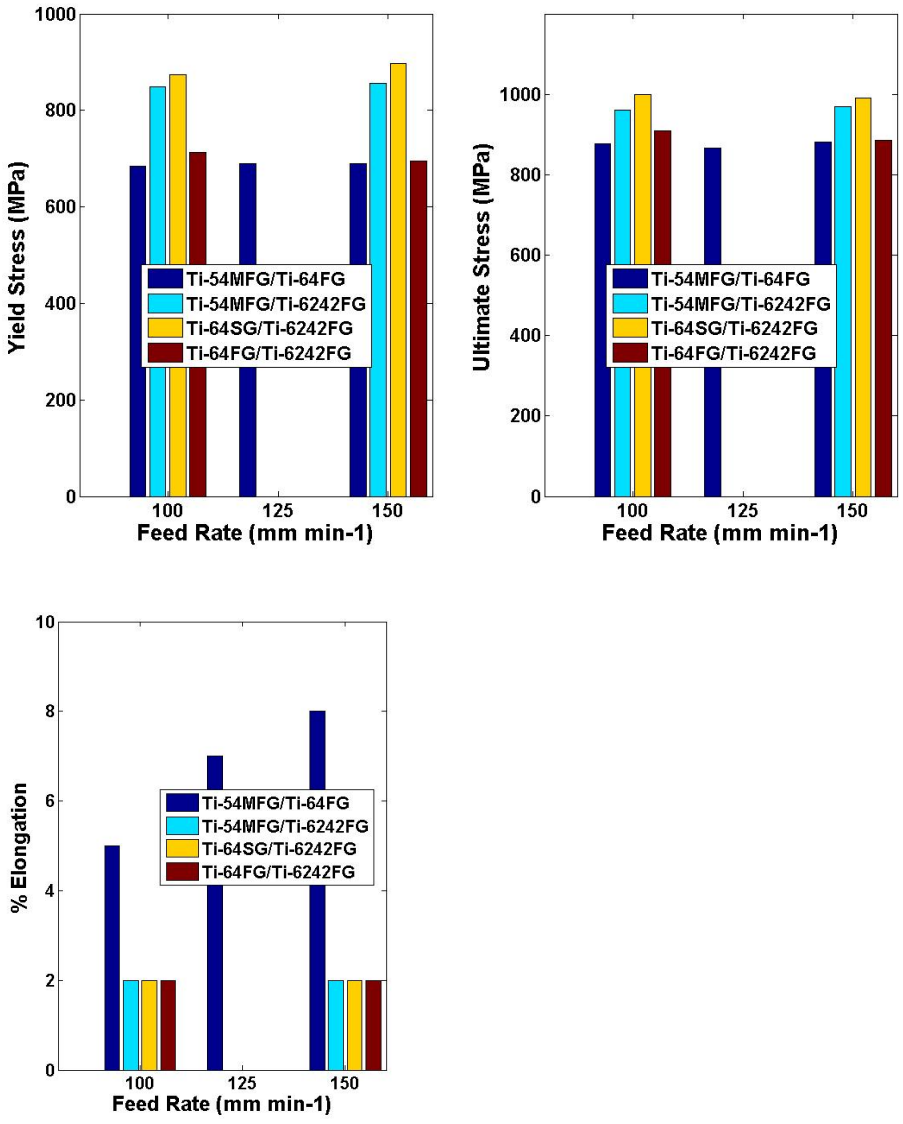

Figure 4.3-10: Effect of Feed Rate on mechanical strength and ductility in dissimilar joined Ti-54MFG with Fine Grained Alloys (Ti-54MFG/Ti-64FG, Ti-54MFG/Ti-6242FG, Ti-64SG/Ti-6242FG, and Ti-64FG/Ti-6242FG)

b. *Influence of Spindle Speed*

The effect of rotation speed on the mechanical behavior of friction stir welded joints was observed by increasing the rotation speed from 225RPM to 325RPM keeping the feed rate constant at 125 mm min-1 as shown in Figure 4.3-11. The increase in rotation speed resulted in increase in yield strength; ultimate strength and the elongation in dissimilar alloy Ti-54MFG/Ti-64FG. In Ti-54MFG/Ti-6242FG, the increase in rotation speed from increased the yield strength and the ultimate strength whereas it decreased in Ti-64FG/Ti-6242FG; and there was no impact on the ductility for both the joints. In Ti-64SG/Ti-6242FG the yield strength increased while the ultimate strength decreased and the ductility did not affect with the spindle speed. In the process when the feed rate was constant, maximum properties in terms of strength were observed at the rotation speed 325RPM for all three of the welded alloys, while the maximum ductility was reached with rotation speed 275RPM. Ti-6242SG/Ti-54MFG alloy showed higher strength than the other dissimilar welded titanium alloys. The rise of maximum 7% in yield strength and of 10 % in ultimate strength was observed in the dissimilar alloys as an effect of increase in rotation speed.

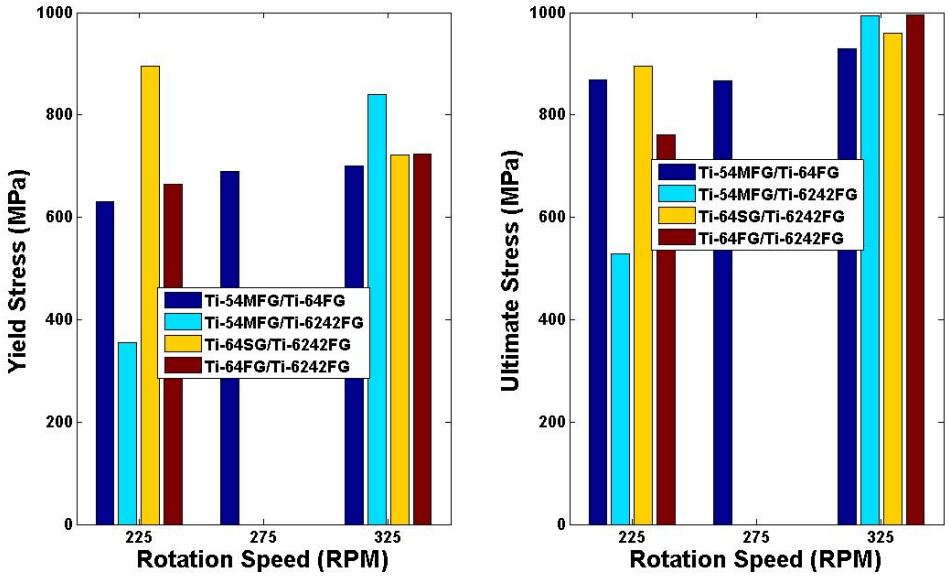

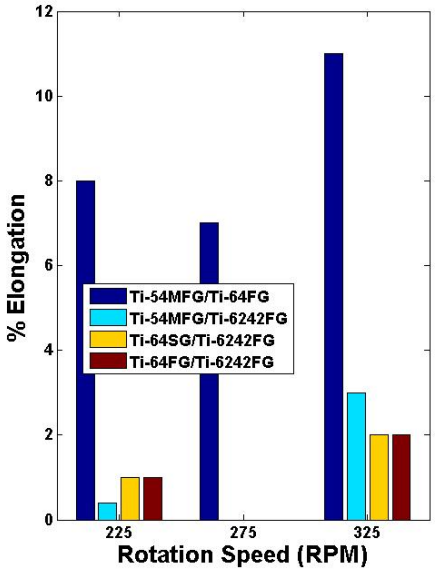

Figure 4.3-11: Effect of Spindle Speed on mechanical strength and ductility of joints in dissimilar joined Ti-Alloys with Fine Grain (Ti-54MFG/Ti-64FG, Ti-54MFG/Ti-6242FG, Ti-64SG/Ti-6242FG, and Ti-64FG/Ti-6242FG)

4.3.3 *Fracture Study*

This fracture study of friction stir welded titanium joints is divided into two parts. The first part presents the fracture study of the friction stir welded joints formed with similar titanium alloys, whereas the second part highlights the fracture study of the joints formed with dissimilar titanium alloys

4.3.3.1 Fracture in Friction Stir Welded Similar Ti-Alloys

The fractured tensile test samples of friction stir welded titanium joints were studied to understand the failure pattern with respect to the feed rate and spindle speed. Figure 4.3-12 shows the fractured samples of different titanium alloys. Most of the samples fractured in the weld zone. Most of the cases showed ductile type of failure. In ductile type of failure two kinds of cases were observed, mixed mode type and of shear type failure. Few cases of brittle failure were also observed in the welded titanium joints. Figure 4.3-13 shows different kinds of failure observed in the welded alloys.

The ductile nature of failure changed from mixed mode to shear in titanium alloys Ti-54MFG/Ti-54MFG with the increase in and feed rate, and in Ti-64SG/Ti-64SG, and Ti-

64FG/Ti-64FG with the increase in speed from 225 RPM to 325RPM at feed rate constant at 125 mm/min. The stress strain curves of these alloys also showed similar results of increase in ductility with that of speed for Ti-54MFG/Ti-54MFG, Ti-64SG/Ti-64SG, and Ti-64FG/Ti-64FG and with that of feed rate for Ti-54MFG/Ti-54MFG. The effect of feed rate did not show specific change in the nature of fracture. Mostly the cases of mixed mode fracture were observed in Ti-64SG/Ti-64SG, Ti-64FG/Ti-64FG, and Ti-6242SG/Ti-6242SG with respect to change in the feed rate. The brittle failure in Ti-6242FG/Ti-6242FG showed low elongation values in their stress strain curves.

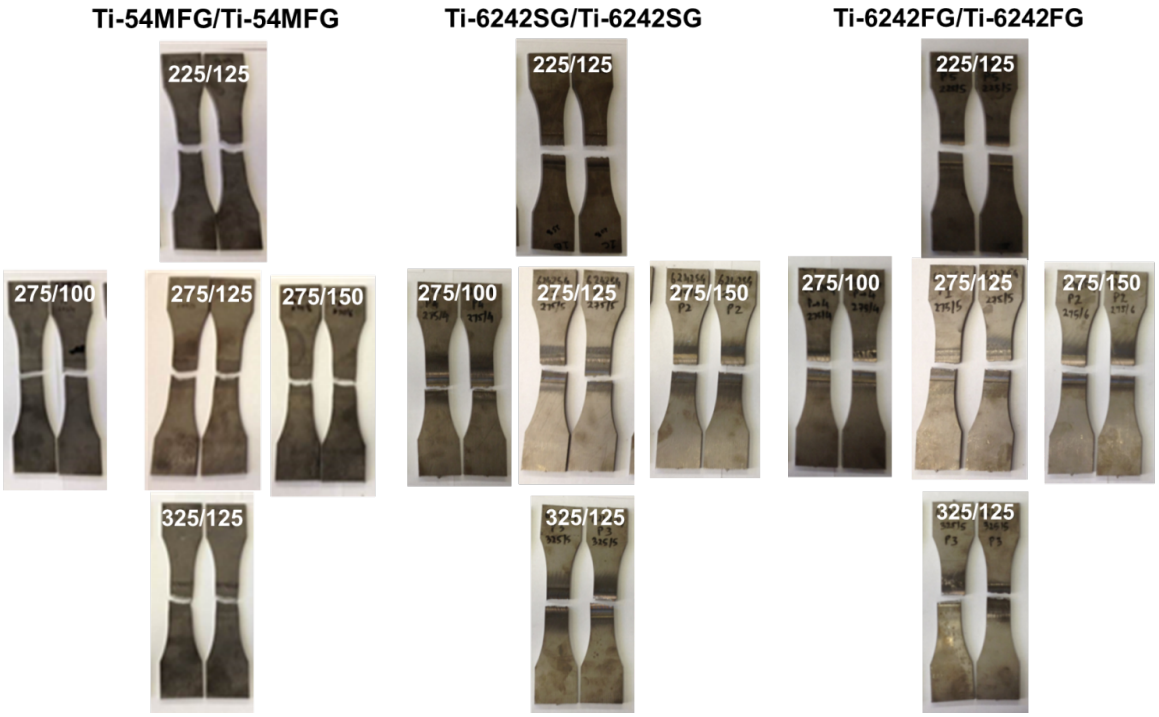

Figure 4.3-12: Fractured FSW Tensile Specimens (Ti-54MFG, Ti-6242SG, and Ti-6242FG at Tool Speed (RPM) and Feed Rate (mm/min)

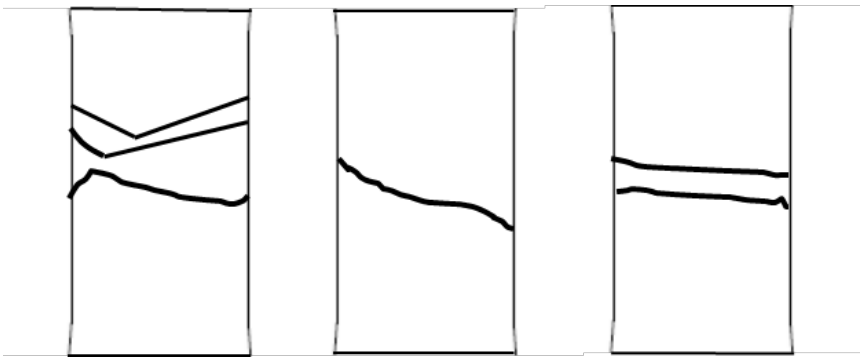

(a) (b) (c)

Figure 4.3-13: Failures in friction stir welded different titanium alloys (a- Mixed Mode, b- Shear, c- Brittle)

4.3.3.2 Fracture in Friction Stir Welded Dissimilar Ti-Alloys

Friction stir welded of dissimilar Ti-alloys were subjected to the tensile tests till the fracture. Figure 4.3-14 shows the fracture occurred in the friction stir welded dissimilar Ti-alloys. Many of dissimilar welded titanium alloys showed ductile type of failure. However in some welded alloys brittle phenomenon was also observed. In the ductile failure, two patterns of failure: mixed mode and shear type was seen following the fracture. In most of the cases, the fracture was observed in the welded region; however there were joints wherein the fracture occurred near the parent material edges. Some cases of edge fracture happened in the advancing side, while some it occurred in the retreating side. The shear type of ductile failure was observed in Ti-64SG/Ti-54MFG at 275RPM/100 mm min-1. In Ti-6242SG/Ti-64SG, the failure occurred at the advancing side. In Ti6242SG/Ti-54MFG, fractured specimens showed failure both at the advancing and the retreating side. The brittle fracture cases included Ti-6242SG/Ti-54MFG -225RPM/125 mm min-1, 275 RPM / 100 mm min-1, Ti-6242SG/Ti-64SG-225RPM/125 mm min-1, 275 RPM/150 mm min-1 and Ti-6242FG/Ti-54MFG-225RPM/125 mm min-1, 275 RPM/150 mm min-1. These joints have recorded low values of ductility in the material behavior test.

Ti-64SG/Ti-54MFG (RPM/mm min-1)

Ti-64SG/Ti-6242SG (RPM/mm min-1)

Ti-6242SG/Ti-54MFG (RPM/mm min-1)

Ti-64FG/Ti-54MFG (RPM/mm min-1)

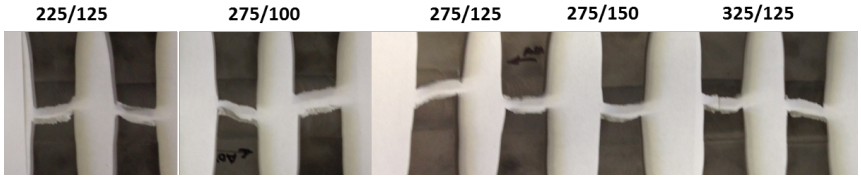

Ti-6242FG/Ti-54MFG (RPM/mm min-1)

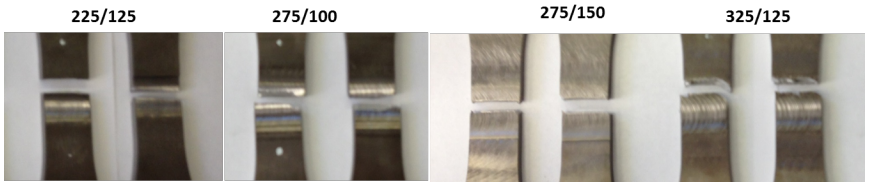

Ti-64SG/Ti-6242FG (RPM/mm min-1)

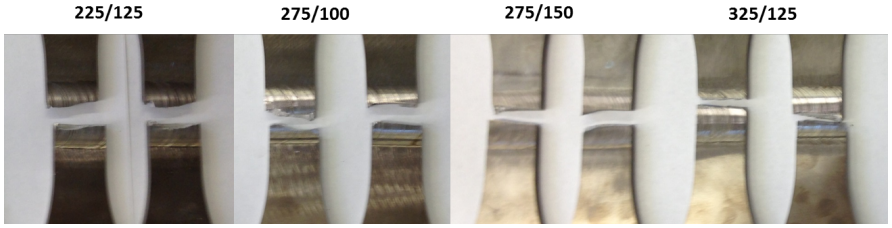

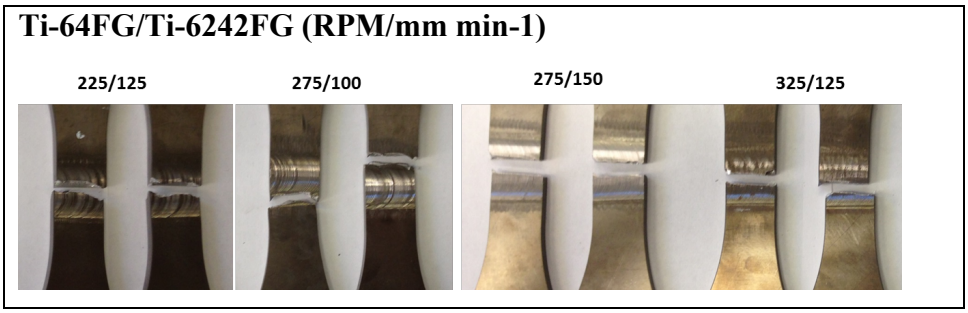

Figure 4.3-14: Fracture in Dissimilar Friction Stir Welded Joints -Ti-54MFG/Ti-64SG, Ti-54MFG/Ti-64SG, Ti-54MFG/Ti-6242SG, Ti-64SG/Ti-6242SG, Ti-64FG/Ti-54MFG, Ti-6242FG/Ti-54MFG, Ti-64SG/Ti-6242FG, and Ti-64FG/Ti-6242FG

4.3.4 *Summary of Joining Processes of Titanium Alloys*

A. Diffusion Bonding of Similar and Dissimilar Titanium Alloys

1. Sound bonds could be obtained in similar and dissimilar titanium alloys with diffusion bonding process at temperatures lower than the β transus temperature of titanium alloys.
2. The effect of bonding temperature on the quality of diffusion bonding showed that the quality of bonding improved as the temperature was increased.
3. The good quality bonds were achieved for most of the similar and dissimilar titanium alloys combinations in the temperature range from $T5^0C$ to $T8^0C$, while at the temperatures $T2^0C$ and $T3^0C$ sound bonds could not be achieved for most of the titanium alloys. The bond strength as high as 200% was achieved using dissimilar titanium alloys.
4. The surface profile measurements of the bonded interface in diffusion bonded dissimilar titanium joints remained unaffected with respect temperature.
5. The hardness at the bonding interface of the diffusion bonded titanium joints increased with the temperature. The hardness varied linearly with respect to temperature.
6. Dissimilar Diffusion Bonded Titanium joints:

6.1 Near-α to β Dissimilar Titanium Joints: In Ti-6242/ Beta 21S the bonding interface showed no visible porosity at temperatures T5, T6, and $T7^0C$.

However at T8^{0}C, thick bond line was evident at the interface suggesting localized concentration of beta material with Ti-6242 material due to inter-diffusion of β-21S alloy constituents. The hardness in β21S region was higher than the hardness in Ti-6242 region. The hardness in the bonding interface lies between the hardness of Ti-6242 and β-21S. The hardness values were found consistent at the temperatures T5, T6, and T7^{0}C. The increase in temperature from T5 to T6 resulted in increasing the yield strength and ultimate strength, however with further increase to T7^{0}C resulted in decreasing the yield strength and ultimate strength.

6.2 Near-α to α+ β Dissimilar Titanium Joints: Ti-64SG /Ti-6242SG yielded good diffusion bonding results. The hardness in Ti-64SG region was higher than the hardness in Ti-6242SG region. The hardness at the bonding interface increased as a function of temperature. The ultimate stress of Ti-6242SG was higher than ultimate stress of Ti-64SG. The yield strength remained unchanged with respect to temperature. In Ti-64SG/Ti-64FG at lower temperatures, bonding quality was poor. A good bonding was obtained at T4^0 and T5^{0}C. The hardness in the bonding interface was lower than the parent material. The hardness in Ti-64SG region was higher than the hardness in Ti-64FG region. The hardness increased with the temperature. The yield strength and ultimate strength slightly increased with the temperature. In Ti-6242SG /Ti-54M a thin bond line was visible at the interface. The temperature T2 and T3^{0}C did not yield good results. The hardness in Ti-6242 region was higher than the hardness in Ti-54M region. The hardness decreased from Ti-6242 region till the interface, and then from the bonding interface, it increased in the Ti-54M regions. Mostly the hardness increased with the temperature rise, except at T7^{0}C where the hardness dropped. The yield strength and ultimate strength improved with the temperature.

6.3 α+ β to α+ β Dissimilar Titanium Joints: In Ti-64SG /Ti-54M the hardness at the interface was slightly lower than the parent material. The hardness was

unaffected with respect to temperature in higher range, whereas it decreased with temperature in low temperature range. For most of the cases, the hardness in Ti-54M regions was higher than in the Ti-64 region. Same results were repeated for yield strength and ultimate strength as well with respect to temperature. In Ti-64FG / Ti-54M good bonding quality results were obtained at lower and higher temperatures. The hardness increased with temperature. The yield strength and ultimate strength also increased with temperature.

6.4 α+ β to β Dissimilar Titanium Joints: For this dissimilar combination Ti-64SG/Beta-21S, good bonding interface results were obtained at temperatures $T5^0$, $T6^0$, and $T7^0$C. The hardness values increased with temperature. The hardness at interface was higher than the parent material. At temperatures $T5^0$ and $T6^0$C, hardness in Ti-64 region was higher than Beta-21S, whereas at $T7^0$C hardness in Beta-21S was higher than Ti-64SG. The ultimate strength and yield strength increased with temperature.

6.5 Comparison of Flexural Properties of Dissimilar Joints with the parent titanium alloys properties: The mechanical properties of diffusion bonded dissimilar titanium alloys were compared with the parent alloys properties to evaluate the bond strength. The temperature where best quality diffusion bond obtained was selected to find the maximum bond strength that can be achieved by diffusion bonding of dissimilar titanium alloys. The highest value of the two alloys was considered to calculate the % of bond strength acquired. Table 4-19 represents the bond strength that was achieved in the diffusion bonding of dissimilar titanium alloys. The bond strength as high as 200% was obtained with Ti-64 and Ti-54M at $T6^0$C. The diffusion bonding of dissimilar titanium alloys produced good bond strength as compared to the parent alloys.

Table 4-19: Dissimilar Diffusion Bonded Ti- Alloys: Bond Strength

Ti-Alloys	Temp (C)	Hardness (HB)	US (MPa)	US: % Parent	YS (MPa)	YS: % Parent
Ti-64/Ti6242	T8	359	984	97	780	79
Ti-64/ β-21S	T7	355	1059	115	950	107
Ti-64/Ti-54M	T6	318	1960	201	1600	181
Ti-64/-Ti64FG	T5	314	1848	195	1500	170
Ti-6242/β-21S	T6	308	636	63	600	61
Ti-6242/Ti-54M	T7	320	2008	198	1575	160

6.6 The bondline hardness as close to 80 % of Ti-64 was achieved with the diffusion bonding process of dissimilar titanium alloys. The bondline hardness increased with the increase of temperature in many cases of diffusion bonded titanium alloy joints.

6.7 Diffusion bonding could be achieved in dissimilar titanium alloys at temperatures lower than the β transus temperature of titanium alloys. At low temperature $T1^0C$ sound bonds were achieved in similar titanium alloy, Ti-54M/Ti-54M and in the dissimilar alloys: Ti-64/ Ti-54M, Ti-6242/ Ti-54M, Beta-21S/ Ti-64FG. The temperatures from $T5^0C$ to $T8^0C$ were found to be the most suitable temperatures for the range of titanium alloys considered in the study. Most of the similar and dissimilar titanium alloys combinations produced good results in the $T5^0$ to $T8^0$ C temperature range. At $T6^0C$, good quality diffusion bonds were obtained for all titanium alloys that included similar as well as dissimilar titanium alloys. The temperatures $T2^0$ and $T3^0C$ were found to be not good for the range of titanium alloys in the study, as sound bonds could not be achieved at these temperatures for most of the titanium alloys.

7. In the cases of good quality joints such as Ti-64SG/Ti-6242SG, the bond line remained unaffected after performing flexure testing. Therefore it demonstrates good joining strength was achieved through diffusion bonding. The fractured surfaces appeared rough and irregular with many micro voids and dimples, demonstrates the case of ductile failure.

B. Friction Stir Welding of Similar and Dissimilar Titanium Alloys

1. Friction Stir Welding joining process produced defect free butt joints with dissimilar titanium alloys. The process showed a very good strength as close as 90% with respect to the parent alloys.
2. The rotation speed of the welding tool showed more influence on the strength of the joints than its feed rate on the mechanical properties in friction stir welded similar and dissimilar titanium alloys.
3. The effect of feed rate and spindle speed resulted average change in yield strength within the similar titanium alloy joints by less than 9 % and in ultimate strength by less than 14 %. The spindle speed 275 RPM showed higher mechanical properties for the joints formed by similar titanium alloys.
4. Lower spindle speed at 225 RPM decreased the mechanical properties of most of the similar titanium alloys. The feed rate 125 mm/min yielded higher as well as lower mechanical properties for the similar titanium alloys. In terms of mechanical properties such as tensile and ultimate strength, the optimum value of spindle speed is 275 RPM.
5. Higher ductility was obtained with spindle speed and feed rate of 325 RPM and 125 mm/min respectively. The titanium alloys Ti-54MFG/Ti-54MFG, Ti-6242SG/Ti-6242SG, and Ti-6242FG/Ti-6242FG produced the highest elongation with this spindle speed and feed rate.
6. In case of similar titanium the spindle speed of 275 RPM, comparatively good mechanical properties were obtained with the feed rate of 100 mm/min. Ti-64SG/Ti-64SG and Ti-64FG/Ti-64FG reached maximum elongation; Ti-54MFG/Ti-54MFG showed maximum yield and ultimate tensile strength; and Ti-6242SG/Ti-6242SG indicated maximum yield strength at 275 RPM/ 100mm/min.
7. In case of dissimilar joints, the optimum feed rate and rotation speed were 125 mm min-and 325RPM respectively. Ti-54MFG/Ti-6242SG showed higher mechanical strength than Ti-6242SG/Ti-64SG and Ti-54MFG/Ti-64SG.

8. The maximum ductility 14% was recorded for Ti-6242SG/Ti-64SG at 275RPM/125 mm min-1.
9. In case of friction stir welded similar titanium joints; the maximum mechanical strength was obtained with Ti-6242SG/Ti-6242SG, while the process condition which produced maximum joint strength in similar alloys was 275RPM and 150 mm min-1. In the friction stir welded joints formed with dissimilar titanium alloys, the maximum strength was achieved with Ti-64SG/Ti-6242FG and the process parameters that resulted in maximum joint strength were 225 RPM and 125 mm min-1.
10. The friction stir welded formed by similar titanium alloys fractured in the weld zone. Most of the titanium joints showed ductile failure except Ti-6242FG/Ti-6242FG which showed brittle failure. The effect of spindle speed was evident than the feed rate on the ductile nature of the failure. The ductile nature changed from mixed mode to shear with the increase in spindle speed in Ti-54MFG/Ti-54MFG, Ti-64SG/Ti-64SG, and Ti-64FG/Ti-64FG.
11. Most of the cases of friction stir welded dissimilar titanium joints showed fracture in the welded region, thus the process showed good joining capability.

Chapter 5. MODELING OF JOINING PROCESSES

The current chapter demonstrates theoretical modeling of diffusion bonding joining process followed by numerical modeling of mechanical behavior of both the diffusion bonding and the friction stir welding processes. Section 5.1 presents theoretical modeling of diffusion bonding process. Section 5.2 presents the probabilistic model developed for predicting diffusion bonding time for dissimilar titanium alloys. Section 5.3 demonstrates numerical modeling of flexure test for dissimilar alloys. The numerical model on mechanical behavior of joints is presented in the last section.

5.1 THEORETICAL MODELING OF DIFFUSION BONDING

The diffusion bonding process was modeled to predict diffusion bonding time of titanium alloys. The diffusion bonding models were applied to predict diffusion bonding time of similar alloys. Three models of diffusion bonding were applied to estimate diffusion bonding time based on the pressure sintering process and the model of grain boundary diffusion coupled with creep. These three models included the oldest model of diffusion bonding time that of Hamilton (1973), the well-established model of bonding time which of Pilling(1988), and the most recent model of diffusion bonding time developed by Fang (2012) which addresses dynamic conditions of diffusion bonding mechanisms. The models were derived using matlab program.

5.1.1 *Modified Hamilton Model*

Hamilton made first attempt to predict the bonding time to attain full interfacial contact between two rough surfaces. The surfaces to be joined consisted of triangular section asperities in point-to point contact. The bonding time defined in Hamilton's model is given by equation 5.1.

$$t_B = \frac{0.8T}{A_{sp} exp\left(Q_{sp}/_{RT}\right)} \left(\frac{1}{3^{1/2}P}\right)^{n_{sp}} \quad (5.1)$$

Here $\dot{\varepsilon} = A_{creep}\sigma^n = A_{sp} exp\left(Q_{sp}/_{RT}\right)\sigma^n$, $d_F = d_0/2$ (5.2)

Where t_B = bonding time, P = bonding pressure, $\dot{\varepsilon}$ = strain rate

In case of diffusion bonding of ultrafine α/ β Ti-alloys, the alpha particle size yields lower flow stress, and thus lower bonding temperatures are feasible for diffusion bonding. However, plastic flow behavior may be affected by static coarsening (during preheating prior to pressurization) and dynamic coarsening (during bonding). The strain rate equation in ultrafine Ti-64 is given by:

$$\dot{\varepsilon} = \left(\frac{ADGb}{kT}\right)\left(\frac{\sigma}{G}\right)^n \left(\frac{b}{d}\right)^p \quad (5.3)$$

Therefore, substituting the strain rate equation in case of ultrafine Ti-64 in equation 4.1 gives the modified form of Hamilton's equation (equation 5.4).

$$t_B = \frac{0.8kT}{ADGb}\left(\frac{d}{b}\right)^n \left(\frac{G}{3^{1/2}P}\right)^n \quad (5.4)$$

Where t_B = bonding time, P = bonding pressure, k= 1.38E-23 J/K (Boltzmaan constant), AD ($\mu m^2/s$) = 5.92E8*exp(-19,840/T(K)), G=20,000MPa, b = beta phase, d = alpha particle diameter, n = 1.67 (creep exponent), p = 2 (constant).

The above model was used to predict diffusion bonding time for ultra fine Ti-6Al-4V with the above properties for different size of alpha particles (d = 1μm, 2 μm, 4 μm, and 6μm). Figure 5-1 shows the results of predicted diffusion bonding time with modified Hamilton Model for Ti-6Al-4V Fine Grain. The effect of grain size and the temperature is evident on the diffusion bonding process. Lower grain size results in lowering the time required to complete the diffusion bonding process. In terms of bonding temperature, it can be seen that the increase in the bonding temperature decreases the bonding time.

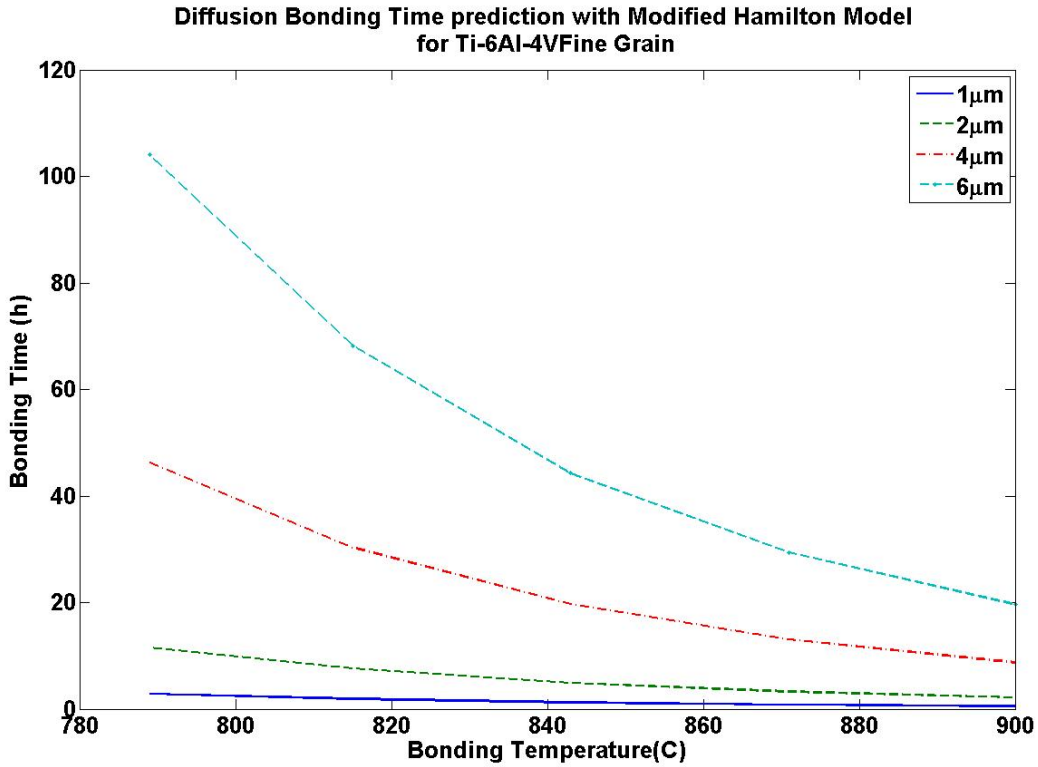

Figure 5.1-1: Bonding Time prediction with Modified Hamilton Model for Ti-6Al-4VFine Grain

5.1.2 *Pilling's Model*

Pilling's model is one of the well-established model to predict bonding time in diffusion bonding of titanium alloy Ti-6Al-4V. The theoretical model to predict bonding time has been derived in the literature survey chapter of the thesis. Before applying the Pilling's model to simulate the bonding time with the current experimental conditions, the established model was derived using the material properties and process conditions as applied in the original Pilling's model. The ode solver in Matlab for used to predict the bonding time for the Ti-6Al-4V alloy.

Pilling's model of bonding time for Ti-64SG was simulated to estimate the bonding time for rate of change of fractional area of interfacial voids. The effect of bonding mechanisms on the process is simulated for the Ti-64SG alloy. The bonding time at

different bonding pressures was also simulated for the various surface finish parameters. The material properties of Ti-6Al-4V are given below [18].

1. Crystallographic and thermal data

- Atomic volume Ω (m^3) :1.78E-29
- Burgers vector *b* (m): 2.9E-10
- Melting Temperature Tm (K) :1933
- Surface energy (Jm^{-2}) :1.7

2. Modulus and plasticity

- Shear modulus at 300K μ (MPa)
    - α = 4.3E4
    - β = 2.05E4
- Temperature dependence, Tm/μdμ/dt
    - α = -1.2
    - β = -0.5
- A_{pl} ($\dot{\varepsilon}$ in reciprocal seonds when sigma in megapascals) = 7.5E-2
- A_{sp} ($\dot{\varepsilon}$ in reciprocal seconds when sigma in megapascals) = 3.8E4
- Activation energy for creep Q_{pl} (kJ $mole^{-1}$) = 150
- Activation energy for superplastic flow Q_{sp} (kJ $mole^{-1}$) = 150
- Stress exponent for creep n_{pl} = 4.3
- Stress exponent for superplastic flow n_{sp} = 1.43

3. Diffusion

- Grain boundary diffusion D_{gb} del_0 (m^3s^{-1})
    - α = 3.6E-16
    - β = 5.4E-17
- Activation Energy Q_{gb} (kJ mol^{-1})
    - α = 97
    - β = 153

1. Effect of bonding mechanisms on the rate of change of fractional area

In the model, as stated earlier, the reduction in the area of non-bonded interface during bonding was visualized into two components: the axial collapse of the cylindrical columns at constant external radius by power law creep and superplastic flow, and secondly, by the transfer of matter from the interfaces which intersect the free surface of the no bonded area by diffusion. The influence of plastic collapse and diffusive flow mechanisms on diffusion bonding in Ti-64SG is shown in Figure 5.1-2. The bonding temperature and pressure were 910^0C and 1 MPa respectively. The initial radius of void was 8 μm. The initial void height was defined as twice the Ra (Ra: Amplitude = 10 μm). The result showed the complete interfacial contact is attained primarily as a result of time-dependent (super) plastic flow of material into the interracial voids, rather than by diffusion, an observation which was in broad agreement with the predictions of the plane strain models of Derby and Wallach. Therefore bonding process could be addressed as ‘solid state’ rather than ‘diffusion.’

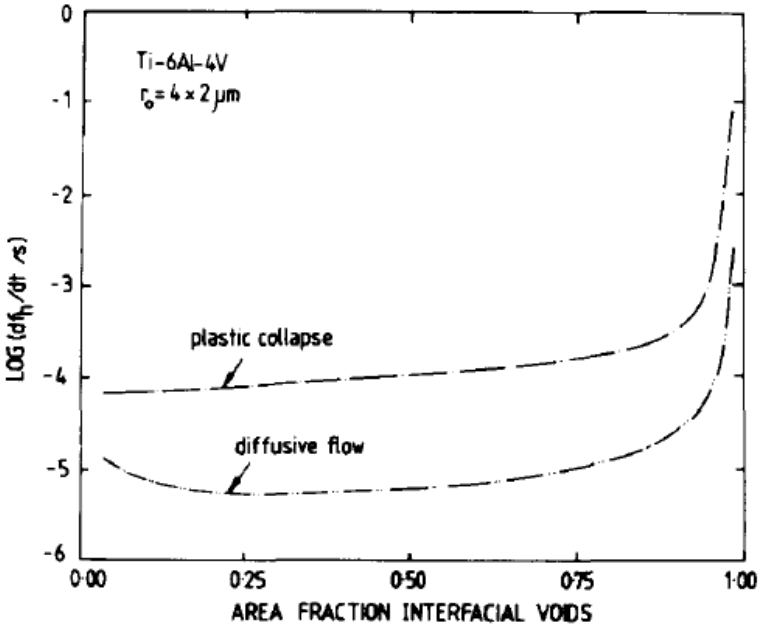

Fig. 6. The relative kinetics of the void closure process by diffusion and plastic collapse for different surface finishes ($T = 910\,^{\circ}C$, $P = 1$ MPa).

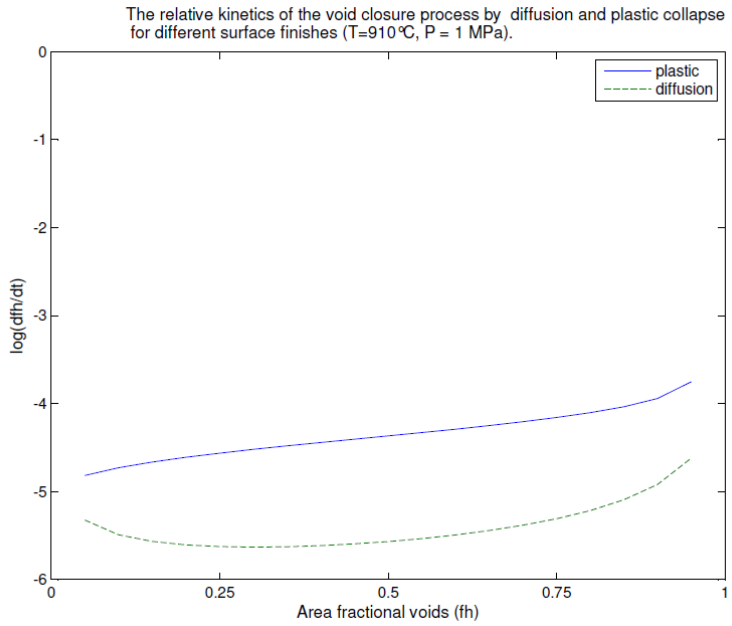

Figure 5.1-2: Relative Kinetics of the void closure by diffusion and plastic collapse for different surface finishes (T= 910^0C, P = 1 MPa) [18]

2. Bonding time at different bonding pressures for various surface finishes

The diffusion bonding process is greatly affected by the surface parameters at the bonding interface. The typical roughness dimensions of various treated surfaces for Ti-64SG are provided in Table 5-1. Measurements of the roughness of as-received and pickled surfaces, ground surfaces and grit blasted surfaces show broadly different asperity geometries. The variation in bonding time with pressure for different surface finishes predicted by the isostatic model is shown in Figure 5.1-3. It is evident that the surface finish exerts greater influence on the time required to attain full interfacial contact. It is explained with two reasons: Firstly, as the voids decrease in size, the surface tension becomes progressively larger with respect to the applied pressure and contributes towards the effective stress in the wall of the cylinder. Secondly, for a fixed amount of diffusion, the fractional change in the volume of the interfacial void increases as the void dimensions decrease, i.e. diffusion is more effective at closing smaller voids.

Table 5-1: Typical roughness dimensions of treated surfaces

Surface	Wavelength (µm)	Amplitude (µm)
As-received and pickled	2.1	0.6
Ground (2540 grit SiC)	2.5	13
Grit blasted	4.5	22
Typical Waviness	100	20

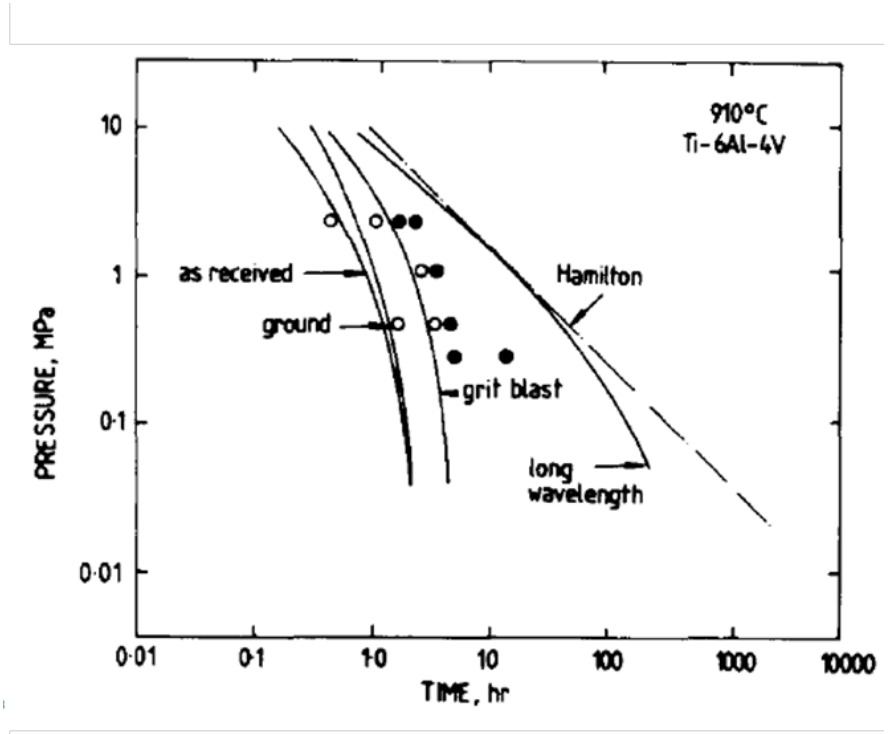

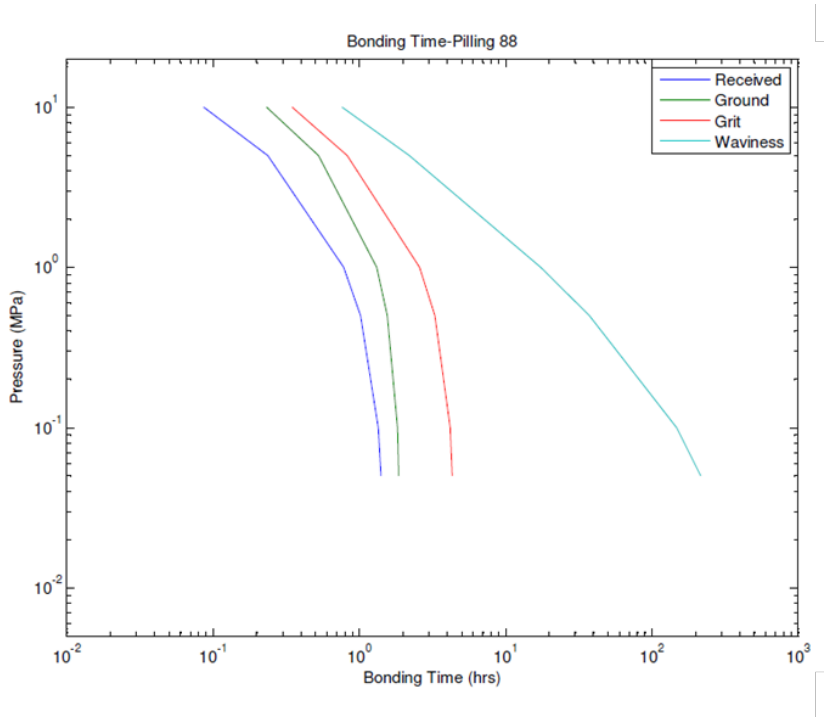

Figure 5.1-3: Bonding time at different pressures for various surface finishes[18]

5.1.3 *Fang's Model [21]*

Fang's model was simulated to understand the effect of different diffusion bonding mechanisms on bonding time. The model encompasses three mechanisms: surface source, interface, and creep for void closure based on dynamic conditions. The chapter 2 provides details on these mechanisms and the dynamic condition applied during void closure. Fang's model was derived in Matlab using ode solver. The results were found at temperature 1123K, pressure 10MPa and the alloys properties were used from Table 5.2. Figure 5.1-4 shows the derived model wherein the bonding area fraction is calculated by applying three mechanisms: surface source, interface and creep for time duration of 1800 seconds. The creep mechanism was found to be the dominating among all the mechanisms contributing towards the void closure.

Table 5-2: Ti-64 alloy properties in Fang's model [21]

Parameter	Symbol	Unit	α-Ti	β-Ti
Atomic volume	Ω	10^{-29} m^3	1.76	1.81
Burgers vector	b	10^{-10} m	2.95	2.86
Melting point	T_m	K	1933	1933
Shear modulus at 300 K	G	10^{10} Pa	4.36	2.05
Surface energy	γ	Jm^{-2}	1.7	1.7
Temperature coefficient of shear modulus	$(T_m/G)(dG/dT)$	—	-1.2	−0.5
Yield strength at 300 K	σ_y	10^6 Pa	—	—
Volume diffusion coefficient (pre-exponential)	D_{0V}	10^{-7} m^2 s^{-1}	8.6×10^{-3}	1.9
Volume diffusion activation energy	Q_V	10^3 J mol^{-1}	150	153
Grain boundary diffusion coefficient (pre-exponential)	$D_{0B}\delta_B$	10^{-16} m^3 s^{-1}	3.6	0.54
Grain boundary diffusion activation energy	Q_B	10^3 J mol^{-1}	97	153
Surface diffusion coefficient (pre-exponential)	D_{0S}	10^{-6} m^2 s^{-1}	5	5
Surface diffusion activation energy	Q_S	10^3 J mol^{-1}	89	89
Surface diffusion layer thickness	δ_S	10^{-10} m	1	1
Creep constant	A	—	7.7×10^4	1×10^5
Creep coefficient (pre-exponential)	D_{0cr}	10^{-7} m^2 s^{-1}	8.6×10^{-3}	1.9
Creep activation energy	Q_{cr}	10^3 J mol^{-1}	150	153
Creep exponent	n	—	4.3	4.3

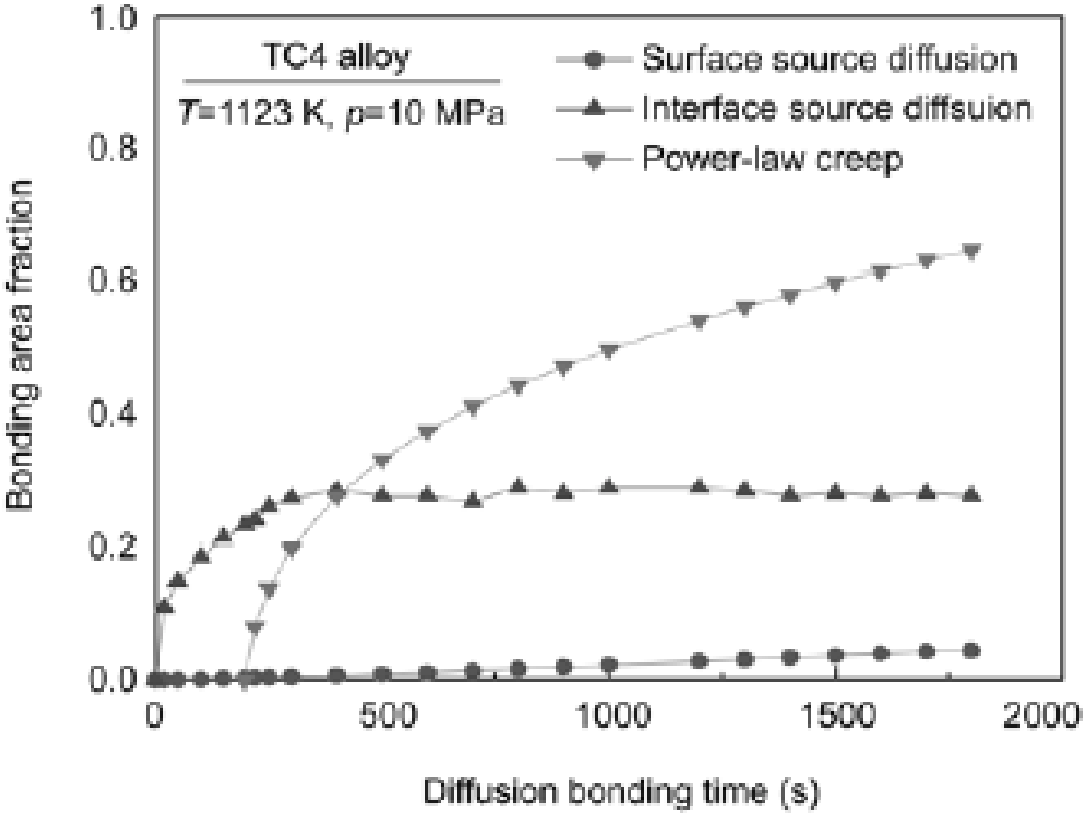

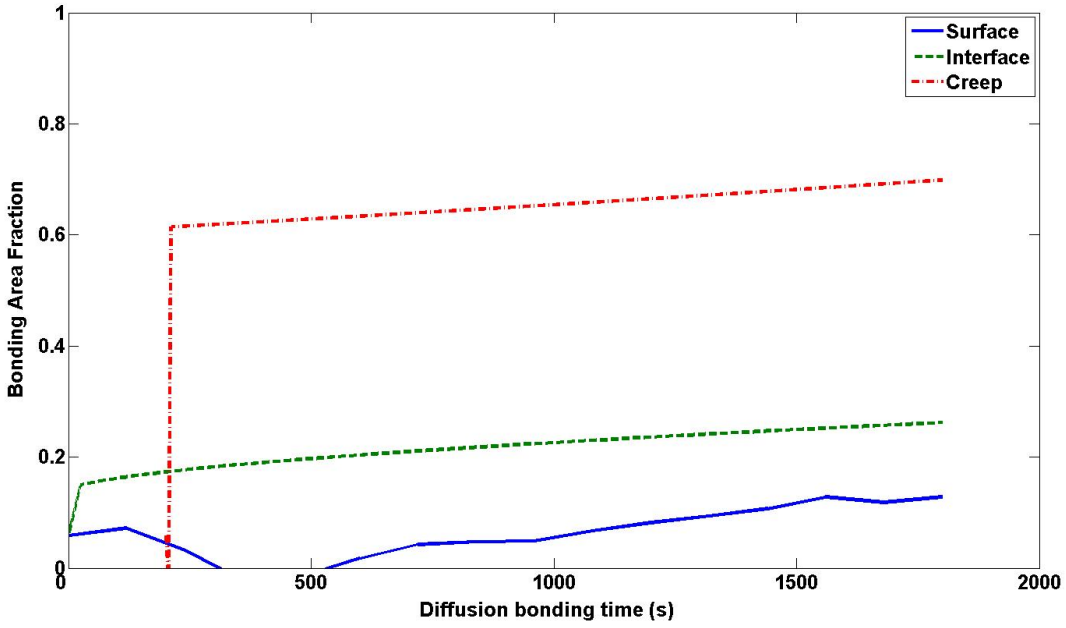

Figure 5.1-4: Modeling of Fang's DB model [21]

5.1.4 *Experimental Bonding Time using Pilling's Model for Ti-64SG, Ti-6242SG, and Ti-54M Alloys*

Piling's model [18] was applied to simulate bonding time with experimental conditions for diffusion bonding of similar titanium alloys. The bonding time was predicted for three different similar alloys Ti-64SG/Ti-64SG, Ti-6242SG/Ti-6242SG, and Ti-54M/Ti-54M. The duplex nature of titanium alloy was used to incorporate material properties of the titanium alloys. The material properties were defined separately for alpha and beta titanium. The proportion of alpha/beta was different for all the three alloys. Ti-6242SG being a near-alpha alloy had lower proportion of beta than the other alloys. In addition to the alpha/beta proportion, the surface profile parameters, the wavelength 'λ' and amplitude 'Ra' and the grain size 'd' were different for these three alloys. The surface profile parameters were used from surface roughness measurements of the parent alloys (Ti-64SG: λ = 31E-6, Ra = 1.361E-6, d = 8E-6; Ti-6242SG: λ = 21E-6, Ra = 0.83E-6, d = 6E-6; and Ti-54M: λ = 36E-6, Ra = 1.8119E-6, d = 5E-6). During the simulation, the pressure was constant between 1-5MPa, and the bonding temperature was varied from 780^0C to 950^0C similar to experimental condition. Figure 5.1-5 shows the predicted diffusion bonding time for different similar titanium alloys using Pilling's model. It is evident that that increase in bonding temperature decreases the bonding time. In terms of different alloys, Ti-6242SG/Ti-6242SG took less time to complete bonding as compared to Ti-64SG/Ti-64SG and Ti-54M/Ti-54M. Both the alpha/beta titanium alloys, Ti-64SG/Ti-64SG and Ti-54M/Ti-54M showed closer results in terms of diffusion bonding time.

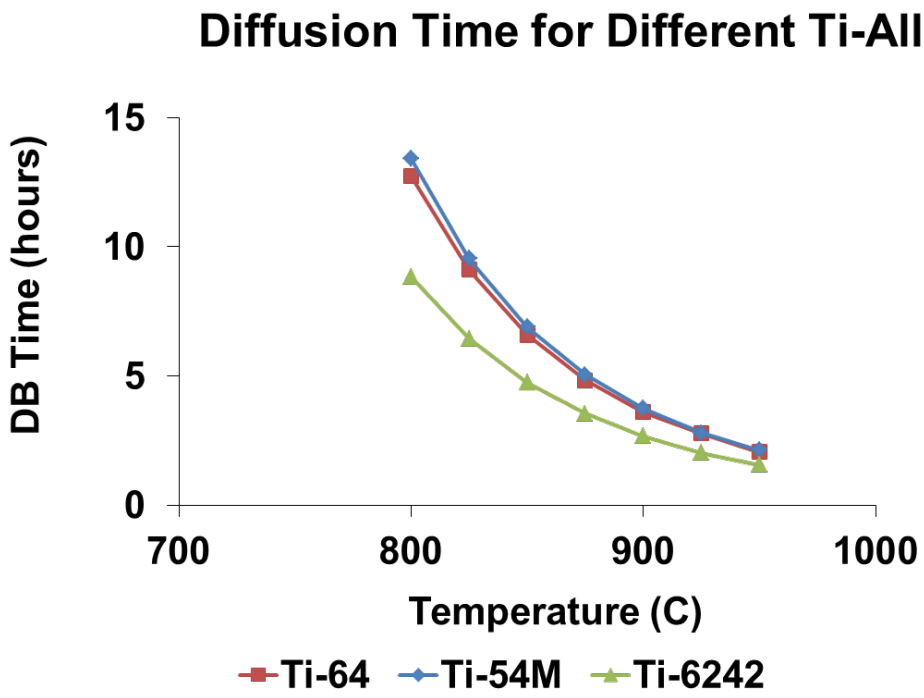

Figure 5.1- 5.1-5: Diffusion Bonding time for different Ti-Alloys (Ti-64SG/Ti-64SG, Ti-6242SG/Ti-6242SG, and Ti-54M/Ti-54M

5.2 MODELING OF DIFFUSION BONDING TIME IN DISSIMILAR TITANIUM ALLOYS

The diffusion bonding of similar alloys has been modelled successfully by many researchers. The different kind of models has modeled the bonding interface region with triangular, cylindrical, elliptical, sine wave geometry. However till date the diffusion bonding time has not been modeled for dissimilar alloys. The joining of dissimilar titanium alloys differs from the similar titanium alloys in following aspects. The geometry at the interface is different. Due to difference in surface profile, grain size, the void shape turns complex and cannot be always be completely circular or elliptical. It can be circular at one side of material and elliptical at the other side of material or can also be of same shape but with different void radius and height. Therefore the geometry is the first aspect that should be addressed while modeling the diffusion bonding time of dissimilar alloys. In the current model the geometry of void at the interface is simplified by making independent surface

profile measurements of both the dissimilar alloys. Then the surface profiles are superimposed to obtain the surface profile at the interface of the bonding. This surface profile produces a cylindrical, elliptical, or sine wave. In addition to that marked amount of scatter is exhibited by the voids on faying surfaces. Hence, the stochastic characteristics are important during the bonding of dissimilar surfaces. Li [24] has developed probabilistic model for prediction of bonding time in diffusion bonding of similar alloys. In the current work, the above probabilistic model is adopted for prediction of diffusion bonding time for dissimilar alloys.

5.2.1 *Probabilistic Modeling of Bonding Time in Dissimilar Ti-Alloys*

A probabilistic model is constructed by identification and characterization of variables, determination of probability density function and cumulative distribution function for random variables based on existing experimental data and experience, followed by combination of the deterministic model with CDF of random variables to construct a probabilistic model. In the model of prediction of diffusion bonding time, variables are distinguished into two categories: external variables and internal variables. External variables include parameters that describe environmental conditions, such as pressure and temperature; internal variables include material properties and its geometric characteristics like surface profile in diffusion bonding.

In the current work, the diffusion bonding of dissimilar alloys Ti-64SG and Ti-6242SG is modeled to calculate the bonding time with these alloys. The model includes the probabilistic feature of the surface to be bonded by assuming void radius and height as random variables. The random variable generation along with numerical integration is then applied to calculate bonding time and its probabilistic distribution of bonding of dissimilar alloys. The following steps were adopted in the model.

1. Surface Profile Measurements

   The surface profiles of Ti-64SG and Ti-6242SG was measured using Mahr profilometer. The typical profile of parent materials is shown in Figure 5.2-1. It can

be seen that that profiles of two parent materials (Ti-64SG and Ti-6242SG) differed from each other in terms of surface roughness parameters. Therefore to find the gemetry of voids, in terms of height and radius of void at the interface of the bond surface, the two surface profiles were superimposed to obtain the interface profile. To superimpose them, the intial value of the profile of one of the parent alloy (Ti-6242SG) was matched with the initial value of profile of the another parent alloy (Ti-64SG). Figure 5.2-2 displays the superimposed profiles of two alloys.

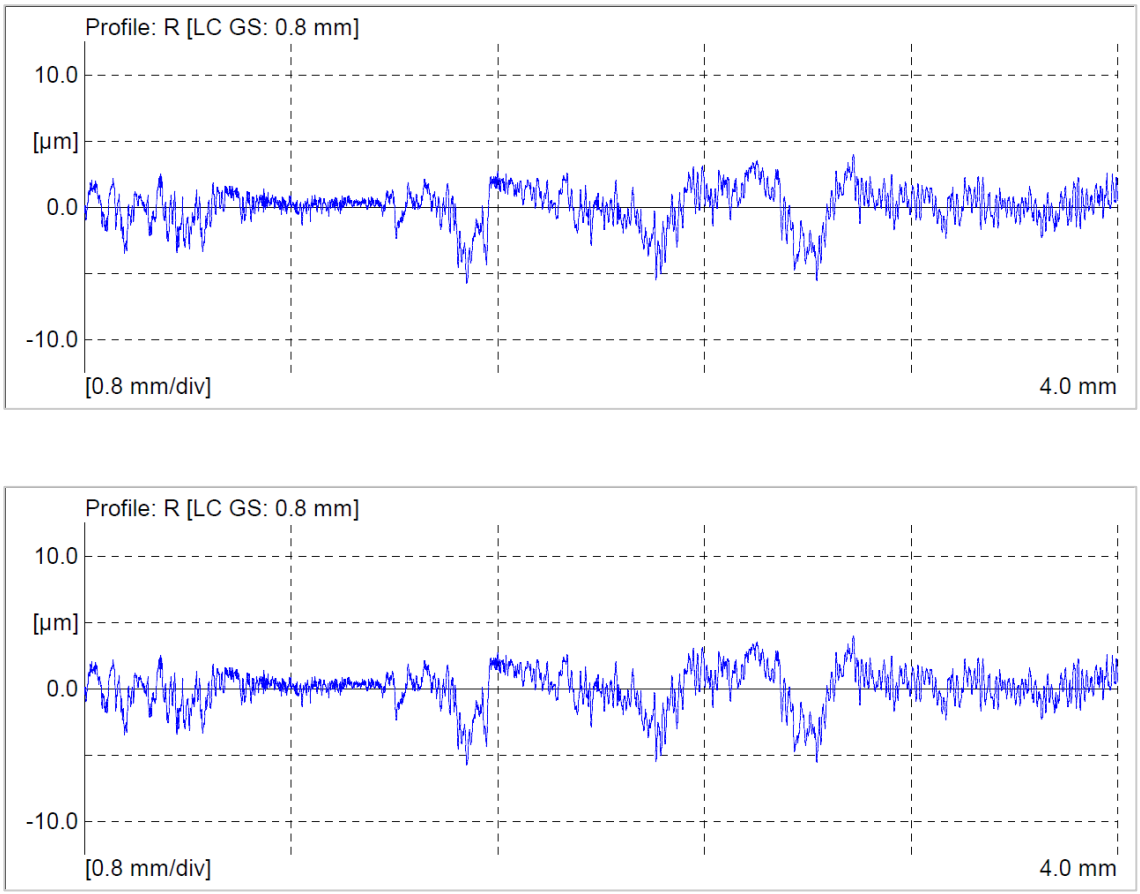

Figure 5.2-1: Typical Surface Profile of Parent Alloys –Ti-64SG/Ti-6242SG

Figure 5.2-2: Surface Profiles of Dissimilar Ti-Alloys Aligned for surface characteristics at Bonding Interface

2. Shape and Geometry of Voids

The SEM observation of diffusion bonded of dissimilar alloy Ti-64/Ti-6242 showed that the surface can be represented by semicircular voids as shown in Figure 5.2-3 (Figure 4.2-45). Therefore in current model cylindrical voids are assumed, similar to Pilling's work. In order to simplify the geometry in the current model, it is assumed that the surface to be bonded has a geometry that consists of parallel, semicircular groves having unit length in unit width. The void radius and height are simplified as constants.

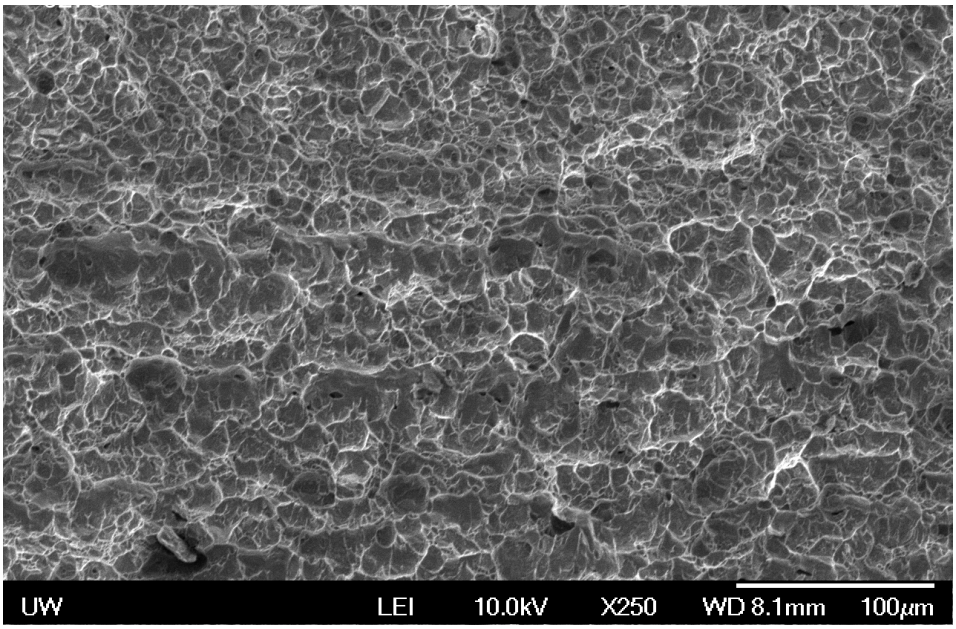

Figure 5.2-3: Microstructure of Fractured surface along bonding interface: Ti-64/Ti-6242, T8^{0}C

3. Applying Diffusion Bonding Mechanisms

In the current work, Pilling's model is utilized to estimate the diffusion bonding time of dissimilar alloys. Pilling's model is derived in chapter 2. Equation 2.1 defined the area of fraction 'A_{f0}' at the initial contact (t = 0), where σ and σ_y are the applied stress and yield stress corresponding to the bond temperature respectively. The bonded fraction can be defined by equation 5.5 (where r_0 is the initial void radius and 'r' is the instantaneous void radius and 'f' is set as$f = (r/r_0)^2$). When the bonding is complete, A_f =1.

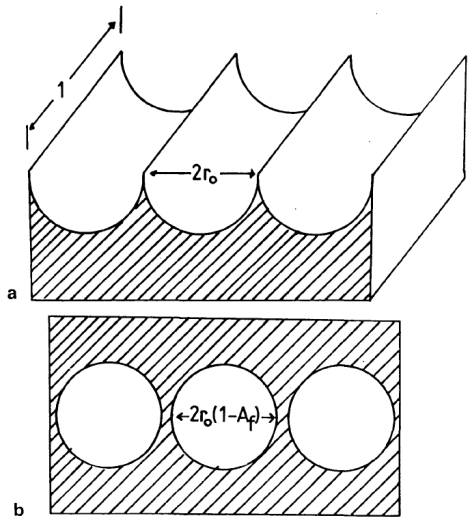

Figure 5.2-4: Pilling Model Void geometry at t = 0 [10]

$$A_{f0} = \frac{\sigma}{\sigma_y} \tag{2.1}$$

$$A_f = \frac{r_0 - r}{r_0} \tag{5.5}$$

The void closure is attributed to the four diffusion bonding mechanisms that include plastic deformation, power law creep, grain boundary diffusion and volume diffusion. The equation 5.6 describes the equation of strain rate as described in Li's model of diffusion bonding [25].The equations from the chapter 2, 2.32 and 2.33 describe the rate of change of bonding due to volume diffusion and grain boundary diffusion respectively. The rate of change in area of fraction 'f' due to plastic deformation is defined in equation 5.4. This equation is obtained through substitutions in the pilling's equation of rate of change of fractional area due to plastic deformation. The total bonding time is obtained by integrating the rate equation given by equation 5.8.

$$\dot{\varepsilon} = \frac{A\, exp^{(-Q_{sp}/RT)}\, \sigma^n}{T} \tag{5.6}$$

$$\left[\frac{df}{dt}\right]_{vol} = -\frac{4\Omega D_v}{kT}\left[\frac{f}{ln\left(\frac{1}{f}\right)-\frac{1-f}{2}}\right]\frac{1}{r_o^2}p \tag{2.32}$$

$$\left[\frac{df}{dt}\right]_{gb} = -\frac{2\Omega D_{gb}\delta}{kT}\left[\frac{1}{ln\left(\frac{1}{f}\right)-\frac{1-f}{2}}\right]\frac{1}{r_o^2}p\left(\frac{1+\frac{h}{d}}{h}\right) \tag{2.33}$$

$$\left[\frac{df}{dt}\right]_{plasticity} = \frac{\dot{\varepsilon}}{\sigma_e}\left(3p\sqrt{f} - \frac{2\gamma\sqrt{f}}{r_0} + \frac{6\gamma}{r_0}\right) \tag{5.7}$$

$$t = \int_{f_0}^{f} \frac{-\sigma_e/\dot{\varepsilon}}{\left(3p\sqrt{f} - \frac{2\gamma\sqrt{f}}{r_0} + \frac{6\gamma}{r_0}\right) + \frac{4\Omega D_v}{kT}\left[\frac{f}{\ln\left(\frac{1}{f}\right) - \frac{1-f}{2}}\right]\frac{1}{r_0^2}p + \frac{2\Omega D_{gb}\delta}{kT}\left[\frac{1}{\ln\left(\frac{1}{f}\right) - \frac{1-f}{2}}\right]\frac{1}{r_0^2}p\left(\frac{1+\frac{h}{d}}{h}\right)} df \tag{5.8}$$

Where A, Q and n are the Dorn constant in power law creep equation, activation energy and creep exponent, respectively; Ω is atomic volume; D_{gb} and D_v and grain boundary and volume diffusivities; δ, d and h are the grain boundary width, grain size and void height respectively.

4. Identification and characterization of Variables

The deterministic model of diffusion bonding time depends on bonding parameters, pressure, temperature, and surface finish of bonding interface and material properties. The pressure and temperature are represented as external variables. The internal variables would include the properties such as σ_y, A_{sp}, n_{sp}, σ^{nsp}, A_{pl}, n_{pl}, σ^{pl}, D_{gb}, D_v, Ω, γ, n, h_o, and r_o. Here some of the variables are dependent on bonding parameters, such as σ_y, D_{gb}, and D_v have dependence on temperature, and would be functions of temperature. Though these variables are treated as deterministic variables in the process, for simplicity only geometric parameters of void, the initial height h_o and the initial radius r_o are considered as random variables.

5. Distribution Fit of Random Variables of Dissimiliar Bonding Interface

   a. Height of the Void

The height of void is calculated at the bonding interface of dissimilar alloys from superimposed surface profile of the two parent alloys. The surface profile measured on surface profilometer consists of 11200 points over 5.6 mm of the length (1 data point = 0.5μm). The profile plot provides the y corrodinate of the profile. To characterize the surface profile from the total profile points, some intital hunderd points were skipped and then 5000 points were used to evaluate the parameters. The surface profile would vary depending on the measurment conditions and

direction of the measurement. Therefore the mean value is found by taking average of the profile points of the aligned profile of both the alloys. Figure 5.2-5 illustrates the superimposed profile of bonding Interface of dissimilar titanium alloys (Ti-64SG/Ti-6242SG). The distance of every profile point of each of the profile from the mean line was caluculated which provided the peak heights of both the profile, represented as peak height '$h1_n$' of one parent alloy and peak height '$h2_n$' of other alloy respectively (where n denotes the profile point number, n=1 to 5000). The total height of the void was calculated by adding height '$h1_n$' of alloy A and height '$h2_n$' of alloy B. The 5000 data points of initial height were used to find the distributuion fit of the dataset of the height of the voids at the interface of dissimilar joining tianium alloys. A number of different kinds of distribution fits were tried in Matlab14 program using distribution fitting toolbox. It is found that height of the void fit reasonnably into inverse gaussian distribution. Figure 5.2-6 shows the inverse gaussian distribution fit of initial height at the bonding interface of dissimilar alloys Ti-64SG/Ti-6242SG. The inverse gaussian distribution is defined by mean μ and shape parameter λ. The probabblity density function of inverse gaussian distribution is defined as follows.

$$f(x;\mu,\lambda) = \left[\frac{\lambda}{2\pi x^3}\right] exp\, \frac{-\lambda(x-\mu)^2}{2\mu^2 x} \qquad (\text{for } x > 0,\ \mu > 0 \text{ and } \lambda > 0) \tag{5.9}$$

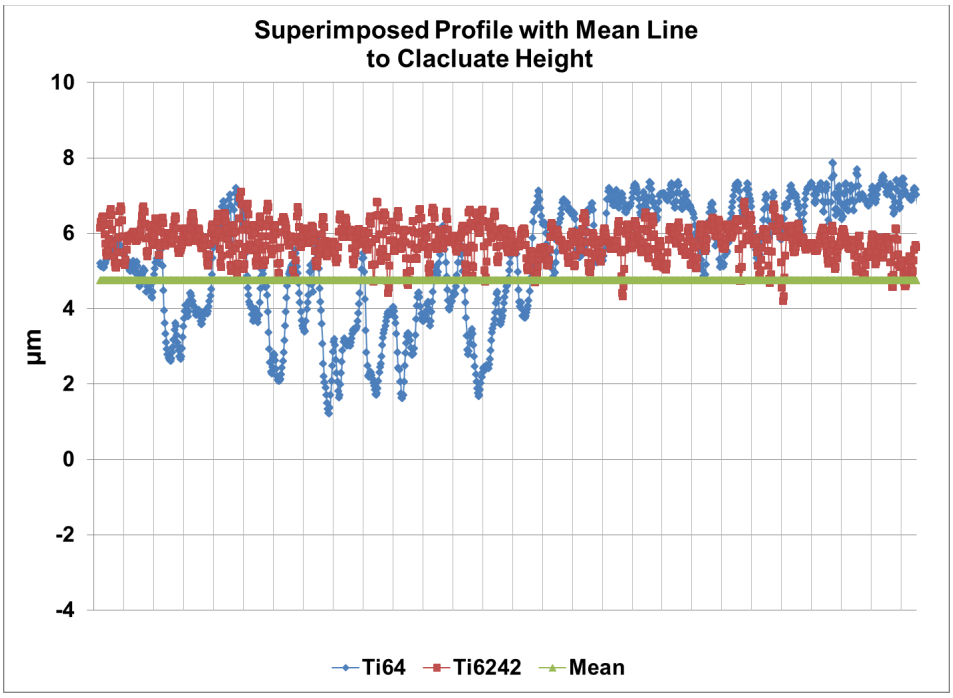

Figure 5.2-5: Superimposed profile of Bonding Interface of Dissimilar Titanium Alloys (Ti-64SG/Ti-6242SG)

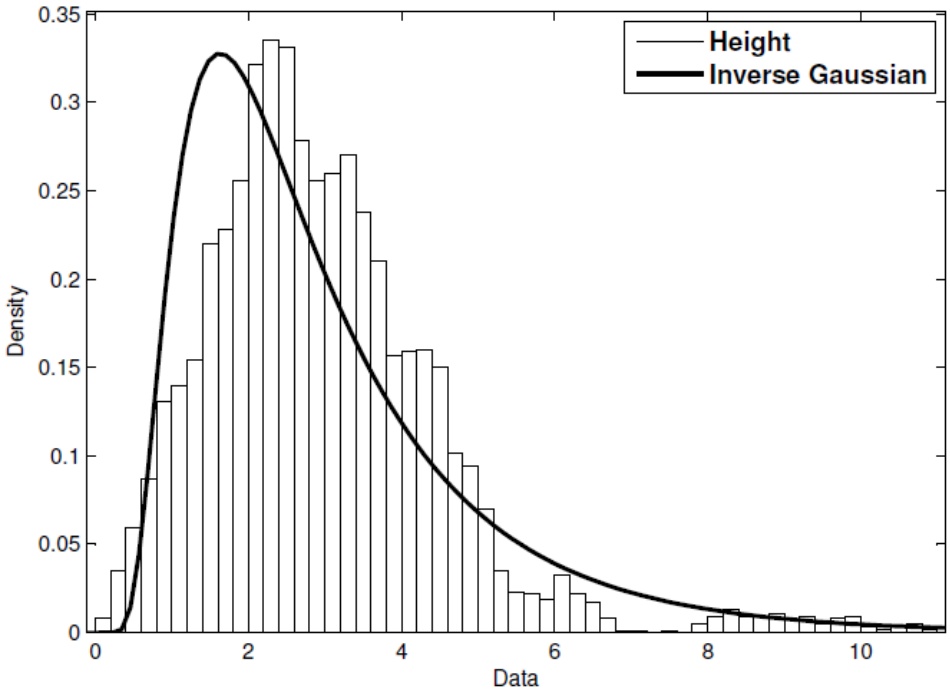

Figure 5.2-6: Distribution Fit of Height of Void at Bonding Interface of Dissimilar Alloys –Ti64SG/Ti-6242SG

b. Width of Void

The width of the profile was found from the profile points in superimposed profile obtained by subtracting them from the mean value of the both the alloys. The revised profile was obtained by plotting the surface profile of the alloys plotted from the mean line of both the profiles is shown in Figure 5.2-7. Further, the profile was separated into several charts, wherein in every chart 150 profile points were plotted to provide closer view of the profile distribution. The the x-axis in the indiviually separated charts was divided into gridlines. In the plot 5 gridlines were placed for every 20 points. From the surface profile characterization, it was known that 1 data point corresponds to 0.5μm and 20 profile points will be equal to 10 μm on the x-axis of the profile coordiante system. Therefore one divison in 20 points would be equal to 2 μm. The number of divisions in profile were counted where aprroaximately the void is formed. The width of the void was then calcualted by multiplying the number of divisions and the spacing of each division on the horizontal axis of the surface profile. A dataset of 32 points was utilized to fit a distribution of width of the void geometry. Figure 5.2-8 illustrates the profiles used to find the spacing between the voids. A number of different kind of distribution fits were tried in Matlab14 program using distribution fitting toolbox. It is found that width of the void reasonably fit into exponential distribution as shown in Figure 5.2-9. The probablity density function of exponential distribution is defined as follows, where 'λ' is the rate paratmeter of the distribution.

$$f(x) = \lambda e^{-\lambda x} \quad (\lambda > 0) \tag{5.10}$$

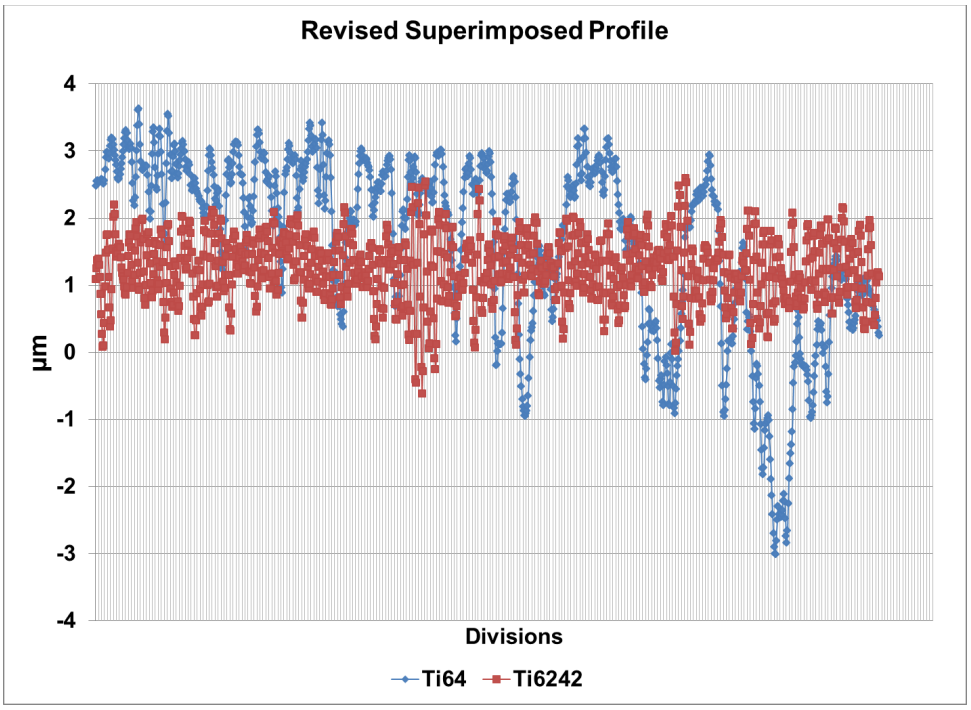

Figure 5.2-7: Revised Superimposed profile at the Bonding Interface of Dissimilar Alloys –Ti64SG/Ti-6242SG (from the mean line of both the profiles)

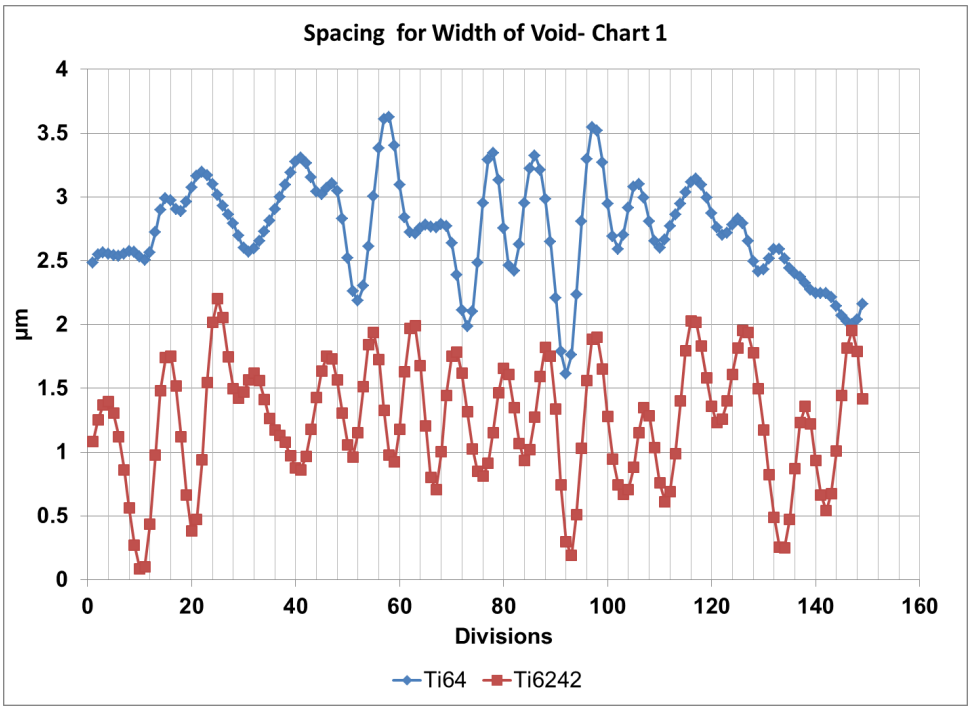

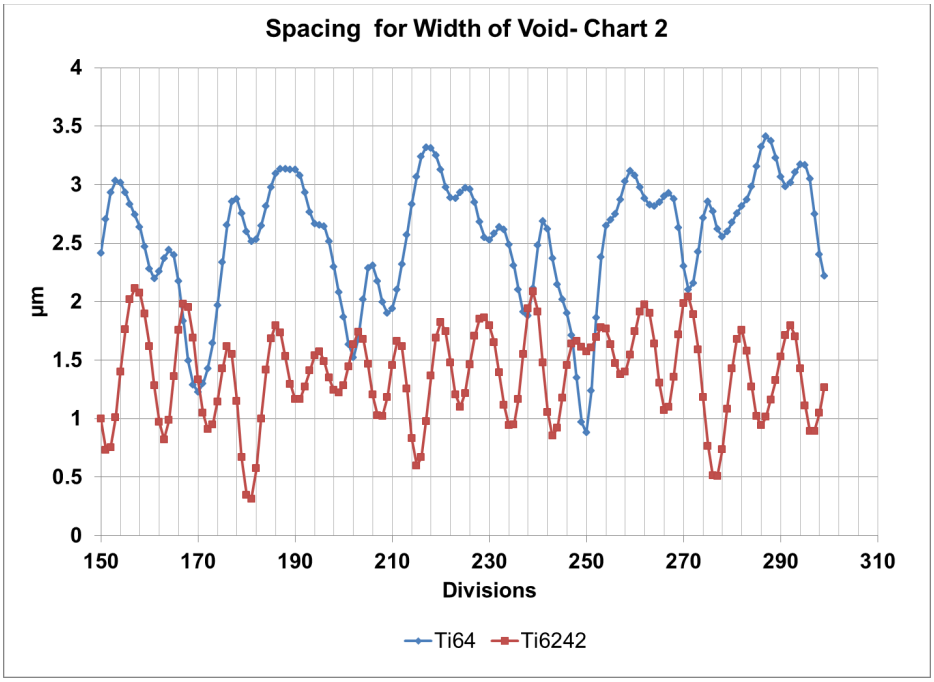
Spacing for Width of Void- Chart 2
µm
4
3.5
3
2.5
2
1.5
1
0.5
0
150
170
190
210
230
250
270
290
310
Divisions
Ti64
Ti6242

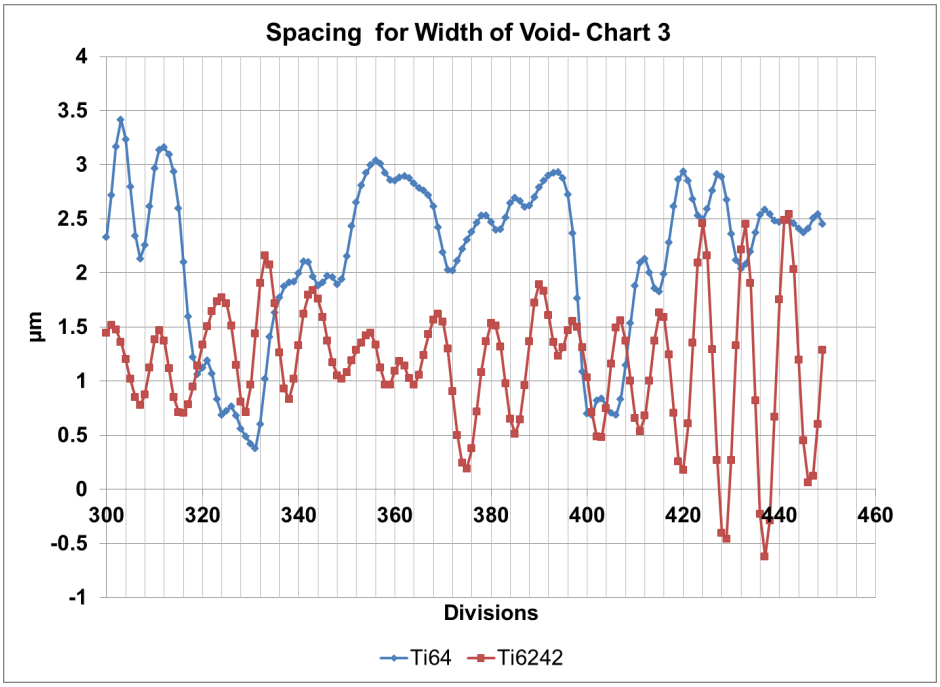
Spacing for Width of Void- Chart 3
µm
4
3.5
3
2.5
2
1.5
1
0.5
0
-0.5
-1
300
320
340
360
380
400
420
440
460
Divisions
Ti64
Ti6242

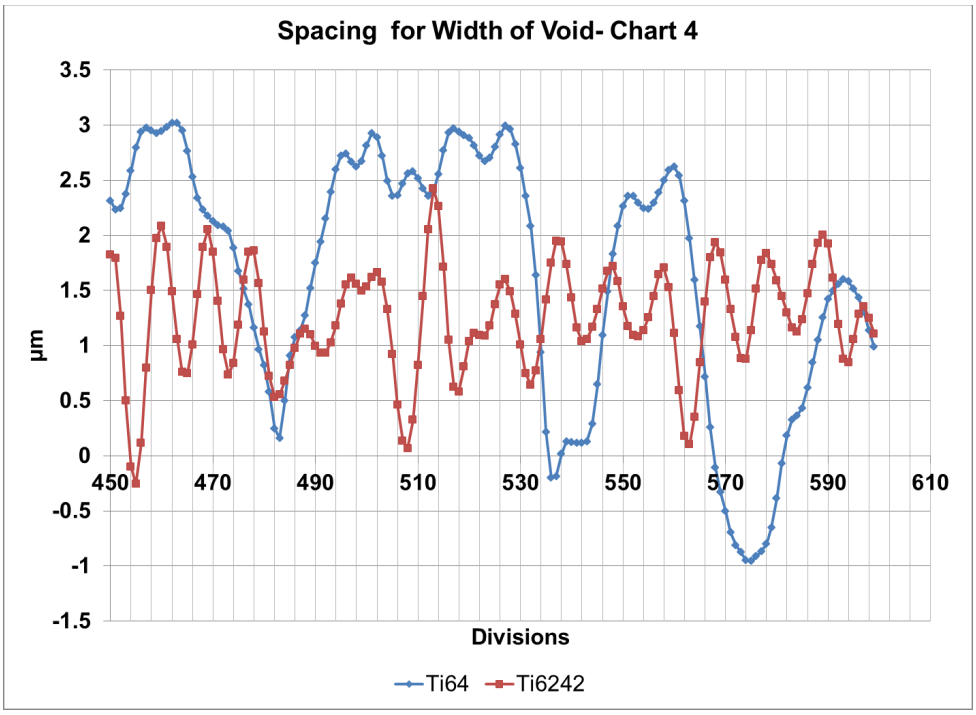
Spacing for Width of Void- Chart 4
3.5
3
2.5
2
1.5
1
0.5
0
-0.5
-1
-1.5
µm
450
470
490
510
530
550
570
590
610
Divisions
Ti64
Ti6242

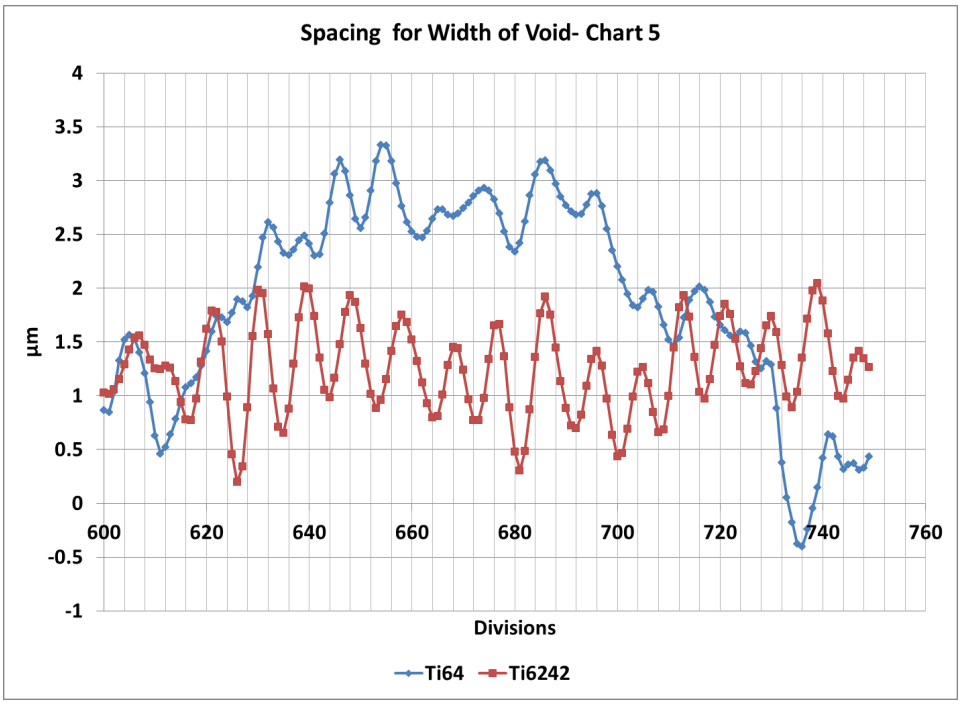
Spacing for Width of Void- Chart 5
4
3.5
3
2.5
2
1.5
1
0.5
0
-0.5
-1
µm
600
620
640
660
680
700
720
740
760
Divisions
Ti64
Ti6242

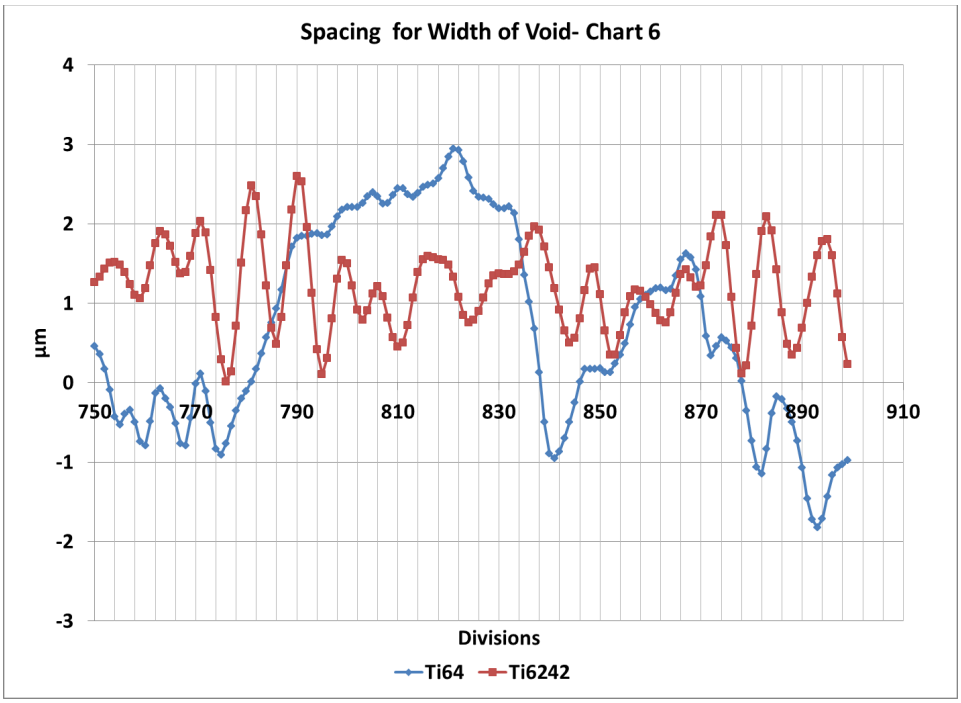

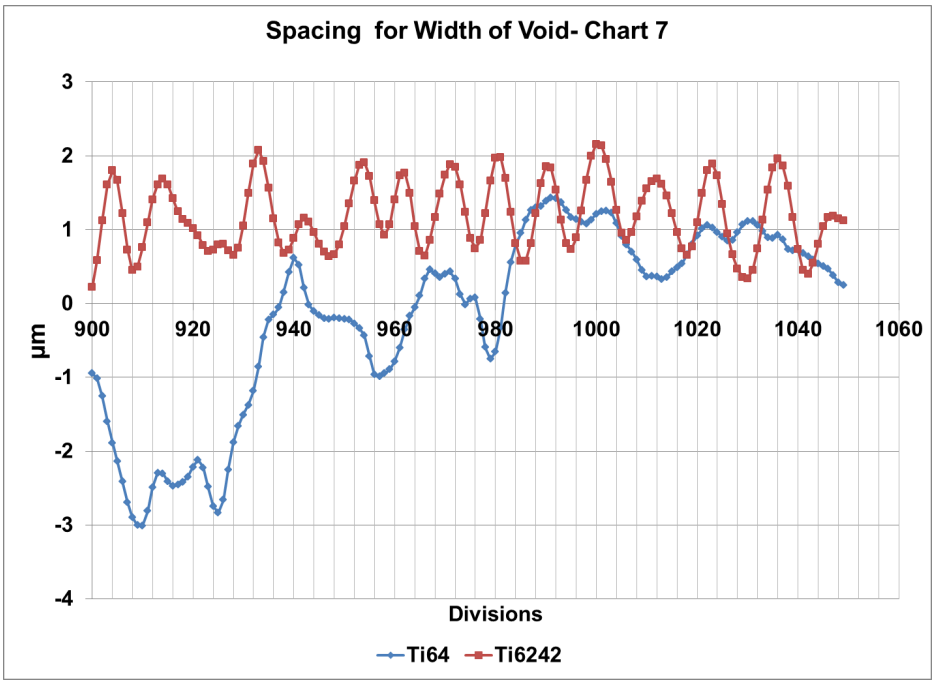

Figure 5.2-8: Surface profile charts for calculating width of void at bonding interface of Dissimilar Alloys –Ti64SG/Ti-6242SG

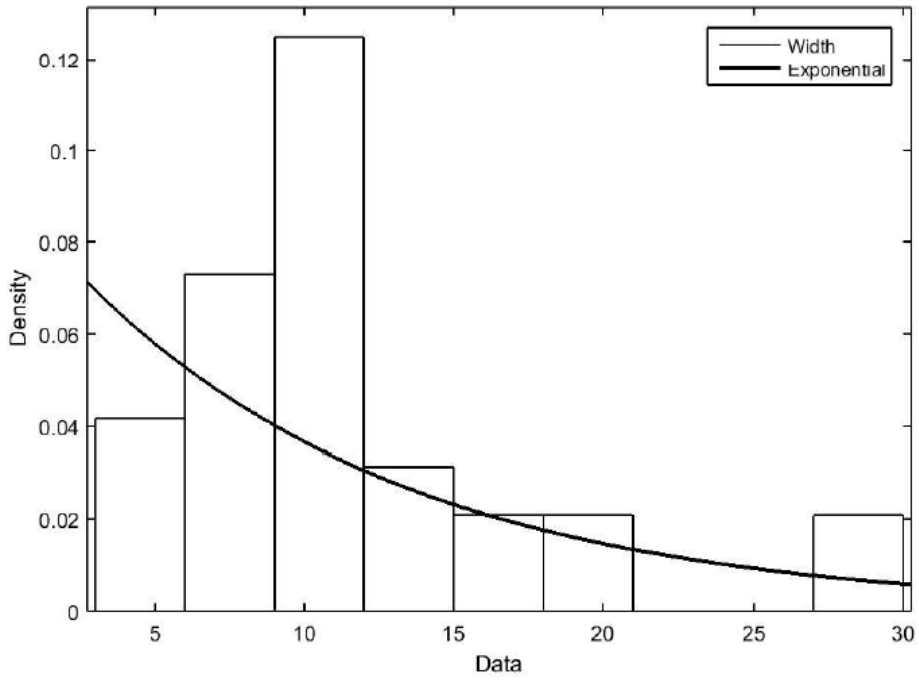

Figure 5.2-9: Distribution fit of width of void at bonding interface of Dissimilar Alloys –Ti64SG/Ti-6242SG

6. Random Number Generation with Numerical Integration to calculate diffusion bonding time

   The samples of random variables were generated using distribution function in Matlab. The distribution functions of inverse gaussian and of exponential were applied to produce random samples of initial height h_0 and initial radius r_0 respectively. The substitution of this sample value in the bonding time equation calculates the bonding time of the process and its CDF. A set of 100 random variables was used to simulate 1 CDF. The process of generating CDF was repeated for 100 times.

7. Material Properties in Bonding Mechanisms of Dissimilar Alloys

   In the duplex alloys such as Ti-64 and Ti-6242 two types of titanium, 'α' and 'β' is present. Therefore in the dissimilar alloys having duplex nature, the variation in the material properties during the bonding mechanisms were taken into consideration with the proportions of 'α' and 'β' present in them.

8. Flow Chart

The steps followed in the characterization of surface profile at the bonding interface of dissimilar alloys are highlighted in the flow chart shown in Figure 5.2-10.

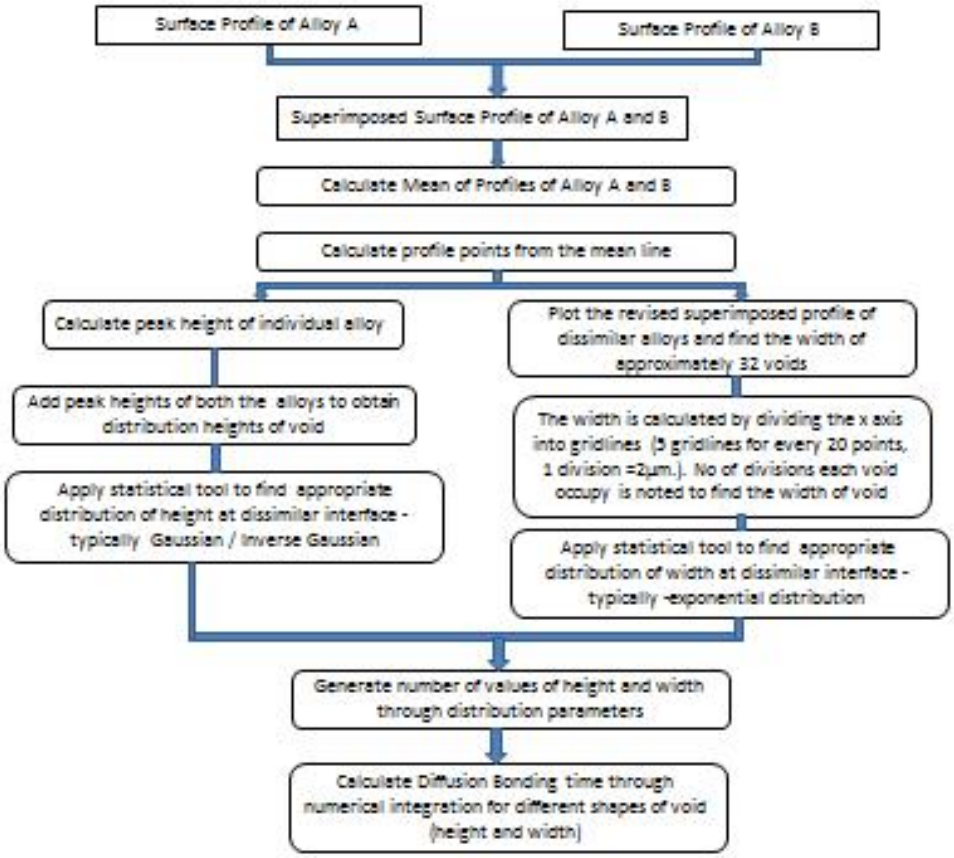

Figure 5.2-10: Flow Chart of Surface Profile Characterization and Bonding Time Estimation at the Joining Interface of Dissimilar Alloys

5.2.2 *Probabilistic Model Results of Diffusion Bonding time in Dissimilar Titanium Alloys*

The new model of modeling of diffusion bonding time in dissimilar titanium alloys was applied to simulate diffusion bonding time in the joining of dissimilar titanium alloys Ti-64SG/Ti-6242SG. The probability density function (pdf) for the height and width of the

void was defined by inverse gaussian and exponential distributions respectively. In the probability density function of height the values of 'μ' and 'λ' were 2.96977E-6 and 6.98841E-6 respectively, while in case of pdf for width of void the value of 'μ' was set to be 10.9375E-6. As stated earlier, the total bonding time was obtained by integrating the strain rate equation given by equation 5.5. The material properties of Ti-6Al-4V were utilized in the model as given below [18, 20, and 25]. In the material data 'α' and 'β' denote the alpha and beta proportions of the properties respectively.

1) Atomic volume
   - Ω_α (m^3) = 1.76E-29;
   - Ω_β (m^3) = 1.81E-29;

2) Burgers vector b (m) = $2.9 \times 10{-}10$

3) Bonding Temperature T (Kelvin), Melting Temperature Tm (Kelvin) = 1973;

4) Pressure P (Pascal)

5) Gas Constant R = 8.314;

6) Boltzmann's constant k (J/K) = 1.38*1E-23;

7) Grain Boundary diffusivity
   - Dgbdel_ α =3.6E-16*exp(-97000/(R*T));
   - Dgbdel_ β =5.4E-17*exp(-153000/(R*T));

8) Volume Boundary diffusivity
   - Dv_ α =8.6E-10*exp(-150000/(R*T));
   - Dv_ β =1.9E-7*exp(-153000/(R*T));

9) Surface energy Se (J m-2)=1.7;

10) Grain size d (m) = 8E-6;

11) Stress exponent n =4.3

12) Shear Modulus G (MPa)
   - G_ α = g α 300*(1+((T-300)/Tm)*(td_g α));
   - G_ β = g b300*(1+((T-300)/Tm)*(td_g β));
     g α 300=4.3E4; g β 300=2.05e4;
     td_g α =-1.2; td_g β =-0.5;

13) Dorn Constant 'A'

- A_ α = α *Docr_ α *exp(-Qocr_ α /(R*T))*((G_ α *1E6*del_ α)/(k*T));
- A_ β = β *Docr_ β *exp(-Qocr_ β /(R*T))*((G_ β *1E6*del_ β)/(k*T));

Docr_ α =6E-7; Docr_b=9E-8;
Qocr_ α =97000; Qocr_ β =153000;
del_ α =5.9e-10; del_ β =5.72e-10;

14) 'α' and 'β' proportions at different temperatures

- T4 = 'α': 0.55 (Ti-64SG+Ti-6242SG), 'β': 0.45(Ti-64SG+Ti-6242SG)
- T5 = 'α': 0.50 (Ti-64SG+Ti-6242SG), 'β': 0.50(Ti-64SG+Ti-6242SG)
- T7 = 'α': 0.45 (Ti-64SG+Ti-6242SG), 'β': 0.55(Ti-64SG+Ti-6242SG)
- T8 = 'α': 0.40 (Ti-64SG+Ti-6242SG), 'β': 0.60(Ti-64SG+Ti-6242SG)

In the current work, the diffusion bonding process was characterized at different bonding temperatures. The adopted model for dissimilar titanium alloys was applied to predict bonding time with constant pressure between 1-5MPa at different temperatures. The estimated CDF value at different temperatures is shown in Figure 5.2-11. These results show reasonable agreement with the experimental conditions.

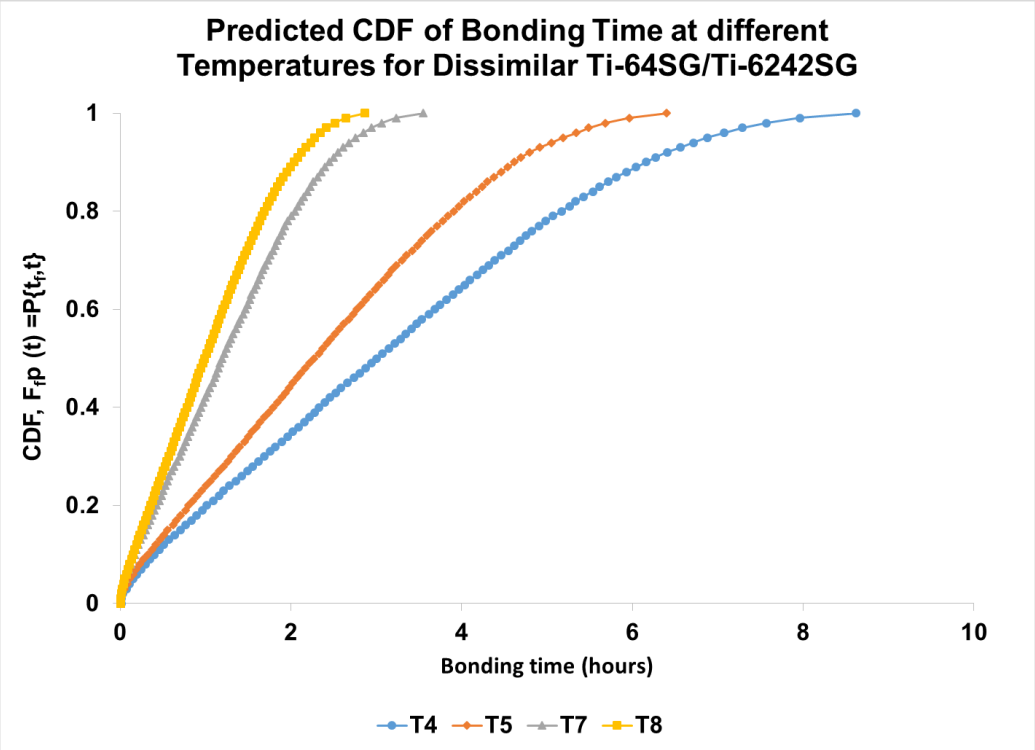

Figure 5.2-11: Predicted CDF of Bonding Time at different temperatures for Dissimilar Ti-64SG/Ti-6242SG

5.2.2.1 Effect of Grain Size on Bonding Time

The effect of grain size was studied on the bonding time of dissimilar titanium joint Ti-64SG/Ti-6242SG. The bonding parameters of pressure and temperature were kept constant at T7^{0}C and pressure between 1-5 MPa. The grain size was increased from 4 to 30µm. The results of effect of grain size on bonding time in Figure 5.2-12 shows that smaller grain size require less time to complete bonding process, which in agreement with the literature.

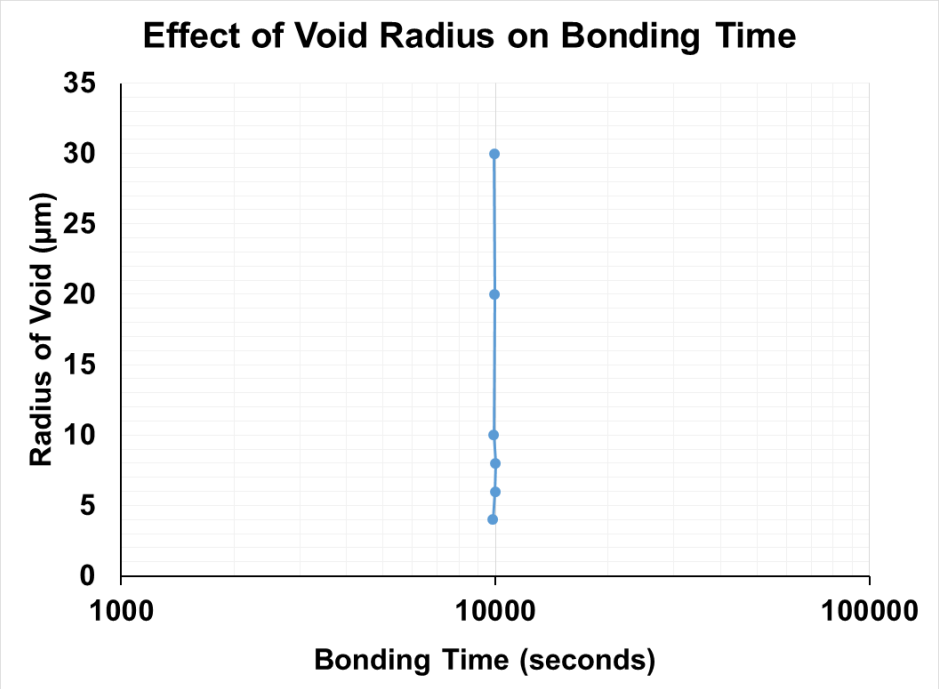

Figure 5.2-12: Effect of Grain size diameter on Bonding Time

5.2.2.2 Effect of Surface Roughness on Bonding Time

The effect of surface roughness was studied on the bonding time of dissimilar titanium joint Ti-64SG/Ti-6242SG. In the simulation of bonding time, pressure and temperature were kept constant at T7^{0}C and 2MPa. In the model effect of void radius was studied by increasing the radius value from 5 to 30µm, while the height of void was generated randomly. Similarly the effect of height of void was studied by increasing the height from 0.5 to 30 µm while generating the radius randomly. The results of effect of surface roughness on the bonding time are shown in Figure 5.2-13. In the cases, the increase in

void radius or height results in higher bonding time which is again in agreement with the literature.

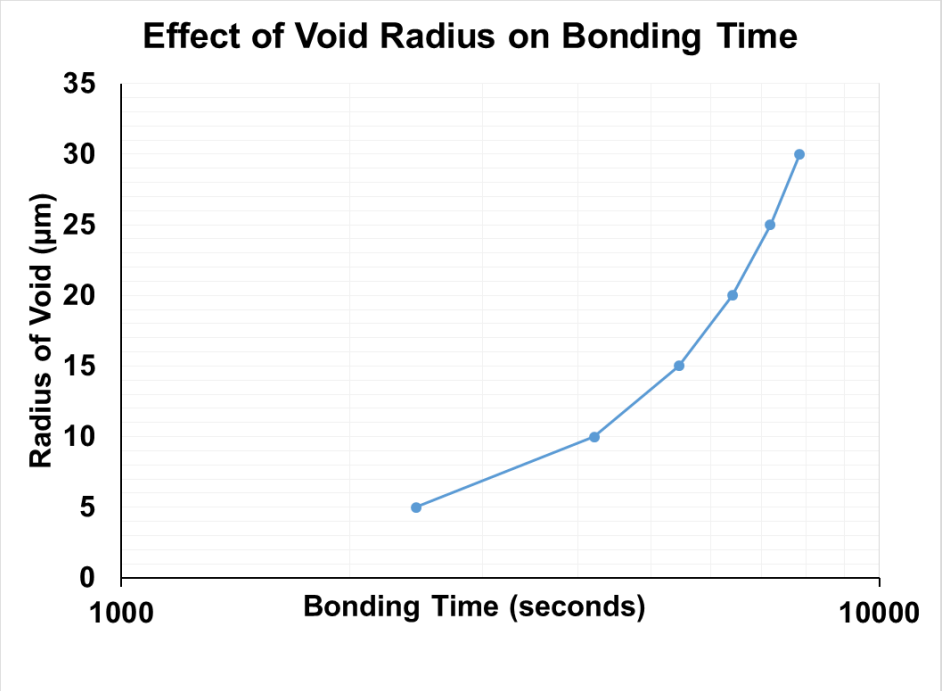

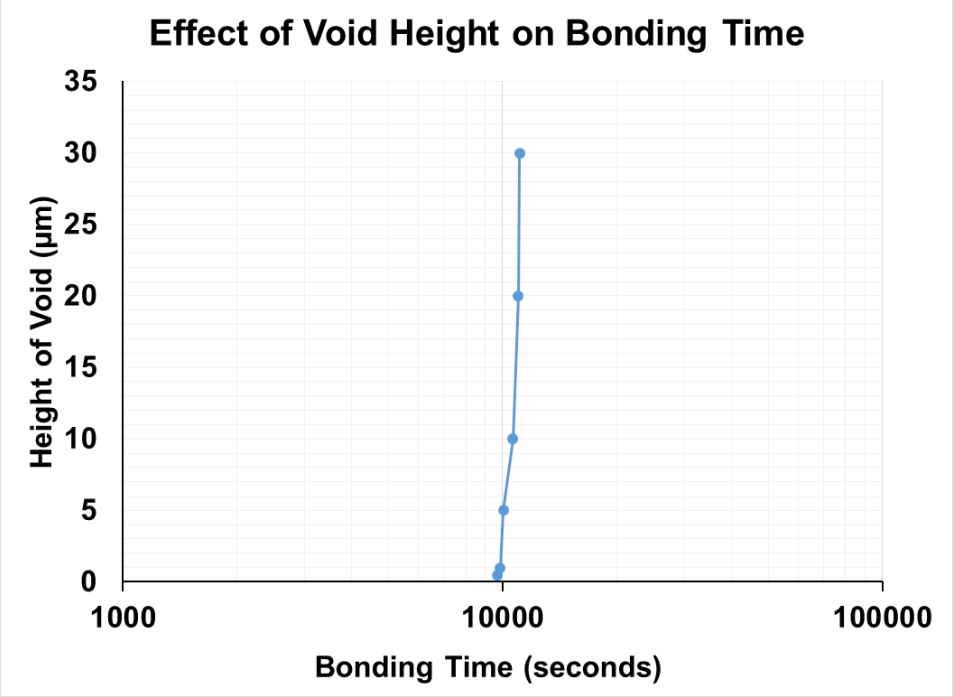

Figure 5.2-13: Effect of Surface Roughness on Bonding Time

5.3 NUMERICAL MODELING OF DIFFUSION BONDING IN SIMILAR TITANIUM ALLOYS

The numerical model of diffusion bonding was developed in Abaqus. As explained in theoretical modeling of diffusion bonding, the geometry of the mating surface can be assumed to in plane strain condition. Therefore, 2-D model was developed with the plane strain condition. In diffusion bonding, the creep is the dominant mechanism amongst the other bonding mechanisms that includes grain boundary diffusion due to surface source and volume source mechanism. Therefore, in the current model, the creep mechanism is considered while studying the void closure in diffusion bonding. The effect of pressure and temperature was studied on void closure in diffusion bonding process.

5.3.1 *Finite Element Modeling*

The 2 D model of diffusion bonding was studied with single void in the center of the sandwiched sheets. The voids are semi elliptical on the both sheets in reverse direction to form ellipse, when both the sheets are brought together in contact. The dimension of the void was 0.0499 mm along minor axis and 0.0626 mm across major axis of the ellipse. The mesh was generated using plane strain linear elements with tree nodes and triangular shape (CPE3), with a refined mesh in the vicinity of the void. A contact condition was defined between the bonding surfaces and boundary conditions were applied using diffusion bonding machine set up. In the model, the lower end corners were constrained in both the direction while the other portion of lower end was constrained in the y- direction. The upper end corners were constrained in the x-direction. The load in terms of bonding pressure was applied on the upper surface. The experimental temperature and pressure conditions were applied to the model. The work piece material is assumed to be isotropic, linear-elastic and strain-hardenable. The creep property is applied with strain hardening model of Abaqus. The creep property was applied with strain hardening model of Abaqus. In the model the coefficients of strain rate were defined from Fang's model of void closure for Ti-64alloy [21].

$$\dot{\varepsilon} = A\left|\frac{\sigma}{G}\right|^{n}$$

Where$\dot{\varepsilon}$ is strain rate, A is creep constant, G is shear modulus, and n is stress exponent.

In the strain rate equation, the creep constant is a function of temperature. Therefore in the study the effect of temperature on diffusion bonding was studied through the creep constant variable in the strain rate equation. Numbers of simulations were run to study the effect of pressure and temperature on the void closure in diffusion bonding. The effect of temperature was studied by varying the temperature from T5, T7, and T8^{0}C keeping pressure constant between 1-5 MPa, while the effect of pressure was evaluated by changing pressure from 1, 2 and 3 MPa with temperature at T7^{0}C. The strain rate equation was calculated separately for each temperature condition and changed accordingly in the simulations of different bonding temperatures. The finite element process was divided into two steps, the static and the visco step. The initial application of the pressure is assumed to occur so quickly that it involves purely elastic response, which is obtained by using the static procedure. The creep response is then developed in a second step, using the quasi-static procedure. A response of 3600-9600 seconds (1-3 hours) was requested similar to experimental condition, sufficient to reach steady-state conditions. During the quasi-static step a tolerance is provided to control the time increment choice and, hence, the accuracy of the transient creep solution.

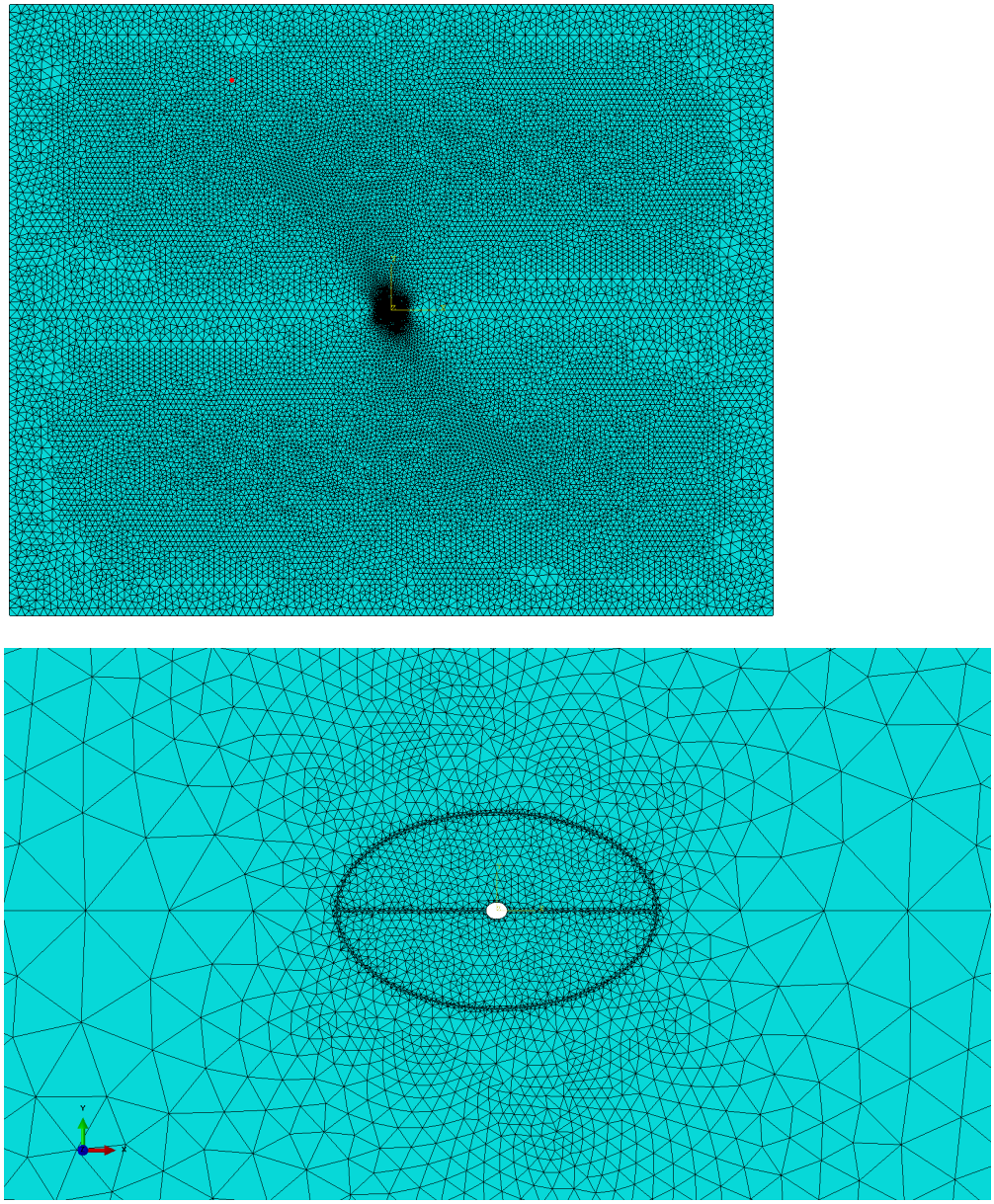

Figure 5.3-1: Meshed FEA model showing refined mesh in the vicinity of the bonding interface

5.3.2 *Simulation Results*

The result of application of bonding pressure and creep was studied on the void closure in diffusion bonding process. The effect of pressure and temperature on bonding was evaluated by measuring the deformation of nodes at the bonding interface. Figure 5.2-2

shows the position of upper and lower nodes those were measured to obtain deformation due to application of different bonding temperatures and pressures. Figure 5.3-3 the effect of bonding condition on the voids which are present at the bonding interface. It can be seen that the elliptical void reduces its dimensions as an effect of bonding pressure and creep mechanism. Figure 5.3-4 and 5 show the effect of bonding temperature and pressure respectively on the closure of void. It is evident that that increase in bonding temperature and pressure results to the increase in void closure, therefore higher the temperature or pressure, higher is the void closure. The area of fraction bonded was found out by calculating the area of void before and after the loading condition. It was found that around 70% of area of fraction is achieved through the creep mechanism. This is in agreement with the Fang's result [21] on void closure of TC4 alloy with different bonding mechanisms, wherein creep contributes to around 70% of void closure, while the other bonding mechanisms, surface source and interface source contribute to remaining 30 % of void closure in diffusion bonding.

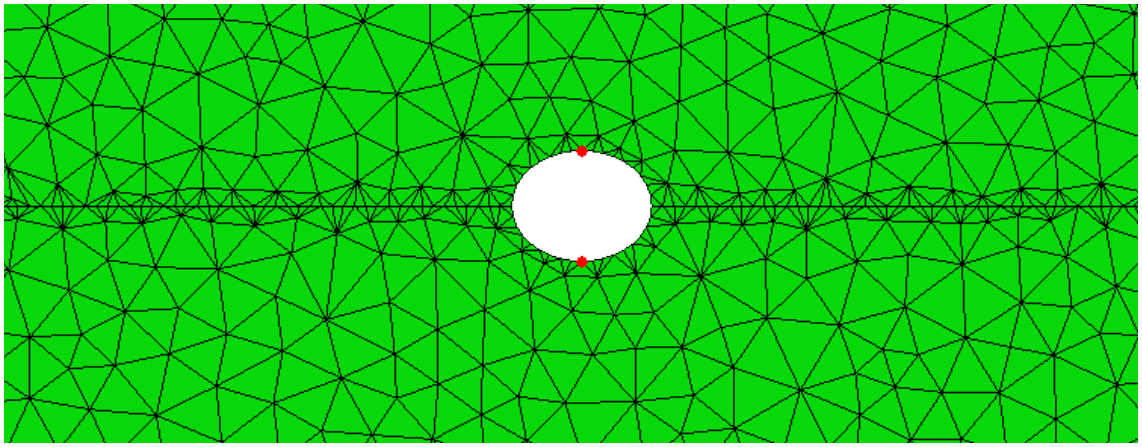

Figure 5.3-3: Nodes Measured to Obtain Deformation

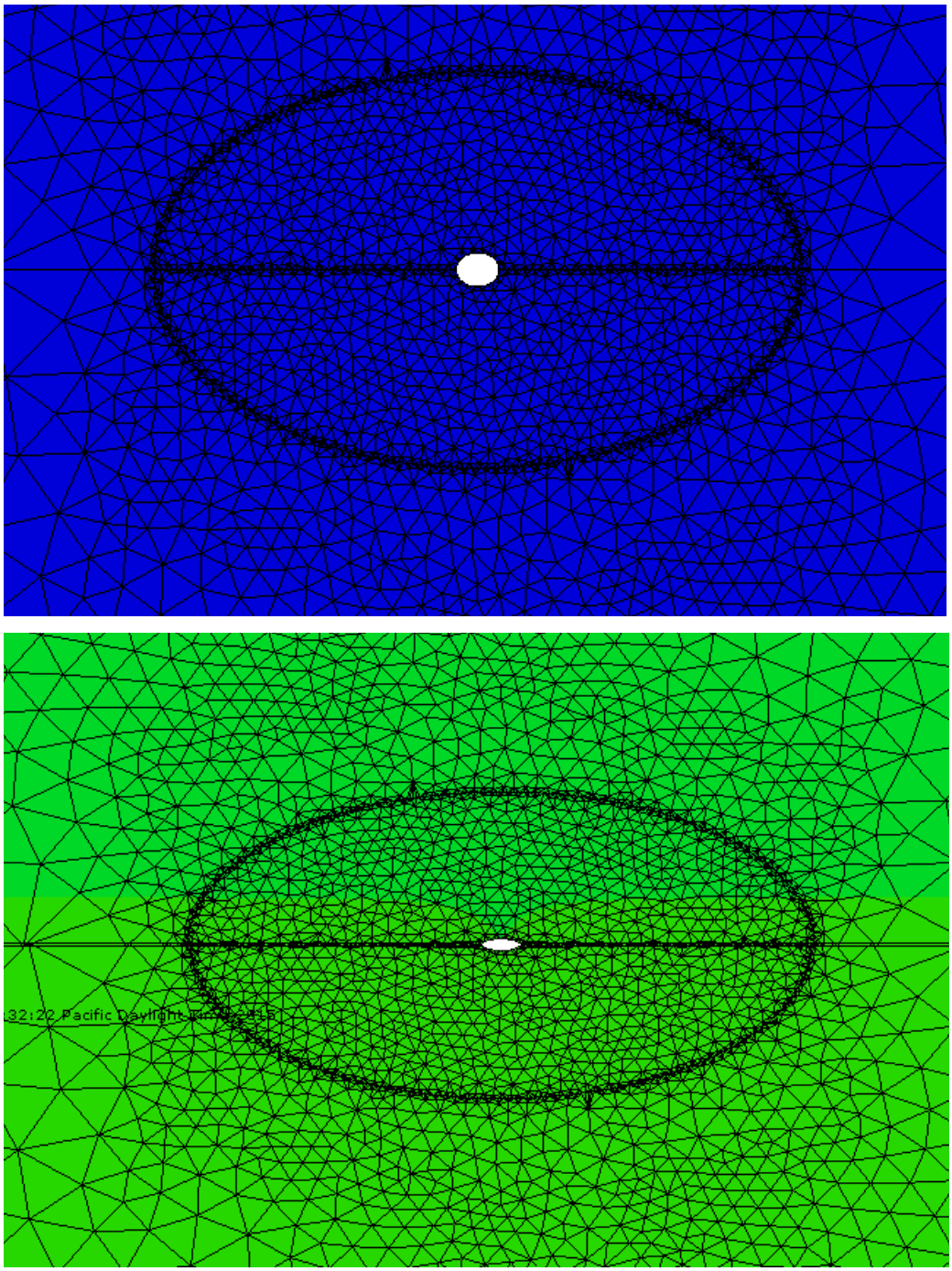

Figure 5.3-2: Void geometry before and after application of bonding condition in Ti-64 at P = (1-5 MPa), T= T7C

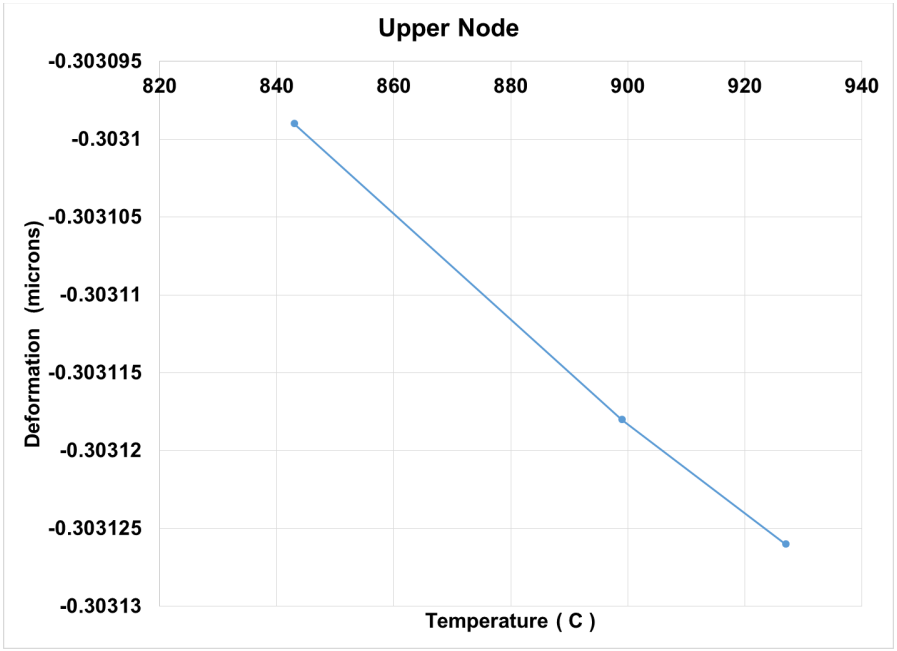

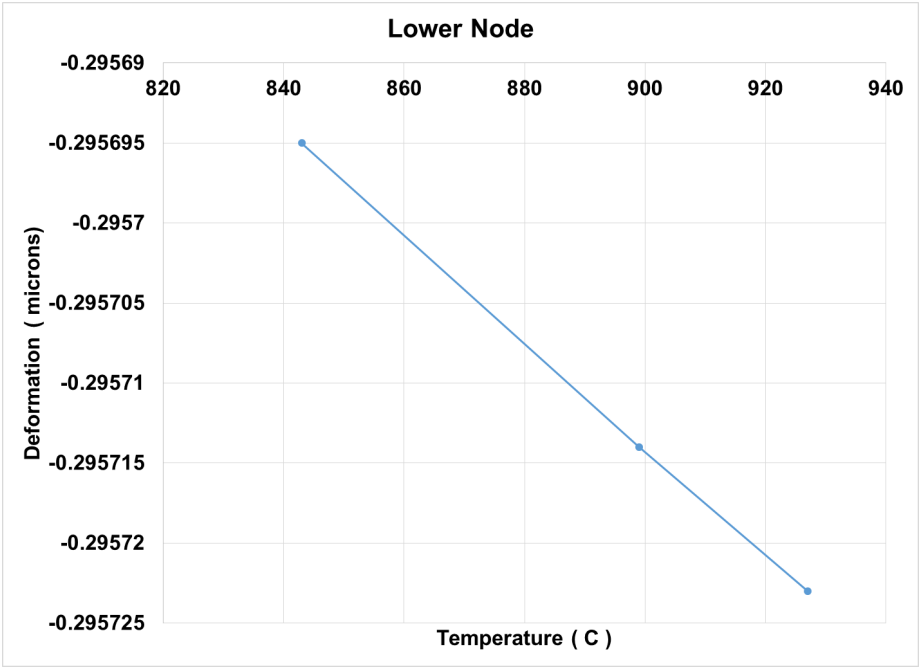

Figure 5.3-4: Effect of Temperature on Void Closure (P=1-5MPa)

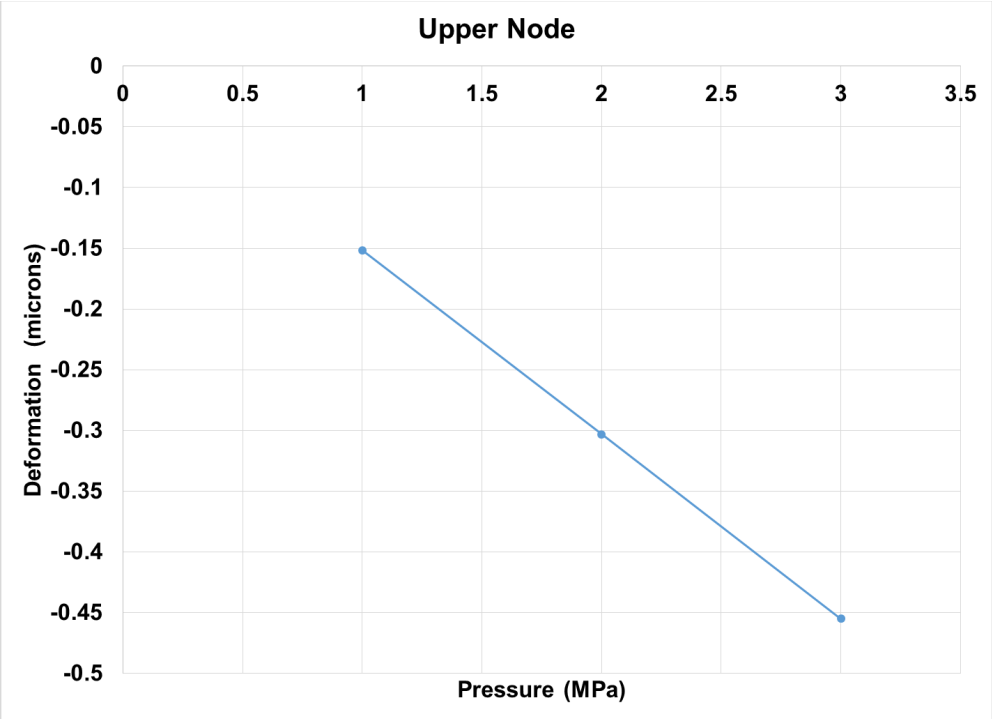

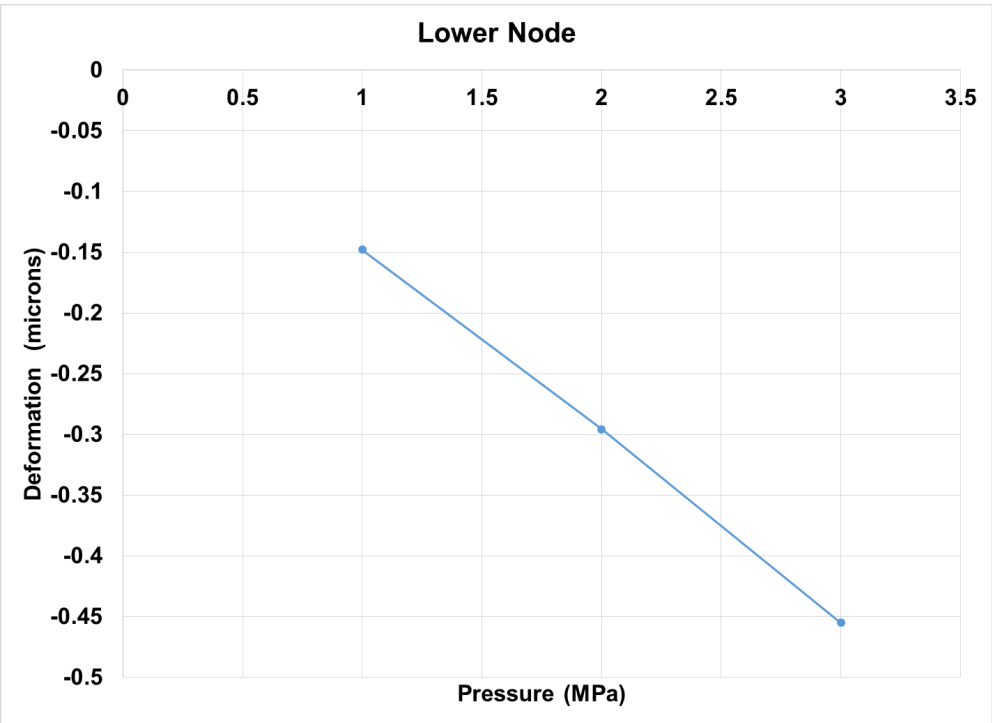

Figure 5.3-5: Effect of Pressure on Void Closure ($T=T7^0C$)

5.4 NUMERICAL MODELING OF FLEXURE TESTING IN DISSIMILAR TITANIUM ALLOYS

The flexure test behavior of diffusion bonded of similar and dissimilar titanium joints was simulated using ansys workbench. The behavior of titanium joints with similar alloys was simulated by using same material model for both of the sheets. However the numerical model of mechanical behavior of dissimilar joint was simulated by using experimental material curves for each of the sheet to be joined and compared to the experimental curves obtained for the dissimilar joints. To develop the model of dissimilar titanium joint included two parent alloys, Ti-64SG / Ti-64SG, Ti-6242/Ti-6242, and the third one was the combination of these alloys, Ti-64SG /Ti-6242. The cases of perfectly bonded were used in the simulation. The solid model of the bending specimen was developed in ansys workbench. The boundary conditions similar to the experimental conditions were applied to obtain the numerical results. For each case, results were obtained for two loading conditions, the load where yield stress was present and the load where ultimate stress was obtained or in other words, at the yielding load and at the maximum loading condition. Each loading condition was simulated for two diffusion bonding temperatures used in preparing diffusion bonding joints. The two diffusion bonding temperatures those applied were T5^{0}C (0.51&0.50Tm) and T8^{0}C (0.56& 0.55 Tm). Therefore, for each alloy 4 simulations were required and hence total 12 simulations were run to obtain the numerical results.

5.4.1 *Finite Element Modeling*

The static structural type of test was adopted for simulating three dimensional model of three point bending of diffusion bonded titanium alloys. The element type ‘20 Node-Hexahedral’ element type was chosen to perform the simulations. The material model of *Bilinear Isotropic Hardening* was applied till the maximum load point in the experimental stress strain curve. In case of Ti-64/Ti-6242 Model, the material properties of parent alloys Ti-64SG / Ti-64SG and Ti-6242/Ti-6242 were applied in the model and the result of it was validated against the Ti-64SG /Ti-6242 experimental data. The element mesh size was 3.75e-4m. At the left end the boundary condition of fixed support was applied whereas at

the right end roller support condition was used. The nodal type of force was applied at the center of the upper alloy in the negative y direction. Table 5-2 shows the dimensions of the rectangular sheets. Both the alloy sheets were equally divided in the height of the bounding box. Figure 5.4-1 show the meshed perfectly bonded sheets along with the load and the boundary conditions. Table 5-3 shows the details on the material data of titanium alloys.

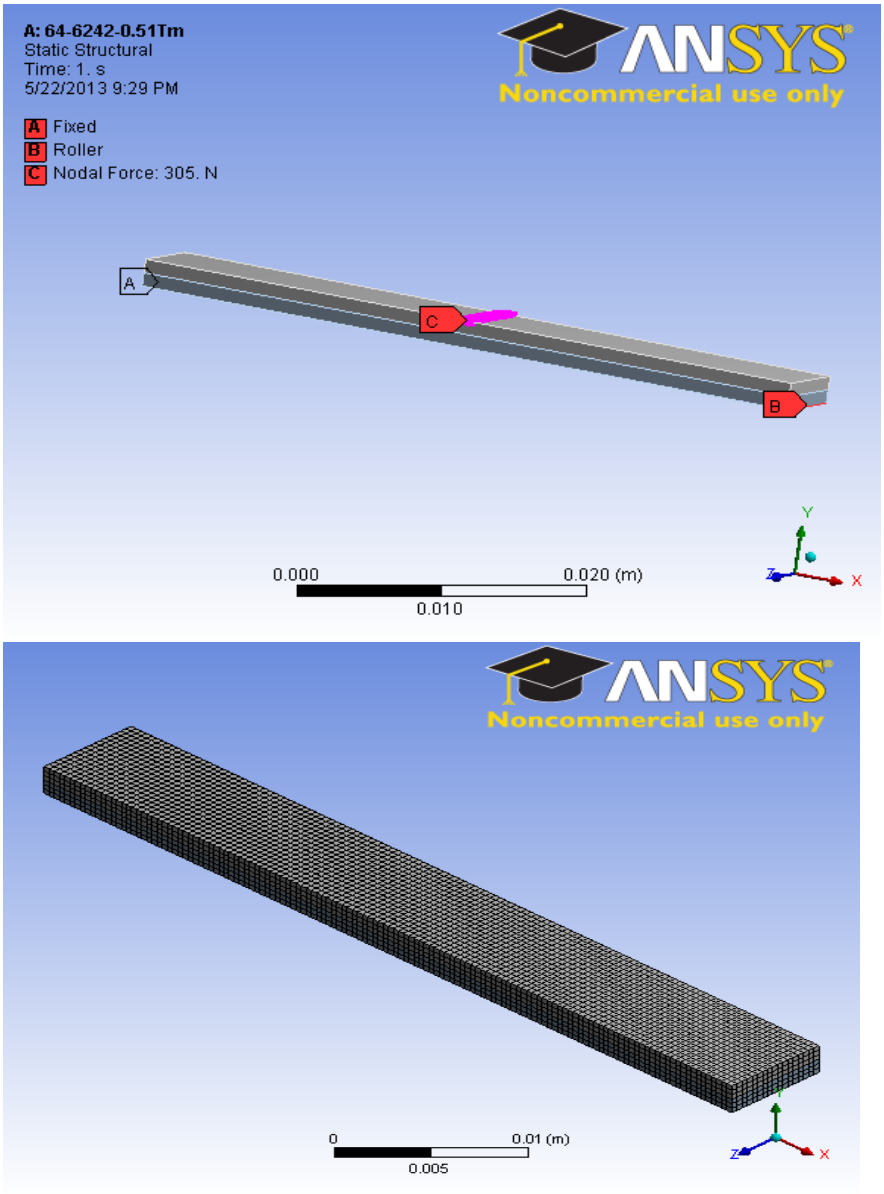

Figure 5.4-1: Perfectly Bonded Meshed sheet with Load and Boundary conditions

Table 5-2: Dimensions of the Rectangular Sheets

Bounding Box	
Length (L) :Length X	50 mm
Height (d):Length Y	2.10±0.07 mm
Width(b):Length Z	7.90±1.62 mm

Table 5-3: Material data of Titanium alloys (Ti-64, Ti-6242, and Ti-64/Ti-6242)

DB Alloy	Temp (C)	Elastic Modulus (GPa)	Yield Strength 0.2 % (MPa)	Tangent Modulus (MPa)	Poisson's Ratio	Load @ yield strength (N)	Load @ Ultimate Strength (N)
Ti-64/Ti-64	T5	58.96	700	3165	0.342	250	269
	T8	62.33	710	6981	0.342	382	404
Ti-6242/Ti-6242	T5	66.18	840	9736	0.32	284	317
	T8	54.93	800	8776	0.32	483	561
Ti-64/Ti-6242	T5	54.19	720	5946	0.331	270	305
	T8	51.90	780	11731	0.331	471	471

5.4.2 *Simulation Results*

The contours of numerical results for the equivalent stress, the normal stress in y direction and the equivalent strain are plotted for Ti-64SG / Ti-64SG, Ti-6242/Ti-6242, and Ti-64SG /Ti-6242 at $T5^0C$ for the maximum load condition are displayed in Figures 5.4-2 to 5. Table 5-4 tabulates the comparison of the numerical results with the experimental results at two points in the stress strain curve, the yield Point and the ultimate Stress, whereas Figure 5.4-6 displays the comparison plots with the experimental results. The bending phenomenon (compression on top, tension on bottom) was observed. The contours of Ti-6242/Ti-6242 were larger than Ti-64SG/ Ti-64SG contours. The dissimilar alloy, Ti-64SG /Ti-6242 contours lie between contours of Ti-64SG/ Ti-64SG and Ti-6242/Ti-6242.The numerical results of parent alloys Ti-64SG/Ti-64SG and Ti-6242/Ti-6242 were in good agreement with experimental results for both cases (yield, ultimate) at both temperatures.

The numerical results of the dissimilar alloy Ti-64SG/Ti-6242 lie within 10%. The ultimate stress in Ti-64SG /Ti-6242 was observed close to Ti-6242.

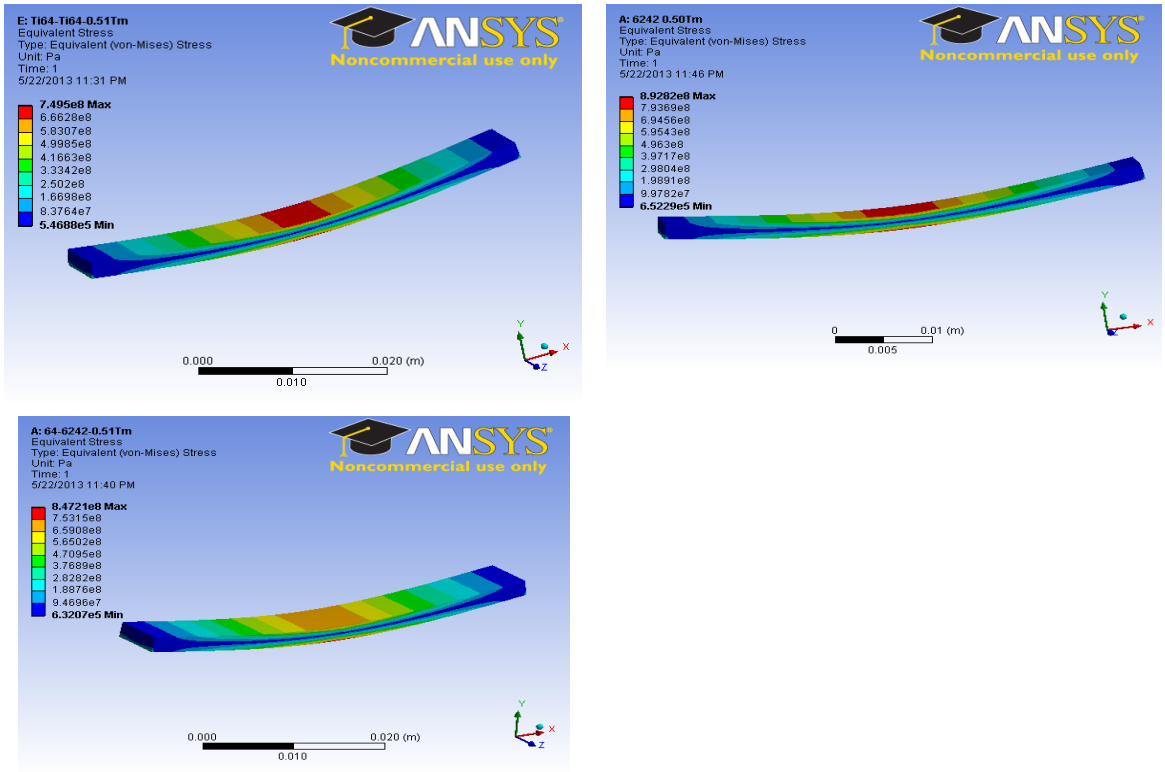

Figure 5.4-2: Contours of Stress/ Strain results – Equivalent Stress at 0.51 Tm: Max load for Ti-64SG/Ti-64SG, Ti-6242/Ti-6242, and Ti-64SG /Ti-6242

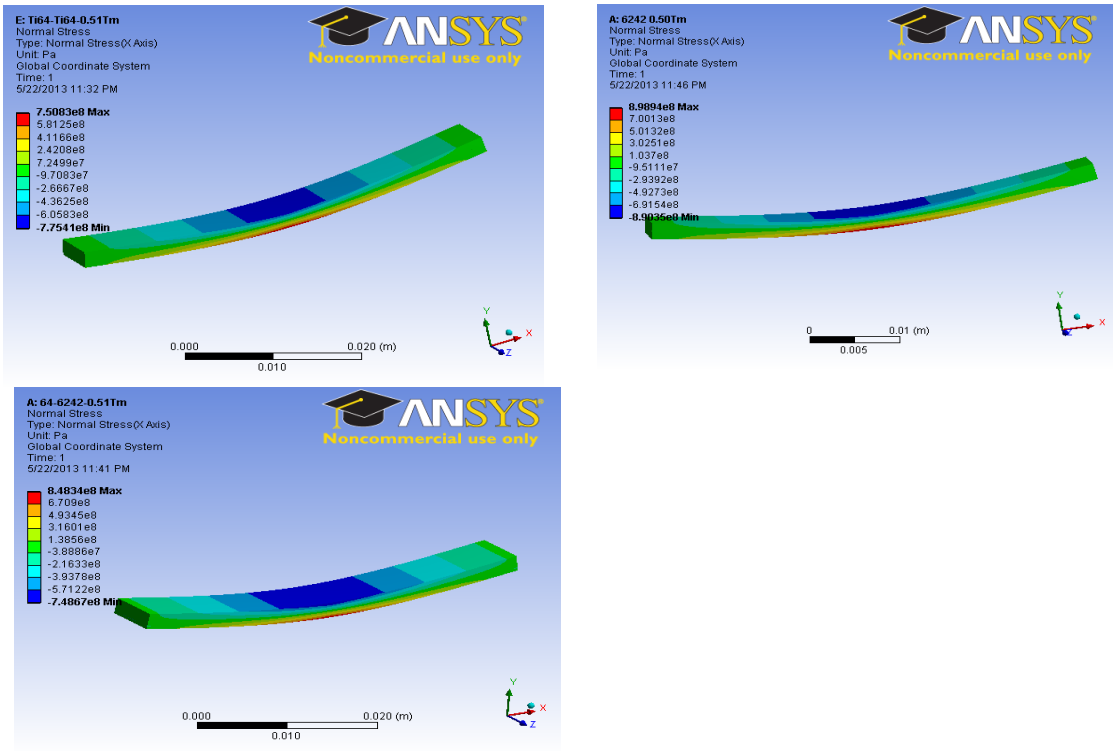

Figure 5.4-3: Contours of Stress/ Strain results –Normal Stress in y direction at 0.51 Tm: Max load for Ti-64SG/Ti-64SG, Ti-6242/Ti-6242, and Ti-64SG /Ti-6242

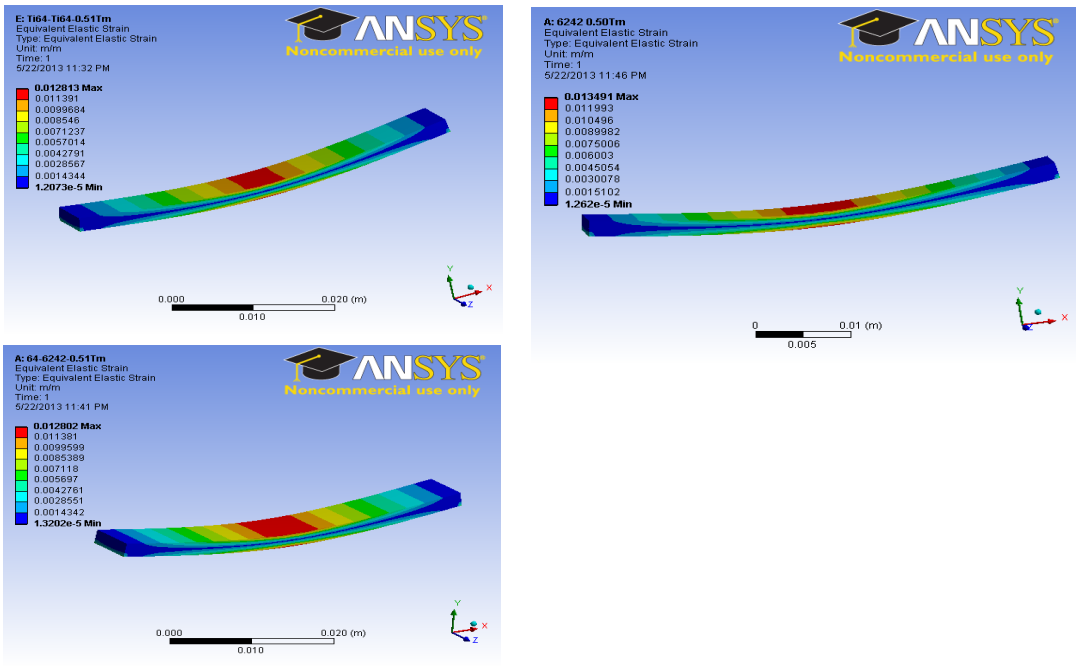

Figure 5.4-5: Contours of Stress/ Strain results – Elastic Strain at 0.51 Tm: Max load for Ti-64SG/Ti-64SG, Ti-6242/Ti-6242, and Ti-64SG /Ti-6242

Table 5-4: Comparison with Experimental Results

DB Alloy	Bonding Temp	Yield Point					Ultimate Stress @ Max Load Point				
		Stress (MPa)			Elastic Strain		Stress (MPa)			Elastic Strain	
			Numerical					Numerical			
		Exp.	Normal	Eqvi.	Exp	Numerical	Exp.	Normal	Eqvi.	Exp.	Numerical
Ti64/ Ti-64	0.51Tm	700	698	709	0.01187	0.01216	754	751	750	0.01278	0.01281
	0.56Tm	710	711	722	0.01139	0.01173	750	752	763	0.01203	0.0124
Ti-6242/ Ti-6242	0.51Tm	840	836	850	0.01269	0.01299	936	898	893	0.01414	0.01349
	0.56Tm	800	799	816	0.01456	0.01506	929	860	850	0.01691	0.01548
Ti-64/ Ti-6242	0.51Tm	720	747	746	0.01329	0.01231	814	848	847	0.01502	0.0128
	0.56Tm	780	757	772	0.01503	0.01376	984	846	843	0.01896	0.01535

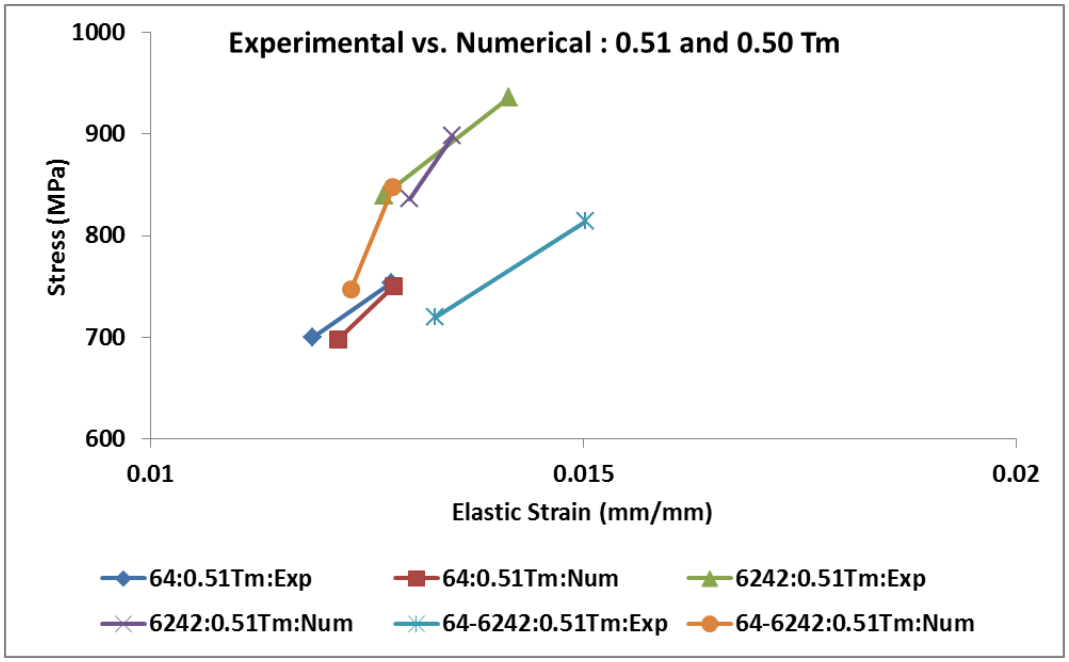

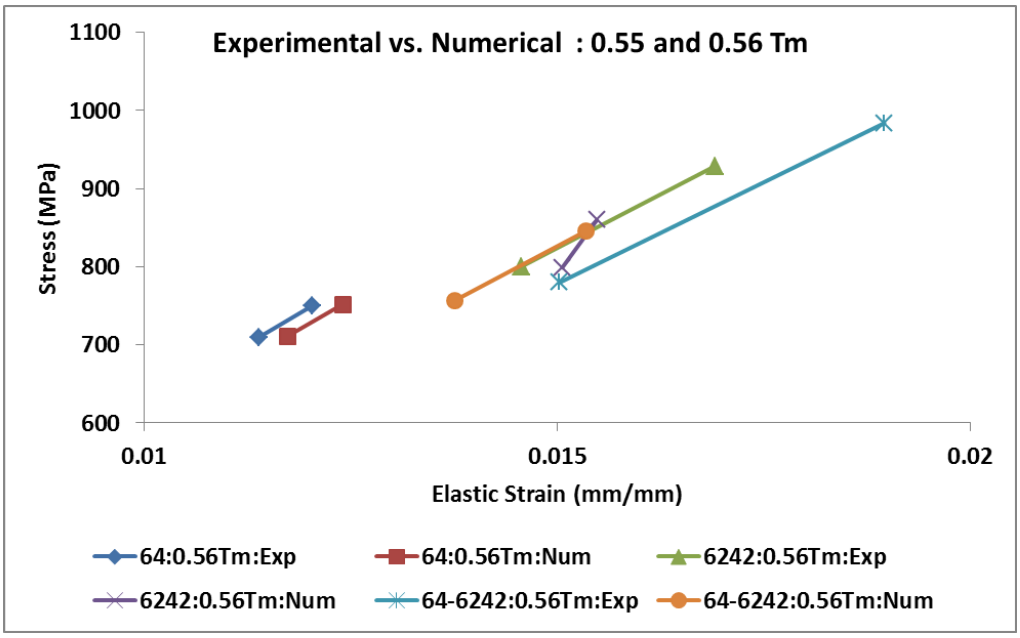

Figure 5.4-6: Comparison with the experimental results

5.5 *NUMERICAL MODELING OF MECHANICAL BEHAVOIR OF WELDED JOINTS*

The tensile behavior of the FSW specimens was modeled using the commercial FEA Modeling software ANSYS WORKBENCH 14.5. Ti-54MFG/Ti-54MFG tensile curve was chosen to simulate finite element model at all the processing conditions. FSW tensile specimen has three regions: two base materials regions present on the either side of the weld, and the weld nugget region. In the geometric model of FEA, these three regions were approximated to one full tensile specimen. The geometric model was then meshed and the boundary conditions were applied to it.

5.5.1 *Finite Element Modeling*

The 3-D model of tensile specimen was generated in ANSYS WORKBENCH using tensile specimen dimension discussed in experimental section. The meshing operation was then performed to produce the finite element model of the specimen. The element type '20 Node- Hexahedral' element type was chosen to perform the simulations. The meshed model was made up of 16,800 and 82,189 elements and nodes respectively (Figure 5.5-1). The experimental stress strain curves showed isotropic hardening behavior in the friction

stir welded specimens. This elastic plastic behavior of the stress strain curve was applied with multi linear isotropic hardening model in the finite element model. Figure 5.5-2 shows the typical multi linear isotropic hardening material curve applied in the model. The boundary conditions and constraints were applied to the model to simulate the conditions of load and constraints applied to the specimens during the actual tensile test. One end of the tensile specimen was fixed (frictionless support) and displacement was incrementally applied to the other end as shown in Figure 5.5-3.

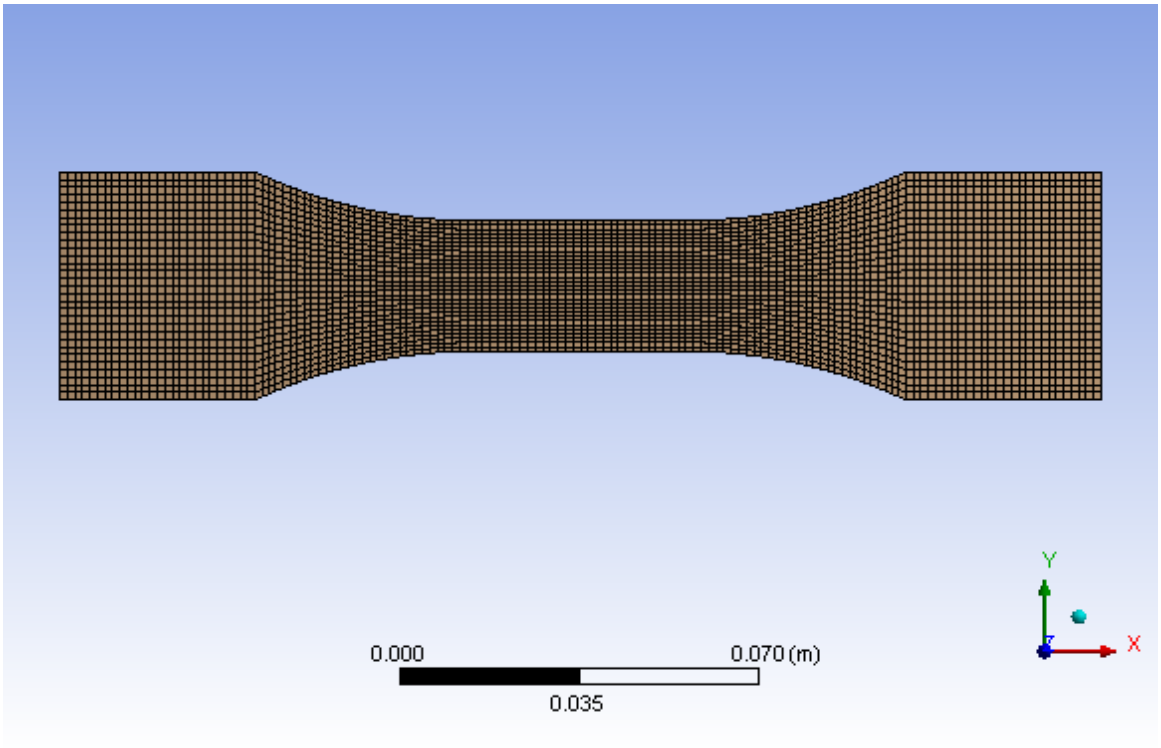

Figure 5.5-1: Meshed FEA Model

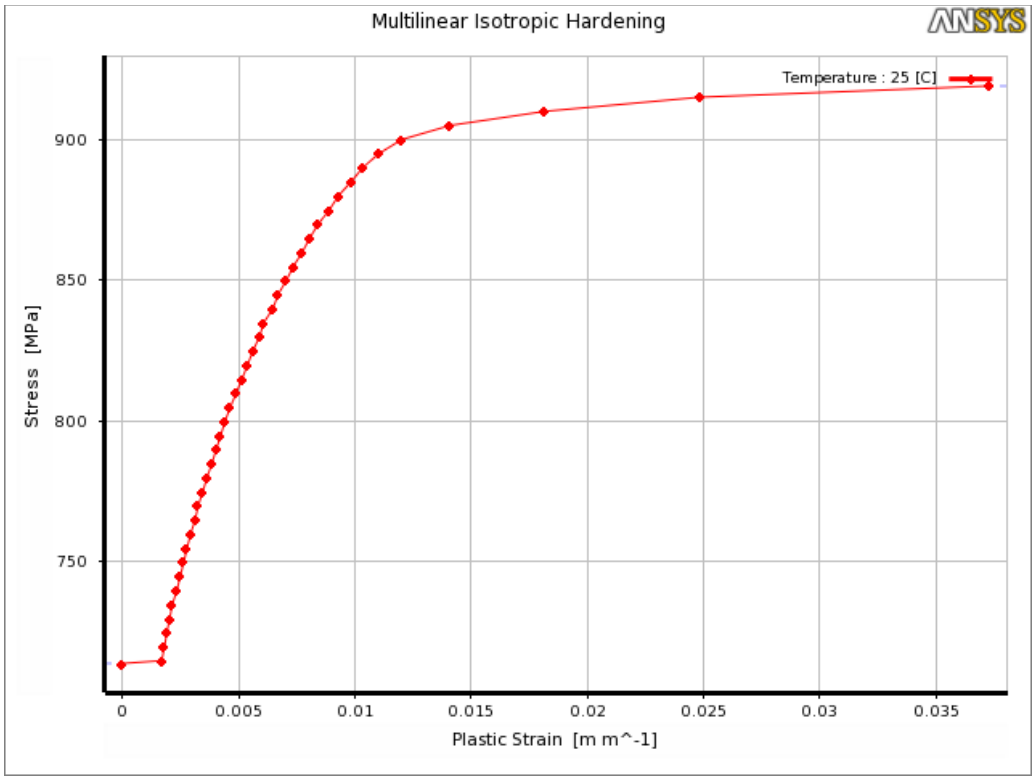

Figure 5.5-2: Material Model (Ti-54MFG/Ti-54MFG -275RPM/125 mm min-1)

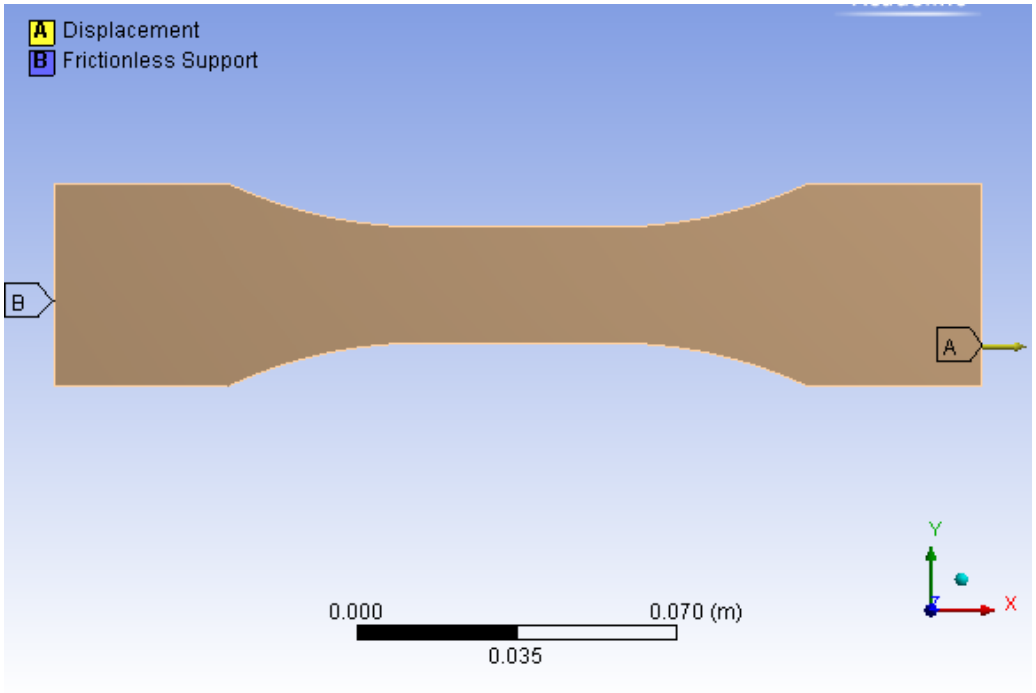

Figure 5.5-3: Boundary and Loading Conditions in FEA model

5.5.2 *Finite Element Results*

The finite element results of stress and strain are plotted for the all the processing conditions were plotted and compered to the experimental results. In the stress strain curve, the equivalent stress was plotted vs total equivalent strain obtained at increments during the simulation. The region of maximum equivalent stress and strain is located in the welded region of the friction stir welded joint. The effect of processing conditions was also studied on the contours of equivalent stress and strain. Figure 5.5-4 shows compares stress strain curve from finite element model with the experimental material curve at different feed rates and rotation speeds. Figures 5.5-5 to 6 show the effect of feed rate on equivalent stress and strain contours respectively. The effect of speed on the contours of stress and strain is shown in Figures 5.5-7 to 8.

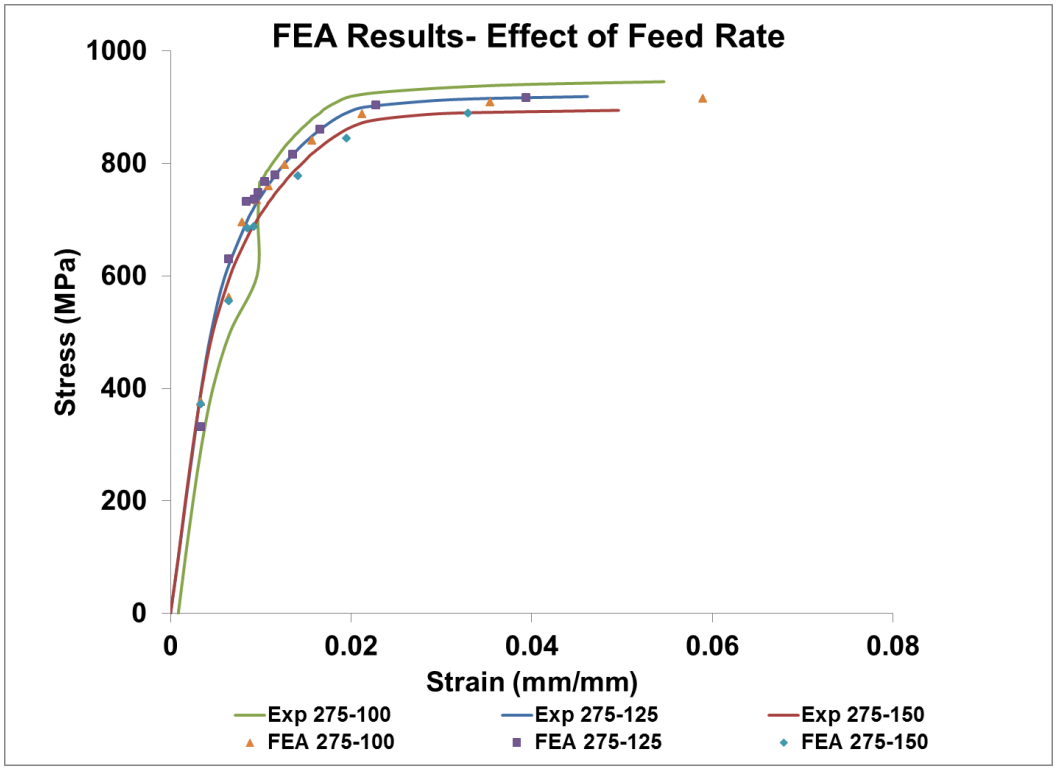

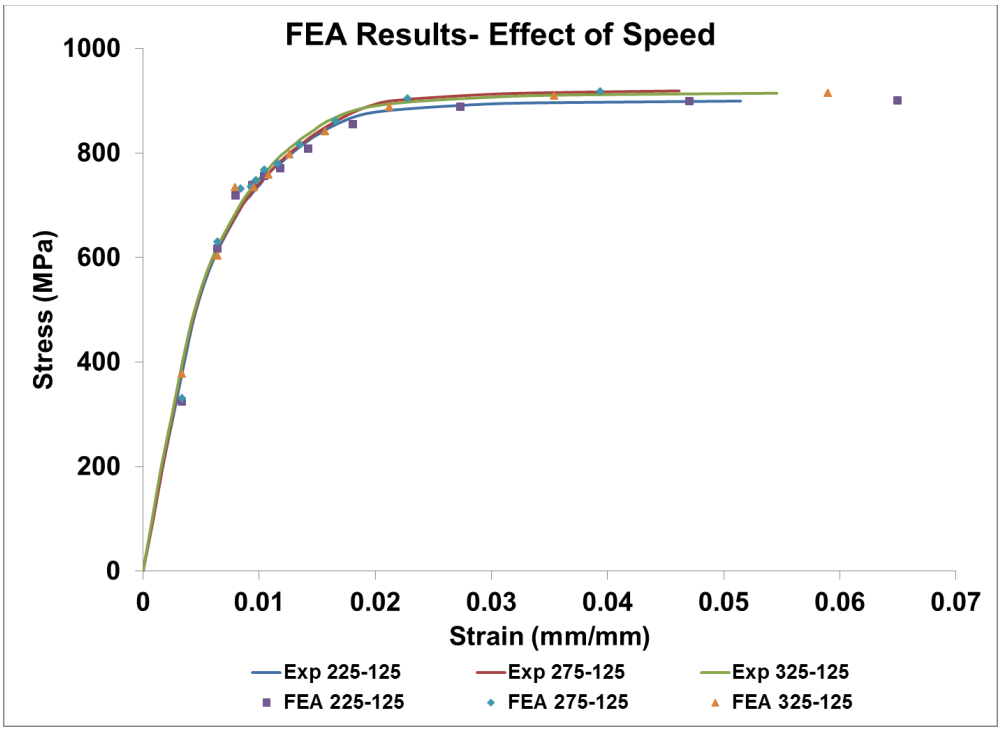

Figure 5.5-4: FSW Stress Strain Curves for Ti-54MFG/Ti-54MFG at different feed rates and rotation speeds- Experimental and FEA

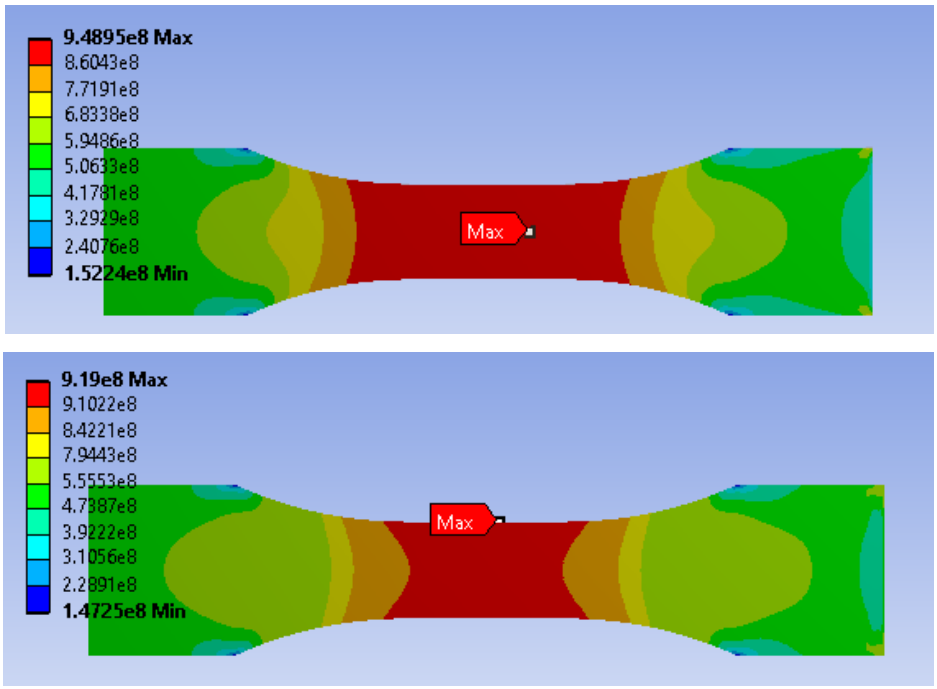

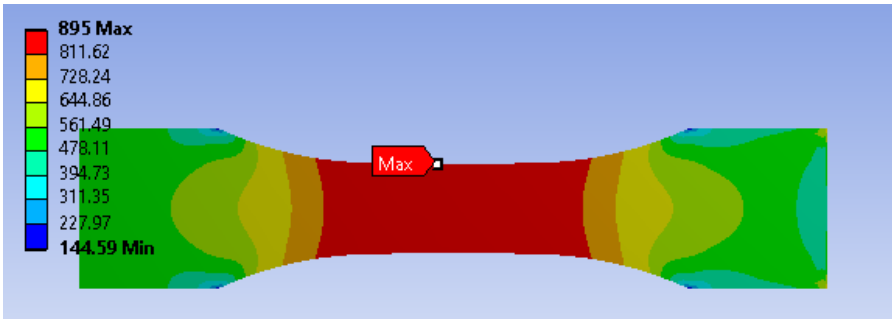

Figure 5.5-5: Effect of Feed Rate on Stress Contours in Ti-54MFG/Ti-54MFG (100, 125, 150 mm min-1 at constant 275 RPM)

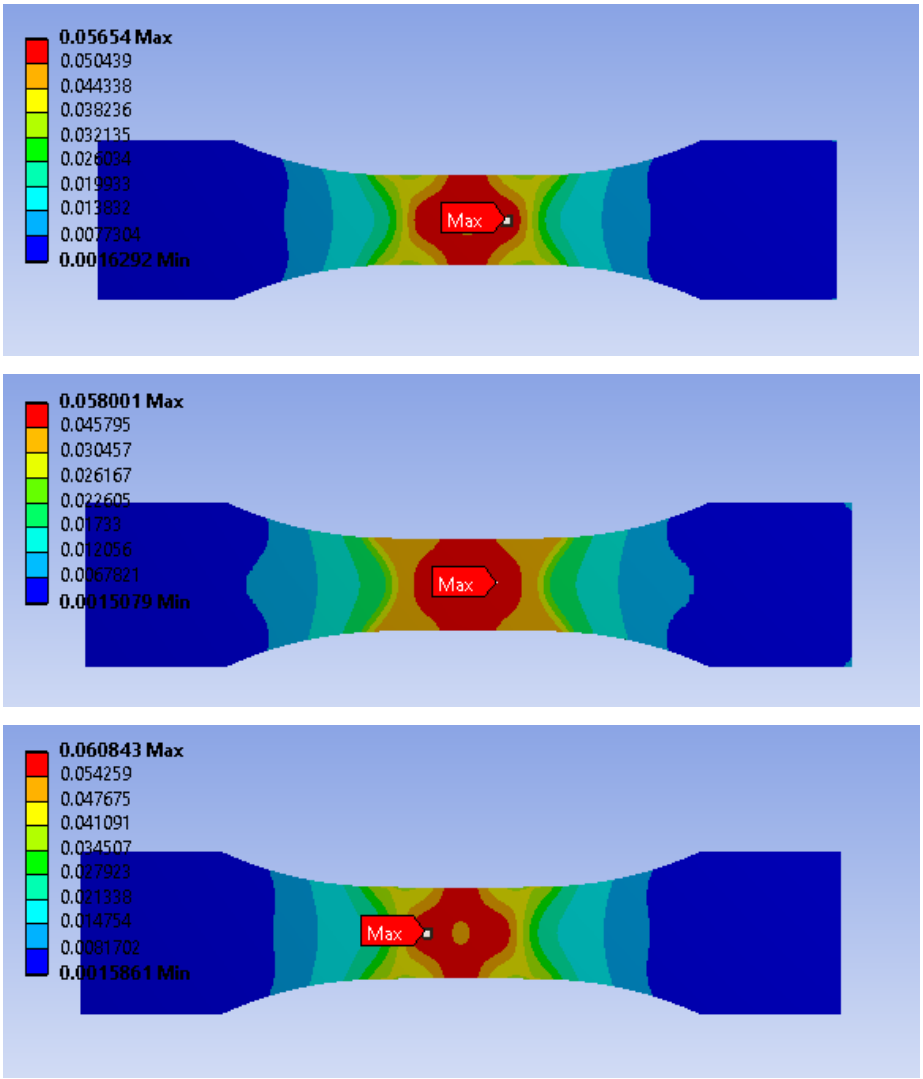

Figure 5.5-6: Effect of feed rate on strain contours in Ti-54MFG/Ti-54MFG (100, 125, 150 mm min-1 at constant 275 RPM)

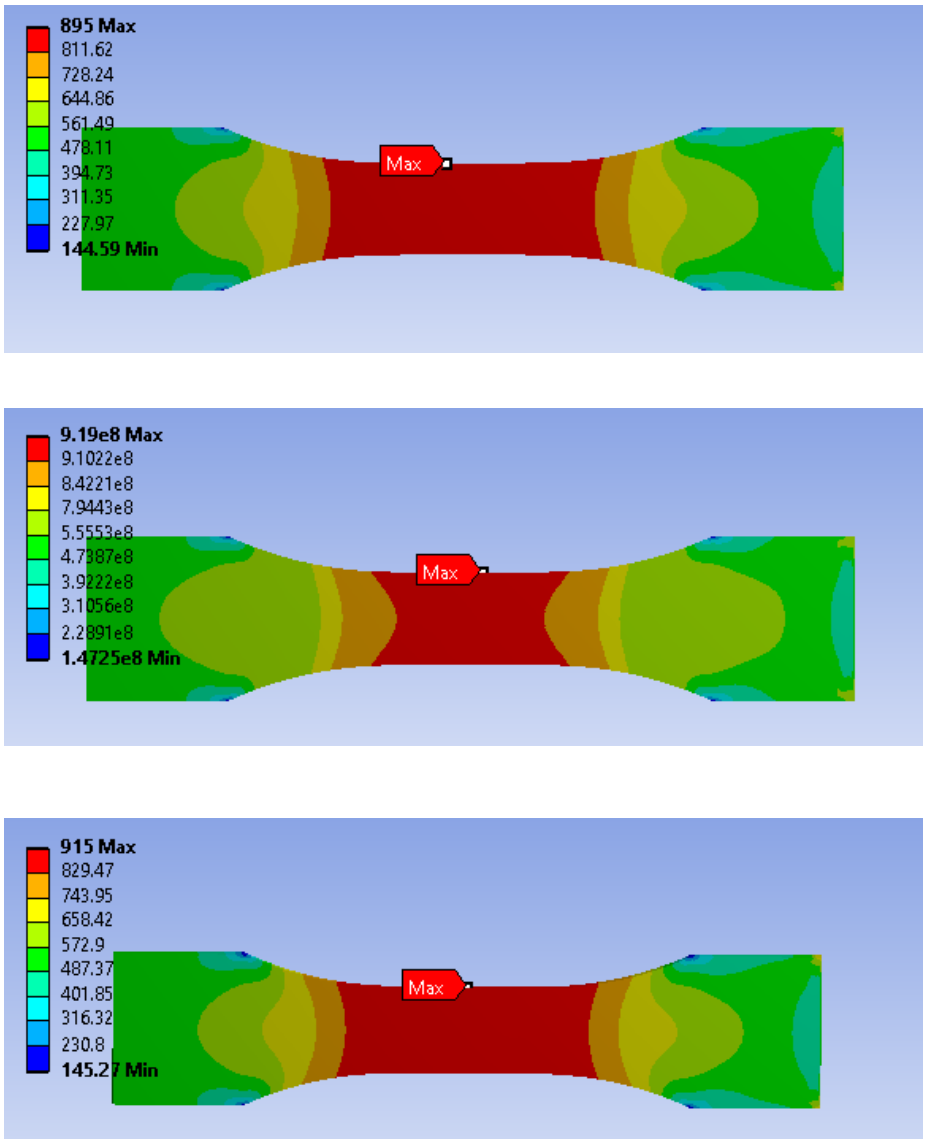

Figure 5.5-7: Effect of speed on stress contours in Ti-54MFG/Ti-54MFG (225,275,325 RPM at constant 125 mm min-1)

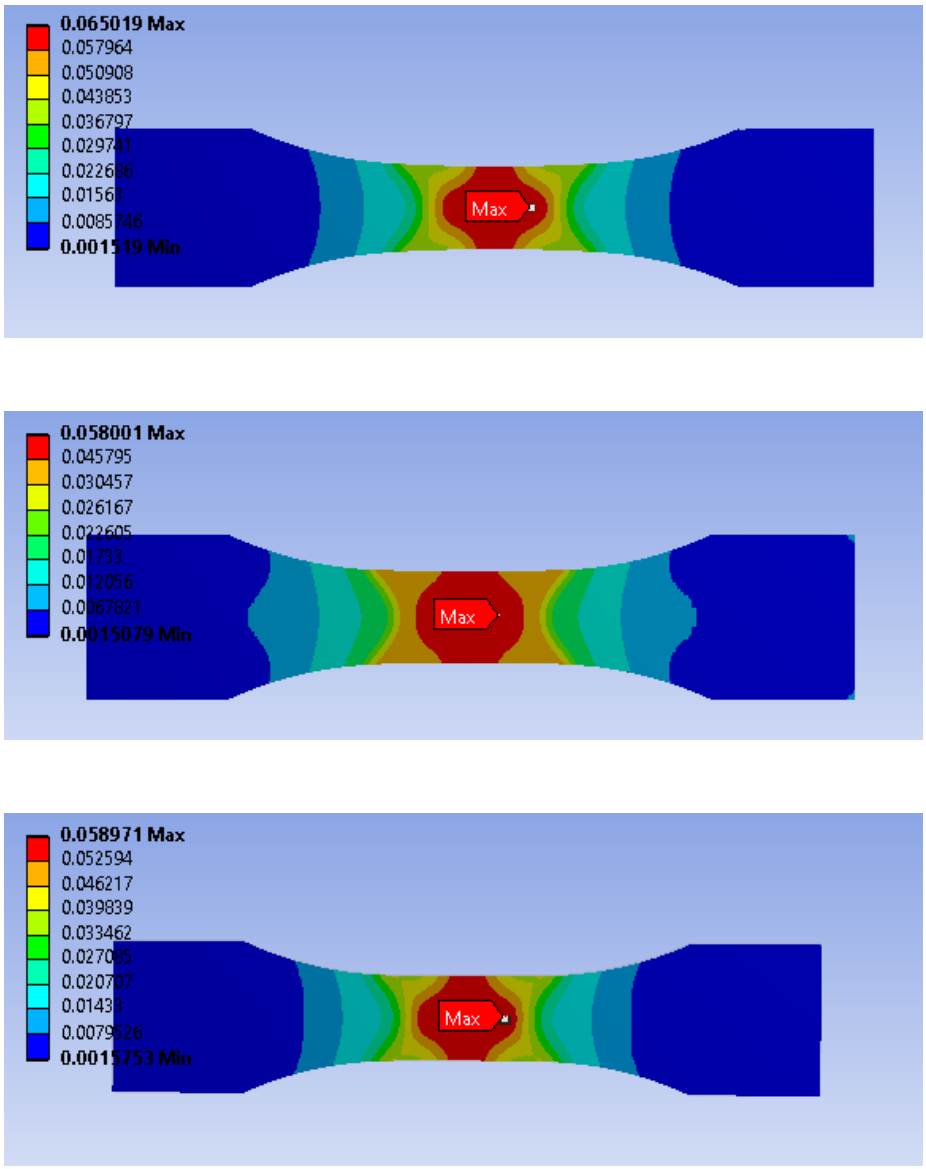

Figure 5.5-8: Effect of speed on strain contours in Ti-54MFG/Ti-54MFG (225,275,325 RPM at constant 125 mm min-1)

5.6 SUMMARY AND CONCLUSION

1. The experimental results of bonding time were compared to the Pilling's model of bonding time for similar titanium alloys, Ti-6242SG/Ti-6242SG, Ti-64SG/Ti-64SG, and Ti-54M/Ti-54M. The simulated results showed reasonable agreement with the experimental results.
2. A probabilistic model was developed to predict diffusion bonding time in dissimilar titanium alloys. The probabilistic model of dissimilar alloys estimates the surface profile present at the bonding interface of dissimilar alloys. In the model, the surface profile of the bonding interface was found out through superimposing profiles of the parent alloys. The geometry was defined with the radius and the height of void at the interface. It was observed that the parameters of height and radius of void show a probability distribution, and therefore the distribution fit tool was applied to fit the data of height and radius into probability distribution. The random values of geometry of the void generated from the distribution fit were used to generate cumulative density function (CDF) of bonding time.
3. The numerical modeling of diffusion bonding in similar titanium alloys was demonstrated with dominant creep mechanism. The results were in agreement with Fang's results [21] of contribution of different bonding mechanisms in diffusion bonding of Ti-64 alloy. It was evident that higher bonding pressure and temperature accelerate the void closure process.
4. The numerical model of flexural testing of dissimilar titanium alloys (Ti-64SG/Ti-6242SG) was developed with the material curves of diffusion bonded parent alloys (Ti-64SG/Ti-64SG and Ti-6242SG/Ti-6242SG). The numerical results of mechanical behavior for diffusion bonded dissimilar alloy joints Ti-64SG/Ti-6242SG lie within 10% of experimental results.
5. In the numerical model of mechanical behavior of friction stir welded joints, the variation of strains in the gage area results imply that there is effect of welding

on the stress and strain distribution across the welded specimen. The location of maximum stress is different from the maximum strain.

6. In the above model, as the feed rate was increased, the location of equivalent stress moved from the right (loading side) to the left side (fixed side) of the specimen. The strain location moved from center region to upper region with the increase in feed rate. The increase in speed transitioned the location of maximum stress from the fixed end to the upper edge, while the maximum strains were seen at the right (loading) side.
7. The numerical results of mechanical performance of friction stir welded similar titanium joints showed strong agreement with the experimental stress strains. They are within 5 % of the experimental results. The difference in the numerical results can be attributed to the assumption of constant thickness, and homogenous material model. There is thinning in the nugget region due to welding process across the base materials. The material curve in the welded region could vary from the base material stress strain curves. This numerical model predicts the mechanical behavior of FSW joints.

Chapter 6. CONCLUSION AND FUTURE WORK

6.1 DIFFUSION BONDING OF SIMILAR AND DISSIMILAR TI-ALLOYS

1. The diffusion bonding process was studied with titanium alloys other than the most popular titanium alloy Ti-64SG. Dissimilar and similar types of diffusion bonded titanium joints were examined to evaluate feasibility of joining titanium alloys to increase and improve its proficiency.
2. Three types of titanium alloys were utilized in the study. The joining of similar type of titanium alloys was studied with near-α to near-α, α + β to α + β and β to β titanium alloys, while diffusion bonding of dissimilar titanium alloys was studied with near-α to α + β, near-α to β, α + β to α + β, and α + β to β alloy combinations.
3. The diffusion bonding of similar and dissimilar titanium alloys was investigated by varying the diffusion temperature while maintaining the pressure and time constant. Twenty three samples made of similar titanium joints and fifty samples of dissimilar titanium joints were examined to assess the diffusion bonding process with these titanium alloys.
4. The bond integrity was evaluated with metallographic examination and mechanical testing. The surface and subsurface characteristics were examined to evaluate the surface characteristics and bonding strength. The surface texture was measured using Mahr-Surface profilometer and the hardness measurement was performed on LECO Micro-Hardness tester.
5. The mechanical strength of diffusion-bonded joints was investigated by conducting flexural testing on Instron machine. The fracture characteristics of diffusion bonded samples were examined through SEM.
6. Sound bonds could be obtained in similar and dissimilar titanium alloys with diffusion bonding process at temperatures lower than the β transus temperature of titanium alloys. The higher bonding temperature showed better results on the quality of diffusion bonding. The good quality of bond was obtained for the cases of Ti-64SG/Ti-64SG, Ti-6242SG/Ti-6242SG, and Beta-21S/Beta-21S with similar titanium alloys. In dissimilar titanium alloys, the good quality of joints was attained

from Ti-64SG/Ti-6242SG, Beta-21S/Ti-64SG, Beta-21S/Ti-6242, Ti-64SG/Ti-54M, and Ti-6242SG/Ti-54M.

7. The fracture results from flexural test of diffusion bonded similar and dissimilar alloy joints showed that in the good bonding cases, the bond line remained unaffected even after performing the testing. Therefore it demonstrates good joining strength was achieved through diffusion bonding. The fractured surfaces were observed rough and irregular with many micro voids and dimples, therefore exhibiting ductile nature of fracture.
8. A probabilistic model was developed to predict diffusion bonding time in dissimilar titanium alloys. The probabilistic model of dissimilar alloys estimates the surface profile present at the bonding interface of dissimilar alloys. The model also addresses the random nature of surface at the interface by using the random values of the geometry of the void present at the bonding interface for joining of dissimilar alloys with diffusion bonding. The variation in material properties is incorporated by using the duplex nature of titanium alloy in terms of alpha and beta proportion.
9. The numerical model of diffusion bonding was developed by applying creep mechanism. The area of fraction bonding was in agreement with the creep mechanism results. In order to obtain full closure of voids, the other bonding mechanism shall also be incorporated in the model.
10. The numerical modeling of mechanical behavior of diffusion bonded dissimilar titanium alloy joints was developed which can be used to obtain flexural strength of dissimilar joints from the parent alloys material curve.

6.2 FRICTION STIR WELDING OF SIMILAR AND DISSIMILAR TI-ALLOYS

1. Friction stir welding was demonstrated with similar and dissimilar titanium alloys at different rotation speeds and feed rates. The joining process produced defect free butt joints with dissimilar titanium alloys. The process showed a very good strength as close as 90% with respect to the parent alloys.

2. Two types titanium alloys, near-α to near-α and α + β to α + β, were utilized to evaluate similar titanium joints using friction stir welding. The strength of friction stir welded dissimilar titanium joints were evaluated from near-α to α + β and α + β to α + β types of titanium alloys. Total numbers of fifty seven samples were used in the study, which included twenty five of similar combinations and thirty two of dissimilar combinations of titanium alloys.
3. The mechanical performance of friction stir welded similar and dissimilar titanium joints was evaluated by conducing tensile tests at room temperature. The global stress strain behavior and nature of fracture of the welded joints was determined from the tensile tests.
4. The rotation speed of the welding tool showed more influence on the strength of the joints than its feed rate on the mechanical properties in friction stir welded similar and dissimilar titanium alloys.
5. The optimum values of process conditions were identified to obtain the friction stir welded joints with different similar and dissimilar titanium alloys. The optimum values of spindle speed and feed rate for the joints formed by similar titanium alloys were 275 RPM/100 mm min-1, whereas it was 325RPM/125 mm min-1 for the joints formed by dissimilar titanium alloys.
6. The process conditions and the titanium joints that yielded maximum joint strength were recognized. The process parameters that produced maximum joint strength were 275RPM and 150 mm min-1 and 225 RPM and 125 mm min-1for similar and dissimilar titanium alloy joints respectively. Among the different similar and dissimilar titanium joints, the highest strength was obtained with Ti-6242SG/Ti-6242SG and with Ti-64SG/Ti-6242FG.
7. Numerical model of mechanical behavior of friction stir welded similar joints was developed and compared with the experimental results. The effect of processing conditions was studied on the maximum stress and strain locations. The region of maximum stresses and strains for different processing conditions were located in the model. The numerical results of mechanical behavior of friction stir welded titanium joint are within 5 % of the experimental results.

6.3 FUTURE WORK

1. The fatigue life of product is very important characteristic of its service life. Therefore, fatigue characterization of the joints formed by diffusion bonding and friction stir welding with similar and dissimilar titanium alloys should be conducted as a part of further research.
2. The experimental work conducted on studying the mechanical performance of diffusion bonded similar and dissimilar titanium alloys was done by varying the bonding temperature while maintaining the bonding pressure and time constant during the process. The effect of other bonding parameters such as pressure and time should also be examined on the quality of joints formed by the bonding process.
3. The theoretical model to predict bonding time of dissimilar titanium alloys mainly addresses geometrical aspect of interface surfaces that have higher impact in the estimation of bonding time. The current model takes into brief consideration of the material properties of the joining alloys. However the model should also include the material aspects of the joining titanium alloys in terms of grain and boundary coefficients, superplastic rate and strain rate.
4. The numerical model to predict the void closure in diffusion bonding model was developed for similar titanium alloys with an idealized single void. However marked amount of scatter is exhibited by the voids on faying surfaces. In order to address this, the model should be extended to multiple voids with various void geometries to study the effect of different geometries on the void closure.
5. The study of friction stir welded titanium joints formed by similar and dissimilar titanium alloys was concentrated on the mechanical performance. The dissimilar titanium friction stir welded joints contains different alloying elements at the weld nugget zone. Therefore the metallurgical characterization of these joints can highlight the impact of mixing of different alloying elements. Hence the metallurgical characterization of the titanium joints should be done to examine the heat zones, and crystallographic phase structures at the weld region.

BIBILOGRAPHY

[1] Gerd Lütjering, James C. Williams, 2007, “Titanium.”

[2] John L. Everhart, 1954, “Titanium and Titanium Alloys.”

[3] Mathew J. Donachie, 1987, “Titanium and Titanium Alloys.”

[4] Heat Resistant Materials ASM Specialty Handbook

[5] D.M.Brunette, P.Tengvall, M.Textor, P.Thomsen, 2001, “Titanium in Medicine”, Metallurgy and Technological Properties, Chapter 3, pp.32, Springer-Verlag, ISBN 3-540-66936-1

[6] Ani Zhechevaa, Wei Shaa, Savko Malinovb, Adrian Longa, 2005, “Enhancing the microstructure and properties of titanium alloys through nitriding and other surface engineering methods,” Surface & Coatings Technology, Vol.200, pp. 2192– 2207

[7] Daniel G. Sanders and Mamidala Ramulu, 2004, “Examination of superplastic forming combined with diffusion bonding for titanium: Perspective from experience,” JMEPEG 13, pp.744-752.

[8] N.F. Kazakov, 1981, "Diffusion Bonding of Materials", Pergamon Press, New York.

[9] J.Pilling, D.W Livesey, J.B.Hawkyard and N.Ridley, 1984, “Solid state bonding in superplastic Ti-6Al-4V,” Metal Science, Vol. 18, pp.117-122.

[10] M. F. Islam, J. Pilling, and N. Ridley,1997, "Effect of surface finish and sheet thickness on isostatic diffusion bonding of superplastic Ti-6AI-4V,” Materials Science and Technology, Vol. 13, pp. 1045-1050.

[11] W.H.King and W.A.Owczarski, 1967, “Diffusion Welding of Commercially Pure Titanium,” Weld. J.Res.Suppl, Vol.46, 289-298.

[12] C.H.Hamilton, 1973, “Tianium Science and Technology (edited by R.IJaffee and H.MBurte”, Vol.1, Plenum Press,New York, pp.625-648.

[13] G.Garmong,N.E.Paton, A.S. Argon, 1975, “Attainment of full interfacial contact during diffusion bonding,” Metallurgical Transactions A, Vol. 6, pp.1269-1279.

[14] I.W.Chen and A.S.Argon, 1981, “Diffusive growth of grain-boundary cavities,” Acta Metallurgica, Vol.29, pp.1759-1768.

[15] Derby B,Wallach E.R, 1980, “Theoretical model for diffusion bonding,” Metal Sci, Vol.16(1), pp.49-56.

[16] Derby B, Wallach E R., 1984, “Diffusion bonding: Development of theoretical model”, Metal Science, Vol.18 (1), pp.427-431.

[17] Hill A, Wallach ER., 1989, “Modeling solid state diffusion bonding”, Acta Metall, Vol.37 (19), pp. 2425-2437.

[18] J.Pilling, 1988, “The Kinetics of Isostatic Diffusion Bonding in Superplastic Materials”, Mater.Sci.Eng, Vol.100, pp. 137-144.

[19] W.Johnson and P.B.Mellor, 1983, Engineering Plasticity, Ellis Hardwood, Chichestrer, pp 219.

[20] J.Pilling, N.Ridley, MF Islam, 1996, “On modeling of diffusion bonding in materials:superplastic Super Alpha-2”, Materials Science and Engineering, Vol. A205, pp. 72-79.

[21] RuiFang Ma, MiaoQuan Li, Hong Li, WeiXin Yu , 2012, “Modeling of void closure in diffusion bonding process based on dynamic conditions”, Science China Technological Sciences, Vol. 55, Issue 9, pp. 2420-2431.

[22] Johnson W, Sowerby R, Venter R.D., 1982, “Plane Strain Slip Fields for Metal Deformation Processes,” Oxford: Pergamon Press, pp 119-121.

[23] M. F. Islam, J. Pilling, and N. Ridley, 1997,“ Effect of surface finish and sheet thickness on isostatic diffusion bonding of superplastic Ti-6Al-4V,” Materials Science and Technology, Vol. 13, pp.1045-1150.

[24] N. Orhan, M. Aksoy, M.Eroglu, “A new model for diffusion bonding and its application to duplex alloys”, 1999, Materials Science and Engineering, Vol. A271, pp.458-468.

[25] Shu-Xin Li, Shan-Tung Tu, Fu-Zhen Xuan, 2005, “A probabilistic model for prediction of bonding time in diffusion bonding,” Materials Science and Engineering, Vol. A 407, pp. 250-255.

[26] W.A. Baeslack III, J.R. Davis, C.E. Cross, 1993, “Selection and Weldability of Conventional Titanium Alloys,” ASM Handbook, Volume 6: Welding, Brazing, and Soldering, pp. 507-523.

[27] Y. Maehara and T.G.Langdon, 1990, “Superplasticity of Steels and Ferrous Alloys”, Mater.Sci.Eng” Vol.A128, pp. 1-13.

[28] N.Ridely, M.T.Salehi, and J.Pilling, 1992 “Isostatic bonding of microduplex stainless steel”, Materials Science and Technology, Vol. 8, pp.791-795.

[29] Shuying Liu, Kuan Xu, Guangbao Liu, Congcong Cao and Zhonghao Heng, 2013, " The evolution characteristics and numerical analysis of diffusion bonding interface structure of titanium alloy/Cu/ Stainless steel," Adv. Mater.Sci., Vol. 33, pp. 224-231.

[30] Ren Jiangwei, Li Yajiang , Feng Tao, 2002" Microstructure characteristics in the interface zone of Ti/Al diffusion bonding," Materials Letters, Vol. 56, Issue 5, pp. 647–652

[31] S.J. Tuppen, M.R. Bache, W.E.Voice, 2005, "A fatigue assessment of dissimilar alloy diffusion bonds," International Journal of Fatigue, Vol.27, pp.651-658.

[32] N.Ridley, Z.C Wang, and G.W Lorimer, 1997, "Diffusion Bonding of Dissimilar Titanium Alloys," Materials Science Forum, Vols. 243-245, pp. 669-674

[33] M.T.Cope, D.R.Evetts, N.Ridley, 1986 "Superplastic Deformation characteristics of two micro duplex titanium alloys," Journal of Materials Science 21, pp. 4003-4008

[34] Thomas, W.; Nicholas, E.; Needham, J.; Murch, M.; Templesmith, P.; Dawes, C.; Great Britain Patent 9125978.8, 1991

[35] R.S. Mishra, Z.Y. Ma, 2005, "Friction stir welding and processing," Materials Science and Engineering, R 50, pp. 1-78.

[36] L.E.Murr, Y.Li, E.A.Trillo, B.M.Nowak, and J.C.McClure, A, 1999, "Comparative Study of Friction Stir Welding of Aluminum Alloys," Aluminum Trans, 1(1), pp. 141-154

[37] L.E.Murr, 2010, "A Review of FSW Research on Dissimilar Metal and Alloy Sytems", Journal of Materials Engineering and Performance, Vol. 19(8), pp.1071-1089.

[38] Won-Bae Lee , Chang-Young Lee , Woong-Seong Chang , Yun-Mo Yeon , Seung-Boo Jung, 2005, "Microstructural investigation of friction stir welded pure titanium", Materials Letters, Vol. 59, pp.3315 – 3318

[39] Xiaocong He, Fengshou Gu, Andrew Ball, 2014, "A review of numerical analysis of friction stir welding, Progress in Materials Science,"Vol. 65, pp.1–66.

[40] Y. N. Zhang, X. Cao, S. Larose and P. Wanjara, 2012, "Review of tools for friction stir welding and processing," Canadian Metallurgical Quarterly, Vol. 51 No. 3, pp. 250-261.

[41] P.D. Edwards and M. Ramulu, 2009, "Effect of Process Conditions on Superplastic Forming Behavior in Titanium 6Al-4V Friction Stir Welds," Science and Technology of Welding & Joining, Vol. 14, No.7, pp. 669-680.

[42] Lienert, T.J., 2007, "Microstructure and Mechanical Properties of Friction Stir Welded Titanium Alloys," Friction Stir Welding and Processing, ASM International, pp.123-154.

[43] A.P. Reynolds, Elizabeth Hood, Wei Tang, 2005, "Texture in friction stir welds of Timetal 21S", Scripta Materialia, Vol.52, pp. 491- 494.

[44] Yu Zhang, Yutaka S. Sato, Hiroyuki Kokawa, Seung Hwan C. Park, Satoshi Hirano, 2008, "Microstructural characteristics and mechanical properties of Ti–6Al–4V friction stir welds,"Materila Science and Engineering, Vol. A 485, pp. 448-455.

[45] H.J. Liu, L. Zhou, Q.W. Liu, 2010, "Microstructural characteristics and mechanical properties of friction stir welded joints of Ti–6Al–4V titanium alloy," Materials and design 31, pp.1650-1655.

[46] M. Ramulu, P.D. Edwards, D.G. Sanders, A.P. Reynolds and T. Trapp, 2010, "Tensile Properties of Friction Stir welded Ti-6AL-4V Butt Joints," Materials & Design, Vol. 30, pp.3056-3061.

[47] D.G. Sanders, M. Ramulu, P.D. Edwards, 2008, "Superplastic forming of friction stir welds in Titanium alloy6Al-4V: prelimianary results", Mat.-wiss.u.Werkstofftech, Vol.39, No. 4-5.

[48] D. Sanders, P. Edwards, M. Ramulu, and G. Grant, 2010, "Optimization of Friction Stir Welding Process for Superplastic Forming and Improved Surface Texture for Titanium Aerospace Structures," Key Engineering Materials, Vol. 433, pp. 153-167.

[49] P.Edwards and M. Ramulu, "Identification of Process Parameters for Friction Stir Welding Ti–6Al–4V", 2010, Journal of Engineering Materials and Technology, Vol.132, pp. 0310061-03100610.

[50] P.Edwards, M. Petersen, M. Ramulu, R. Boyer., 2010, "Mechanical Performance of Heat treated Ti-6Al-4V Friction Stir Welds," Key Engineering Materials, Vol.436, pp. 213-221.

[51] P. Edwards and M. Ramulu., 2010, "Peak Temperatures during Friction Stir Welding of Ti-6Al-4V," Science and Technology of Welding & Joining, Vol.15, No.6, pp. 468-472.

[52] Paul Edwards, 2010, "Friction Stir Welding of Ti-6Al-4V Sheet and Plate for Aerospace Structures," Doctoral Dissertation.

[53] Yu Zhang, Yutaka S. Sato, Hiroyuki Kokawa, Seung Hwan C. Park, Satoshi Hirano, 2008, "Microstructural characteristics and mechanical properties of Ti–6Al–4V friction stir welds,"Materila Science and Engineering, Vol. A 485, pp. 448-455.

[54] H.J. Liu, L. Zhou, Q.W. Liu, 2010,"Microstructural characteristics and mechanical properties of friction stir welded joints of Ti–6Al–4V titanium alloy ," Materials and design 31, pp.1650-1655.

[55] Liu Hui-jie, Zhou, Li, 2010," Microstructural zones and tensile characteristics of friction stir welded joint of TC4 titanium alloy," Trans. Nonferrous Met. Soc. China, Vol.20, pp. 1873-1878.

[56] P.Alvarez, G.Janeiro, A.A.M da Silva, E. Aldanondo and A. Echeverria, " Material Flow and mixing patterns during dissimilar FSW," 2010, Science and Technology, Vol. 15, No. 8, pp.648-653.

[57] A.Esmaeilli, M.K. Besharati Givi and H.R. Zareie Rajani, "Investigation of weld defects in dissimiliar friction stir welding of aluminum to brass by radiography," Science and Technology, 2012, Vol. 17, 539-543.

[58] Masayuki Aonuma and Kazuhiro Nakata, Dissimilar Metal Joining of 2024 and 7075 Aluminium Alloys to Titanium Alloys by Friction Stir Welding, 2011, Materials Transactions, Vol. 52, No. 5, pp. 948 to 952.

[59] Gerhard Welsch, Rodney Boyer, E. W. Collings, 2007, "Materials Properties Handbook: Titanium Alloys."

[60] M. Armendia, A. Garay, L.M. Iriarte, P.J. Arrazola, 2010, "Comparison of the machinabilities of Ti-6Al-4V and TIMETALTi-5Al-4V-0.6Mo-0.4Fe using uncoated WC–Co tools," Journal of Materials Processing Technology, Vol. 210, Issue 2, pp.197–203.

[61] R.R.Boyer, 1996, "An overview on the use of titanium in the aerospace industry," Materials Science and Engineering A213, pp.103-114.

[62] Franna Pitt, M.Ramulu, 2004, "Influence of Grain Size and Microstructure on Oxidation Rates in Titanium Alloy Ti-6Al-4V Under Superplastic Forming Conditions", Journal of Materials Engineering and Performance, Vol.13, pp. 727-734.

[63] Larry D. Hefti, May 2010, "Fine Grain Titanium 6AL-4V for Superplastic Forming and Diffusion Bonding of Aerospace products", JOM, Vol.62 No.5, pp. 42-45.

[64] M. Es-Souni, 2000, "Primary, secondary and anelastic creep of a high temperature near a-Ti alloy Ti-6Al-2Sn-2Zr-2MoSi", Materials Characterization, Vol.45, pp. 153-164.

[65] http://www.matweb.com/Search/MaterialGroupSearch.aspx?GroupID

[66] Brian Griffiths, 2001, "Manufacturing Surface Technology-Surface Integrity and Functional Performance", pp.109-128

APPENDIXES

The appendix section includes the collection of data of the experimental work done on diffusion bonding and friction stir welded joints for similar and dissimilar titanium alloys. The data comprises of micrographs; microstructures; tables of mechanical testing results; compilation of surface roughness parameters, surface profiles and charts of surface parameters; matlab programs; and numerical code applied in the modeling (abaqus code of modeling diffusion bonding).

A. DIFFUSION BONDED TI- JOINTS SPECIMEN THICKNESSES

S.No	Type of Ti-Alloy	Type of Ti-Alloy	Ti-Alloy/Ti-Alloy	Original Thickness
1	Near-α	Near-α	Ti-6242/Ti-6242	1.016/1.016
2	α + β	α + β	Ti-54M/Ti-54M	2.540/2.540
3			Ti-64SG/Ti-64SG	1.016/1.016
4			Ti-64FG/Ti-64FG	2.540/2.540
5	β	β	β-21S/ β-21S	0.6858/0.6858
6	Near-α	α + β	Ti-6242/Ti-54M	1.016/2.540
7			Ti-6242/ Ti-64SG	1.016/1.016
8			Ti-6242/ Ti-64FG	1.016/2.540
9	Near-α	β	Ti-6242/ β-21S	1.016/0.6858
10	α + β	α + β	Ti-54M /Ti-64SG	2.540/1.016
11			Ti-54M/ Ti-64FG	2.540/2.540
12			Ti-64SG /Ti-64FG	1.016/2.540
13	α + β	β	Ti-54M/ β-21S	2.540/0.6858
14			Ti-64SG/ β-21S	1.016/0.6858
15			Ti-64FG/ β-21S	2.540/0.6858

B. MICROSTRUCTURES OF DIFFUSION BONED TITANIUM ALLOYS JOINTS- SIMILAR AND DISSIMILAR ALLOYS

Beta-21S/Beta-21S

T1

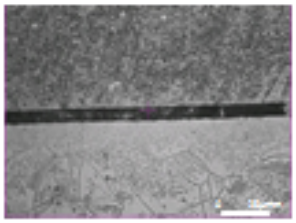

T2

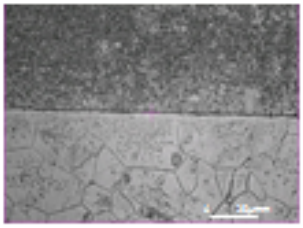

T5

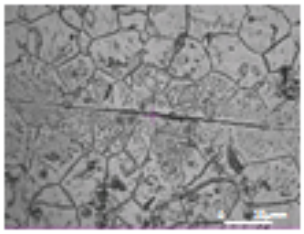

T6

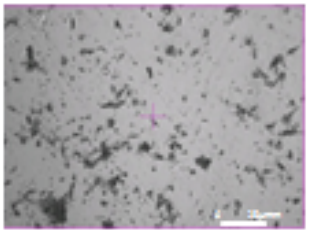

T7

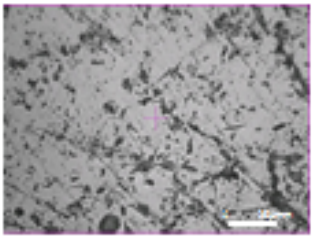

T8

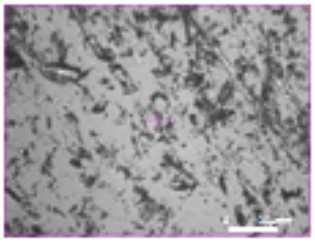

Ti-54M/Ti-54M

T1

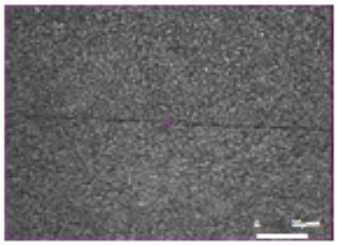

T2

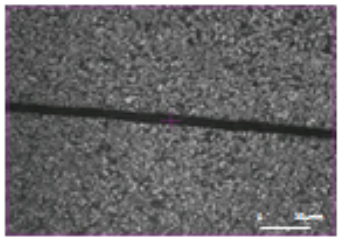

T3

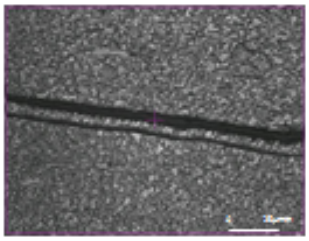

T4

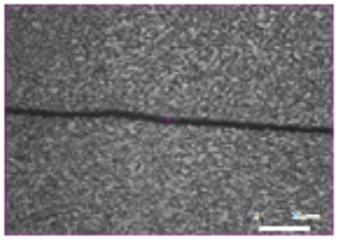

T5

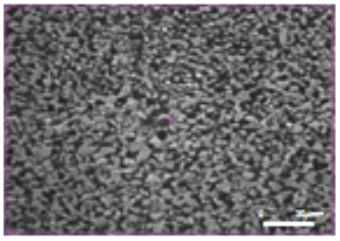

T3-EXTRA

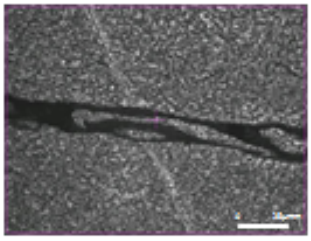

Ti-64FG/Ti-64FG

T1

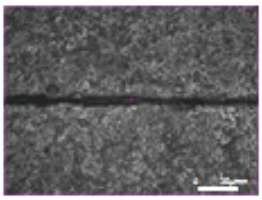

T2

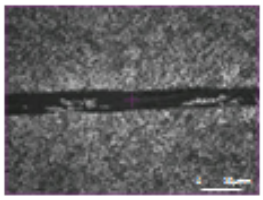

T3

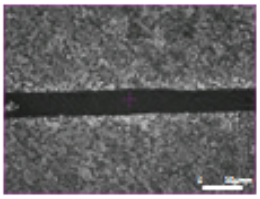

T4

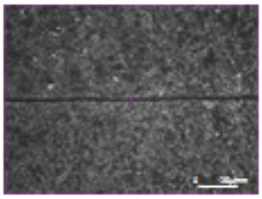

T2-EXTRA

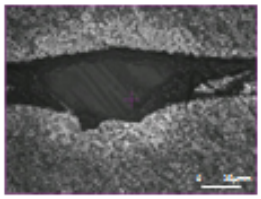

T2-EXTRA

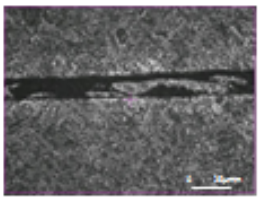

T3-EXTRA

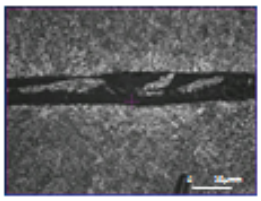

Ti-64SG/Ti-54M

T1

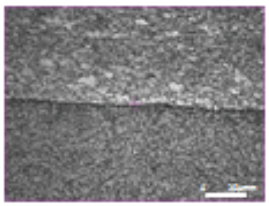

T2

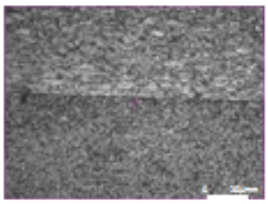

T3

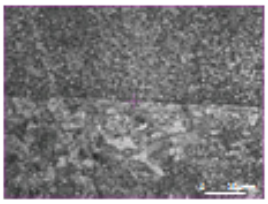

T4

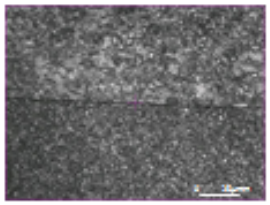

T5

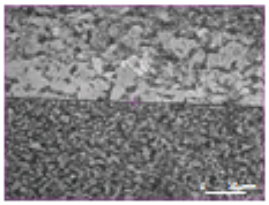

T6

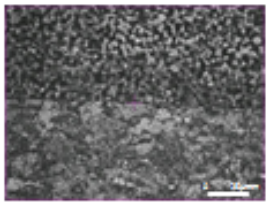

T7

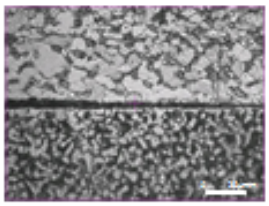

Ti-6242/Ti-54M

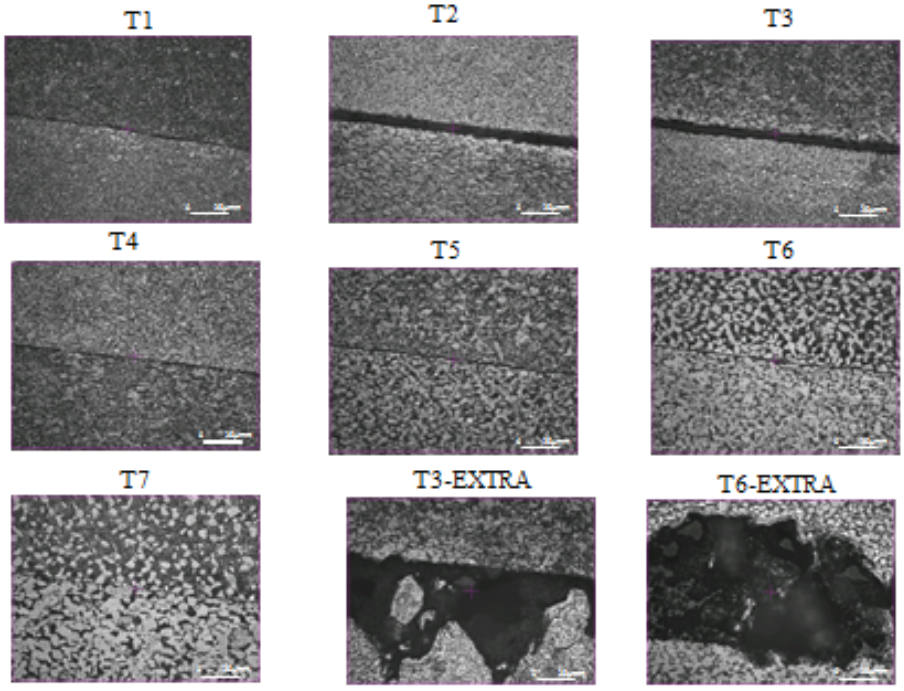

Beta-21S/Ti-54M

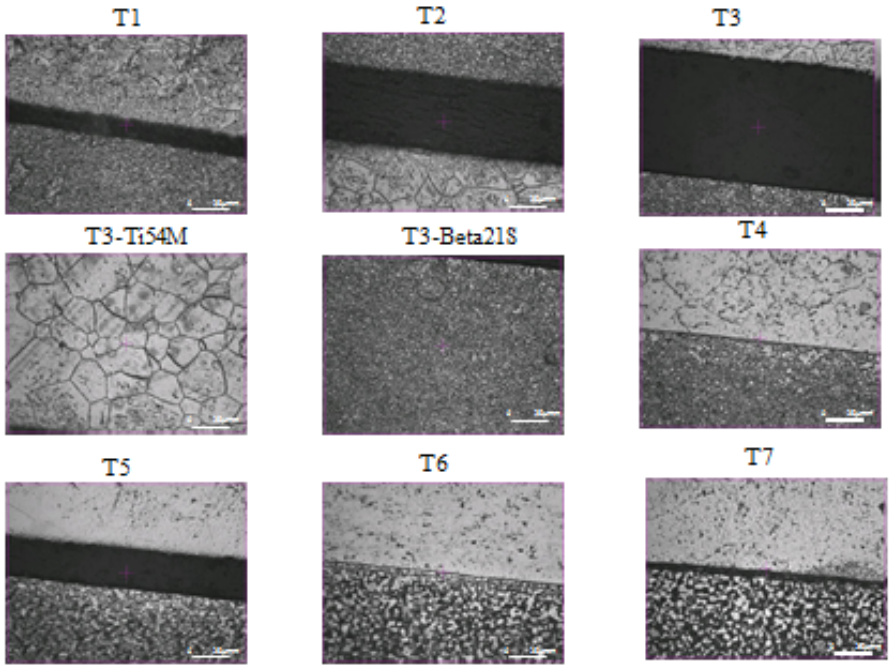

Ti-6242/Ti-64FG

T1

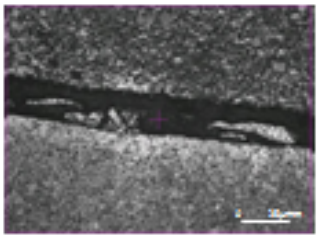

T2

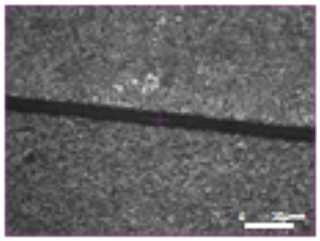

T3

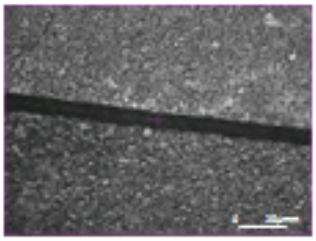

T4

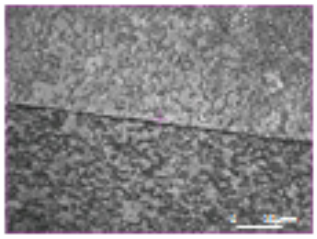

T5

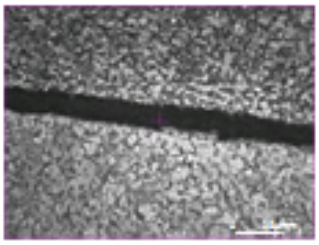

Ti-64FG/Beta-21S

T1

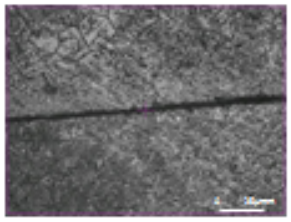

T2

T3

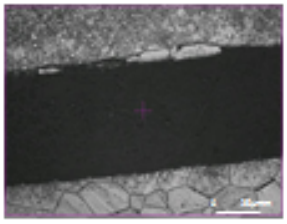

T4

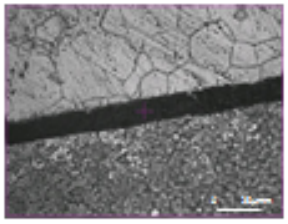

T5

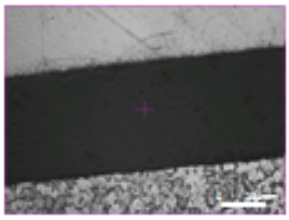

T2 -EXTRA

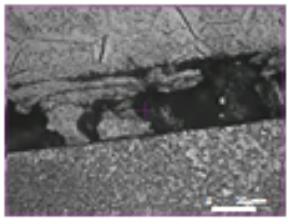

Ti-64SG/Ti64FG

T1

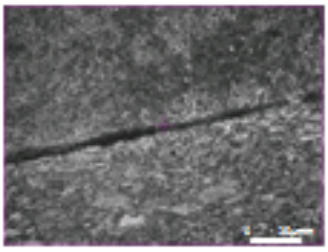

T2

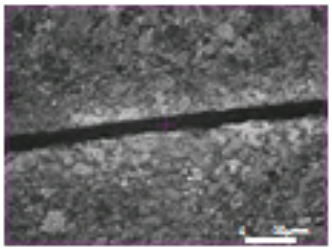

T3

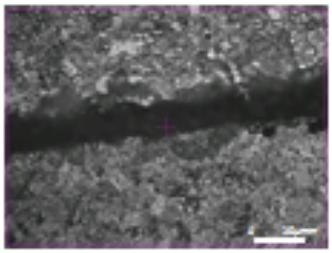

T4

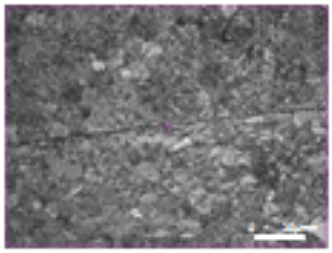

T5

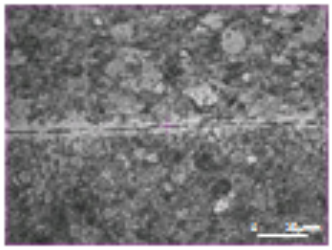

Ti-64FG/Ti-54M

T1

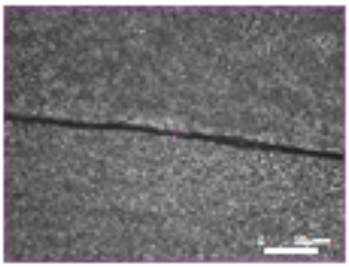

T2

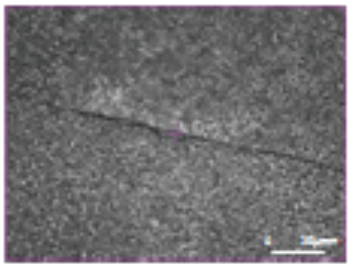

T3

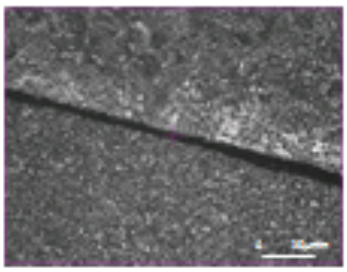

T4

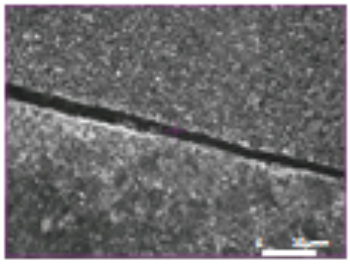

T5

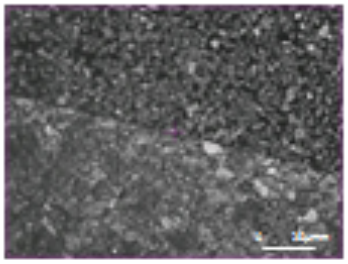

T2-EXTRA

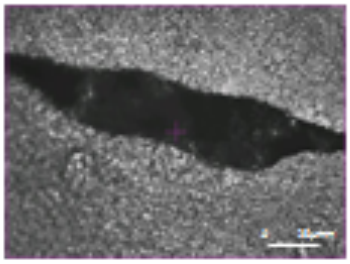

Beta-21S/Ti-64SG

T4

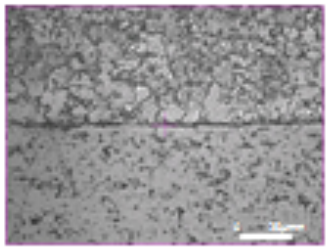

T5

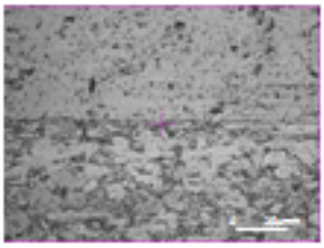

T6

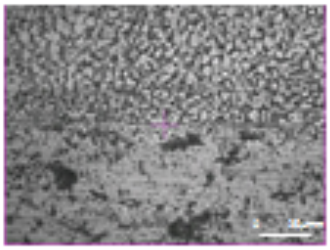

T7

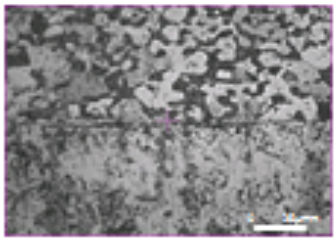

T8

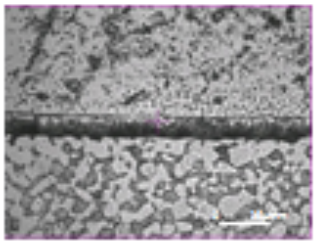

C.HARDNESS MICROGRAPHS FOR SIMILAR AND DISSIMILAR DIFFUSION BONDED TI-ALLOY JOINTS

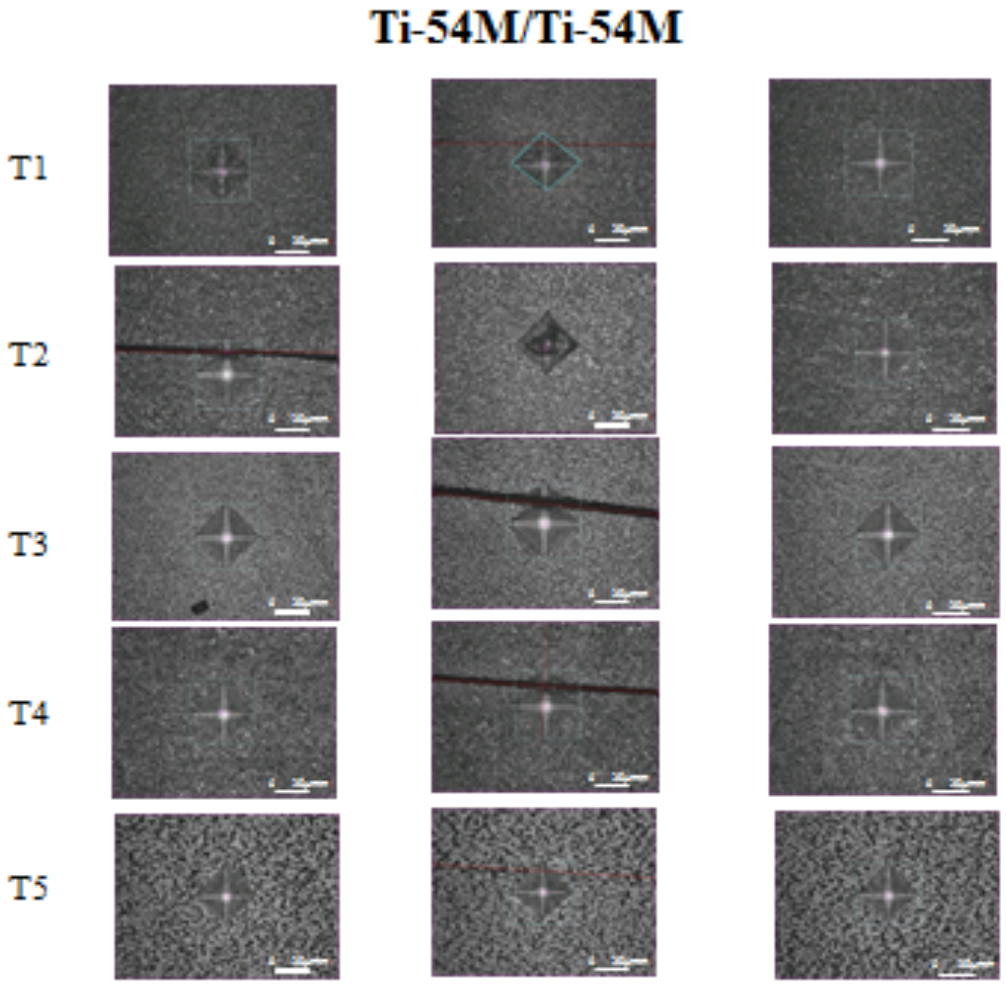

Ti-6242/Ti-6242

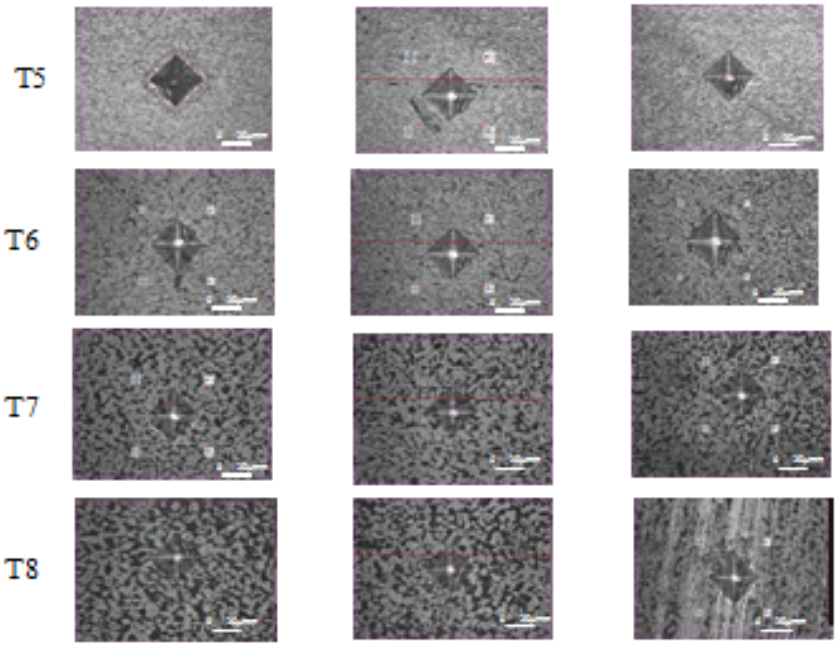

Ti-64SG/Ti-64SG

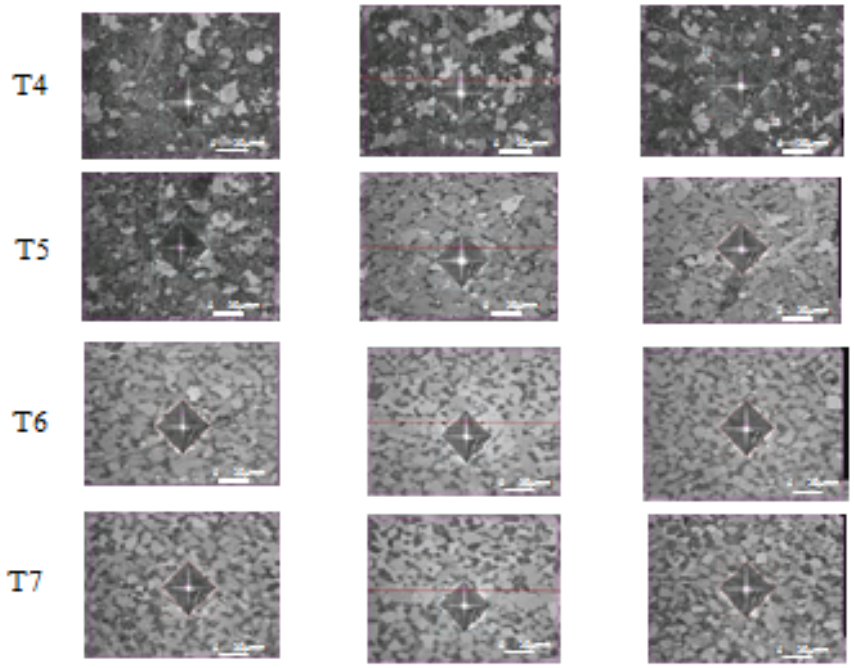

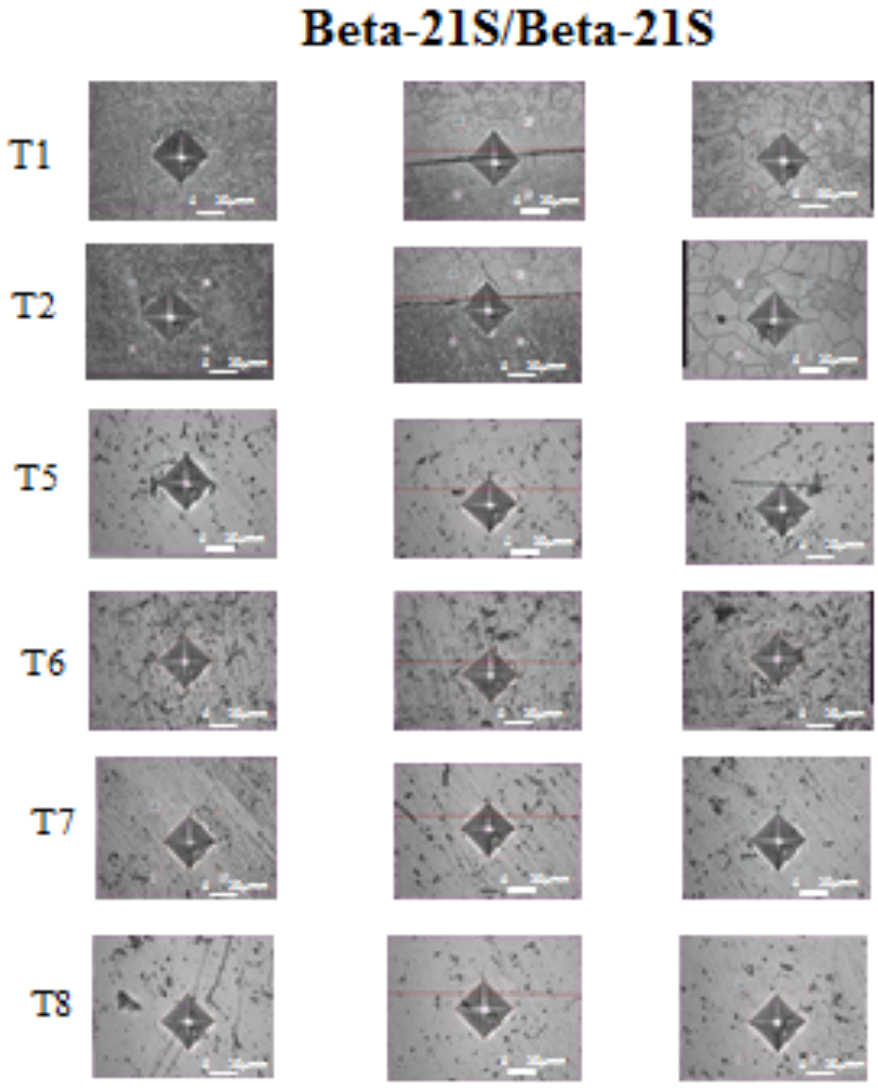
Beta-21S/Beta-21S
T1
T2
T5
T6
T7
T8

Ti-6242SG/Beta-21S

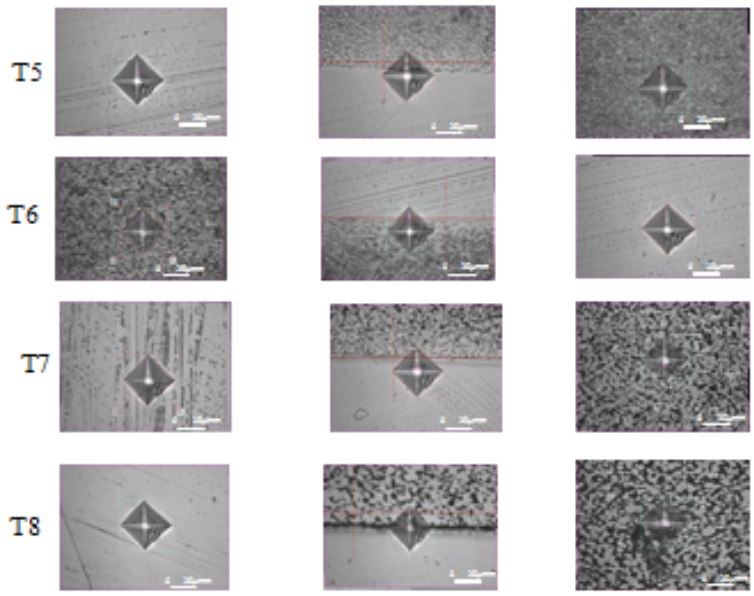

Beta-21S/Ti-64SG

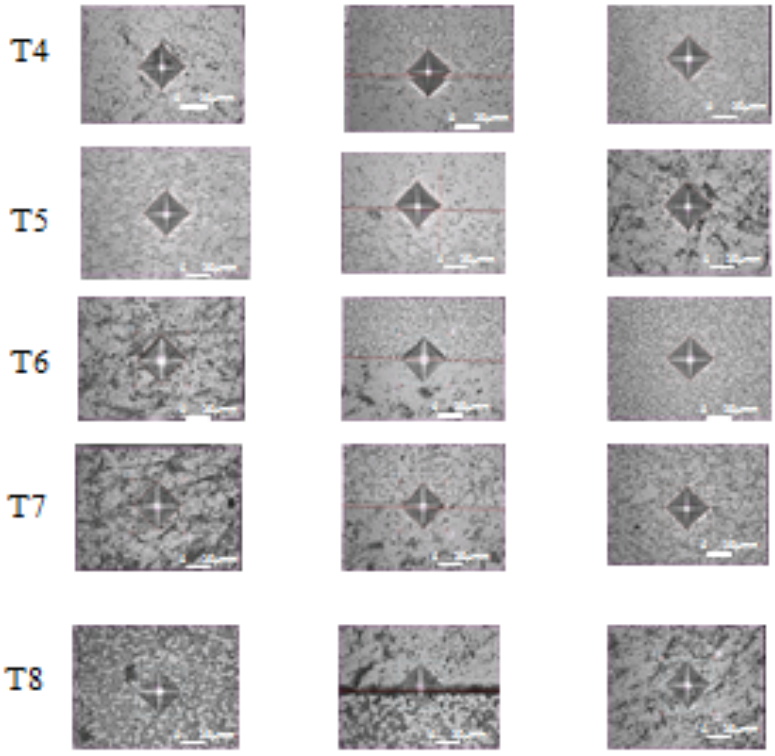

Ti-6242SG/Ti-64SG

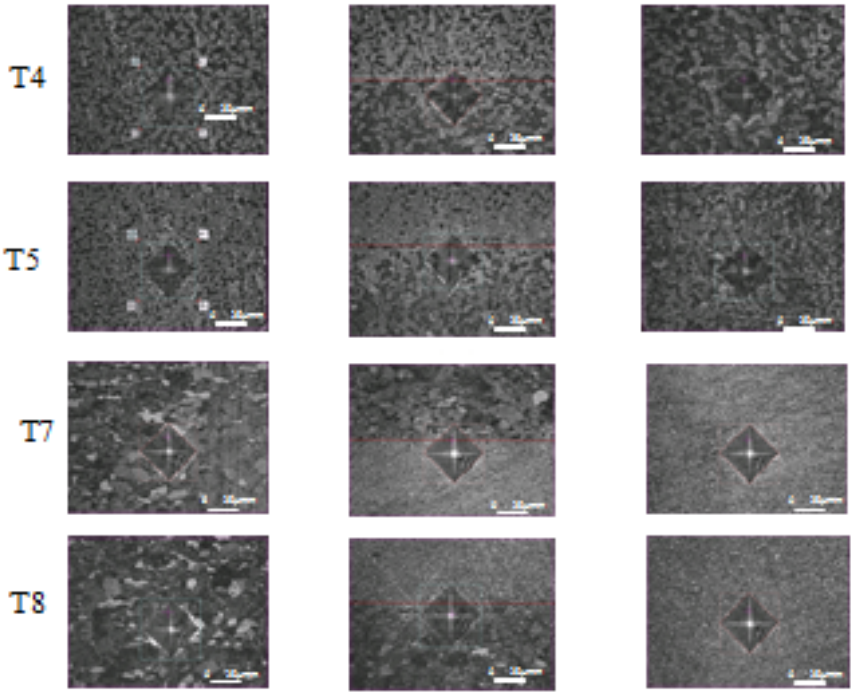

Beta-21S/Ti-64FG

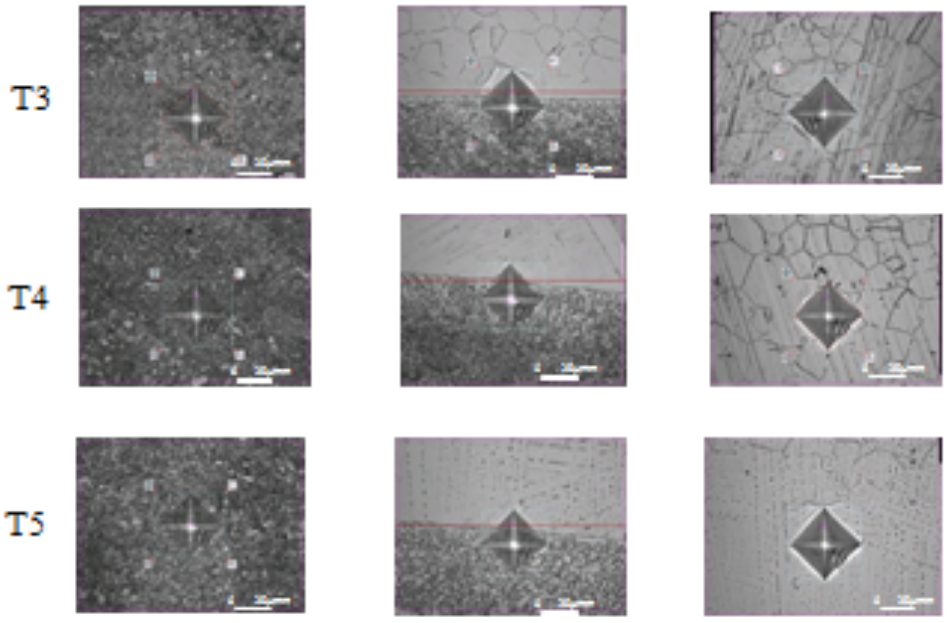

Ti-64FG/Beta-21S

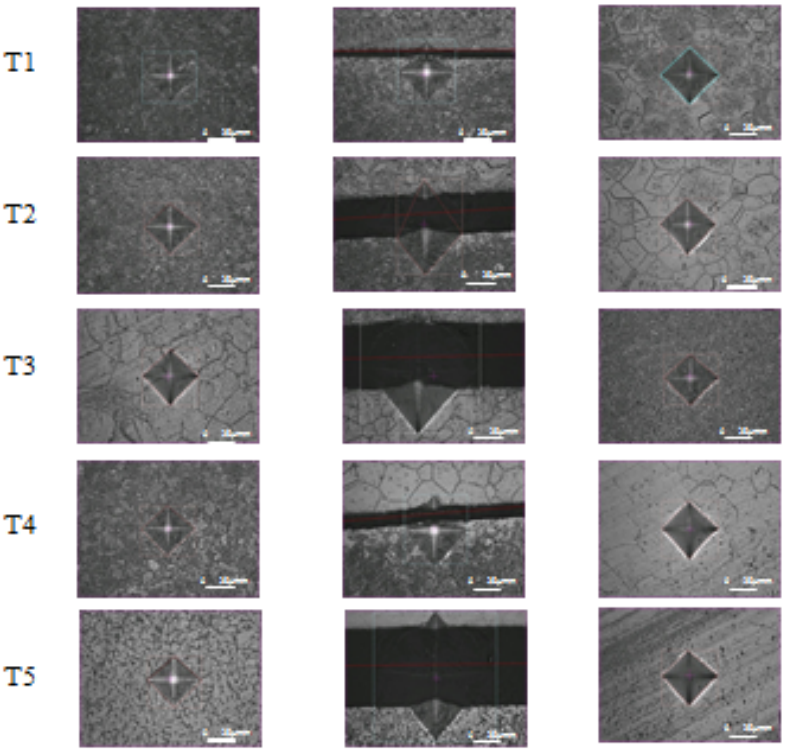

Ti-6242/Ti-54M

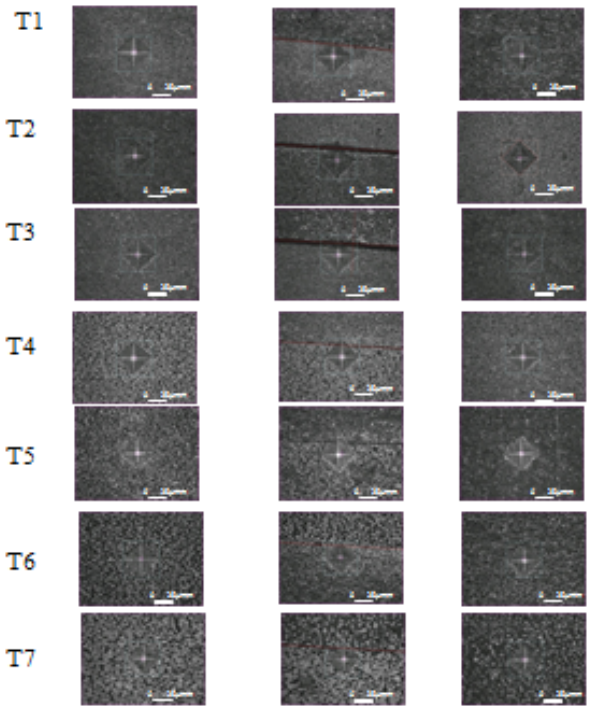

Ti-54M/Beta-21S

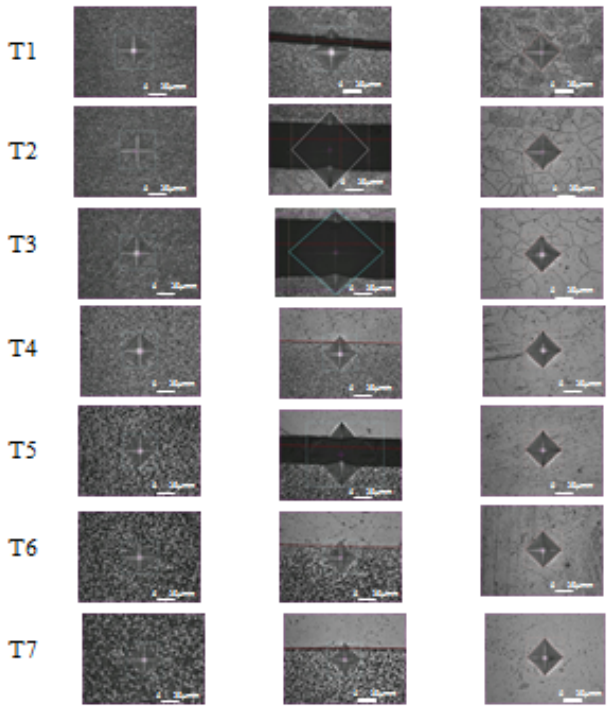

Ti-64SG/Ti-54M

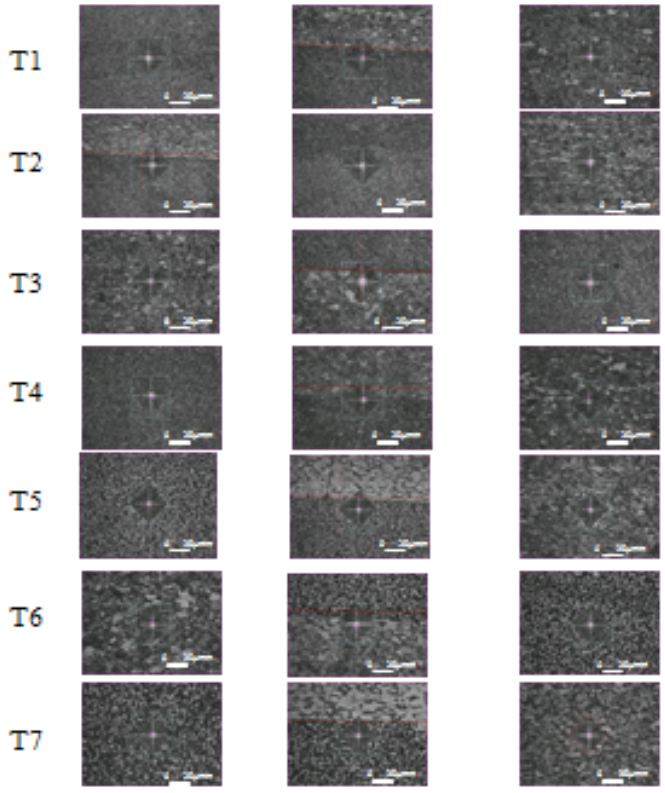

Ti-6242/Ti-64FG

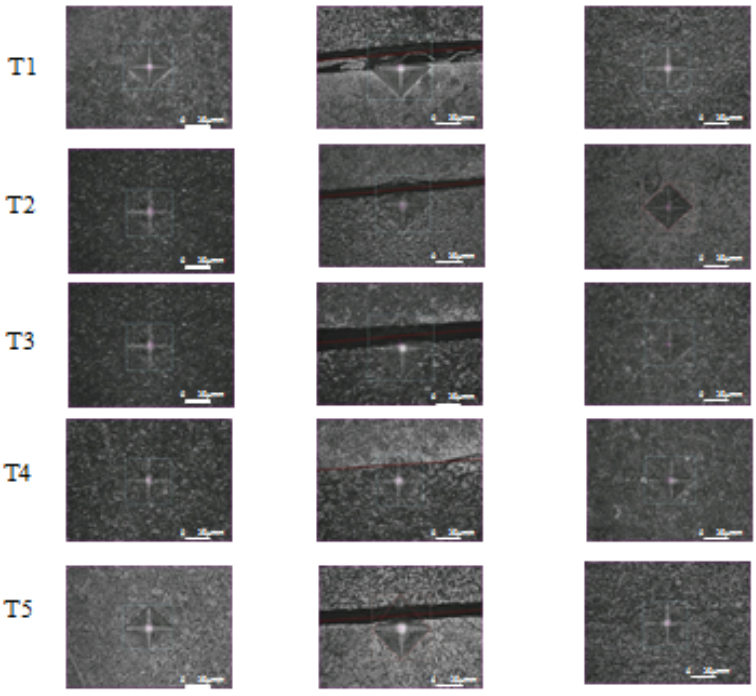

Ti-64SG/Ti64FG

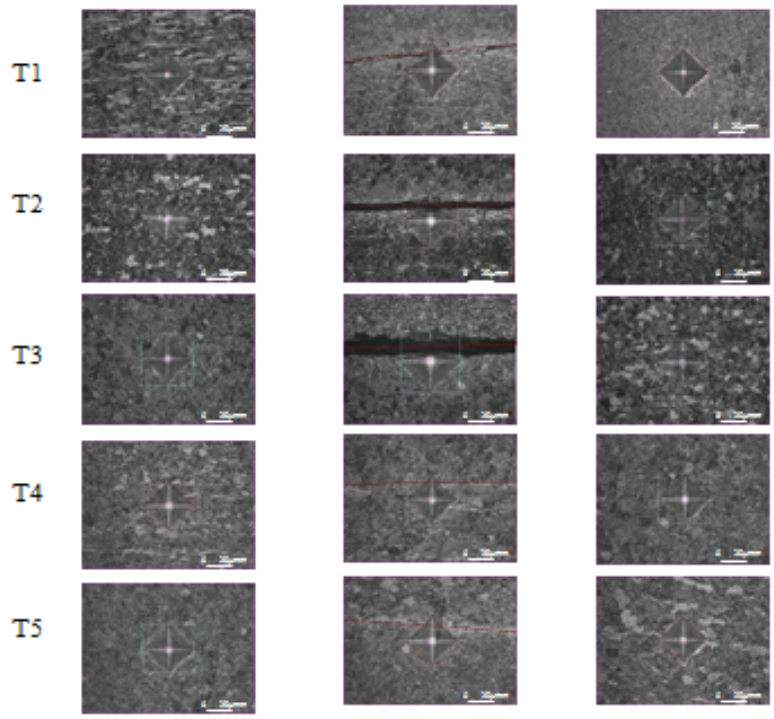

D: ULTIMATE STRESS EFFICIENCY OF DIFFUSION BONDED DISSIMILAR TI-ALLOYS

The ultimate stresses results of dissimilar titanium joints were compared with their respective parent-parent alloy joints and joint efficiency was evaluated with respect to the parent diffusion bonded alloy joints.

Table D**:** Ultimate Stress Efficiency of Diffusion bonded Dissimilar Ti-Alloys

	T (C)	Ultimate Stress (MPa)			% Joint Efficiency	
		β21S/Ti54M	β21S	Ti-54M	β21S	Ti-54M
β21S / Ti-54M	T1	1175	429	1563	174.05	-24.82
	T2	1368	573	1508	138.91	-9.24
	T3	1028		1492		-31.13
	T4	1666		1547		7.71
	T5	1556	426	1660	264.79	-6.28
	T6	1704	403		323.06	
	T7	1693	239		608.81	

	T (C)	Ultimate Stress (MPa)			% Joint Efficiency	
		β21S /64	β21S	Ti-64	β21S	Ti-64
β21S / Ti-64	T4	626		723		-13.34
	T5	705	426	754	65.25	-6.58
	T6	685	403	625	70.01	9.64
	T7	1059	239	651	343.64	62.64
	T8	527	324	750	62.51	-29.72

	T (C)	Ultimate Stress (MPa)			% Joint Efficiency	
		Ti64FG/β21S	Ti-64FG	β21S	β21S	Ti-64FG
Ti-64FG / β21S	T1	1752	1649	429	308.58	6.2
	T2	1567	1083	573	173.52	44.68
	T3	1165	1710			-31.87
	T4	1416	1558			-9.13
	T5	1133		426	165.76	

	T (C)	Ultimate Stress (MPa)			% Joint Efficiency	
		Ti-6242/β21S	Ti-6242	β21S	β21S	Ti-6242
Ti6242/β21S	T5	613	936	426	43.73	-34.54
	T6	636	854	403	58	-25.48
	T7	518	854	239	117.04	-39.3
	T8	523	929	324	61.18	-43.7

	T (C)	Ultimate Stress (MPa)			% Joint Efficiency	
		Ti-64/Ti54M	Ti-64	Ti-54M	Ti-54M	Ti-64
Ti-64 /Ti-54M	T1	1725		1563	10.39	
	T2	1692		1508	12.21	
	T3	1703		1492	14.11	
	T4	1786	723	1547	15.45	147.17
	T5	1828	754	1660	10.1	142.26
	T6	1960	625			213.81
	T7	1882	651			189.02

	T (C)	Ultimate Stress (MPa)			% Joint Efficiency	
		Ti-64FG/Ti-54M	Ti-64FG	Ti-54M	Ti-54M	Ti-64FG
Ti64FG/Ti-54M	T1	1590	1649	1563	1.75	-3.6
	T2	1545	1083	1508	2.48	42.69
	T3	1584	1710	1492	6.13	-7.4
	T4	1577	1558	1547	1.93	1.19
	T5	1794		1660	8.09	

	T (C)	Ultimate Stress (MPa)			% Joint Efficiency	
		Ti-6242/ Ti-54M	Ti-6242	Ti-54M	Ti-54M	Ti-6242
Ti-6242 /Ti-54M	T1	1722		1563	10.22	
	T2	1744		1508	15.69	
	T3	1302		1492	-12.78	
	T4	1523		1547	-1.54	
	T5	1740	936	1660	4.84	85.83
	T6	1948	854			128.05
	T7	2008	854			135.18

	T (C)	Ultimate Stress (MPa)			% Joint Efficiency	
		Ti64/Ti64FG	Ti-64	Ti-64FG	Ti-64	Ti-64FG
Ti-64 /Ti-64FG	T1	1512		1649		-8.31
	T2	1474		1083		36.17
	T3	1471		1710		
	T4	1892	723	1558	161.77	
	T5	1848	754		144.9	

	T (C)	Ultimate Stress (MPa)			% Joint Efficiency	
		Ti-6242/ Ti-64	Ti-6242	Ti-64	Ti-64	Ti-6242
Ti-6242/Ti-64	T4	751		723		
	T5	814	936	754	7.86	-13.11
	T6	832	854	625	33.2	-2.59
	T7	870	854	651	33.56	1.88
	T8	984	929	750	31.19	5.95

	T (C)	Ultimate Stress (MPa)			% Joint Efficiency	
		Ti-6242/ Ti-64FG	Ti-6242	Ti-64FG	Ti-64FG	Ti-6242
Ti-6242 /Ti-64FG	T1	1483		1649	-10.09	
	T2	1513		1083	39.77	
	T3	1469		1710	-14.1	
	T4	1807		1558	15.95	
	T5	1356	936			44.84

E: SURFACE PROFILES OF DIFFUSION BONDED SIMILAR AND DISSIMILAR TITANIUM ALLOY JOINTS

E.1 Surface Profiles of Bondline of the DB Joints

The surface profiles measured at the bondline of the diffusion bonded joints formed by similar and dissimilar titanium alloys are shown below. The surface profiles were measured at all the bonding temperatures. Here T1,T2,……T8 in the brackets denote the bonding temperatures. The surface profiles displayed are in the ascending order of the bonding temperatures provided in the brackets.

1. β-21S/ β-21S (T5,T6,T7,T8)

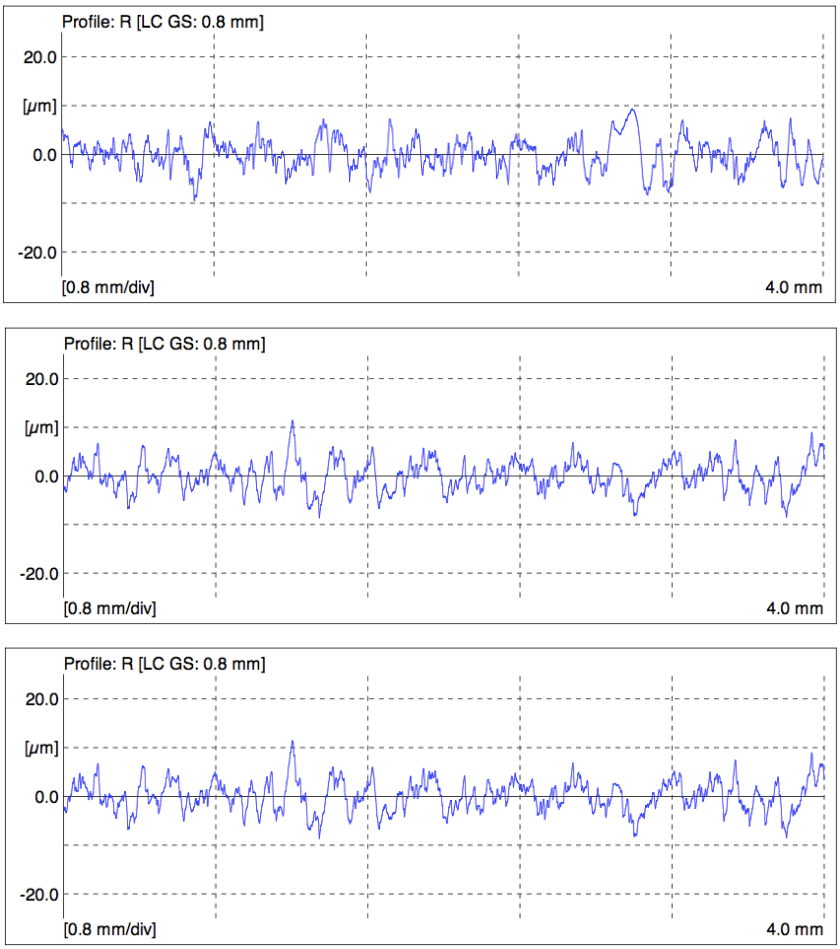

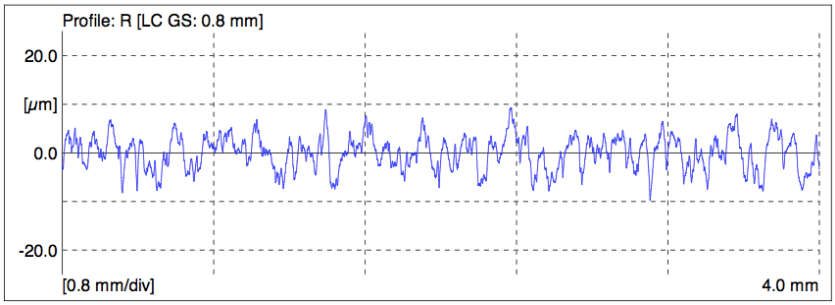
Profile: R [LC GS: 0.8 mm]
20.0
[μm]
0.0
-20.0
[0.8 mm/div]
4.0 mm

2. Ti-54M/ Ti-54M (T4,T5,T6,T7, and T8)

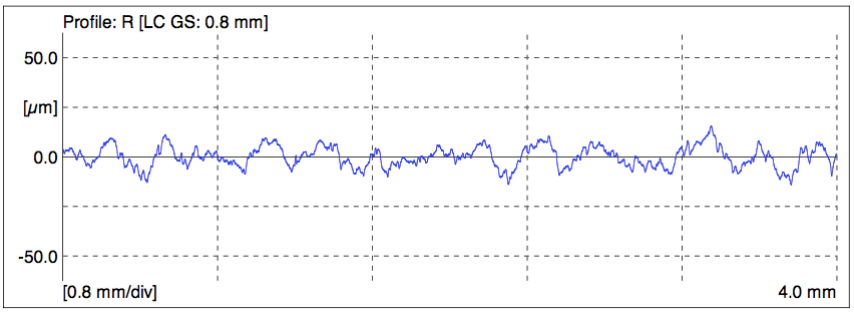

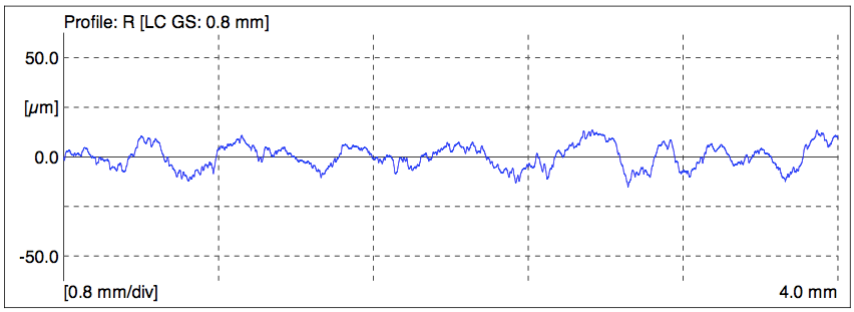

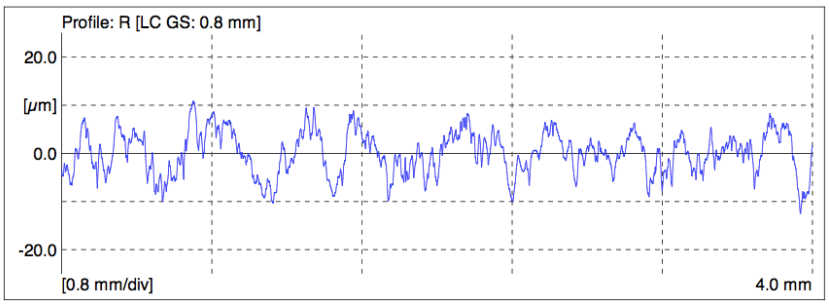

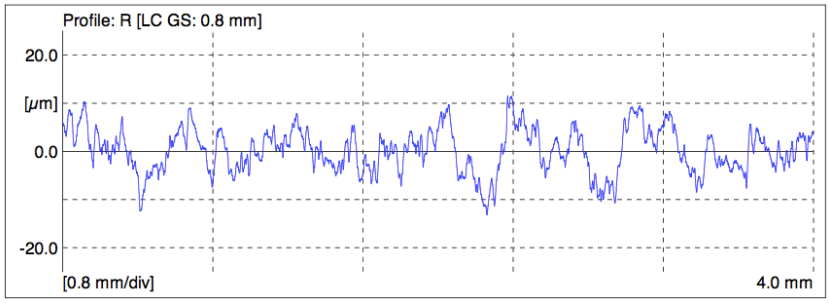

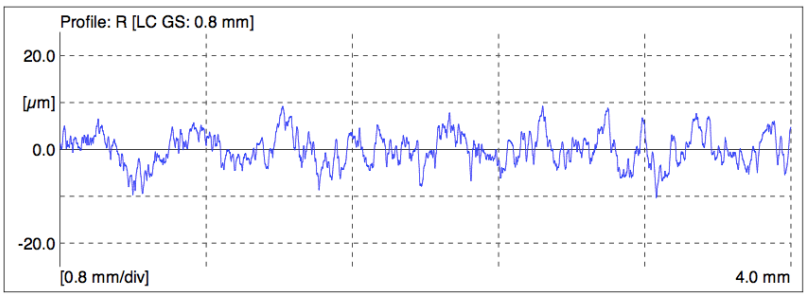

3. Ti-6Al-4V / Ti-6Al-4V (T4,T5,T6,T7)

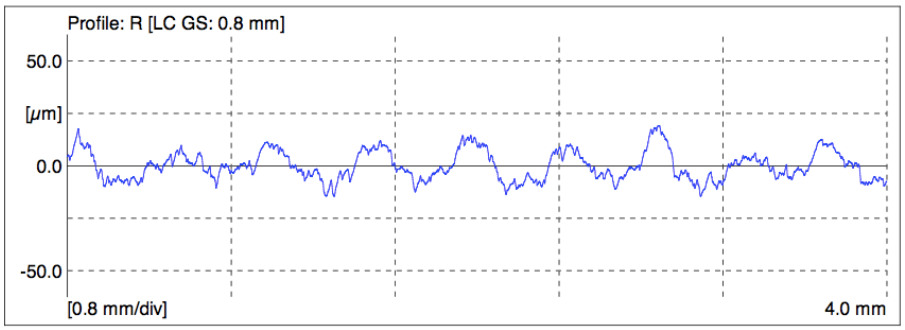

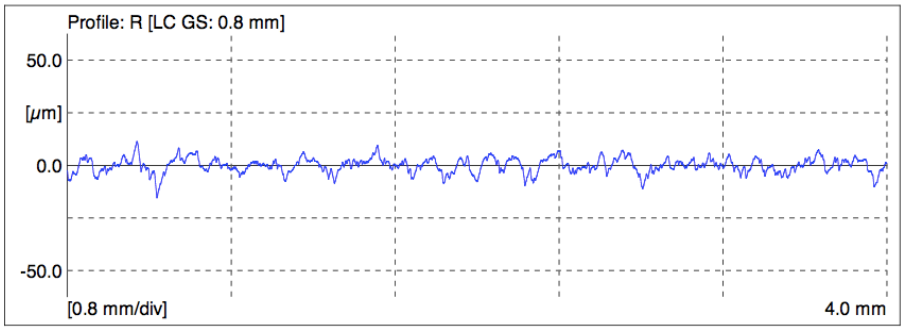

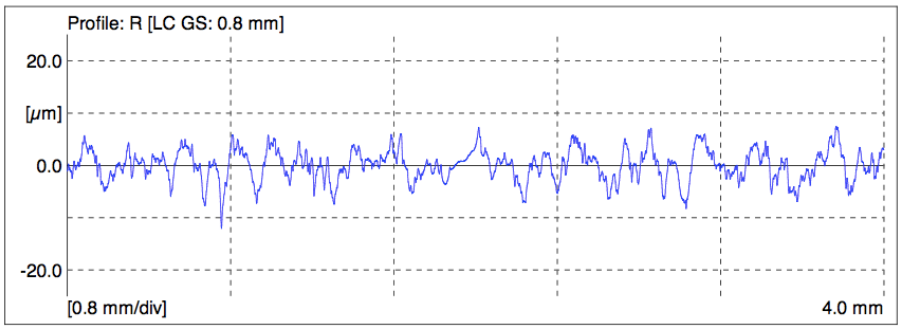

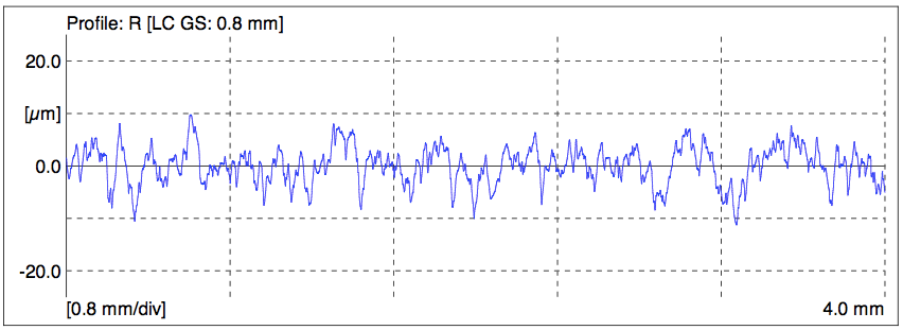

4. Ti-6Al-4V FG/ Ti-6Al-4V FG (T1,T2,T3,T4)

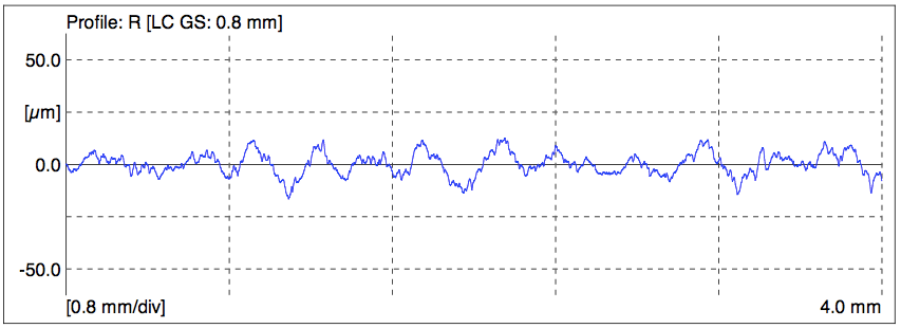

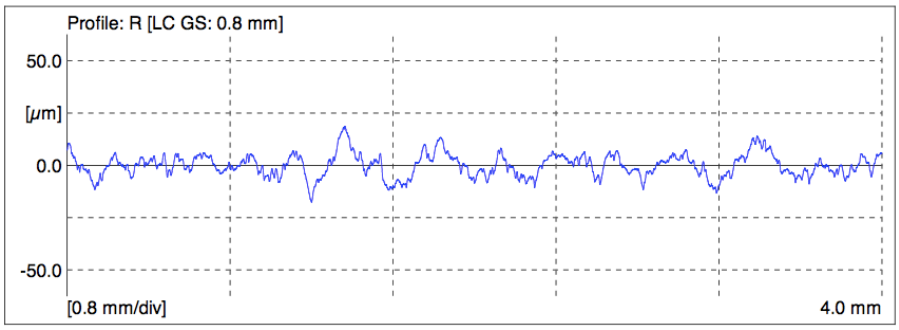

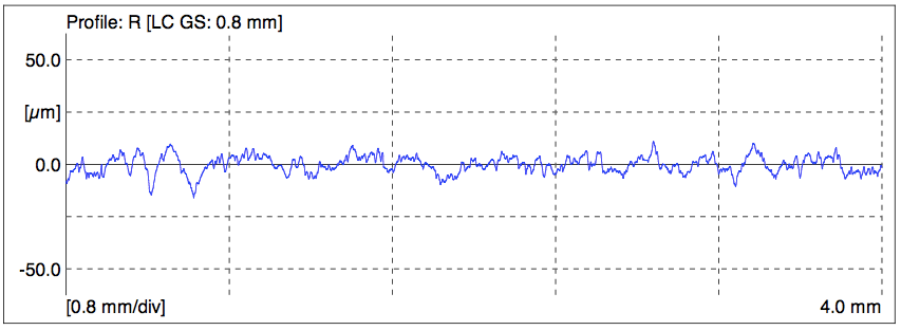

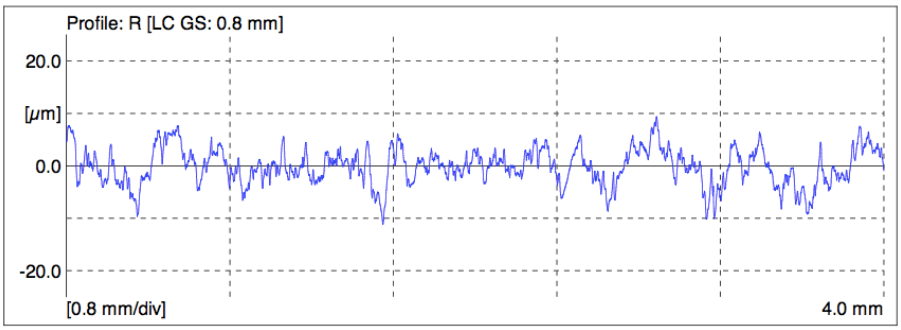

5. Ti-6242/ Ti-6242 (T5,T6,T7,T8)

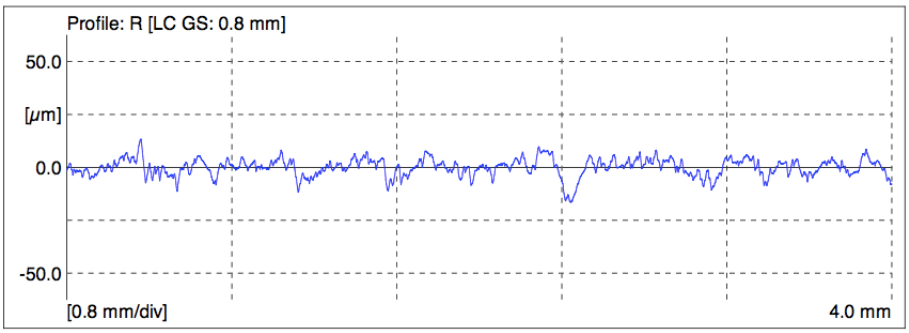

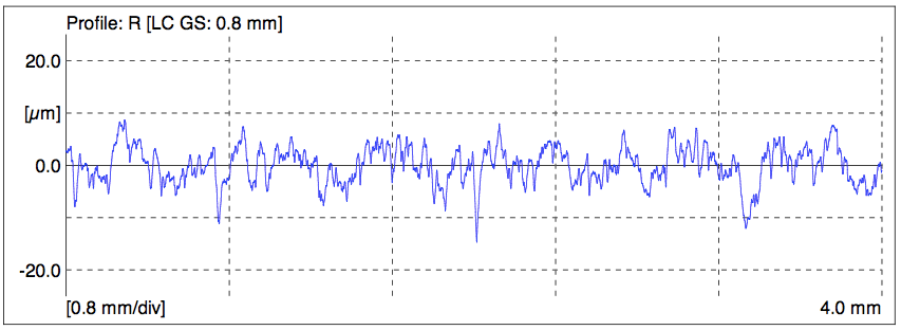

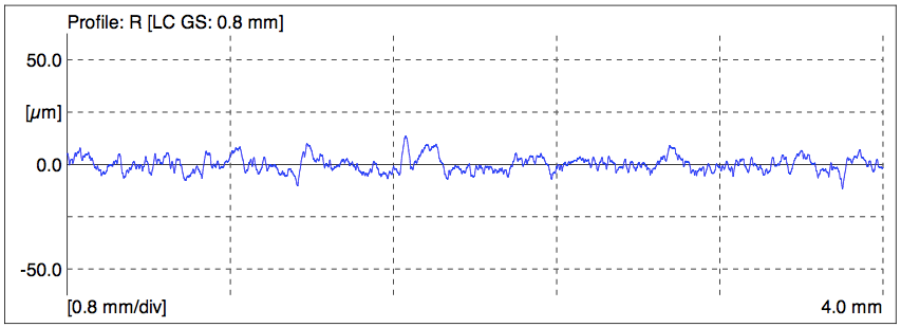

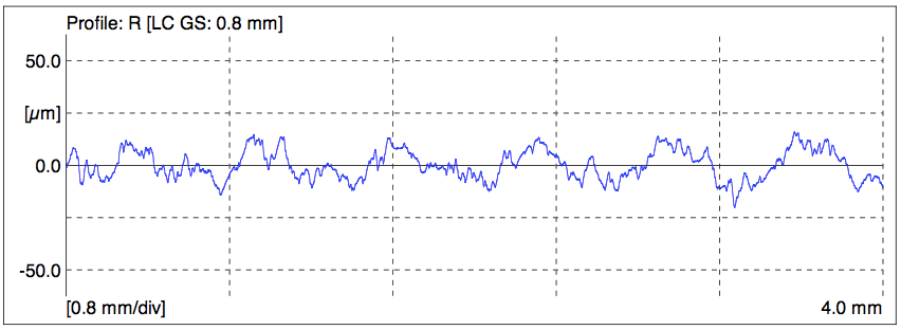

6. β-21S /Ti-54M (T1,T2,T3,T4,T5,T6,T7)

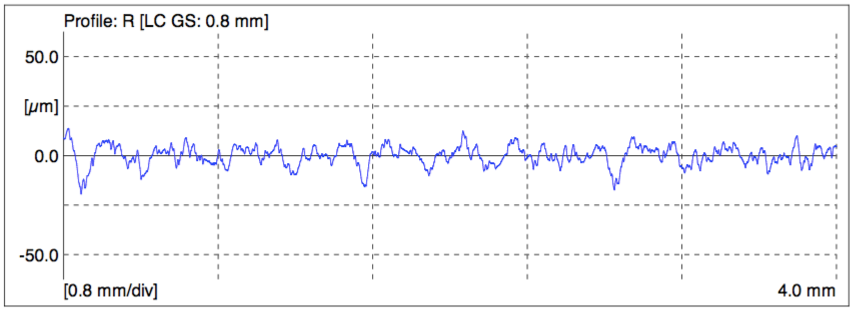

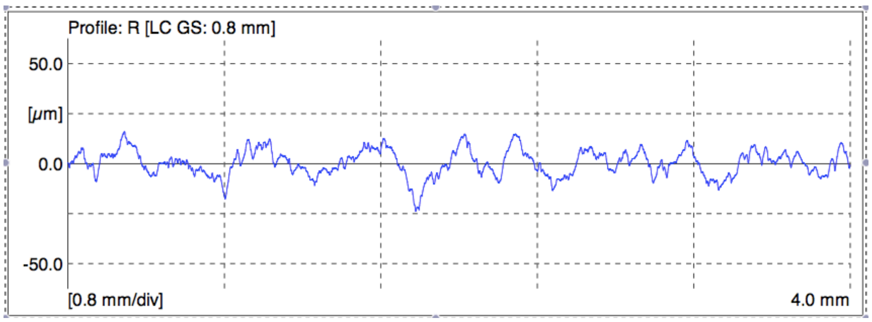

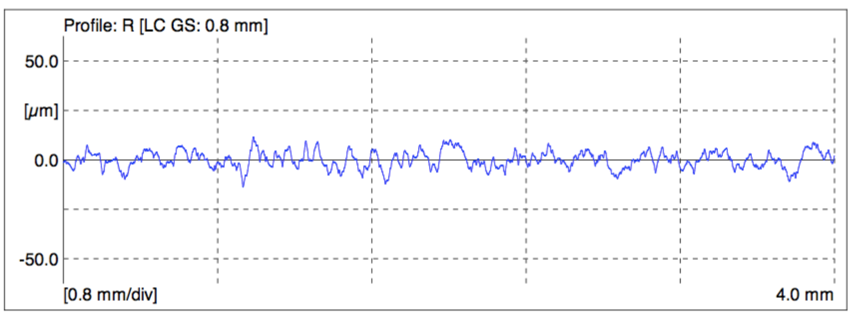

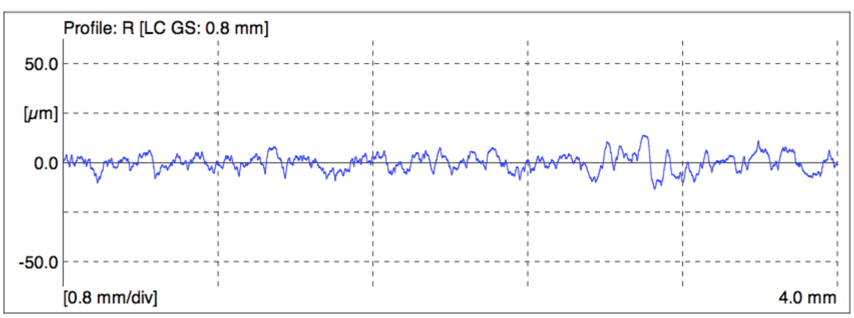

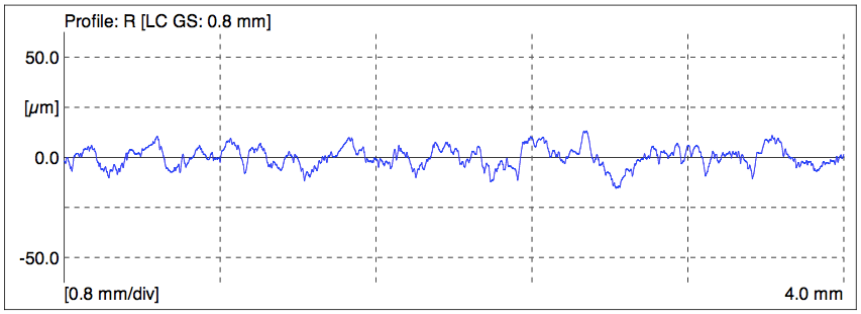
Profile: R [LC GS: 0.8 mm]
50.0
[µm]
0.0
-50.0
[0.8 mm/div]
4.0 mm

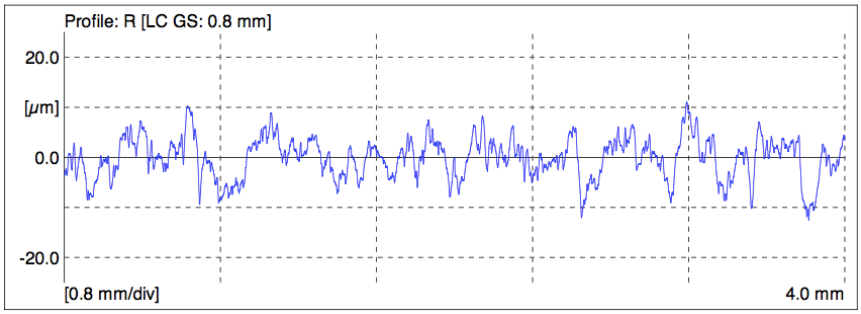
Profile: R [LC GS: 0.8 mm]
20.0
[µm]
0.0
-20.0
[0.8 mm/div]
4.0 mm

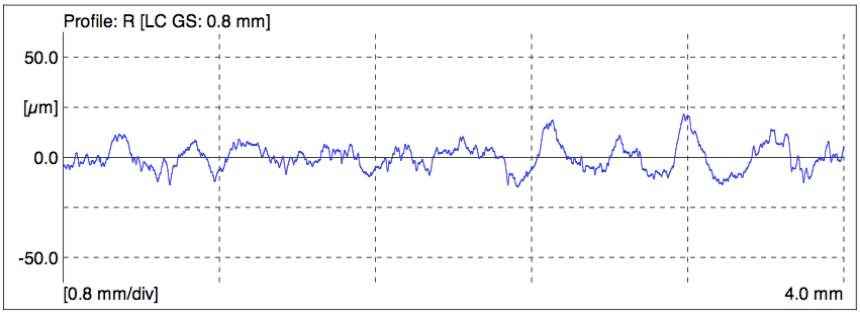
Profile: R [LC GS: 0.8 mm]
50.0
[µm]
0.0
-50.0
[0.8 mm/div]
4.0 mm

7. β-21S /Ti-64 (T4,T5,T6,T7,T8)

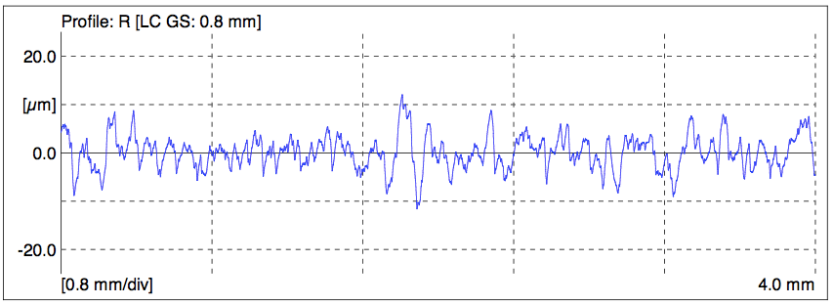

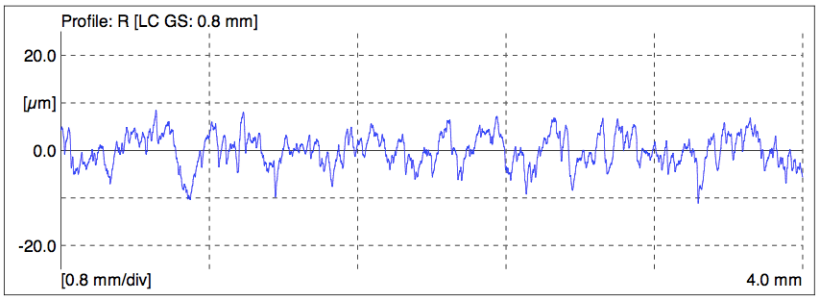

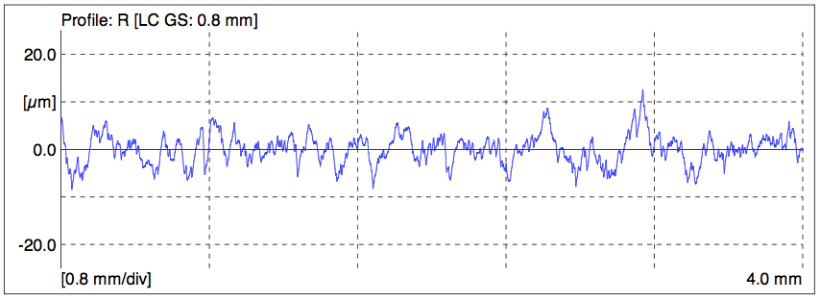

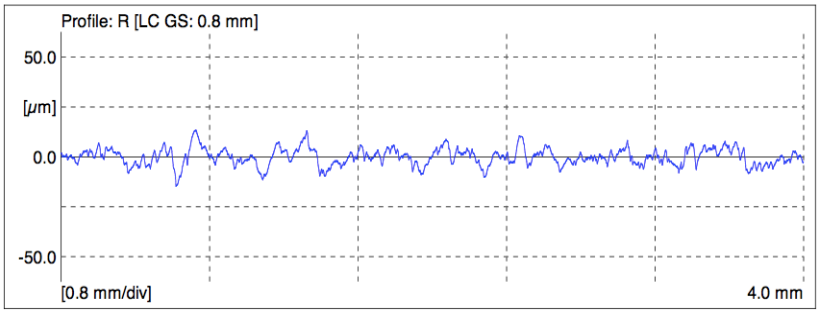

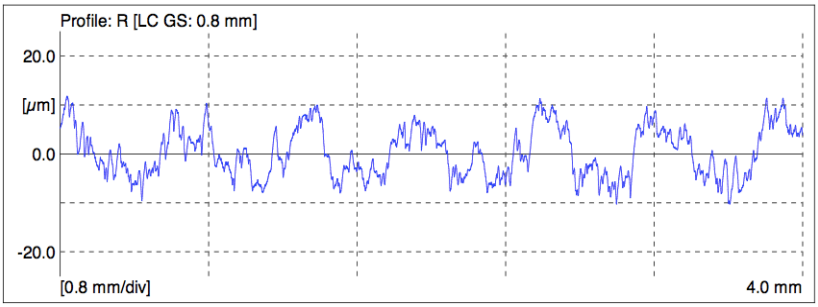

8. β-21S /Ti-64FG

    a. β-21S /Ti-64FG - Batch 1 (T3,T4,T5,T6)

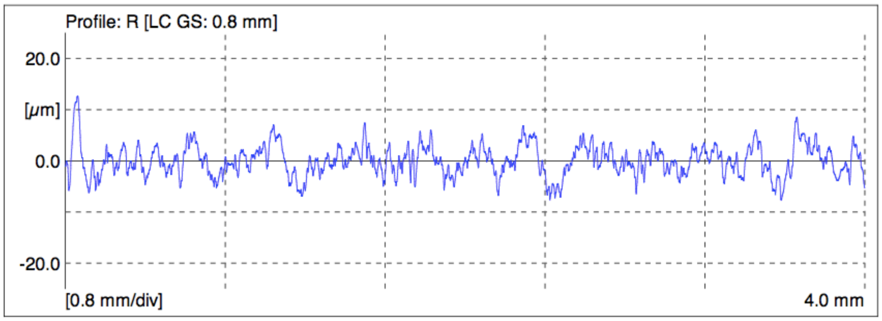

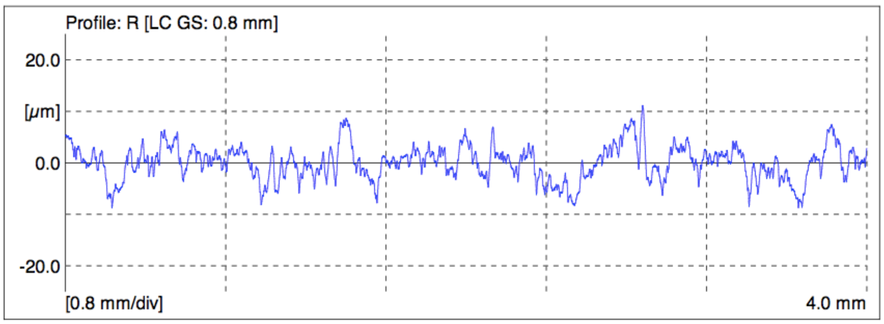

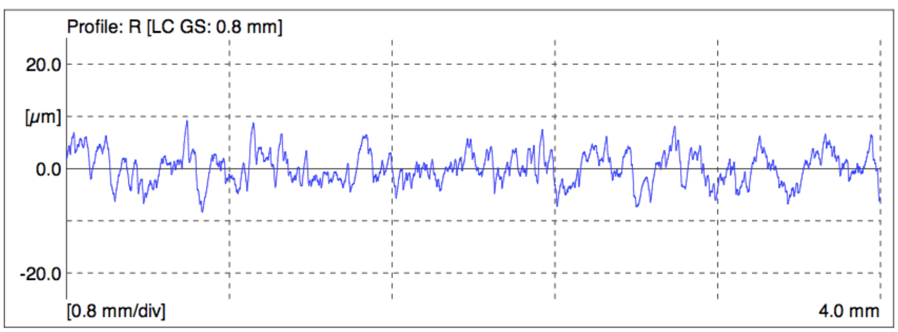

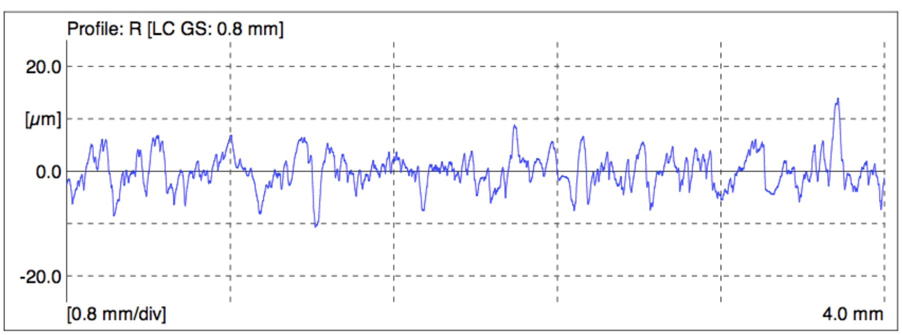

b. β-21S /Ti-64FG - Batch 2 (T1,T2,T3,T4,T5)

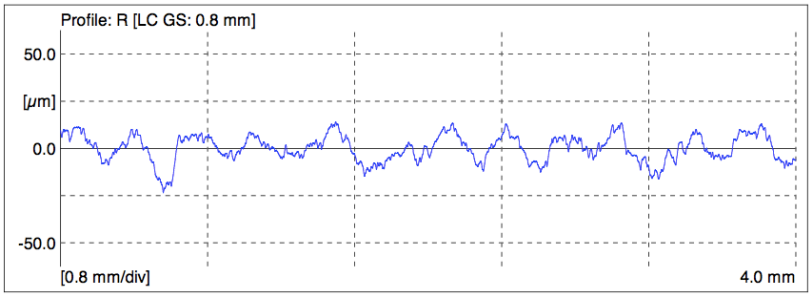

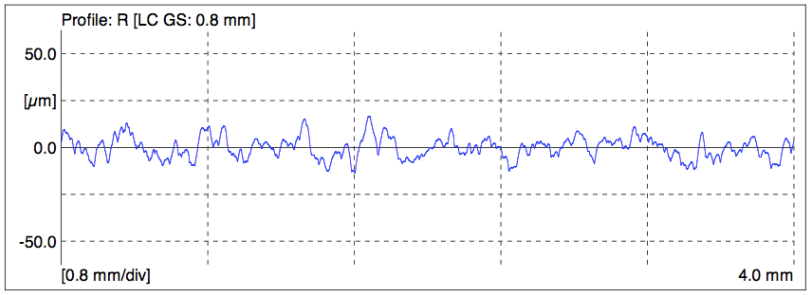

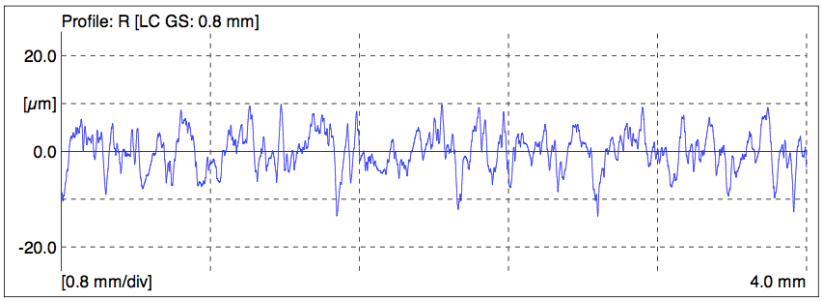

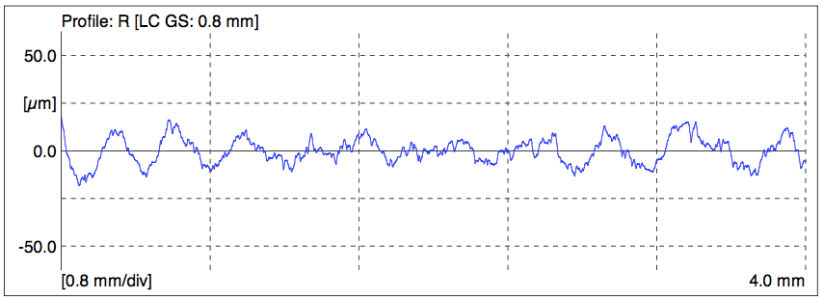

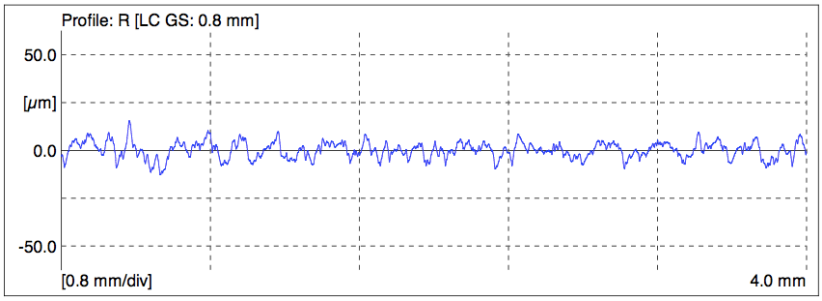

9. Ti-6242/ β-21S (T5,T6,T7,T8)

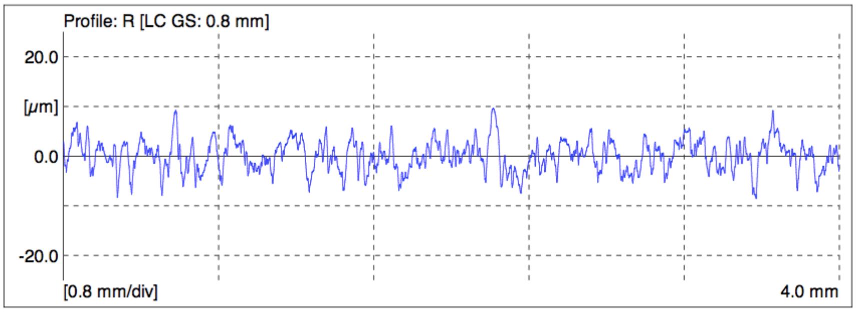

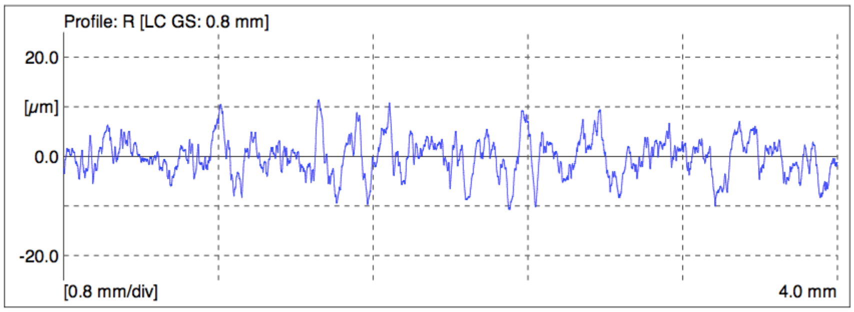

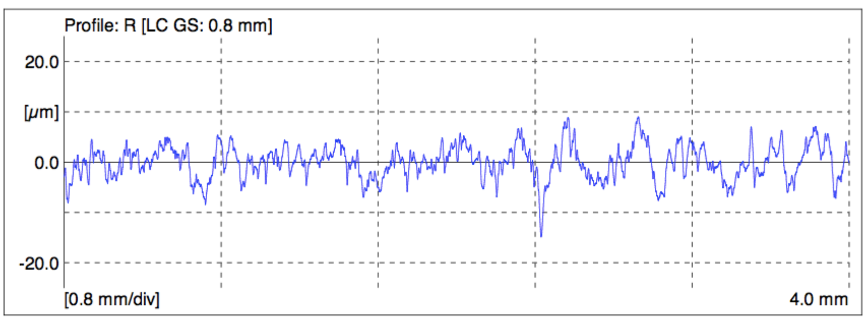

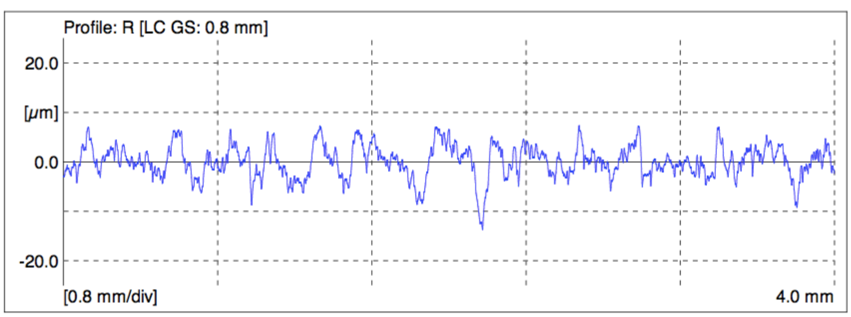

10. Ti-64/Ti-54M (T1,T2,T3,T4,T5,T6,T7)

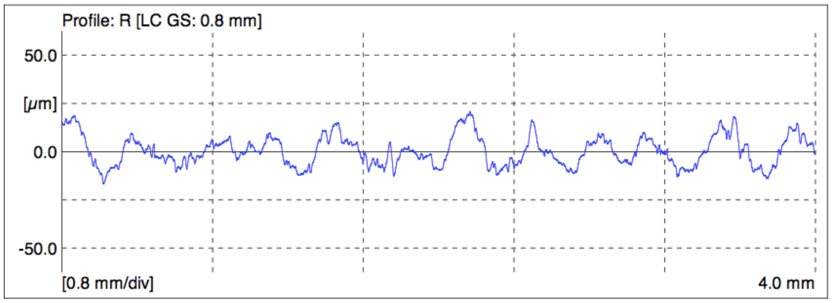

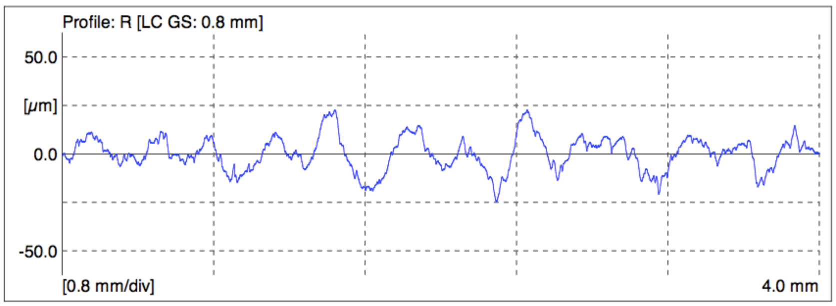

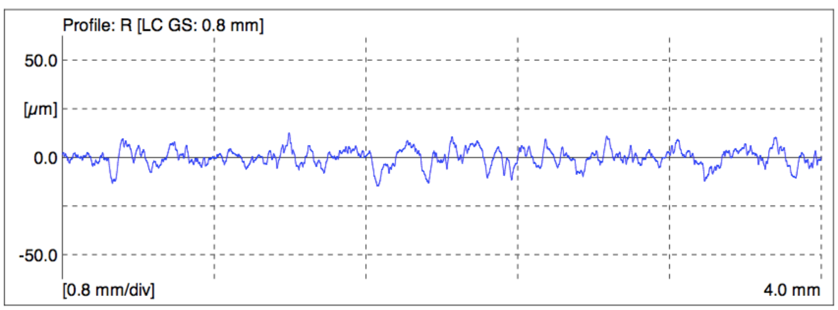

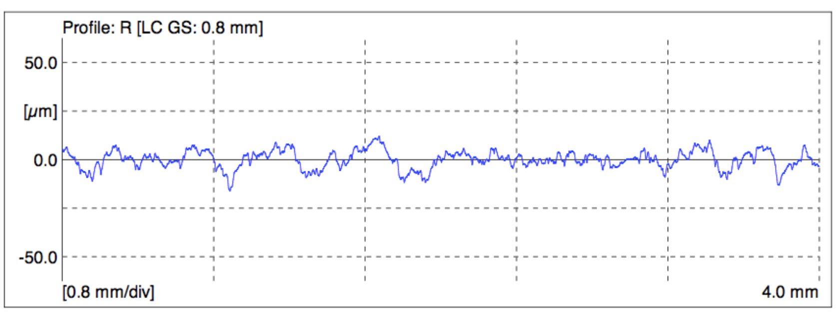

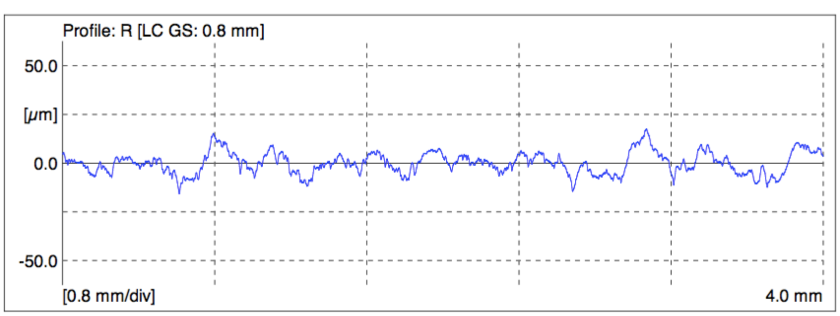

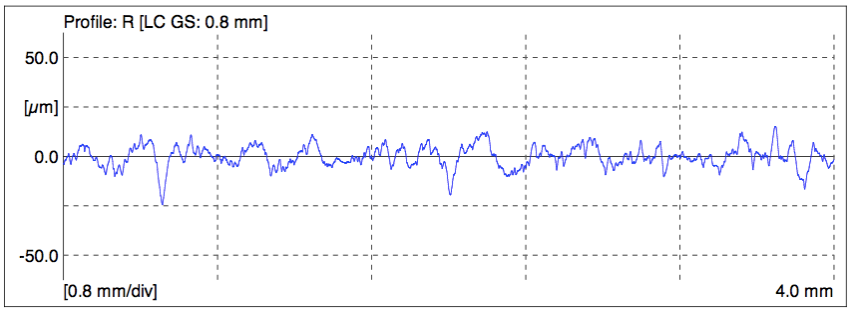
Profile: R [LC GS: 0.8 mm]
50.0
[μm]
0.0
-50.0
[0.8 mm/div]
4.0 mm

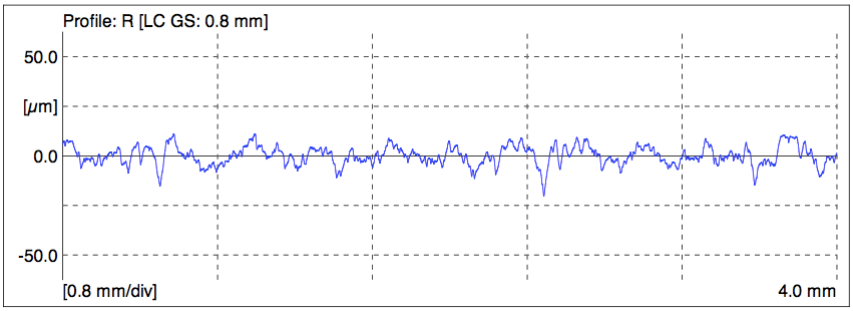
Profile: R [LC GS: 0.8 mm]
50.0
[μm]
0.0
-50.0
[0.8 mm/div]
4.0 mm

11. Ti-64FG/Ti-54M (T1,T2,T3,T4,T5)

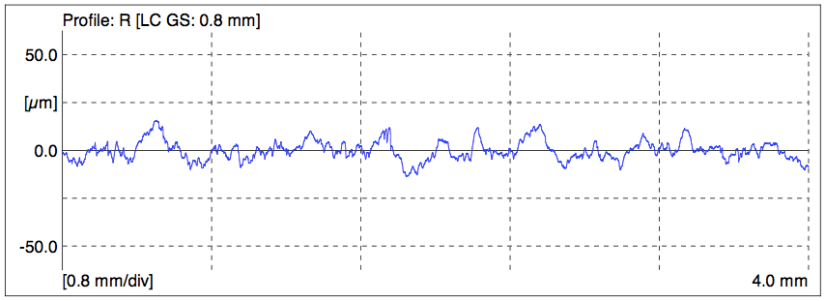

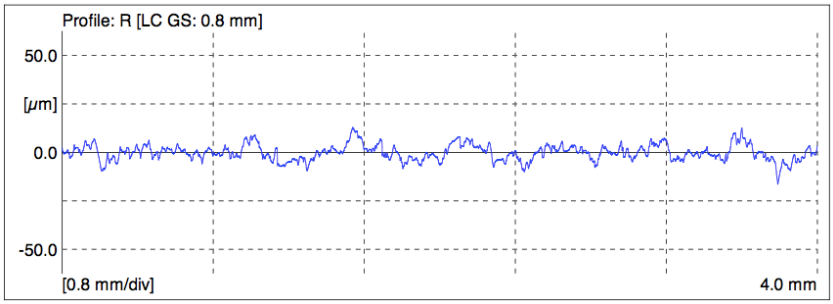

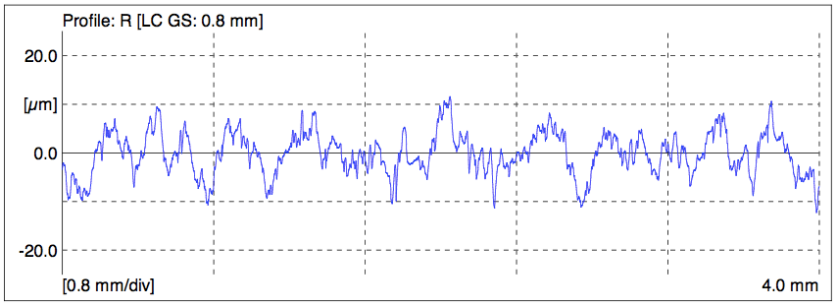

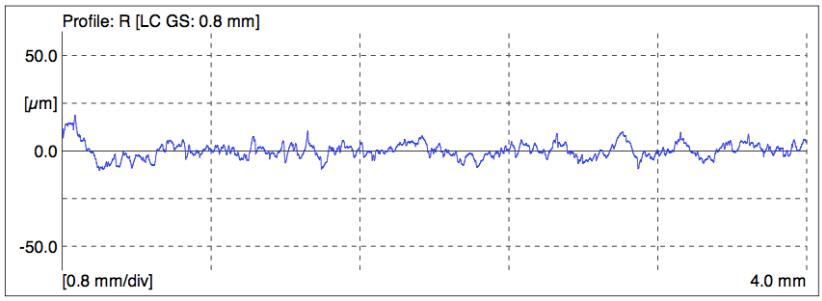

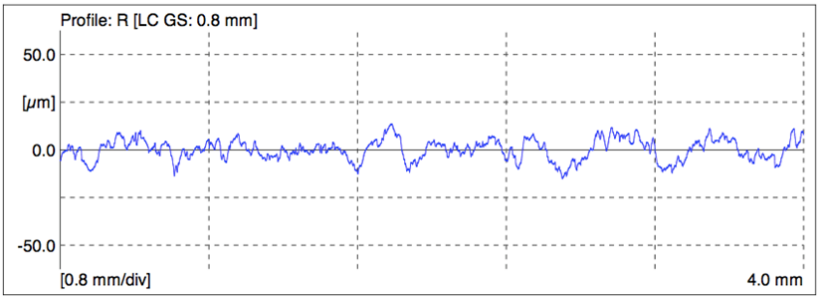

12. Ti-6242/Ti-54M (T1,T2,T3,T4,T5,T6,T7)

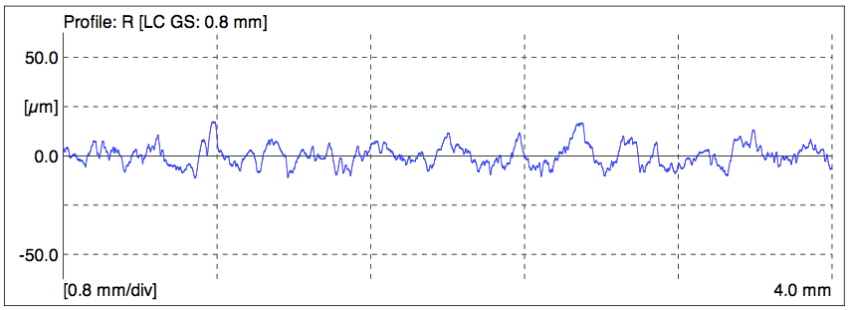

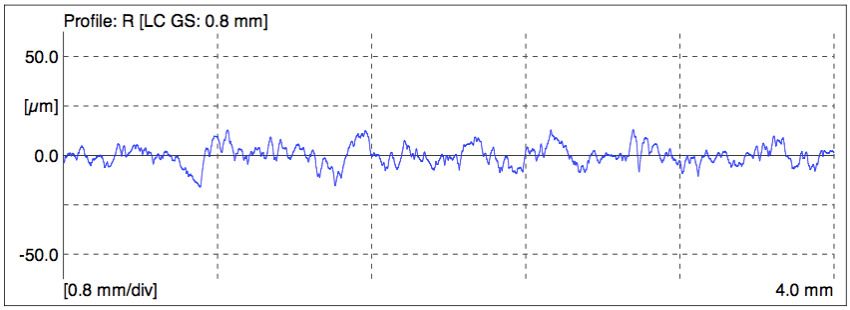

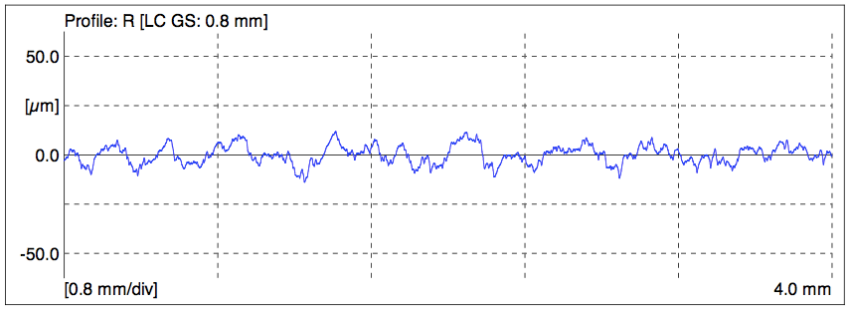

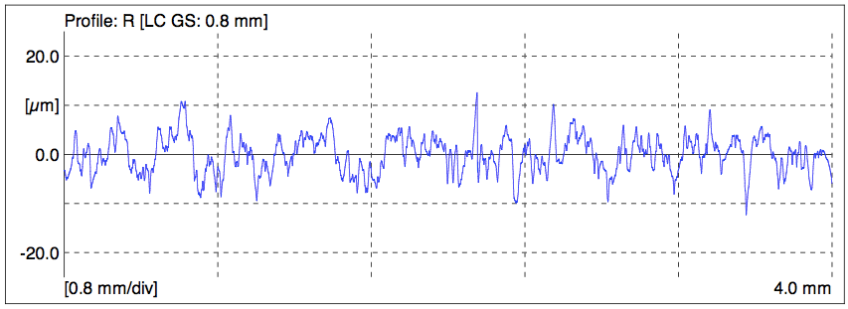

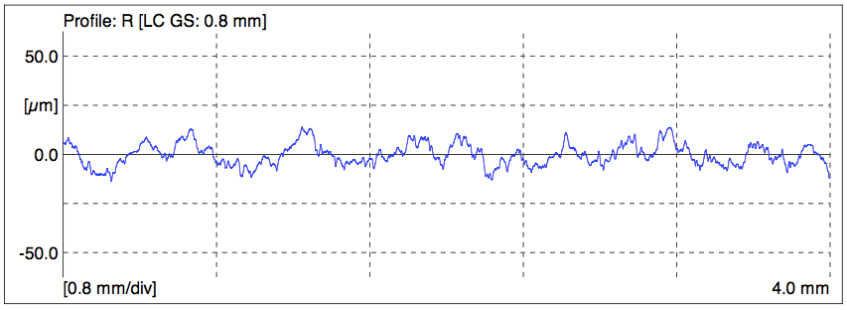

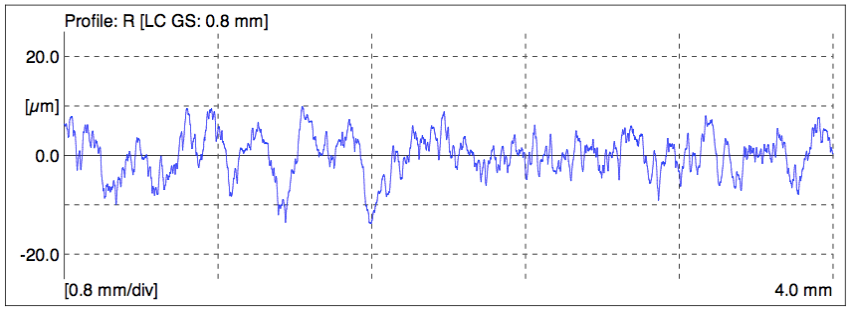
Profile: R [LC GS: 0.8 mm]
20.0
[µm]
0.0
-20.0
[0.8 mm/div]
4.0 mm

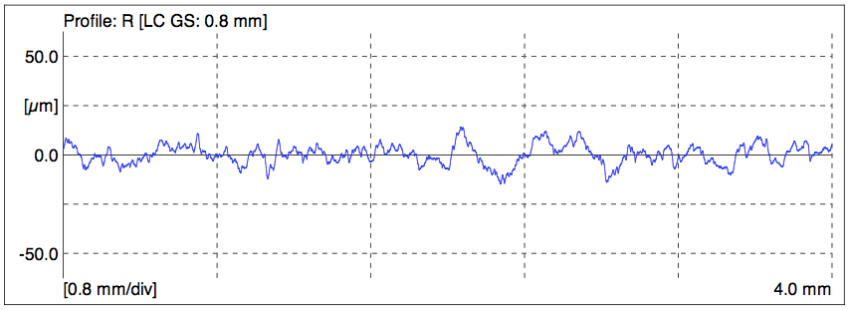
Profile: R [LC GS: 0.8 mm]
50.0
[µm]
0.0
-50.0
[0.8 mm/div]
4.0 mm

13. Ti-64SG/Ti-64FG (T1,T2,T3,T4,T5)

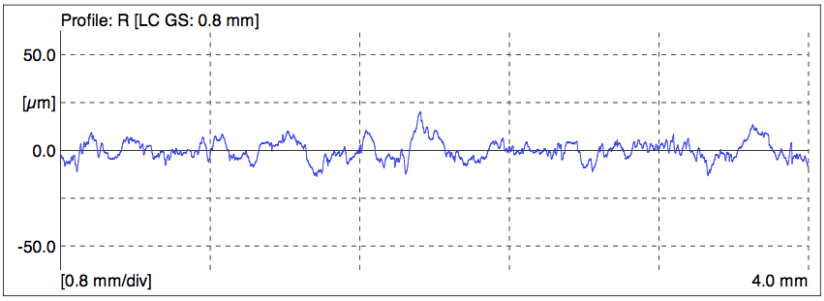

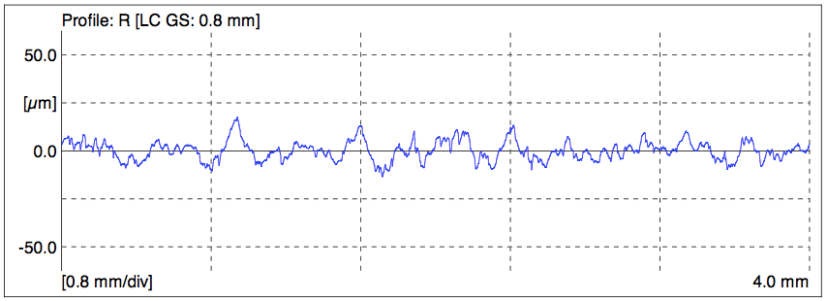

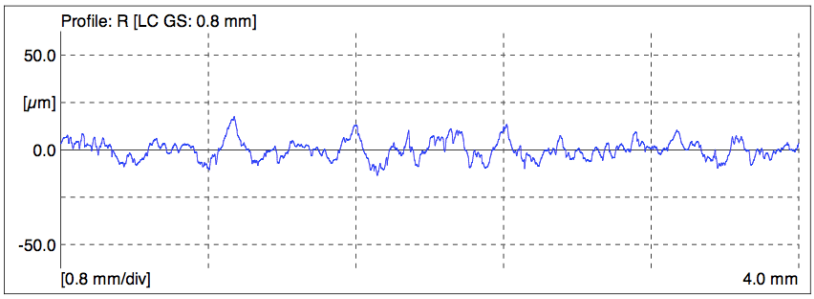

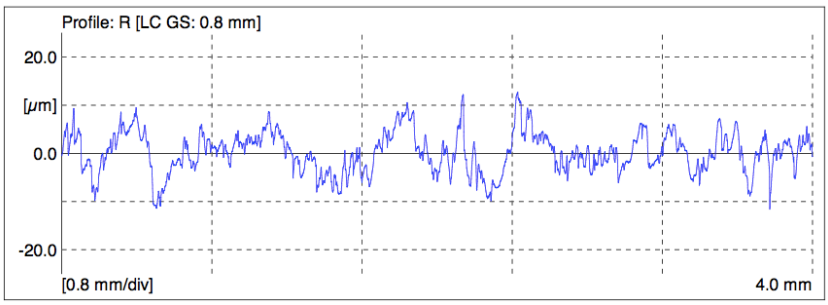

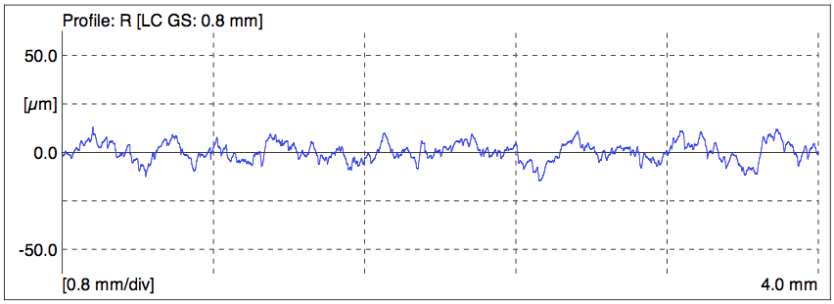

14. Ti-6242/Ti-64 (T4,T5,T7,T8)

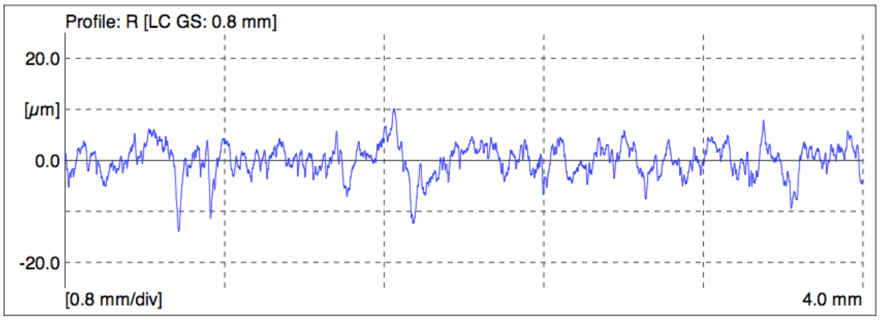

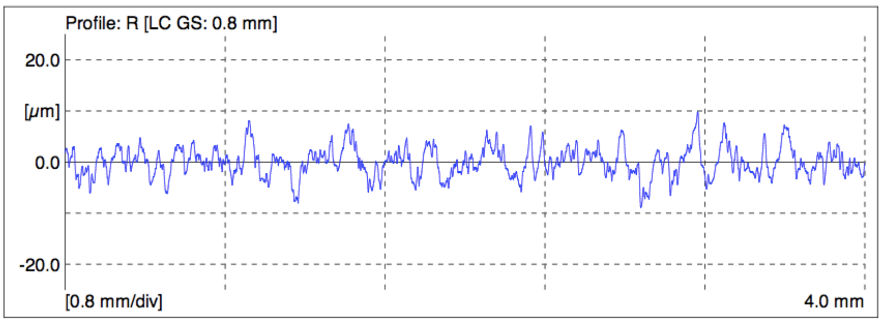

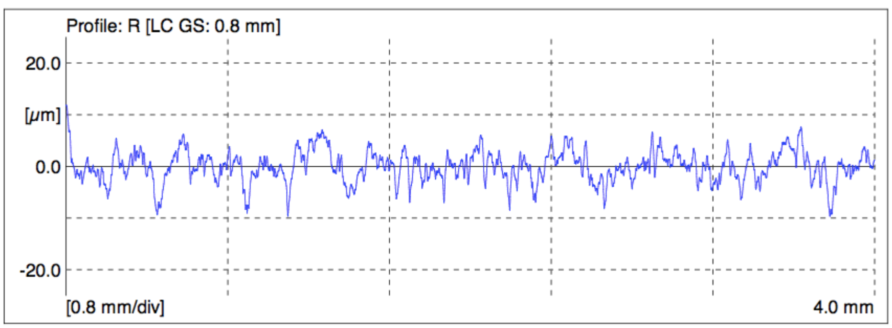

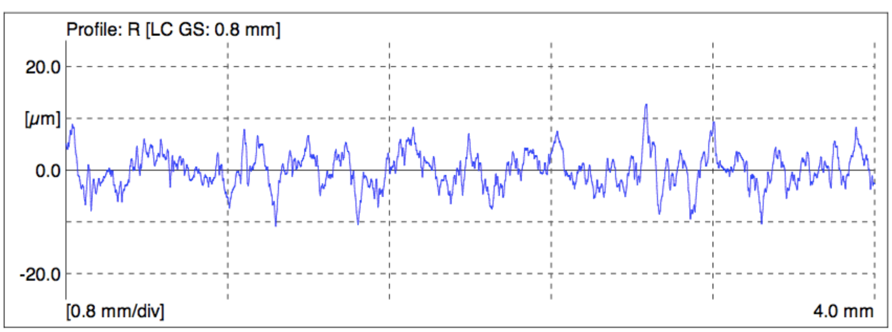

15. Ti-6242/Ti-64FG (T1,T2,T3,T4,T5)

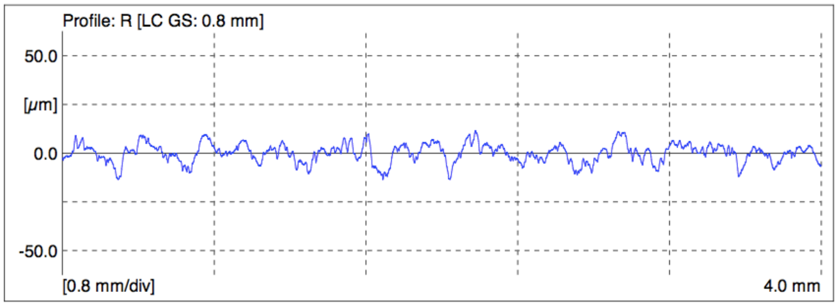

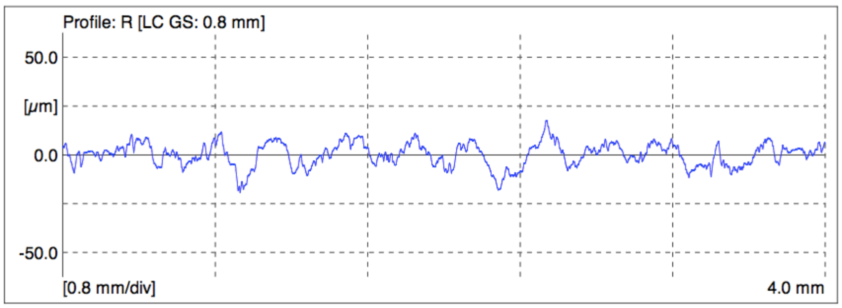

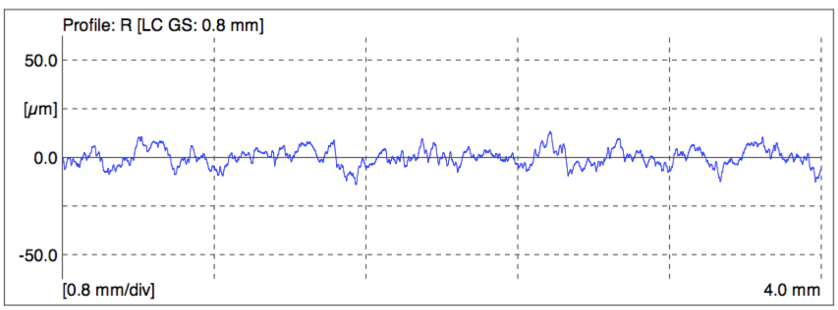

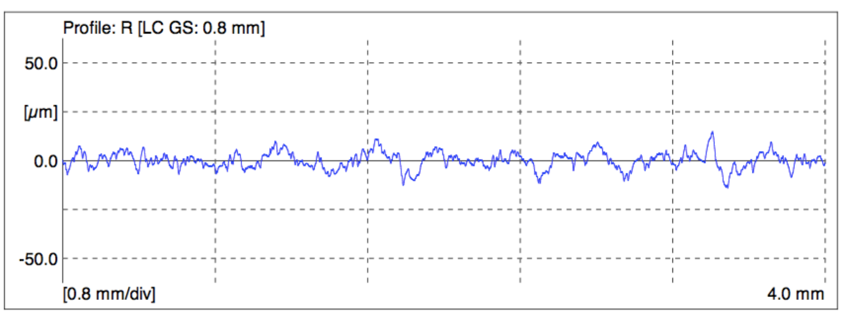

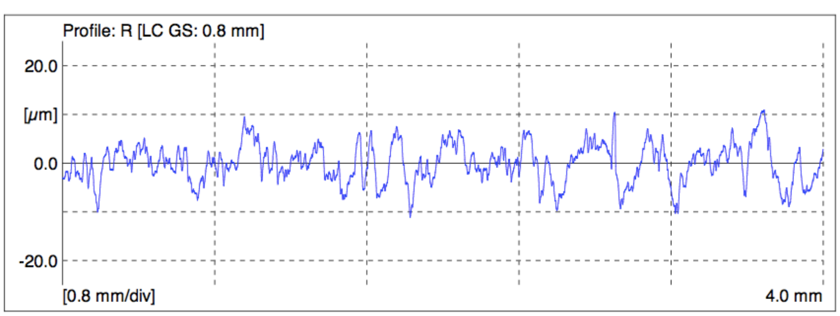

E.2. SURFACE PROFILE PARAMETERS (BD: BONDLINE)

The surface parameters measured at different bonding temperatures are listed below. The definitions of profile parameters included are (Ra: Center Line Average or Arithmetic Mean; Rq: Root Mean Square (RMS) Average; Rz: Peak to Valley Height within Sampling Length; Rt: Peak to Valley Height within Entire Length (Maximum Height of the Profile); Rsk: Skewness; Rku: Kurtosis)

Ti-Joint	Parameter (µm)	Location	Temperatures (C)				
			T4	T5	T6	T7	T8
Ti-64SG/Ti-64SG	Ra	Ti-64	3.833	2.263	2.263	2.331	2.310
		BD	5.718	2.779	2.332	2.794	2.641
		Ti-64	8.330	2.86	3.327	3.202	3.598
	Rq	Ti-64	4.608	2.818	2.818	2.877	3.017
		BD	6.913	3.538	2.970	3.523	3.293
		Ti-64	10.136	3.643	3.999	3.983	4.566
	Rz	Ti-64	19.091	13.080	13.080	14.417	16.226
		BD	27.876	19.475	15.053	17.491	16.024
		Ti-64	39.980	16.556	17.559	17.973	22.358
	Rt	Ti-64	24.710	16.580	16.580	18.620	24.270
		BD	33.850	26.880	19.510	20.990	19.530
		Ti-64	51.220	21.810	23.070	22.890	26.840
	Rsk	Ti-64	-0.020	-0.270	-0.270	-0.260	3.06
		BD	0.380	-0.430	-0.280	-0.270	2.950
		Ti-64	0.320	-0.310	-0.100	-0.330	2.790
	Rku	Ti-64	2.310	2.800	2.800	-0.330	4.180
		BD	2.420	3.610	3.030	-0.300	2.860
		Ti-64	2.740	2.960	2.510	-0.400	3.210

Ti-Joint	Parameters (µm)	Location	Temperatures (C)			
			T5	T6	T7	T8
Ti-6242SG/Ti-6242SG	Ra	Ti-6242	2.522	3.124	3.155	3.376
		BD	3.183	2.827	5.946	2.857
		Ti-6242	3.022	2.480	8.081	3.043
	Rq	Ti-6242	3.132	3.978	3.918	4.204
		BD	4.172	3.524	7.053	3.594
		Ti-6242	3.922	3.216	9.224	3.908
	Rz	Ti-6242	16.453	20.178	18.318	19.694
		BD	20.886	18.124	28.157	17.904
		Ti-6242	19.830	16.943	32.923	19.335
	Rt	Ti-6242	19.470	30.070	21.660	22.800
		BD	29.750	23.340	36.100	25.170
		Ti-6242	26.700	22.88	38.980	25.030
	Rsk	Ti-6242	-0.190	0.040	-0.010	-0.270
		BD	-0.690	-0.380	0.140	0.480
		Ti-6242	-0.060	-0.280	0.020	-0.110
	Rku	Ti-6242	2.940	3.990	2.820	2.760
		BD	4.340	3.300	2.160	3.350
		Ti-6242	3.480	3.860	1.800	3.460

Ti-Joint	Surface Parameter (µm)	Location	Temperatures (C)					
			T1	T2	T5	T6	T7	T8
β21S/β21S	Ra	Beta-21S	3.121	2.200	2.524	2.393	2.235	4.031
		BD	2.251	2.654	2.604	2.507	2.559	2.828
		Beta-21S	3.210	2.827	3.307	3.373	3.285	3.178
	Rq	Beta-21S	3.930	2.822	3.238	3.102	2.816	5.103
		BD	2.881	3.468	3.271	3.108	3.203	3.452
		Beta-21S	4.047	3.536	4.210	4.162	4.033	4.060
	Rz	Beta-21S	19.154	15.296	17.072	15.942	15.567	24.735
		BD	15.753	19.094	15.327	15.767	16.198	15.971
		Beta-21S	20.432	17.066	22.970	19.895	19.133	19.775
	Rt	Beta-21S	22.700	19.110	24.100	20.820	20.740	32.090
		BD	18.120	29.260	18.890	20.040	19.260	19.020
		Beta-21S	25.520	22.870	28.100	27.990	25.140	24.780
	Rsk	Beta-21S	-0.160	-0.450	-0.350	-0.210	-0.190	-0.390
		BD	-0.250	-0.470	0.000	0.110	-0.290	-0.170
		Beta-21S	-0.220	0.030	0.350	-0.080	-0.290	0.630
	Rku	Beta-21S	3.020	3.640	3.620	3.440	3.650	3.210
		BD	3.330	4.490	2.900	2.980	2.940	2.490
		Beta-21S	3.020	3.140	3.450	2.960	2.930	3.720

Ti-Joint	Parameters (µm)	Location	Temperatures (C)				
			T4	T5	T6	T7	T8
Ti-54M/Ti-54M	Ra	Ti-54M	3.029	7.820	2.741	2.289	2.363
		BD	4.317	5.002	3.627	3.717	2.773
		Ti-54M	11.151	2.316	6.719	8.53	5.208
	Rq	Ti-54M	3.781	9.608	3.508	2.855	2.999
		BD	5.250	5.928	4.419	4.568	3.423
		Ti-54M	13.404	2.860	8.160	10.355	6.447
	Rz	Ti-54M	18.552	35.868	17.597	14.012	15.259
		BD	23.116	23.732	19.281	19.767	16.591
		Ti-54M	45.760	13.342	30.480	36.823	26.195
	Rt	Ti-54M	25.390	48.490	24.160	18.850	18.33
		BD	29.780	28.750	23.360	24.730	19.54
		Ti-54M	60.990	14.540	38.440	50.85	35.52
	Rsk	Ti-54M	0.130	0.490	-0.120	-0.020	-0.2
		BD	-0.020	0.040	-0.180	-0.010	0.04
		Ti-54M	0.550	-0.260	0.110	0.1	-0.01
	Rku	Ti-54M	3.020	2.710	3.430	2.940	3.1
		BD	2.460	2.160	2.400	2.670	2.72
		Ti-54M	2.460	2.570	2.430	2.59	2.55

Ti-Joint	Parameters (µm)	Location	Temperatures (C)			
			T1	T2	T5	T6
Ti-64FG/Ti-64FG	Ra	Ti-64FG	8.677	2.457	8.348	1.940
		BD	4.233	4.345	3.327	2.731
		Ti-64FG	2.425	8.583	2.669	4.204
	Rq	Ti-64FG	10.400	3.072	10.137	2.492
		BD	5.300	5.480	4.116	3.459
		Ti-64FG	3.040	10.781	3.294	5.079
	Rz	Ti-64FG	39.629	15.227	39.840	13.385
		BD	22.765	25.406	19.195	16.092
		Ti-64FG	14.845	40.658	15.770	20.296
	Rt	Ti-64FG	54.110	21.070	46.720	17.290
		BD	29.170	36.390	26.850	20.540
		Ti-64FG	18.140	59.230	18.900	29.9
	Rsk	Ti-64FG	-0.220	-0.100	0.120	-0.090
		BD	-0.060	0.130	-0.430	-0.330
		Ti-64FG	0.190	0.460	-0.250	0.18
	Rku	Ti-64FG	2.440	2.980	2.250	3.580
		BD	2.900	3.310	3.280	3.010
		Ti-64FG	2.780	3.290	2.590	2.77

Ti-Joint	Parameters (μm)	Location	Temperatures (C)						
			T1	T2	T3	T4	T5	T6	T7
Ti-6242/Ti-54M	Ra	Ti-6242	2.721	5.389	3.093	2.48	6.251	2.643	6.128
		BD	4.32	3.808	3.765	3.018	4.551	3.361	3.961
		Ti-54M	4.554	2.555	5.665	3.379	3.349	4.599	2.914
	Rq	Ti-6242	3.504	6.723	3.915	3.16	7.929	3.343	7.465
		BD	5.367	4.686	4.918	3.733	5.559	4.263	4.985
		Ti-54M	5.798	3.191	7.425	4.28	4.173	5.726	3.688
	Rz	Ti-6242	17.52	28.611	19.268	16.493	33.114	16.178	29.535
		BD	24.193	20.897	22.822	20.144	23.517	19.297	22.764
		Ti-54M	25.456	15.871	30.481	18.264	20.568	24.296	18.972
	Rt	Ti-6242	26.26	40.85	23.41	21.65	43.07	21.2	36.91
		BD	28.55	25.74	28.97	24.89	27.62	23.71	28.93
		Ti-54M	38.03	24.02	45.74	24.87	26.34	27.33	24.79
	RSm	Ti-6242	158.94	407.56	142.28	108.76	461	126.86	419.22
		BD	205	263.1	154.04	141.09	266.42	151.64	218.82
		Ti-54M	283.62	130.69	380.94	164.84	159.98	270	117.05
	Rsk	Ti-6242	0.62	-0.1	0.14	-0.12	0.47	-0.1	-0.02
		BD	0.58	-0.07	-0.11	-0.06	0.13	-0.39	-0.09
		Ti-54M	0.12	0.36	0.63	-0.27	0.11	0.16	-0.1
	Rku	Ti-6242	4.76	3.06	3.01	3.49	3.08	3.12	2.5
		BD	3.18	2.6	3.29	2.9	2.53	3.15	2.98
		Ti-54M	3.31	3.57	4.23	2.98	2.94	2.49	3.35

Ti-Joint	Parameters (µm)	Location	Temperatures (C)				
			T4	T5	T6	T7	T8
Ti-6242SG/Ti-64SG	Ra	Ti-6242SG	1.832	2.637	2.470	3.124	2.971
		BD	2.443	2.244	2.231	2.294	2.710
		Ti-64SG	3.303	2.041	3.230	2.812	2.971
	Rq	Ti-6242SG	2.267	3.475	3.115	3.950	3.867
		BD	3.152	2.877	2.890	3.006	3.426
		Ti-64SG	4.142	2.626	4.019	3.527	3.867
	Rz	Ti-6242SG	11.861	18.113	13.912	18.896	20.516
		BD	17.209	14.345	13.662	16.940	18.648
		Ti-64SG	19.241	13.279	18.616	18.071	20.516
	Rt	Ti-6242SG	14.150	27.010	19.650	21.920	28.720
		BD	24.020	18.830	20.320	21.560	23.630
		Ti-64SG	23.710	16.670	22.79	22.660	28.720
	Rsk	Ti-6242SG	-0.070	-0.080	0.050	-0.320	-0.440
		BD	-0.660	0.130	0.230	-0.200	0.060
		Ti-64SG	-0.380	0.120	-0.280	-0.270	-0.440
	Rku	Ti-6242SG	2.760	3.870	3.150	2.930	4.200
		BD	4.530	3.220	3.840	3.610	3.300
		Ti-64SG	3.220	3.210	2.820	3.200	4.200

Ti-Joint	Parameters (µm)	Location	Temperatures (C)				
			T4	T5	T6	T7	T8
Ti-6242/Ti-64FG	Ra	Ti-6242	2.617	2.729	4.224	4.345	2.743
		BD	3.79	4.88	3.642	3.188	3.306
		Ti-64FG	8.876	7.21	2.437	2.914	3.851
	Rq	Ti-6242	3.445	3.477	5.414	5.273	3.417
		BD	4.808	5.99	4.537	3.971	4.223
		Ti-64FG	11.193	8.705	3.141	3.563	4.824
	Rz	Ti-6242	17.876	18.646	25.671	21.655	17.169
		BD	21.509	25.324	21.061	18.465	21.293
		Ti-64FG	36.565	33.776	17.087	16.963	22.107
	Rt	Ti-6242	26.23	24.87	35.51	26.64	24.69
		BD	25.15	37.11	27.28	22.16	28.99
		Ti-64FG	63.37	39.67	20.66	20.91	29.37
	RSm	Ti-6242	116.8	117.86	258.77	320.04	129.09
		BD	211.58	273.19	155.31	155.28	144.37
		Ti-64FG	456.88	441.93	110.17	183.19	272.86
	Rsk	Ti-6242	0.01	-0.16	0.06	-0.08	-0.07
		BD	-0.37	-0.33	-0.06	-0.15	-0.1
		Ti-64FG	-0.14	0.21	0.16	0.04	-0.13
	Rku	Ti-6242	4.06	3.33	3.38	2.46	3.01
		BD	2.94	2.93	2.76	2.75	3.43
		Ti-64FG	3.27	2.31	3.39	2.61	3.3

Ti-Joint	Parameters (µm)	Location	Temperatures (C)			
			T5	T6	T7	T8
Ti-6242SG/Bea-21S	Ra	Ti-6242	2.959	2.909	3.714	2.817
		BD	2.494	2.601	3.035	2.542
		Beta-21S	2.454	2.962	2.715	3.080
	Rq	Ti-6242	3.856	3.563	4.872	3.486
		BD	3.106	3.302	3.851	3.268
		Beta-21S	3.141	3.730	3.501	3.990
	Rz	Ti-6242	19.894	16.616	24.837	16.884
		BD	15.337	15.573	18.606	15.963
		Beta-21S	16.176	19.079	17.801	20.566
	Rt	Ti-6242	25.510	20.210	33.850	20.910
		BD	18.160	23.870	22.200	21.150
		Beta-21S	21.640	23.040	28.370	28.760
	Rsk	Ti-6242	0.120	-0.340	-0.270	0.000
		BD	0.090	-0.290	-0.100	-0.340
		Beta-21S	0.090	-0.040	-0.810	0.110
	Rku	Ti-6242	3.520	2.700	3.660	2.760
		BD	2.900	3.480	3.070	3.710
		Beta-21S	3.300	3.070	5.210	3.820

Ti-Joint	Parameters (µm)	Location	Temperatures (C)						
			T1	T2	T3	T4	T5	T6	T7
Ti-64/Ti-54M	Ra	Ti-64	9.321	8.981	2.913	3.98	6.091	2.783	2.679
		BD	6.35	6.865	3.504	3.664	4.409	4.204	3.782
		Ti-54M	3.426	3.477	7.027	2.742	3.311	4.81	5.285
	Rq	Ti-64	11.326	10.687	3.807	4.852	7.598	3.534	3.393
		BD	7.702	8.656	4.486	4.657	5.536	5.434	4.769
		Ti-54M	4.238	4.395	8.782	3.45	4.353	5.887	6.623
	Rz	Ti-64	39.792	37.702	19.81	22.604	29.051	17.823	18.005
		BD	31.294	34.558	22.315	21.123	25.611	27.949	24.764
		Ti-54M	20.295	20.616	35.1	16.728	21.731	24.585	28.063
	Rt	Ti-64	54.37	53.76	33.96	27.34	38.95	23.92	8.23
		BD	37.68	47.11	27.13	28.08	33.42	39.62	31.44
		Ti-54M	26.23	28.34	47.6	21.84	30.69	32.48	34.05
	RSm	Ti-64	379.300	415.440	131.040	293.000	411.720	150.040	126.770
		BD	317.410	339.500	139.550	204.720	295.380	173.180	172.450
		Ti-54M	144.020	170.21	365.750	150.630	148.460	298.750	298.810
	Rsk	Ti-64	0.360	0.160	0.230	0.100	0.250	-0.130	-0.260
		BD	0.480	-0.010	-0.400	-0.410	0.150	-0.510	-0.220
		Ti-54M	-0.090	0.060	0.100	-0.030	0.640	0.210	0.430
	Rku	Ti-64	2.570	2.560	5.100	2.710	2.810	3.300	3.040
		BD	2.500	2.910	3.310	3.070	2.860	4.250	3.330
		Ti-54M	2.800	3.240	2.720	2.960	4.670	2.460	3.070

Ti-Joint	Parameters (µm)	Location	Temperatures(C)				
			T1	T2	T3	T4	T5
Ti-64FG//Ti-54M	Ra	Ti-64FG	3.269	6.559	5.227	2.480	3.702
		BD	3.922	3.514	3.169	3.142	4.433
		Ti-54M	6.394	2.45	2.989	7.217	7.608
	Rq	Ti-64FG	4.235	7.960	6.310	3.245	4.649
		BD	5.075	4.383	4.150	4.032	5.447
		Ti-54M	8.021	3.183	3.916	8.903	9.707
	Rz	Ti-64FG	21.035	29.114	24.899	17.966	21.358
		BD	23.054	20.726	20.221	20.291	24.098
		Ti-54M	30.682	17.506	20.605	33.426	36.573
	Rt	Ti-64FG	28.150	36.730	33.360	21.860	28.150
		BD	23.054	23.930	28.860	29.270	28.640
		Ti-54M	45.340	22.680	28.500	48.380	45.480
	RSm	Ti-64FG	126.070	378.280	313.060	121.450	156.000
		BD	179.830	193.690	141.350	178.91	242.000
		Ti-54M	399.560	119.790	106.130	506.930	539.250
	Rsk	Ti-64FG	-0.040	0.110	-0.080	-0.35	0.030
		BD	0.340	-0.260	0.640	0.000	-0.180
		Ti-54M	0.160	-0.410	-0.670	0.180	-0.010
	Rku	Ti-64FG	3.45	2.43	2.34	3.76	2.98
		BD	3.29	2.78	4.38	3.39	2.52
		Ti-54M	3.21	4.14	4.19	2.7	2.65

Ti-Joint	Parameters (µm)	Location	Temperatures(C)				
			T1	T2	T3	T4	T5
Ti-64SG/Ti-64FG	Ra	Ti-64SG	2.938	3.557	3.421	5.526	4.817
		BD	4.069	3.960	3.358	3.409	3.926
		Ti-64FG	5.036	5.374	5.217	3.115	3.263
	Rq	Ti-64SG	3.674	4.547	4.249	7.213	5.849
		BD	5.094	5.057	4.268	4.248	4.86
		Ti-64FG	6.313	6.781	6.554	4.099	4.111
	Rz	Ti-64SG	17.991	22.165	20.567	27.625	24.845
		BD	23.905	23.164	19.229	19.578	22.312
		Ti-64FG	26.107	29.163	27.221	19.528	19.786
	Rt	Ti-64SG	22.220	33.640	24.770	42.670	31.44
		BD	33.720	30.930	25.270	24.310	27.77
		Ti-64FG	36.680	36.180	39.720	30.25	24.6
	RSm	Ti-64SG	114.440	144.920	159.190	378.780	290.21
		BD	211.03	231.810	131.830	229.130	185.17
		Ti-64FG	256.500	449.000	468.810	143.380	126.4
	Rsk	Ti-64SG	0.150	0.250	-0.090	-0.050	-0.32
		BD	0.330	0.340	0.040	0.090	0.01
		Ti-64FG	-0.010	0.580	0.230	0.960	-0.26
	Rku	Ti-64SG	2.81	3.47	2.82	3.19	2.49
		BD	3.4	3.13	3.08	2.84	2.72
		Ti-64FG	2.97	3.16	2.85	5.83	3.03

Ti-Joint	Parameters (µm)	Location	Temperatures (C)						
			T1	T2	T3	T4	T5	T6	T7
Beta-21S/Ti-54M	Ra	Beta-21S	3.947	6.253	2.837	2.736	4.213	3.692	5.094
		BD	3.879	5.272	3.393	3.377	4.076	3.247	5.282
		Ti-54M	5.504	3.149	4.591	4.676	3.035	2.570	2.922
	Rq	Beta-21S	5.008	7.839	3.474	3.521	5.407	4.550	6.494
		BD	4.973	6.534	4.211	4.259	5.049	4.102	6.610
		Ti-54M	7.012	3.906	5.655	5.621	3.778	3.278	3.605
	Rz	Beta-21S	24.061	29.398	18.083	18.34	25.838	21.260	27.921
		BD	25.098	29.785	20.543	19.431	22.986	9.590	27.096
		Ti-54M	28.897	19.480	23.769	22.850	17.599	16.949	16.901
	Rt	Beta-21S	30.920	40.06	23.08	23.85	33.850	30.670	36.510
		BD	33.280	39.840	25.420	27.260	28.660	23.6	36.330
		Ti-54M	37.580	25.84	34.790	27.150	22.030	21.860	20.500
	RSm	Beta-21S	146.750	329.09	119.08	132.77	253.17	322.55	317.91
		BD	148.700	376.60	140.2	130.350	205.18	170.98	305.79
		Ti-54M	357.670	140.54	282.42	364.80	131.55	114.00	123.58
	Rsk	Beta-21S	-0.320	-0.09	0.04	-0.51	0.550	-0.020	0.100
		BD	-0.630	-0.160	-0.090	-0.040	-0.140	-0.380	0.370
		Ti-54M	0.560	-0.210	0.200	-0.290	-0.210	-0.210	-0.410
	Rku	Beta-21S	3.400	2.92	2.87	3.77	3.360	3.060	3.060
		BD	3.780	3.170	2.730	3.170	2.850	2.930	3.120
		Ti-54M	3.020	3.030	2.870	2.290	2.920	3.500	2.850

Ti-Joint	Parameter (µm)	Location	Temperatures (C)				
			T4	T5	T6	T7	T8
Beta-21S/Ti-64SG	Ra	Beta-21S	1.894	2.317	2.801	3.139	3.087
		BD	2.670	2.786	2.399	4.367	3.336
		Ti-64SG	3.225	2.152	3.446	9.910	2.853
	Rq	Beta-21S	2.466	2.912	3.676	3.989	3.899
		BD	3.467	3.412	3.075	5.065	4.241
		Ti-64SG	4.002	2.770	4.860	12.507	3.609
	Rz	Beta-21S	13.623	15.426	17.989	18.713	19.011
		BD	16.612	16.832	15.161	19.693	21.215
		Ti-64SG	18.504	15.056	19.981	53.923	18.320
	Rt	Beta-21S	17.770	18.150	27.430	25.110	22.560
		BD	23.650	19.640	21.050	22.07	28.160
		Ti-64SG	23.860	18.100	29.800	79.410	23.010
	Rsk	Beta-21S	-0.200	-0.080	0.410	0.120	0.060
		BD	0.160	-0.320	0.110	0.400	-0.050
		Ti-64SG	0.050	0.210	1.310	0.720	-0.060
	Rku	Beta-21S	3.650	3.120	4.690	3.100	2.920
		BD	3.470	2.760	3.340	2.030	3.340
		Ti-64SG	2.750	3.430	5.740	4.160	3.240

Ti-Joint	Parameters (µm)	Location	Temperatures (C)			
			T3	T4	T5	T6
Beta-21S/Ti--64FG	Ra	Beta-21S	3.098	3.004	2.162	3.002
		BD	2.375	2.595	2.554	2.519
		Ti-64FG	3.172	3.004	3.372	4.195
	Rq	Beta-21S	3.834	3.748	2.787	3.679
		BD	3.024	3.317	3.335	3.070
		Ti-64FG	3.983	3.748	4.308	5.604
	Rz	Beta-21S	18.025	17.477	14.035	16.943
		BD	15.196	16.149	16.952	14.620
		Ti-64FG	20.652	17.477	20.429	23.146
	Rt	Beta-21S	21.110	20.270	17.600	20.080
		BD	20.260	19.930	24.670	17.570
		Ti-64FG	27.070	20.270	25.430	34.23
	Rsk	Beta-21S	0.060	-0.190	0.320	-0.020
		BD	0.34	0.000	0.230	0.200
		Ti-64FG	-0.220	-0.190	0.250	-0.510
	Rku	Beta-21S	2.630	2.780	3.470	2.510
		BD	3.670	3.080	3.970	2.580
		Ti-64FG	3.390	2.780	3.190	3.790

Ti-Joint	Parameters (µm)	Location	Temperatures (C)				
			T4	T5	T6	T7	T8
Ti-64FG/Beta-21S	Ra	Ti-64FG	2.722	2.999	5.725	3.107	3.968
		BD	5.762	4.583	3.260	5.577	3.425
		Beta-21S	8.708	5.271	4.771	7.321	2.945
	Rq	Ti-64FG	3.412	3.813	7.150	4.049	4.963
		BD	7.006	5.656	4.109	6.816	4.258
		Beta-21S	10.485	6.784	5.949	9.296	3.661
	Rz	Ti-64FG	15.657	19.521	29.323	20.622	21.398
		BD	27.752	24.993	21.757	26.356	20.238
		Beta-21S	38.356	29.757	27.605	33.614	17.449
	Rt	Ti-64FG	20.140	27.250	39.120	27.450	28.270
		BD	37.650	30.370	23.460	35.710	28.360
		Beta-21S	54.560	42.020	33.82	44.070	19.530
	RSm	Ti-64FG	122.700	132.790	489.640	157.080	272.890
		BD	302.270	217.250	126.180	327.770	144.280
		Beta-21S	419.060	305.730	148.270	454.190	105.870
	Rsk	Ti-64FG	0.000	-0.040	0.400	0.360	-0.280
		BD	-0.350	0.070	-0.330	-0.030	-0.060
		Beta-21S	0.160	-0.150	-0.590	0.190	-0.190
	Rku	Ti-64FG	3.020	3.250	3.030	4.240	2.900
		BD	2.780	2.710	2.970	2.440	2.940
		Beta-21S	2.420	3.550	3.120	2.620	2.790

F.LOAD DISPLACEMENT CURVES OF FRICTION STIR WELDED TITANIUM JOINTS

The load displacement curves of the friction stir welded tensile samples for similar and dissimilar titanium alloys subjected to tensile tests are included in this section.

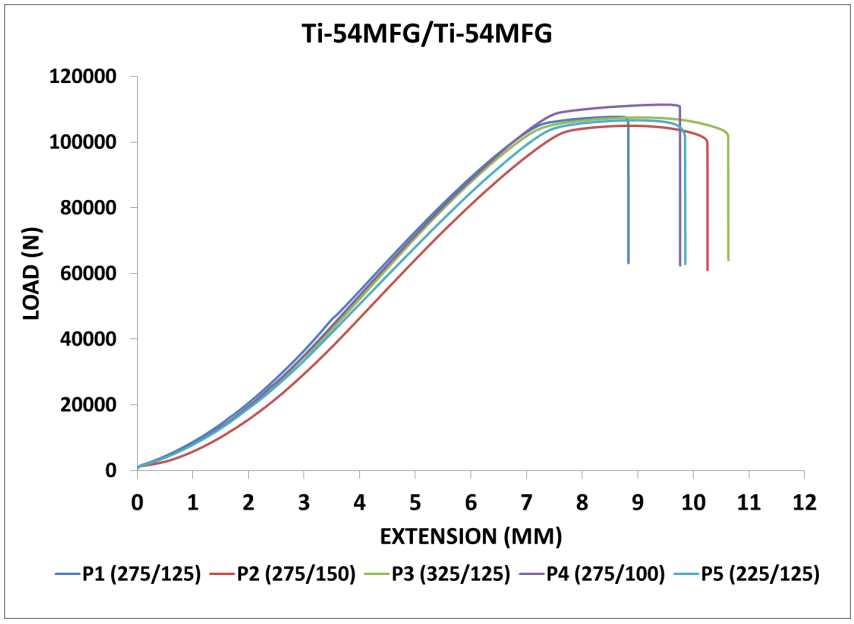

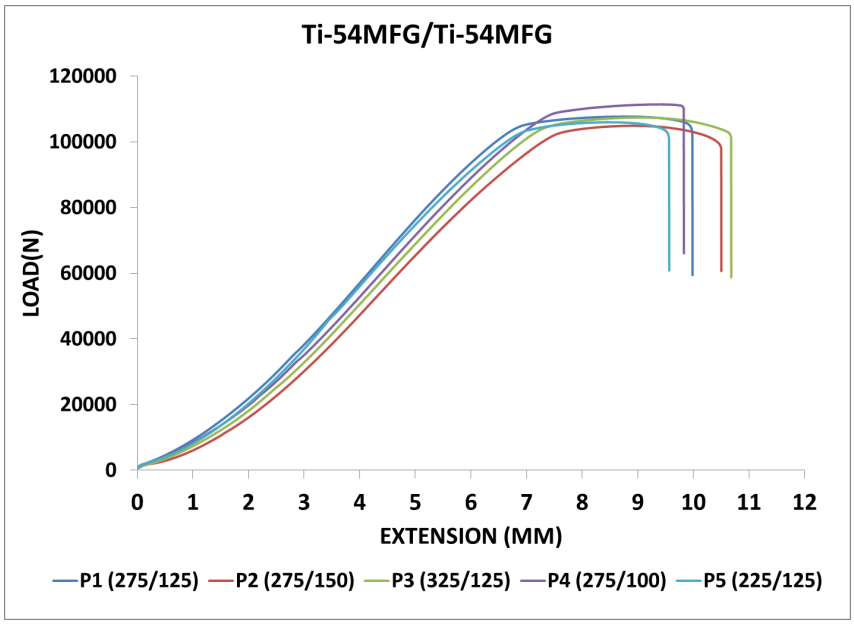

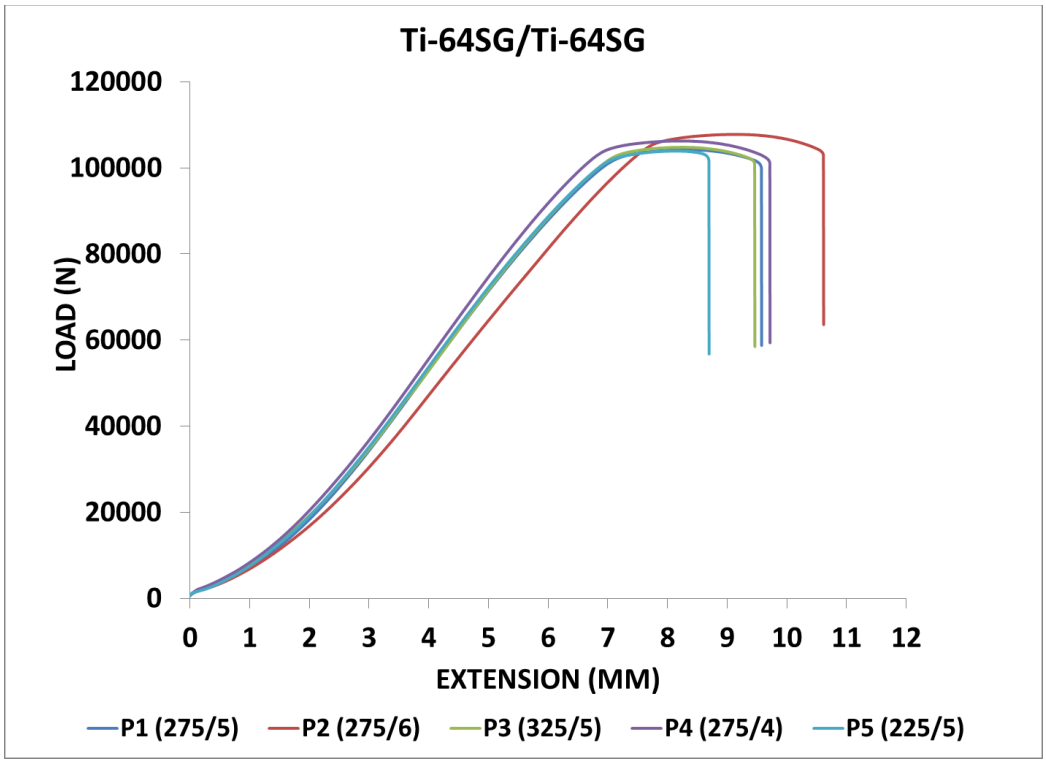
Ti-64SG/Ti-64SG
120000
100000
80000
60000
40000
20000
0
LOAD (N)
0 1 2 3 4 5 6 7 8 9 10 11 12
EXTENSION (MM)
P1 (275/5)
P2 (275/6)
P3 (325/5)
P4 (275/4)
P5 (225/5)

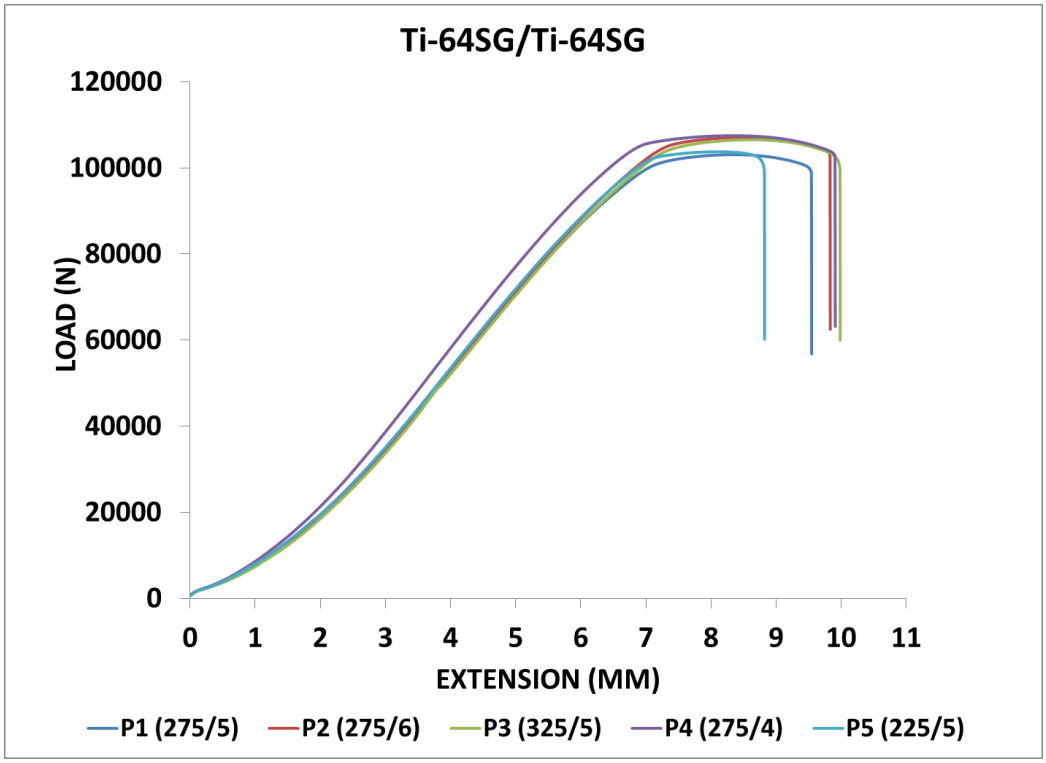
Ti-64SG/Ti-64SG
120000
100000
80000
60000
40000
20000
0
LOAD (N)
0 1 2 3 4 5 6 7 8 9 10 11
EXTENSION (MM)
P1 (275/5)
P2 (275/6)
P3 (325/5)
P4 (275/4)
P5 (225/5)

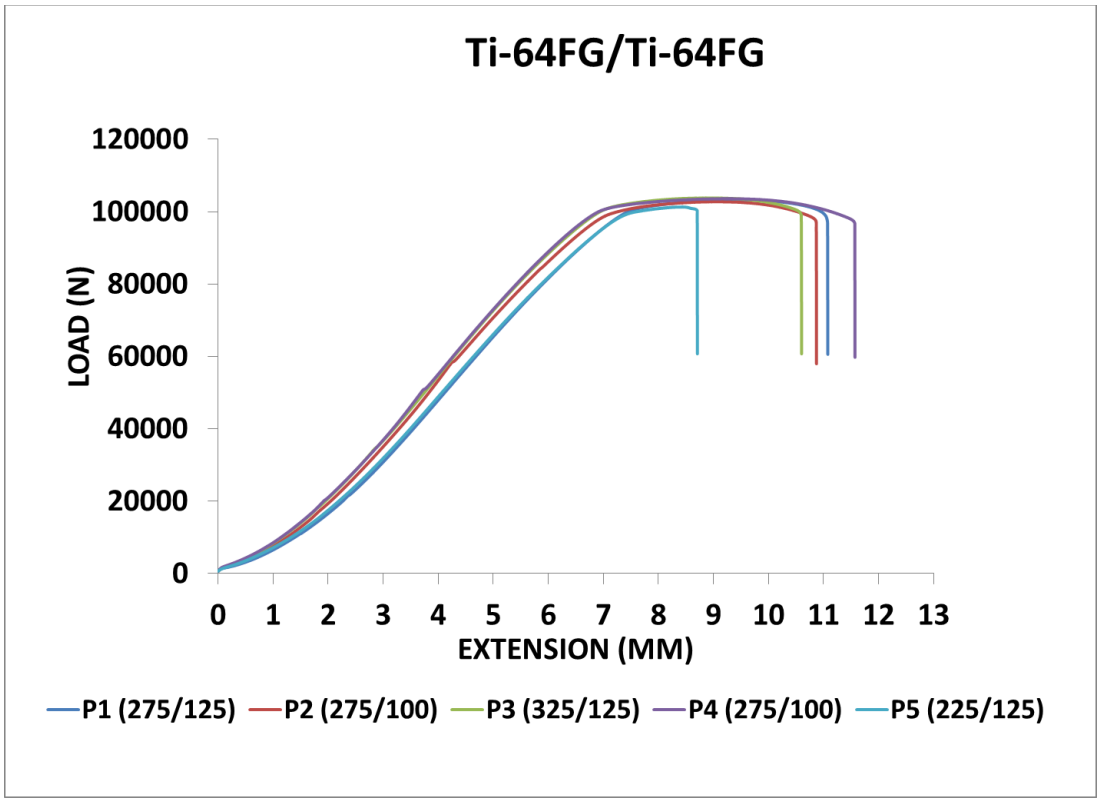
Ti-64FG/Ti-64FG
120000
100000
80000
60000
40000
20000
0
LOAD (N)
0 1 2 3 4 5 6 7 8 9 10 11 12 13
EXTENSION (MM)
P1 (275/125)
P2 (275/100)
P3 (325/125)
P4 (275/100)
P5 (225/125)

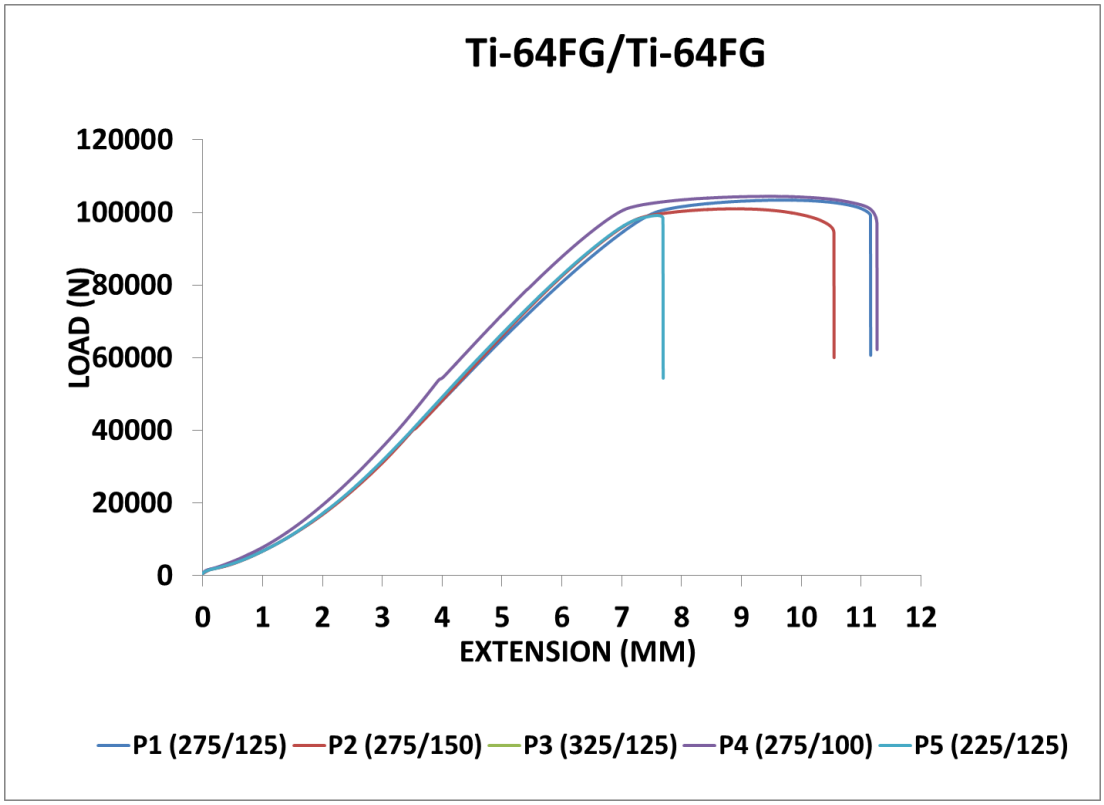
Ti-64FG/Ti-64FG
120000
100000
80000
60000
40000
20000
0
LOAD (N)
0 1 2 3 4 5 6 7 8 9 10 11 12
EXTENSION (MM)
P1 (275/125)
P2 (275/150)
P3 (325/125)
P4 (275/100)
P5 (225/125)

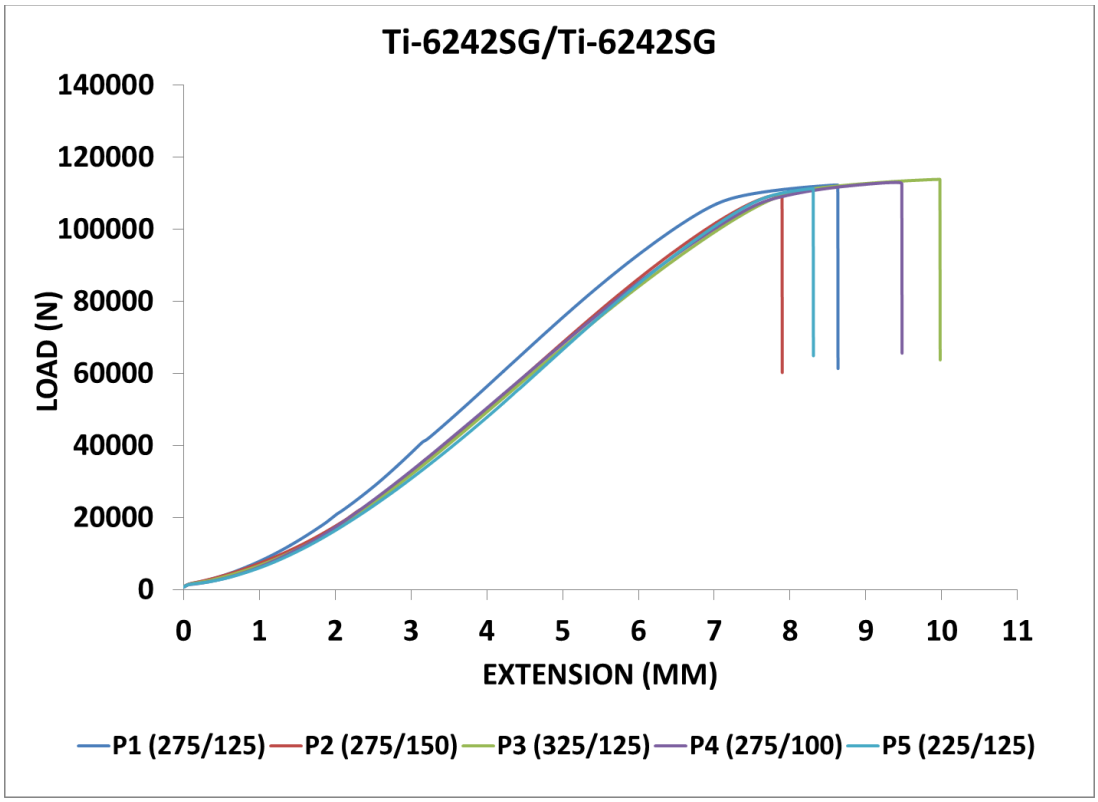
Ti-6242SG/Ti-6242SG
140000
120000
100000
80000
60000
40000
20000
0
LOAD (N)
0 1 2 3 4 5 6 7 8 9 10 11
EXTENSION (MM)
P1 (275/125)
P2 (275/150)
P3 (325/125)
P4 (275/100)
P5 (225/125)

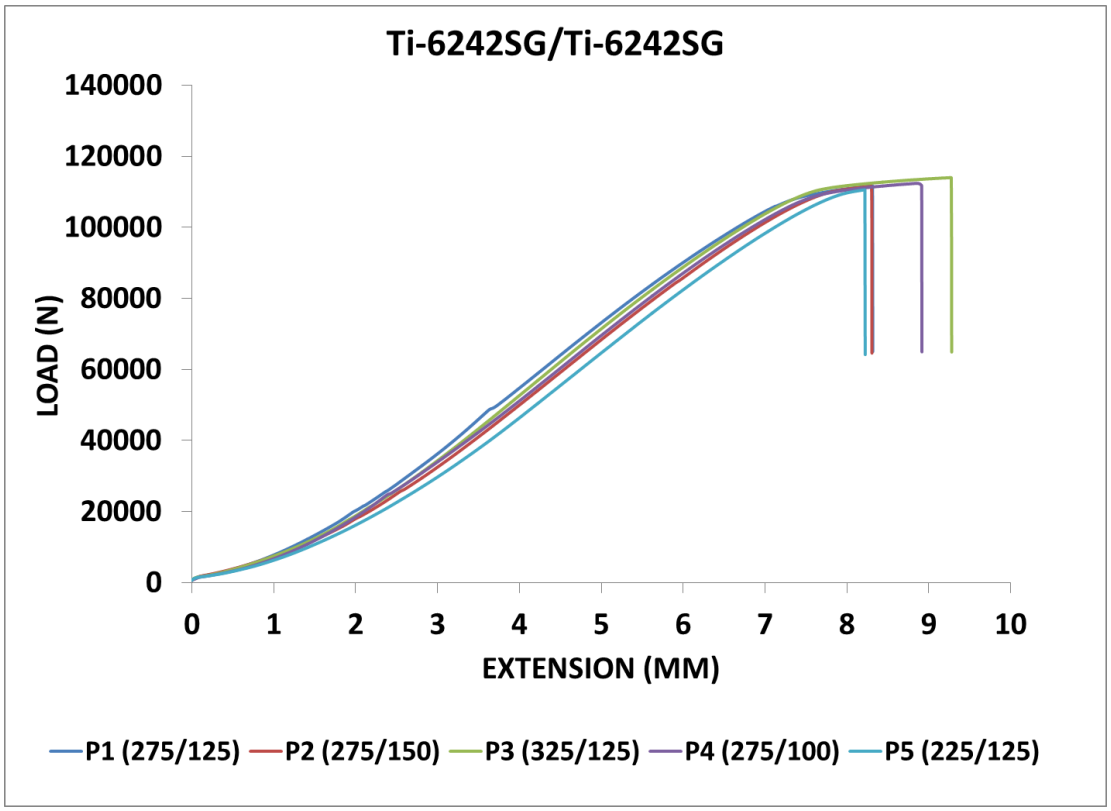
Ti-6242SG/Ti-6242SG
140000
120000
100000
80000
60000
40000
20000
0
LOAD (N)
0 1 2 3 4 5 6 7 8 9 10
EXTENSION (MM)
P1 (275/125)
P2 (275/150)
P3 (325/125)
P4 (275/100)
P5 (225/125)

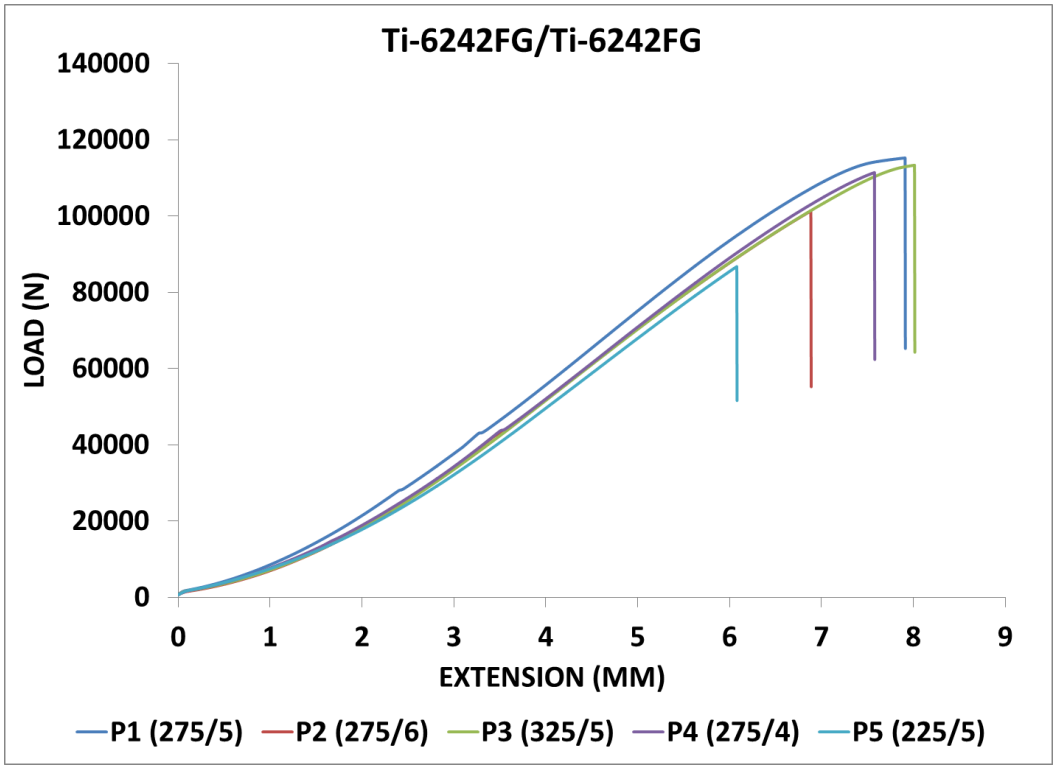
Ti-6242FG/Ti-6242FG
140000
120000
100000
80000
60000
40000
20000
0
LOAD (N)
0
1
2
3
4
5
6
7
8
9
EXTENSION (MM)
P1 (275/5)
P2 (275/6)
P3 (325/5)
P4 (275/4)
P5 (225/5)

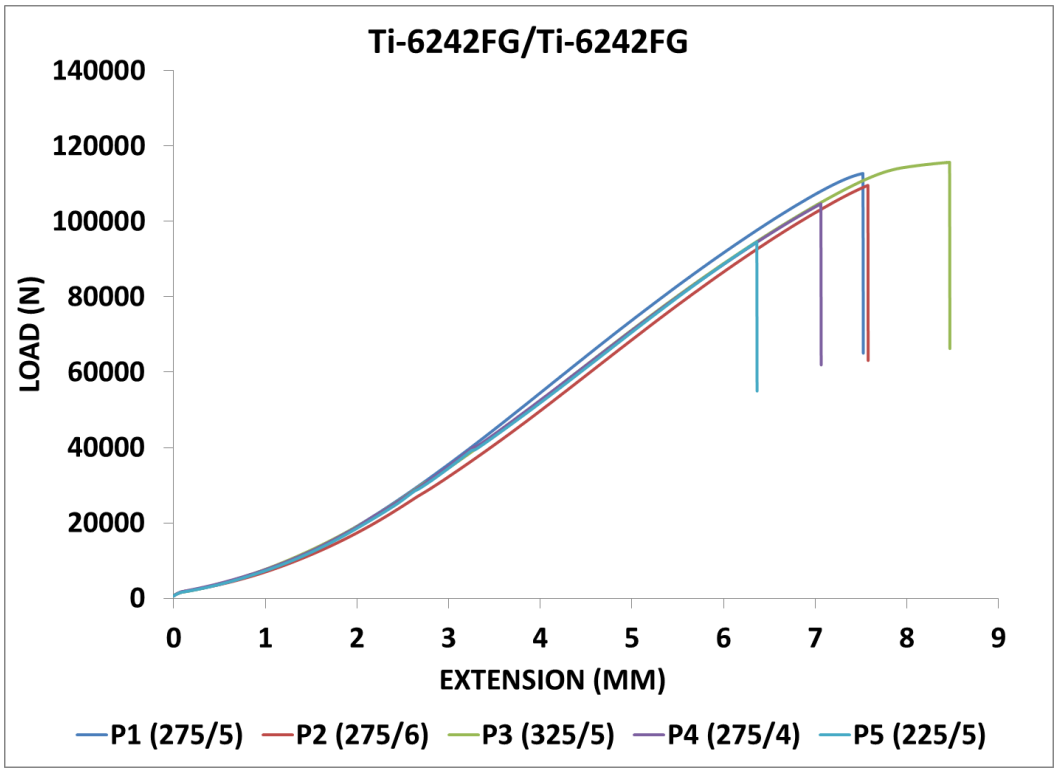
Ti-6242FG/Ti-6242FG
140000
120000
100000
80000
60000
40000
20000
0
LOAD (N)
0
1
2
3
4
5
6
7
8
9
EXTENSION (MM)
P1 (275/5)
P2 (275/6)
P3 (325/5)
P4 (275/4)
P5 (225/5)

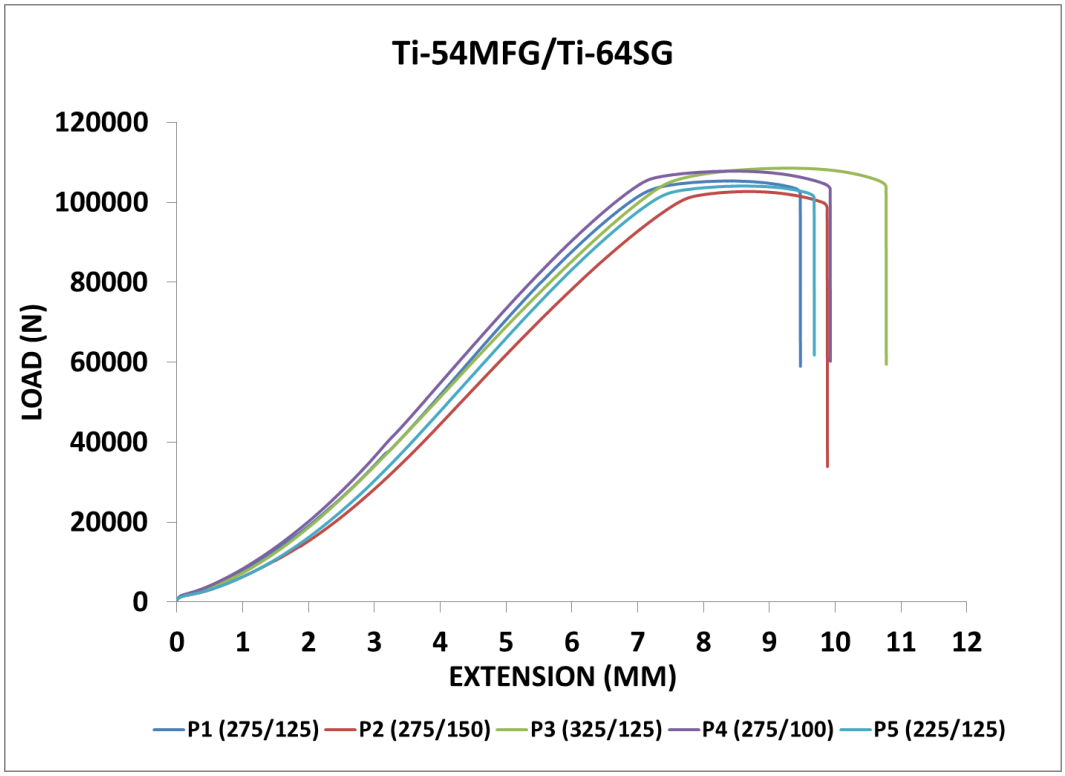
Ti-54MFG/Ti-64SG
120000
100000
80000
60000
40000
20000
0
LOAD (N)
0 1 2 3 4 5 6 7 8 9 10 11 12
EXTENSION (MM)
P1 (275/125)
P2 (275/150)
P3 (325/125)
P4 (275/100)
P5 (225/125)

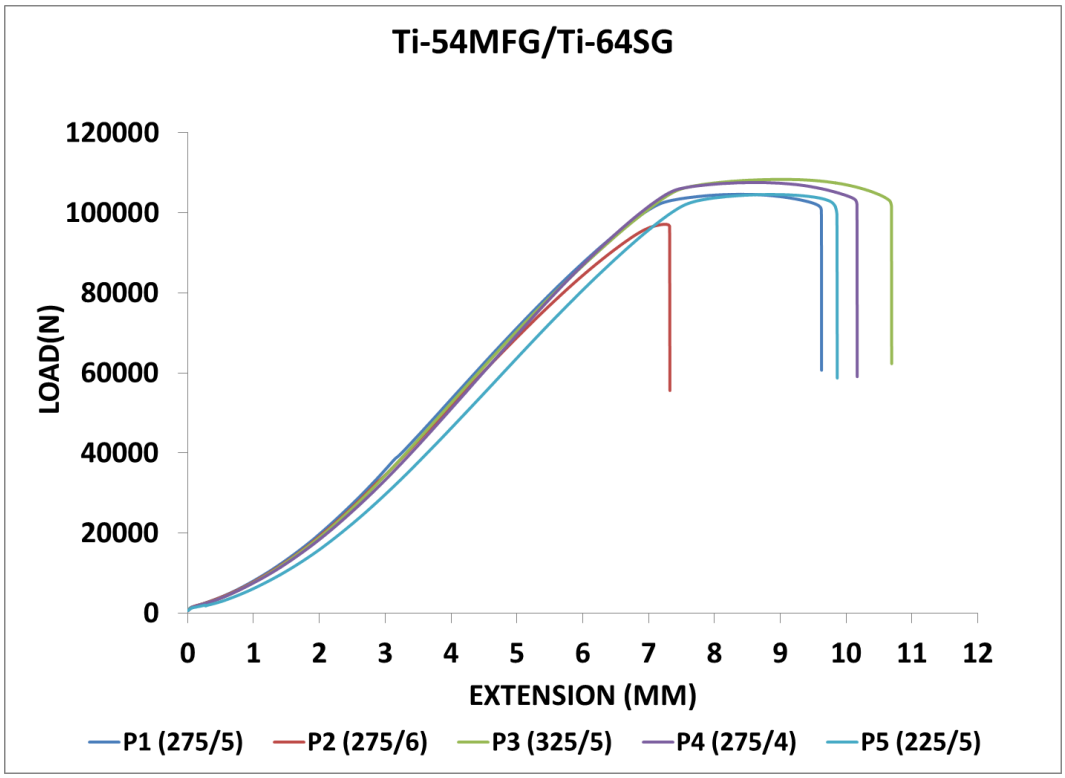
Ti-54MFG/Ti-64SG
120000
100000
80000
60000
40000
20000
0
LOAD(N)
0 1 2 3 4 5 6 7 8 9 10 11 12
EXTENSION (MM)
P1 (275/5)
P2 (275/6)
P3 (325/5)
P4 (275/4)
P5 (225/5)

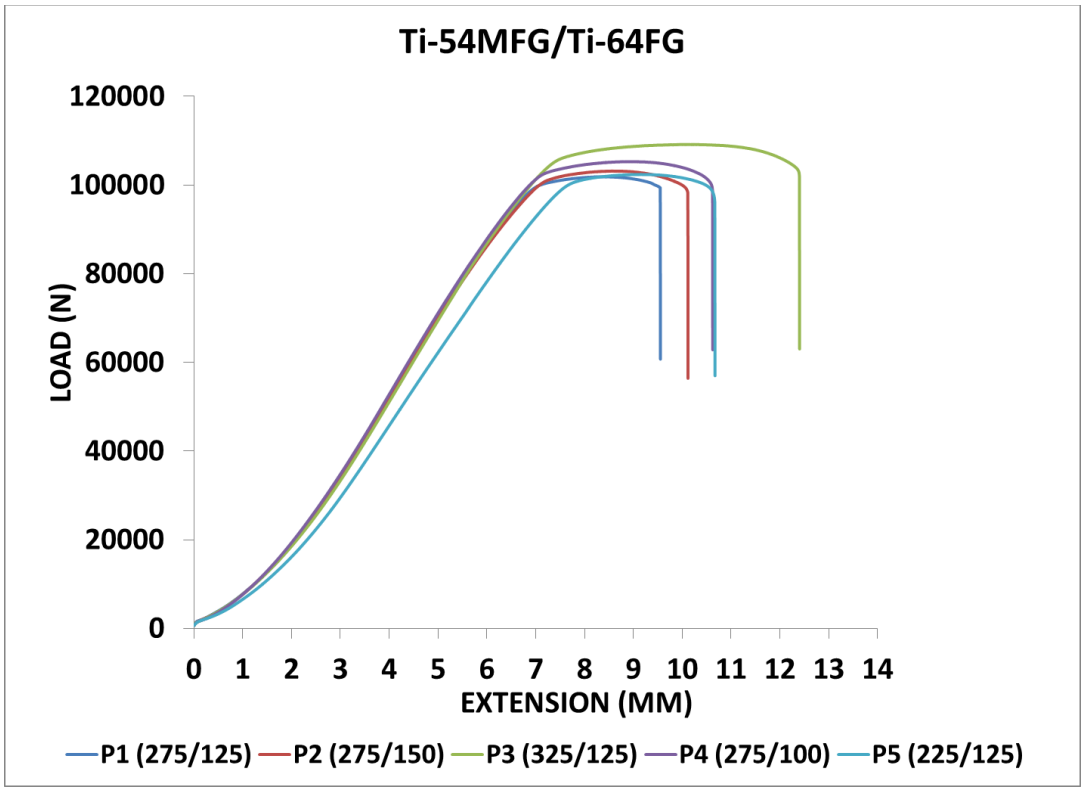
Ti-54MFG/Ti-64FG
120000
100000
80000
60000
40000
20000
0
LOAD (N)
0 1 2 3 4 5 6 7 8 9 10 11 12 13 14
EXTENSION (MM)
P1 (275/125)
P2 (275/150)
P3 (325/125)
P4 (275/100)
P5 (225/125)

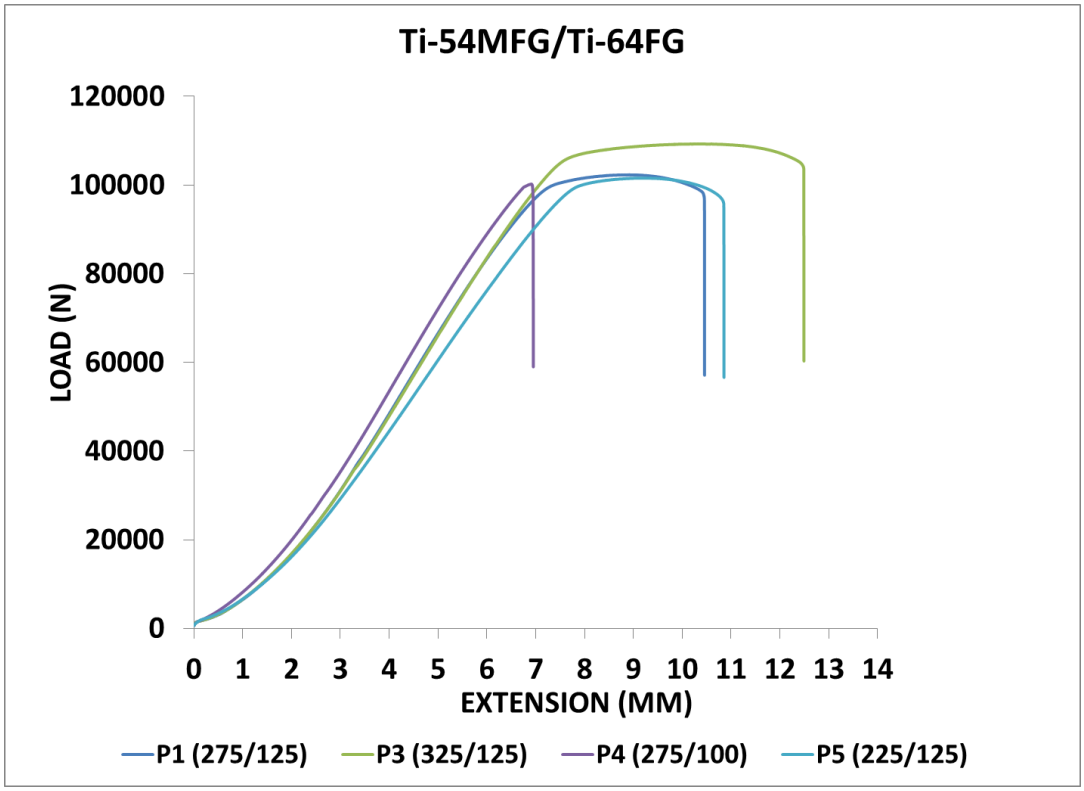
Ti-54MFG/Ti-64FG
120000
100000
80000
60000
40000
20000
0
LOAD (N)
0 1 2 3 4 5 6 7 8 9 10 11 12 13 14
EXTENSION (MM)
P1 (275/125)
P3 (325/125)
P4 (275/100)
P5 (225/125)

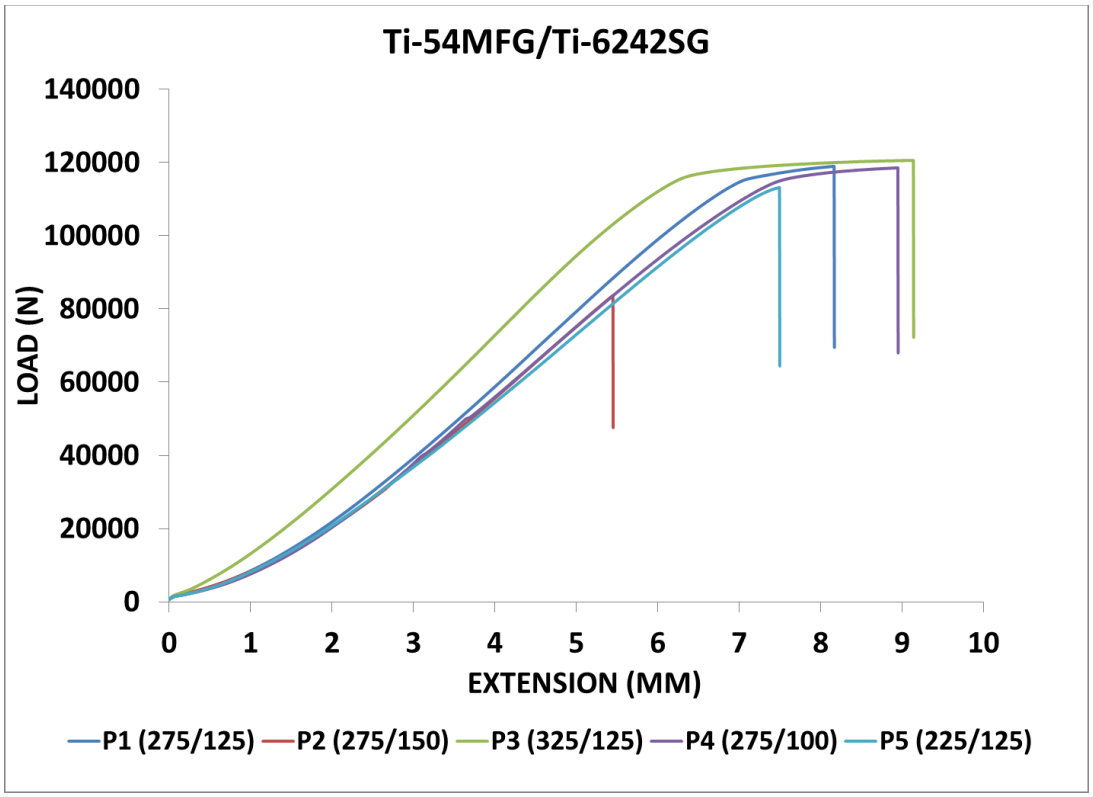
Ti-54MFG/Ti-6242SG
140000
120000
100000
80000
60000
40000
20000
0
LOAD (N)
0 1 2 3 4 5 6 7 8 9 10
EXTENSION (MM)
P1 (275/125) P2 (275/150) P3 (325/125) P4 (275/100) P5 (225/125)

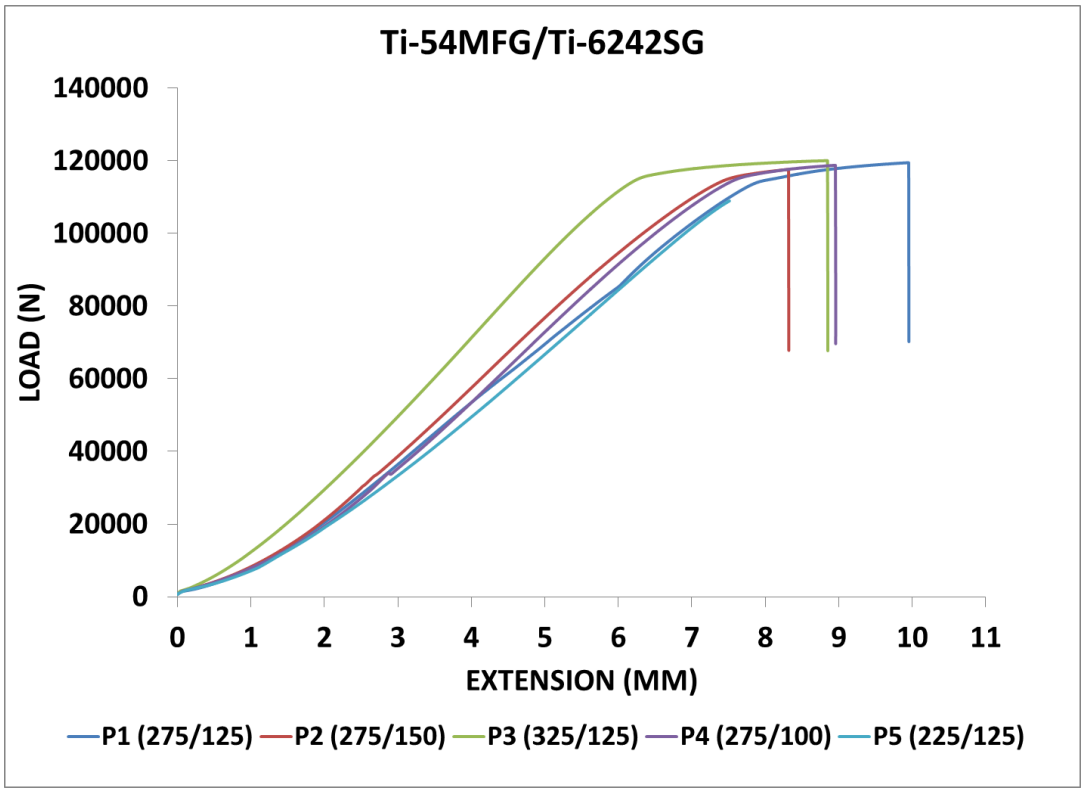
Ti-54MFG/Ti-6242SG
140000
120000
100000
80000
60000
40000
20000
0
LOAD (N)
0 1 2 3 4 5 6 7 8 9 10 11
EXTENSION (MM)
P1 (275/125) P2 (275/150) P3 (325/125) P4 (275/100) P5 (225/125)

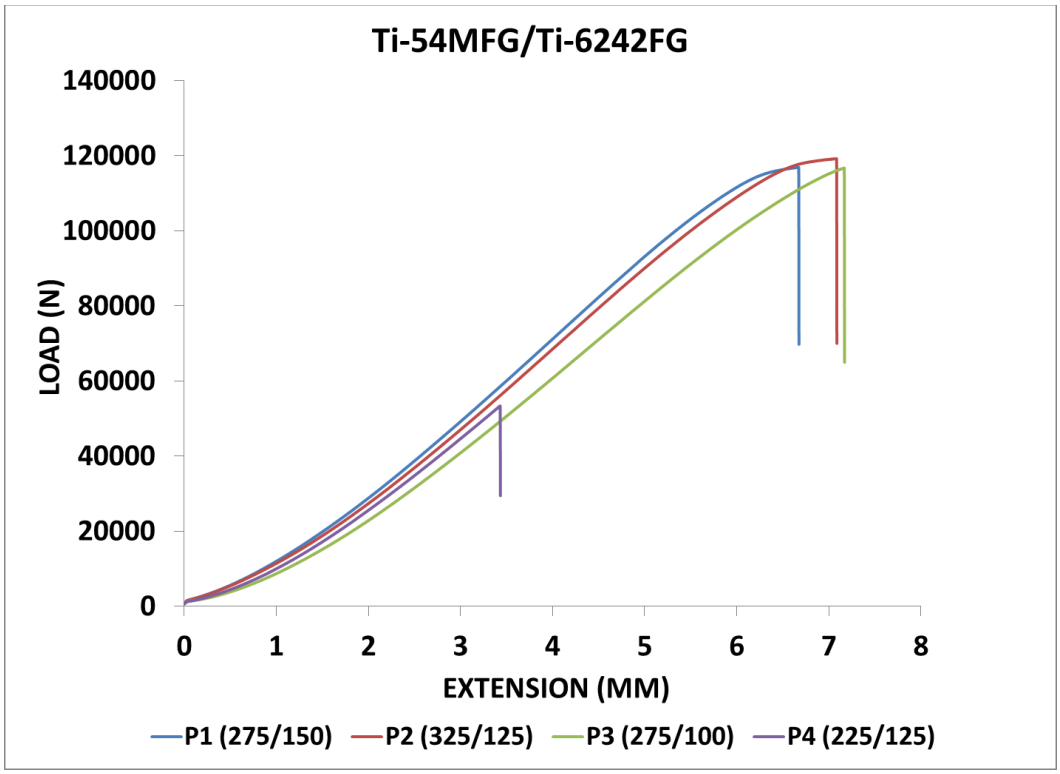
Ti-54MFG/Ti-6242FG
140000
120000
100000
80000
60000
40000
20000
0
LOAD (N)
0
1
2
3
4
5
6
7
8
EXTENSION (MM)
P1 (275/150)
P2 (325/125)
P3 (275/100)
P4 (225/125)

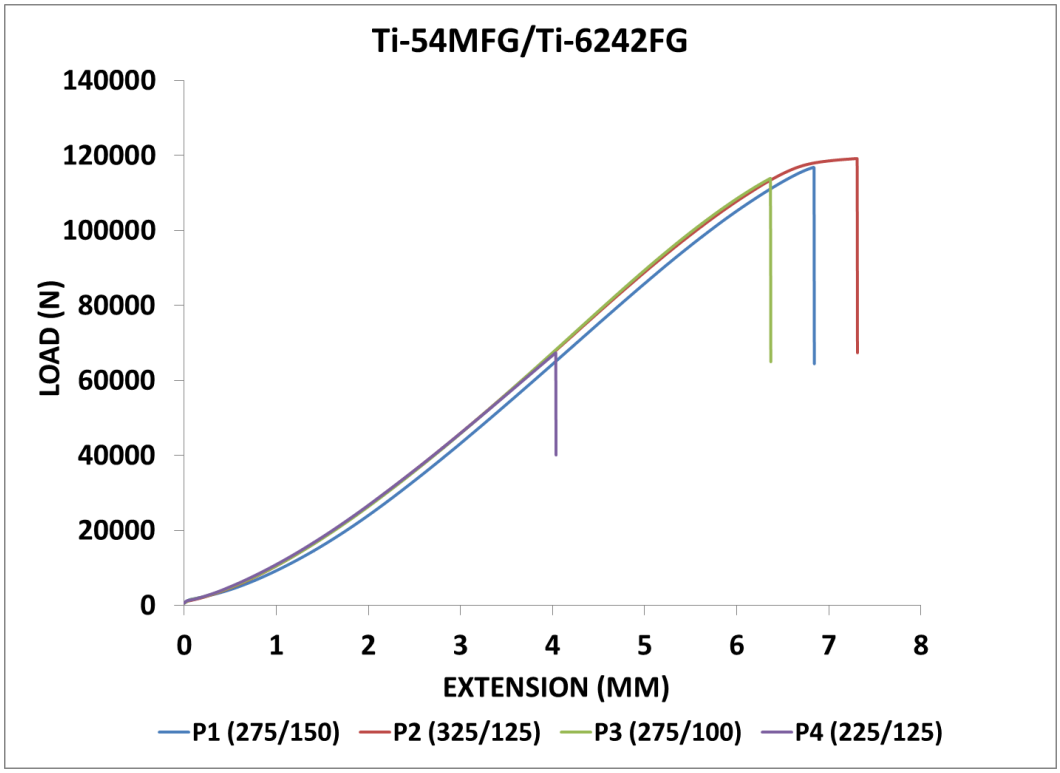
Ti-54MFG/Ti-6242FG
140000
120000
100000
80000
60000
40000
20000
0
LOAD (N)
0
1
2
3
4
5
6
7
8
EXTENSION (MM)
P1 (275/150)
P2 (325/125)
P3 (275/100)
P4 (225/125)

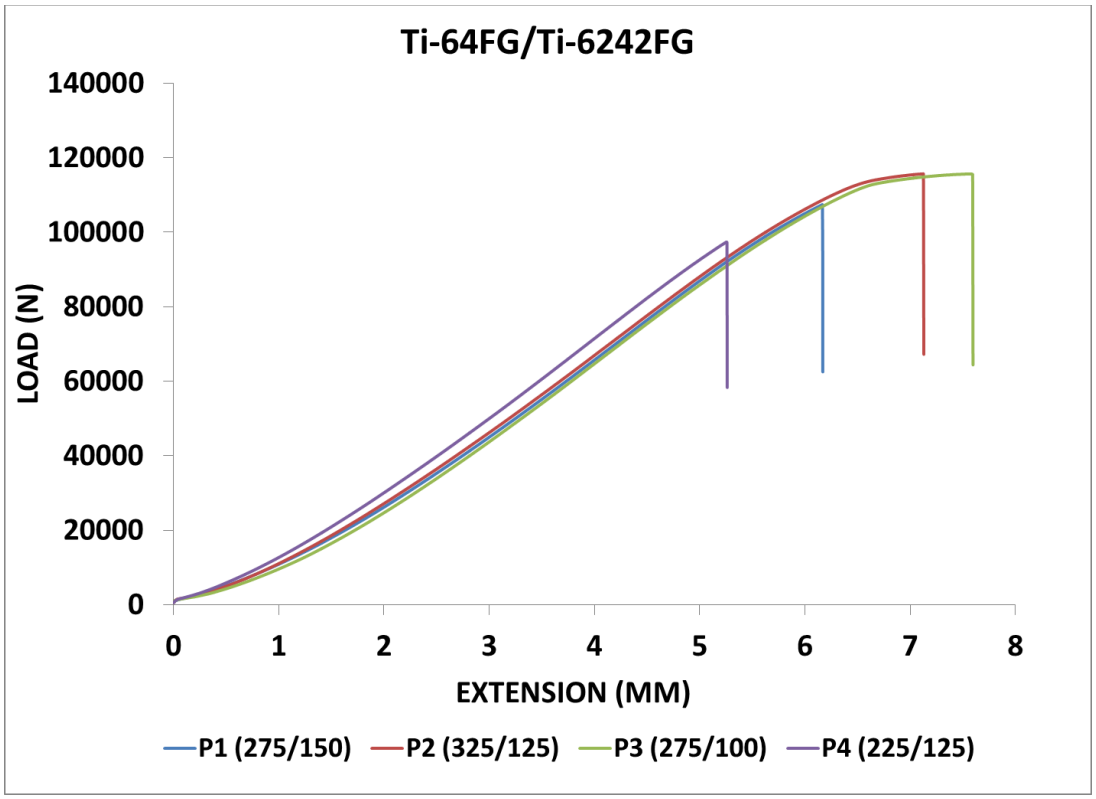
Ti-64FG/Ti-6242FG
140000
120000
100000
80000
60000
40000
20000
0
LOAD (N)
0
1
2
3
4
5
6
7
8
EXTENSION (MM)
P1 (275/150)
P2 (325/125)
P3 (275/100)
P4 (225/125)

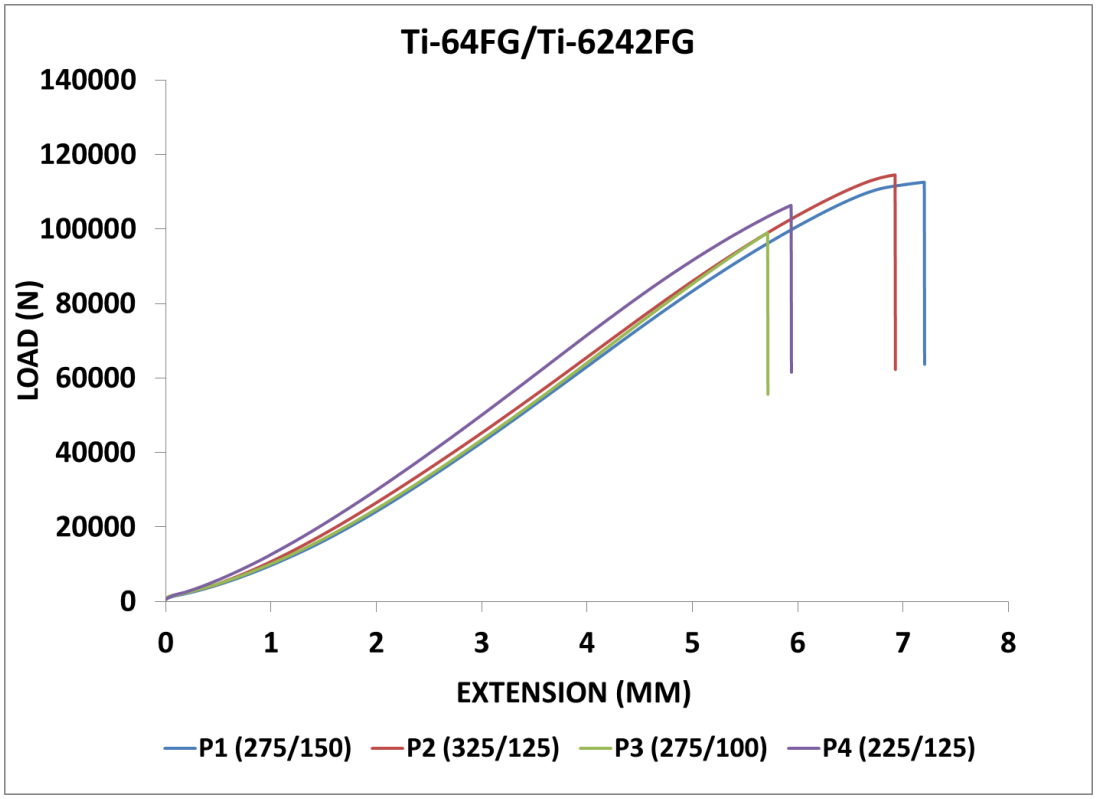
Ti-64FG/Ti-6242FG
140000
120000
100000
80000
60000
40000
20000
0
LOAD (N)
0
1
2
3
4
5
6
7
8
EXTENSION (MM)
P1 (275/150)
P2 (325/125)
P3 (275/100)
P4 (225/125)

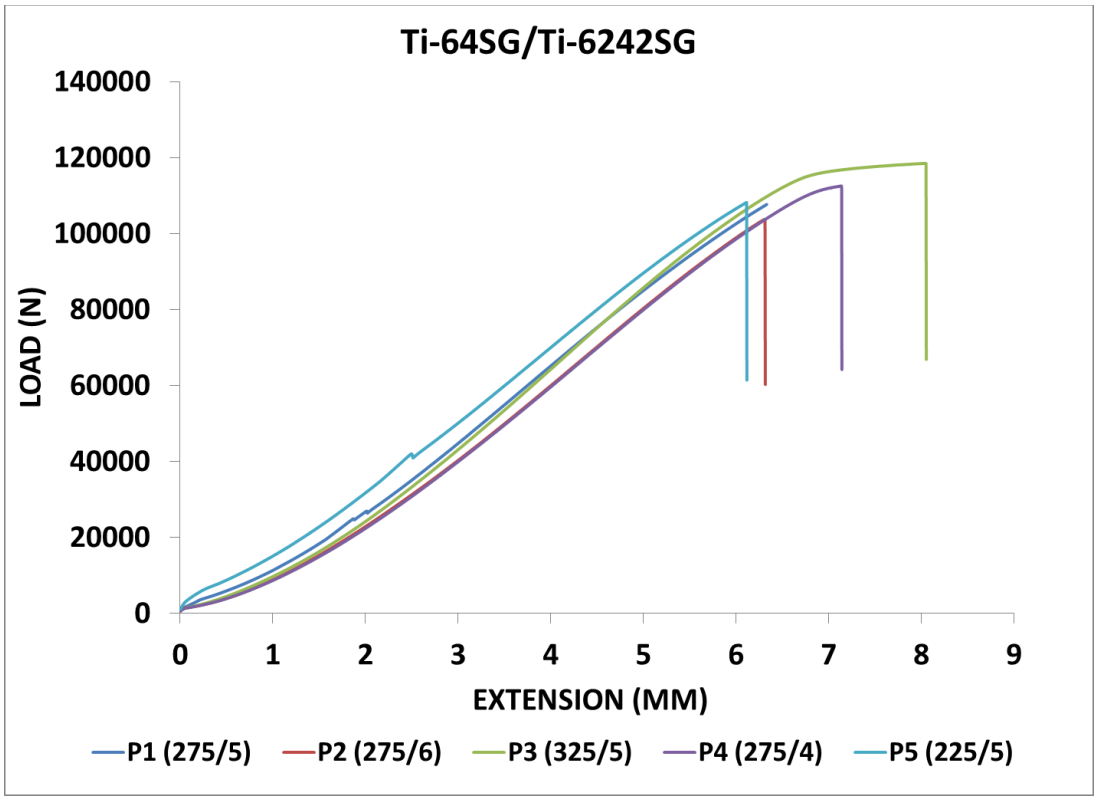
Ti-64SG/Ti-6242SG
LOAD (N)
140000
120000
100000
80000
60000
40000
20000
0
0 1 2 3 4 5 6 7 8 9
EXTENSION (MM)
P1 (275/5)
P2 (275/6)
P3 (325/5)
P4 (275/4)
P5 (225/5)

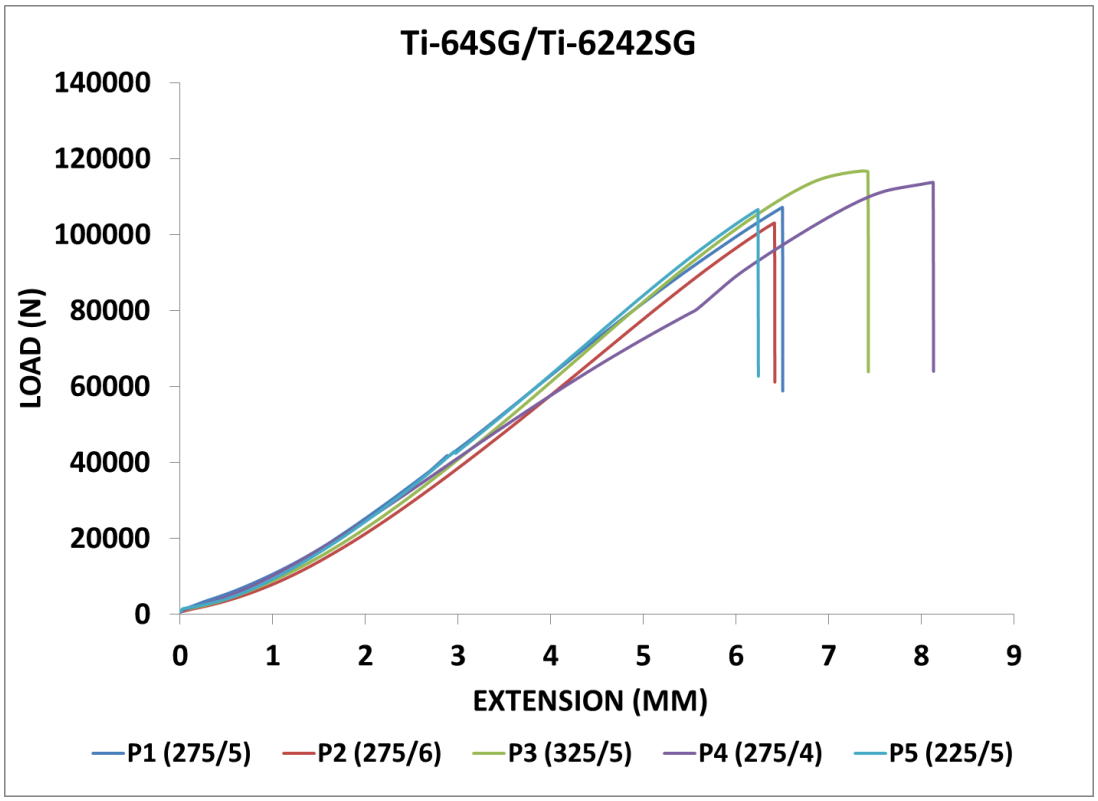
Ti-64SG/Ti-6242SG
LOAD (N)
140000
120000
100000
80000
60000
40000
20000
0
0 1 2 3 4 5 6 7 8 9
EXTENSION (MM)
P1 (275/5)
P2 (275/6)
P3 (325/5)
P4 (275/4)
P5 (225/5)

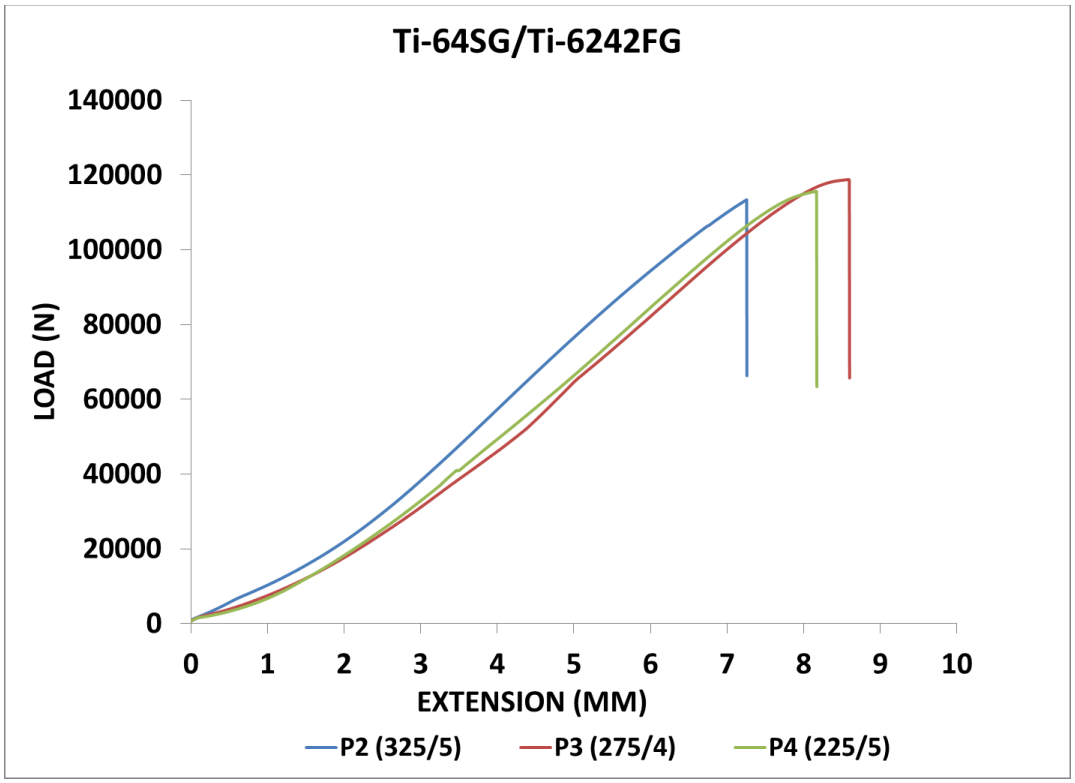
Ti-64SG/Ti-6242FG
140000
120000
100000
80000
60000
40000
20000
0
LOAD (N)
0
1
2
3
4
5
6
7
8
9
10
EXTENSION (MM)
P2 (325/5)
P3 (275/4)
P4 (225/5)

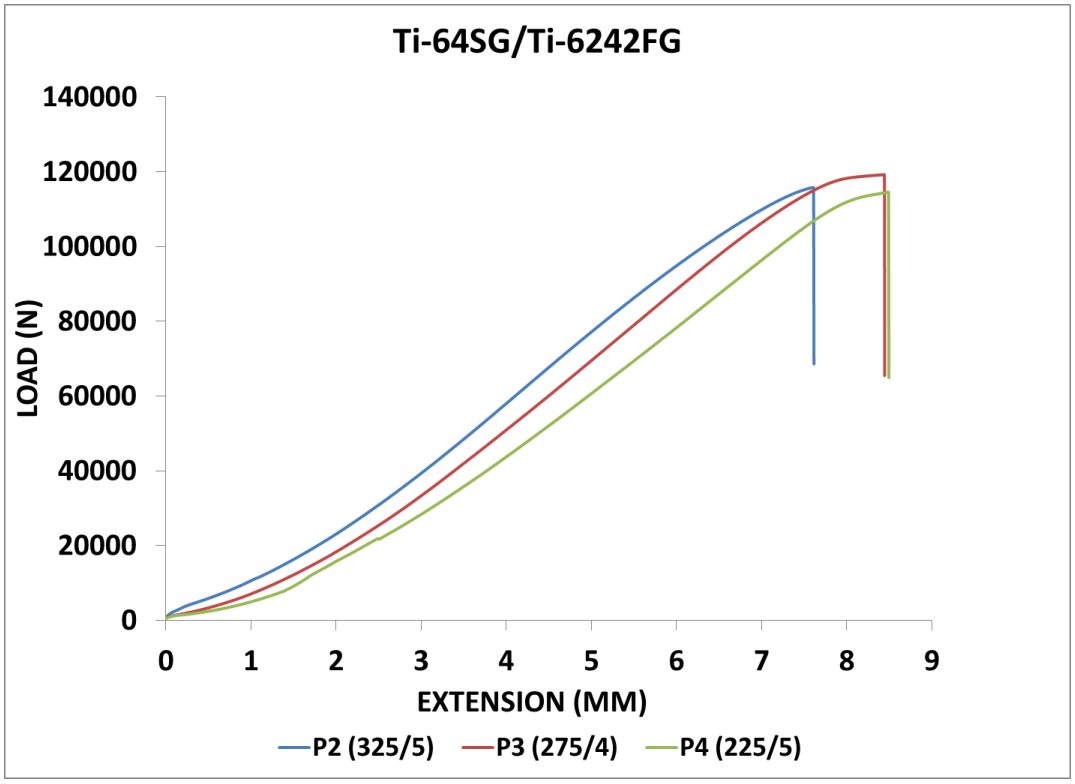
Ti-64SG/Ti-6242FG
140000
120000
100000
80000
60000
40000
20000
0
LOAD (N)
0
1
2
3
4
5
6
7
8
9
EXTENSION (MM)
P2 (325/5)
P3 (275/4)
P4 (225/5)

G. SURFACE PROFILES FOR FRICTION STIR WELDED SIMILAR AND DISSIMLAR TITANIUM JOINTS

G.1 Surface Profiles of Weld Nugget

The surface profiles of the nugget region of the friction stir welded joints formed from similar and dissimilar titanium alloys are included in this section. The profiles measured in the both transverse and the longitudinal directions are present. The measurements performed at the different process conditions of spindle speed and the feed rate are shown for all the welded joints.

1) Ti-54MFG/Ti-54MFG Weld Nugget in Transverse direction RPM/ mm min-1 (225/125, 275/100, 275/125, 275/150, 325/125)

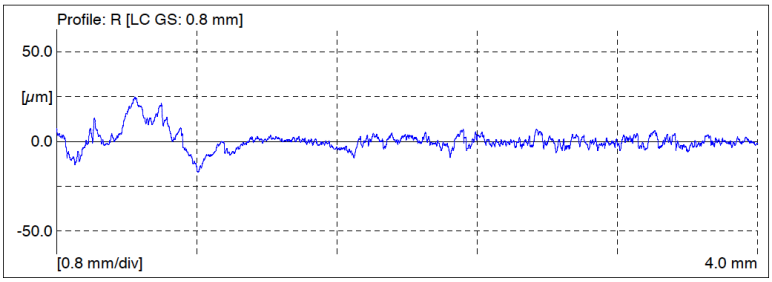

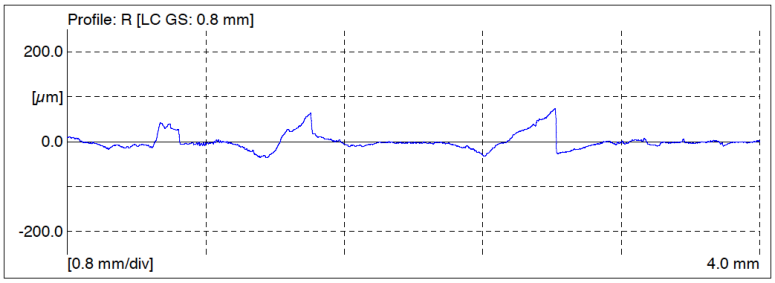

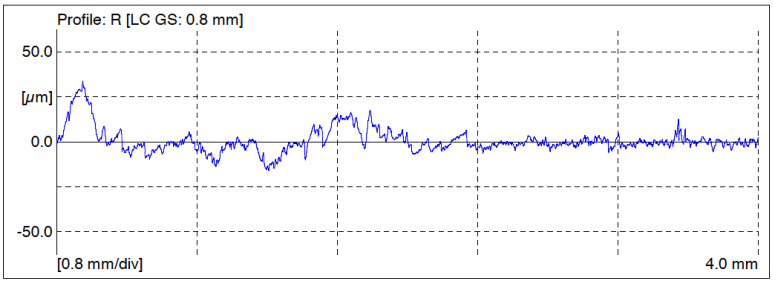

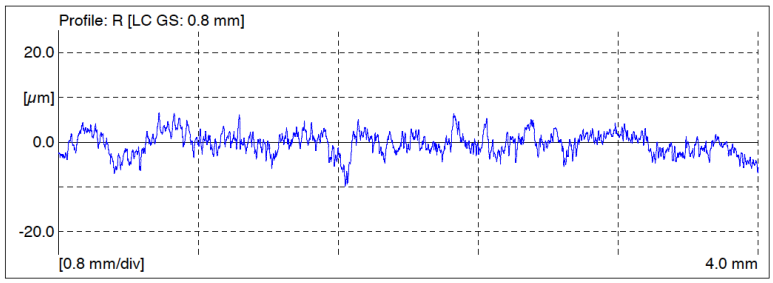
Profile: R [LC GS: 0.8 mm]
20.0
[µm]
0.0
-20.0
[0.8 mm/div]
4.0 mm

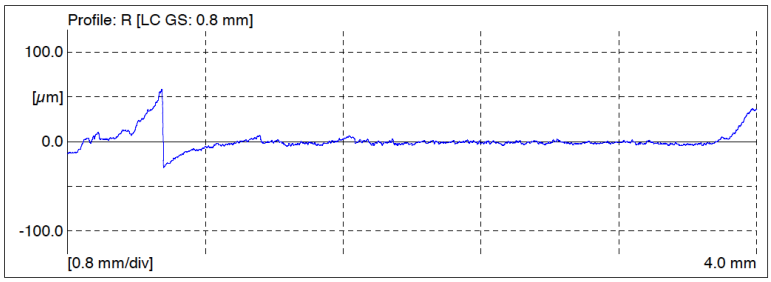
Profile: R [LC GS: 0.8 mm]
100.0
[µm]
0.0
-100.0
[0.8 mm/div]
4.0 mm

2) Ti-54MFG/Ti-54MFG Weld Nugget in Longitudinal direction RPM/ mm min-1 (225/125, 275/100, 275/125, 275/150, 325/125)

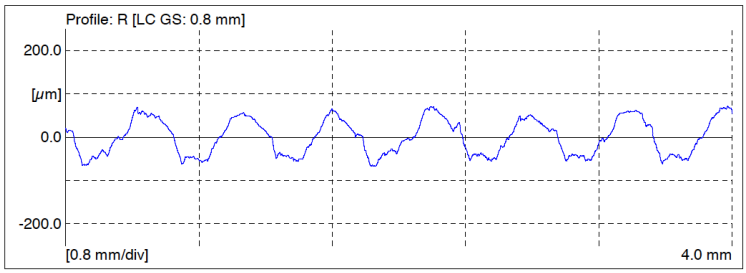

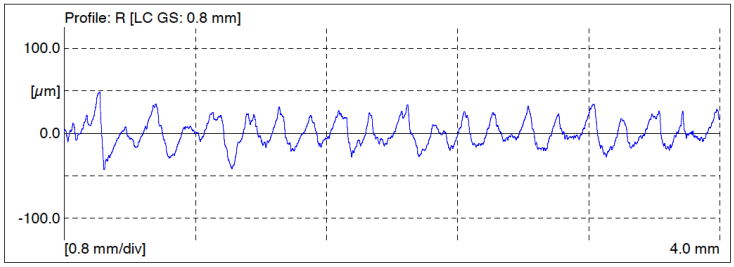

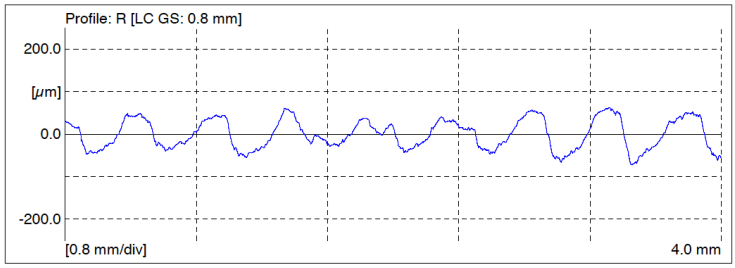

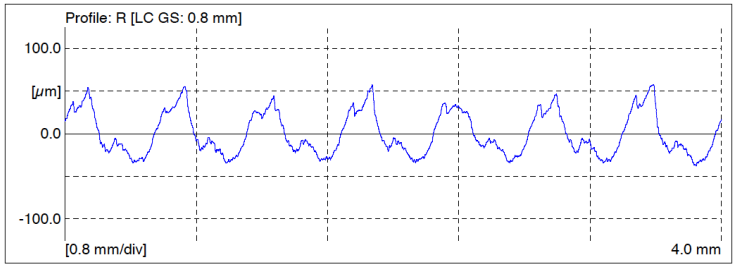

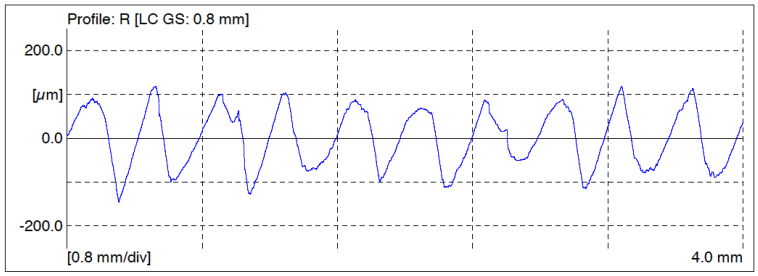

3) Ti-64SG/Ti-64SG Weld Nugget inTransverse direction RPM/ mm min-1 (225/125, 275/100, 275/125, 275/150, 325/125)

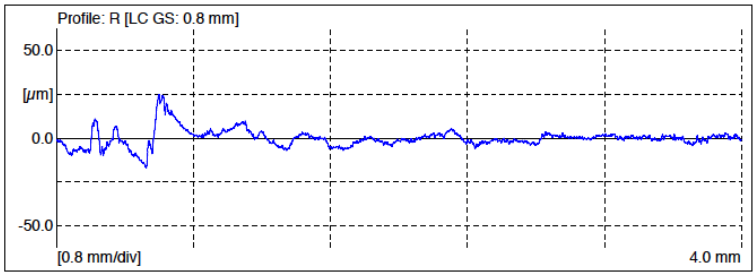

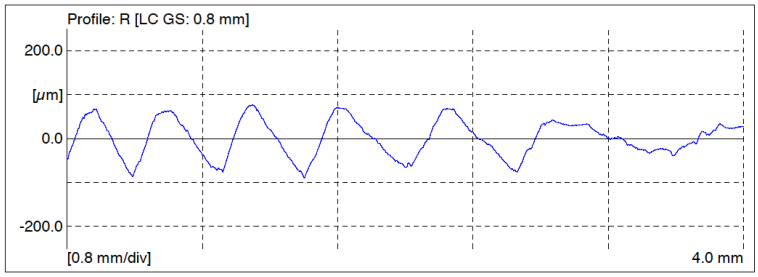

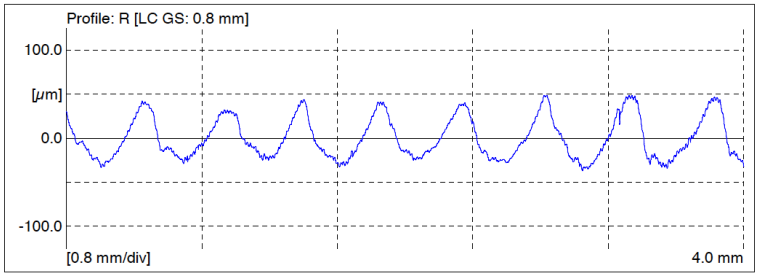

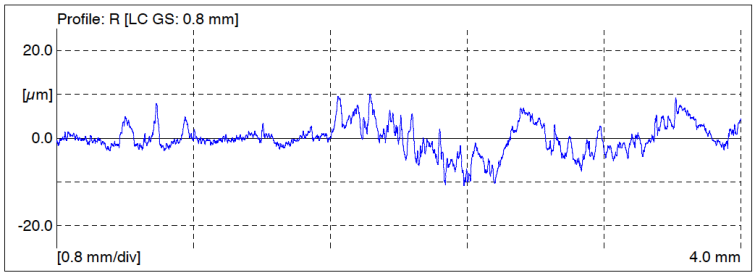

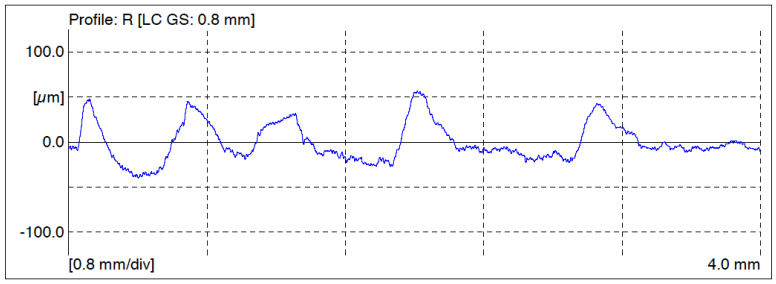

4) Ti-64SG/Ti-64SG Weld Nugget in Longitudinal direction RPM/ mm min-1 (225/125, 275/100, 275/125, 275/150, 325/125)

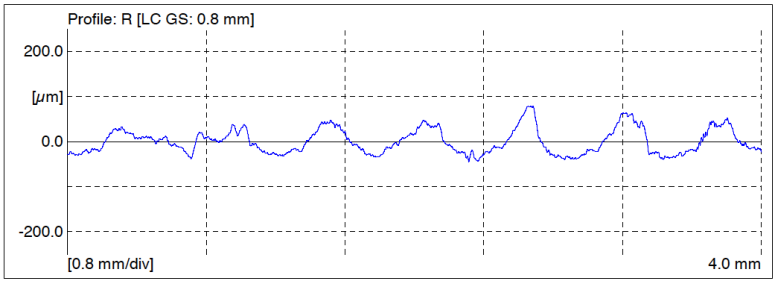

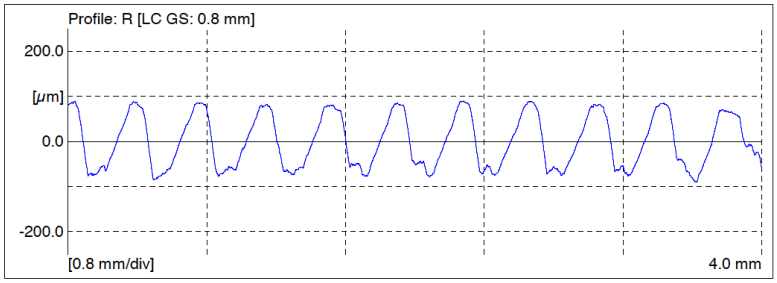

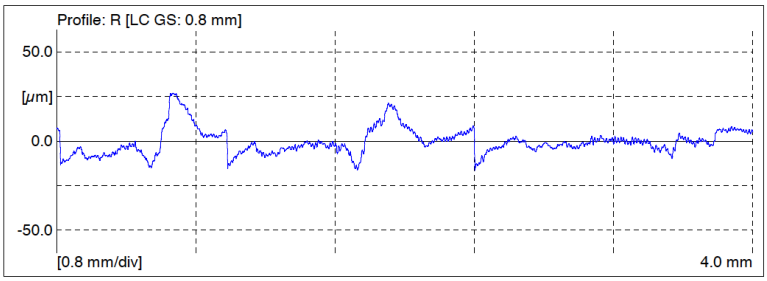

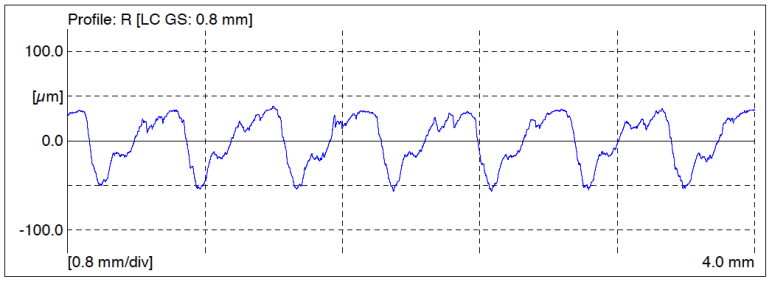

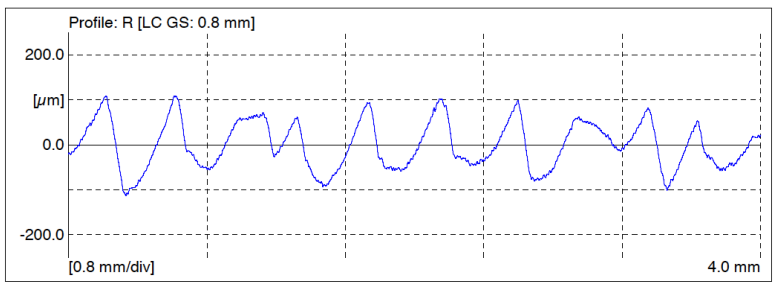

5) Ti-64SG/Ti-64SG Weld Nugget in Transverse direction RPM/ mm min-1 (225/125, 275/100, 275/125, 275/150, 325/125)

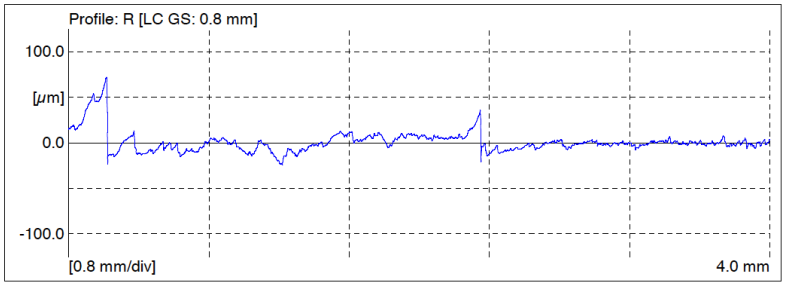

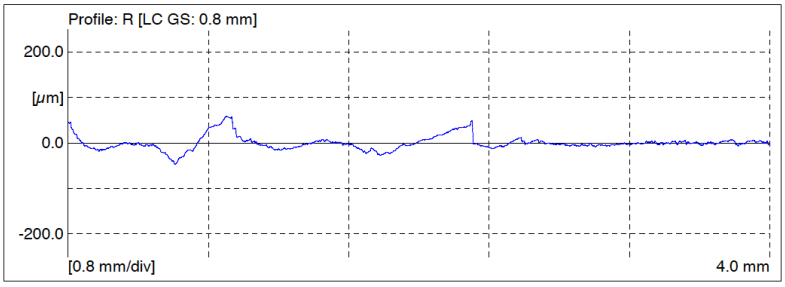

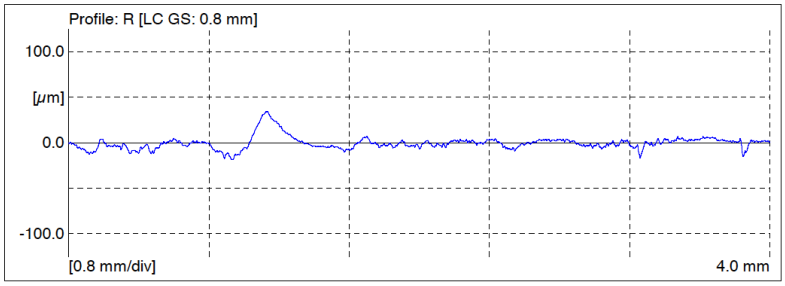

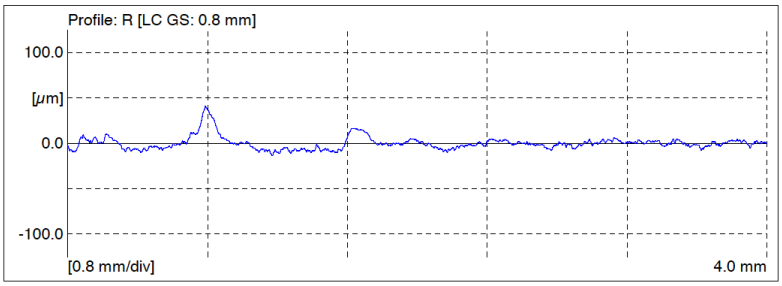

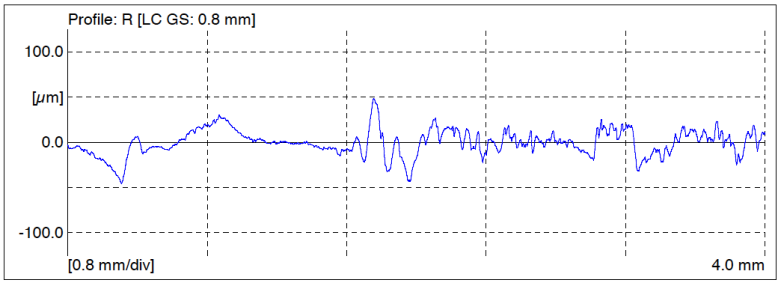

6) Ti-64FG/Ti-64FG Weld Nugget in Longitudinal direction RPM/ mm min-1 (225/125, 275/100, 275/125, 275/150, 325/125)

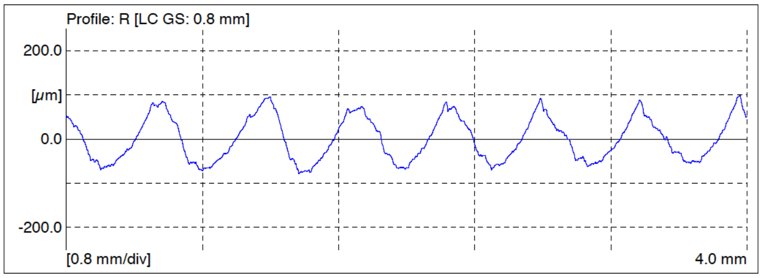

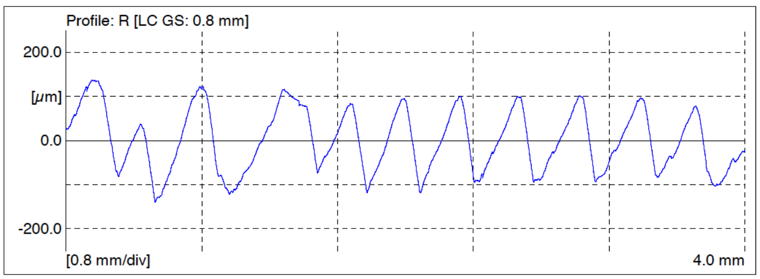

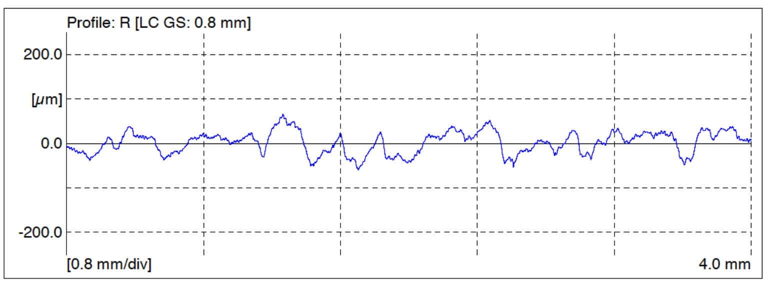

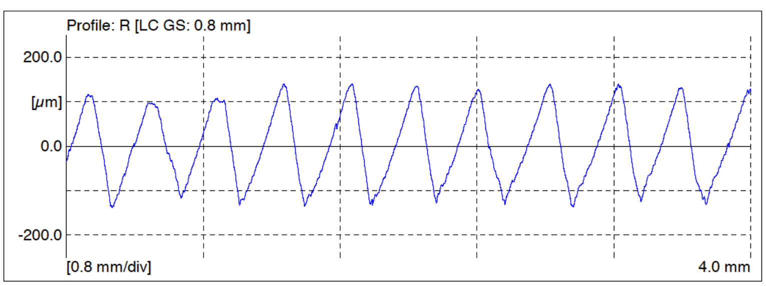

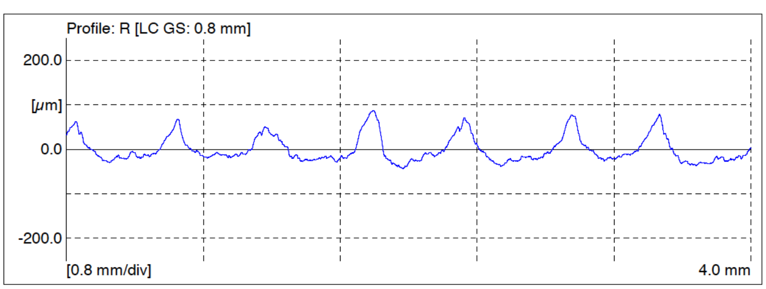

7) Ti-6242SG/Ti-6242SG Weld Nugget in Transverse direction RPM/ mm min-1 (225/125, 275/100, 275/125, 275/150, 325/125)

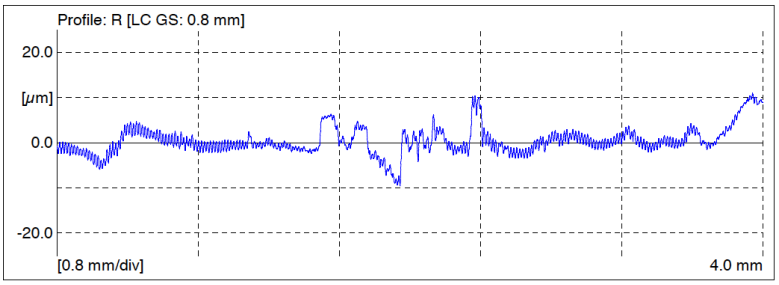

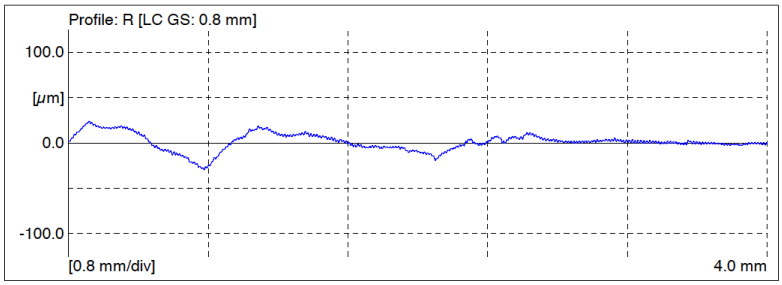

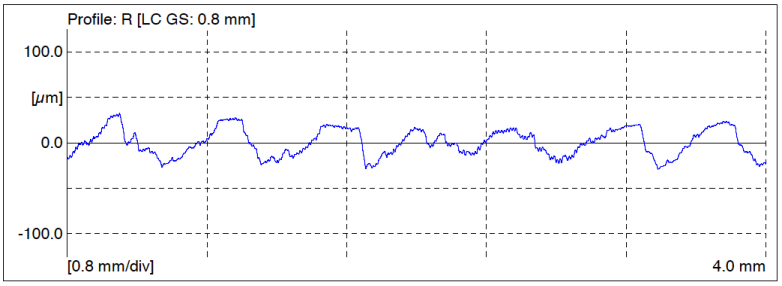

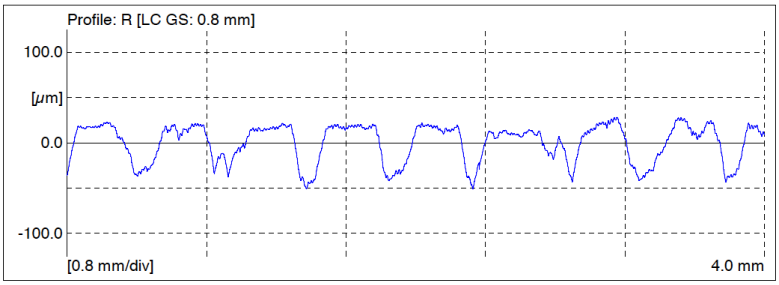

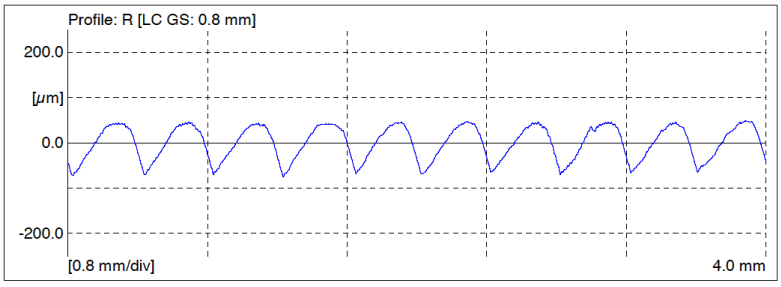

8) Ti-6242SG/Ti-6242SG Weld Nugget in Longitudinal direction RPM/ mm min-1 (225/125, 275/100, 275/125, 275/150, 325/125)

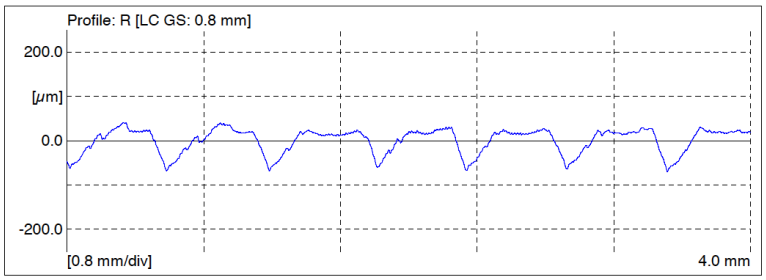

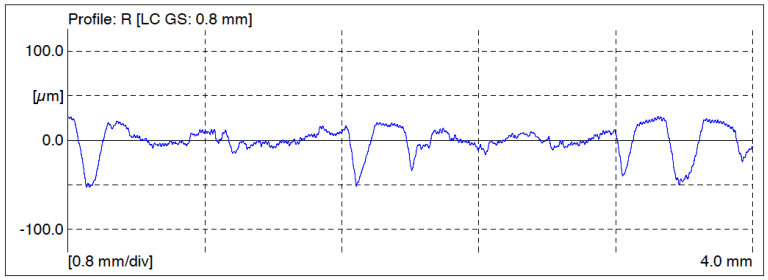

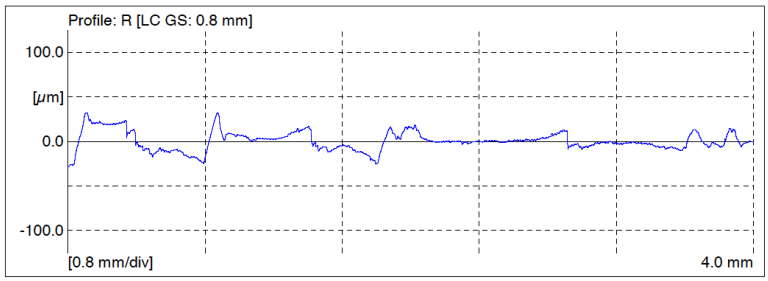

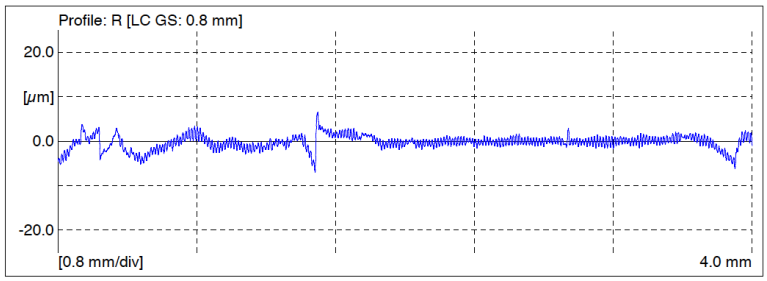

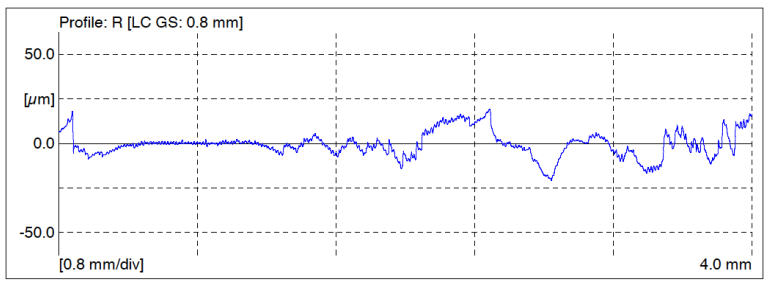

9) Ti-6242FG/Ti-6242FG Weld Nugget in Transverse direction RPM/ mm min-1 (225/125, 275/100, 275/125, 275/150, 325/125)

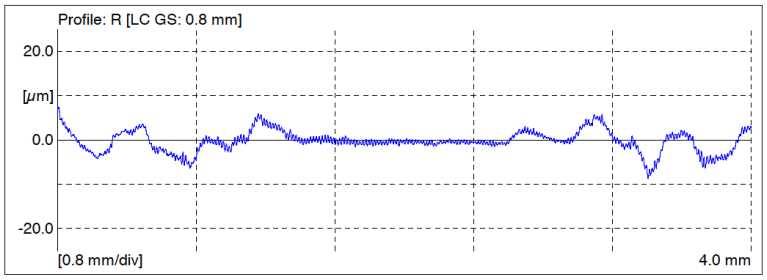

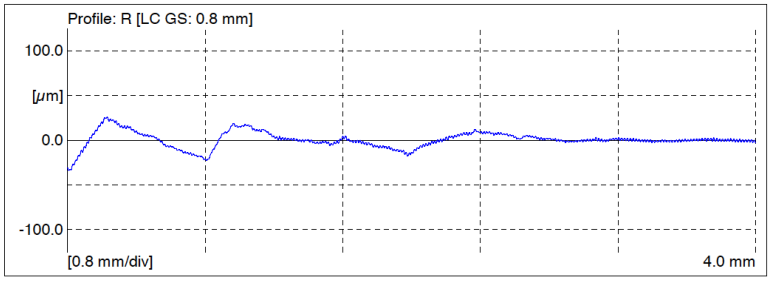

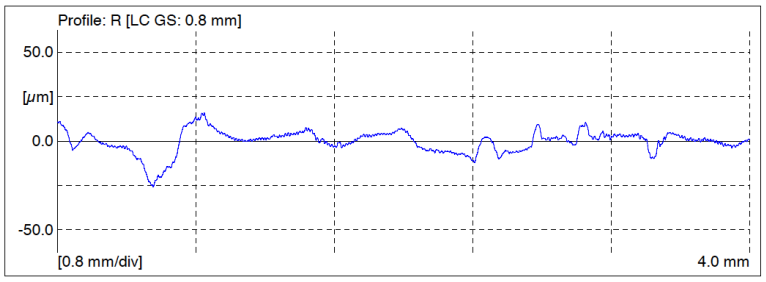

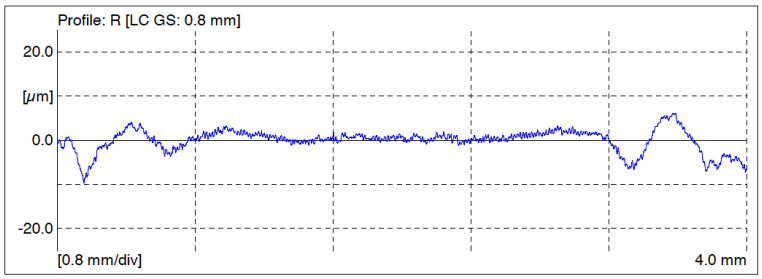

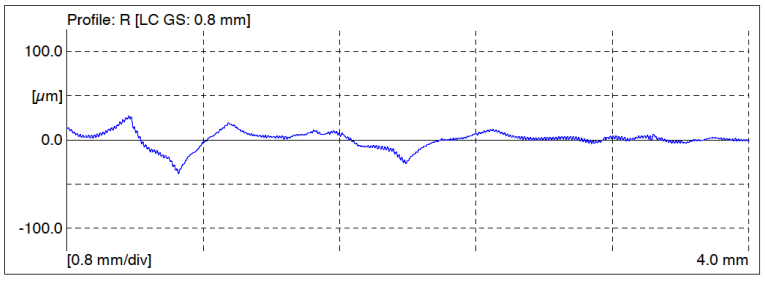

10) Ti-6242FG/Ti-6242FG Weld Nugget in Longitudinal direction RPM/ mm min-1 (225/125, 275/100, 275/125, 275/150, 325/125)

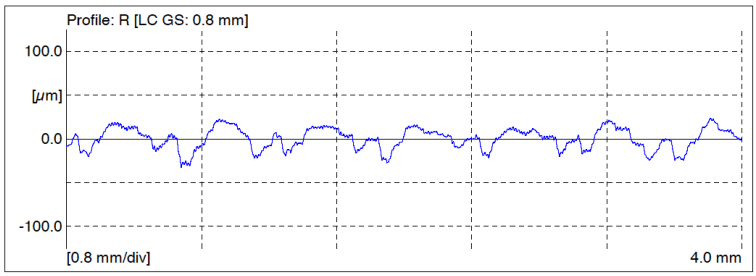

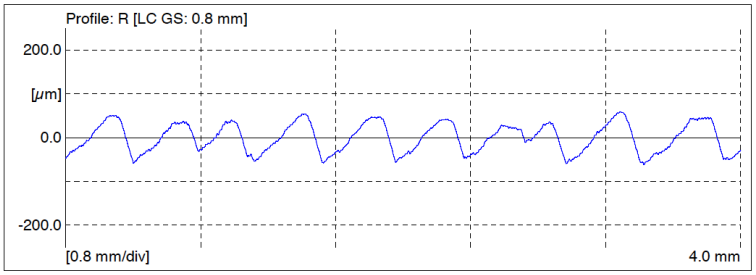

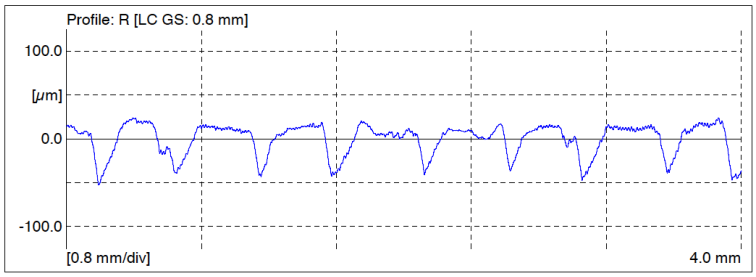

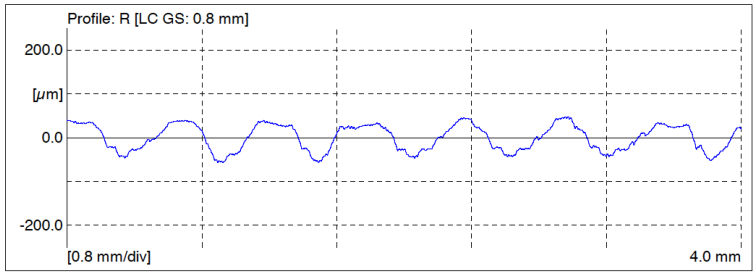

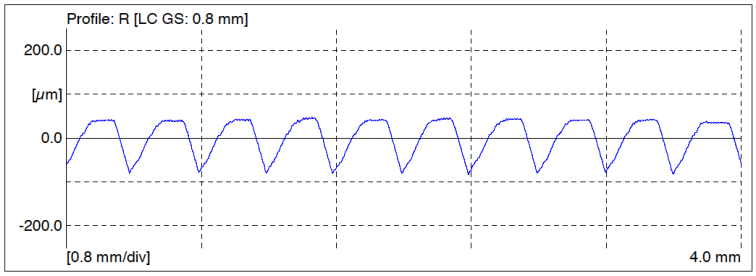

11) Ti-54MFG/Ti-64SG Weld Nugget in Transverse direction RPM/ mm min-1 (275/125, 275/100, 275/150, 325/125)

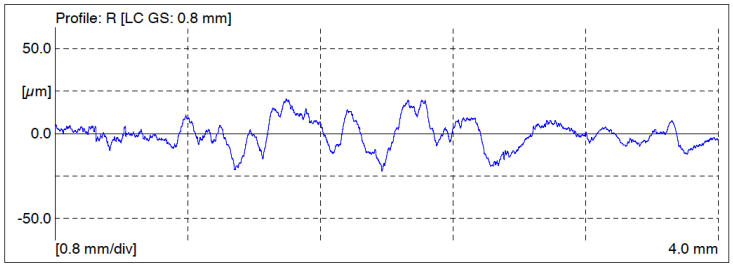

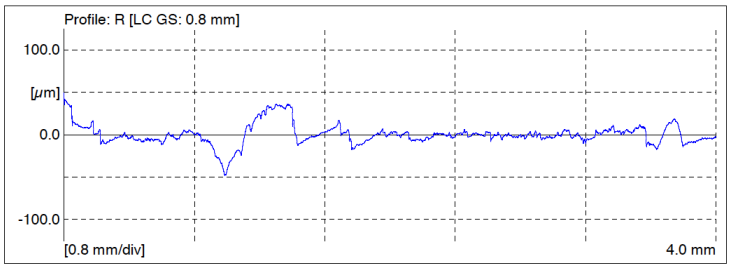

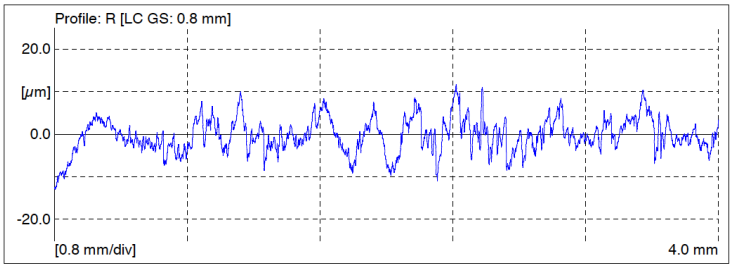

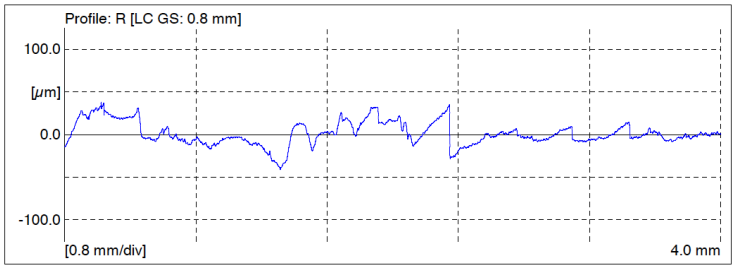

12) Ti-54MFG/Ti-64SG Weld Nugget in Longitudinal direction RPM/ mm min-1 (275/125, 275/100, 275/150, 325/125)

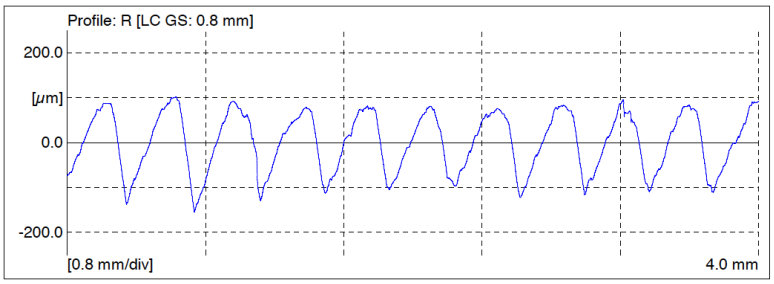

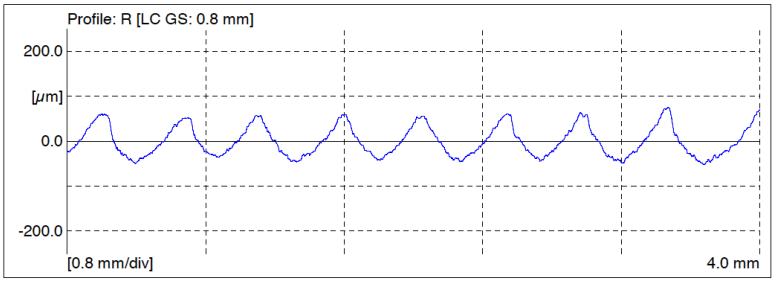

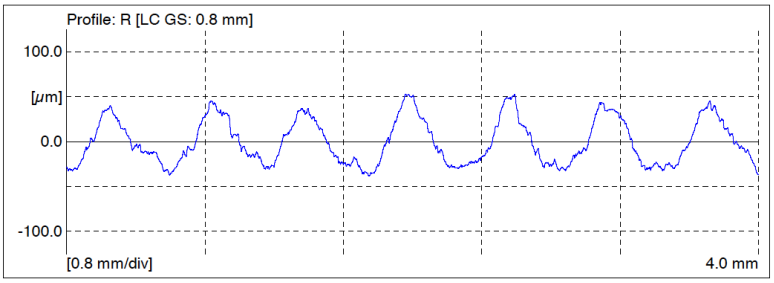

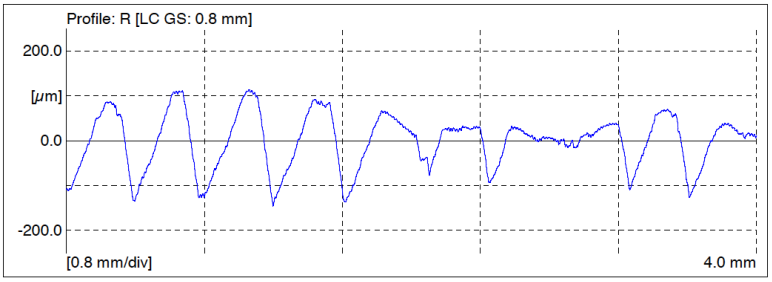

13) Ti-54MFG/Ti-6242SG Weld Nugget in Transverse direction RPM/ mm min-1 (225/125, 275/100, 275/125, 275/150, 325/125)

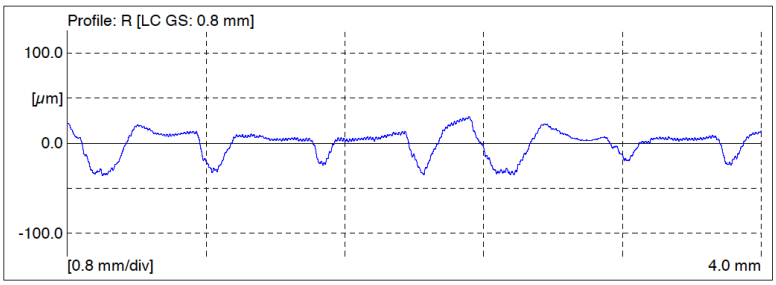

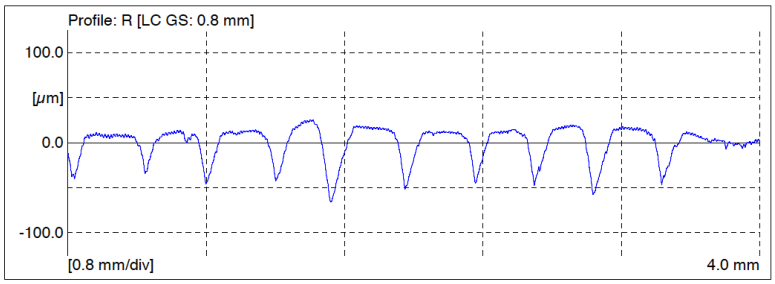

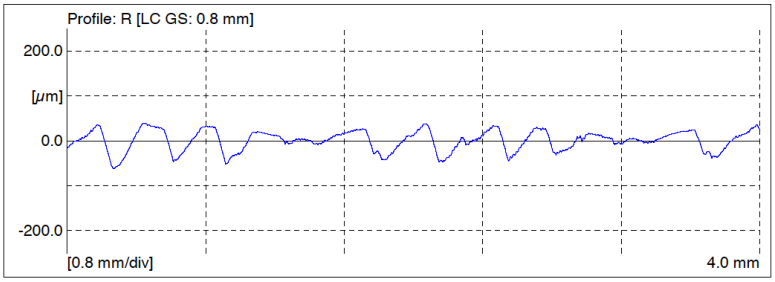

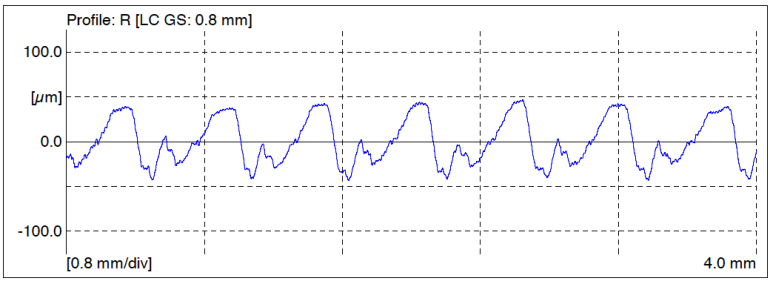

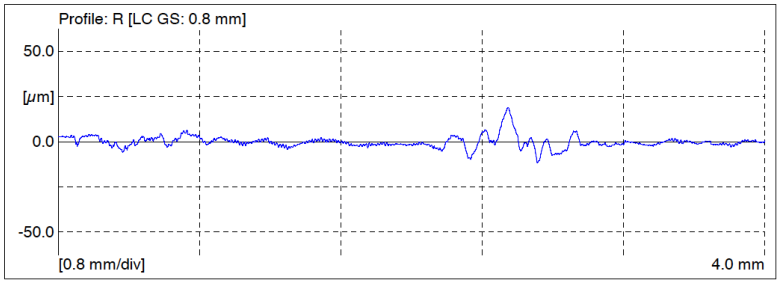

14) Ti-54MFG/Ti-6242SG Weld Nugget in Longitudinal direction RPM/ mm min-1 (225/125, 275/100, 275/125, 275/150, 325/125)

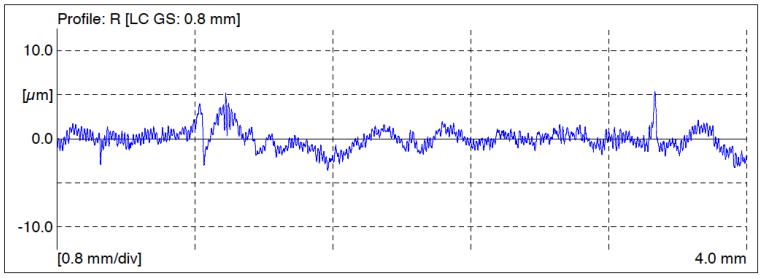

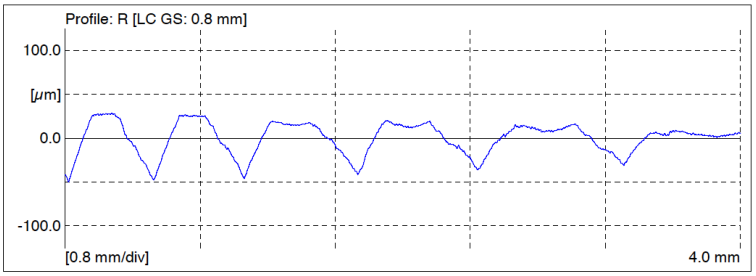

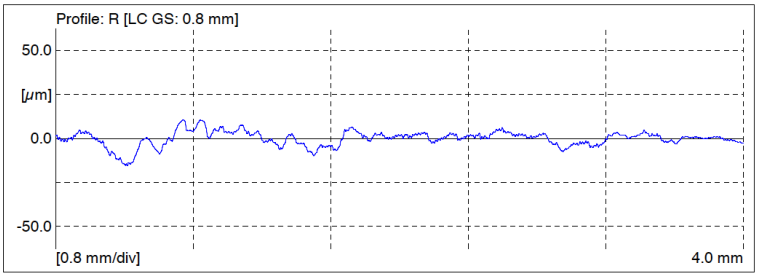

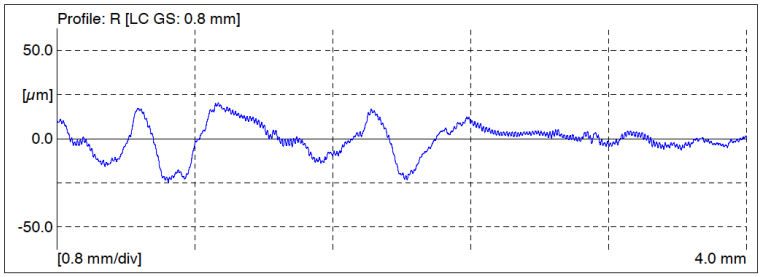

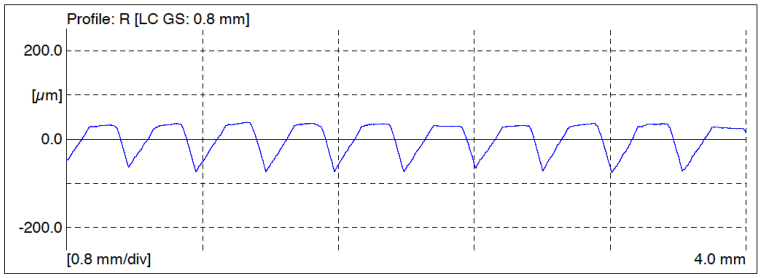

15) Ti-64SG/Ti-6242SG Weld Nugget in Transverse direction RPM/ mm min-1 (225/125, 275/100, 275/125, 275/150, 325/125)

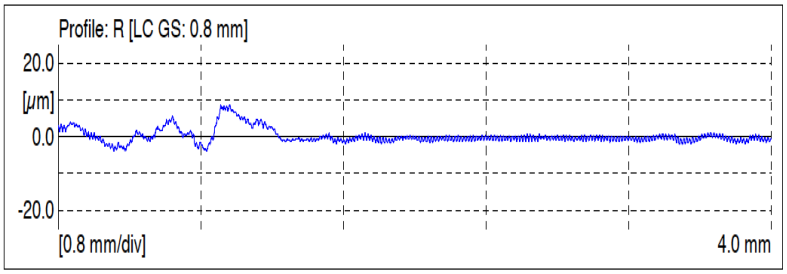

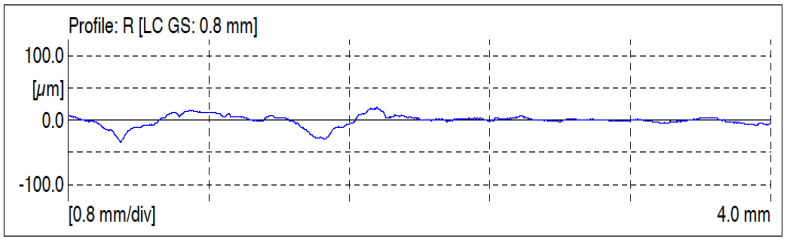

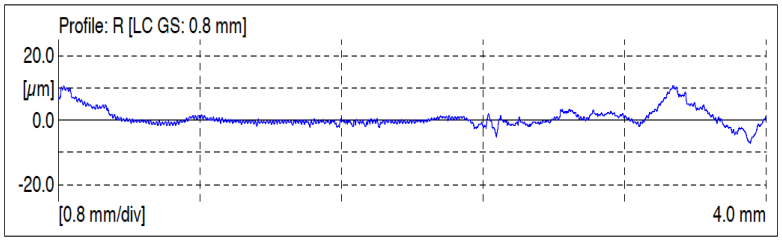

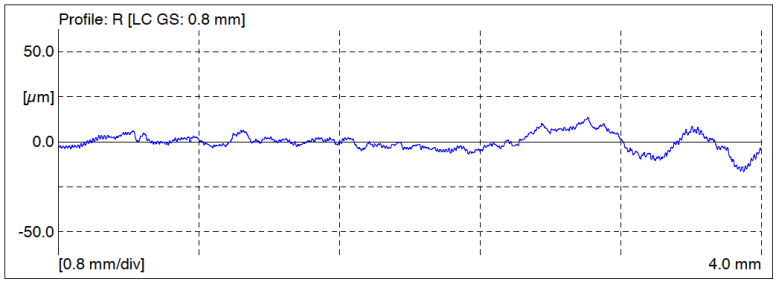

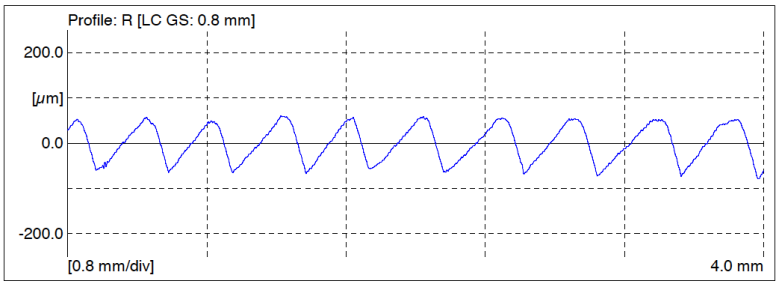

16) Ti-64SG/Ti-6242SG Weld Nugget in Longitudinal direction RPM/ mm min-1 (225/125, 275/100, 275/125, 275/150, 325/125)

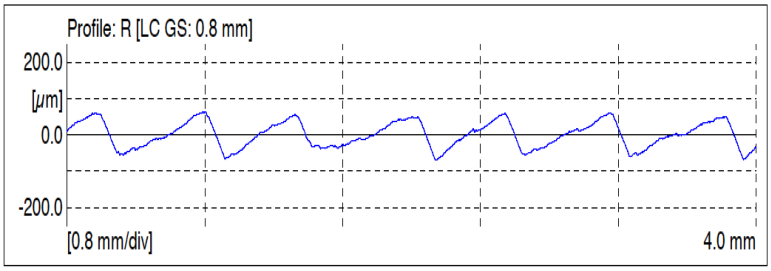

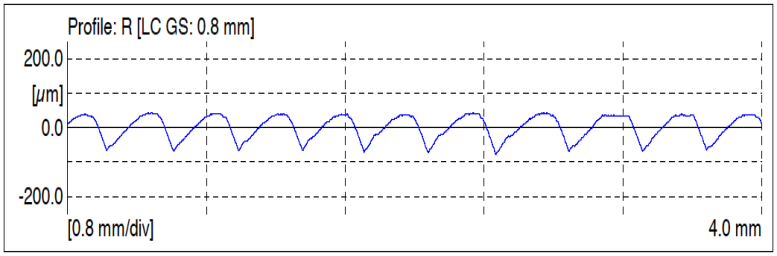

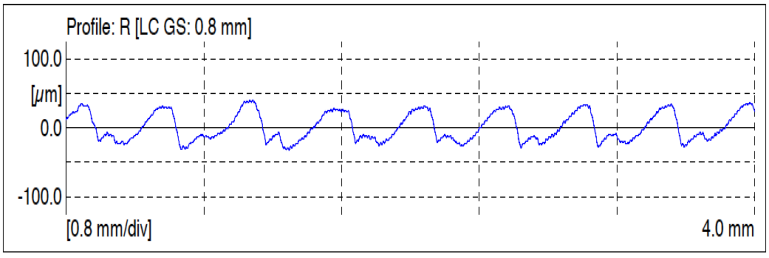

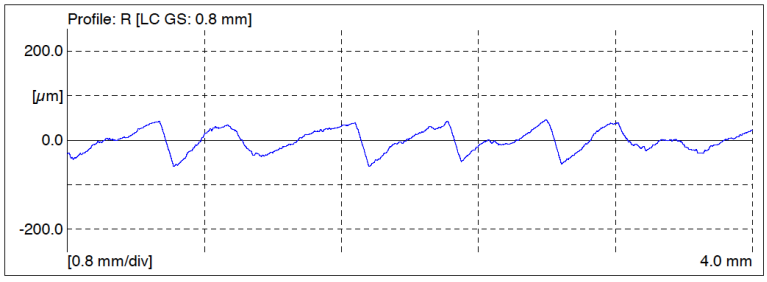

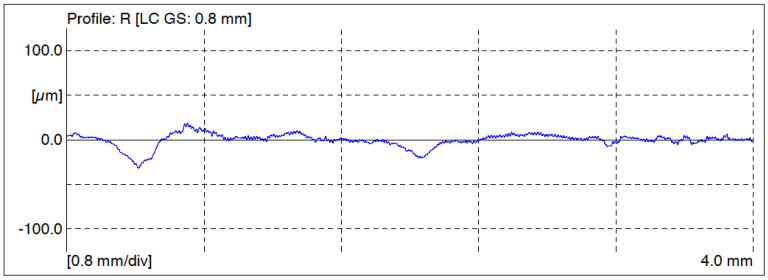

17) Ti-54MFG/Ti-64FG Weld Nugget in Transverse direction RPM/ mm min-1 (225/125, 275/100, 275/125, 275/150, 325/125)

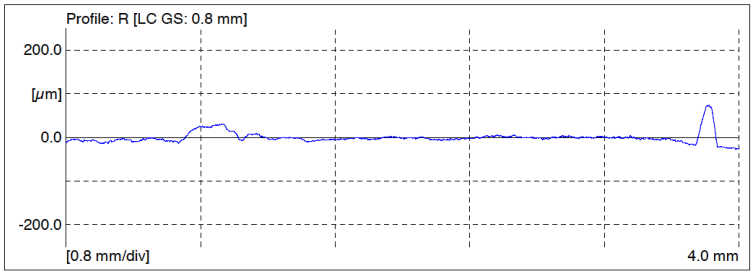

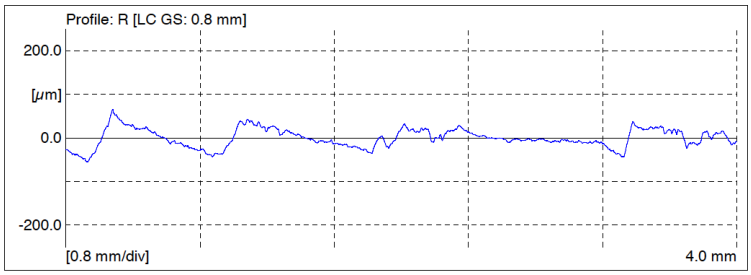

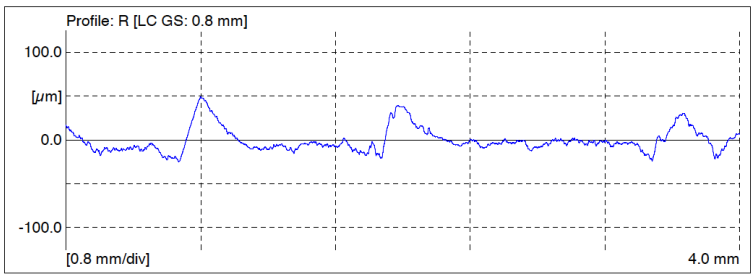

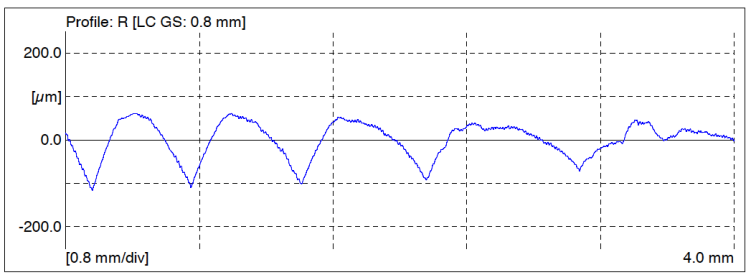

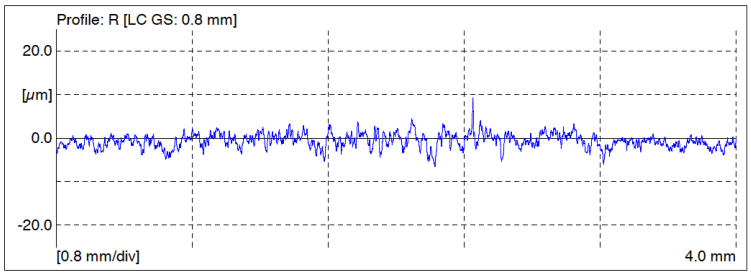

18) Ti-54MFG/Ti-64FG Weld Nugget in Longitudinal direction RPM/ mm min-1 (225/125, 275/100, 275/125, 275/150, 325/125)

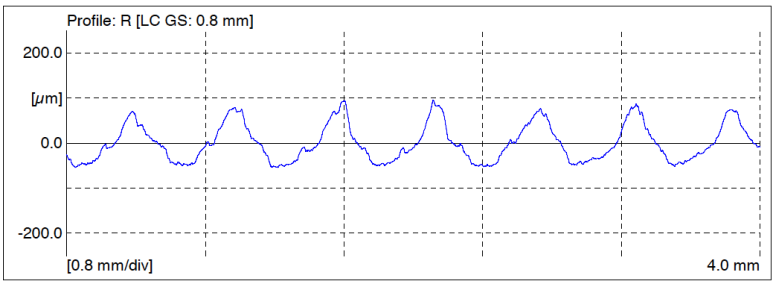

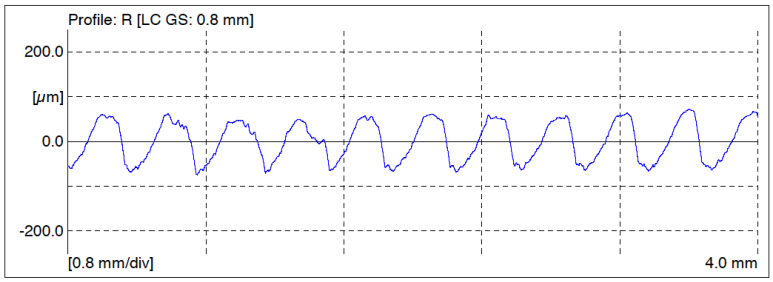

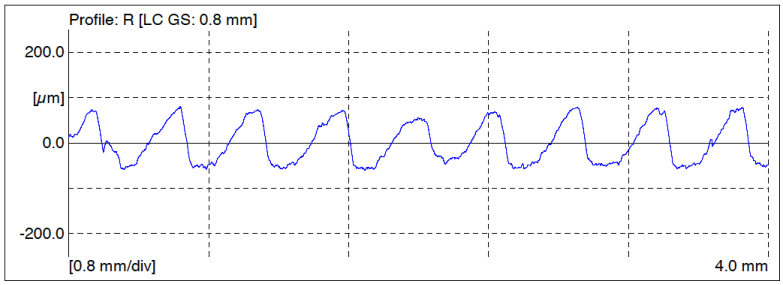

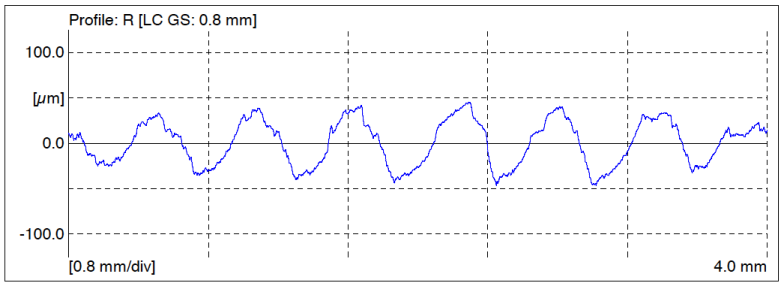

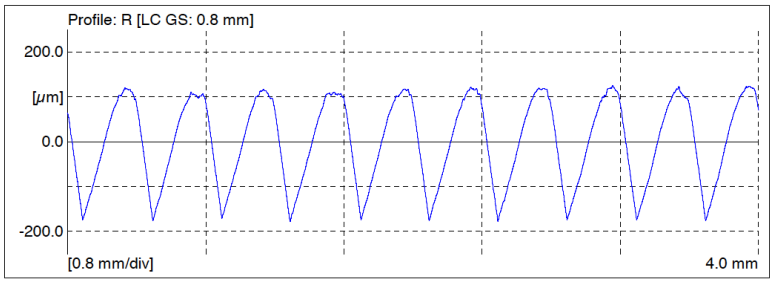

19) Ti-54MFG/Ti-6242FG Weld Nugget in Transverse direction RPM/ mm min-1 (275/100, 275/150, 325/125)

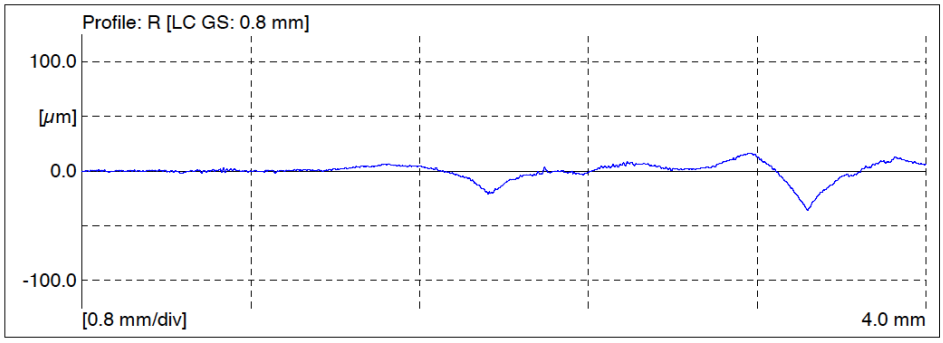

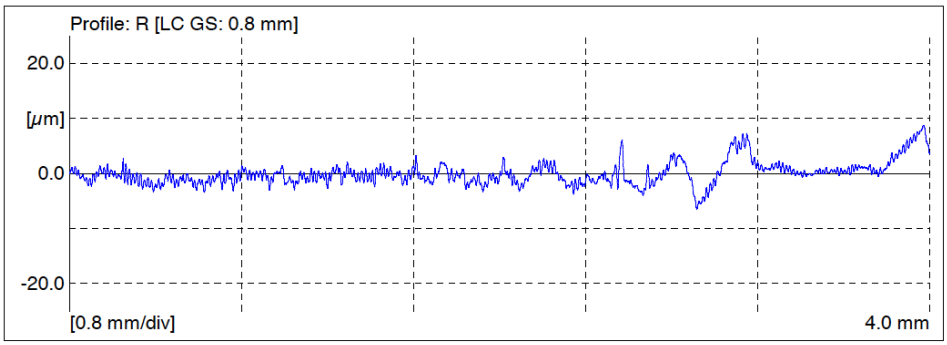

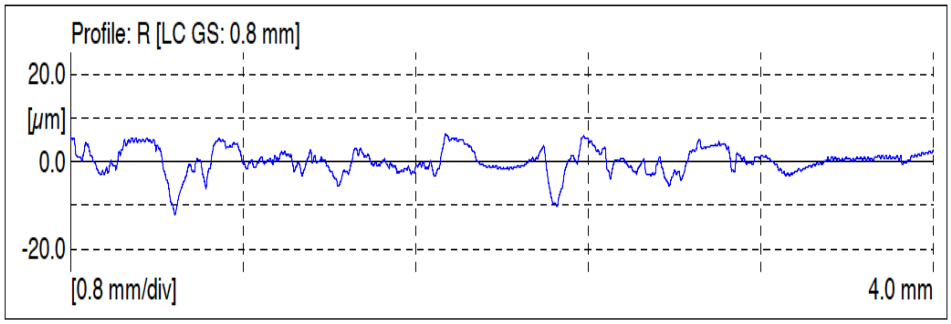

20) Ti-54MFG/Ti-6242FG Weld Nugget in Longitudinal direction RPM/ mm min-1 (225/125, 275/100, 275/150, 325/125)

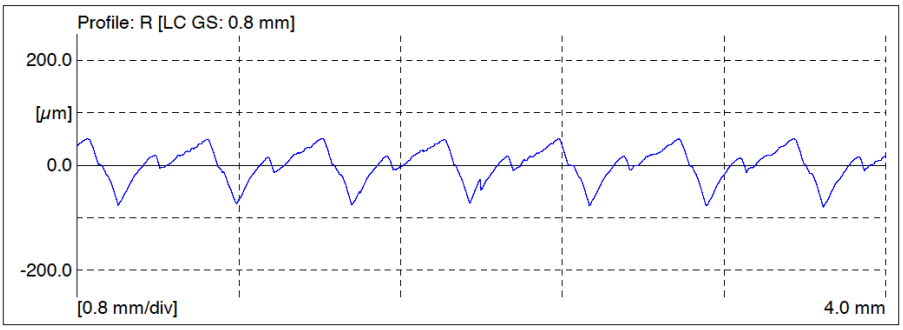

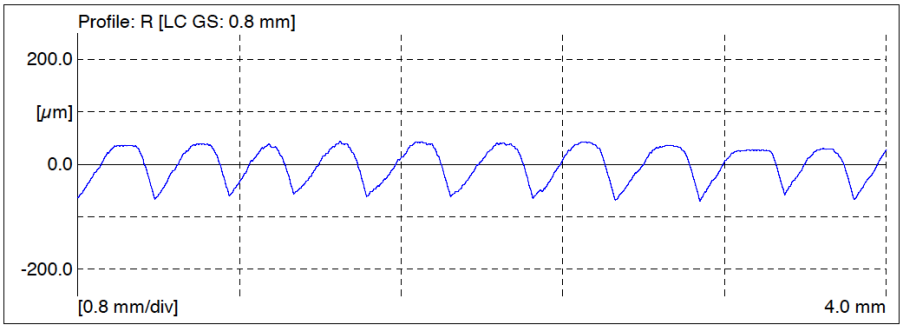

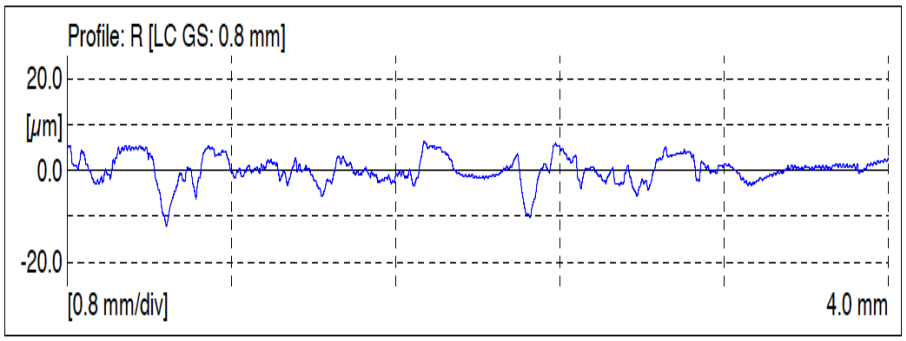

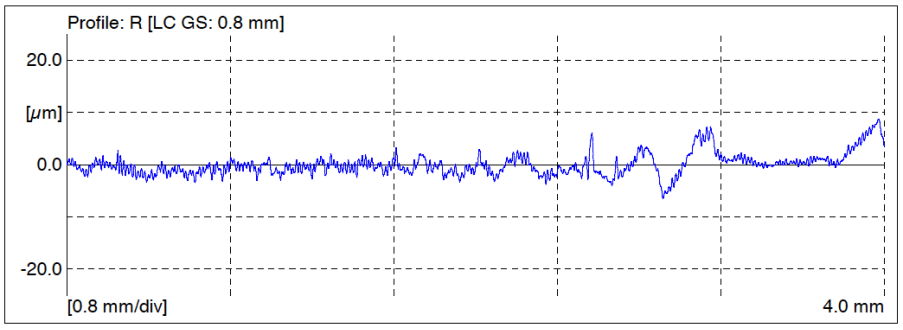

21) Ti-64SG/Ti-6242FG Weld Nugget in Transverse direction RPM/ mm min-1 (225/125, 275/100, 275/150, 325/125)

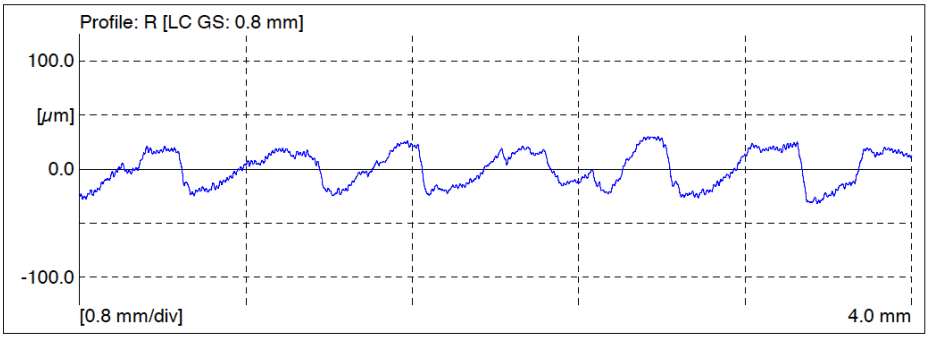

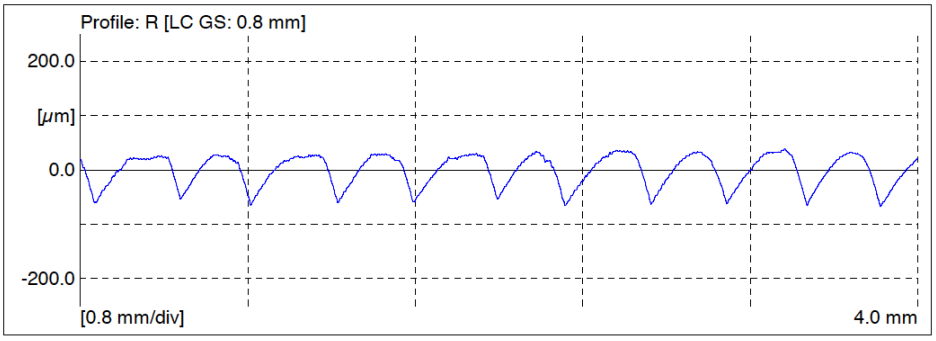

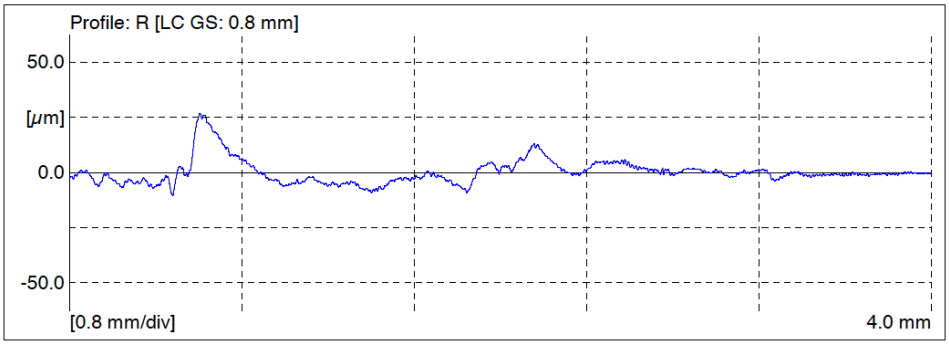

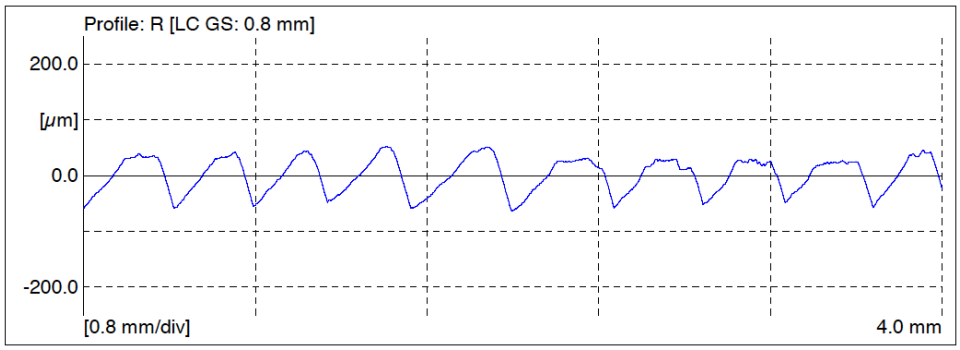

22) Ti-64SG/Ti-6242FG Weld Nugget in Longitudinal direction RPM/ mm min-1 (225/125, 275/100, 275/150, 325/125)

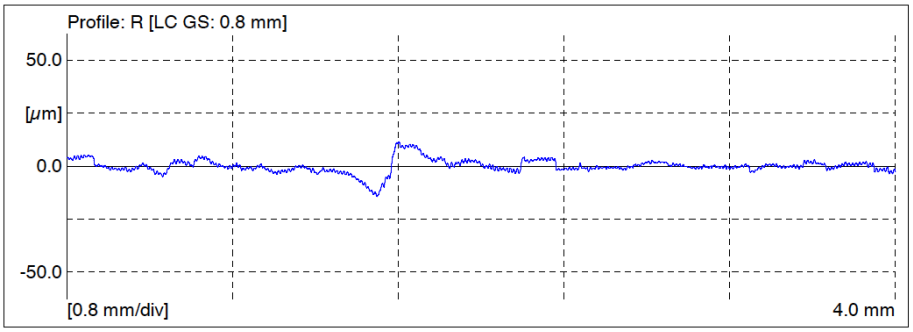

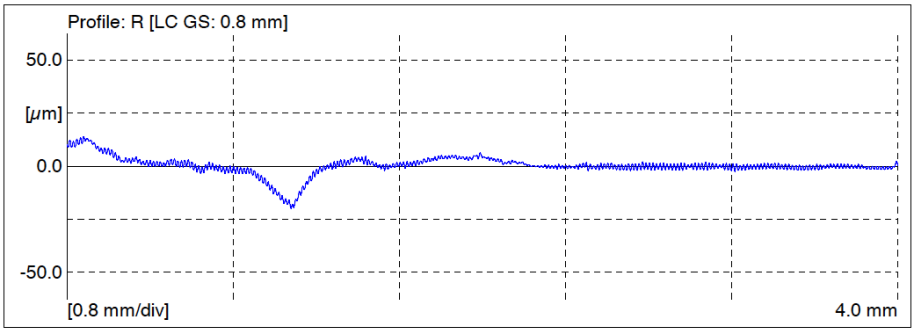

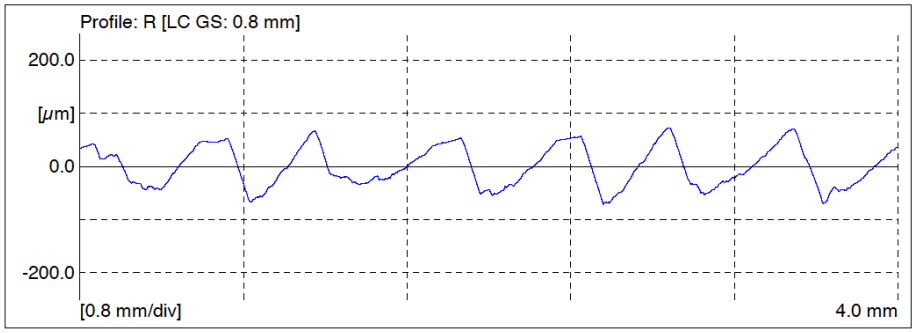

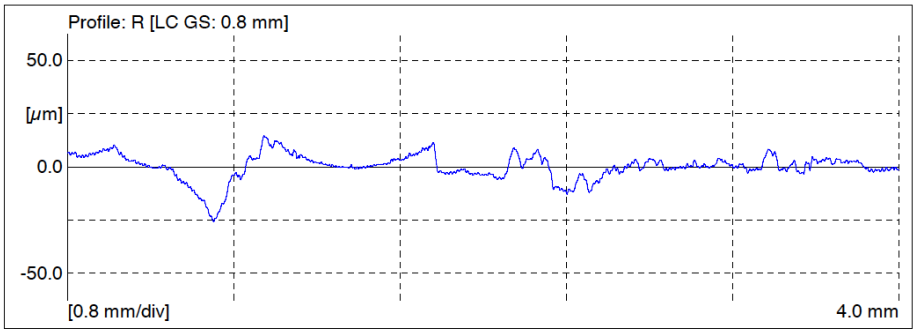

23) Ti-64FG/Ti-6242FG Weld Nugget in Transverse direction RPM/ mm min-1 (225/125, 275/100, 275/150, 325/125)

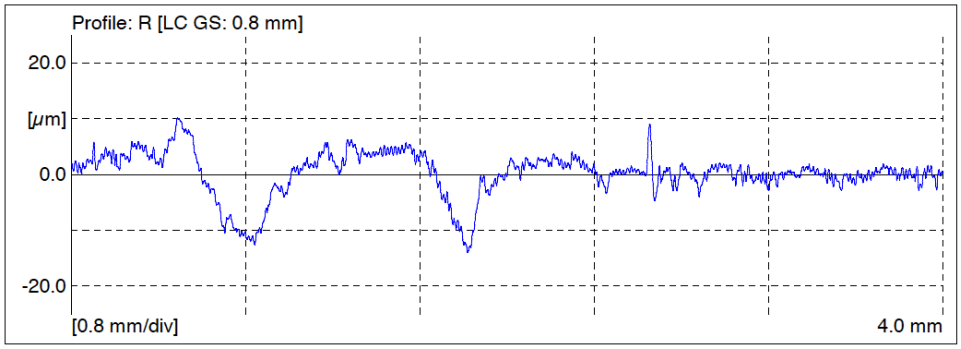

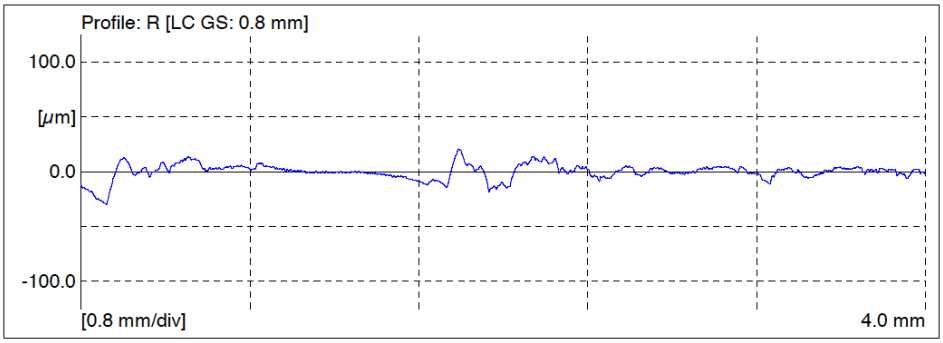

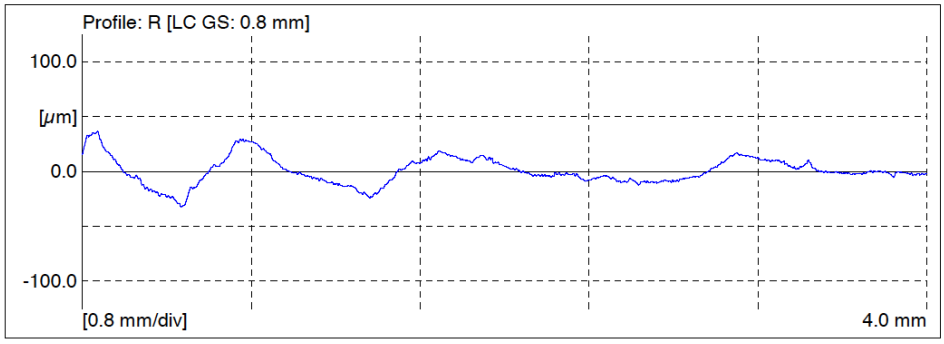

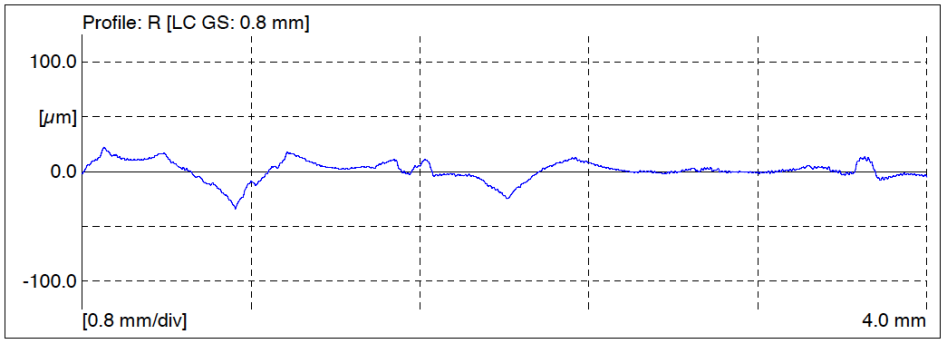

24) Ti-64FG/Ti-6242FG Weld Nugget in Longitudinal direction RPM/ mm min-1 (225/125, 275/100, 275/150, 325/125)

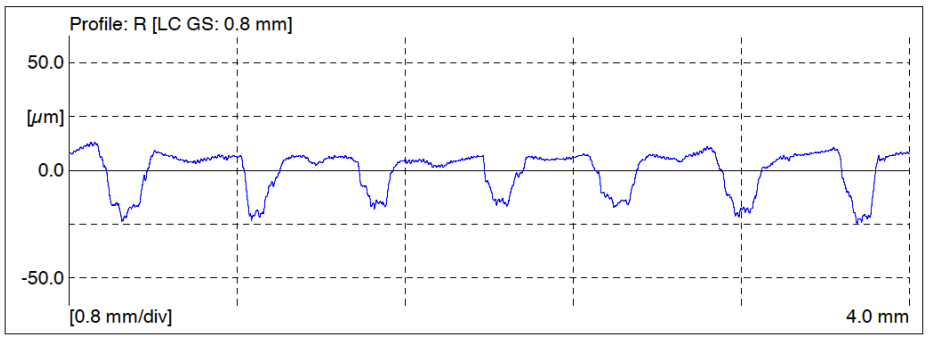

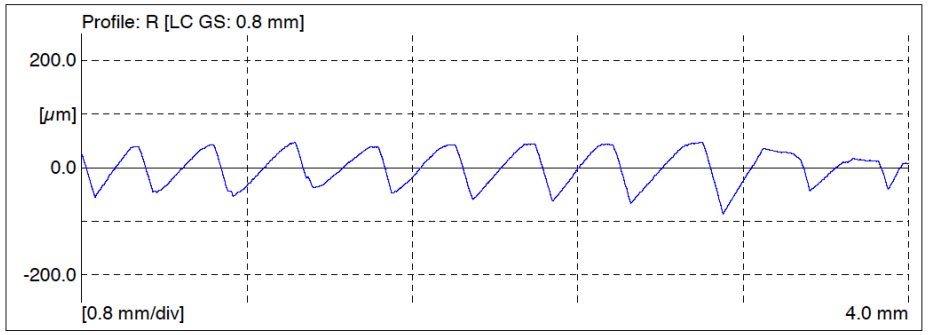

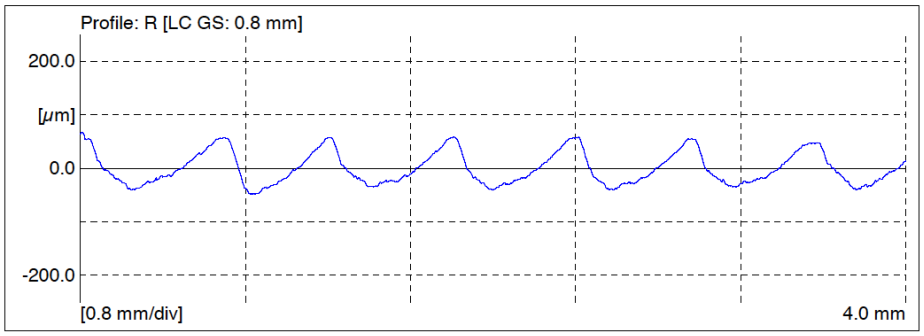

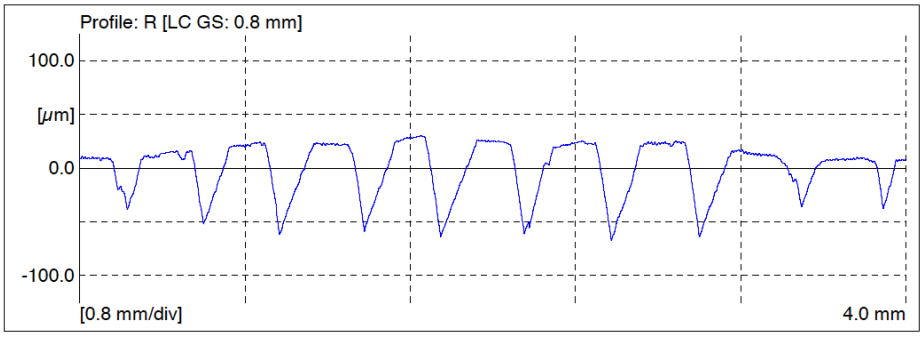

G.2. Surface profile parameters for Friction Stir Welded Similar and Dissimilar Ti-Joints

The surface parameters were measured for friction stir welded titanium joints in the longitudinal and transverse direction at three locations (Parent Alloy1, Weld Nugget, and Parent Alloy2) are listed below. The definitions of profile parameters included are (Ra: Center Line Average; Rq: Root Mean Square (RMS) Average; Rz: Peak to Valley Height within a Sample Length; Rmax: Maximum Roughness Height within a Sample Length; Rt: Maximum Height of the Profile; RSm: Mean width of the roughness profile elements; Rsk: Skewness; Rku: Kurtosis)

Ti-Joint	Surface Parameter (μm)	Location	Longitudinal				
			225/125	275/100	275/125	275/150	325/125
Ti-54MFG/Ti-54MFG	Ra	Ti-54M	1.293	1.523	1.565	1.582	1.695
		Weld Nugget	35.955	12.314	30.294	22.01	56.479
		Ti-54M	1.481	1.005	1.073	1.206	1.357
	Rq	Ti-54M	1.58	1.947	2.106	1.997	2.158
		Weld Nugget	40.572	15.219	34.38	24.925	64.234
		Ti-54M	1.9	1.234	1.347	1.543	1.832
	Rz	Ti-54M	8.858	12.165	12.585	11.513	13.18
		Weld Nugget	127.54	68.057	111.099	87.137	221.525
		Ti-54M	11.135	7.172	8.97	9.658	13.648
	Rmax	Ti-54M	10.1	13.1	17.9	13.8	15.6
		Weld Nugget	138	90.9	135.4	95.5	264.5
		Ti-54M	16.1	7.9	14.2	11.6	16.5
	Rt	Ti-54M	10.1	13.6	19.4	14.1	15.6
		Weld Nugget	139.7	90.9	135.4	95.5	264.5
		Ti-54M	16.1	8.6	14.2	12.2	17
	RSm	Ti-54M	21.8	32.5	34.7	30.6	31.9
		Weld Nugget	578.8	185	474.7	569	394.4
		Ti-54M	28.7	21.2	21.1	25.9	23.3
	Rsk	Ti-54M	0.03	0.53	0.91	0.12	0.52
		Weld Nugget	0.08	0.2	0	0.46	-0.09
		Ti-54M	-0.62	0.06	-0.07	-0.21	-1.14
	Rku	Ti-54M	2.61	3.75	6.54	3.27	3.84
		Weld Nugget	1.6	2.78	1.77	1.94	1.81
		Ti-54M	4.01	2.75	3.95	3.92	7.06

Ti-Joint	Surface Parameter (µm)	Location	Transverse				
			225/125	275/100	275/125	275/150	325/125
Ti-54MFG/Ti-54MFG	Ra	Ti-54M	1.321	1.648	4.422	1.653	1.638
		Weld Nugget	3.589	11.6	4.287	1.97	5.355
		Ti-54M	1.415	1.313	1.307	1.308	2.767
	Rq	Ti-54M	1.623	2.128	5.916	2.088	2.104
		Weld Nugget	5.541	17.704	6.793	2.478	10.21
		Ti-54M	1.798	1.615	1.608	1.612	3.906
	Rz	Ti-54M	8.826	12.286	31.215	11.501	13.341
		Weld Nugget	20.404	62.559	25.521	12.649	32.324
		Ti-54M	10.644	8.527	8.625	8.873	24.871
	Rmax	Ti-54M	9.2	16.2	38	15.3	16.8
		Weld Nugget	40.3	105.4	43.5	16.2	88
		Ti-54M	12.6	9.7	10.3	10	39.7
	Rt	Ti-54M	9.6	16.2	38	15.3	16.8
		Weld Nugget	41.7	109.2	49.4	16.3	88
		Ti-54M	12.9	10.3	10.3	10.2	39.7
	RSm	Ti-54M	25.7	41.4	145.1	46.2	44
		Weld Nugget	160.9	938.3	244.4	105.3	1226
		Ti-54M	24.2	22.7	28.5	25.1	45.3
	Rsk	Ti-54M	-0.14	0.56	-1.14	0.55	0.5
		Weld Nugget	1.38	1.47	1.92	-0.6	2.49
		Ti-54M	-0.32	0.1	0.04	-0.07	-0.61
	Rku	Ti-54M	2.65	4.08	4.87	3.65	4.16
		Weld Nugget	7.41	6.03	8.33	3.21	12.08
		Ti-54M	3.33	2.68	2.7	2.73	5.6

Ti-Joint	Surface Parameter (µm)	Location	Longitudinal				
			225/125	275/100	275/125	275/150	325/125
Ti-64SG/Ti-64SG	Ra	Ti-64SG	1.028	1.17	0.971	1.31	1.594
		Weld Nugget	23.231	52.169	5.444	24.434	44.558
		Ti-64SG	2.162	1.381	0.844	0.719	1.617
	Rq	Ti-64SG	1.275	1.645	1.181	1.637	2.015
		Weld Nugget	27.521	57.773	7.347	27.418	52.115
		Ti-64SG	2.641	1.748	1.091	0.932	2.031
	Rz	Ti-64SG	6.966	8.449	5.788	8.871	11.037
		Weld Nugget	93.056	168.329	28.198	90.574	182.167
		Ti-64SG	13.476	9.901	6.863	6.564	11.316
	Rmax	Ti-64SG	7.9	14.9	6.5	15	15.1
		Weld Nugget	119.8	174.7	41.81	92.7	221.5
		Ti-64SG	14.1	11.6	8.2	8.2	12
	Rt	Ti-64SG	8.5	15.1	6.5	15	15.3
		Weld Nugget	123.7	179.2	43.21	95.5	221.5
		Ti-64SG	15.2	13	8.96	9	13.7
	RSm	Ti-64SG	20.9	23.7	20.7	20.6	33.3
		Weld Nugget	571	380	636.7	566	437.5
		Ti-64SG	20.6	26.7	36.49	26.5	35.3
	Rsk	Ti-64SG	0.07	-1.64	0	0.39	0.28
		Weld Nugget	0.61	0.17	0.88	-0.39	0.05
		Ti-64SG	0.03	0.2	0.3	0.51	-0.07
	Rku	Ti-64SG	2.77	10.7	2.49	4.68	3.53
		Weld Nugget	2.52	1.5	4.68	1.88	2.06
		Ti-64SG	2.54	3.2	4.12	5.25	2.93

Ti-Joint	Surface Parameter (µm)	Location	Transverse				
			225/125	275/100	275/125	275/150	325/125
Ti-64SG/Ti-64SG	Ra	Ti-64SG	1.433	1.337	0.713	1.504	1.27
		Weld Nugget	3.221	34.875	20.065	2.539	16.758
		Ti-64SG	1.738	1.765	0.994	1.528	1.672
	Rq	Ti-64SG	1.788	1.683	0.894	1.861	1.664
		Weld Nugget	4.929	41.107	23.142	3.403	20.675
		Ti-64SG	2.193	2.295	1.246	1.907	2.106
	Rz	Ti-64SG	9.553	9.5	4.847	10.376	10.453
		Weld Nugget	17.54	129.844	77.991	13.843	63.032
		Ti-64SG	12.938	14.402	7.005	10.472	11.781
	Rmax	Ti-64SG	10.1	10.9	6.26	11.4	17.4
		Weld Nugget	42	167.4	85.87	20.9	87.6
		Ti-64SG	15.9	20.8	9.49	12.8	12.6
	Rt	Ti-64SG	11.4	12.2	6.26	11.9	17.9
		Weld Nugget	42	167.4	85.87	20.9	96.6
		Ti-64SG	16.8	20.8	9.49	12.8	13.9
	RSm	Ti-64SG	53.1	31.4	22.22	24	48
		Weld Nugget	453.5	626.1	478.43	298.7	725.4
		Ti-64SG	45.4	40.4	28.17	27.5	35.9
	Rsk	Ti-64SG	-0.17	-0.16	-0.24	0.01	0.8
		Weld Nugget	1.19	-0.07	0.5	-0.17	0.62
		Ti-64SG	0.02	0.72	0.18	0.02	-0.09
	Rku	Ti-64SG	2.82	3.09	3.29	2.78	7.45
		Weld Nugget	8.45	2.04	1.97	3.53	2.82
		Ti-64SG	3.33	5.67	3.15	2.85	2.91

Ti-Joint	Surface Parameter (µm)	Location	Longitudinal				
			225/125	275/100	275/125	275/150	325/125
Ti-64FG/Ti-64FG	Ra	Ti-64FG	1.015	1.089	0.957	1.003	1.148
		Weld Nugget	43.11	60.105	21.024	23.851	69.621
		Ti-64FG	0.993	1.589	1.008	1.923	1.096
	Rq	Ti-64FG	1.252	1.329	1.169	1.21	1.391
		Weld Nugget	48.743	69.311	24.68	29.308	79.976
		Ti-64FG	1.205	2.635	1.256	2.732	1.33
	Rz	Ti-64FG	6.678	7.201	6.643	6.063	7.418
		Weld Nugget	160.011	227.702	96.479	108.092	269.765
		Ti-64FG	6.85	11.695	7.663	18.826	6.962
	Rmax	Ti-64FG	7.7	9.5	8	6.7	9.1
		Weld Nugget	174.8	277	116.1	130.3	275.8
		Ti-64FG	7.6	28.5	9.9	23.7	7.7
	Rt	Ti-64FG	7.7	9.6	8	6.8	9.1
		Weld Nugget	176.9	277	124.3	130.3	278.2
		Ti-64FG	7.6	28.5	10	25.8	7.7
	RSm	Ti-64FG	18.8	18.8	18.7	18.4	18.8
		Weld Nugget	571.5	357.4	382.7	559.8	385.9
		Ti-64FG	19.1	24.7	19	40.2	18
	Rsk	Ti-64FG	-0.3	-0.11	-0.04	0.07	-0.1
		Weld Nugget	0.24	0.09	0.01	1.04	0.1
		Ti-64FG	-0.06	-3.35	-0.11	-1.19	0.08
	Rku	Ti-64FG	2.97	2.76	2.71	2.37	2.56
		Weld Nugget	1.74	1.86	2.19	3.17	1.75
		Ti-64FG	2.63	23.36	3.32	7	2.47

Ti-Joint	Surface Parameter (µm)	Location	Transverse				
			225/125	275/100	275/125	275/150	325/125
Ti-64FG/Ti-64FG	Ra	Ti-64FG	1.326	1.092	1.236	1.21	1.281
		Weld Nugget	7.135	10.14	4.717	4.683	10.819
		Ti-64FG	1.399	1.356	1.311	1.369	1.375
	Rq	Ti-64FG	1.726	1.363	1.552	1.518	1.597
		Weld Nugget	11.767	15.408	7.134	7.154	14.255
		Ti-64FG	1.766	1.674	1.631	1.69	1.703
	Rz	Ti-64FG	9.58	7.637	8.71	8.364	9.005
		Weld Nugget	43.824	56.384	24.655	31.189	60.576
		Ti-64FG	10.386	8.857	9.151	9.141	9.09
	Rmax	Ti-64FG	14	8.5	9.6	11.2	9.4
		Weld Nugget	95.4	91.5	52.8	51.5	91.5
		Ti-64FG	14	9.9	9.8	12.5	10.3
	Rt	Ti-64FG	14.7	9.1	10.9	11.2	10.1
		Weld Nugget	96.5	105.6	52.8	54.7	93.8
		Ti-64FG	14	9.9	10.6	12.5	11.2
	RSm	Ti-64FG	29.7	31.5	35.9	36.2	31.5
		Weld Nugget	520.4	525.8	337.6	430.2	224.4
		Ti-64FG	30.8	25.1	24.4	29.2	26.8
	Rsk	Ti-64FG	-0.92	-0.1	0	0.03	-0.1
		Weld Nugget	2.67	1.01	1.42	2.15	-0.31
		Ti-64FG	0.06	-0.09	-0.05	0.04	0.03
	Rku	Ti-64FG	5.59	2.92	2.9	3.42	2.84
		Weld Nugget	12.9	5.74	8.68	11.01	3.81
		Ti-64FG	3.28	2.67	2.83	2.8	2.72

Ti-Joint	Surface Parameter (µm)	Location	Longitudinal				
			225/125	275/100	275/125	275/150	325/125
Ti-6242SG/Ti-6242SG	Ra	Ti-6242SG	0.845	0.821	1.277	0.642	0.676
		Weld Nugget	23.786	11.455	7.756	1.183	5.099
		Ti-6242SG	0.925	0.959	0.788	0.658	0.68
	Rq	Ti-6242SG	1.034	1.008	2.586	0.765	0.848
		Weld Nugget	27.953	15.86	10.448	1.601	7.075
		Ti-6242SG	1.152	1.167	1.295	0.786	0.813
	Rz	Ti-6242SG	5.099	5.406	9.835	3.807	4.025
		Weld Nugget	101.685	57.224	40.402	8.092	28.651
		Ti-6242SG	6.16	5.908	5.837	3.767	3.94
	Rmax	Ti-6242SG	5.74	6.4	30.84	4.24	6.28
		Weld Nugget	109.73	79	60.79	13.46	40.13
		Ti-6242SG	7.55	6.95	13.38	4.27	4.3
	Rt	Ti-6242SG	5.99	6.4	30.84	4.39	6.28
		Weld Nugget	111.4	79.26	60.86	13.46	40.13
		Ti-6242SG	7.55	7.17	13.38	4.27	4.3
	RSm	Ti-6242SG	21.55	23.95	23.26	18.14	20.45
		Weld Nugget	582.58	434.75	943.13	42.79	248.8
		Ti-6242SG	27.04	22.48	20.56	19.59	19.38
	Rsk	Ti-6242SG	-0.1	-0.08	5.74	0.06	-0.17
		Weld Nugget	-0.91	-1.19	0.35	-0.96	-0.01
		Ti-6242SG	-0.19	-0.12	4.02	-0.17	-0.1
	Rku	Ti-6242SG	2.61	2.69	48.96	2.28	3.16
		Weld Nugget	2.52	4.63	3.48	4.66	3.45
		Ti-6242SG	2.97	2.57	30.41	2.3	2.32

Ti-Joint	Surface Parameter (µm)	Location	Transverse				
			225/125	275/100	275/125	275/150	325/125
Ti-6242SG/Ti-6242SG	Ra	Ti-6242SG	0.677	0.772	0.762	0.749	0.778
		Weld Nugget	2.106	6.856	17.894	12.657	32.685
		Ti-6242SG	0.706	0.696	1.09	0.897	0.948
	Rq	Ti-6242SG	0.809	0.905	0.945	0.938	0.968
		Weld Nugget	3.041	9.38	20.572	14.787	36.882
		Ti-6242SG	0.859	0.895	1.757	1.115	1.167
	Rz	Ti-6242SG	4.183	4.13	5.117	5.266	5.075
		Weld Nugget	12.824	27.813	69.307	50.142	116.811
		Ti-6242SG	4.360	5.227	12.302	5.721	6.017
	Rmax	Ti-6242SG	5.39	4.42	6.05	5.590	6.14
		Weld Nugget	19.95	53.55	72.69	59.68	118.91
		Ti-6242SG	4.88	11.43	38.66	6.95	7.17
	Rt	Ti-6242SG	5.39	4.42	6.1	5.790	6.14
		Weld Nugget	20.52	53.55	78.99	61.54	123.76
		Ti-6242SG	4.96	11.43	38.66	6.95	7.17
	RSm	Ti-6242SG	18	17.37	25.59	35.960	30.33
		Weld Nugget	177.84	1337.5	480.25	572.17	398.44
		Ti-6242SG	19.79	18.61	24.23	25.01	25.12
	Rsk	Ti-6242SG	-0.06	-0.01	-0.02	-0.020	0
		Weld Nugget	1.08	-0.1	-0.74	0.08	-0.39
		Ti-6242SG	-0.07	0.62	4.37	0.01	0.02
	Rku	Ti-6242SG	2.46	2.07	2.77	2.940	2.84
		Weld Nugget	5.43	3.61	2.2	1.95	1.74
		Ti-6242SG	2.54	10.11	53.93	2.8	2.6

Ti-Joint	Surface Parameter (µm)	Location	Longitudinal				
			225/125	275/100	275/125	275/150	325/125
Ti-6242FG/Ti-6242FG	Ra	Ti-6242FG	0.887	1.126	0.751	0.758	0.818
		Weld Nugget	9.953	28.878	14.517	26.617	35.538
		Ti-6242FG	0.893	0.89	2.053	0.865	0.818
	Rq	Ti-6242FG	1.108	1.478	0.929	0.937	1.026
		Weld Nugget	12	32.791	17.851	29.511	40.052
		Ti-6242FG	1.095	1.086	2.931	1.066	1.021
	Rz	Ti-6242FG	6.58	8.28	5.211	5.135	5.538
		Weld Nugget	45.827	108.655	66.913	90.721	125.626
		Ti-6242FG	5.483	5.642	17.729	5.61	5.538
	Rmax	Ti-6242FG	7.69	10.9	6.37	5.87	7.45
		Weld Nugget	51.76	120.93	75.87	97.26	129.41
		Ti-6242FG	6.01	6.05	23.31	5.95	7.29
	Rt	Ti-6242FG	9.06	10.9	7.09	5.93	7.45
		Weld Nugget	56.31	120.93	76.15	105.23	129.89
		Ti-6242FG	6.01	6.36	23.31	6.17	7.29
	RSm	Ti-6242FG	27.65	46.95	28.88	24.29	31.82
		Weld Nugget	411.33	435	476.79	565.67	402.89
		Ti-6242FG	24.46	24.59	93.96	23.15	23.34
	Rsk	Ti-6242FG	-0.01	0.21	-0.35	-0.14	-0.18
		Weld Nugget	-0.29	-0.1	-1.12	-0.19	-0.5
		Ti-6242FG	-0.06	-0.02	-1.33	-0.01	0.02
	Rku	Ti-6242FG	3.25	3.86	3.22	2.91	2.9
		Weld Nugget	2.33	1.71	3.05	1.63	1.81
		Ti-6242FG	2.55	2.58	6.76	2.68	2.97

Ti-Joint	Surface Parameter (µm)	Location	Transverse				
			225/125	275/100	275/125	275/150	325/125
Ti-6242FG/Ti-6242FG	Ra	Ti-6242FG	0.689	0.719	0.638	0.651	0.642
		Weld Nugget	1.775	6.051	4.571	1.771	6.732
		Ti-6242FG	0.662	0.622	0.61	0.618	0.671
	Rq	Ti-6242FG	0.844	0.858	0.753	0.779	0.775
		Weld Nugget	2.413	8.841	6.319	2.502	9.544
		Ti-6242FG	0.782	0.737	0.722	0.741	0.783
	Rz	Ti-6242FG	4.47	4.119	3.624	4.044	3.866
		Weld Nugget	8.93	29.727	22.791	7.74	29.851
		Ti-6242FG	3.873	3.774	3.735	3.985	3.632
	Rmax	Ti-6242FG	5.94	5.17	4.29	4.58	4.93
		Weld Nugget	13.75	59.64	38.98	13.75	65.01
		Ti-6242FG	4.19	4.7	4.24	6.27	3.79
	Rt	Ti-6242FG	5.99	5.3	4.77	5	5.14
		Weld Nugget	16.03	59.64	41.5	15.84	65.01
		Ti-6242FG	4.3	4.7	4.58	6.27	3.88
	RSm	Ti-6242FG	18.85	17.13	17.75	18.42	18.68
		Weld Nugget	451.25	689.83	560	623.2	1171.25
		Ti-6242FG	17.37	17.07	17.54	18.13	16.84
	Rsk	Ti-6242FG	0.07	-0.08	0.01	0.04	-0.02
		Weld Nugget	-0.57	-0.23	-1.19	-1.06	-0.81
		Ti-6242FG	-0.02	-0.02	0.06	0.02	0.05
	Rku	Ti-6242FG	2.94	2.35	2.17	2.38	2.43
		Weld Nugget	3.72	4.57	5.55	4.45	4.89
		Ti-6242FG	2.25	2.23	2.3	2.67	2.03

Ti-Joint	Surface Parameter (µm)	Location	Transverse				
			225/125	275/100	275/125	275/150	325/125
Ti-64SG/Ti-54MFG	Ra	Ti-64SG		1.455	1.749	1.692	1.179
		Weld Nugget		57.543	28.656	21.951	48.49
		Ti-54MFG		3.13	1.805	1.561	1.354
	Rq	Ti-64SG		1.879	2.254	2.192	1.487
		Weld Nugget		65.565	33.366	24.973	60.052
		Ti-54MFG		4.256	2.421	2.041	1.749
	Rz	Ti-64SG		11.989	13.102	11.67	8.55
		Weld Nugget		216.14	112.228	82.475	207.619
		Ti-54MFG		22.485	13.853	12.927	10.476
	Rmax	Ti-64SG		14.5	16.3	14.2	9.9
		Weld Nugget		257.1	127	91.2	259.4
		Ti-54MFG		32.1	19.4	16.4	16.1
	Rt	Ti-64SG		17.5	16.8	14.5	10
		Weld Nugget		257.1	127	91.2	259.4
		Ti-54MFG		33.3	19.4	20.1	16.1
	RSm	Ti-64SG		27.1	36.5	32	22.7
		Weld Nugget		378.1	475.4	575.3	451.6
		Ti-54MFG		73.2	33.6	31.9	25.8
	Rsk	Ti-64SG		-0.43	-0.78	-0.68	-0.27
		Weld Nugget		-0.28	0.43	0.37	-0.44
		Ti-54MFG		-1.33	-0.36	0.54	-0.79
	Rku	Ti-64SG		4.59	4.48	3.67	3.25
		Weld Nugget		1.8	1.96	1.85	2.47
		Ti-54MFG		6.29	4.63	5.18	5.45

Ti-Joint	Surface Parameter (µm)	Location	Transverse				
			225/125	275/100	275/125	275/150	325/125
Ti-64SG/Ti-54MFG	Ra	Ti-64SG		1.403	1.493	1.216	1.957
		Weld Nugget		6.407	7.997	3.137	10.2
		Ti-54MFG		2.55	1.466	2.819	2.675
	Rq	Ti-64SG		1.736	1.844	1.504	2.424
		Weld Nugget		8.184	12.19	3.995	13.565
		Ti-54MFG		3.326	1.817	3.636	3.586
	Rz	Ti-64SG		8.905	10.316	8.31	13.018
		Weld Nugget		30.631	46.537	18.695	44.383
		Ti-54MFG		16.19	9.415	19.898	17.893
	Rmax	Ti-64SG		9.6	12.2	10	17.4
		Weld Nugget		42	84.2	20.1	63.4
		Ti-54MFG		22.2	10.8	33.5	25.4
	Rt	Ti-64SG		9.6	12.5	10.3	17.4
		Weld Nugget		42.6	97.6	24.6	79.1
		Ti-54MFG		22.2	11.7	33.6	25.4
	RSm	Ti-64SG		36.4	30.1	27.7	55.7
		Weld Nugget		327.9	368.8	158.3	438.3
		Ti-54MFG		77.7	29.8	22.8	75.6
	Rsk	Ti-64SG		-0.09	-0.06	-0.01	-0.48
		Weld Nugget		-0.12	0.46	-0.24	0.42
		Ti-54MFG		-0.61	0.12	0.99	-0.76
	Rku	Ti-64SG		2.67	2.86	2.86	3.15
		Weld Nugget		2.95	6.07	3.15	3.38
		Ti-54MFG		3.8	2.76	7.14	4.6

Ti-Joint	Surface Parameter (µm)	Location	Longitudinal				
			225/125	275/100	275/125	275/150	325/125
Ti-6242SG/Ti-54MFG	Ra	Ti-6242SG	0.721	0.605	0.599	0.706	0.537
		Weld Nugget	0.875	14.794	3.12	6.71	29.926
		Ti-54MFG	0.816	0.764	0.753	0.779	0.536
	Rq	Ti-6242SG	0.861	0.736	0.73	0.848	0.697
		Weld Nugget	1.159	18.064	4.239	8.995	33.802
		Ti-54MFG	0.995	0.942	0.94	0.952	0.746
	Rz	Ti-6242SG	4.056	3.604	3.882	4.182	3.871
		Weld Nugget	6.15	60.999	16.296	28.258	109.835
		Ti-54MFG	4.929	5.227	5.505	4.754	4.924
	Rmax	Ti-6242SG	4.5	4.82	4.58	4.85	5.07
		Weld Nugget	8.77	78.59	26.1	41.74	111.49
		Ti-54MFG	5.39	6.51	6.4	5.61	8.29
	Rt	Ti-6242SG	4.67	4.82	4.93	5.19	5.07
		Weld Nugget	8.96	78.59	26.1	44.92	114.1
		Ti-54MFG	5.5	6.51	6.74	6.68	8.3
	RSm	Ti-6242SG	18.14	19.98	18.51	18.51	47.33
		Weld Nugget	97.61	692.4	518	715.5	407.44
		Ti-54MFG	23.96	28.21	25.99	20.83	44.94
	Rsk	Ti-6242SG	-0.03	-0.05	-0.07	-0.04	-0.45
		Weld Nugget	0.28	-0.69	-0.9	-0.53	-0.61
		Ti-54MFG	-0.02	0.02	0.2	-0.16	-0.61
	Rku	Ti-6242SG	2.28	2.62	2.67	2.47	3.71
		Weld Nugget	4.55	2.69	4.75	3.28	1.98
		Ti-54MFG	2.47	2.72	3.1	2.73	8.01

Ti-Joint	Surface Parameter (µm)	Location	Transverse				
			225/125	275/100	275/125	275/150	325/125
Ti-6242SG/Ti-54MFG	Ra	Ti-6242SG	0.689	0.749	0.892	0.677	0.418
		Weld Nugget	11.737	14.242	18.166	22.234	2.16
		Ti-54MFG	0.849	1.035	0.811	0.692	0.558
	Rq	Ti-6242SG	0.857	0.928	1.105	0.835	0.529
		Weld Nugget	14.819	18.373	22.37	25.698	3.264
		Ti-54MFG	1.043	1.302	0.966	0.834	0.724
	Rz	Ti-6242SG	4.67	4.928	6.036	4.625	3.283
		Weld Nugget	51.961	72.653	85.169	84.882	13.9
		Ti-54MFG	5.53	7.191	4.563	4.007	4.538
	Rmax	Ti-6242SG	4.96	6.22	6.83	5.13	5.31
		Weld Nugget	64.92	91.34	102.22	87.47	30.75
		Ti-54MFG	5.92	8.08	5.28	4.48	5.21
	Rt	Ti-6242SG	5.43	6.33	6.83	5.25	5.68
		Weld Nugget	65.33	91.34	102.22	89.94	30.75
		Ti-54MFG	6.15	8.08	5.76	4.54	5.66
	RSm	Ti-6242SG	26.68	26.94	24.98	22.56	23.61
		Weld Nugget	593.58	381.94	469.69	574.5	289.81
		Ti-54MFG	22.18	30.63	19.72	18.42	46.4
	Rsk	Ti-6242SG	0.07	-0.06	-0.2	0.01	-0.5
		Weld Nugget	-0.88	-1.37	-0.48	0.28	1.26
		Ti-54MFG	-0.17	0.4	0.08	0.02	-0.79
	Rku	Ti-6242SG	2.79	2.92	2.78	2.74	5.43
		Weld Nugget	2.89	4.04	2.51	1.77	10.53
		Ti-54MFG	2.68	3.12	2.29	2.32	4.22

Ti-Joint	Surface Parameter (µm)	Location	Longitudinal				
			225/125	275/100	275/125	275/150	325/125
Ti-6242SG/Ti-64SG	Ra	Ti-6242SG	0.773	0.817	0.593	0.59	0.78
		Weld Nugget	30.358	29.791	18.024	20.339	4.988
		Ti-64SG	0.713	0.651	0.747	0.441	0.884
	Rq	Ti-6242SG	0.931	0.983	0.73	0.735	0.979
		Weld Nugget	35.251	33.813	20.166	24.575	7.504
		Ti-64SG	0.876	0.815	0.892	0.609	1.121
	Rz	Ti-6242SG	4.489	4.864	3.904	3.928	5.38
		Weld Nugget	119.994	112.211	64.961	88.876	23.312
		Ti-64SG	4.641	4.581	4.724	4.047	6.492
	Rmax	Ti-6242SG				4.85	8.52
		Weld Nugget				101.91	50.3
		Ti-64SG				4.99	10.84
	Rt	Ti-6242SG	5.21	5.45	4.71	4.85	8.86
		Weld Nugget	133.17	120.96	71.96	105.2	50.3
		Ti-64SG	5.87	5.42	5.93	5.29	10.84
	RSm	Ti-6242SG				32.11	19.6
		Weld Nugget				591.67	524.17
		Ti-64SG				30.27	25.89
	Rsk	Ti-6242SG				-0.04	-0.48
		Weld Nugget				-0.31	-1.6
		Ti-64SG				-1.33	0.47
	Rku	Ti-6242SG				2.92	4.69
		Weld Nugget				2.23	6.44
		Ti-64SG				6.79	5.43

Ti-Joint	Surface Parameter (µm)	Location	Transverse				
			225/125	275/100	275/125	275/150	325/125
Ti-6242SG/Ti-64SG	Ra	Ti-6242SG	0.48	0.429	0.477	0.437	1.081
		Weld Nugget	1.266	5.783	1.74	3.737	34.079
		Ti-64SG	0.651	0.912	0.616	0.46	0.708
	Rq	Ti-6242SG	0.592	0.542	0.632	0.568	1.325
		Weld Nugget	1.964	8.715	2.785	4.893	38.848
		Ti-64SG	0.814	1.141	0.769	0.588	0.868
	Rz	Ti-6242SG	3.175	3.2	3.741	3.744	6.922
		Weld Nugget	6.002	27.742	9.274	14.455	126.979
		Ti-64SG	4.33	6.087	4.026	3.214	4.824
	Rmax	Ti-6242SG				5.73	7.68
		Weld Nugget				25.18	131.77
		Ti-64SG				3.64	6.06
	Rt	Ti-6242SG	3.95	4	5.65	5.73	7.68
		Weld Nugget	12.62	53.88	17.75	30.16	139.75
		Ti-64SG	4.99	6.99	4.9	4.09	6.61
	RSm	Ti-6242SG				24.12	25.22
		Weld Nugget				556.83	419.25
		Ti-64SG				43.62	19.39
	Rsk	Ti-6242SG				-0.3	-0.14
		Weld Nugget				-0.35	-0.15
		Ti-64SG				-0.7	-0.2
	Rku	Ti-6242SG				4.77	2.69
		Weld Nugget				3.7	1.71
		Ti-64SG				3.67	2.93

Ti-Joint	Surface Parameter (µm)	Location	Longitudinal				
			225/125	275/100	275/125	275/150	325/125
Ti-64FG/Ti-54MFG	Ra	Ti-64FG	1.493	1.113	0.895	2.16	1.068
		Weld Nugget	34.349	39.53	40.244	21.885	83.821
		Ti-54MFG	1.093	1.522	1.156	1.402	1.619
	Rq	Ti-64FG	2.021	1.353	1.087	3.245	1.271
		Weld Nugget	41.1	43.804	44.843	24.619	94.403
		Ti-54MFG	1.355	2.129	1.835	2.082	2.034
	Rz	Ti-64FG	12.959	7.553	5.896	21.231	6.358
		Weld Nugget	137.269	129.797	133.586	77.928	298.084
		Ti-54MFG	7.904	12.097	9.93	14.071	12.9
	Rmax	Ti-64FG	17.6	8.4	6.4	26.4	7.1
		Weld Nugget	147.2	138	139.1	89.1	302.8
		Ti-54MFG	9.8	16.7	23	22.3	12.9
	Rt	Ti-64FG	19.7	8.8	6.8	27.8	7.1
		Weld Nugget	149.1	146.2	141.3	91.8	303.3
		Ti-54MFG	4.093	17.3	23	22.3	13.2
	RSm	Ti-64FG	26.3	18.8	18.1	41.4	17.4
		Weld Nugget	575	373.6	461.9	561.5	399.8
		Ti-54MFG	21.8	30.3	23.1	28.4	33.5
	Rsk	Ti-64FG	-0.92	-0.02	0.09	-1.73	0.01
		Weld Nugget	0.55	-0.02	0.32	-0.05	-0.3
		Ti-54MFG	-0.13	-0.87	-3.73	-1.58	0.27
	Rku	Ti-64FG	6.21	2.59	2.62	8.01	2.28
		Weld Nugget	2.14	1.5	1.6	1.71	1.69
		Ti-54MFG	2.98	5.75	31.37	9.5	3

Ti-Joint	Surface Parameter (µm)	Location	Transverse				
			225/125	275/100	275/125	275/150	325/125
Ti-64FG/Ti-54MFG	Ra	Ti-64FG	1.228	1.245	1.138	1.298	1.198
		Weld Nugget	7.104	17.265	10.114	1.39	33.699
		Ti-54MFG	1.59	1.373	1.49	1.701	1.837
	Rq	Ti-64FG	1.514	1.542	1.396	1.734	1.484
		Weld Nugget	12.326	21.236	13.735	1.781	41.239
		Ti-54MFG	1.984	1.723	2.036	2.374	2.436
	Rz	Ti-64FG	8.41	8.238	7.492	11.285	7.772
		Weld Nugget	40.232	76.349	53.709	9.604	132.347
		Ti-54MFG	11.705	9.626	13.767	15.376	14.393
	Rmax	Ti-64FG	9.7	9.7	7.9	14.4	9.1
		Weld Nugget	101	120.4	74.4	14.5	177.6
		Ti-54MFG	13.6	12.9	20.9	19.2	17.8
	Rt	Ti-64FG	9.7	9.9	8.5	15.3	9.1
		Weld Nugget	101	120.4	74.4	15.7	178.1
		Ti-54MFG	14.8	13.4	20.9	21.5	18.9
	RSm	Ti-64FG	30.8	28.3	39.4	38.2	34.4
		Weld Nugget	1014	714.4	1084.3	80.9	768.5
		Ti-54MFG	28.8	26.9	33	39	37.5
	Rsk	Ti-64FG	0.14	-0.07	0.03	-0.76	-0.05
		Weld Nugget	2.57	-0.1	1.24	-1.04	-0.77
		Ti-54MFG	-0.16	-0.2	-0.93	-1.16	1.03
	Rku	Ti-64FG	2.75	2.72	2.69	5.14	2.68
		Weld Nugget	14.51	2.69	4.62	3.59	2.74
		Ti-54MFG	3.09	3.36	7.35	6.99	5.87

Ti-Joint	Surface Parameter (µm)	Location	Longitudinal				
			225/125	275/100	275/125	275/150	325/125
Ti-6242FG/Ti-54MFG	Ra	Ti-6242FG	1.009	0.695		0.92	0.597
		Weld Nugget	25.187	29.264		5.568	27.996
		Ti-54MFG	0.978	0.351		0.835	0.455
	Rq	Ti-6242FG	1.31	0.889		1.136	0.764
		Weld Nugget	31.805	33.125		6.915	33.992
		Ti-54MFG	1.25	0.452		1.097	0.567
	Rz	Ti-6242FG	6.759	4.757		5.772	3.909
		Weld Nugget	126.984	105.862		29.04	123.297
		Ti-54MFG	7.053	2.584		6.815	3.144
	Rmax	Ti-6242FG	10.03	5.56			5.04
		Weld Nugget	131.48	113.11			161.25
		Ti-54MFG	7.72	3.62			3.32
	Rt	Ti-6242FG	10.51	5.6		7.18	5.04
		Weld Nugget	131.49	114.56		32.5	168.89
		Ti-54MFG	7.83	3.62		9.6	3.53
	RSm	Ti-6242FG	85.92	56.74			68.18
		Weld Nugget	437.19	384.1			389.72
		Ti-54MFG	66.31	30.06			33.91
	Rsk	Ti-6242FG	-1.14	-0.26			-0.61
		Weld Nugget	-0.6	-0.49			-0.38
		Ti-54MFG	-0.59	0.54			-0.22
	Rku	Ti-6242FG	4.77	3.12			3.6
		Weld Nugget	2.67	1.82			2.61
		Ti-54MFG	3.5	3.97			2.89

Ti-Joint	Surface Parameter (µm)	Location	Transverse				
			225/125	275/100	275/125	275/150	325/125
Ti-6242FG/Ti-54MFG	Ra	Ti-6242FG	1.051	0.422		0.721	0.342
		Weld Nugget		4.987		2.155	1.496
		Ti-54MFG	0.597	0.497		0.616	0.444
	Rq	Ti-6242FG	1.496	0.624		0.894	0.421
		Weld Nugget		7.858		2.892	2.117
		Ti-54MFG	0.782	0.637		0.777	0.553
	Rz	Ti-6242FG	8.182	3.623		4.737	2.255
		Weld Nugget		20.917		11.845	8.331
		Ti-54MFG	3.848	3.954		4.555	3.042
	Rmax	Ti-6242FG	9.48	6.41			2.4
		Weld Nugget		49.27			13.75
		Ti-54MFG	4.87	5.61			3.31
	Rt	Ti-6242FG	9.55	6.89		5.93	2.5
		Weld Nugget		52.38		18.33	15.16
		Ti-54MFG	5.76	5.65		6.1	3.82
	RSm	Ti-6242FG	108.93	25.47			22.56
		Weld Nugget		759.25			120.54
		Ti-54MFG	70.65	52.23			57.29
	Rsk	Ti-6242FG	-1.57	2.81			0.12
		Weld Nugget		-1.64			1.12
		Ti-54MFG	-0.81	-0.01			-0.22
	Rku	Ti-6242FG	6.44	22.46			2.65
		Weld Nugget		7.16			5.61
		Ti-54MFG	4.7	4.09			2.96

Ti-Joint	Surface Parameter (µm)	Location	Longitudinal				
			225/125	275/100	275/125	275/150	325/125
Ti-6242FG/Ti-64SG	Ra	Ti-6242FG	0.736	0.55		0.526	0.659
		Weld Nugget	2.173	2.581		32.393	4.21
		Ti-64SG	0.797	1.171		1.477	0.733
	Rq	Ti-6242FG	0.88	0.674		0.668	0.776
		Weld Nugget	3.252	4.371		37.032	6.024
		Ti-64SG	0.972	1.497		2.119	0.927
	Rz	Ti-6242FG	4.186	3.584		4.029	3.735
		Weld Nugget	12.54	11.722		124.665	21.835
		Ti-64SG	5.003	8.454		10.918	4.786
	Rmax	Ti-6242FG	4.94	4.42		4.68	4.6
		Weld Nugget	25.72	24.53		143.99	35.99
		Ti-64SG	5.37	9.9		14.34	5.95
	Rt	Ti-6242FG	5.09	4.53		5.06	4.6
		Weld Nugget	25.95	33.9		143.99	40.21
		Ti-64SG	5.4	10.52		14.94	5.95
	RSm	Ti-6242FG	18.33	17.53		43.56	17.52
		Weld Nugget	337.85	165.45		568.67	538.3
		Ti-64SG	22.82	34.31		152.25	28.41
	Rsk	Ti-6242FG	0.01	-0.1		-0.33	0.03
		Weld Nugget	-0.35	-1.01		0.07	-1.16
		Ti-64SG	-0.04	0.67		-2	-0.21
	Rku	Ti-6242FG	2.23	2.77		3.48	2.18
		Weld Nugget	7.07	8.4		1.82	5.88
		Ti-64SG	2.49	3.91		7.74	3.11

Ti-Joint	Surface Parameter (µm)	Location	Transverse				
			225/125	275/100	275/125	275/150	325/125
Ti-6242FG/Ti-64SG	Ra	Ti-6242FG	0.809	0.953		0.376	0.808
		Weld Nugget	14.665	24.706		3.648	27.033
		Ti-64SG	0.613	0.767		0.473	0.682
	Rq	Ti-6242FG	0.987	1.155		0.459	1.008
		Weld Nugget	16.361	28.67		5.545	30.667
		Ti-64SG	0.754	0.984		0.613	0.811
	Rz	Ti-6242FG	4.913	5.669		2.521	5.56
		Weld Nugget	52.187	97.63		17.702	103.451
		Ti-64SG	3.979	5.28		3.719	3.713
	Rmax	Ti-6242FG	5.63	6.47		3.18	6.9
		Weld Nugget	56.68	106.67		37.21	115.14
		Ti-64SG	4.42	8.77		4.36	4.58
	Rt	Ti-6242FG	5.86	6.47		3.18	7.27
		Weld Nugget	61.76	106.67		37.21	115.76
		Ti-64SG	4.63	8.77		4.68	4.71
	RSm	Ti-6242FG	22.63	21.32		19.69	25.67
		Weld Nugget	577.25	376.15		700.5	405.67
		Ti-64SG	21.71	23.15		40.56	17.98
	Rsk	Ti-6242FG	-0.01	-0.03		-0.1	-0.33
		Weld Nugget	-0.07	-0.73		2	-0.26
		Ti-64SG	-0.15	-0.53		-0.67	0
	Rku	Ti-6242FG	2.56	2.41		2.69	3.2
		Weld Nugget	1.65	2.18		8.96	1.83
		Ti-64SG	2.68	4.61		4.06	2.3

Ti-Joint	Surface Parameter (µm)	Location	Longitudinal				
			225/125	275/100	275/125	275/150	325/125
Ti-6242FG/Ti-64FG	Ra	Ti-6242FG	0.668	0.687		0.682	0.663
		Weld Nugget	7.944	26.845		25.983	20.079
		Ti-64FG	0.584	0.286		0.306	0.577
	Rq	Ti-6242FG	0.829	0.862		0.866	0.828
		Weld Nugget	9.454	31.226		30.263	24.133
		Ti-64FG	0.811	0.355		0.381	0.786
	Rz	Ti-6242FG	4.433	4.539		4.917	4.317
		Weld Nugget	31.748	102.41		100.239	81.067
		Ti-64FG	4.501	1.88		2.182	4.229
	Rmax	Ti-6242FG	5.1	5.24		5.72	4.68
		Weld Nugget	36.91	133.37		107.78	93.98
		Ti-64FG	6.67	2.49		2.68	6.32
	Rt	Ti-6242FG	5.66	5.56		6.05	5.23
		Weld Nugget	38.03	133.37		115.68	97.69
		Ti-64FG	6.67	2.49		2.68	6.32
	RSm	Ti-6242FG	60.83	69.13		53.77	62.44
		Weld Nugget	577	392.22		576.92	431.69
		Ti-64FG	60.15	23.69		21.91	29.88
	Rsk	Ti-6242FG	0.12	-0.51		-0.51	-0.52
		Weld Nugget	-1.06	-0.37		0.48	-0.94
		Ti-64FG	-1.37	0.08		0.02	-0.54
	Rku	Ti-6242FG	2.86	3.17		3.47	2.99
		Weld Nugget	2.69	2.05		2	2.78
		Ti-64FG	7.88	2.87		2.92	5.74

Ti-Joint	Surface Parameter (µm)	Location	Transverse				
			225/125	275/100	275/125	275/150	325/125
Ti-6242FG/Ti-64FG	Ra	Ti-6242FG	0.377	0.582		0.42	0.422
		Weld Nugget	2.796	4.835		9.485	6.439
		Ti-64FG	0.525	0.475		0.556	0.551
	Rq	Ti-6242FG	0.473	1.79		0.696	0.522
		Weld Nugget	3.993	6.981		12.311	8.879
		Ti-64FG	0.654	0.594		0.689	0.702
	Rz	Ti-6242FG	2.826	9.316		4.366	2.805
		Weld Nugget	15.369	25.955		39.081	31.108
		Ti-64FG	3.525	3.053		3.515	3.779
	Rmax	Ti-6242FG	2.98	21.31		12.86	3.42
		Weld Nugget	21.36	43.45		68.78	56.14
		Ti-64FG	3.8	3.42		3.76	4.43
	Rt	Ti-6242FG	3.29	21.31		12.86	3.47
		Weld Nugget	24.14	50.82		68.78	56.14
		Ti-64FG	4.17	3.57		4.01	4.43
	RSm	Ti-6242FG	22.25	84.66		18.54	20.32
		Weld Nugget	289.35	361.3		1194.5	1384.5
		Ti-64FG	40.2	61.04		42.96	55.62
	Rsk	Ti-6242FG	-0.05	7.65		0.01	-0.1
		Weld Nugget	-1	-1.12		0.4	-0.56
		Ti-64FG	-0.21	-0.13		-0.05	-0.18
	Rku	Ti-6242FG	3.02	70.91		20.99	2.81
		Weld Nugget	4.77	6.04		3.32	4.19
		Ti-64FG	2.89	2.8		2.65	3.04

G.3 Effect of Feed Rate and Spindle Speed on (Ra) at Weld Nugget

This section illustrates the graphs of effect of the process parameters, the spindle speed and the feed rate, on the surface roughness of the weld nugget. The profile parameter 'Ra' is plotted for the cases of similar and dissimilar friction stir welded titanium joints. For most of the cases feed rate had more influence on the profile in the longitudinal direction, while effect of speed was observed in the transverse direction.

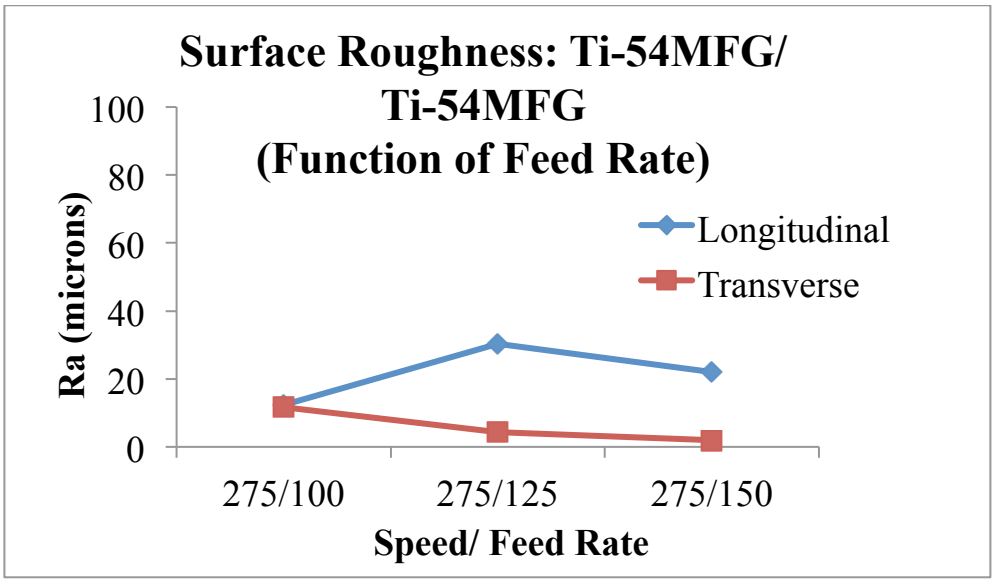

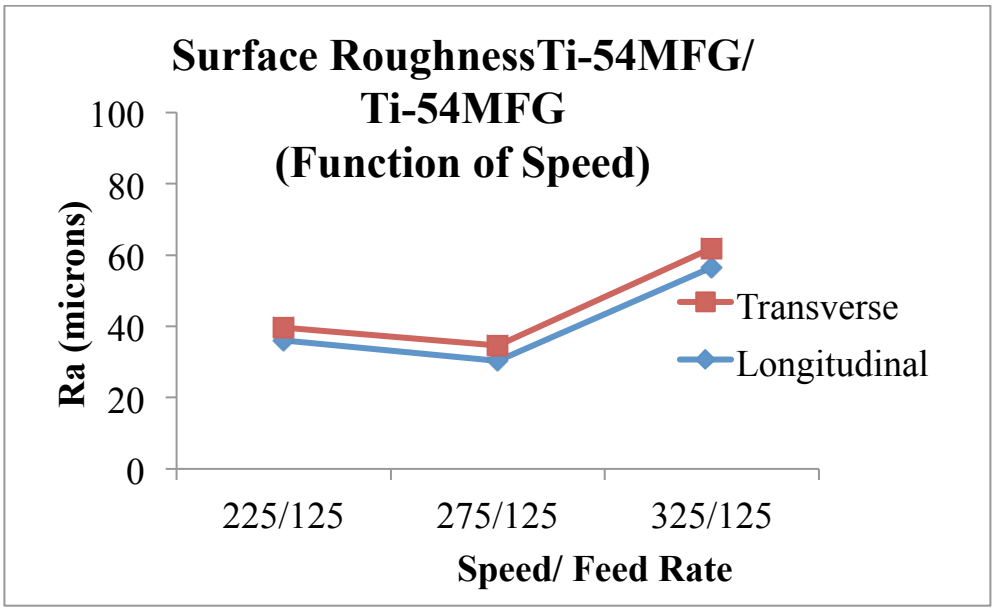

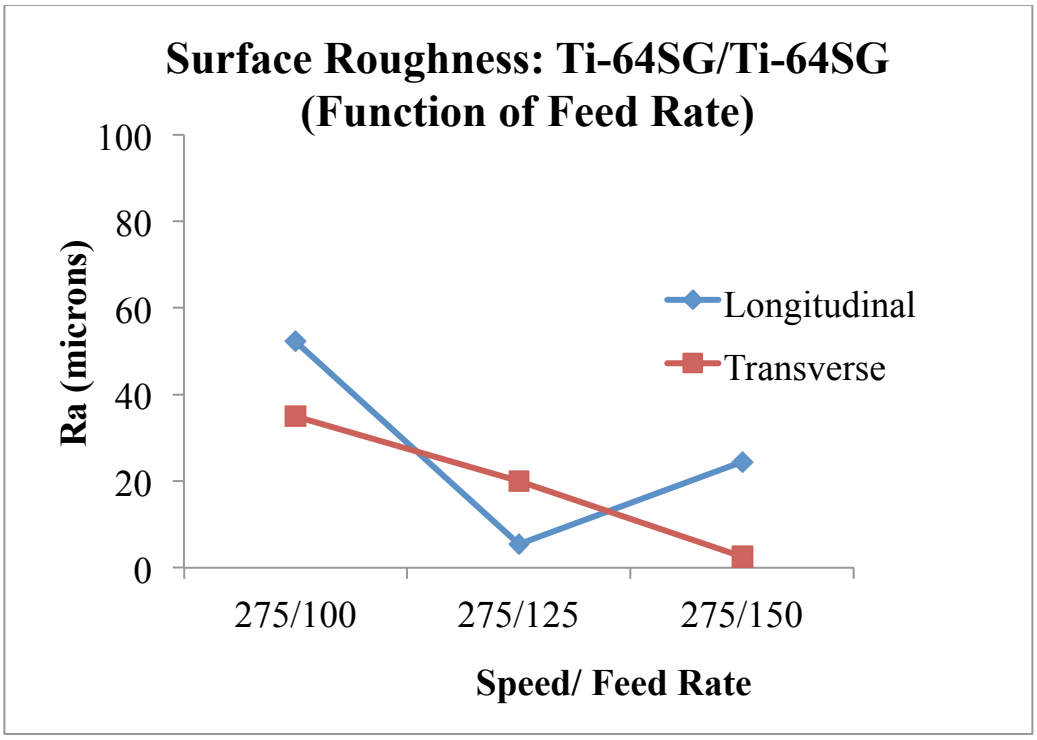
Surface Roughness: Ti-64SG/Ti-64SG
(Function of Feed Rate)
100
80
60
40
20
0
Ra (microns)
Longitudinal
Transverse
275/100
275/125
275/150
Speed/ Feed Rate

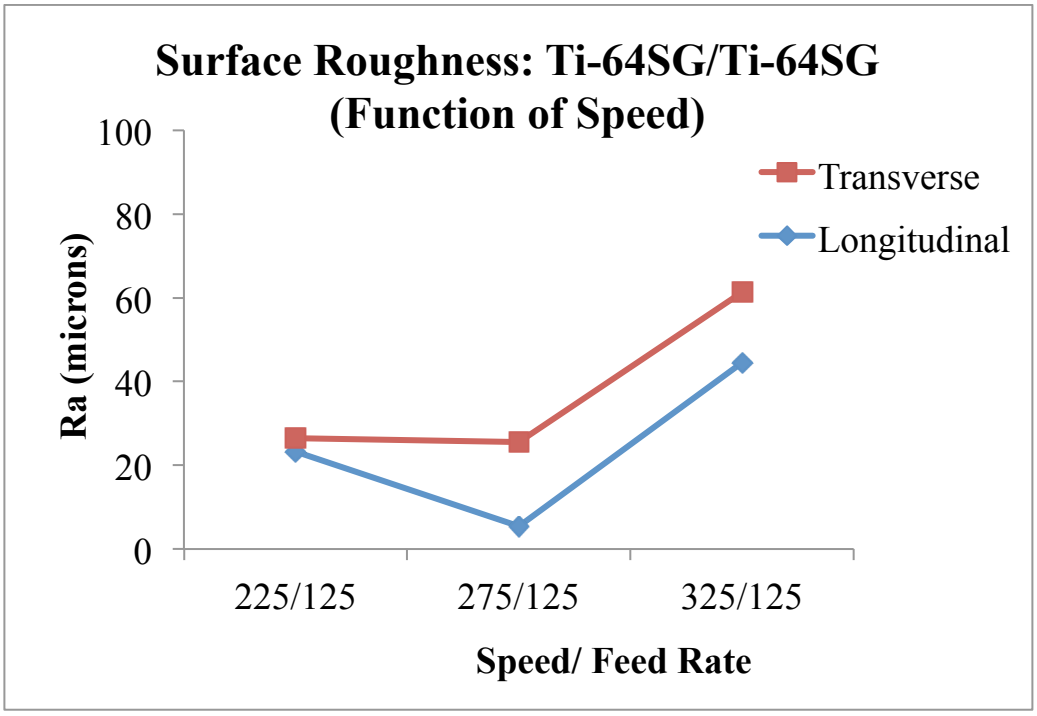
Surface Roughness: Ti-64SG/Ti-64SG
(Function of Speed)
100
80
60
40
20
0
Ra (microns)
Transverse
Longitudinal
225/125
275/125
325/125
Speed/ Feed Rate

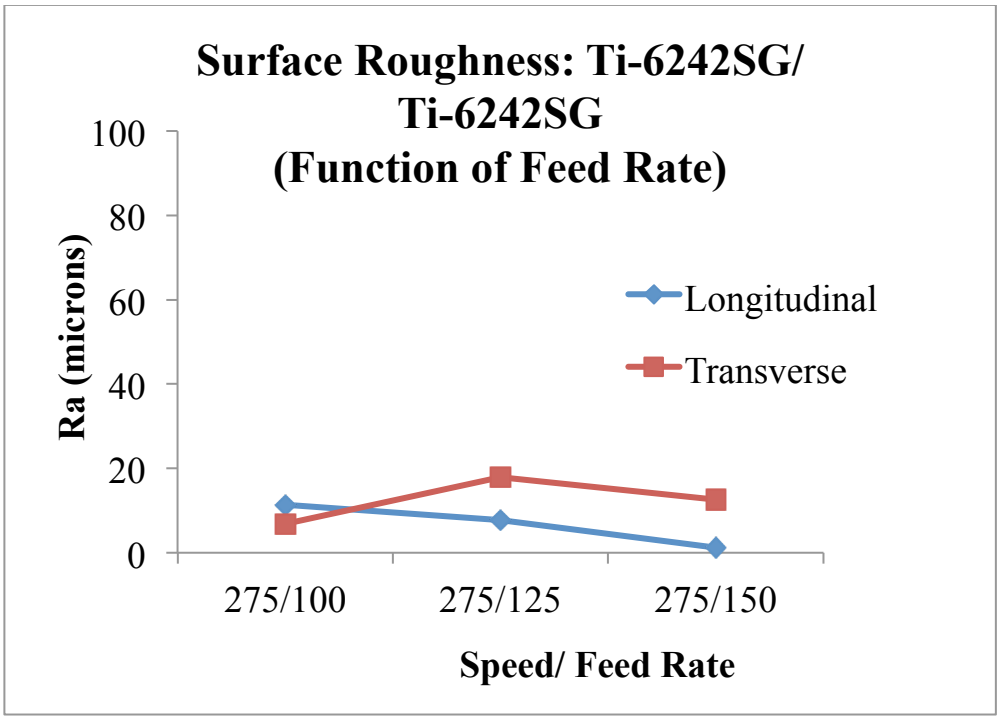
Surface Roughness: Ti-6242SG/ Ti-6242SG (Function of Feed Rate)
Ra (microns)
100
80
60
40
20
0
Longitudinal
Transverse
275/100
275/125
275/150
Speed/ Feed Rate

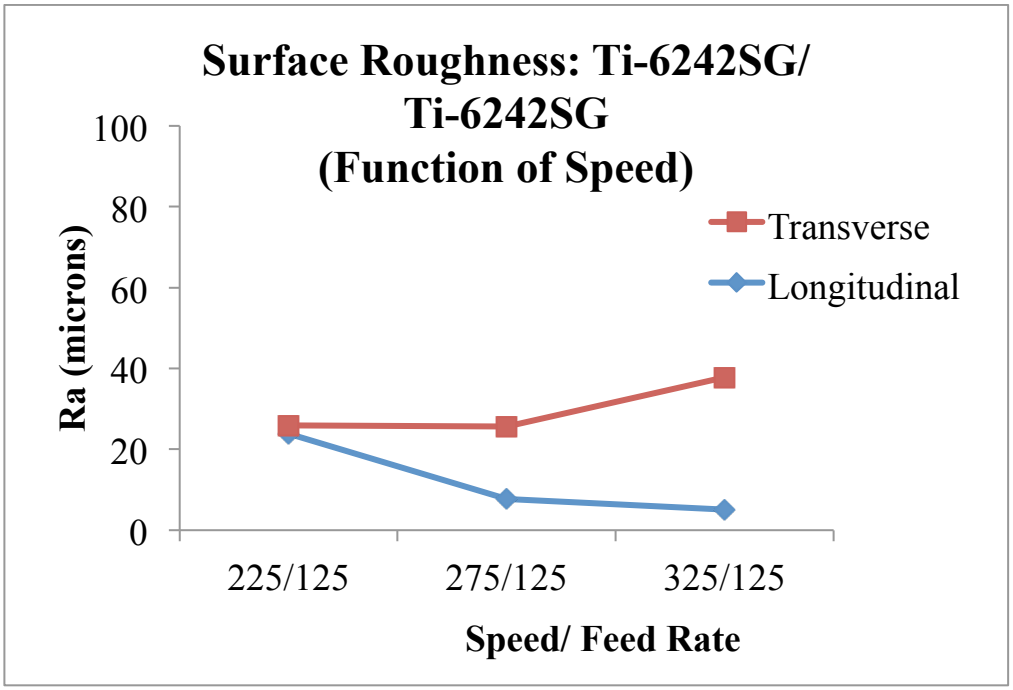
Surface Roughness: Ti-6242SG/ Ti-6242SG (Function of Speed)
Ra (microns)
100
80
60
40
20
0
Transverse
Longitudinal
225/125
275/125
325/125
Speed/ Feed Rate

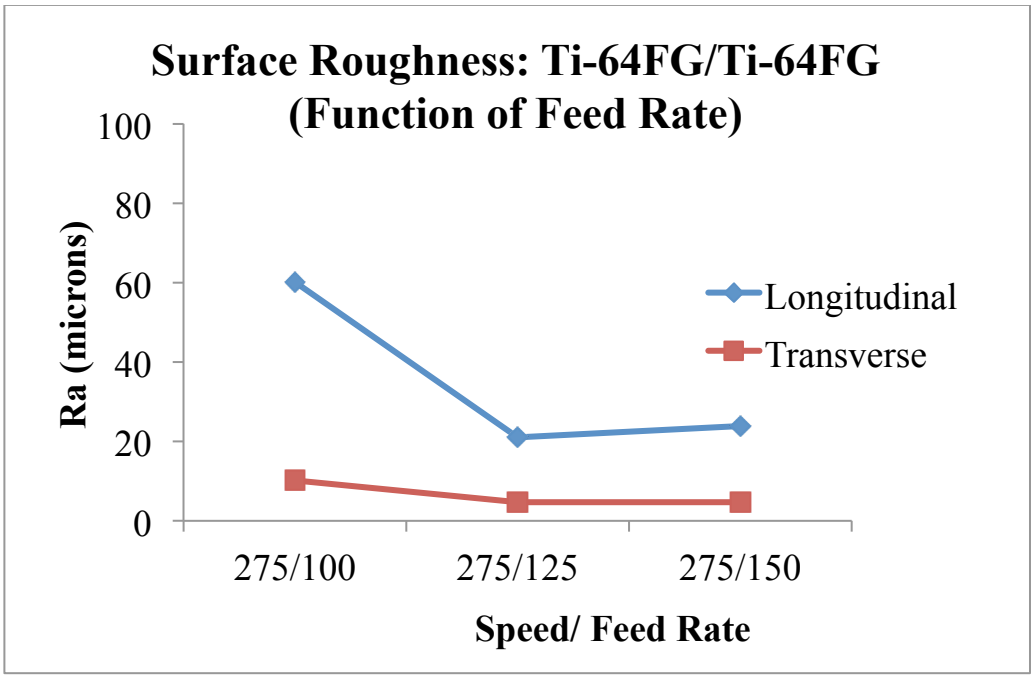
Surface Roughness: Ti-64FG/Ti-64FG
(Function of Feed Rate)
Ra (microns)
100
80
60
40
20
0
275/100
275/125
275/150
Speed/ Feed Rate
Longitudinal
Transverse

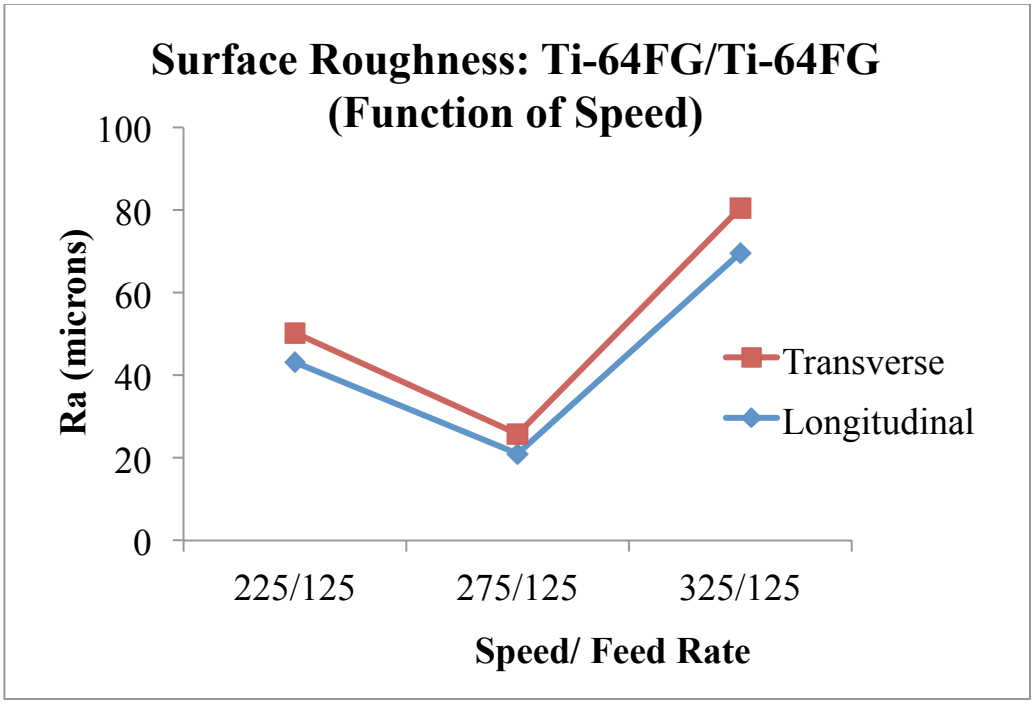
Surface Roughness: Ti-64FG/Ti-64FG
(Function of Speed)
Ra (microns)
100
80
60
40
20
0
225/125
275/125
325/125
Speed/ Feed Rate
Transverse
Longitudinal

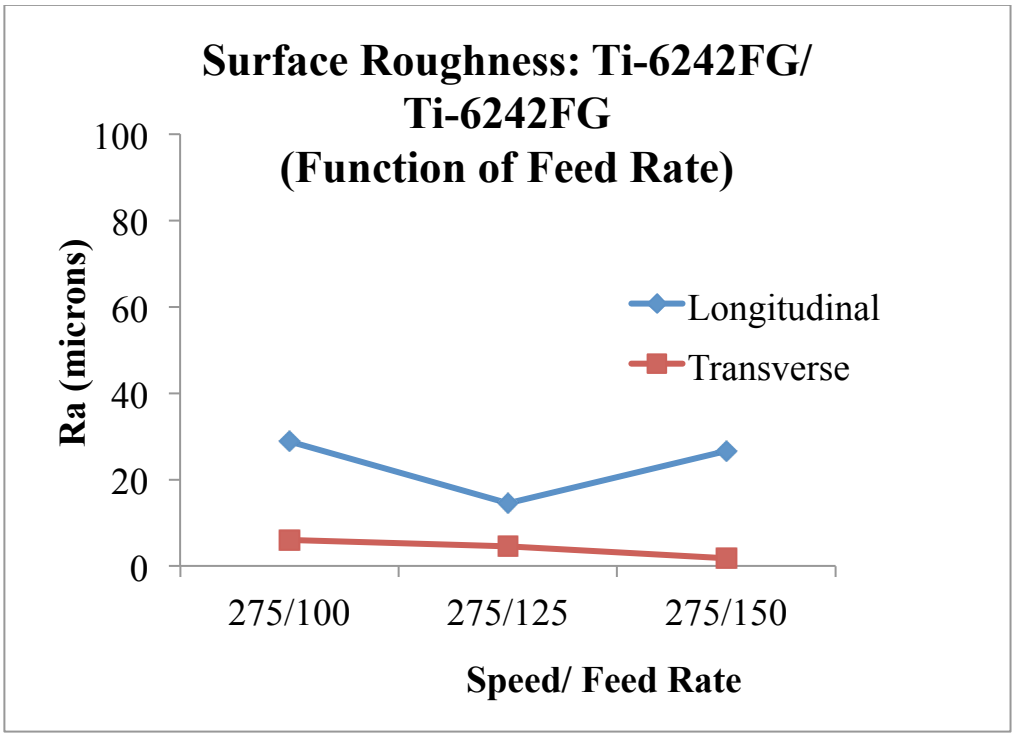
Surface Roughness: Ti-6242FG/ Ti-6242FG (Function of Feed Rate)
Ra (microns)
100
80
60
40
20
0
Longitudinal
Transverse
275/100
275/125
275/150
Speed/ Feed Rate

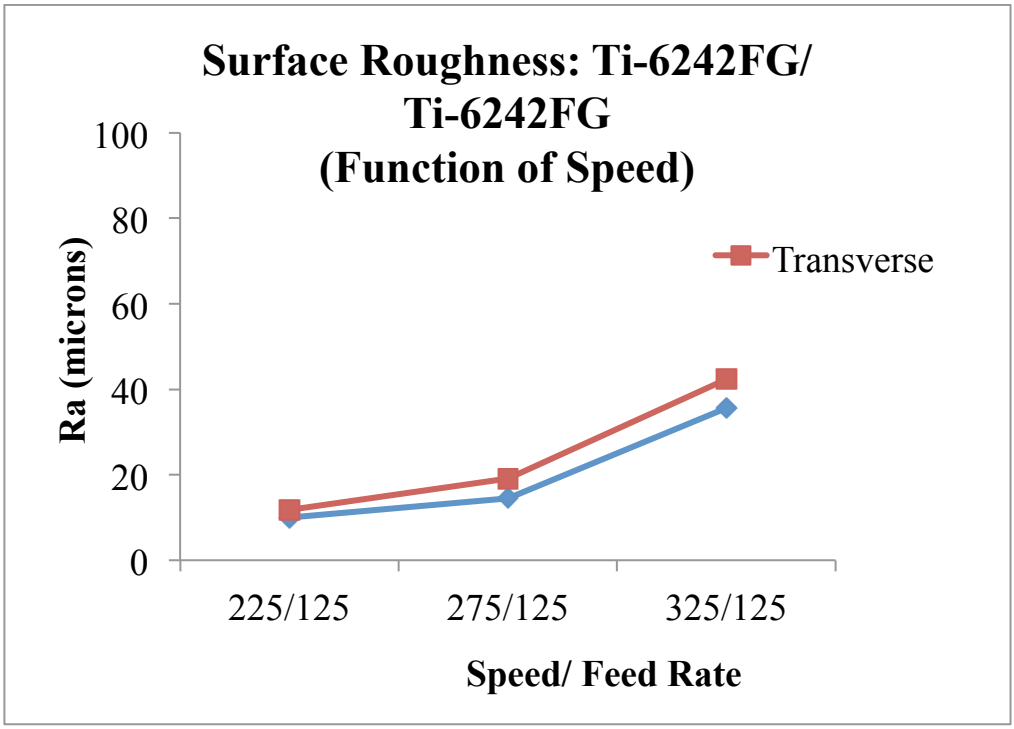
Surface Roughness: Ti-6242FG/ Ti-6242FG (Function of Speed)
Ra (microns)
100
80
60
40
20
0
Transverse
225/125
275/125
325/125
Speed/ Feed Rate

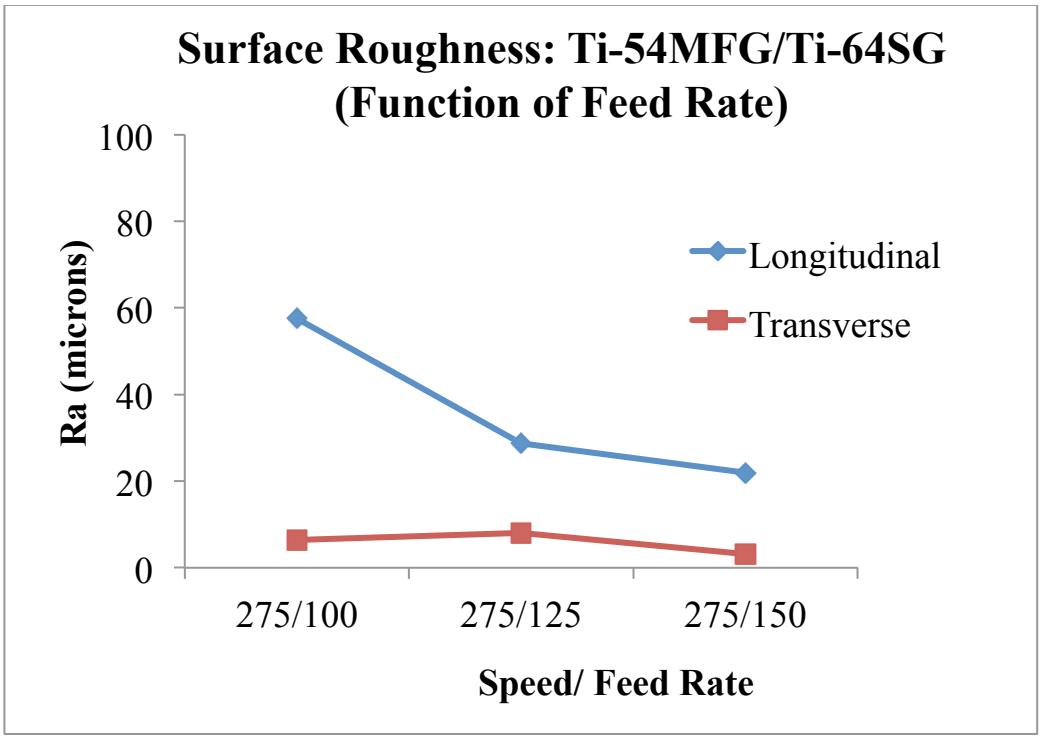
Surface Roughness: Ti-54MFG/Ti-64SG
(Function of Feed Rate)
100
80
60
40
20
0
Ra (microns)
Longitudinal
Transverse
275/100
275/125
275/150
Speed/ Feed Rate

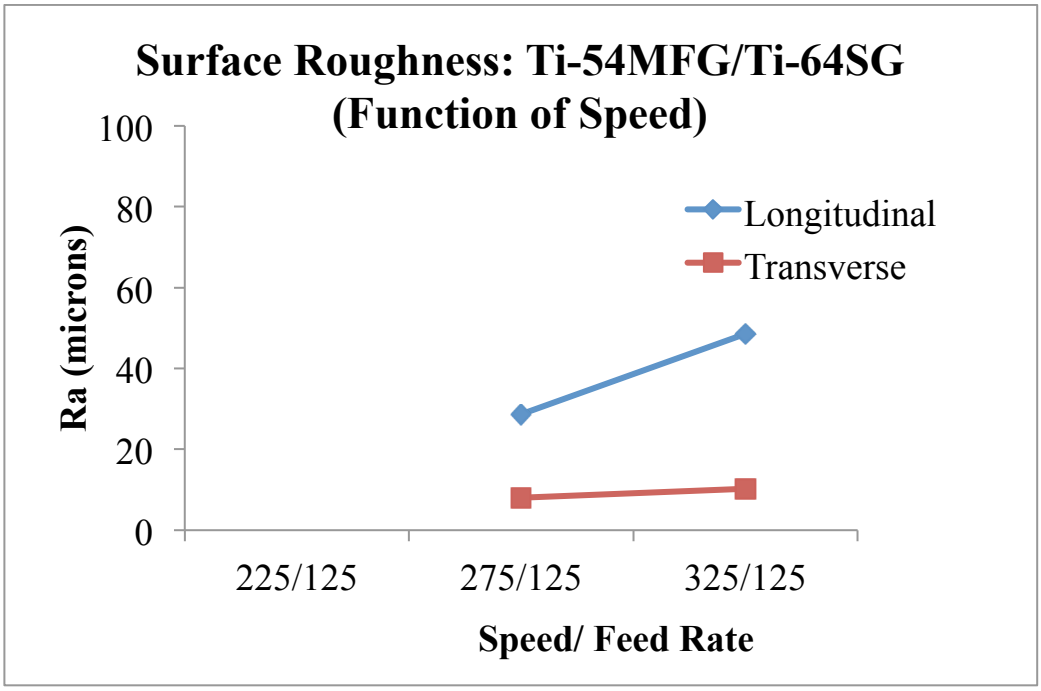
Surface Roughness: Ti-54MFG/Ti-64SG
(Function of Speed)
100
80
60
40
20
0
Ra (microns)
Longitudinal
Transverse
225/125
275/125
325/125
Speed/ Feed Rate

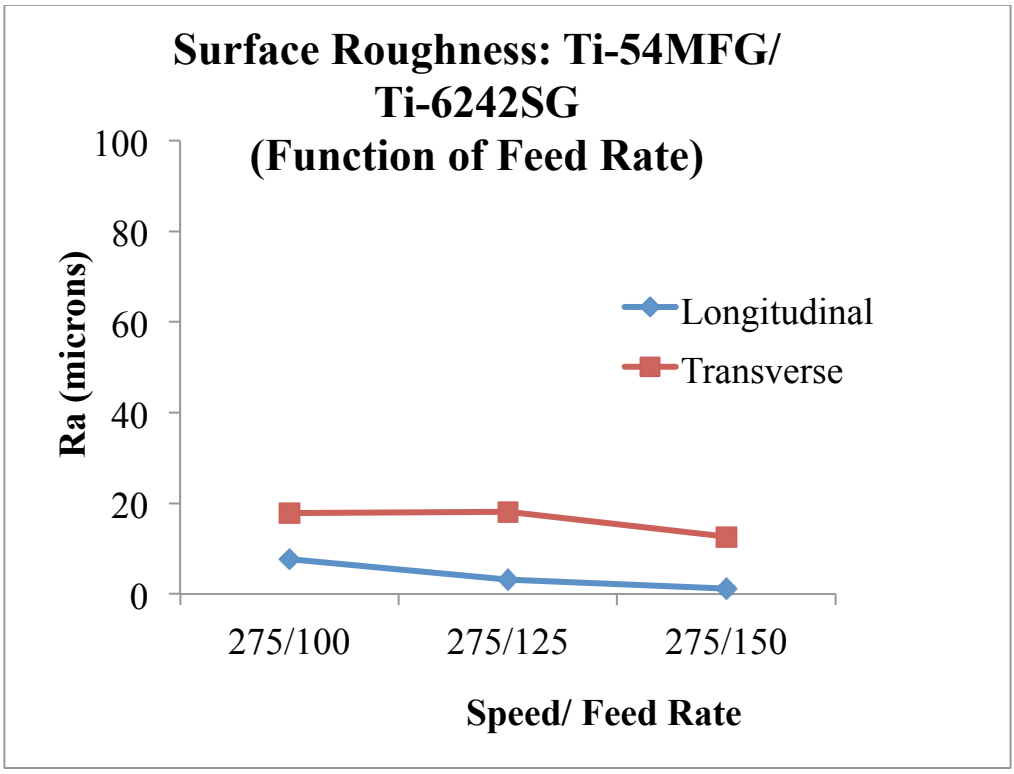
Surface Roughness: Ti-54MFG/ Ti-6242SG (Function of Feed Rate)
Ra (microns)
100
80
60
40
20
0
Longitudinal
Transverse
275/100
275/125
275/150
Speed/ Feed Rate

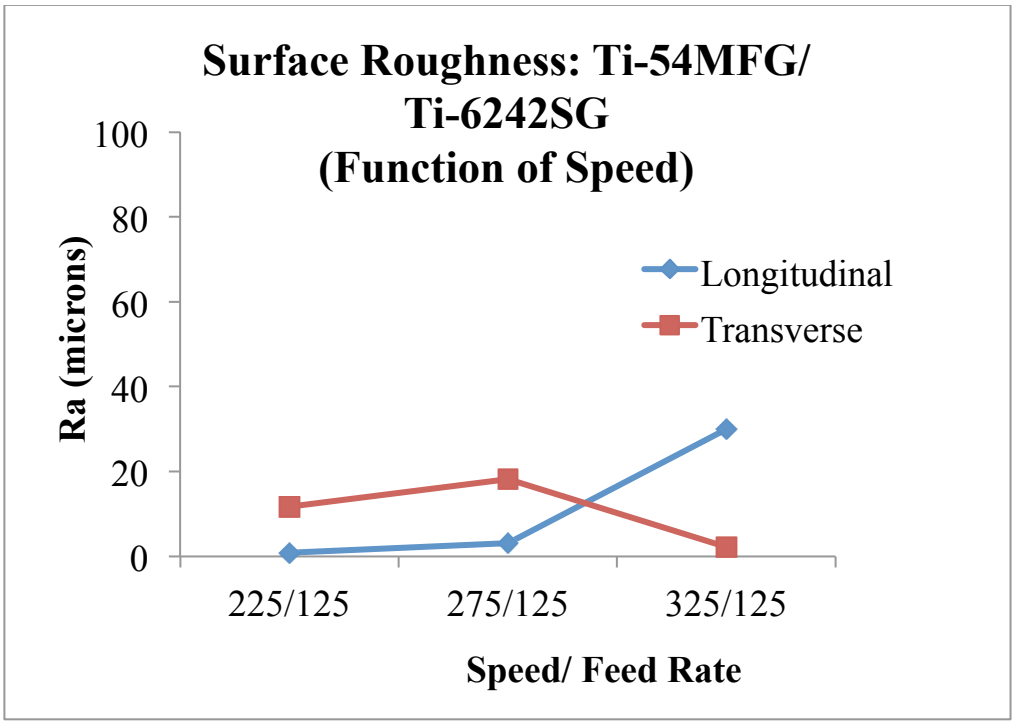
Surface Roughness: Ti-54MFG/ Ti-6242SG (Function of Speed)
Ra (microns)
100
80
60
40
20
0
Longitudinal
Transverse
225/125
275/125
325/125
Speed/ Feed Rate

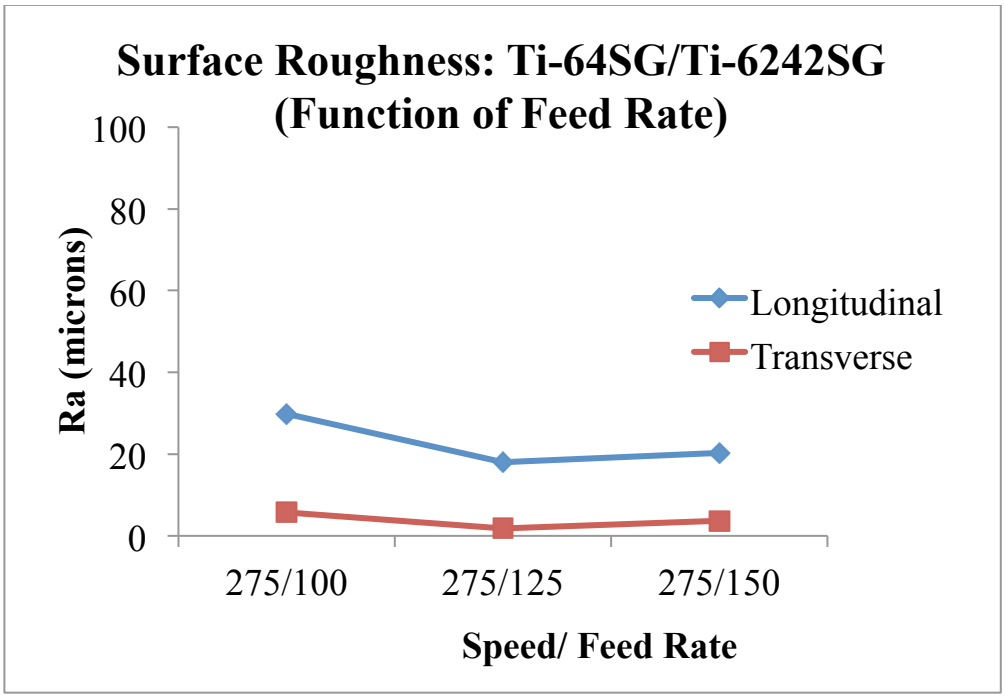
Surface Roughness: Ti-64SG/Ti-6242SG
(Function of Feed Rate)
100
80
60
40
20
0
Ra (microns)
Longitudinal
Transverse
275/100
275/125
275/150
Speed/ Feed Rate

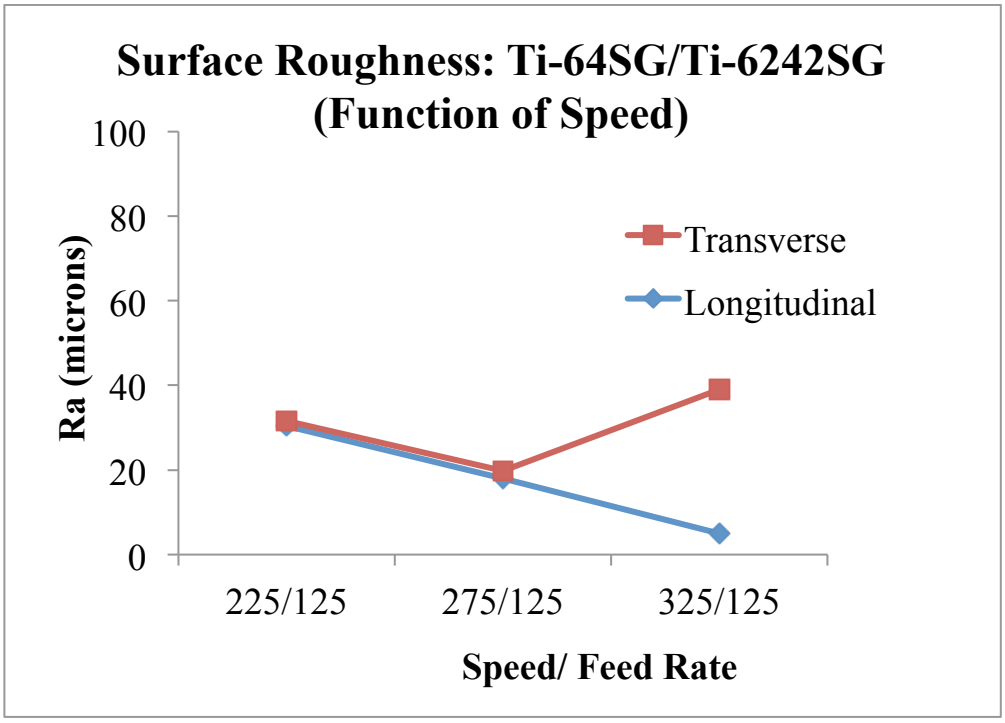
Surface Roughness: Ti-64SG/Ti-6242SG
(Function of Speed)
100
80
60
40
20
0
Ra (microns)
Transverse
Longitudinal
225/125
275/125
325/125
Speed/ Feed Rate

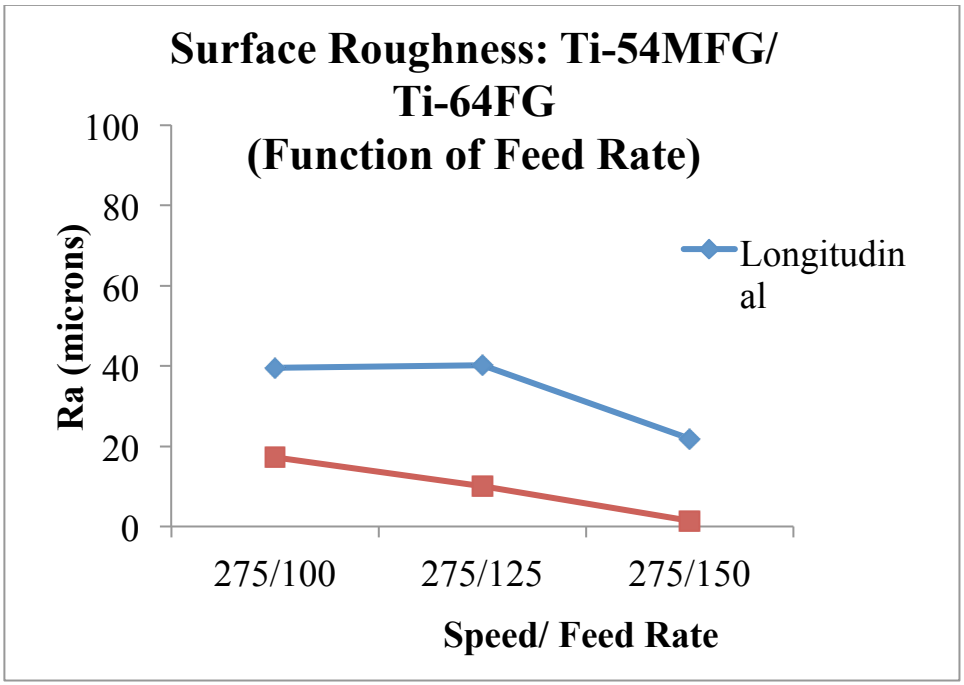
Surface Roughness: Ti-54MFG/ Ti-64FG (Function of Feed Rate)
Ra (microns)
100
80
60
40
20
0
Longitudinal
275/100
275/125
275/150
Speed/ Feed Rate

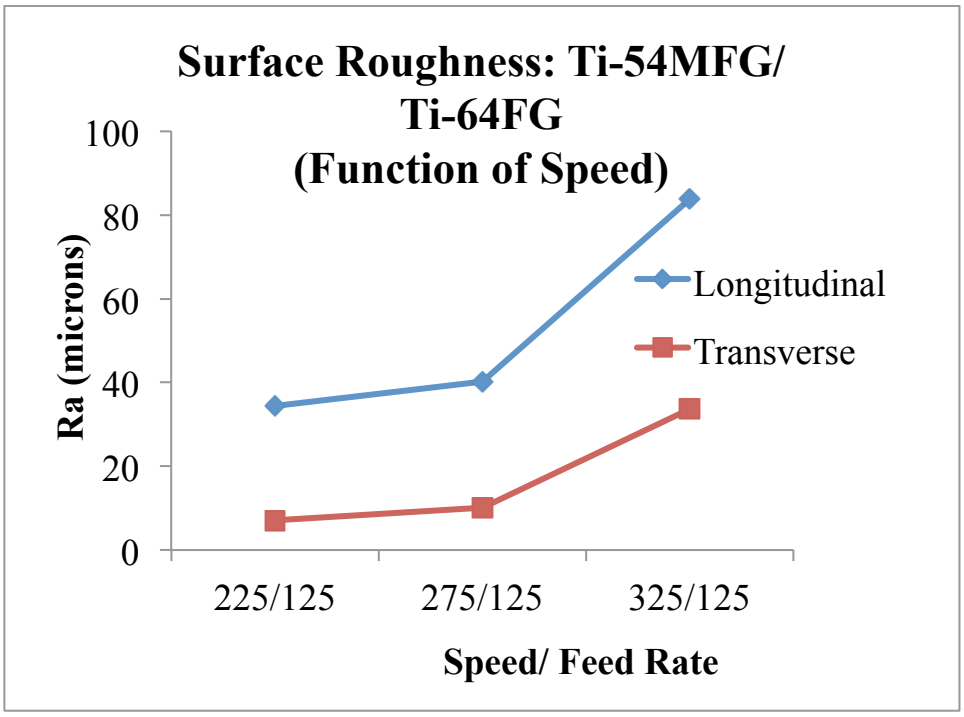
Surface Roughness: Ti-54MFG/ Ti-64FG (Function of Speed)
Ra (microns)
100
80
60
40
20
0
Longitudinal
Transverse
225/125
275/125
325/125
Speed/ Feed Rate

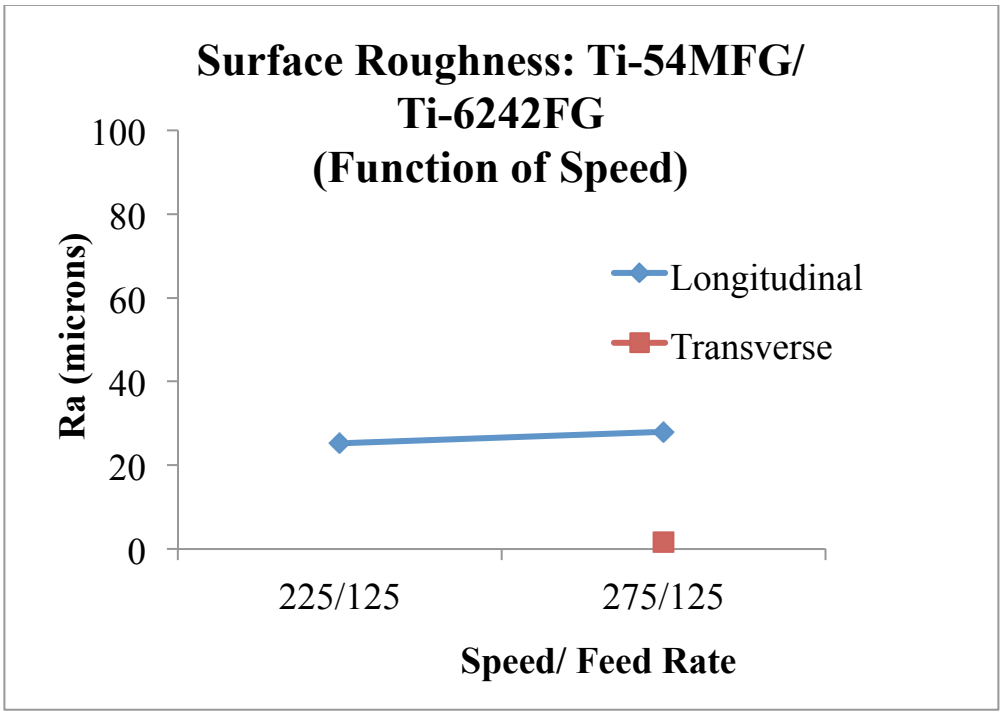
Surface Roughness: Ti-54MFG/ Ti-6242FG (Function of Speed)
Ra (microns)
100
80
60
40
20
0
Longitudinal
Transverse
225/125
275/125
Speed/ Feed Rate

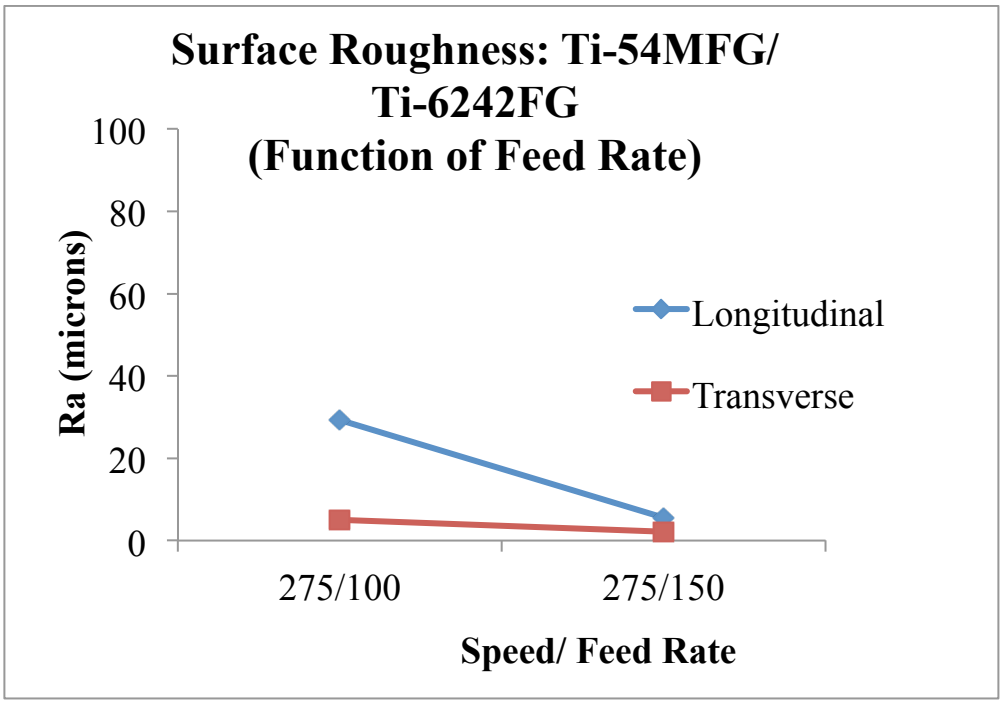
Surface Roughness: Ti-54MFG/ Ti-6242FG (Function of Feed Rate)
Ra (microns)
100
80
60
40
20
0
Longitudinal
Transverse
275/100
275/150
Speed/ Feed Rate

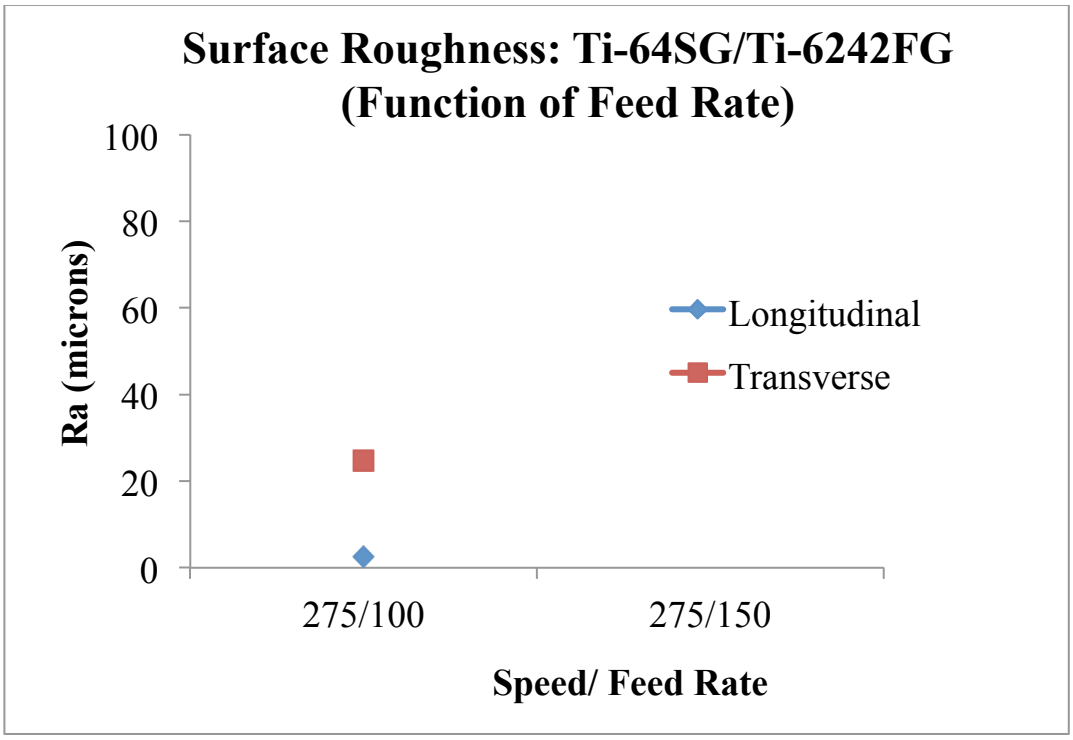
Surface Roughness: Ti-64SG/Ti-6242FG
(Function of Feed Rate)
Ra (microns)
100
80
60
40
20
0
Longitudinal
Transverse
275/100
275/150
Speed/ Feed Rate

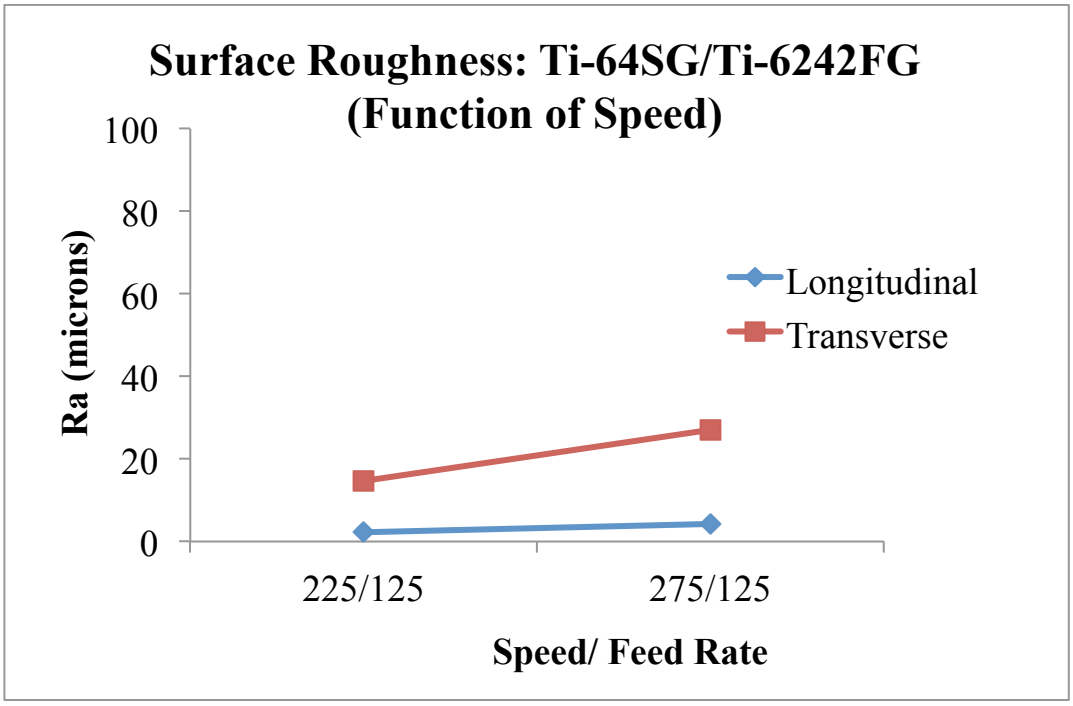
Surface Roughness: Ti-64SG/Ti-6242FG
(Function of Speed)
Ra (microns)
100
80
60
40
20
0
Longitudinal
Transverse
225/125
275/125
Speed/ Feed Rate

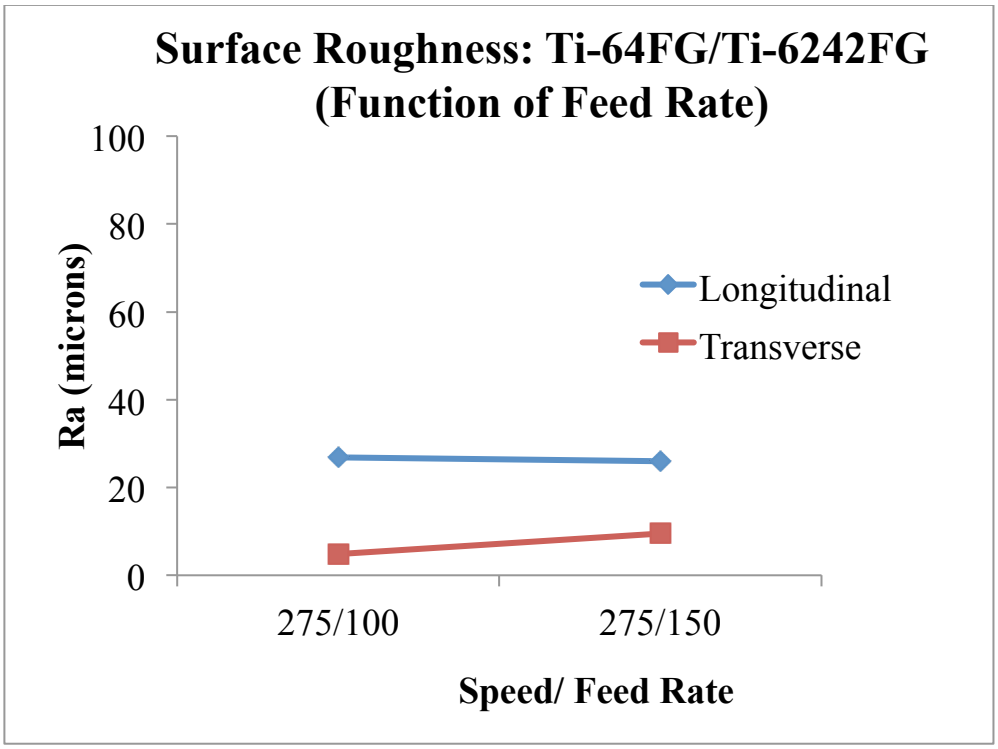
Surface Roughness: Ti-64FG/Ti-6242FG
(Function of Feed Rate)
100
80
60
40
20
0
Ra (microns)
Longitudinal
Transverse
275/100
275/150
Speed/ Feed Rate

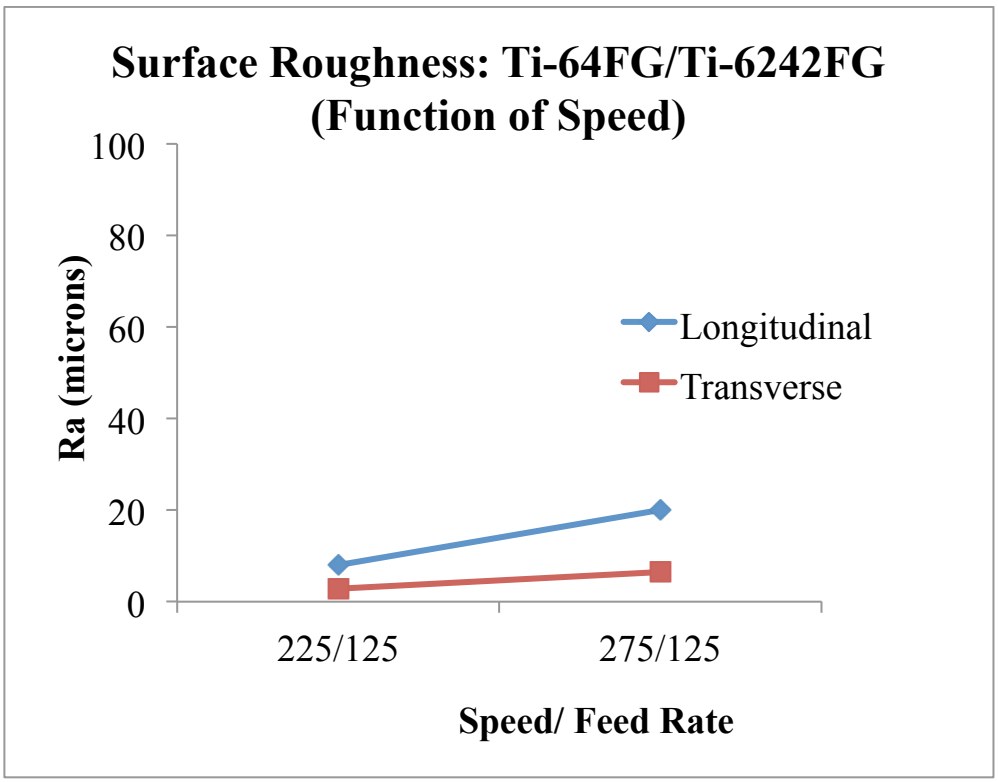
Surface Roughness: Ti-64FG/Ti-6242FG
(Function of Speed)
100
80
60
40
20
0
Ra (microns)
Longitudinal
Transverse
225/125
275/125
Speed/ Feed Rate

H.MATLAB PROGRAMS

1. Bonding time with Modified Hamilton Equation

```
clc
clear all

% Bonding time with Modified Hamilton Equation%

P=2E6; %Bonding Pressure in Pascal
k=1.38E-23; % Boltzman constant (J/K)
Tc=900;   %Temperature in Celsius
T=Tc+273;  % Temperature in Kelvin
AD= 5.92E8*exp(-19840/T)*1E-12% Constant(m^2/s)

G=20000E6; %Shear Modulus in Pascal
b=0.287E-9; %m
n=1.67;
p=2;
d=6E-6; % alpha particle diameter

%Bonding Time tb

tb=((0.8*k*T)/(AD*G*b))*((d/b)^p) * ((G/(3^0.5*P))^n)
tb/3600
```

2. Pilling's Model :Rate of change of fractional area of interfacial voids

```
% Pilling's Model:Rate of change of fractional area of interfacial
voids%

clear all
clc

av=1.78E-29; % alpha  Atomic Volume (m^3)
av_a=av
av_b=av
b=2.9E-10; % Burgers vector (m)
Tm=1933; % Melting Temperature (K)
Se= 1.7; % Surface Energy (J/m^2)

nsp=2.05;
T=910+273; % (Diffusion temperature K)
P=1E6;  %diffusion Pressure (MPa)
R=8.314;  %(J-mol-1-K-1)
k=1.38*1E-23; %Boltzmann's constant (J/K)

wl=10E-6 %wavelength (m)
```

```
ro=8E-6 %external radius r_o (m)
Ra=10E-6
ho=2*Ra % outer height of void (m)
d=8E-6; % grain size (m)
bt=-4.593+0.0041*T % beta component
al=1-bt  % alpha component

% Diffusion %
%Dv=5.9E-3*exp(-330000/(R*T));
%Dgbdel=3E-12*exp(-202000/(R*T));  % "Dgb"  Grain boundary diffusion
(m^3-s-1)


% Void closure process is evaluated by plastic and diffusion collapse

% *** Plastic Collapse Calcualtions *** %

%Fractional Area fh (Non bonded surface) is defined by  (r_h^2)/(r_o^2
)
% sig_z=(-P* r_o^2)/((r_o^2 -r_h^2 ) )
% Se =Surface Tension
% Radial Stress or sig_r =  ((P-(-2?)?r_o )+(f_h^(1/2)-1))/(1-f_h )
% Circumferential Stress or sig_t =  ((-P-(-
2?)?r_o)+(f_h^(1/2)+1))/(1-f_h )
% Von mises Stress or sig=((0.5*((sig_r-sig_t)^2+(sig_t-
sig_z)^2+(sig_z-sig_r)^2))^0.5)*1E-6
%
% Strain rate in radial direction or edot_r=edot*(sig_r-
0.5*(sig_t+sig_z))/(sig*1E6)
%  Differential change in non bonded area(plastic collapse) or
dfhbydt_pl=-2*edot_r*(1-fh)

% **** Diffusion Collapse Calcualtions *** %

% *** Program Calculations *** %
% In the program, 'fh':Fractional Area (Non bonded surface)is varied
from 0.05 to 0.95
%'ro' (outer radius of void) = wl/2 ho (outer height of void)=2*Ra (m)
%The stress, strain  and other required calculations are made
% The differential change in nonbonded fractional area is evaluated by
plastic and difusive collapse

sizfh=40;
fh=zeros(sizfh,1);
fhp=zeros(sizfh,1);

intfh = 0.025;
incrementfh = 0.025;
for i=1:sizfh
    fh(i) = intfh + (i-1)*incrementfh

    sig_r=(P-(2*Se/ro))*(((fh(i)^0.5)-1)/(1-fh(i)))
sig_t=(-P-(2*Se/ro))*(((fh(i)^0.5)+1)/(1-fh(i)))
```

```
    sig_z= -P/(1-fh(i))
    sig=((0.5*((sig_r-sig_t)^2+(sig_t-sig_z)^2+(sig_z-sig_r)^2))^0.5)*1E-6

    Dv=5.9E-3*exp(-330000/(R*T));
    Dgbdel=3E-12*exp(-202000/(R*T));


    edot=((1.28E9*exp(-308000/(R*T))*(sig^nsp)))
    edot_r=edot*((sig_r-0.5*(sig_t+sig_z))/(sig*1E6))
    edot_z=edot*((sig_z-0.5*(sig_t+sig_r))/(sig*1E6))

    dfhbydt_pl(i)=-2*edot_r*(1-fh(i))
     l_pl(i)=log10( dfhbydt_pl(i))   % log plot_plastic collapse %
    h(i)=ho*fh(i)


       dvbydt_al(i) = -al*((4*av*Dv)/(k*T))*(fh(i))/ (log(1/fh(i))-((1-
    fh(i))/2))*(P/(ro^2))
       dvbydt_bt(i) = -bt*((4*av*Dv)/(k*T))*(fh(i))/ (log(1/fh(i))-((1-
    fh(i))/2))*(P/(ro^2))

       dgbbydt_al(i) = -al*((2*Dgbdel*av_a)/(k*T))*(1/ (log(1/fh(i))-((1-
    fh(i))/2)))*(P/(ro^2))*((1+(h/d))/h)
       dgbbydt_bt(i) = -bt*((2*Dgbdel*av_b)/(k*T))*(1/ (log(1/fh(i))-((1-
    fh(i))/2)))*(P/(ro^2))*((1+(h/d))/h)

       dfhbydt_d(i)= dvbydt_al(i) + dvbydt_bt(i)+ dgbbydt_al(i) +
    dgbbydt_bt(i)
       l_d(i)=log10( dfhbydt_d(i)) % log plot_diffusive collapse %
       fhp(i)=1-fh(i)
    end

    plot(fhp,l_pl,fhp,l_d,'--'),legend('plastic','diffusion'),xlabel('fhp:
    Area Fraction Bonded'),ylabel('log(dfh/dt)')
```

3. *Pilling's Model: Bonding time with pressure for different Surface Finishes*

```
    % Pilling's Model: Bonding time with pressure for different Surface
    Finishes %

clc
clear all

T=927+273;
Tm=1973;
P=2;
ga300=4.3E4;
gb300=2.05e4;
td_ga=-1.2;
```

```
td_gb=-0.5;
bt=0.70;
al=1-bt;
g_a=ga300*(1+((T-300)/Tm)*(td_ga));
g_b=gb300*(1+((T-300)/Tm)*(td_gb));
g=al*g_a+bt*g_b;
sig_y=1E-3*g;
fc=P/sig_y;
fh=1-fc

upper=fh;
lower=0.0;
inc=0.00001;
FINALSUM=0;
counter=1;
start=upper;
while(counter<=((upper-lower)/inc)+1)
    value(counter)= pilling3(start);
    FINALSUM=FINALSUM+value(counter).*inc;
    counter=counter+1;
    start=start-inc;
end
-FINALSUM
-FINALSUM/3600


function [ dydt ] =pilling3(fh)
av_a=1.76E-29;
av_b=1.81E-29;
T=927+273;
P=2E6;
R=8.314;
k=1.38*1E-23; %Boltzmann's constant (J/K)

Dgbdel_a=3.6E-16*exp(-97000/(R*T));
Dgbdel_b=5.4E-17*exp(-153000/(R*T));
Se=1.7;
nsp=1.43;
npc=4.3;
wl=21e-6;
ro=wl/2;  %ro=wl/2;
Ra=0.83E-6;
ho=Ra/2; %ho=Ra/2;
bt=0.70;
al=1-bt;
d=8E-6;

sig_r=((P-2*Se/ro)*((sqrt(fh)-1)/(1-fh)));
sig_t=((-P-2*Se/ro)*((sqrt(fh)+1)/(1-fh)));

sig_z=(-P/(1-fh));
sig=(sqrt(0.5*((sig_r-sig_t)^2+(sig_t-sig_z)^2+(sig_z-sig_r)^2)))*1E-6;
```

```
edot=((3.8E4/T)*exp(-150000/(R*T))*(sig^nsp))+((7.5E-2/T)*exp(-
150000/(R*T))*(sig^npc));

edot_r=edot*(sig_r-0.5*(sig_t+sig_z))/(sig*1E6);
%edot_r=edot*((1E-6*sig_r-0.5*(1E-6*sig_t+1E-6*sig_z))/(sig));
edot_z=edot*((sig_z-0.5*(sig_t+sig_r))/(sig*1E6));

dfhbydt_pl=-2*edot_r.*(1-fh)
 h=ho*fh;

   N=round(1+(h/d));

   dvbydt_al = (-2*pi*Dgbdel_a*av_a*sig_z*(1-fh))/ (k*T*(log(1/fh)-((1-
fh)/2)));
   dvbydt_bt = (-2*pi*Dgbdel_b*av_b*sig_z*(1-fh))/ (k*T*(log(1/fh)-((1-
fh)/2)));
   dvbydt = al* dvbydt_al+ bt* dvbydt_bt

   dfhbydt_d=-N*((1/(pi*ro^2*h))*dvbydt);

   dydt=1/(dfhbydt_pl+dfhbydt_d);

end
```

4. *Fang's Model: Program to calculate initial values for ode solver to calculate area of bonded fraction*

```
clear all
clc

p= 10; % pressure (MPa)
h=1.15; % initial height of void(1E-6m)
c=5.01;% inital width of void (1E-6m)
a= 5.52;% half of the distance between the centers of two adjacent voids
(10-6m)
%a=5.22;
e=a-c % half of bonding length in bonding interface(1E-6m)
nu= 1.7; %Surface energy(J/m^2)
T=1123; % Temperature in Kelvin
ra=(h^2/c)  % radius of curvature of void neck (1E-6m)%
sig_y= 884-0.92*(T-273) % Yeild Stress (MPa)
K=sig_y/(3^(0.5)); % Material's Shear yeild strength (MPa) %
sig_dash = (p*a-nu)/e  % (MPa) %
sig_bar=2*K*(1+(ra/e))*log(1+(e/ra)) % (MPa)

x0 = [1e-12;0.1e-12]
dx = 1e-10;
for i=1:20;
```

```
    i;
    J0 = jacobFD('f2',x0,dx);
    x1 = x0 - inv(J0)*f2(x0)

    x0 = x1;
end
e_y=x1(1);
h_y=x1(2);
e_y1=(p*a-nu)/(2*K*(1+((h_y^2)/(e_y*(a-e_y))))*log(1+((e_y*(a-
e_y))/(h_y^2))));
h_y1=h*(a-(pi*c/4))/(a-((pi/4)*(a-e_y)));
Apd=e_y1/a;
function [J] = jacobFD(f,x,delx)
% Calculates the Jacobian of the
% system of non-linear equations:
% f(x) = 0, through finite differences.
% The Jacobian is built by columns

[m n] = size(x);
for j = 1:m
xx = x;
xx(j) = x(j) + delx;
f_xx  = feval(f,xx);
f_x = feval(f, x);
J(:,j) = (f_xx-f_x)/delx;
%J(:,j) = (f(xx)-f(x))/delx;
end;
% end

function [f] = f2(x)
% f2(x) = 0, with x = [x(1);x(2)]
% represents a system of 2 non-linear equations
p= 10; % pressure (MPa)
h=1.15; % initial height of void(10-6m)
c=5.01;% inital width of void (10-6m)
a= 5.52;%5.25 half of the distance between the centers of two adjacent
voids (10-6m)
e=a-c; % half of bonding length in bonding interface(10-6m)
nu= 1.7; %Surface energy(J/m^2)
T=1123; % Temperature in Kelvin

ra=(h^2/c);   % radius of curvature of void neck (10-6m)%
sig_y= 884-0.92*(T-273); % Yeild Stress (MPa)

e_y=x(1);
h_y=x(2);

K=sig_y/(3^0.5);
f1= -e_y +((p*a-nu)/(2*K*(1+((h_y^2)/(e_y*(a-e_y))))*log(1+((e_y*(a-
e_y))/(h_y^2)))));
f2=-h_y+(h*(a-(pi*c/4))/(a-((pi/4)*(a-e_y))));

f = [f1;f2];
```

5. *Fang's Model: ode solver to calculate area of bonded fraction by surface source, interface and creep mechanisms*

```
% Fang's Model: ode solver to calculate area of bonded fraction %

 clc
 clear all

[t1,y1] = ode45('fangsurface',0:120:1800,[1.266E-6  0.3241E-6 ])
[t2,y2] = ode23('fanginterface',0:25:1800,[1.266E-6  0.3241E-6]);
[t3,y3] = ode45('fangcreep',0:0.075:1800,[1.266E-6  0.3241E-6]);

A1=y1(:,end);
B1=[A1]/5.52e-6;
A2=y2(:,end) ;
B2=A2/5.52e-6 ;
A3=y3(:,end);
B3=A3/5.52e-6 ;

plot(t1,B1,t2,B2,'--',t3,B3,'-.','LineWidth',3)

set(gca,'YLim',[0 1])
set(gca,'XLim',[0 2000])
ax.YTick = [0, 0.2, 0.4, 0.6, 0.8, 1];
legend('Surface','Interface','Creep')
xlabel('Diffusion bonding time (s)','FontSize',12,'FontWeight','bold')
ylabel('Bonding Area Fraction','FontSize',12,'FontWeight','bold')
set(gca,'FontSize',12,'fontWeight','bold')



function [ dydt ] = fangsurface(t,y1)

dydt = zeros(size(y1));

h = y1(1);
e = y1(2);


bt=0.687;
al=1-bt;

%UNTITLED3 Summary of this function goes here
%   Detailed explanation goes here
Dos=5E-6;  %surface diffusion coefficient (pre-exponental)
Qs=89E3; %Surface diffusion activation energy
R=8.314; %Gas constant (J/(mol-K)
```

```
T= 1123; %Absolute Diffusion bonding temperature (K)
Ds= Dos*exp(-Qs/(R*T));  %Surface coefficient (m^2/s)
av_al=1.76E-29; %atomic volume(m^3)
av_bt=1.81E-29;
k=1.38*1E-23; %Boltzmann's constant (J/K)
nu= 1.7; %Surface energy(J/m^2)
p= 10E6; % pressure (MPa)
%h12=1.15; % initial height of void(1E-6m)
% inital width of void (1E-6m)
a= 5.26E-6;% half of the distance between the centers of two adjacent
voids (10-6m)
c=a-e; % half of bonding length in bonding interface(1E-6m)
ra=(h^2)/c;
dels=1*1E-10;
Dov_al=8.6E-10;
Dov_bt=1.9E-7;
Qv_al=150E3;
Qv_bt=153E3;

R=8.314;

n=4.3;

Tm=1933;


Dos=5E-6;
Qs=89E3;
Ds_al=Dos*exp(-Qs/(R*T));


ds_al=0.46*(Ds_al*dels*nu*av_al*t/(k*T))^0.25;
ds_bt=0.46*(Ds_al*dels*nu*av_al*t/(k*T))^0.25;
ds=al*ds_al+bt*ds_bt;

Dv_al=Dov_al*exp(-Qv_al/(R*T));
Dv_bt=Dov_bt*exp(-Qv_bt/(R*T));

function F=myfun(x)
a= 5.26E-6;% half of the distance between the centers of two adjacent
voids (10-6m)
c=a-e; % half of bonding length in bonding interface(1E-6m)
F=[(x(1).^2/(c).^2)+(x(2).^2/(h).^2)-1;
ds.^2-x(2).^2-(x(1)-c).^2];
end

x0=[0.170E-6 0.170E-6];
[x,fval]=fsolve(@myfun,x0);
m=x(2)/x(1);


theta1=atand(m);
```

```
rb1=(((c^2*sin((theta1))^2)+h^2*cos((theta1))^2)^(1.5))/(c*h);


if ra~=rb1
 V1dot_al=(2*av_al*Ds*dels*nu/(ra*k*T))*((1/ra)-(1/rb1));
 V1dot_bt=(2*av_bt*Ds*dels*nu/(ra*k*T))*((1/ra)-(1/rb1));
 V1dot=al*V1dot_al+ bt*V1dot_bt;

 V2dot_al=(2*av_al*Dv_al*nu/(k*T))*((1/ra)-(1/rb1));
 V2dot_bt=(2*av_bt*Dv_bt*nu/(k*T))*((1/ra)-(1/rb1));
 V2dot=al*V2dot_al+ bt*V2dot_bt;


 V12dot=V1dot+V2dot;

 dydt(1) = 4*V12dot/(pi*c);

 dydt(2)=((4*V12dot/(pi*c))*c)/h;

end
end


function [ dydt ] = fanginterface(t2,y2)

dydt = zeros(size(y2));

h = y2(1);
e = y2(2);


a= 5.52E-6;% half of the distance between the centers of two adjacent
voids (10-6m)
c=a-e;% inital width of void (1E-6m)
%e=a-c; % half of bonding length in bonding interface(1E-6m)

bt=0.687;
al=1-bt;

p= 10e6; % pressure (Pa)

R=8.314;
av_al=1.76E-29; %atomic volume(m^3)
av_bt=1.81E-29;
k=1.38*1E-23; %Boltzmann's constant (J/K)
n=4.3;
T= 1123;
Tm=1933;
Qb_al=97E3;
Qb_bt=153E3;
```

```
nu= 1.7; %Surface energy(J/m^2)

ga300=4.36E10;
gb300=2.05e10;
td_ga=-1.2;
td_gb=-0.5;
G_al=ga300*(1+((T-300)/Tm)*(td_ga));
G_bt=gb300*(1+((T-300)/Tm)*(td_gb));

A_al=7.7E4;
A_bt=1E5;
Docr_al=8.6E-10;
Docr_bt=1.9E-7;
Qcr_al=150E3;
Qcr_bt=153E3;

b_al=2.95E-10;
b_bt=2.86E-10;

Ac_al=A_al*Docr_al*exp(-Qcr_al/(R*T))*((G_al*b_al)/(k*T));
Ac_bt=A_bt*Docr_bt*exp(-Qcr_bt/(R*T))*((G_bt*b_bt)/(k*T));

delb_al=2*b_al;
delb_bt=2*b_bt;
Dobdelb_al=3.6E-16;
Dobdelb_bt=5.4E-17;

Db_al=Dobdelb_al*exp(-Qb_al/(R*T));
Db_bt=Dobdelb_bt*exp(-Qb_bt/(R*T));
Ac=7.5585e10

db_al=((Db_al*av_al*p)/(Ac_al*k*T*((p*1E-9)/(G_al*1E-9))^(n)))^(1/3);
db_bt=((Db_bt*av_bt*p)/(Ac_bt*k*T*((p*1E-9)/(G_bt*1E-9))^(n)))^(1/3);

Db=al*Db_al+bt*Db_bt
G=G_al*al+bt*G_bt


av=al*av_al+bt*av_bt

db=((Db*av*p)/(Ac*k*T*((p*1E-9)/(G*1E-9))^(n)))^(1/3);

ra=(h^2)/c;

if (db >= e);
    l=e;
else
   l = db;
end
```

```
sigI=((2*a*l*p)+(3*((l-2*c)*((e-l)*((1/l)+(1/ra))-((2*l*(e-
l)))/ra)))*nu)/(2*l^2+3*(l-2*c)*(e-l));


Dov_al=8.6E-10;
Dov_bt=1.9E-7;
Qv_al=150E3;
Qv_bt=153E3;

Dv_al=Dov_al*exp(-Qv_al/(R*T));
Dv_bt=Dov_bt*exp(-Qv_bt/(R*T));

V3dot_al=((3*Db_al*delb_al*av_al)/(2*k*T*l))*(sigI-(nu/l)-(nu/ra));
V3dot_bt=((3*Db_bt*delb_bt*av_bt)/(2*k*T*l))*(sigI-(nu/l)-(nu/ra));
V3dot=al*V3dot_al+bt*V3dot_bt;

V4dot_al=((3*Dv_al*av_al*ra)/(k*T*l))*(sigI-(nu/l)-(nu/ra));
V4dot_bt=((3*Dv_bt*av_bt*ra)/(k*T*l))*(sigI-(nu/l)-(nu/ra));
V4dot=al*V4dot_al+bt*V4dot_bt;


dydt(1)=-(V3dot+V4dot)/e;

dydt(2)=((-(V3dot+V4dot)/e)/h)*(a*((4/pi)-1)+e);

end
function [ dydt ] = fangcreep(t3,y3)

dydt = zeros(size(y3));

h = y3(1);
e = y3(2);


a= 5.52E-6;% half of the distance between the centers of two adjacent
voids (10-6m)
c=a-e;% inital width of void (1E-6m)

bt=0.687;
al=1-bt;

p= 10e6; % pressure (Pa)

R=8.314;
av_al=1.76E-29; %atomic volume(m^3)
av_bt=1.81E-29;
k=1.38*1E-23; %Boltzmann's constant (J/K)
n=4.3;
T= 1123;
Tm=1933;
Qb_al=97E3;
Qb_bt=153E3;
```

```
nu= 1.7; %Surface energy(J/m^2)

ga300=4.36E10;
gb300=2.05e10;
td_ga=-1.2;
td_gb=-0.5;
G_al=ga300*(1+((T-300)/Tm)*(td_ga));
G_bt=gb300*(1+((T-300)/Tm)*(td_gb));

A_al=7.7E4;
A_bt=1E5;
Docr_al=8.6E-10;
Docr_bt=1.9E-7;
Qcr_al=150E3;
Qcr_bt=153E3;

b_al=2.95E-10;
b_bt=2.86E-10;

Ac_al=A_al*Docr_al*exp(-Qcr_al/(R*T))*((G_al*b_al)/(k*T))
Ac_bt=A_bt*Docr_bt*exp(-Qcr_bt/(R*T))*((G_bt*b_bt)/(k*T))
Ac=7.5585e10;
delb_al=2*b_al;
delb_bt=2*b_bt;
Dobdelb_al=3.6E-16;
Dobdelb_bt=5.4E-17;

Db_al=Dobdelb_al*exp(-Qb_al/(R*T));
Db_bt=Dobdelb_bt*exp(-Qb_bt/(R*T));

Db=al*Db_al+bt*Db_bt
G=G_al*al+bt*G_bt

av=al*av_al+bt*av_bt

db=((Db*av*p)/(Ac*k*T*((p*1E-9)/(G*1E-9))^(n)))^(1/3);

if (db >= e);
    l=e;

ra=(h^2)/c;
sigI=((2*a*l*p)+(3*((l-2*c)*((e-l)*((1/l)+(1/ra))-((2*l*(e-
l)))/ra)))*nu)/(2*l^2+3*(l-2*c)*(e-l));



Dov_al=8.6E-10;
Dov_bt=1.9E-7;
Qv_al=150E3;
Qv_bt=153E3;

Dv_al=Dov_al*exp(-Qv_al/(R*T));
Dv_bt=Dov_bt*exp(-Qv_bt/(R*T));
```

```
V3dot_al=((3*Db_al*av_al)/(2*k*T*l))*(sigI-(nu/l)-(nu/ra));
V3dot_bt=((3*Db_bt*av_bt)/(2*k*T*l))*(sigI-(nu/l)-(nu/ra));
V3dot=al*V3dot_al+bt*V3dot_bt;

V4dot_al=((3*Dv_al*av_al*ra)/(2*k*T*l))*(sigI-(nu/l)-(nu/ra));
V4dot_bt=((3*Dv_bt*av_bt*ra)/(2*k*T*l))*(sigI-(nu/l)-(nu/ra));
V4dot=al*V4dot_al+bt*V4dot_bt;

dydt(1)=-(V3dot+V4dot)/e;
dydt(2)=((-(V3dot+V4dot)/e)/h)*(a*((4/pi)-1)+e);

else
    l=db;

S=-1;

fun = @(z) (a./(a-c*(1-((z.^2)./(h.^2))).^0.5)).^n;

upper=h;
lower=0.0;
inc=0.0001;
f=-1e-8;
counter=1;
start=h;
while(counter<=((upper-lower)/inc)+1)
    value(counter)= creepzfun(start);
    f=f+value(counter).*inc;
    counter=counter+1;
    vstart=start-inc;
end

dydt_al(1)=(S*Ac_al*(abs((p)/(G_al)))^n)*f;
dydt_bt(1)=(S*Ac_bt*(abs((p)/(G_bt)))^n)*f;
dydt(1)=al*dydt_al(1)+bt*dydt_bt(1)
dydt(2)=-(dydt(1)/h)*(a*((4/pi)-1)+e)

end

function y = creepzfun(z)
   y =  (a./(a-c*(1-((z.^2)./(h.^2))).^0.5)).^n
end

end
```

6. *Program to calculate diffusion bonding time with dissimilar titanium alloys*

```
clc
clear all
```

```
Pr=2;
Tc=899;
T=Tc+273;
Tm=1973;
ga300=4.3E4;
gb300=2.05e4;
td_ga=-1.2;
td_gb=-0.5;

G_a=ga300*(1+((T-300)/Tm)*(td_ga));
G_b=gb300*(1+((T-300)/Tm)*(td_gb));

bt=0.55;
al=1-bt;

G=al*G_a+bt*G_b;

G1=6.2E4*(1+((T-300)/Tm)*(1-1.2));

sig_y=1E-3*G;
fo=Pr/sig_y;

fh=1-fo;


upper=fh;
lower=0;
inc=0.001;
k=round((upper-lower)/inc) ;

m=1;
n=100;
XFINAL=zeros(n+1,1);

for j=1:m

DBTIME=zeros(n,1);
DBTIME2=zeros(n,1);
h=zeros(n,1);
ro=zeros(n,1);



pd= makedist('InverseGaussian','mu',2.96977E-6,'lambda',6.98841E-6);
h=random(pd,n,1);
pd= makedist('Exponential','mu',10.9375e-6);
ro=random(pd,n,1);

for i=1:n


DBTIME(i)=0;
```

```
counter=1;
start=upper;

while(counter<=((upper-lower)/inc)+1)
    value(counter)= diffusionpdf2(start,h(i),ro(i));


   DBTIME(i)=DBTIME(i)+value(counter).*inc;
    counter =counter+1;
    start=start-inc;
end
-DBTIME(i);
DBTIME2(i)=DBTIME(i)/3600;
end
DBTIME2;
[F,X,Flo,Fup] = ecdf(DBTIME2);
XFINAL = XFINAL  + X;
end

XFINAL = XFINAL/m;
plot(XFINAL,F);


function [ dydt ] =diffusionpdf2(fh,h,ro)


av_a=1.76E-29;
av_b=1.81E-29;

Tc=899;
T=Tc+273;
P=2E6;
R=8.314;
k=1.38*1E-23; %Boltzmann's constant (J/K)

Dgbdel_a=3.6E-16*exp(-97000/(R*T));
Dgbdel_b=5.4E-17*exp(-153000/(R*T));

Dv_a=8.6E-10*exp(-150000/(R*T));
Dv_b=1.9E-7*exp(-153000/(R*T));

Se=1.7;

bt=0.55;
al=1-bt;
d=8E-6;
ht=h1;
sig_r=((P-2*Se/ro)*((sqrt(fh)-1)/(1-fh)));
sig_t=((-P-2*Se/ro)*((sqrt(fh)+1)/(1-fh)));

sig_z=(-P./(1-fh));
```

```
sig=(sqrt(0.5*((sig_r-sig_t).^2+(sig_t-sig_z).^2+(sig_z-sig_r).^2)))*1E-
6;

Tm=1973;
Dgb_a=6E-7;
Dgb_b=9E-8;
Qgb_a=97000;
Qgb_b=153000;
A=1.2E-9;
n1=1.43;
del_a=5.9e-10;
del_b=5.72e-10;
ga300=4.3E4;
gb300=2.05e4;
td_ga=-1.2;
td_gb=-0.5;

G_a=ga300*(1+((T-300)/Tm)*(td_ga));
G_b=gb300*(1+((T-300)/Tm)*(td_gb));

Ac_a=A*Dgb_a*exp(-Qgb_a/(R*T))*((G_a*1E6*del_a)/(k*T));
Ac_b=A*Dgb_b*exp(-Qgb_b/(R*T))*((G_b*1E6*del_b)/(k*T));
edot=al*(Ac_a*(sig/G_a)^n1)+bt*(Ac_b*(sig/G_b)^n1);

dfbydtp = (-edot/(sig))*((3*P*fh.^0.5)-((2*Se*fh.^0.5)/ro)+((6*Se)/ro));

dfbydtgb_a= ((-2*av_a*Dgbdel_a)./(k*T))*(1./((log(1./fh))-((1-
fh)./2)))*(1./(ro.^2))*((1+(ht/d))./ht)*P;
dfbydtgb_b= ((-2*av_b*Dgbdel_b)./(k*T))*(1./((log(1./fh))-((1-
fh)./2)))*(1./(ro.^2))*((1+(ht/d))./ht)*P;
dfbydtgb=al*dfbydtgb_a+bt*dfbydtgb_b;

dfbydtvol_a=(-(4*av_a*Dv_a)./(k*T))*(fh./((log(1./fh))-((1-
fh)./2)))*((1./(ro).^2))*P;
dfbydtvol_b=(-(4*av_b*Dv_b)./(k*T))*(fh./((log(1./fh))-((1-
fh)./2)))*((1./(ro).^2))*P;
dfbydtvol=al*dfbydtvol_a+bt*dfbydtvol_b;

dydt=(-(sig)./edot)./(dfbydtp +dfbydtgb+dfbydtvol);

end
```

I. ABAQUS PROGRAM OF DIFFUSION BONDING

*Heading

** Job name: 2dfinal Model name: Model-1

** Generated by: Abaqus/CAE 6.14-2

*Preprint, echo=NO, model=NO, history=NO, contact=NO

**

```
** PARTS
**
*Part, name=Part-1
*Node

*Element, type=CPE3

*Nset, nset=Set-1, generate
   1,  9558,     1
*Elset, elset=Set-1, generate
    1,  18636,      1
** Section: Section-1
*Solid Section, elset=Set-1, material=Material-1-Copy2
50.,
*End Part
**
**
** ASSEMBLY
**
*Assembly, name=Assembly
**
*Instance, name=Part-1-1, part=Part-1
*End Instance
**
*Instance, name=Part-1-2, part=Part-1
        0.,          0.,          0.
        0.,          0.,          0.,          0.,          0.,          1.,         180.
*End Instance
**
*Nset, nset="Complete body", instance=Part-1-1, generate
   1,  9558,     1
*Nset, nset="Complete body", instance=Part-1-2, generate
```

```
   1,  9558,     1
*Elset, elset="Complete body", instance=Part-1-1, generate
    1,  18636,      1
*Elset, elset="Complete body", instance=Part-1-2, generate
    1,  18636,      1
*Nset, nset=Fixed, instance=Part-1-2

*Elset, elset=Fixed, instance=Part-1-2

*Nset, nset=Set-4, instance=Part-1-2
 4, 5
*Nset, nset=Set-5, instance=Part-1-2

*Elset, elset=Set-5, instance=Part-1-2

*Nset, nset=Set-6, instance=Part-1-1
 4, 5
*Nset, nset=Set-7, instance=Part-1-1
 3, 6
*Nset, nset=Set-8, instance=Part-1-2
 3, 6
*Nset, nset="Side Ends", instance=Part-1-1

 479, 480
*Nset, nset="Side Ends", instance=Part-1-2

 479, 480
*Elset, elset="Side Ends", instance=Part-1-1

*Elset, elset="Side Ends", instance=Part-1-2

*Elset, elset=_Load_S2, internal, instance=Part-1-1
```

*Elset, elset=_Load_S3, internal, instance=Part-1-1

*Elset, elset=_Load_S1, internal, instance=Part-1-1

*Surface, type=ELEMENT, name=Load
_Load_S2, S2
_Load_S3, S3
_Load_S1, S1
*Elset, elset="_lower contact_S3", internal, instance=Part-1-2

*Elset, elset="_lower contact_S2", internal, instance=Part-1-2

*Elset, elset="_lower contact_S1", internal, instance=Part-1-2

*Surface, type=ELEMENT, name="lower contact"
"_lower contact_S3", S3
"_lower contact_S2", S2
"_lower contact_S1", S1
*Elset, elset="_lower contact 2_S3", internal, instance=Part-1-2

*Elset, elset="_lower contact 2_S2", internal, instance=Part-1-2

*Elset, elset="_lower contact 2_S1", internal, instance=Part-1-2
 280, 337, 462, 562, 637, 1815, 1850, 4177, 4178, 4179, 4180, 4182, 4184, 4186, 4245, 4246
 4248, 4250, 4252
*Surface, type=ELEMENT, name="lower contact 2"
"_lower contact 2_S3", S3
"_lower contact 2_S2", S2
"_lower contact 2_S1", S1
*Elset, elset="_upper contact_S3", internal, instance=Part-1-1

```
*Elset, elset="_upper contact_S2", internal, instance=Part-1-1

*Elset, elset="_upper contact_S1", internal, instance=Part-1-1

*Surface, type=ELEMENT, name="upper contact"
"_upper contact_S3", S3
"_upper contact_S2", S2
"_upper contact_S1", S1
*Elset, elset="_upper contact 2_S3", internal, instance=Part-1-1
  155, 1753, 1851, 1910, 2040, 2145, 2225, 2369
*Elset, elset="_upper contact 2_S2", internal, instance=Part-1-1

*Elset, elset="_upper contact 2_S1", internal, instance=Part-1-1

*Surface, type=ELEMENT, name="upper contact 2"
"_upper contact 2_S3", S3
"_upper contact 2_S2", S2
"_upper contact 2_S1", S1
*End Assembly
*Amplitude, name=Amp-1, time=TOTAL TIME, definition=SMOOTH STEP
           0.,             0.,             1.,             1.
**
** MATERIALS
**
*Material, name=Material-1
*Conductivity
6.,
*Creep
 3.7607e-14, 4.3,  0.
*Density
 4.43e-09,
```

```
*Elastic
 113.8, 0.342
*Plastic, hardening=JOHNSON COOK
880., 695., 0.36,  0.8,1900., 293.
*Specific Heat
526.,
*Material, name=Material-1-Copy
*Creep
 1.72828e-24,5.,0.
*Elastic
 2e+07, 0.3
*Material, name=Material-1-Copy2
*Creep
 4.0445e-14, 4.3,  0.
*Elastic
113800., 0.342
**
** INTERACTION PROPERTIES
**
*Surface Interaction, name=IntProp-1
1.,
*Surface Behavior, pressure-overclosure=HARD
**
** PREDEFINED FIELDS
**
** Name: Predefined Field-1   Type: Temperature
*Initial Conditions, type=TEMPERATURE
"Complete body", 927.
**
** INTERACTIONS
**
** Interaction: Int-1
```

```
*Contact Pair, interaction=IntProp-1, type=SURFACE TO SURFACE
"lower contact", "upper contact"
** ----------------------------------------------------------------
**
** STEP: Step-1
**
*Step, name=Step-1, nlgeom=NO
*Static
1., 1., 1e-05, 1.
**
** BOUNDARY CONDITIONS
**
** Name: BC-3 Type: Displacement/Rotation
*Boundary
Set-4, 1, 1
Set-4, 2, 2
Set-4, 6, 6
** Name: BC-4 Type: Displacement/Rotation
*Boundary
Set-5, 2, 2
** Name: BC-5 Type: Displacement/Rotation
*Boundary
Set-6, 1, 1
**
** LOADS
**
** Name: Load-1   Type: Pressure
*Dsload, amplitude=Amp-1
Load, P, 2.
**
** OUTPUT REQUESTS
**
```

*Restart, write, frequency=0

**

** FIELD OUTPUT: F-Output-1

**

*Output, field, frequency=10

*Node Output

CF, NT, RF, U

*Element Output, directions=YES

LE, PE, PEEQ, PEMAG, S, TEMP

*Contact Output

CDISP, CSTRESS, SJD, SJDA, SJDT, SJDTA

**

** HISTORY OUTPUT: H-Output-1

**

*Output, history

*Energy Output

ALLAE, ALLCD, ALLDMD, ALLEE, ALLFD, ALLIE, ALLJD, ALLKE, ALLKL, ALLPD, ALLQB, ALLSD, ALLSE, ALLVD, ALLWK, ETOTAL

*Contact Output

SJD, SJDA, SJDT, SJDTA

*End Step

** --

**

** STEP: Step-2

**

*Step, name=Step-2, nlgeom=NO, inc=72000

*Visco, cetol=5e-06

7200., 7200., 0.072, 7200.

**

** OUTPUT REQUESTS

**

*Restart, write, frequency=0

```
**
** FIELD OUTPUT: F-Output-1
**
*Output, field, frequency=10
*Node Output
CF, NT, RF, U
*Element Output, directions=YES
LE, PE, PEEQ, PEMAG, S, TEMP
*Contact Output
CDISP, CSTRESS
**
** HISTORY OUTPUT: H-Output-1
**
*Output, history
*Energy Output
ALLAE, ALLCD, ALLDMD, ALLEE, ALLFD, ALLIE, ALLJD, ALLKE, ALLKL,
ALLPD, ALLQB, ALLSD, ALLSE, ALLVD, ALLWK, ETOTAL
*End Step
```

CURRICULAM VITAE

NEHA KULKARNI

24515 SE 46th Terrace - Issaquah, WA 98029

(337) 288-5433 ▪ nbhagat@u.washington.edu ▪ nehamech2004@gmail.com

US PERSON STATUS

- Yes: Permanent Resident.

EDUCATION

UNIVERSITY OF WASHINGTON (UW)
August 2015

PhD in Mechanical Engineering (GPA: 3.69/4.0)

Thesis: Study of the Mechanical Performance of Similar and Dissimilar Titanium Alloy Joints formed by Diffusion bonding (DB) and Friction Stir Welding (FSW) Processes.

(Advisor: Dr. Ramulu Mamidala, Professor, UW, Seattle)

UNIVERSITY OF LOUISIANA AT LAFAYETTE (ULL)
2009

Master of Science in Mechanical Engineering (GPA: 4.0/4.0)

Thesis: Strain Formations in an Oval Aluminum Stamp Formed Die.

(Advisor: Dr. William Emblom, Assistant Professor, ULL, Lafayette)

VISVESVARAYA NATIONAL INSTITUTE OF TECHNOLOGY (VNIT), India.

2004

Bachelor of Engineering in Mechanical Engineering (GPA: 3.6/4.0)

PROFESSIONAL EXPERIENCE

UNIVERSITY OF WASHINGTON
April 2010- Current

Research Assistant, Department of Rehabilitation Medicine (under Dr. Murray Maitland, Associate Professor, UW, Division of Physical Therapy)

- Working on developing a novel prosthetic foot in collaboration with an interdisciplinary team of engineers, prosthetists, biomechanics researchers and prosthetic users.
- Contributed to the identification and implementation of conceptual designs for building prosthetic foot.

- Designed tools, materials, processes and fixtures for material testing,
- Designed and performed failure tests for parts and assemblies of the prosthetic foot prototype.

Research Assistant, Mechanical Engineering (under Dr. Ramulu Mamidala, Professor, UW, Seattle)

- Worked on a project funded by Boeing Research and Technology group for quality evaluation of solid state joining of similar and dissimilar titanium alloys with DB and FSW processes applied in aircraft structure, landing gears, and fuselage among others.
- Demonstrated strong analytical skills by collecting, organizing, synthesizing and analyzing engineering data gathered from a large number of experiments.
- Developed mathematical and numerical models for diffusion bonding of dissimilar materials to optimize diffusion bonding process.
- Developed numerical model for tensile behavior of friction stir welded joints.
- Performed mechanical testing to evaluate joint strength properties for friction stir welded and diffusion bonded titanium joints by conducting tensile tests and flexural testing on Instron Machine.
- Performed hardness measurements on LECO Micro-Hardness Tester and surface texture analysis using Mahr-Surface Profilometer and analyzed fractography of the fractured samples with scanning electron microscope (SEM).
- Published research papers and presented research in multiple conferences.
- Lead a team of graduate students to prepare a poster for a research symposium.

Teaching Assistant, Mechanical Engineering (under Dr. Ramulu Mamidala, Professor, UW, Seattle)

- Teaching assistant for graduate courses: Modern Manufacturing Processes and Fatigue of Materials.
- Demonstrated excellent communication skills by explaining challenging concepts to students.
- Led the class in absence of the professor by organizing and delivering class lectures. Organized instructional materials and evaluated students' homework, and tests.

Visiting Scientist, Mechanical Engineering (under Dr. Ramulu Mamidala, Professor, UW, Seattle)

- Developed numerical model of shot peening using FEA and studied residual stresses and surface profile for single shot and multiple shots as a function of shot peening parameters (ball size and velocity) for three materials (Steel, Al-7075, and Ti-6Al-4V).

UNIVERSITY OF LOUISIANA AT LAFAYETTE
Aug 2007 – Dec 2009

Research Assistant, Mechanical Engineering (under Dr. Emblom, Assistant Professor, ULL, Lafayette)

- Performed FEA analysis of Hishida die and of an oval aluminum stamp formed die for optimization of draw bead and blank holder trajectories to maximize draw depth.

CUMMINS INDIA LTD, a part of CUMMINS INC., USA
Aug 2004 – Aug 2007

Manager, Program Management-New Product Introduction (NPI) Department

- Worked on a Six Sigma (DMAIC) project to reduce time-overrun of the NPI projects.
- Organized and conducted pre-milestone reviews of projects to gauge compliance against requirements.
- Collaborated with team members the functional area activities of projects, coordinated and monitored milestone review requirements.
- Managed NPI training program, prepared tutorials and handouts for various functional areas (technical, operations, marketing, and customer care) and coordinated training program activities.

Graduate Trainee Engineer, Operations Management (OMP) Training Program

- Led a project for engineering process improvement using "Design of Experiments (DOE)" for Electric Discharge Machining (EDM) used in manufacturing injector cups.
- Participated in improving manufacturing methods by implementation of lean principles and technologies.
- Participated in design reviews and in implementation of manufacturing plans.
- Supported the assembly lines by development and implementation of production and tooling methodologies.
- Established centralized communication system for all CNC machines in the "Cylinder Head Manufacturing Division" in collaboration with cross functional teams.

PROFICIENCIES

- Lean and Kaizen: Implemented at various projects of process capability improvement for injector cup machining and for setting up work instructions for assembling engines at Cummins India Ltd.
- FEA: Applied Ansys Workbench in doctoral research for simulating tensile and flexural behavior of titanium joints. Applied Abaqus in modeling diffusion bonding process. Applied LS-Dyna in modeling shot peening process and in Master's thesis for modeling oval pan profile.

- CAD and CAM: Applied Pro-E and Solidworks in metal forming and solid state joining modeling. Applied Gibbs CAM in graduate level course.
- Mechanical Testing: Conducted tensile and flexural testing on Instron machine.
- Six Sigma: Worked as a Six Sigma team member to reduce the time-overrun of projects for the introduction of new Generator Sets at Cummins India Ltd.
- Statistical tools: DOE, Measurement systems analysis, Failure Mode Effects Analysis (FMEA), Hypothesis Testing, and Regression Analysis applied at Cummins India Ltd.

RESEARCH PUBLICATIONS AND CONFERENCES

- N. Kulkarni and M. Ramulu, "Experimental Study of Mechanical Performance in Friction Stir Welded Dissimilar Titanium Alloys," 2015 SEM Annual Conference and Exposition on Experimental and Applied Mechanics, (June 8-11, 2015), Costa Rica, California.
- N. Kulkarni and M. Ramulu, "Experimental and Numerical Analysis of Mechanical Behavior in Friction Stir Welded Different Titanium Alloys," To appear in Proceedings of the ASME 2014 International Mechanical Engineering Congress & Exposition IMECE2014, (November 14-20, 2014), Montreal, Canada.
- N. Kulkarni, M. Ramulu, and D.G. Sanders "Experimental Study on the Quality of Dissimilar Titanium Joints through Diffusion Bonding," Poster presentation at International Titanium Association Conference-TITANIUM USA 2014, (September 21-24, 2014), Chicago, Illinois.
- N. Kulkarni, H. Bae, R. Mamidala , "A three-dimensional single and multiple shot simulation of shot penning for Steel, Aluminium and Titanium alloys," to be published in Proceedings of the 12th International Conference on Shot Peening, (September 15-18, 2014), Goslar, Germany.
- N. Kulkarni, M. Ramulu, D. Sanders and L. Hefti, "Experimental Investigation of Flexural Behavior of Diffusion Bonded Dissimilar joints of Titanium Alloys," Presented at the 25th Advanced Aerospace Materials and Processes (AeroMat) Conference and Exposition, (June 16-19, 2014), Orlando, Florida.
- M. Ramulu, N. Kulkarni, K. Gangwar, T.Morton and V. Aditya, "Experimental Study to Develop Joining Methods for New or Modified High Temperature Titanium Alloys: Metallurgical Characterizations, Microstructural Integrity and Mechanical Performance," Poster presentation at the JCATI Symposium at WSU, (April 21, 2014), Pullman, WA.
- N. Kulkarni and M. Ramulu, "Flexural Behavior of Diffusion Bonded Titanium Joint," Presented at the International Conference on Computational & Experimental Engineering and Sciences (ICCES) Conference, (May 24-28 2013), Seattle.
- N. Kulkarni, W.J. Emblom, T. Kozman, J. Lee, and K.J. Weinmann, "The Development of a Strain Model for an Oval Aluminum Stamp Formed Pan," Transactions of the North American Manufacturing Research Institution of the Society of Manufacturing Engineers (NAMRI of SME), May 2010.

ACADEMICS

Experimental Stress Analysis… Fracture Mechanics… Fatigue of Materials…Elasticity… Metal Forming… Finite Element Analysis… Mechanical Engineering Analysis…Thermodynamics… Combustion… Advanced System Dynamic and Controls… Computer Aided Machining… Machine Design… Heat Transfer.

HONORS / ACTIVITIES

- Invited for Poster Presentation at International Titanium Association Conference Titanium 2014, (September 21-24, 2014), Chicago, Illinois.
- Awarded Superior Student recognition by the University of Louisiana at Lafayette.
- Certification from International Society of Agile Manufacturing for attending seminar on "Inter-Disciplinary Seminar Series on Application of Lean Six Sigma in Industry, Healthcare & Services."
- Participated in "Graduate Student Poster Contest" at University of Louisiana at Lafayette.
- Won 2nd place in a "24hrs hand-made model-making contest" at VNIT, India.